UNIVERSITY OF CALIFORNIA

Los Angeles

Developing Inorganic Approaches to Polymerization and Bioconjugation

A dissertation submitted in partial satisfaction of the requirements for the degree Doctor of Philosophy in Chemistry

by

Marco Stefano Messina

2019

ABSTRACT OF THE DISSERTATION

Developing Inorganic Approaches to

Polymerization and Bioconjugation

by

Marco Stefano Messina

Doctor of Philosophy in Chemistry

University of California, Los Angeles, 2019

Professor Heather Dawn Maynard, Chair

Multi-disciplinary approaches to problem solving are needed given the increasing complexity of fundamental scientific questions. This dissertation undertakes a holistic approach to research and tackles challenges spanning the biology, chemistry, and materials interface. The central theme for most projects involves applying inorganic and main group chemistry to develop new bioconjugation strategies or polymerization methodologies to access novel materials. Chapter One provides an overview of the dissertation projects and provides insight on the project inceptions.

Chapter Two describes efforts in understanding the effects of trehalose polymers towards protein stabilization. The stabilization capability of polymers made from a set of styrenyl-based trehalose monomer regioisomers were studied. Polymers of each trehalose monomer regioisomer

and one polymer which contained all three isomers combined were synthesized. All polymer regioisomers stabilized insulin to a similar degree towards agitation and heat stress.

Chapter Three details the initial discovery that icosahedral boron-rich cluster compounds of the type $B_{12}(OR_{12})$—where "R" can be any alkyl or aryl group— could be utilized as strong one-electron photooxidants thereby initiating the polymerization of olefins. The perfunctionalized clusters are able to initiate polymerization of a range of styrene substrates under blue LED irradiation. Also demonstrated, is the visible light initiated, metal free cationic polymerization of isobutylene into poly(isobutylene).

Chapter Four introduces carborane-based chain-transfer agents (CTA's) to be used in reversible addition-fragmentation chain-transfer (RAFT) polymerization. The CTA's mediate the controlled polymerization of olefin-based monomers to produce monodisperse carborane terminated polymers. The carborane-based scaffold serves as a general ^{1}H NMR spectroscopic handle used to elucidate polymer molecular weight. Binding of carborane into the hydrophobic cavity of β-cyclodextrin was demonstrated by isothermal titration calorimetry thereby validating its potential use as an affinity label. The carborane RAFT agents also act as Raman active probes.

Chapter Five explores the reactivity of gold(III) organometallic complexes in the context of bioconjugation chemistry. The gold(III) organometallic complexes mediated the conjugation of small molecule substrates which included heterocycles, an anti-cancer drug, biotin, and low molecular weight PEG to cysteine residues on biomolecules. The bioconjugation reactions proceeded rapidly, with high efficiency, and in a broad pH range.

The Dissertation of Marco Stefano Messina is approved.

Dean Ho

Alexander M. Spokoyny

Heather D. Maynard, Committee Chair

University of California, Los Angeles

2019

This dissertation is dedicated to my mother. I love you.

TABLE OF CONTENTS

LIST OF FIGURES

LIST OF TABLES

LIST OF SCHEMES

LIST OF ABBREVIATIONS

(4-Cl)-PS = 4-chloro-polystyrene
AIBN = Azobisisobutyronitrile
CH_2Cl_2 = Dichloromethane
CS_2 = Carbon Disulfide
CTA = Chain transfer agent
CV = Cyclic Voltammetry
Da = Dalton
DARPin = Designed ankyrin repeat protein
DFT = Density functional theory
DMF = *N*,*N*-dimethylformamide
DPBS = Dulbecco's phosphate buffered saline
FGF2 = Fibroblast growth factor 2
GPC = Gel permeation chromatography
GSH = Glutathione
HCl = Hydrochloric acid
HEPES = 2-[4-(2-hydroxyethyl)piperazin-1-yl]ethanesulfonic acid
HOMO = Highest occupied molecular orbital
HPLC = High-performance liquid chromatography
HRP = Horseradish peroxidase
ICP-AES = Inductively coupled plasma atomic emission spectroscopy
ITC = Isothermal titration calorimetry
K_a = Association constant
kDa = kilodalton
LC-MS = Liquid chromatography mass spectrometry
LUMO = Lowest unoccupied molecular orbital
MALS = Multi-angle light scattering
MeCN = Acetonitrile
M_n = Number average molecular weight
M_w = Weight average molecular weight
Na_2CO_3 = Sodium carbonate
NaOH = Sodium hydroxide
NIPAAm = *N*-isopropylacrylamide
NMR = Nuclear magnetic resonance
pDNA = Plasmid deoxyribonucleic acid
PEG = poly(ethylene glycol)
PMA = poly(methyl acrylate)
pNIPAAm = poly(*N*-isopropylacrylamide)
PS = poly(styrene)
RAFT = Reversible addition-fragmentation chain transfer
siRNA = Small-interfering ribonucleic acid
TBA = Tetrabutyl ammonium
TBAF = Tetrabutyl ammonium fluoride
TCEP = Tris(2-carboxyethyl)phosphine

TD-DFT = Time-dependent density functional theory
TFA = Trifluoroacetic acid
THF = Tetrahydrofuran
TMS = Trimethylsilyl
UV-Vis = Ultraviolet-visible
β-Gal = β-galactosidase

ACKNOWLEDGEMENTS

"It may be that the gulfs will wash us down:

It may be we shall touch the Happy Isles,

And see the great Achilles, whom we knew.

Tho' much is taken, much abides; and tho'

We are not now that strength which in old days

Moved earth and heaven, that which we are, we are;

One equal temper of heroic hearts,

Made weak by time and fate, but strong in will

To strive, to seek, to find, and not to yield."

-Alfred, Lord Tennyson

As I reflect on all of the people who have had the greatest influence in my life and during my dissertation studies, no one played a larger role than my mother. Raising a child as a single parent, while working and earning a PhD, takes a great amount of strength and resilience, the stresses and hardships of which surpass even the most daunting NIH R01 proposals or lifeless and deteriorating scientific research projects. Thank you, mom, for the sacrifices you have made which have allowed me to freely pursue my interests.

Thank you also to my grandparents and to all of my aunts: Lydia, Christi, Vicky. Thank you to my father and my family in Italy, reconnecting with you all has definitely been a source of happiness for me. Thank you for the support from afar! I hope I will be able to visit you all more, if I ever earn more than a graduate student stipend. I love you all. Finally, thank you to my (probably) thousands of cousins and extended family in the states and abroad.

I would like to thank my wife, Kathryn, for marrying me. Not a day goes by where I do not spend time with myself, so I do realize how challenging life with me can be. Finding Kathryn has been the single most important achievement of my graduate career. Kathryn, thank you for being my constant source of support and motivation. Thank you also to my in-laws for welcoming me to the family and for the support.

Thank you, Heather, for taking a chance and hiring me. Dealing with my stubbornness for five years is no small task. You have given me a great deal of freedom to pursue new ideas, collaborations, and general life opportunities, I am extremely lucky to have ended up under your guidance, I have learned so much! Thank you for your support, dedication to mentorship, and constant guidance in all things academia. Though I will be indebted to you forever, I promise to accept all invitations for all of the themed journal issues in your honor and to nominate you for all of the awards.

Thank you Alex for allowing me to sit in on your group meetings early on in my graduate career and for giving me the freedom to run wild in your laboratory. Your mentorship and close guidance has been vital to my development as a scientist. You have opened many opportunities for me, I am grateful for all that you have done. Thank you also for being a great friend, I look forward to many years of exchanging great wine. Hopefully one day I will be able to repay all of the coffee and other beverages that you provided. I would also like to thank the other members on my committee, Ellen Sletten and Dean Ho, who have guided me throughout my graduate career. Thank you to my undergraduate advisor, Mark Olson, who set me on this trajectory. I never would have made it this far without your guidance.

I would like to thank Dr. JK for his mentorship throughout my career and for being one of my groomsmen. I appreciate your thoughtfulness and friendship over the years, I have no doubt

you will be incredibly successful in everything you do. Thank you to both Sam and Eric for being great friends and for being involved in mine and Kathryn's wedding (Sam as officiant and Eric as a groomsman). I have learned so much from both of you and have really come to cherish our small dinner parties.

Thank you to Paul Chong, Omar Ebrahim, and Ramya Pathuri, my undergraduate colleagues. You all have contributed immensely to the projects and mentoring you three has been an incredibly fun experience. I am sure that I was the one to learn more from you all than you have learned from me. Thank you also to Hayden, I can't think of anyone more talented and hard-working to lead many of the new research directions formed before I left. You will have an extremely successful research career and I can't wait to see where life takes you!

Thank you to the post-doc crew in Alex's group. Whether you all like it or not, you have all played a significant role in my development, and have really shaped the way that I think about chemistry. Jon, you really have a knack for breathing new life into projects. Your drive and hunger are Brady-esque and I look forward to the day when you release a book/system which rivals "TB12". Thank you for all of the hours you spent with me, your support, and most importantly, for being part of my wedding. You are a great friend and I look forward to all of the success life has to offer you! Liban, your presence was greatly missed in the group after you moved on to the working world! We needed your witty remarks and your ability to argue with Alex for hours during group meetings. You always stuck up for us, but most importantly, you stuck it to the man, hopefully we can meet up across the pond someday. Julia, I have learned a great deal from you in a short amount of time, you really pushed me to become a better scientist. Xin, thank you for all of your support and guidance in everything synthesis.

I would also like to thank the rest of the members from both the Maynard and Spokoyny research groups, there are so many to list! Thank you, Arvind, Kathleen, Neil, Madeline, Pri, Doug, Kyle, Mikayla, Nik, Jane, Emma, Jacquelin, Natalie, Uland, Cait, Maltish, Peter, En-Wei, Nick, June, Daniele, Muhammet, Wixtrom, Kent, Jessica, Rebecca, Harry, Kierstyn, Zee, Nick, Mary, Rafal, and Dahee.

I would like to thank the NSF Bridge-to-Doctorate (Grant HRD-1400789) and Predoctoral Fellowship (Grant DGE-0707424) and the UCLA Christopher S. Foote Fellowship for funding throughout my graduate career.

Chapter 1 is reproduced with permission from Messina, M. S.; Ko, J. H.; Yang, Z.; Strouse, M. J.; Houk, K. N.; Maynard, H. D. Effect of trehalose polymer regioisomers on protein stabilization. *Polym. Chem.* **2017**, *8*, 4781-4788. Dr. Jeong Hoon Ko (JK) contributed greatly to the experimental work. Dr. Zhongyue Yang and Prof. Ken Houk contributed to the computational studies. Dr. M. Jane Strouse contributed to the NMR studies.

Chapter 2 is reproduced with permission from Messina, M. S.; Axtell, J. C.; Wang, Y.; Chong, P.; Wixtrom, A. I.; Kirlikovali, K. O.; Upton, B. M.; Hunter, B. M.; Shafaat, O. S.; Khan, S. I.; Winkler, J. R.; Gray, H. B.; Alexandrova, A. N.; Maynard, H. D.; Spokoyny, A. M. Visible-Light Induced Olefin Activation using 3D Aromatic Boron-Rich Cluster Photooxidants. *J. Am. Chem. Soc.* **2016**, *138*, 6952-6955. Copyright 2016 American Chemical Society. Dr. Jonathan Axtell contributed to much of the experimental work, like many of the projects, a monumental team effort! Dr. Alex Wixtrom, Dr. Kent Kirlikovali, and Paul Chong contributed to the synthesis and characterization of cluster compounds. Yiqun Wang and Prof. Anastassia Alexandrova contributed to the computational studies. Dr. Saeed Khan contributed to the X-ray crystallographic studies. Dr. Brianna Upton contributed to the polymer characterization.

Bryan Hunter, Oliver Shafaat, Dr. Jay Winkler, Prof. Harry Gray contributed to the photophysical studies.

Chapter 3 is reproduced with permission from Messina, M. S.; Graefe, C. T.; Chong, P.; Ebrahim, O. M.; Pathuri, R. S.; Bernier, N. A.; Mills, H. A.; Rheingold, A. L.; Frontiera, R. R.; Maynard, H. D.; Spokoyny, A. M. Carborane RAFT Agents as Tunable and Functional Molecular Probes for Polymer Materials. *Polym. Chem.* **2019**, *10*, 1660-1667. Copyright 2019 Royal Society of Chemistry. Christian Graefe and Prof. Renee Frontiera contributed to the Raman studies. Paul Chong, Omar Ebrahim, Ramya Pathuri, and Harrison Mills contributed greatly to the experimental work (small molecule and/or polymer synthesis). Nicholas Bernier was the ITC data wizard. Dr. Arnold Rheingold was responsible for the X-ray crystallographic studies.

Chapter 4 is reproduced with permission from Messina, M. S.; Stauber, J. M.; Waddington, M. A.; Rheingold, A. L.; Maynard, H. D.; Spokoyny, A. M. Organometallic Gold(III) Reagents for Cysteine Arylation. *J. Am. Chem. Soc.* **2018**, 140, 7065-7069. Copyright 2019 American Chemical Society. Dr. Julia Stauber contributed greatly to the synthesis of many of the organometallic compounds and the experimental work, this was a colossal team effort! Mary Waddington helped with the synthesis of the peptides and with the LC-MS studies as well. Dr. Arnold Rheingold was responsible for the X-ray crystallographic studies.

VITA

Education

University of California, Los Angeles (UCLA) Los Angeles, CA (2014-Present)

- Ph.D. Candidate in Organic Chemistry

Texas A&M University- Corpus Christi (TAMUCC) Corpus Christi, TX (2009-2014)

- B.S. Chemistry, with Honors
- Minor: Philosophy

Research Experience

7/2014 – present Graduate Researcher, Department of Chemistry and Biochemistry, UCLA.

Advisors: Heather D. Maynard and Alexander M. Spokoyny

1/2012 – 7/2014 Undergraduate Researcher, Department of Physical and Environmental Sciences, TAMUCC.

Advisor: Mark A. Olson

6/2013 – 8/2013 Undergraduate Researcher, Department of Chemistry, Massachusetts Institute of Technology (MIT).

Advisor: Jeremiah A. Johnson

Selected Awards

- Aduro-Berkeley Postdoctoral Fellowship (2019-2021)
- Boehringer-Ingelheim-UCLA Dissertation Award for Excellence in Organic Chemistry (2019)
- John Stauffer Fellowship, UCLA (2019)
- Christopher S. Foote Fellowship, UCLA (2017)
- NSF- Predoctoral Fellowship (GRFP) (2016-2019)
- Ford Fellowship Honorable Mention (2015)
- NSF- Bridge-to-Doctorate Fellowship (2014-2016)
- Eugene V. Cota-Robles Fellowship (2014-2019)
- UCLA Competitive Edge (2014)
- NSF- LSAMP Research Fellow, National Science Foundation. (2012 – 2014)
- SACNAS National Conference Travel Scholarship (2012)
- NSF- ACE Research Fellow, National Science Foundation (2012 – 2014)
- Welch Research Fellow, Welch Foundation. (2012)

Publications (*Denotes corresponding author; †Denotes equal contribution)

Axtell, J. C.*; **Messina, M. S.**; Liu, J.-Y.; Galaktionova, D.; Schwan, J.; Porter, T. M.; Savage, M. D.; Wixtrom, A. I.; Rheingold, A. L.; Kubiak, C. P.; Winkler, J. R.; Gray, H. B.*; Kral, P.*; Alexandrova, A. N.*; Spokoyny, A. M.* "Photooxidative Generation of Dodecaborate-Based Weakly Coordinating Anions." *Inorg. Chem.* **2019**, DOI: 10.1021/acs.inorgchem.9b00935.

Messina, M. S.*; Graefe, C. T.; Chong, P.; Ebrahim, O. M.; Pathuri, R. S.; Bernier, N. A.; Mills, H. A.; Rheingold, A. L.; Frontiera, R. R.*; Maynard, H. D.*; Spokoyny, A. M.* "Carborane RAFT Agents as Tunable and Functional Molecular Probes for Polymer Materials" *Polym. Chem.* **2019**, *10, 1660*-1667.

Messina, M. S.†; Stauber, J. M.†; Waddington, M. A.; Rheingold, A. L.; Maynard, H. D.*; Spokoyny, A. M.* "Organometallic Gold(III) Reagents for Cysteine Arylation" *J. Am. Chem. Soc.* **2018**, 140, 7065-7069.

Messina, M. S.†; Ko, J. H.†; Yang, Z.; Strouse, M. J.; Houk, K. N.; Maynard, H. D.* "Effect of Trehalose Polymer Regioisomers on Protein Stabilization" *Polym. Chem.* **2017**, *8*, 4781-4788.

Dziedzic, R. M.; Martin, J. L.; Axtell, J. C.; Saleh, L. M. A.; Ong, T.-C.; Yang, Y.-F.; **Messina, M. S.**; Rheingold, A. L.; Houk, K. N.; Spokoyny, A. M.* "Cage-Walking: Vertex Differentiation by Palladium-Catalyzed Isomerization of B(9)-Bromo-meta-Carborane" *J. Am. Chem. Soc*. **2017**, *139*, 7729-7732.

Qian, E. A.; Wixtrom, A. I.; Axtell, J. C.; Saebi, A.; Jung, D.; Rehak, P.; Han, Y.; Moully, E. H.; Mosallaei, D.; Chow, S.; **Messina, M. S.**; Wang, J. Y.; Royappa, A. T.; Rheingold, A. L.; Maynard, H. D.; Král, P.; Spokoyny, A. M.* "Atomically Precise Organomimetic Cluster Nanomolecules (OCNs) Assembled via Perfluoroaryl-thiol S_NAr chemistry" *Nature Chem*. **2017**, *9*, 333-340.

Messina, M. S.†; Axtell, J. C.†; Wang, Y.; Chong, P.; Wixtrom, A. I.; Kirlikovali, K. O.; Upton, B. M.; Hunter, B. M.; Shafaat, O. S.; Khan, S. I.; Winkler, J. R.; Gray, H. B.; Alexandrova, A. N.; Maynard, H. D.; Spokoyny, A. M.* "Visible-Light Induced Olefin Activation using 3D Aromatic Boron-Rich Cluster Photooxidants" *J. Am. Chem. Soc.* **2016**, *138*, 6952-6955.

Olson, M. A.*; **Messina, M. S.**; Thompson, J. R.; Dawson, T. J.; Goldner, A.; Gaspar, D.; Vazquez, M.; Lehrman, J. A.; Sue, A. C.-H. "Reversible Morphological Changes of Assembled Supramolecular Amphiphiles Triggered by pH-Modulated Host-Guest Interactions" *Org. Biomol. Chem.* **2016**, *14*, 5714-5720. *New Talent Issue*.

Olson, M. A.*; Thompson, J. R.; Dawson, T. J.; Hernandez, C. M.; **Messina, M. S.**; O'Neal, T. "Template-Directed Self-Assembly by way of Molecular Recognition at the Micellar-Solvent Interface: Modulation of the Critical Micelle Concentration" *Org. Biomol. Chem.* **2013**, *11*, 6483-6492.

Patents and Patent Applications

Spokoyny, A. M.; Maynard, H. D.; Qian, E.; **Messina, M. S.**; Wixtrom, A. I.; Axtell, J. C.; Kirlikovali, K. O.; Gonzalez, A. "Aromatic Boron-Rich Cluster Photooxidants", United States Patent: 2017/018755; International: WO/2017/143348 A2.

Chapter 1

General Introduction

1.1 General Overview

The general need for multi-disciplinary strategies to tackle challenges at the interface of multiple fields has shaped my PhD studies and this dissertation. Against this backdrop, I have spent my dissertation studies bridging the research themes of two groups by developing main-group and organometallic-based systems for polymerization and bioconjugation. The broad theme throughout each project is in the development of new materials or in the development of methodologies to access specific materials, and the foundation of each project lies in chemical synthesis.

The first project consists of synthesizing styrenyl trehalose-based polymers for protein stabilization, the ultimate goal of which was to determine if the modification site of the styrene substituent on the trehalose monomers would affect the overall ability of the polymers to stabilize a therapeutically relevant protein to agitation and heat stress.[1] The Maynard group has previously shown that trehalose-based polymers are able to stabilize an array of proteins to heat stress and have also studied the effect that different polymer backbones have on the stabilization of proteins.[2-4] However, we had yet to understand if different monomer regioisomers would have a significant effect on the overall stabilization capability of the polymers. During the synthesis of the styrenyl-based trehalose monomer, we observed the formation of four regioisomeric products in which styrene was substituted at either the 2-O, 3-O, 4-O, or 6-O position of trehalose. This led to a study where we isolated each of the trehalose monomer regioisomers, with the exception of the 3-O substituted product due to <1% yield, and polymerized each one using free-radical polymerization. Additionally, we prepared a polymer containing all of the monomer regioisomers. Ultimately, we found that all polymers were able to stabilize the protein insulin to agitation and minor heat stress,

indicating that the regioisomers could be pooled together in order to increase the overall yield of the monomer synthesis thus avoiding tedious purification techniques.[1]

Through the course of these studies I had encountered difficulties in polymer characterization. GPC analysis of the trehalose-based polymers consistently produced low molecular weight readings as all of the polymer samples were eluting from the column late into the method.[1,5] Additionally, calculation of the polymer molecular weight by ^{1}H NMR of controlled polymerization reactions did not match the polymer molecular weight by GPC and in all cases the trehalose polymers again eluted close to the solvent elution on the GPC spectra. Ultimately, because the hydroxyl groups on trehalose can interact with the GPC columns thereby introducing inaccurate results, we acetyl protected the trehalose polymers in order to determine polymer molecular weight through back-calculation by GPC.

This problem inspired a strategy to address an idea which had been passed around the Maynard laboratory for some time. This idea was to develop a polymer initiator which could also act as a spectroscopic probe in order to determine polymer molecular weight by end-group analysis using ^{1}H NMR. This type of initiator would need to be substituted with a motif which exhibited a shift in the ^{1}H NMR spectrum significantly different from most commonly used polymer materials and was also strong enough in intensity for accurate integration. This strategy could then be used to determine the molecular weight of polymer materials which were not amenable to traditional GPC techniques. Having become familiar with the carborane-based research projects in the Spokoyny group, the idea of using a carborane-based scaffold to incorporate on the polymer chain-end took shape and ultimately led to the third chapter of the dissertation.

We opted to develop an *ortho*-carborane-based chain-transfer agent to be used in RAFT polymerization processes.[6] The *o*-carborane scaffold is highly tunable, as the boron vertices can

be easily functionalized using reported techniques. *O*-carborane also has unique electronic properties. Carbon atoms attached to the boron vertices most distal to the carbon vertices (B(9) and B(12)) encounter a shielding effect which results in a resonance that appears far upfield (methyl C-*H* ≈ 0.2 ppm) in the ^{1}H NMR spectrum. Carborane is also able to bind into hydrophobic pockets within proteins, a characteristic which could play a role in affinity labeling processes.[7-9] Additionally, the B-H vibration resonates at ~2350-2600 cm^{-1} which is a typically silent region in the Raman spectrum of biological samples and is also unique amongst other commonly used Raman probes which rely on the vibration signal of alkynes and nitriles.[10] All of these characteristics would make carborane-based RAFT agents unique amongst other commonly used RAFT agents and would bridge the themes of main-group chemistry with controlled radical polymerization techniques.[6]

We were able to synthesize a set of carborane RAFT agents in an efficient manner using straight-forward synthetic techniques. The carborane RAFT agents were proficient in mediating the RAFT polymerization of styrene, acrylate, and acrylamide based monomers producing polymers of controlled molecular weights. In all cases, the ^{1}H resonances from the methyl substituents on the B(9) and B(12) vertices of carborane were sufficiently upfield from any of the ^{1}H resonances exhibited by the polymers themselves, which made for facile determination of polymer molecular weight through end-group analysis using ^{1}H NMR spectroscopy. The polymer molecular weight determined by end-group analysis matched closely with the molecular weight determined by GPC across a range of polymers. We performed ITC to measure the extent of binding of the *ortho*-carborane terminated polymers to β-cyclodextran as a model system and found 2:1 binding of *ortho*-carborane to β-cyclodextran with strong binding affinity (K_a = 9.37 x 10^{4} M^{-1}) which is advantageous for its use in affinity labeling applications.[6] Additionally, the

carborane terminated polymers exhibited a Raman signal at 2549 cm^{-1}, a silent region in the Raman spectra of biological samples, indicating that the carborane RAFT agents could also serve as Raman active probes.[6]

The second chapter of this dissertation was a project that spawned out of the Spokoyny group, but again allowed me the ability to bridge the research themes of inorganic cluster-based chemistry with polymerization techniques. This project involved our initial discovery that persubstituted boron-rich clusters of the type $B_{12}(OCH_2Ar)$ (where Ar = C_6H_5 (**1**) or C_6F_5 (**2**)) could act as powerful one-electron photooxidants for the initiation and subsequent polymerization of olefins.[11] We found the formation of polymer upon leaving a solution of 4-methoxystyrene in the presence of **1** under ambient laboratory lighting. Ultimately this initial observation led to us performing control experiments which determined that polymerization occurs only in the presence of both visible light and the cluster compounds. Because both of the boron-rich cluster derivatives absorb at 450 nm, we performed all polymerization reactions under blue LED irradiation. After observing low polymer yields in the presence of **1**, we hypothesized that addition of electron-withdrawing groups on the periphery of the cluster would increase the oxidation potential of the compound to generate a more reactive species and synthesized **2** under this hypothesis. Due to the higher oxidation potential of exhibited by **2** (0.5V higher than **1** vs SCE), we were able to polymerize a large array of electron-rich or -poor styrene substrates with varying functionality. Additionally, we were able to demonstrate the first example of a visible-light initiated and metal free polymerization of the completely unactivated olefin monomer isobutylene into highly branched poly(isobutylene) using **2**.[11]

The final chapter of this dissertation involves the use of organometallic gold(III) reagents for the modification of cysteine amino acid residues on peptides and proteins.[12] The goal was to

broaden the scope of transition-metal based complexes able to carry out the chemoselective modification of biomolecules in biologically relevant conditions. Moreover, I saw this as an opportunity to develop an organometallic-based approach for the construction of protein-polymer conjugates thereby harnessing the expertise of both the Maynard and Spokoyny groups. The hypothesis at the beginning of the project was that the thiophilicity and electrophilicity exhibited by gold(III) oxidative addition complexes should enable for chemoselectivity towards cysteine amino acid residues and facilitate reductive elimination to transfer aryl-containing molecules to cysteine, a process termed cysteine arylation. We began this project using carborane stabilized gold(III) oxidative addition complexes harboring small molecule aryl groups and found them successful in undergoing cysteine arylation on peptides. However, we observed decreased product yields upon higher fractions of water in the reaction media.[12] This posed a challenge as it is essential for new biomolecule modification strategies to exhibit high efficiency in biologically relevant solvent conditions. After multiple failed attempts to modify the ligand system on our caborane stabilized gold(III) oxidative addition complexes, we turned to a commercially available gold(I) precursor stabilized by an Me-Dalphos ligand framework. Using a modified synthetic approach developed by the Bourissou group, we were able to synthesize an array of gold(III) organometallic reagents harboring pharmaceutically relevant aryl substrates, which included heterocycles, an anti-cancer drug, a short-chain PEG, and a fluorescent dye. The MeDalphos stabilized gold(III) reagents were able to efficiently modify a range of unprotected peptide and protein substrates in a variety of conditions. The bioconjugation reactions proceeded rapidly (<5 min) in a large pH window (0.5-14), at ambient temperature, and in low micromolar concentrations. Using this methodology we were able to generate peptide macrocycles, transfer

pharmaceutically relevant molecules onto the surface of peptides and proteins, and transfer a short-chain PEG onto a therapeutically relevant protein in completely aqueous conditions.[12]

Future work in this area is focused on using gold(III) chemistry as a platform to develop protein-polymer conjugates by either grafting-to or grafting-from. This includes taking advantage of the chemoselectivity of the gold(I)-based reagents to undergo oxidative addition across Aryl-I bonds in the presence of other $Csp^{2/3}$-X bonds. This characteristic will enable us to develop gold(III) oxidative addition complexes harboring prototypical ATRP initiators which we can then transfer to cysteine amino acid residues on proteins in order to build a polymer from the protein surface. Additionally, we can develop gold(III) oxidative addition complexes modified with polymers in order to efficiently transfer polymers directly to proteins.

1.2 References

1 Messina, M. S.; Ko, J. H.; Yang, Z.; Strouse, M. J.; Houk, K. N.; Maynard, H. D. *Polym. Chem.* **2017**, *8*, 4781-4788.

2 Mancini, R. J.; Lee, J.; Maynard, H. D. *J. Am. Chem. Soc.* **2012**, *134*, 8474-8479.

3 Pelegri-O'Day, E. M.; Lin, E.-W.; Maynard, H. D. *J. Am. Chem. Soc.* **2014**, *136*, 14323-14332.

4 Lee, J.; Lin, E.-W.; Lau, U. Y.; Hedrick, J. L.; Bat, E.; Maynard, H. D. *Biomacromolecules* **2013**, *14*, 2561-2569.

5 Pelegri-O'Day, E. M.; Paluck, S. J.; Maynard, H. D. *J. Am. Chem. Soc.* **2017**, *139*, 1145-1154.

6 Messina, M. S.; Graefe, C. T.; Chong, P.; Ebrahim, O. M.; Pathuri, R. S.; Bernier, N. A.; Mills, H. A.; Rheingold, A. L.; Frontiera, R. R.; Maynard, H. D.; Spokoyny, A. M. *Polym. Chem.* **2019**, *10*, 1660-1667.

7 Zheng, Z.; Jiang, W.; Zinn, A. A.; Knobler, C. B.; Hawthorne, M. F. *Inorg. Chem.* **1995**, *34*, 2095-2100.

8 Teixidor, F.; Barberà, G.; Vaca, A.; Kivekäs, R.; Sillanpää, R.; Oliva, J.; Viñas, C. *J. Am. Chem. Soc.* **2005**, *127*, 10158-10159.

9 Spokoyny, A. M.; Lewis, C. D.; Teverovskiy, G.; Buchwald, S. L. *Organometallics* **2012**, *31*, 8478-8481.

10 Kennedy, D. C.; Duguay, D. R.; Tay, L.-L.; Richeson, D. S.; Pezacki, J. P. *Chem. Commun.* **2009**, 6750-6752.

11 Messina, M. S.; Axtell, J. C.; Wang, Y.; Chong, P.; Wixtrom, A. I.; Kirlikovali, K. O.; Upton, B. M.; Hunter, B. M.; Shafaat, O. S.; Khan, S. I.; Winkler, J. R.; Gray, H. B.;

Alexandrova, A. N.; Maynard, H. D.; Spokoyny, A. M. *J. Am. Chem. Soc.* **2016**, *138*, 6952-6955.

12 Messina, M. S.; Stauber, J. M.; Waddington, M. A.; Rheingold, A. L.; Maynard, H. D.; Spokoyny, A. M. *J. Am. Chem. Soc.* **2018**, *140*, 7065-7069.

Chapter 2

Effect of Trehalose Polymer Regioisomers on Protein Stabilization

2.1 Introduction

Proteins are widely used as therapeutics in the pharmaceutical industry, feed-stock additives in the agricultural industry, and biochemical reagents in the laboratory setting. However, many proteins are prone to inactivation when exposed to outside stressors such as heat,[1] pH changes,[2] agitation,[3] and desiccation,[4] and their instability during the production, storage, and transport increases their cost.[5] To prevent denaturation and thereby prolong protein activity, excipients such as sugars and polymers are often added to protein formulations.[6]

Trehalose, a non-reducing disaccharide formed by α,α-1,1-linked glucose units,[7] is upregulated in lower-level organisms such as tardigrades during long periods of desiccation.[8,9] This increase in trehalose concentration imparts stability to the organism by protecting the cell membrane and proteins.[10] The mechanism of trehalose protein stabilization is under debate and there exist several different hypotheses.[11-13] The three main hypotheses include water replacement,[13] mechanical entrapment (vitrification),[10] and water entrapment.[14] In the water replacement theory, trehalose forms direct hydrogen bonds with the protein, effectively replacing water molecules and acting as the protein hydration shell. The mechanical entrapment hypothesis suggests that trehalose forms a glassy matrix around the protein, thereby reducing the mobility of the protein and allowing it to retain its tertiary structure. The water entrapment theory states that trehalose molecules trap water molecules around the protein to form a water hydration layer between the protein and trehalose. While the exact mechanism, or the combination of multiple mechanisms, responsible for the stabilization of proteins by trehalose remains to be fully determined,[15] the stability that trehalose imparts on proteins remains clear. It is this feature that has enabled its use as an excipient in a range of protein therapeutic formulations such as

Herceptin®, Avastin®, and Advate®.[16] Trehalose has also been effective as an excipient for the stabilization of reverse transcriptase,[17] as an embedding medium for preserving protein structure during electron crystallography,[18] and as an additive to improve shelf-life of food/ pharmaceutical/cosmetic products.[16]

Motivated by these features of trehalose, we developed polymeric materials based on trehalose that stabilize proteins ranging from enzymes,[19-21] growth factors,[22,23] hormones,[24] and antibodies[22,25] to various stressors including heat, lyophilization, agitation, and direct electron beam irradiation. Other groups have also used trehalose containing polymers in the prevention of amyloid beta (Aβ) aggregation[26] and small interfering RNA (siRNA) and plasmid DNA (pDNA) delivery.[27,28] Previously, we have explored the effect of the polymer back- bone identity on the overall stabilization properties of trehalose glycopolymers by comparing polystyrene and polymethacrylate backbones as excipients to stabilize horseradish peroxidase (HRP) to heat and β-galactosidase (β-Gal) to lyophilization.[20] Slight differences in stabilizing effect were observed for different polymer backbones at low equivalents of the polymer, but at higher equivalents all of the polymers stabilized the proteins, regardless of polymer backbone.

We were thus motivated to systematically investigate the effect of the point of linkage on trehalose while keeping the polymer backbone the same. To study possible differences between trehalose regioisomers on protein stabilization, we prepared styrenyl trehalose monomers with trehalose modified at the 2-O, 3-O, 4-O, or 6-O positions (Scheme 2-1). The resulting polymers, as well as a polymer containing all of the regioisomers, were then tested as excipients for the stabilization of the model protein insulin to mechanical agitation. The results are described herein.

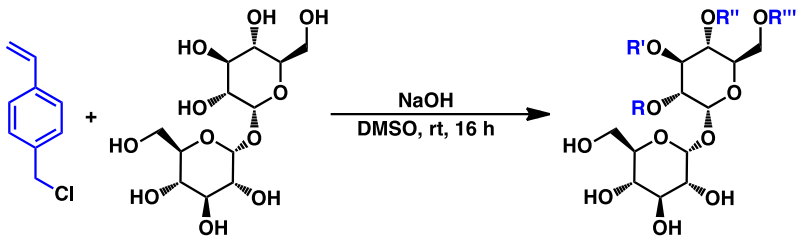

Scheme 2-1. Synthesis of trehalose monomer regioisomers.

2.2 Results and Discussion

The styrenyl trehalose monomers were synthesized using a single-step Williamson etherification. While the synthetic route does not require protecting group strategies, it does result in four regioisomeric monomers **O2**, **O3**, **O4**, and **O6**. Fortunately, the isomers exhibited significantly different retention times on the HPLC (Table 2-1, top), which allowed us to separate the monomers.

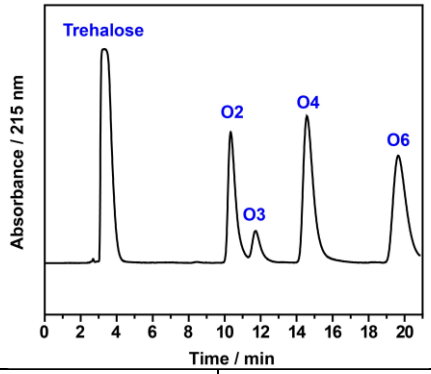

Monomer	Isolated Yield
O2	11%
O3	<1%
O4	39%
O6	13%
OA	64%

Table 2-1. HPLC trace and yields for trehalose monomer regioisomers.

The identity of each regioisomer was assigned after extensive characterization by NMR spectroscopy (COSY, HMBC, and HSQC) (Figure A1–A20). Although the regioisomers were expected to exhibit very similar characteristics, the coupling of the geminal benzyl protons in the ^{1}H NMR spectra varied significantly, with **O4** exhibiting strong coupling (10.8 Hz) indicative of nonequivalent geminal protons in significantly different environments and large Δδ (0.16 ppm; Figure 2-1 B) and **O2** and **O6** exhibiting similarly strong coupling (Figure 2-1 A and C), while **O3** did not show any benzyl proton coupling (Figure A6). This spectroscopic data gave us an indication that each monomer likely adopts a different conformation in solution. Direct NMR observation of through-space correlation in aqueous environment was not possible due to the broadening of the trehalose hydroxyl proton signals in water. Therefore, we computationally explored the differences in the aqueous conformation of the regioisomers.

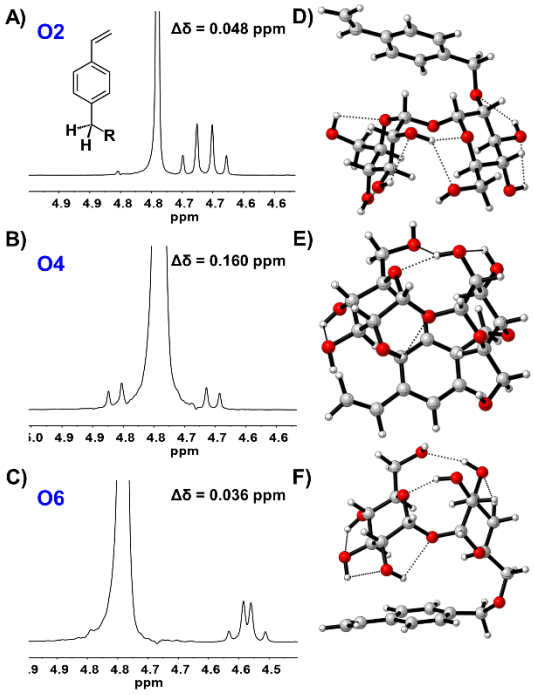

Figure 2-1. Benzyl region of ^{1}H NMR for monomers **O2**, **O4**, and **O6**, and their corresponding lowest energy conformations in aqueous solution.

Briefly, for each isomer a conformational search was con- ducted using Maestro 10.4 and select conformers were optimized by density functional theory (DFT) calculation at B3LYP-D3/6-31G(d) level of theory in Gaussian 09.[29] As shown by the lowest energy conformers for each isomer (Figure 2-1 D–F), all of the isomers retain the so-called clam shell conformation, in which the disaccharide is bent at the anomeric position, bringing the two glucose rings in close proximity that is characteristic for trehalose.[30,31] All of the stable conformations (defined prior to the calculations as within 2 kcal mol^{-1} energy with respect to the most stable conformation) retain the clam shell conformation (Figure A52) as opposed to the higher energy more open conformation (Figure A53). However, **O6** has a single most stable conformation within 4 kcal mol^{-1} (i.e., 99.9% of the population will be in this conformation at any given time according to Boltzmann distribution), and **O4** has two stable conformations within 2 kcal mol^{-1} that only differ by 0.1 kcal mol^{-1} in energy. **O2** has multiple stable conformations within 2 kcal mol^{-1}. These results suggest that **O6** and **O4** have a relatively rigid conformation while other regioisomers are more flexible and fluctuate among the multiple low energy conformations. This result is reasonable, since **O2** substitution would cause the most steric hindrance to the opposite ring due to the spatial proximity of the vinyl benzyl unit, while **O6** would cause the least hindrance. Furthermore, both of the lowest-energy conformations of **O4** show that one of the benzyl protons is proximal to the oxygen of the adjacent hydroxyl on C3 (2.41 and 1.92 Å for the two lowest energy conformers, (Figure 2-1E)), which would explain the exceptionally large $\Delta\delta$ of **O4** benzyl protons in the ^{1}H NMR spectrum (Figure 2-1B).

The yields for all of the regioisomers are provided in Table 2-1; **OA** denotes the combined yield of all of the monomer regioisomers. Interestingly, **O4** was the most favored product. This observed regioselectivity was unexpected, as the primary hydroxyl (**O6**) would be anticipated as

the major product in a simple S_N2 reaction such as Williamson etherification. Based on literature reports of metal-trehalose ionic complexation,[32,33] we hypothesized that ionic complexation of sodium with trehalose may be responsible for the reduced nucleophilicity of the primary hydroxyl. It has been reported that sugars complex with cations in the following order: $Ca^{2+} > Mg^{2+} > Na^{+} > K^{+}$,[32] and the crystal structure of Ca^{2+} with trehalose indicates that 2-O, 3-O, and 6-O chelate the cation.[33] One would therefore expect that the use of potassium hydroxide in place of sodium hydroxide would result in a relatively looser ion pairing at 6-O and increased modification at the primary hydroxyl due to its intrinsically higher nucleophilicity, if ionic complexation were responsible for the unusual selectivity. Indeed, the yield of **O6** relative to **O4** was increased when potassium hydroxide was used as the base or when less sodium hydroxide was used than in the reaction (Table A1). This was further supported by the increased relative yield of **O6** at higher temperature or in water, both of which would attenuate the effect of ionic complexation (Table A2). In water **O6** was the major product as expected. However, the absolute yield of the monomers in water was low even in the presence of a phase transfer catalyst, which was likely due to the hydrolysis of the vinylbenzyl chloride.

Modulation of sugar hydroxyl reactivity by intramolecular hydrogen bonds[34] and metal ions[35] has been previously observed. Benzoylation of methyl α-D-glucopyranoside in pyridine showed that hydroxyl reactivity followed the order 6-OH > 2-OH > 3-OH > 4-OH.[34] However, different reaction conditions changed the reactivity, sometimes even favoring the secondary alcohol 2-OH over the primary 6-OH when mannose was methylated in the presence of silver oxide.[34] Miller et al. leveraged the calcium complexation of fructose to selectively modify the 3′-OH secondary hydroxyl of the fructose unit in a glycosyl acceptor in the presence of four primary hydroxyls in the donor and the acceptor.[35] Our observation on the interesting chemical reactivity

of trehalose adds to the body of work on regioselectivity of sugars.

With the monomer regioisomers assigned, we then targeted polymers made from each regioisomer monomer separately (**P2**, **P4**, and **P6**) and also one containing all regioisomers together (**PA**) (Figure 2-2). The polymer containing all of the monomer regioisomers was synthesized by pooling the mixture purified from HPLC (**OA**). The polymer from **O3** was not pursued due to the low yield of the monomer. The polymers were all synthesized using free radical polymerization with AIBN as the initiator in DMF and water mixtures at 90 °C.

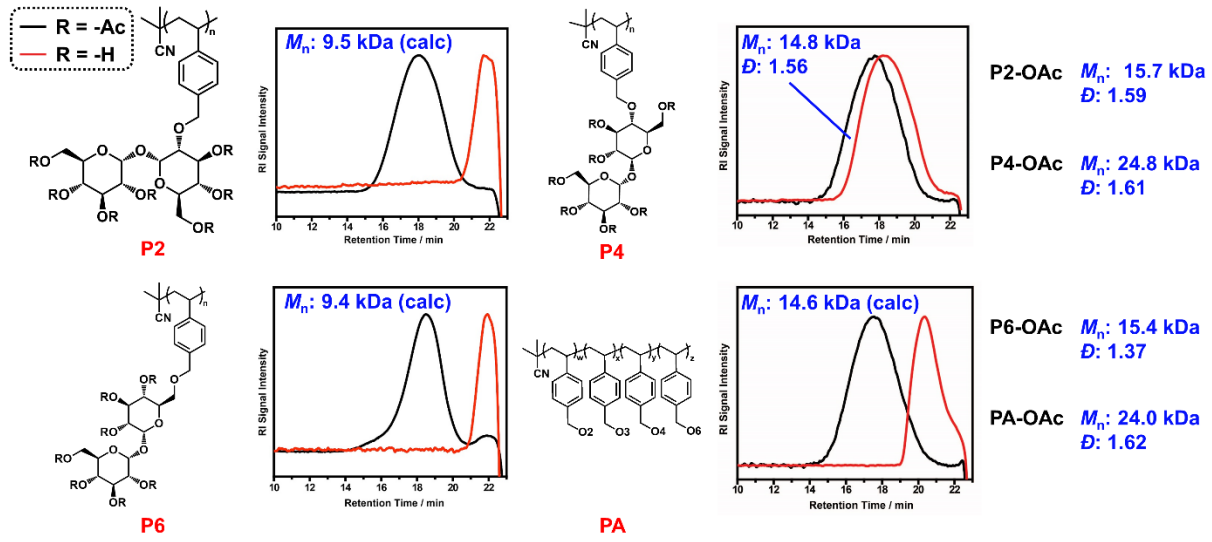

Figure 2-2. Polymer structures of **P2**, **P4**, **P6**, and **PA**. GPC traces with corresponding molecular weight and dispersity for acetyl protected (black) and unprotected (red) polymers. The molecular weights for the unprotected polymers are provided above the GPC traces. For **P2**, **P6**, and **PA** these were calculated from the GPC of the acetylated polymers.

Polymerization of **O2**, **O6**, and **OA** resulted in polymers (**P2**, **P6**, and **PA**), which ran close to the solvent elution on the GPC spectra, initially suggesting that the M_n of polymers were very small (<2 kDa; Figure 2-2). We have previously observed that trehalose polymers with free

hydroxyl groups can interact with GPC columns in DMF giving erroneous results.[23] Thus, to better characterize the molecular weight, we acetylated each polymer (**P2-OAc**, **P4-OAc**, **P6-OAc**, and **PA-OAc**). This was accomplished by treating a small portion of the polymer in solution with excess acetic anhydride in dry pyridine and stirring at room temperature for 48 hours. The motivation was that by increasing the hydrophobicity of the polymer, the polymers from different regioisomers would be similarly solvated by the organic mobile phase (DMF) for accurate GPC analysis. Indeed, acetyl protected polymers showed larger M_n (15.4–24.8 kDa, Figure 2), which allowed us to back-calculate the original polymer molecular weight. Since **P4** did not give erroneous GPC readings as the other polymers, we used this polymer as a control to test the accuracy of estimating M_n in this manner. The M_n for **P4-OA**c was 24.8 kDa, which gives a calculated weight for **P4** of 15.1 kDa. This result is very close to the 14.8 kDa M_n determined by GPC of **P4** prior to acetylation (Figure 2-2). This method provided us molecular weights between 9.4–14.8 kDa for all the polymers. We also tested to see if the mixture of monomers could be acetylated first and then polymerized. Indeed, the polymerization proceeded smoothly to yield **PA-OA**c that was subsequently deprotected as **PA** (see Appendix A for details).

We then utilized the polymers to prevent aggregation of a protein during heating to body temperature and agitation, since this is one way therapeutic proteins are degraded. Insulin was employed as the model protein, since it is an important and widely used therapeutic protein for the treatment of diabetes. Insulin solutions are prone to aggregation when agitated, which makes transportation and storage difficult.[3] Inactivation of insulin, even in small amounts, poses a risk to patients due to improper insulin dosage.[36]

Samples were prepared of insulin and polymer at 1 and 10 weight equivalents (wt equiv.)

in DPBS in 1.5 mL screw-top dram vials. The protein samples were stressed at 37 °C with 250 rpm agitation for 3 hours. Using this method, large insoluble insulin aggregates were visually observed (Figure A50). In order to quantify the amount of intact (non-aggregated) insulin, we utilized HPLC. HPLC has been frequently employed to separate degradation products from the protein thereby enabling accurate quantification of intact insulin.[37] After stress, samples were filtered through 0.2 μm syringe filters to ensure removal of insulin aggregates and analyzed via HPLC.

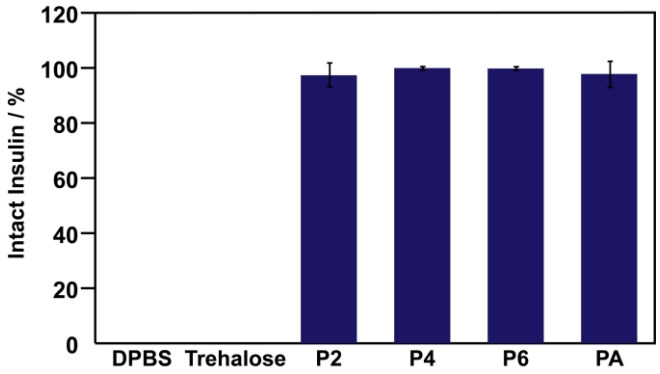

Figure 2-3. Stabilization of insulin using 10 wt equiv. of polymer. Samples were heated to 37 °C with 250 rpm agitation for 3 hours. Intact insulin quantified by HPLC. There is no statistical difference between polymers (n = 3). Note that DPBS and trehalose have zero intact insulin %.

None of the polymers prevented aggregation at 1 wt. equiv. (Figure A51). However, all of the polymers prevented aggregation of insulin similarly (97–100%) at 10 wt. equiv., whereas samples of insulin stressed without added polymer or with 10 wt. equiv. of trehalose aggregated completely (Figure 2-3) meaning that zero percent intact insulin was observed by HPLC. This agrees with previous observations that trehalose in polymeric form is a better stabilizer than trehalose.[19,20,26] Since there were no statistical differences in stabilization between polymers at 10

wt equiv., we conclude that the trehalose monomer regioisomers can be combined to achieve higher monomer yield, and all polymers can be utilized interchangeably, at least with the protein insulin.

The computational studies have shown that while there seem to be differences in conformational flexibility between the monomer regioisomers, all of the stable conformations still possess the clam shell conformation of trehalose (Figure A52), and it is mostly the vinyl benzyl substituent that moves in the conformations for each isomer. Studies have pointed to the axial α,α-(1→1) linkage that results in the clam shell conformation as being important for the protective ability of trehalose.[30,31] Indeed, we have observed that trehalose polymers have superior protein stabilizing ability over polymers from other sugars such as lactose that have more open conformations.[23] More thorough investigation is needed in the future to conclusively decouple the effects of conformational rigidity and the clam shell conformation on protein stabilization; in other words, more work will need to be done to determine if it is the clam shell conformation and the spatial arrangement of the hydroxyl groups itself or the molecular rigidity that results from the clam shell that is responsible for the stabilization. Nonetheless, we observe that the site of attachment of the trehalose to the polymer backbone does not have significant influence on the stabilizing ability. It should also be noted that the trehalose polymer stabilizes better than trehalose, likely due to the cluster glycoside effect from increased local concentration[23,28] and/or the nonionic surfactant character of the hydrophilic sugar side chain attached to the hydrophobic backbone.[20,23] Together, our findings offer an interesting view on the synthesis of trehalose monomers and provide us with data suggesting that monomer regioisomers can be pooled to increase trehalose polymer yields without reducing protein stabilization ability.

2.3 Conclusions

In conclusion, we synthesized four trehalose regioisomers containing an ether-linked styrene moiety positioned at the 2-O, 3-O, 4-O, or 6-O position of trehalose. The substitution position of each monomer was rigorously identified via NMR spectroscopy. NMR data suggested that each regioisomer adopted a distinct conformation in solution and computational methods were employed to explore this. Calculations gave insight into the relative rigidity of the trehalose regioisomers in solution, with monomers **O6** and **O4** being the least flexible with only one or two stable conformations, and monomer **O2** showing multiple stable conformations suggesting that it is conformationally flexible. Despite the differences in conformational flexibility, all monomer regioisomers retained the native clam shell conformation of trehalose. We then probed the stabilization capability of each trehalose regioisomer in polymeric form. Polymers containing each monomer separately and one containing all monomer regioisomers together were synthesized via free radical polymerization. The stabilization capability of the polymers as excipients against mechanical agitation with moderate heating was then tested using insulin as a model protein. There was no substantial difference in the stabilization capability between each polymer; the different polymers prevented protein aggregation (>97%) while there was no intact insulin with trehalose itself or free protein. We conclude that different regioisomers may be combined to achieve higher yields of the polymer material while being able to effectively stabilize proteins, at least insulin, to mechanical stress.

Acknowledgements

H. D. M. thanks the NSF (CHE-1507735) for funding. M. S. M. thanks the NSF Bridge-to-Doctorate (HRD-1400789) and the Predoctoral (GRFP) (DGE-0707424) Fellowships and

UCLA for the Christopher S. Foote Fellowship. The AV 500 NMR data was obtained on equipment supported by the NSF (CHE-1048804). The authors would like to thank Dr. En-Wei Lin for the synthesis of **P4-OAc**, and Dr. Peter Dornan and Professor Mike Jung for the helpful discussion on the origin of regioselectivity in the monomer synthesis. K. N. H. thanks NSF (CHE-1361104) for financial support. Computational resources were provided by the UCLA Institute for Digital Research and Education (IDRE) and the Extreme Science and Engineering Discovery Environment (XSEDE), which is supported by the NSF (OCI-1053575).

2.4 References

1. Oobatake, M.; Ooi, T. *Prog. Biophys. Mol. Biol.*, **1993**, *59*, 237–284.
2. Chi, E. Y.; Krishnan, S.; Randolph, T. W.; Carpenter, J. F. *Pharm. Res.*, **2003**, *20*, 1325–1336.
3. Sluzky, V.; Tamada, J. A.; Klibanov, A. M.; Langer, R. *Proc. Natl. Acad. Sci. U. S. A.*, **1991**, *88*, 9377–9381.
4. Wang, W. *Int. J. Pharm.*, **2000**, *203*, 1–60.
5. Kintzing, J. R.; Interrante, M. V. F.; Cochran, J. R. *Trends Pharmacol. Sci.*, **2016**, *37*, 993–1008.
6. Kamerzell, T. J.; Esfandiary, R.; Joshi, S. B.; Middaugh, C. R.; Volkin, D. B. *Adv. Drug Delivery Rev.*, **2011**, *63*, 1118– 1159.
7. Teramoto, N.; Sachinvala, N. D.; Shibata, M. *Molecules*, **2008**, *13*, 1773–1816.
8. Westh, P.; Ramløv, H. *J. Exp. Zool.*, **1991**, *258*, 303–311.
9. Crowe, L. M.; Reid, D. S.; Crowe, J. H. *Biophys. J.*, **1996**, *71*, 2087–2093.
10. Crowe, J. H.; Carpenter, J. F.; Crowe, L. M. *Annu. Rev. Physiol.*, **1998**, *60*, 73–103.
11. Katyal, N.; Deep, S. *Phys. Chem. Chem. Phys.*, **2014**, *16*, 26746–26761.
12. Paul, S.; Paul, S. *J. Phys. Chem. B*, **2015**, *119*, 1598–1610.
13. Moiset, G.; López, C. A.; Bartelds, R.; Syga, L.; Rijpkema, E.; Cukkemane, A.; Baldus, M.; Poolman, B.; Marrink, S. J. *J. Am. Chem. Soc.*, **2014**, *136*, 16167–16175.
14. Lins, R. D.; Pereira, C. S.; Hünenberger, P. H. *Proteins: Struct., Funct., Bioinf.*, **2004**, *55*, 177–186.
15. Jain, N. K.; Roy, I. *Protein Sci.*, **2009**, *18*, 24–36.
16. Ohtake, S.; Wang, Y. J. *J. Pharm. Sci.*, **2011**, *100*, 2020– 2053.

17. Carninci, P.; Nishiyama, Y.; Westover, A.; Itoh, M.; Nagaoka, S.; Sasaki, N.; Okazaki, Y.; Muramatsu, M.; Hayashizaki, Y. *Proc. Natl. Acad. Sci. U. S. A.*, **1998**, *95*, 520– 524.

18. Hirai, T.; Murata, K.; Mitsuoka, K.; Kimura, Y.; Fujiyoshi, Y. *J. Electron Microsc.*, **1999**, *48*, 653–658.

19. Mancini, R. J.; Lee, J.; Maynard, H. D. *J. Am. Chem. Soc.*, **2012**, *134*, 8474–8479.

20. Lee, J.; Lin, E.-W.; Lau, U. Y.; Hedrick, J. L.; Bat, E.; Maynard, H. D. *Biomacromolecules*, **2013**, *14*, 2561– 2569.

21. Lee, J.; Ko, J. H.; Lin, E.-W.; Wallace, P.; Ruch, F.; Maynard, H. D. *Polym. Chem.*, **2015**, *6*, 3443–3448.

22. Bat, E.; Lee, J.; Lau, U. Y.; Maynard, H. D. *Nat. Commun.*, **2015**, *6*, 6654.

23. Pelegri-O'Day, E. M.; Paluck, S. J.; Maynard, H. D. *J. Am. Chem. Soc.*, **2017**, *139*, 1145–1154.

24. Liu, Y.; Lee, J.; Mansfield, K. M.; Ko, J. H.; Sallam, S.; Wesdemiotis, C.; Maynard, H. D. *Bioconjugate Chem.*, **2017**, *28*, 836–845.

25. Lau, U. Y.; Saxer, S. S.; Lee, J.; Bat, E.; Maynard, H. D. *ACS Nano*, **2015**, *10*, 723–729.

26. Wada, M.; Miyazawa, Y.; Miura, Y. *Polym. Chem.*, **2011**, *2*, 1822–1829.

27. Sizovs, A.; Xue, L.; Tolstyka, Z. P.; Ingle, N. P.; Y. Wu, Y.; M. Cortez, M.; Reineke, T. M. *J. Am. Chem. Soc.*, **2013**, *135*, 15417–15424.

28. Tolstyka, Z. P.; Phillips, H.; Cortez, M.; Wu, Y.; Ingle, N.; Bell, J. B.; Hackett, P. B.; Reineke, T. M. *ACS Biomater. Sci. Eng.*, **2015**, *2*, 43–55.

29. Frisch, M. J.; Trucks, G. W.; Schlegel, H. B.; Scuseria, G. E.; Robb, M. A.; Cheeseman, J. R.; Scalmani, G.; Barone, V.; Mennucci, B.; Petersson, G. A.; H. Nakatsuji, H.; Caricato, M.; Li, X.; Hratchian, H. P.; Izmaylov, A. F.; Bloino, J.; Zheng, G.; Sonnenberg, J. L.;

Hada, M.; Ehara, M.; Toyota, K.; Fukuda, R.; Hasegawa, J.; Ishida, M.; Nakajima, T.; Honda, Y.; Kitao, O.; Nakai, H.; Vreven, T.; Montgomery Jr., J. A.; Peralta, J. E.; Ogliaro, F.; Bearpark, M. J.; Heyd, J.; Brothers, E. N.; Kudin, K. N.; Staroverov, V. N.; Kobayashi, R.; Normand, J.; Raghavachari, K.; Rendell, A. P.; Burant, J. C.; Iyengar, S. S.; Tomasi, J.; Cossi, M.; Rega, N.; Millam, N. J.; Klene, M.; Knox, J. E.; Cross, J. B.; Bakken, V.; Adamo, C.; Jaramillo, J.; Gomperts, R.; Stratmann, R. E.; Yazyev, O.; Austin, A. J.; Cammi, R.; Pomelli, C.; Ochterski, J. W.; Martin, R. L.; Morokuma, K.; Zakrzewski, V. G.; Voth, G. A.; Salvador, P.; Dannenberg, J. J.; Dapprich, S.; Daniels, A. D.; Farkas, Ö.; Foresman, J. B.; Ortiz, J. V.; Cioslowski, J.; Fox, D. J. Gaussian 09, Gaussian, Inc., Wallingford, CT, USA, **2009**.

30. Albertorio, F.; Chapa, V. A.; Chen, X.; Diaz, A. J.; Cremer, P. S. *J. Am. Chem. Soc.*, **2007**, *129*, 10567–10574.
31. Sakakura, K.; Okabe, A.; Oku, K.; Sakurai, M. *J. Phys. Chem. B*, **2011**, *115*, 9823–9830.
32. Oku, K.; Kurose, M.; Kubota, M.; Fukuda, S.; Kurimoto, M.; Tujisaka, Y.; Sakurai, M. *Biosci., Biotechnol., Biochem.*, **2005**, *69*, 7–12.
33. Fujimoto, T.; Oku, K.; Tashiro, M.; Machinami, T. *J. Carbohydr. Chem.*, **2006**, *25*, 521–532.
34. Lawandi, J.; Rocheleau, S.; Moitessier, N. *Tetrahedron*, **2016**, *72*, 6283–6319.
35. Pelletier, G.; Zwicker, A.; Allen, C. L.; Schepartz, A.; Miller, S. J. *J. Am. Chem. Soc.*, **2016**, *138*, 3175–3182.
36. Pryce, R. *Br. Med. J.*, **2009**, *338*, a2218.
37. Oliva, A.; Fariña, J.; Llabrés, M. *Int. J. Pharm.*, **1996**, *143*, 163–170.
38. Lundquist, J. J.; Toone, E. J. *Chem. Rev.*, **2002**, *102*, 555–578.

2.5 Appendix A

2.5.1 Materials

Trehalose was purchased from The Healthy Essential Management Corporation (Houston, TX), dried with ethanol, and stored under vacuum. Azobisisobutyronitrile (AIBN) (98%) was purchased from Sigma-Aldrich and recrystallized from acetone before using. 4-Vinylbenzyl chloride (90%) was purchased from Sigma-Aldrich. Insulin, human recombinant (Cat. No. 91077C; Lot No. 15L255-D) was purchased from Sigma Aldrich. Sodium hydroxide (≥97%, Pellets/Certified ACS), *N*,*N*- dimethylformamide (DMF) (≥99.8%, Certified ACS), dimethyl sulfoxide (DMSO) (≥99.9%, Certified ACS), Eppendorf LoBind® microcentrifuge tubes (0.5 mL and 1.5 mL), and pyridine (≥99%, Certified ACS) were purchased from Fisher Scientific. Pyridine was dried via distillation over calcium hydride and stored over 3 Å molecular sieves. Spectra/Por® 3 dialysis membrane standard RC tubing (MWCO: 3.5 kDa) was used for dialysis of polymers. Deuterated solvents (Cambridge Isotope Laboratories) for NMR spectroscopic analyses were used as received.

2.5.2 Analytical techniques

NMR spectra were recorded on Bruker AV 400, 500, or DRX 500 MHz spectrometers. Chemical shifts are reported in ppm relative to the residual signal of the solvent (D_2O: δ 4.79 ppm, $CDCl_3$: δ 7.26 ppm, or $(CD_3)_2SO$: δ 2.50 ppm). ^{1}H NMR spectra are reported as follows: chemical shift (δ ppm), multiplicity (t = triplet, d = doublet, dd = doublet of doublets, m = multiplet), coupling constant (Hz), and integration. ^{1}H NMR spectra were acquired with a relaxation of 2 s for small molecules and 30 s for polymers with an acquisition time of 3.27 s and 30° pulse angle. Gel permeation chromatography (GPC) was conducted on a Shimadzu high performance liquid chromatography (HPLC) system with a refractive index RID-10A, one Polymer Laboratories

PLgel guard column, and two Polymer Laboratories PLgel 5 μm mixed D columns. Eluent was DMF with LiBr (0.1 M) at 50 °C (flow rate: 0.80 mL min^{-1}). Calibration was performed using near-monodisperse pMMA standards from Polymer Laboratories. HPLC purification of trehalose monomers was performed on a Shimadzu HPLC system with a refractive index and UV detector RID-10A monitoring at λ = 254 and 220 nm, and one Luna 5 μm C18(2) 100 Å LC column (250 × 21.2 mm) with 40% MeOH and 60% H_2O isocratic eluent mixture at a flow rate of 20 mL min^{-1}. The same HPLC system, equipped with an analytical Luna 5 μm C18(2) 100 Å column (250 × 460 mm), was utilized for detection of insulin with a gradient solvent system (water: acetonitrile = 30:70 to 40:60 + 0.1% trifluoroacetic acid over 15 min at 1 mL min^{-1}). Thermogravimetric analysis (TGA) was performed on a PerkinElmer Diamond TG/DTA instrument with a ramping rate of 10 °C per minute. Infrared (IR) spectra were obtained with a PerkinElmer Spectrum One instrument equipped with a universal ATR assembly; spectra are reported in wavenumbers ($\tilde{\nu}$). Mass spectra were acquired on a Waters Acquity Ultra Performance Liquid Chromatography (UPLC) connected to a Waters LCT-Premier XE Time of Flight Instrument controlled by MassLynx 4.1 software. The mass spectrometer was equipped with a Multi-Mode Source operated in the electrospray mode. Trehalose samples were separated using an Acquity BEH C18 1.7 μm column (2.1 × 50 mm) and were eluted with a gradient of 5–50% or 10–45% solvent B over 6 min (solvent A: water, solvent B: acetonitrile, both with 0.2% formic acid (vol/vol)). Mass spectra were recorded in the negative ion mode in the m/z range of 70–2000 with leucine enkephalin (Sigma L9133) as the lock mass standard. Mass spectra were also collected on a Thermo Scientific Exactive Plus mass spectrometer with IonSense Direct Analysis in Real Time (DART-MS) ID-CUBE. Samples of insulin were stressed in a New Brunswick Scientific Excella E24 Incubator Shaker.

2.5.3 Computational methods

Conformers for regioisomer **O2**, **O4**, and **O6** were searched by using Maestro 9.4 with OPLS_2015 force field in implicit water. For each regioisomer, the ensemble of conformers con sists of those whose energies are within 10 kcal mol^{-1} from the lowest one. This ensemble typically includes ~400 structures. The structures were then clustered to 25 representative structures for **O2**, 33 for **O4**, and 42 for **O6** using the chemical informatics tool in Maestro 9.4. These structures were then optimized using B3LYP/6-31 g(d) with SMD water model in Gaussian 09.[29] Frequency analysis was conducted to confirm that the structures are stationary points on the potential energy surface with no imaginary frequency. Thermal energies are calculated by using simple harmonic oscillator model. The reported energies are Gibbs free energies at 298.15 K and 1 bar.

2.5.4 Synthesis of Trehalose Regioisomers

6-O-(4-Vinylbenzyl ether)-α,α-trehalose (**O6**), 4-O-(4-vinyl- benzyl ether)-α,α-trehalose (**O4**), 3-O-(4-vinylbenzyl ether)- α,α-trehalose (**O3**), 2-O-(4-vinylbenzyl ether)-α,α-trehalose (**O2**). NaOH (4.44 g, 1.14×10^{-1} mol) was added to DMSO (100 mL) and stirred for 5 min. Trehalose (4.86 g, 1.42×10^{-2} mol) was then added to the reaction flask. Once trehalose dissolved, 4-vinylbenzyl chloride (0.4 mL, 2.55×10^{-3} mol) was added dropwise and reaction turned yellow. The reaction was stirred for 12 hours at 25 °C and was then precipitated in a mixture of cold hexanes (1.6 L) and dichloromethane (400 mL). Precipitate was collected via filtration and dried under reduced pressure to afford a yellow-white solid. The solid was dissolved in H_2O (50 mL) and neutralized with 12 N hydrochloric acid (HCl). Once neutralized, MeOH (50 mL) was added and the solution mixed. The solution was then filtered through a 0.45 μm cellulose acetate filter and purified via preparative HPLC (40% MeOH in H_2O). MeOH was removed under reduced pressure and water

was removed via lyophilization to afford compounds **O2**, **O3**, **O4**, and **O6** in 11%, <1%, 39%, and 13% yield, respectively, as fluffy white powders. The combined yield for all the regioisomers was 64%.

O2: HPLC retention time (peak intensity): 10.3 minutes. ^{1}H NMR (500 MHz in D_2O, 298 K): δ = 7.47–7.45 (m, 2H), 7.35–7.33 (m, 2H), 6.77–6.71 (m, 1H), 5.84–5.80 (d, J = 17.69 Hz, 1H), 5.30–5.28 (d, J = 11.42 Hz, 1H), 5.23–5.22 (d, J = 3.68 Hz, 1H), 5.14–5.13 (d, J = 4.05 Hz, 1H), 4.69–4.61 (m, 2H), 3.91–3.51 (m, 10H), 3.45–3.39 (m, 2H); ^{13}C NMR (125 MHz in D_2O, 298 K): δ = 137.5, 136.6, 136.2, 128.9, 126.4, 114.7, 93.5, 91.4, 78.7, 73.2, 72.4, 72.2, 72.0, 72.0, 71.0, 69.8, 69.2, 60.6, 60.1; IR $\tilde{\nu}$ (cm^{-1}): 3294 (br), 2923, 1635, 1362, 1043, 988, 827, 803; LC-MS (±1.0) observed (predicted): $[M+HCOO]^-$ 503.1762 (503.1765).

O3: HPLC retention time (peak intensity): 11.7 minutes. ^{1}H NMR (500 MHz in D_2O, 298 K): δ = 7.53–7.45 (q, 4H), 6.83–6.78 (dd, 1H), 5.88–5.85 (d, J = 17.86 Hz, 1H), 5.33–5.31 (d, J = 11.02 Hz, 1H), 5.20–5.19 (m, 2H), 4.86 (s, 2H), 3.91–3.82 (m, 6H), 3.78–3.73 (m, 3H), 3.67–3.64 (m, 1H), 3.57–3.53 (t, J = 9.63 Hz, 1H), 3.47–3.43 (t, J = 9.63 Hz, 1H); ^{13}C NMR (125 MHz in D_2O, 298 K): δ = 137.3, 136.2, 128.9, 126.2, 114.4, 93.2, 93.0, 81.3, 74.8, 72.4, 72.2, 72.1, 70.9, 70.8, 69.6, 69.3, 60.4, 60.3. IR $\tilde{\nu}$ (cm^{-1}): 3301 (br), 2932, 1628, 1512, 1406, 1358, 1285, 1259, 1216, 1146, 1105, 1080, 1027, 986, 943, 910, 827, 802; DART-MS observed (predicted): $[M-H]^-$ 457.17040 (457.17044).

O4: HPLC retention time (peak intensity): 14.6 minutes. ^{1}H NMR (500 MHz in D_2O, 298 K): δ = 7.53–7.41 (q, 4H), 6.83–6.78 (dd, 1H), 5.89–5.85 (d, J = 17.73 Hz, 1H), 5.34–5.32 (d, J = 10.97 Hz, 1H), 5.19–5.16 (m, 2H), 4.89–4.84 (d, J = 10.81 Hz), 4.71–4.69 (d, J = 10.81 Hz, 1H), 3.99–3.95 (t, J = 9.62, 1H), 3.86–3.79 (m, 5H), 3.76–3.72 (m, 2H), 3.68–3.66 (m, 1H), 3.63–3.59 (m,

1H), 3.54–3.50 (t, J = 9.46 Hz, 1H), 3.45–3.41 (t, J = 9.62 Hz, 1H); ^{13}C NMR (125 MHz in D_2O, 298 K): δ = 137.5, 136.6, 136.2, 129.2, 126.3, 114.6, 93.2, 93.0, 77.7, 74.6, 72.6, 72.4, 72.0, 71.1, 71.1, 70.9, 69.6, 60.4, 60.2; IR $\tilde{\nu}$ (cm^{-1}): 3234 (br), 2930, 1629, 1360, 1107, 1043, 992, 913, 827, 805; LC-MS (± 1.0) observed (predicted): $[M+HCOO]^-$ 503.1720 (503.1765).

O6: HPLC retention time (peak intensity): 19.7 minutes. ^{1}H NMR (500 MHz in D_2O, 298 K): δ = 7.52–7.38 (q, 4H), 6.82–6.76 (dd, 1H), 5.87–5.84 (d, J = 17.51 Hz, 1H), 5.32–5.30 (d, J = 11.03 Hz, 1H), 5.17–5.15 (m, 2H), 4.62–4.56 (q, 2H), 3.97–3.94 (m, 1H), 3.85–3.79 (m, 5H), 3.76–3.70 (m, 2H), 3.64–3.60 (m, 2H), 3.47–3.41 (q, 2H); ^{13}C NMR (125 MHz in D_2O, 298 K): δ = 137.3, 136.8, 136.2, 128.7, 126.3, 114.5, 93.3, 93.2, 72.6, 72.5, 72.4, 72.1, 70.9, 78.8, 70.7, 69.9, 69.6, 68.6, 60.5; IR $\tilde{\nu}$ (cm^{-1}): 3328 (br), 2928, 1630, 1512, 1407, 1365, 1212, 1147, 1105, 1076, 1032, 987, 942, 909, 826, 805, 718; LC-MS (± 1.0) observed (predicted): $[M+HCOO]^-$ 503.1765 (503.1765).

2.5.5 Representative free radical polymerization (P4)

O4 (531 mg, 1.16 mmol, 33 eq.) and AIBN (5.77 mg, 35.1 μmol, 1 eq.) were dissolved in H_2O (3.63 mL) and DMF (7.27 mL). The mixture was added to a dry Schlenk tube and subjected to five freeze–pump–thaw cycles. The polymerization was started by immersing the Schlenk tube in a 90 °C oil bath. The polymerization was stopped after 21 hours by cooling with liquid nitrogen and exposing the reaction to air. The polymer was purified via dialysis (MWCO = 3.5 kDa) against H_2O for three days and lyophilized to produce a fluffy white solid.

P2: M_n = 1.9 kDa (M_n calculated from acetylated polymer, vide infra for details: 9.5 kDa); M_w = 2.1 kDa; $Đ$ = 1.09; ^{1}H NMR (500 MHz in DMSO) δ: 7.06, 6.38, 5.06, 4.90, 4.51, 4.39, 3.71, 3.51,

3.36, 3.21, 2.27–0.43; IR: $\tilde{\nu}$ (cm^{-1}): 3351, 2950, 1623, 1425, 1400, 1362, 1150, 1080, 991, 804. TGA weight loss onset temperature: 263 °C.

P4: M_n = 14.8 kDa (M_n calculated from acetylated polymer: 15.1 kDa); M_w = 23.2 kDa; $Đ$ = 1.56; ^{1}H NMR (500 MHz in DMSO) δ: 7.03, 6.40, 5.11, 4.92, 4.85, 4.78, 4.60, 4.41, 3.77, 3.65, 3.58, 3.49, 3.16, 2.11–0.66; IR: $\tilde{\nu}$ (cm^{-1}): 3342, 2928, 1637, 1423, 1359, 1148, 1104, 1039, 987, 846, 803, 706. TGA weight loss onset temperature: 286 °C.

P6: M_n = 1.8 kDa (M_n calculated from acetylated polymer: 9.4 kDa); M_w = 1.9 kDa; $Đ$ = 1.05; ^{1}H NMR (500 MHz in DMSO) δ: 7.05, 6.47, 4.90, 4.80, 4.68, 4.41, 3.89, 3.69, 3.58, 3.49, 3.17, 2.03–0.63; IR: $\tilde{\nu}$ (cm^{-1}): 3344, 2924, 2162, 1636, 1423, 1362, 1147, 1076, 1034, 989, 940, 847, 806, 706. TGA weight loss onset temperature: 274 °C.

PA (all isomers mixed): M_n = 4.4 kDa (M_n calculated from acetylated polymer: 14.6 kDa); M_w = 5.4 kDa; $Đ$ = 1.21; ^{1}H NMR (500 MHz in DMSO) δ: 7.02, 6.42, 5.07, 4.91, 4.82, 4.55, 4.41, 3.88, 3.58, 3.49, 3.16, 2.49, 2.18–0.66; IR: $\tilde{\nu}$ (cm^{-1}): 3348, 2922, 1430, 1362, 1041, 990, 804. TGA weight loss onset temperature: 284 °C.

2.5.6 Representative polymer acetylation (P4)

P4 (11.5 mg, 25.1 μmol, 1 eq.) was dissolved in dry pyridine (1.0 mL) and added to a dry and degassed round bottom flask. After five minutes of stirring, acetic anhydride (59.3 μL, 0.627 mmol, 25 eq.) was added dropwise. The solution stirred at room temperature for 48 hours. After 48 hours, the polymer was precipitated twice from cold diethyl ether. The precipitate was then collected and freeze-dried from benzene to afford product as a white powder. Deacetylated polymer molecular weights (provided above) were calculated using the following equation:

[M_nP-OH] = [M_nP-**OAc**] x ((MW $O_{monomer}$) / (MW **OAc**$_{monomer}$)).

P2-OAc: M_n = 15.7; M_w = 25.0 kDa; $Đ$ = 1.59; ^{1}H NMR (400 MHz in $CDCl_3$) δ: 6.93, 6.41, 5.43, 5.28, 5.09, 5.01, 4.89, 4.57, 4.25, 4.07, 3.93, 2.09, 2.08, 2.01, 0.15, 0.14, 0.11, 0.10.

P4-OAc: M_n = 19.6 kDa; M_w = 31.7 kDa; $Đ$ = 1.62; ^{1}H NMR (400 MHz in $CDCl_3$) δ: 6.89, 6.36, 5.52, 5.44, 5.28, 5.23, 5.05, 5.02, 4.99, 4.49, 4.22, 4.05, 3.96, 3.54, 2.07, 2.05, 2.01, 1.26, 1.20.

P6-OAc: M_n = 15.4 kDa; M_w = 21.2 kDa; $Đ$ = 1.37; ^{1}H NMR (400 MHz in $CDCl_3$) δ: 6.85, 6.29, 5.47, 5.30, 5.04, 4.36, 4.25, 4.09, 4.03, 4.00, 3.50, 2.07, 2.05, 2.02, 2.02, 1.91, 1.84.

PA-OAc: M_n: 24.0 kDa; M_w = 35.0 kDa; $Đ$ = 1.62; ^{1}H NMR (500 MHz in $CDCl_3$) δ: 7.55–6.03, 5.07, 4.51–4.15, 3.71, 3.53, 3.32, 2.07–0.50.

2.5.7 Insulin aggregation studies

A solution of insulin (1.0 mg mL^{-1}) was prepared by dissolving insulin in Dulbecco's phosphate-buffered saline (DPBS, pH 7.4). Aliquots of the insulin solution (100 μL) were mixed with DPBS buffer (control, 100 μL) or stock solutions (100 μL) containing 1 or 10 weight equivalents of **P2**, **P4**, **P6**, or **PA** dis- solved in DPBS in 1.5 mL screw-top dram vials. These samples were taped horizontally for maximum surface area and stressed at 37 °C in an incubating shaker set to 250 rpm for 3 hours. After 3 hours, the samples were removed from the shaker and placed in a 4 °C refrigerator until analytical HPLC analysis.

2.5.8 Supplementary Procedures, Figures, and Tables

2.5.8.1 Synthesis of O2, O3, O4, and O6 using different bases – representative example

The reaction was conducted as in the experimental section of the manuscript, with different molar equivalents of base (entry 1 corresponds to the original condition). A representative reaction condition (entry 2) is detailed as follows: Potassium hydroxide (573 mg, $1.02x10^{-2}$ mol) was suspended in dry dimethyl sulfoxide (9.5 mL) and stirred at room temperature. Trehalose (437 mg, $1.28x10^{-3}$ mol) was then added and stirred until it dissolved. 4-Vinylbenzyl chloride (40 μL, $2.55x10^{-4}$ mol) was added dropwise. The reaction was stirred for 12 hours at 25 ˚C and was then precipitated into a mixture of cold hexanes (160 mL) and dichloromethane (40 mL). The precipitate was collected via filtration and dried under reduced pressure, and the resulting solid was analyzed by HPLC (40% MeOH in H_2O).

Table A1. Modulation of regioselectivity in monomer synthesis using different hydroxyl bases.

Entry	Base		Regioisomer ratio O2 : O3 : O4 : O6[a]
	Base used	Mol. eq. relative to trehalose	
1	NaOH	8	1 : 0.21 : 3.38 : 1.42
2	KOH	8	1 : 0.24 : 1.49 : 1.44
3	NaOH	1	1 : 0.36 : 1.45 : 1.34
4	KOH	1	1 : 0.35 : 1.02 : 1.36

[a] Ratio calculated from HPLC chromatogram AUC.

2.5.8.2 Synthesis of O2, O3, O4, and O6 in water or at a higher temperature

The reaction was conducted as in the experimental section of the manuscript, except at a different temperature (50 °C) or in water. Briefly, 8 equivalents of NaOH and 1 equivalent of trehalose were dissolved in DMSO (to make 0.15 M trehalose), and 0.2 equivalent of 4-vinylbenzyl chloride was added dropwise and the reaction was allowed to stir for 15 to 21 hours at respective temperature. The reaction was neutralized with dilute hydrochloric acid, and analyzed by LC-MS. The reactions in water was conducted both with (entry 3) and without (entry 2) the phase transfer catalyst

(tetrabutylammonium hydrogensulfate) at 0.2 molar equivalents with respect to the added trehalose.

Table A2. The effect of solvent and temperature on regioselectivity

Entry	Solvent	Temperature	Additive	Regioisomer ratio O2 + O3[a] : O4 : O6[b]
1	DMSO	50 °C	None	1 : 2.27 : 2.12
2	Water	23 °C	None	1 : 3.78 : 4.61
3	Water	23 °C	Tetrabutylammonium hydrogensulfate	1 : 2.01 : 3.34

[a] Due to the low overall yield and weak signal, O2 and O3 peaks were overlapping.
[b] Ratio calculated from UPLC-MS chromatogram.

2.5.8.3 Representative Polymer Acetylation: Acetylation of P4

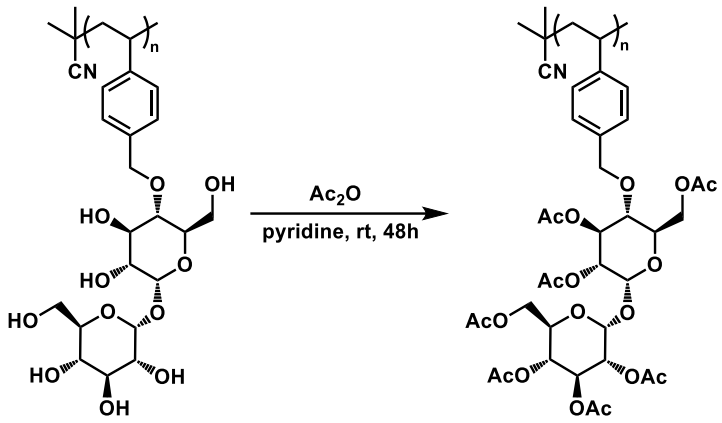

P4 (11.5 mg, 25.1 μmol, 1 eq.) was dissolved in dry pyridine (1.0 mL) and added to a dry and degassed round bottom flask. After five minutes of stirring, acetic anhydride (59.3 μL, 0.627 mmol, 25 eq.) was added dropwise. The solution stirred at room temperature for 48 hours. After 48 hours, the polymer was precipitated twice from cold diethyl ether. The precipitate was then collected and freeze-dried from benzene to afford product as a white powder. The polymer was characterized by DMF GPC.

Deacetylated polymer molecular weight was calculated using the following equation:

$[M_n \text{ P-OH}] = [M_n \text{ P-OAc}]*((\text{MW O}_{monomer})/(\text{MW OAc}_{monomer}))$.

2.5.8.4 Representative Monomer Acetylation: Acetylation of OA (OA-OAc)

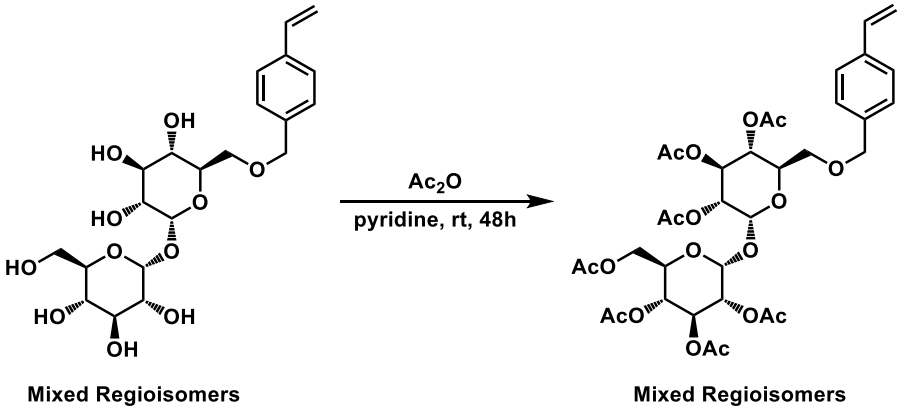

OA (199.6 mg, 0.435 mmol, 1 eq.) was dissolved in dry pyridine (1.4 mL) and added to a dry and degassed round bottom flask. After five minutes of stirring, acetic anhydride (823 µL, 8.70 mmol, 20 eq.) was added dropwise. The solution was stirred at room temperature for 48 hours. After 48 hours, solvent was removed under reduced pressure to yield a white solid. The solid was dissolved in dichloromethane (≈10 mL) and washed with H_2O (≈10 mL) once. Organic layer was collected and washed with brine (≈10 mL) once. The organic layer was collected, dried over $MgSO_4$, and filtered. Solvent was removed under reduced pressure and flash chromatography was performed (dichloromethane:ethyl acetate; 9:1) to afford product as a white solid. Yield= 72%.

2.5.8.5 Free Radical Polymerization of OA-OAc (PA-OAc)

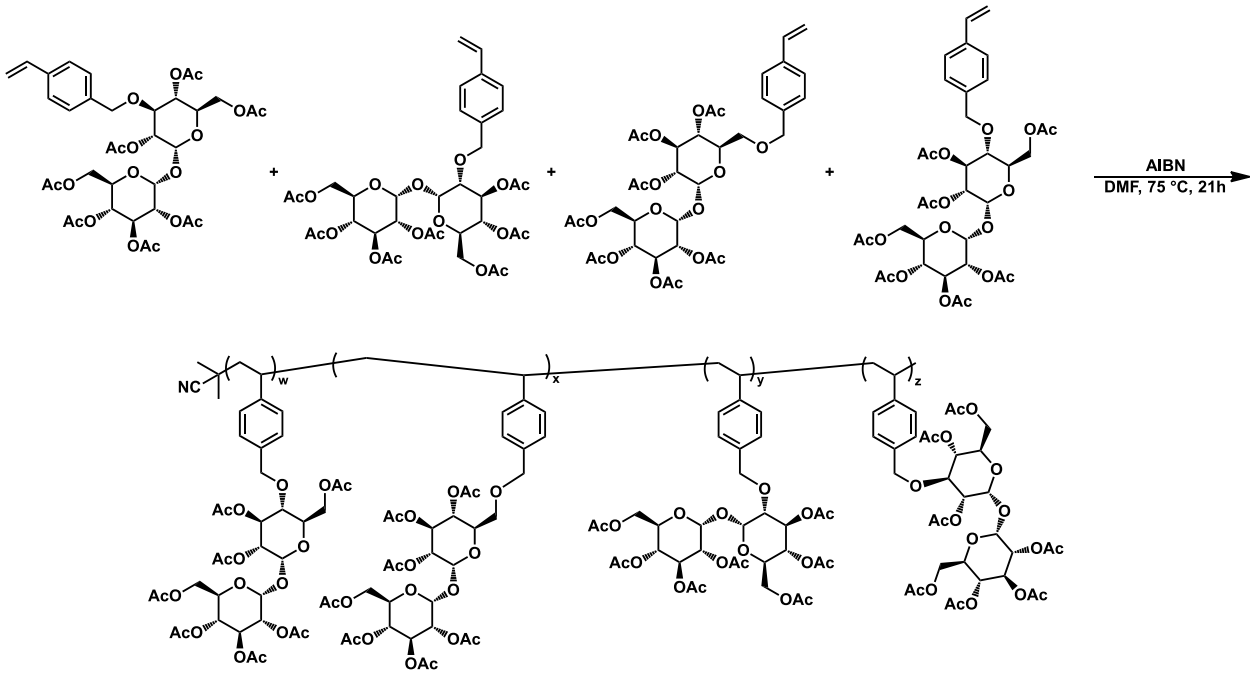

OA (690.0 mg, 0.917 mmol, 43 eq.) and AIBN (3.5 mg, 21.0 µmol, 1eq.) were dissolved in DMF (3.06 mL). The mixture was added to a dry Schlenk tube and subjected to five freeze-pump-thaw cycles. Polymerization was started by immersing the Schlenk tube in a 75 °C oil bath. After 21 hours, the polymer was precipitated from cold diethyl ether. Crude solid was collected via filtration and rinsed with cold diethyl ether to afford the product as a white solid.

2.5.8.6 Representative Polymer Acetyl Deprotection: Deprotection of PA-OAc

PA-OAc (73.4 mg, 97.5 μmol, 1 eq.) was dissolved in $CHCl_3$ (2 mL) and MeOH (2mL). To this was added sodium methoxide (27 μL, 0.488 mmol, 5 eq.) dropwise. The solution was stirred at room temperature for 2 hours. After two hours, the precipitate was collected via centrifugation and dried. Resulting white solid was dissolved in water (~10 mL) and neutralized with 0.1 N HCl. Product was purified via dialysis (MWCO= 3,500 Da) for three days. Lyophilization afforded product as a fluffy white solid.

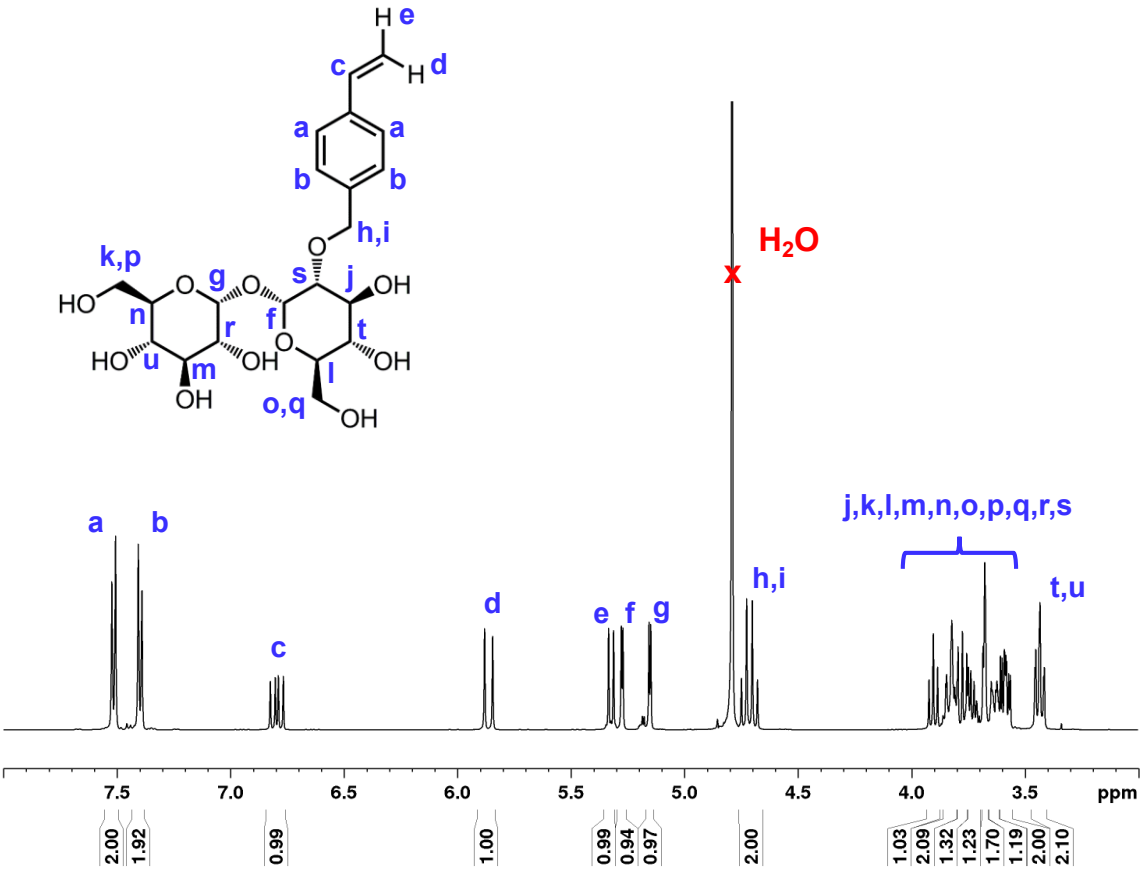

Figure A1. ^{1}H NMR spectrum of **O2** in D_2O at 298 K.

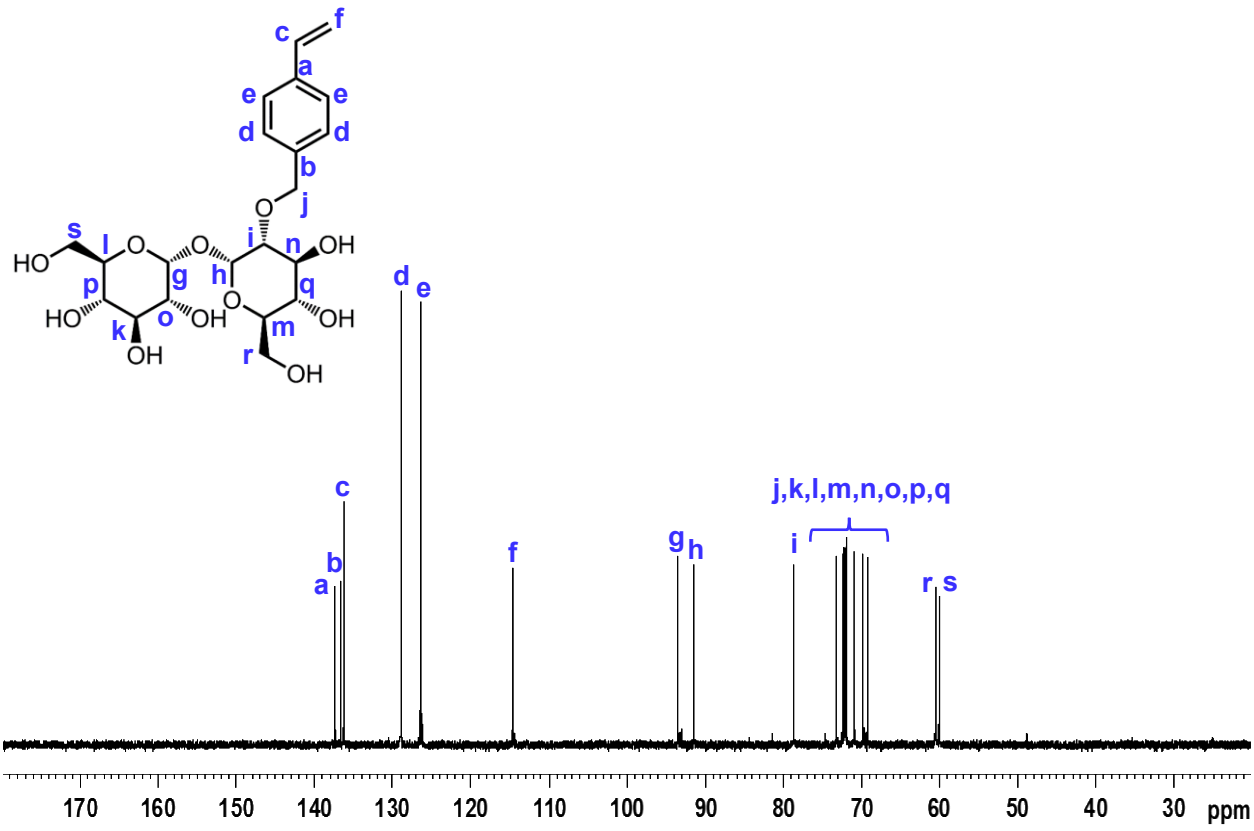

Figure A2. ^{13}C NMR spectrum of **O2** in D_2O at 298 K.

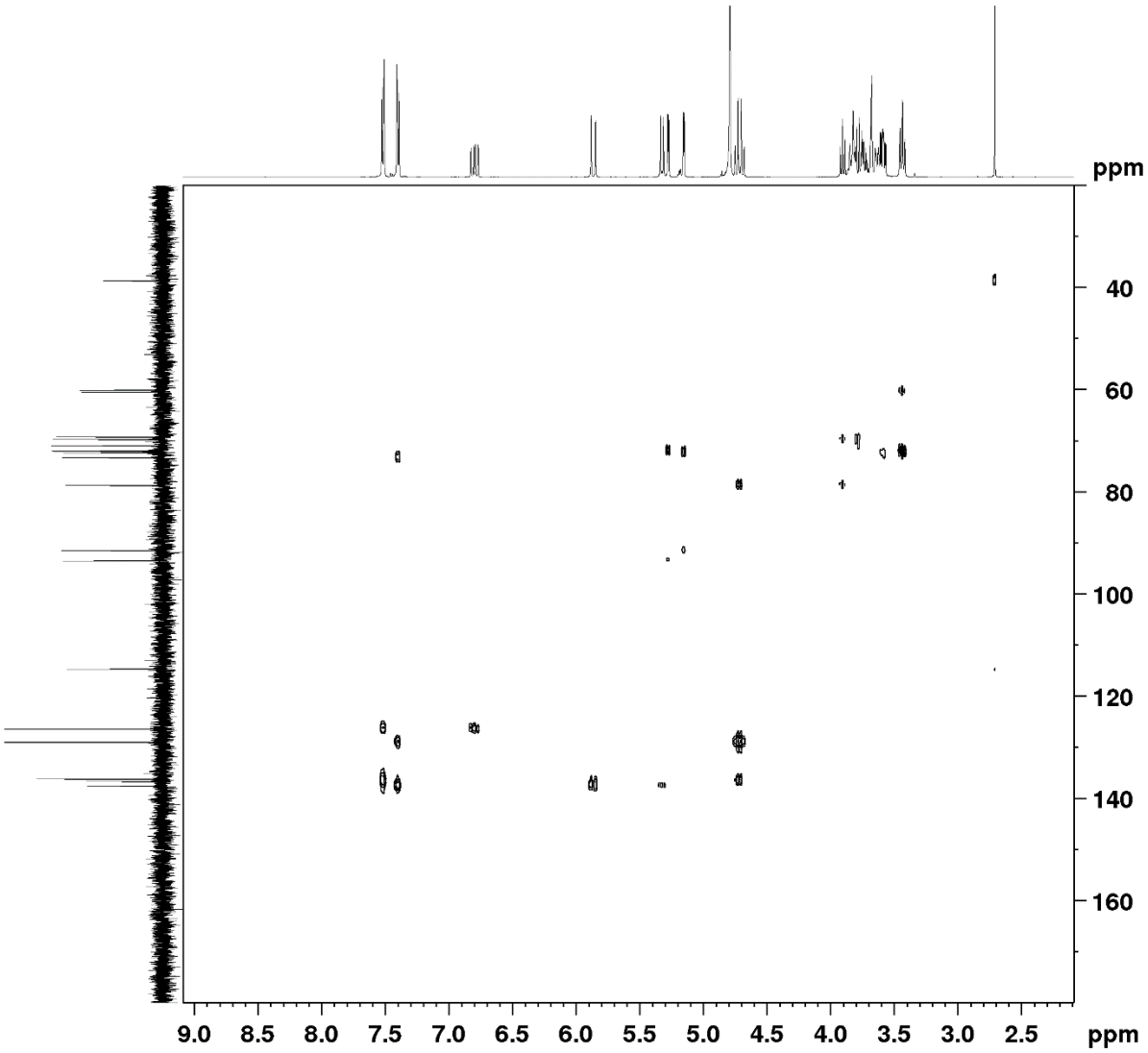

Figure A3. HMBC spectrum of **O2** in D2O at 298 K.

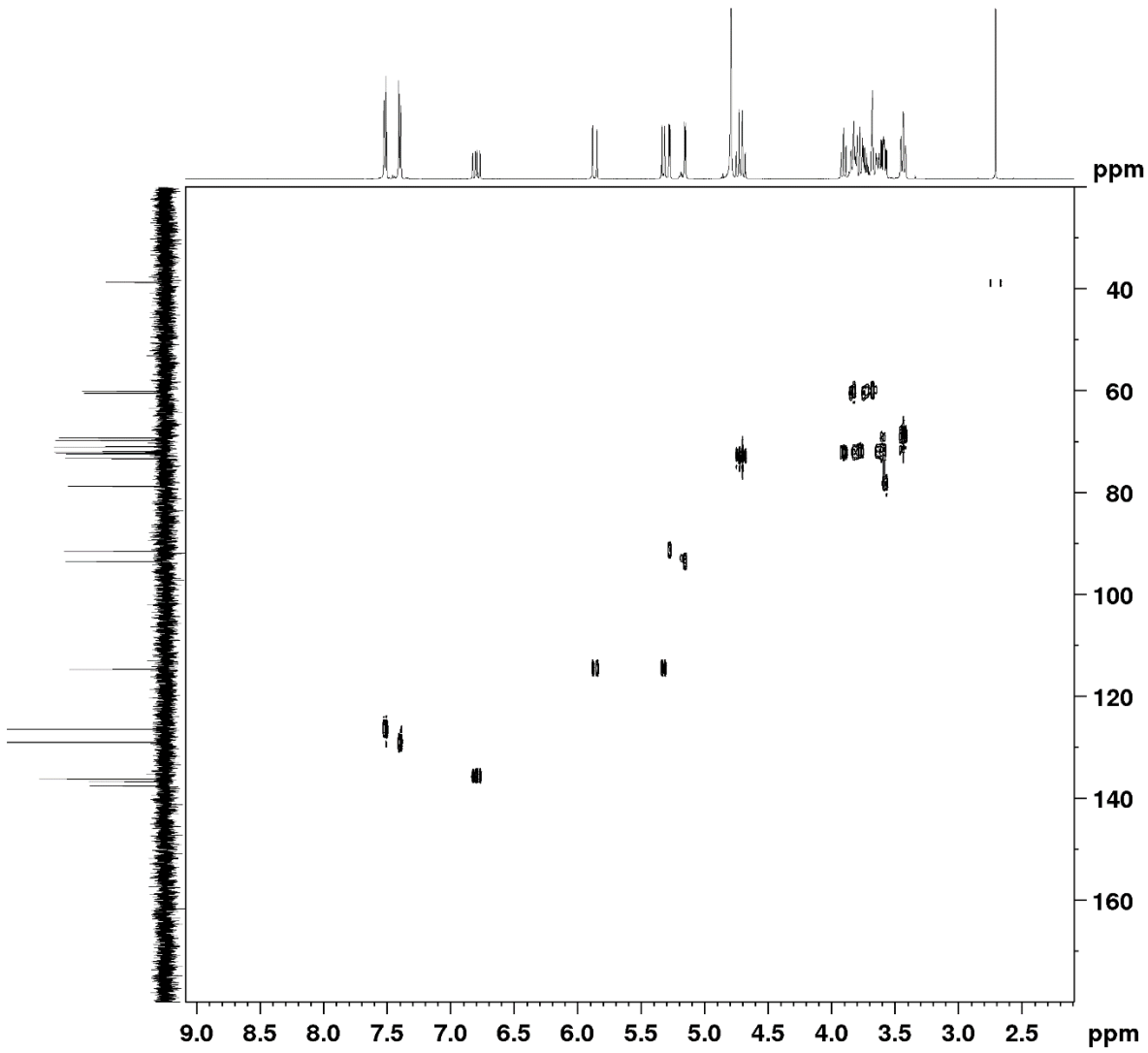

Figure A4. HSQC spectrum of **O2** in D_2O at 298 K.

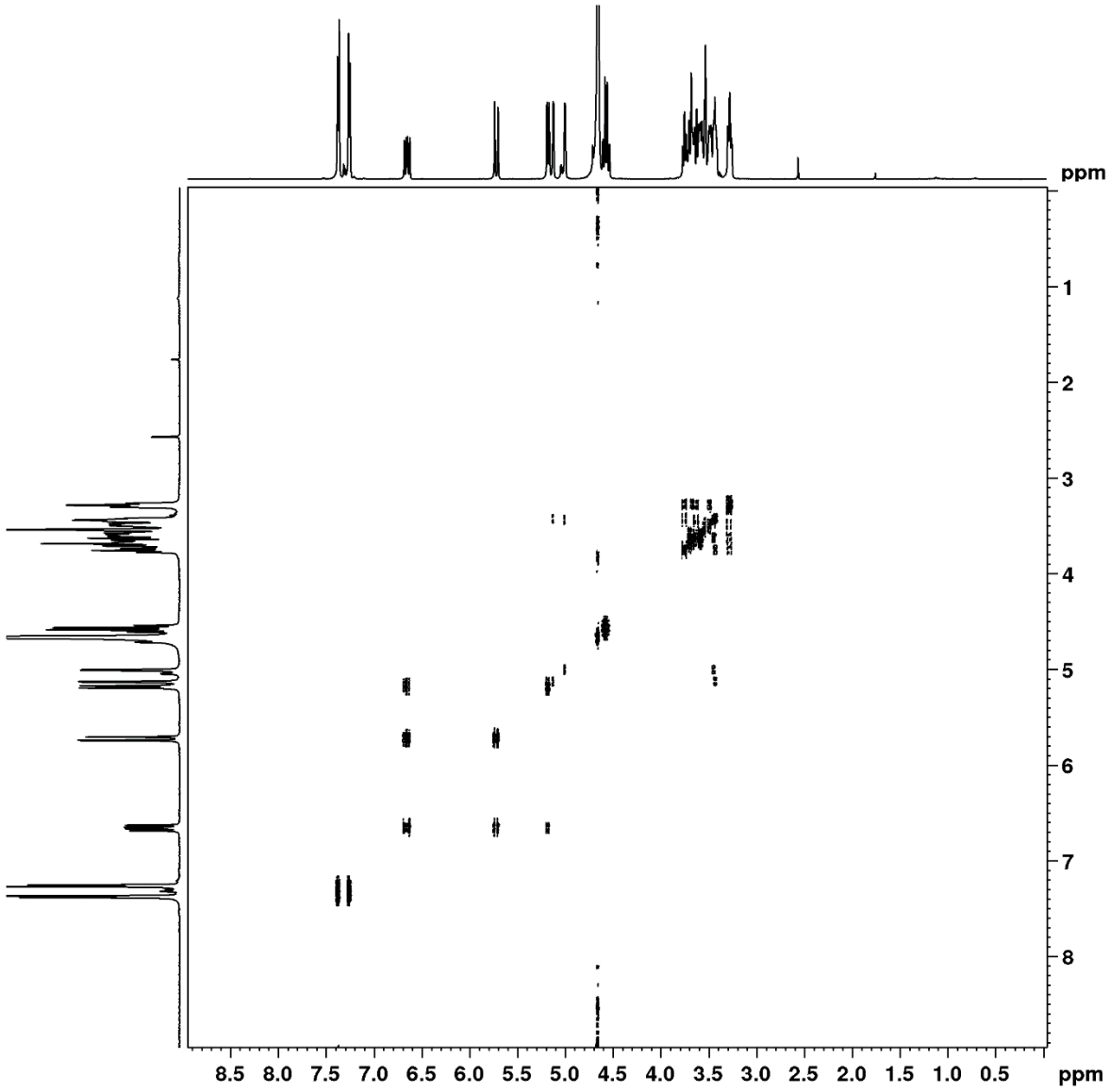

Figure A5. COSY spectrum of **O2** in D_2O at 298 K.

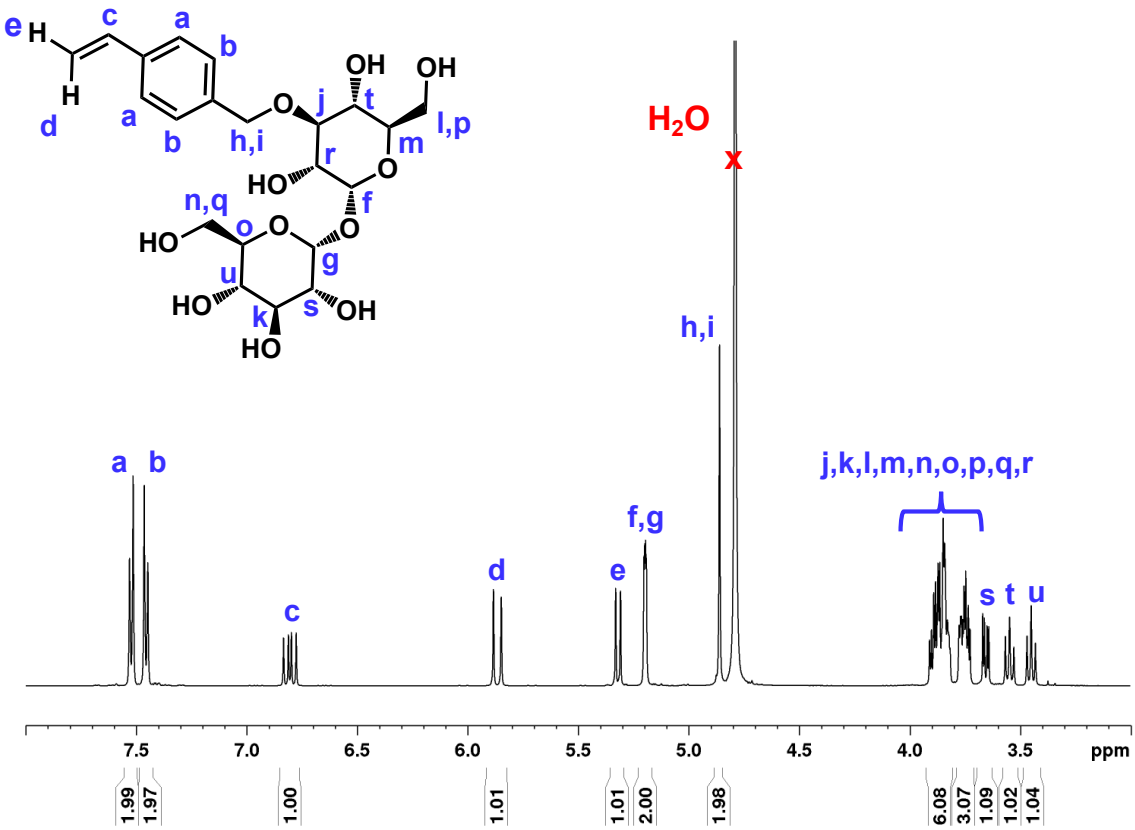

Figure A6. ^{1}H NMR spectrum of **O3** in D_2O at 298 K.

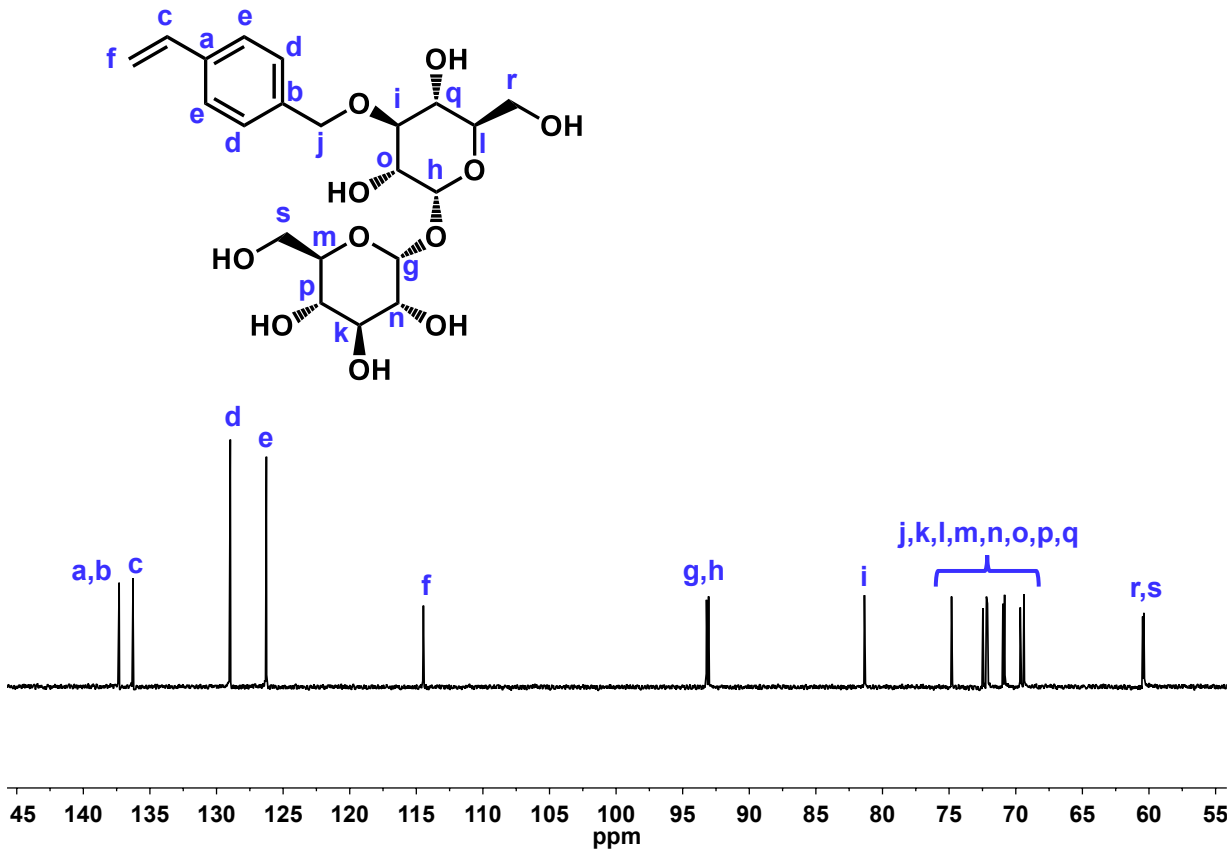

Figure A7. ^{13}C NMR spectrum of **O3** in D_2O at 298 K.

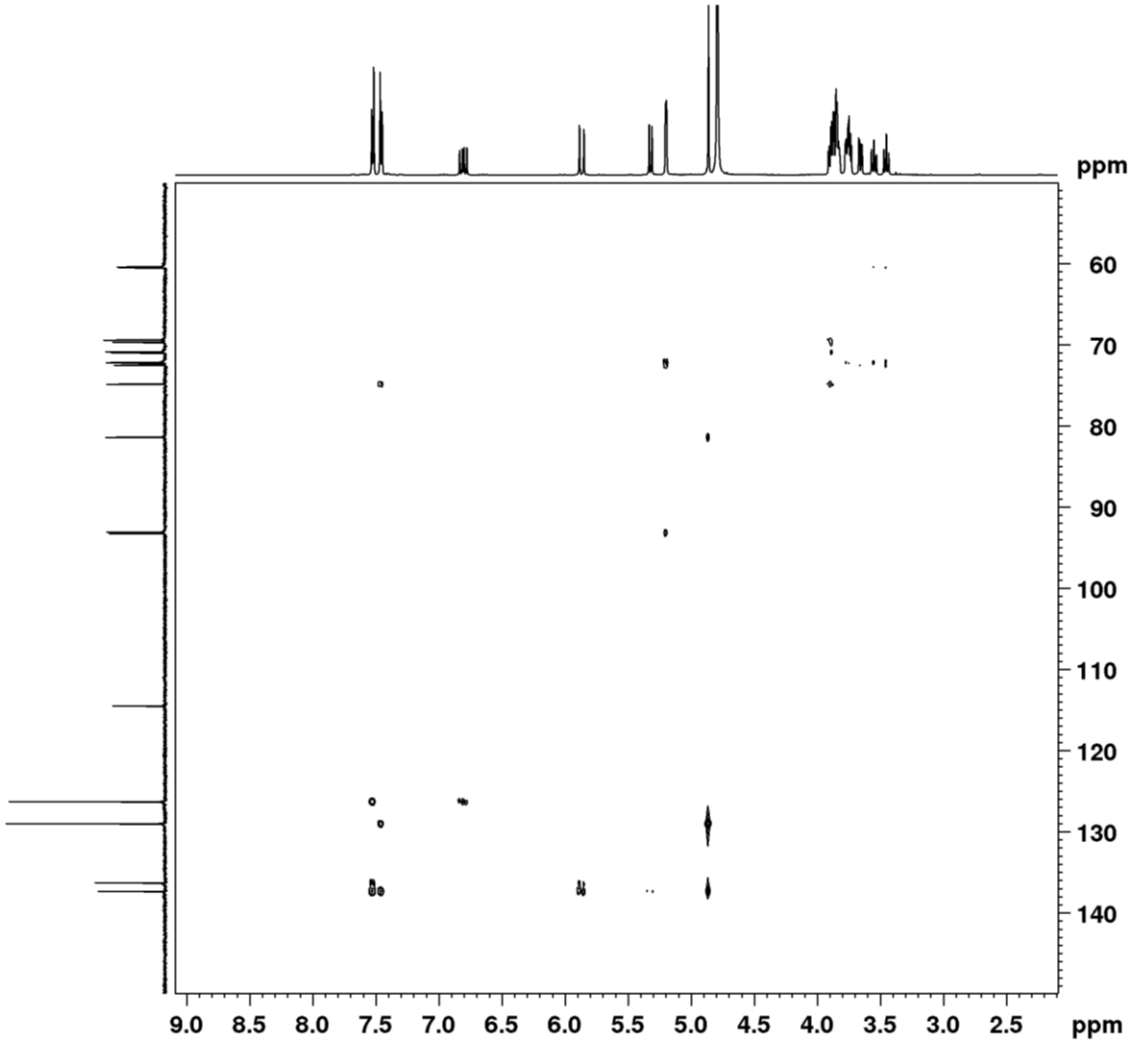

Figure A8. HMBC spectrum of **O3** in D_2O at 298 K.

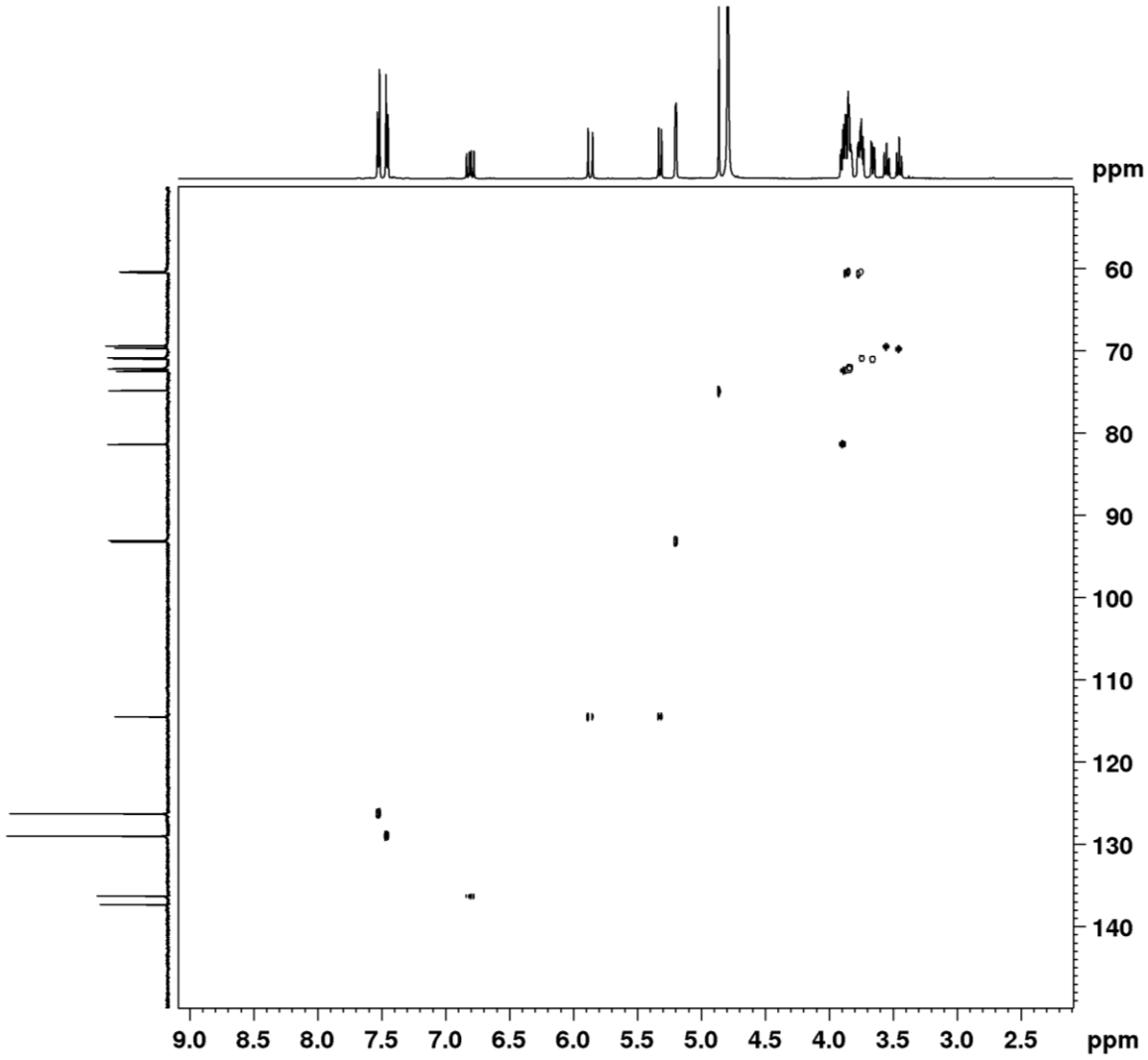

Figure A9. HSQC spectrum of **O3** in D_2O at 298 K.

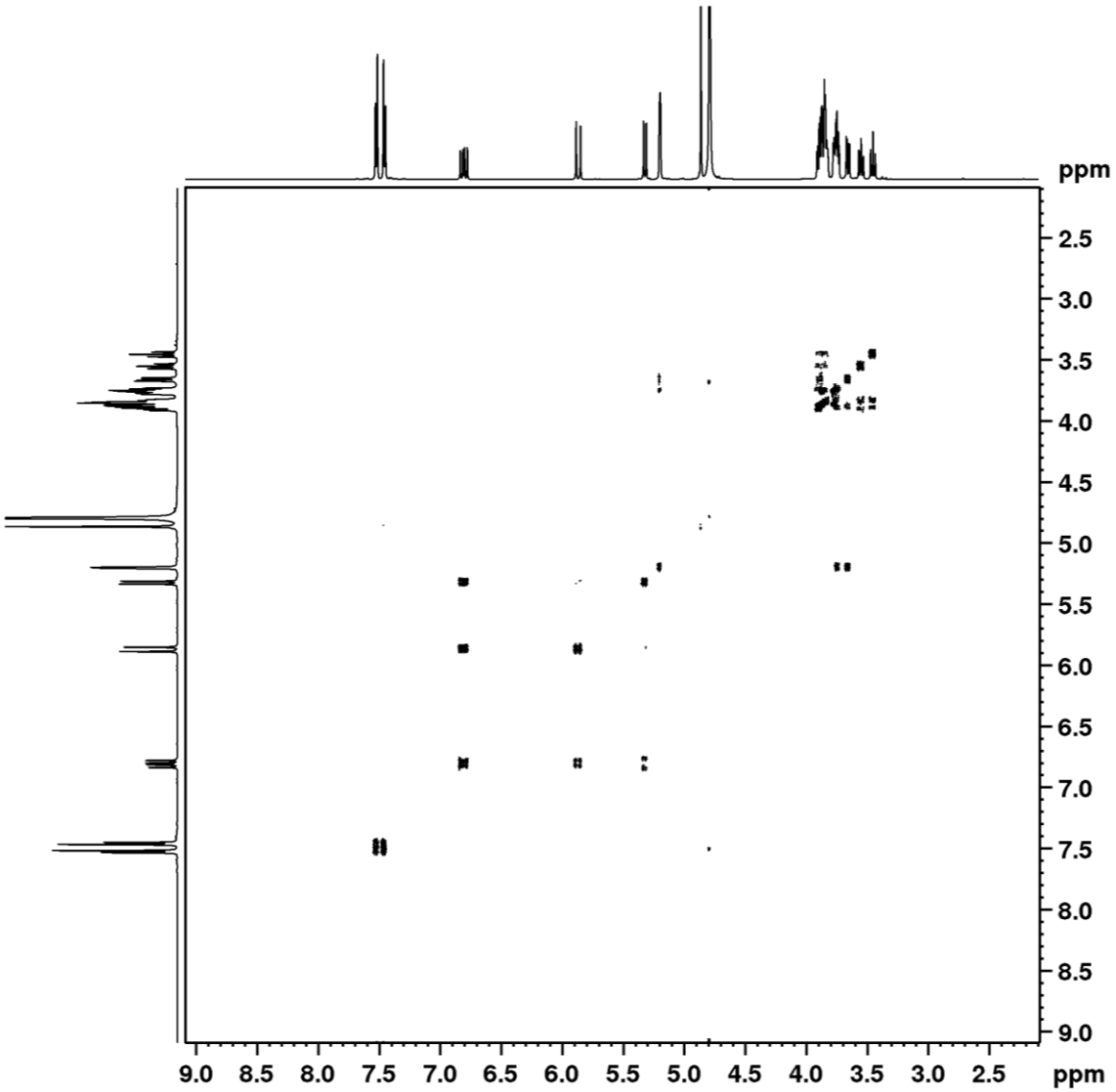

Figure A10. COSY spectrum of **O3** in D_2O at 298 K.

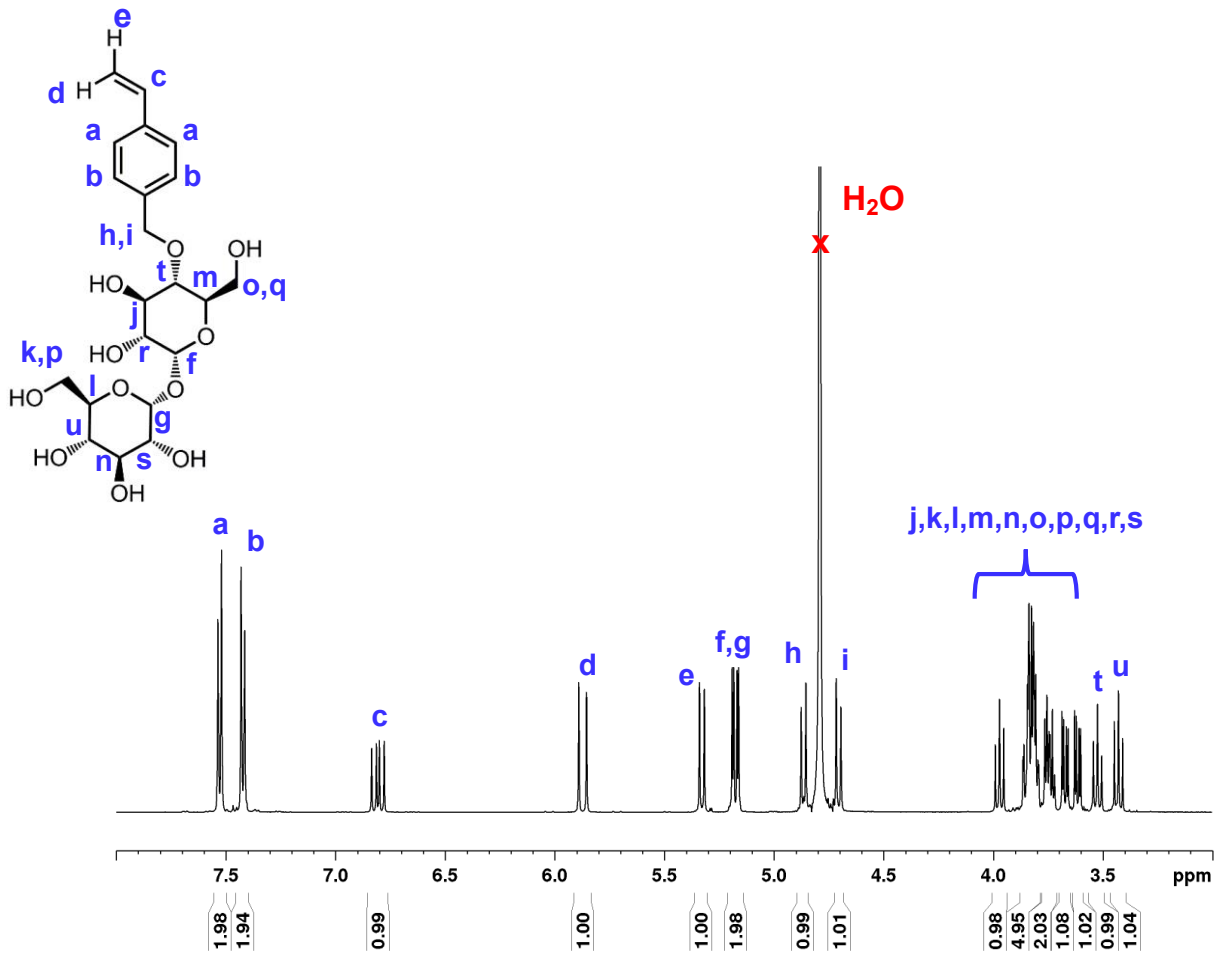

Figure A11. ^{1}H NMR spectrum of **O4** in D_2O at 298 K.

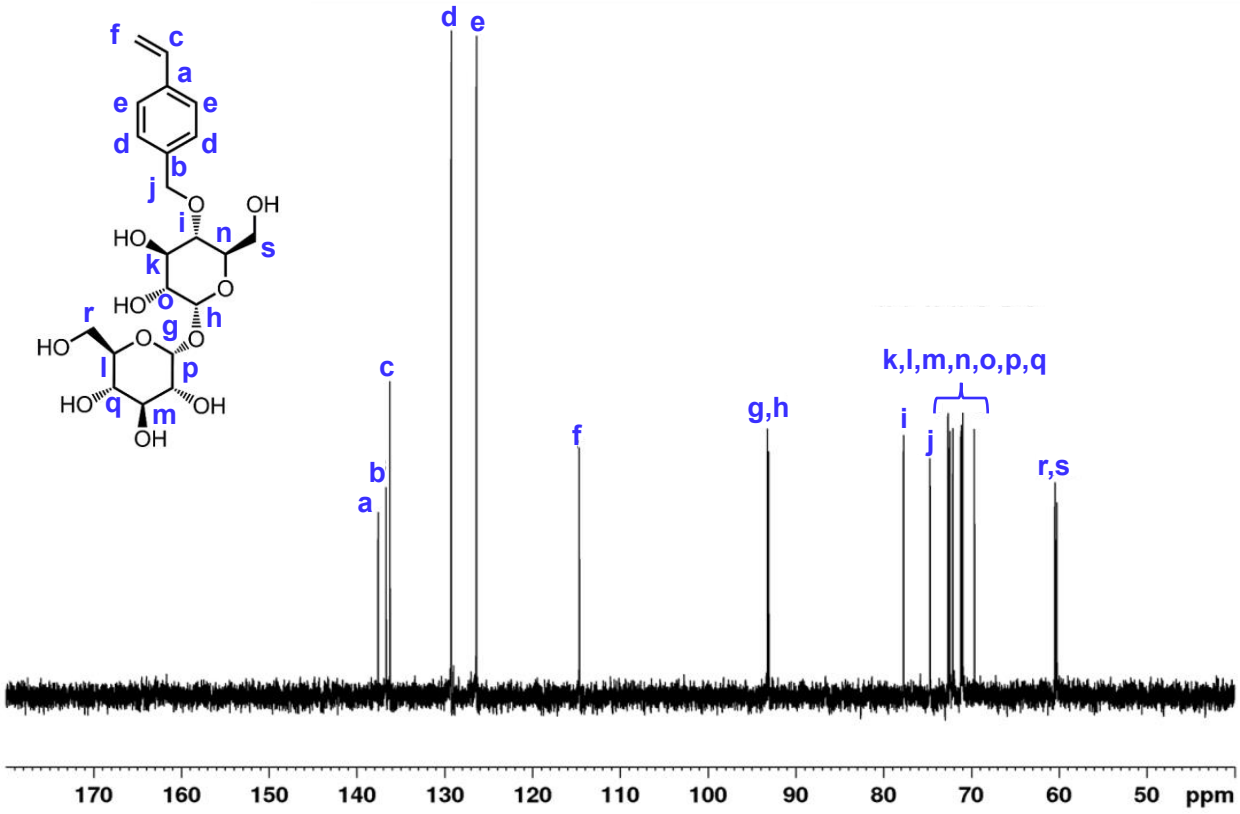

Figure A12. ^{13}C NMR spectrum of **O4** in D_2O at 298 K.

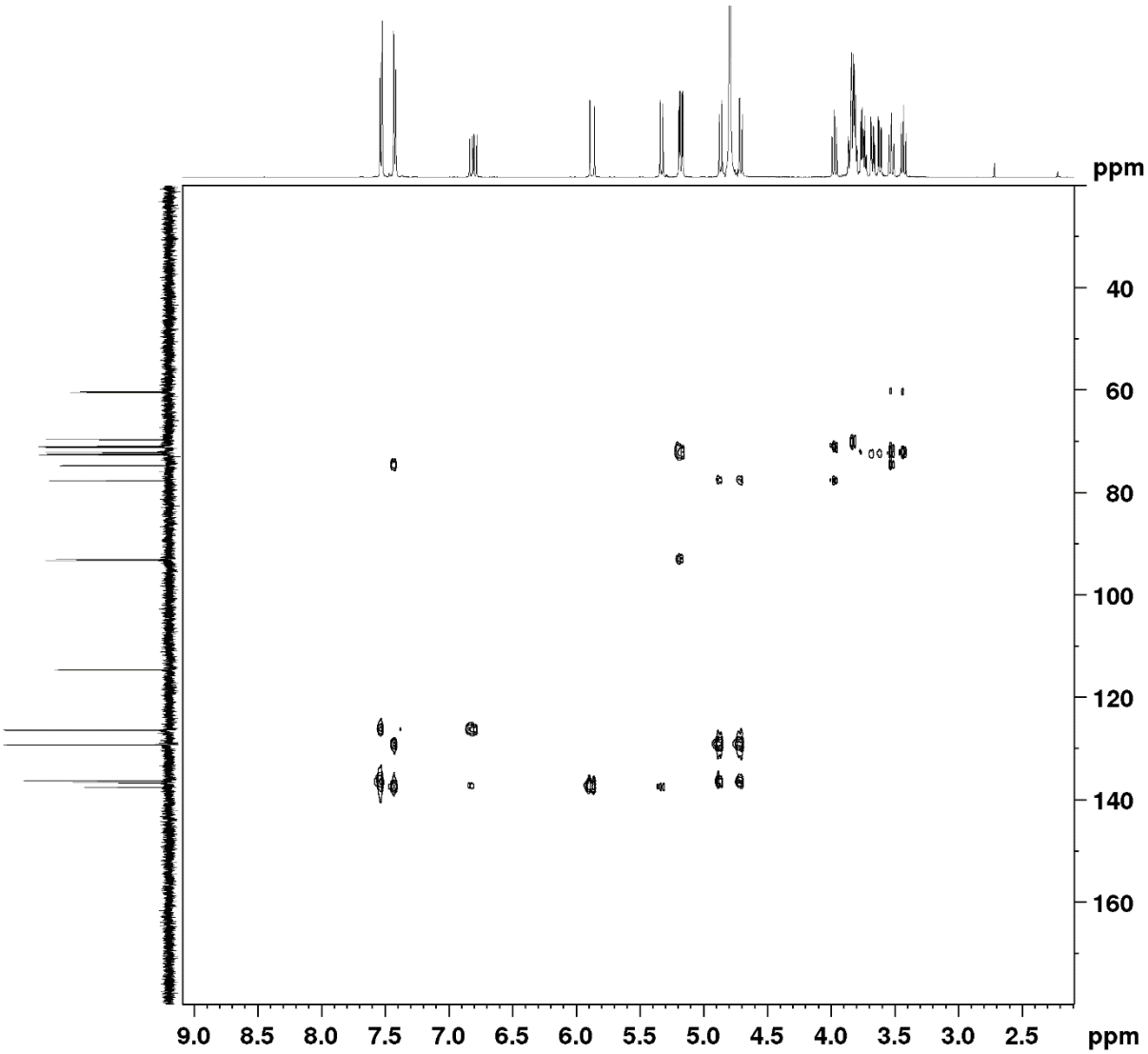

Figure A13. HMBC spectrum of **O4** in D_2O at 298 K.

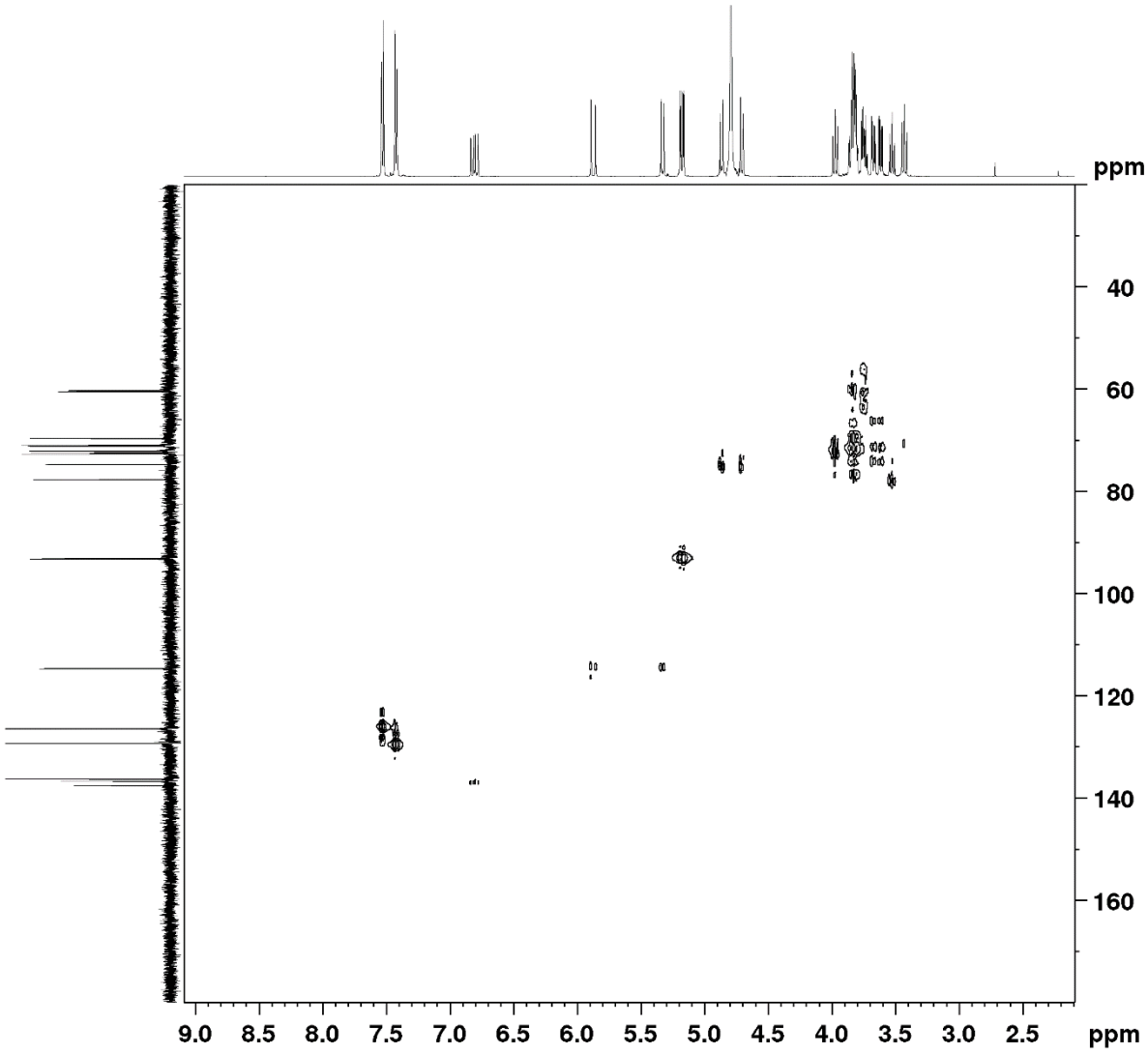

Figure A14. HSQC spectrum of **O4** in D_2O at 298 K.

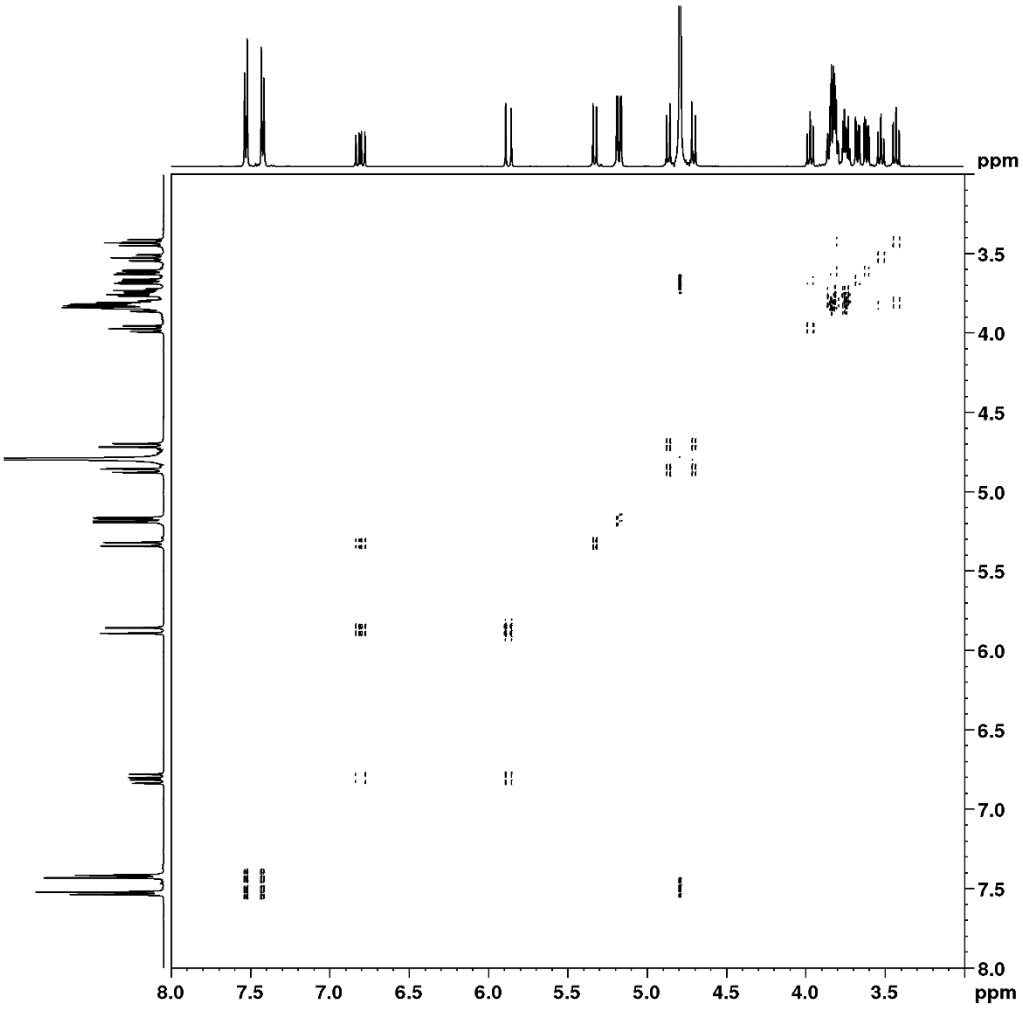

Figure A15. COSY spectrum of **O4** in D_2O at 298 K.

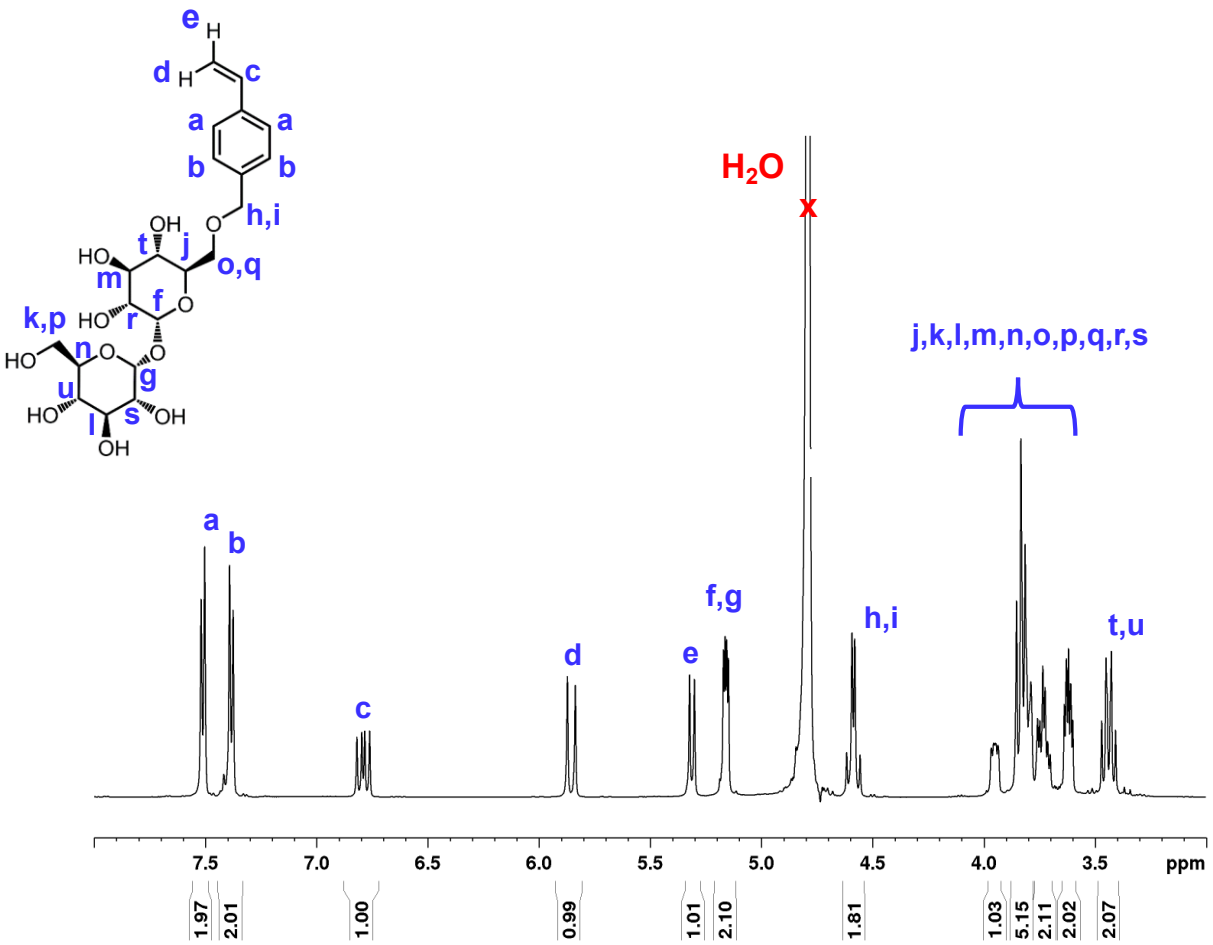

Figure A16. ^{1}H NMR spectrum of **O6** in D_2O at 298 K.

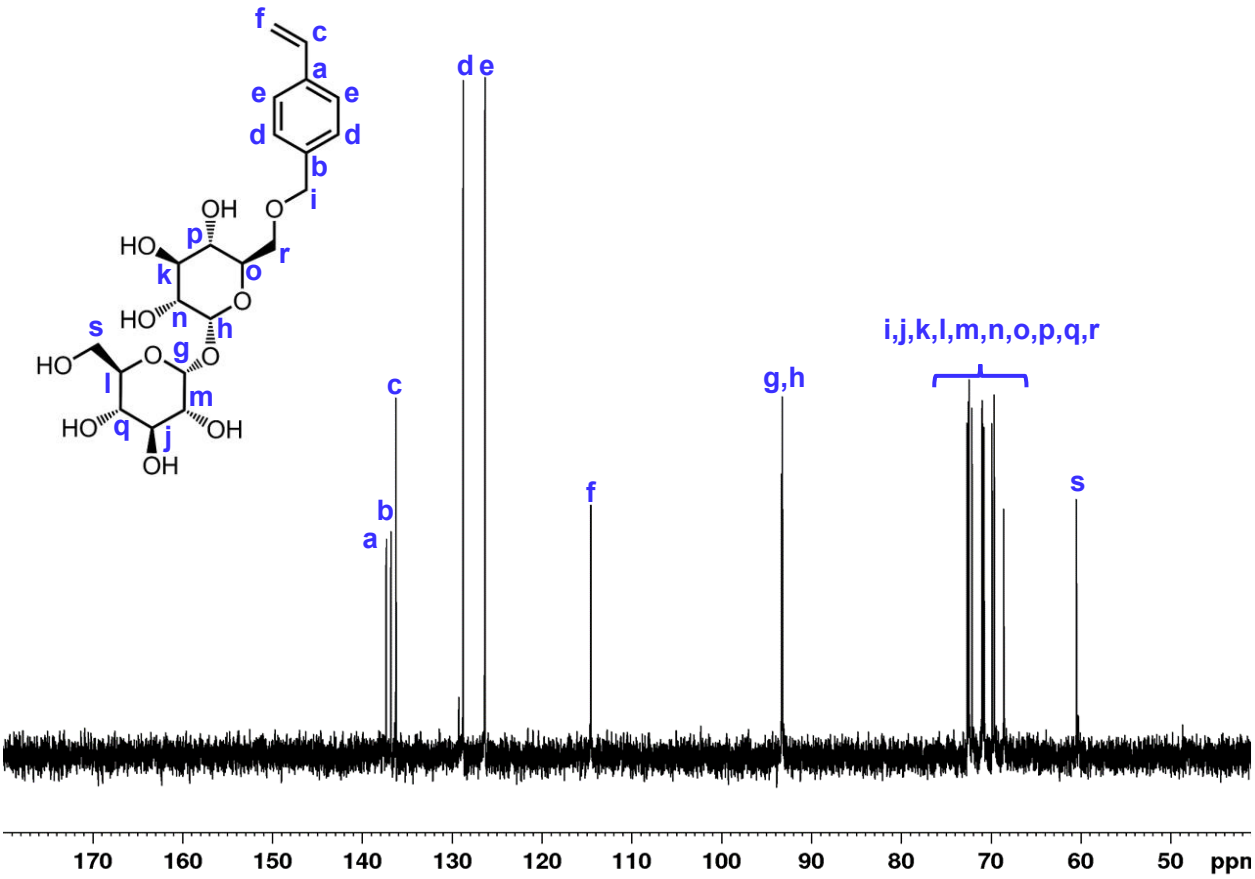

Figure A17. ^{13}C NMR spectrum of **O6** in D_2O at 298 K.

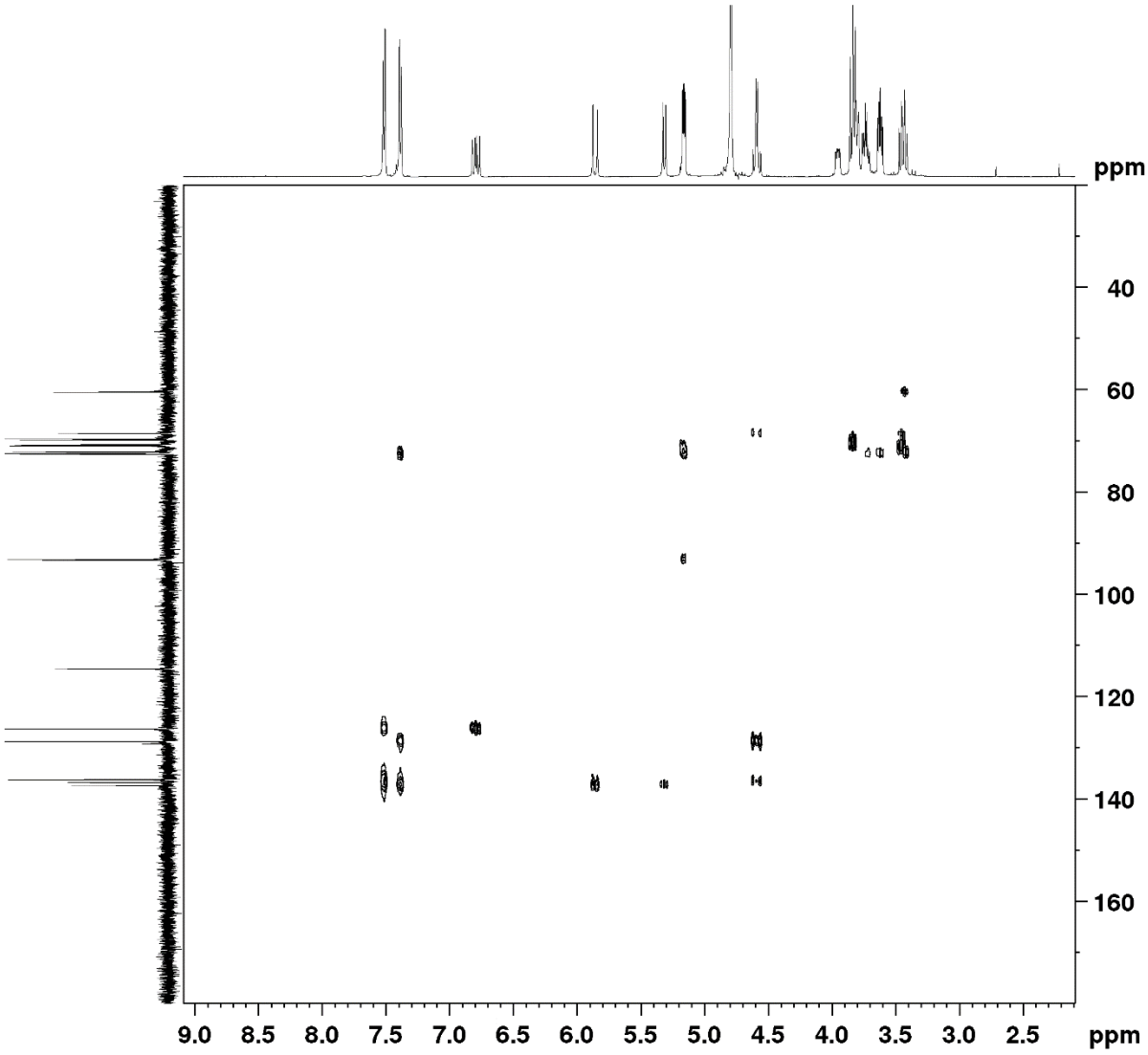

Figure A18. HMBC spectrum of **O6** in D_2O at 298 K.

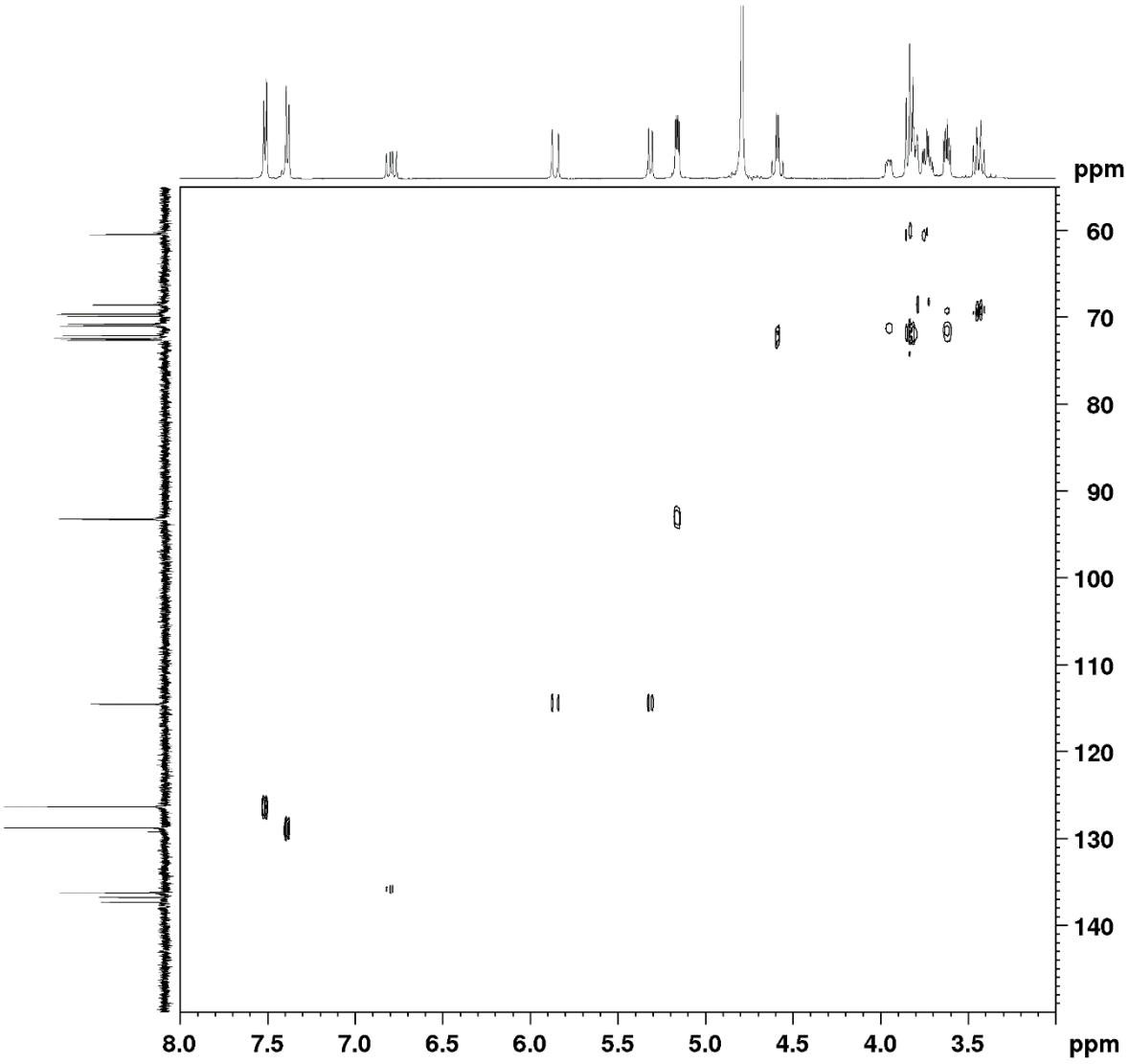

Figure A19. HSQC spectrum of **O6** in D_2O at 298 K.

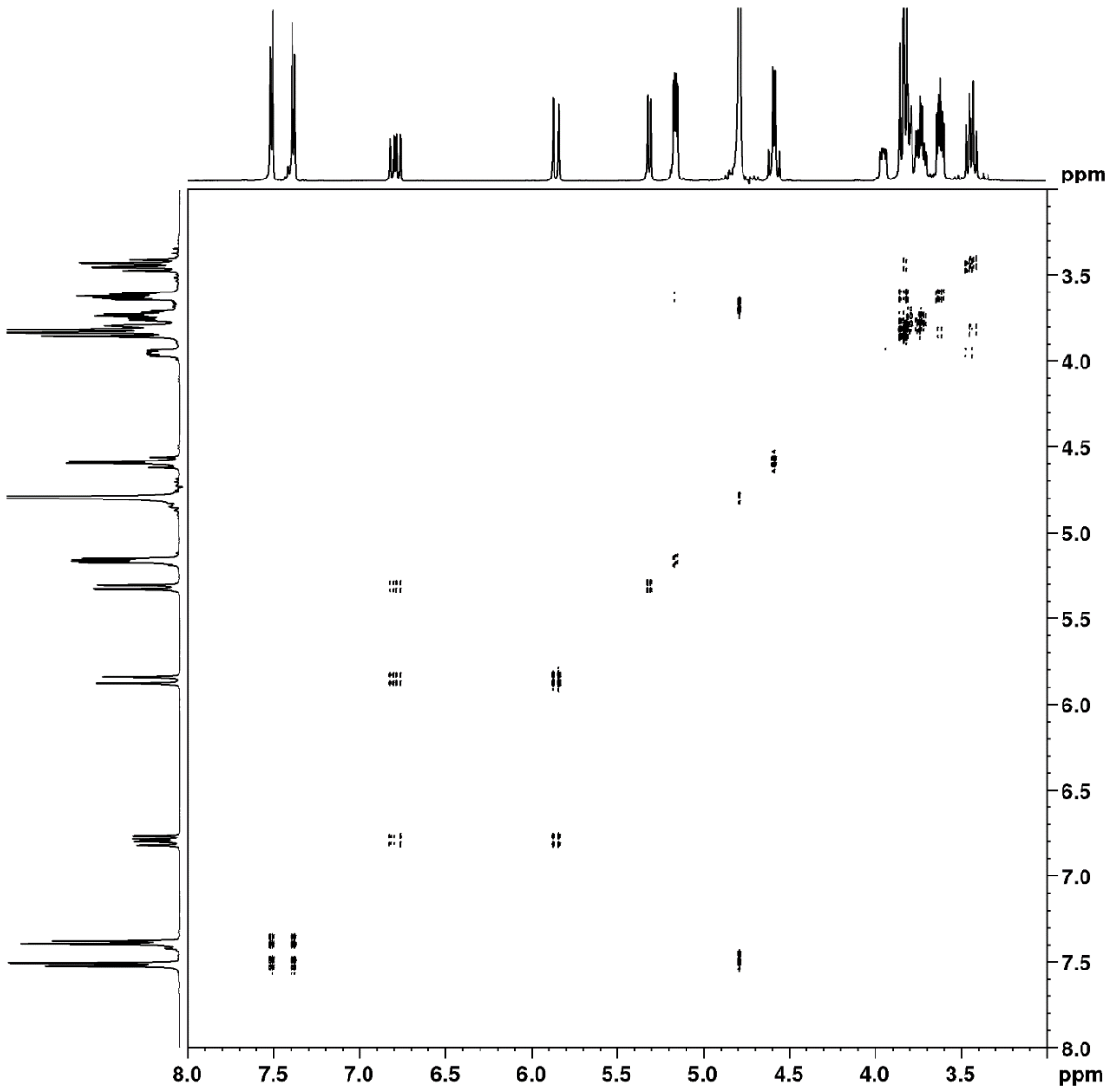

Figure A20. COSY spectrum of **O6** in D_2O at 298 K.

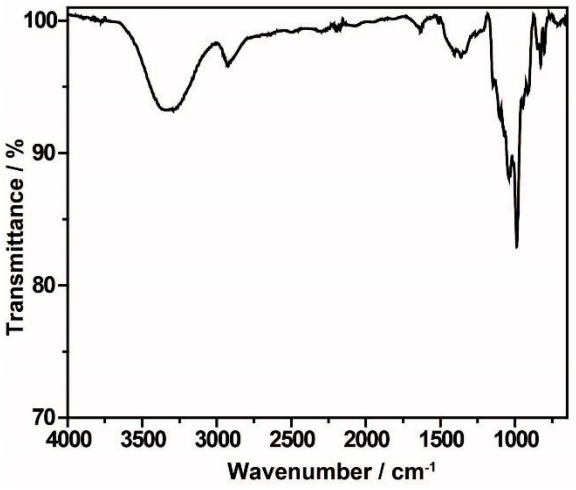

Figure A21. IR spectrum of **O2**.

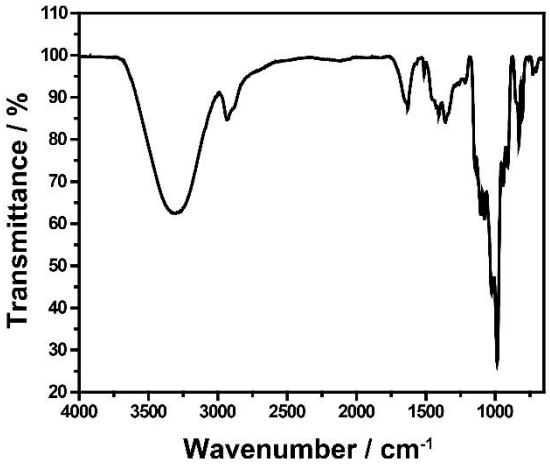

Figure A22. IR spectrum of **O3**.

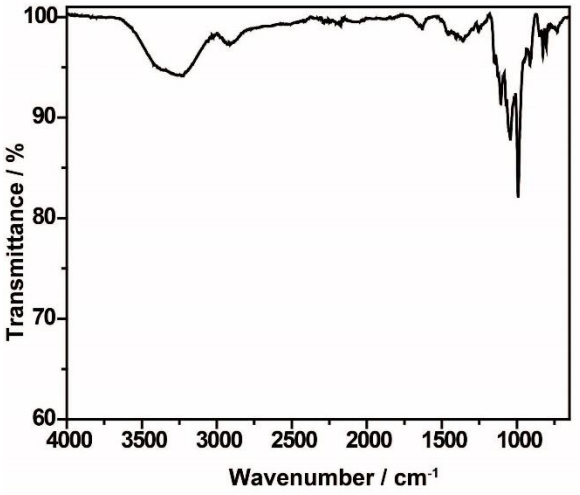

Figure A23. IR spectrum of **O4**.

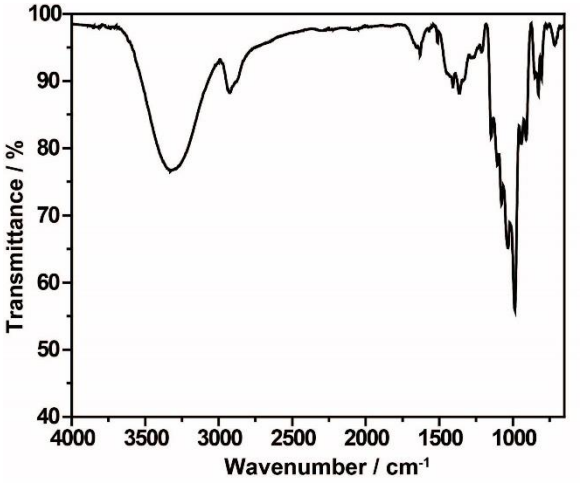

Figure A24. IR spectrum of **O6**.

2.5.8.7 Polymer Characterization

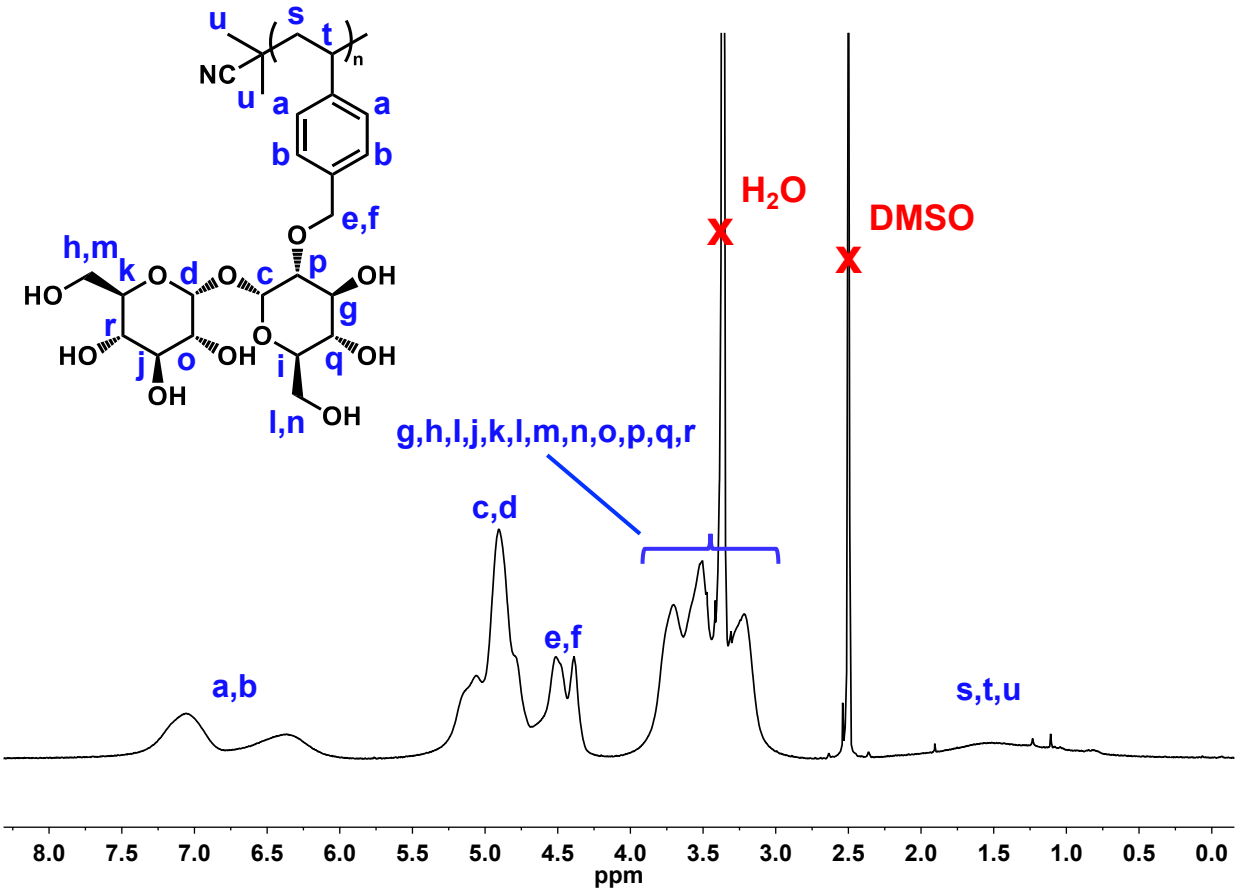

Figure A25. ^{1}H NMR spectrum of **P2** in DMSO-d_6 at 298K.

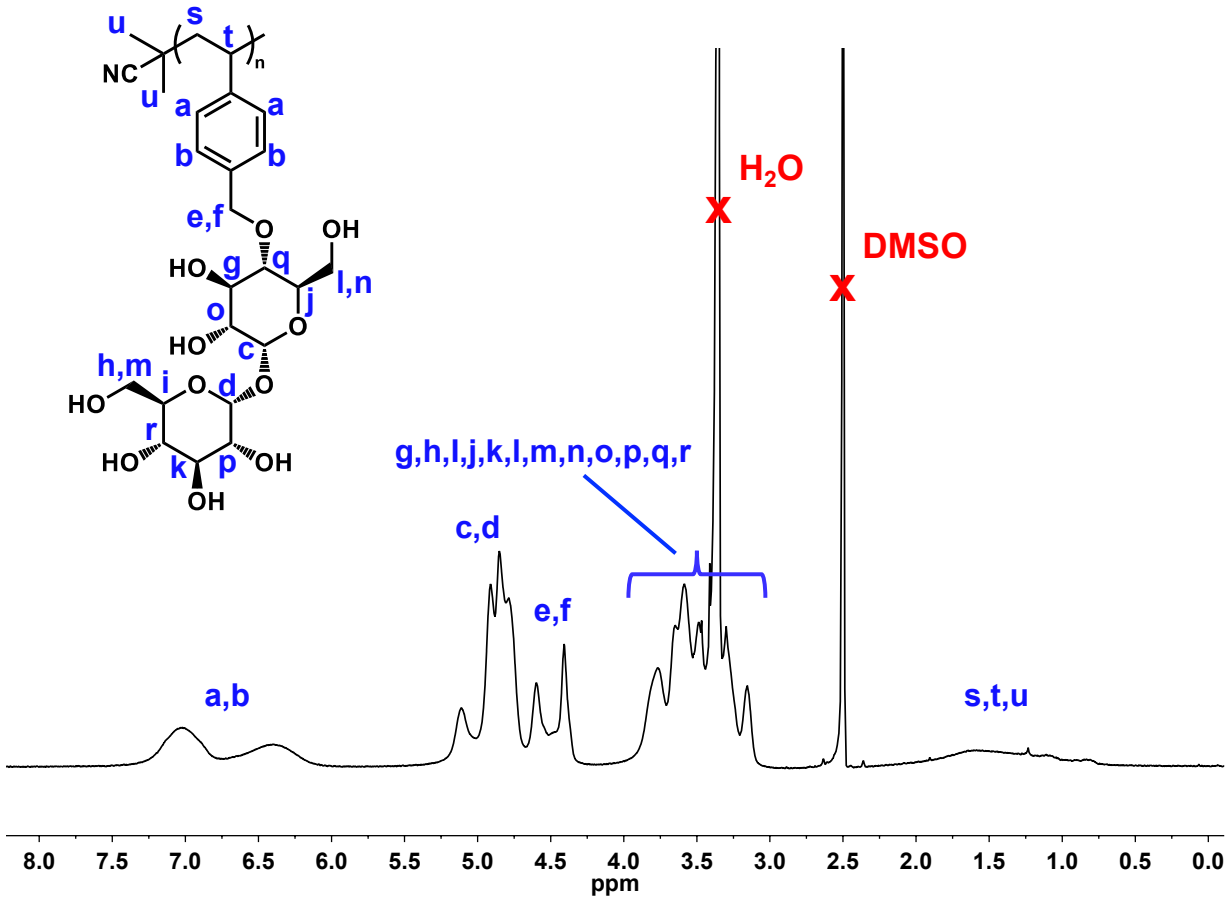

Figure A26. ^{1}H NMR spectrum of **P4** in DMSO-d_6 at 298K.

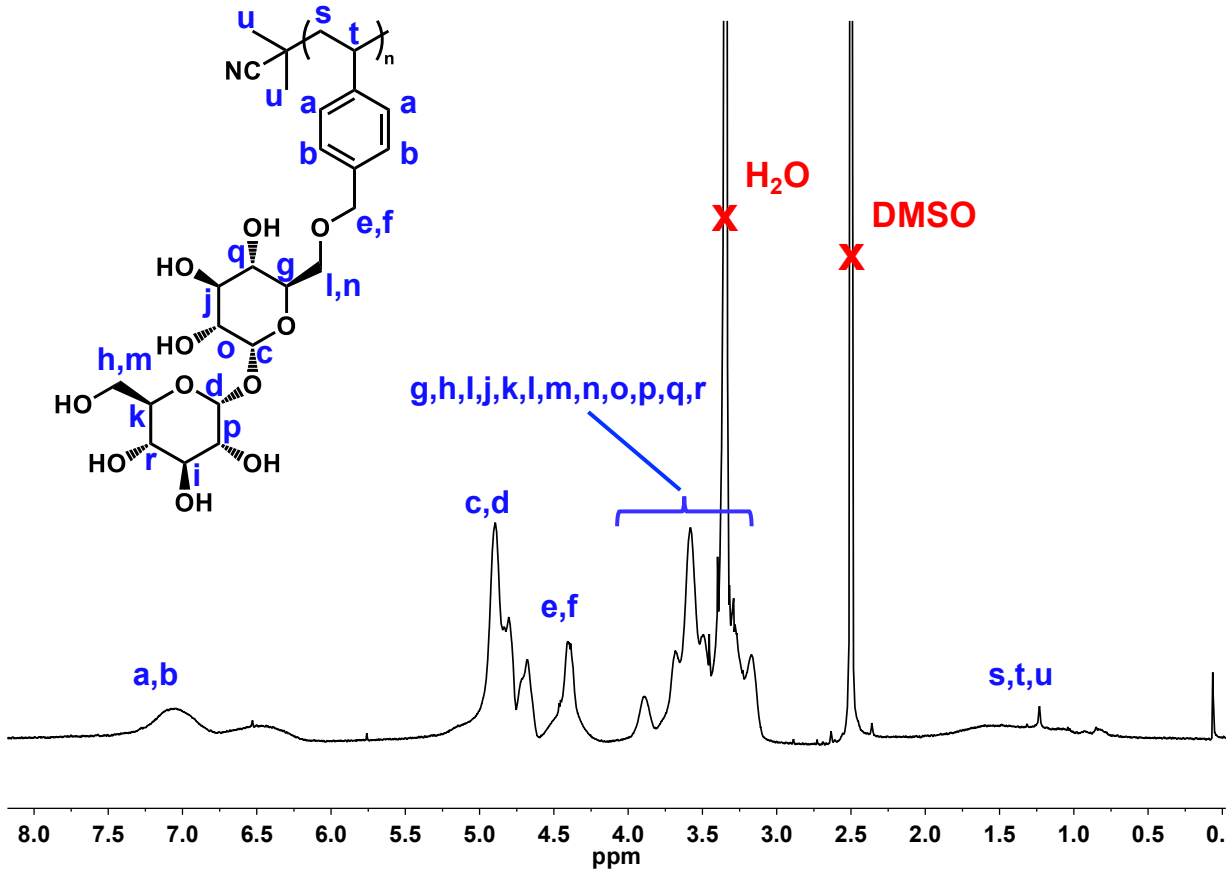

Figure A27. ^{1}H NMR spectrum of **P6** in DMSO-d_6 at 298K.

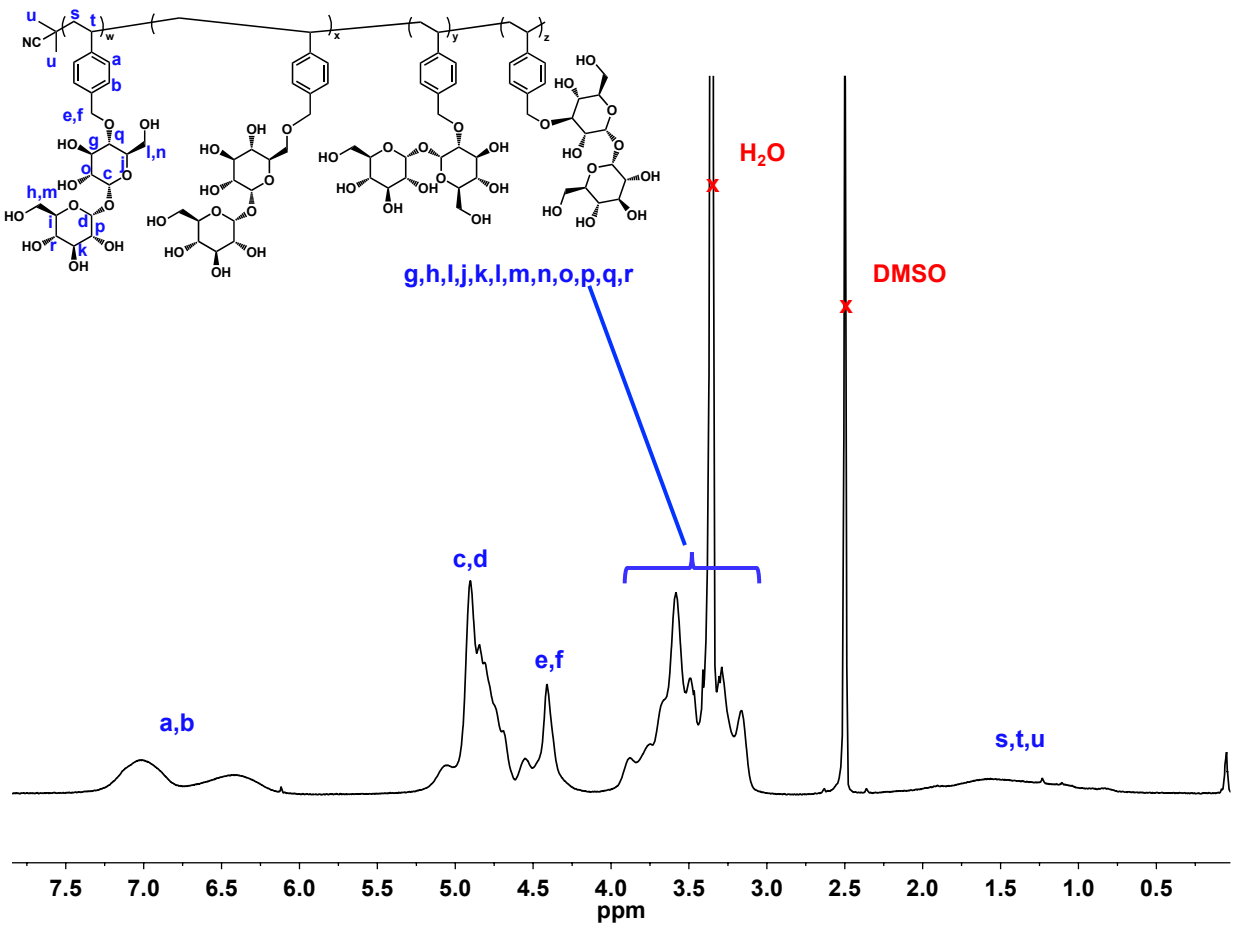

Figure A28. ^{1}H NMR spectrum of **PA** in DMSO-d_6 at 298K.

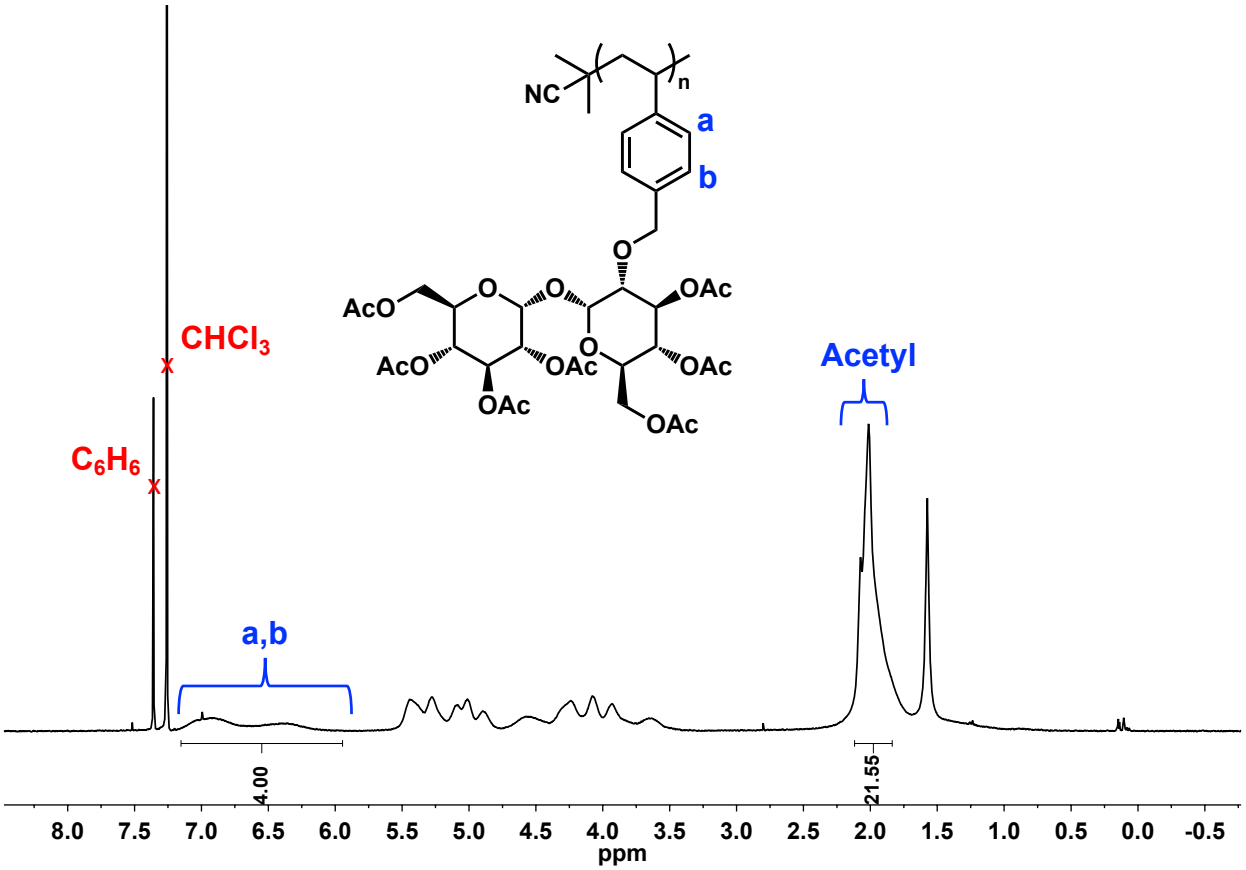

Figure A29. ^{1}H NMR spectrum of acetylated **P2-OAc** in $CDCl_3$ at 298 K.

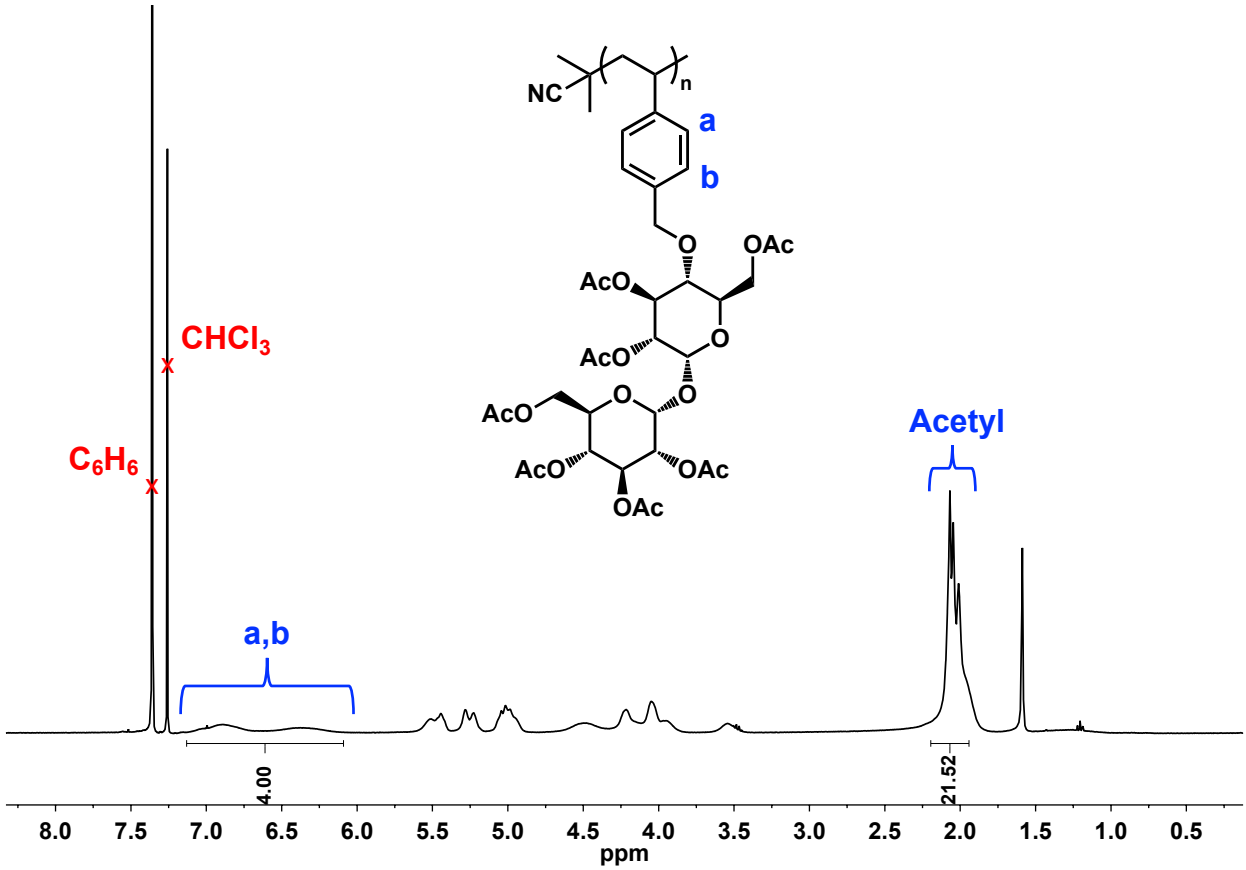

Figure A30. ^{1}H NMR spectrum of acetylated **P4-OAc** in $CDCl_3$ at 298 K.

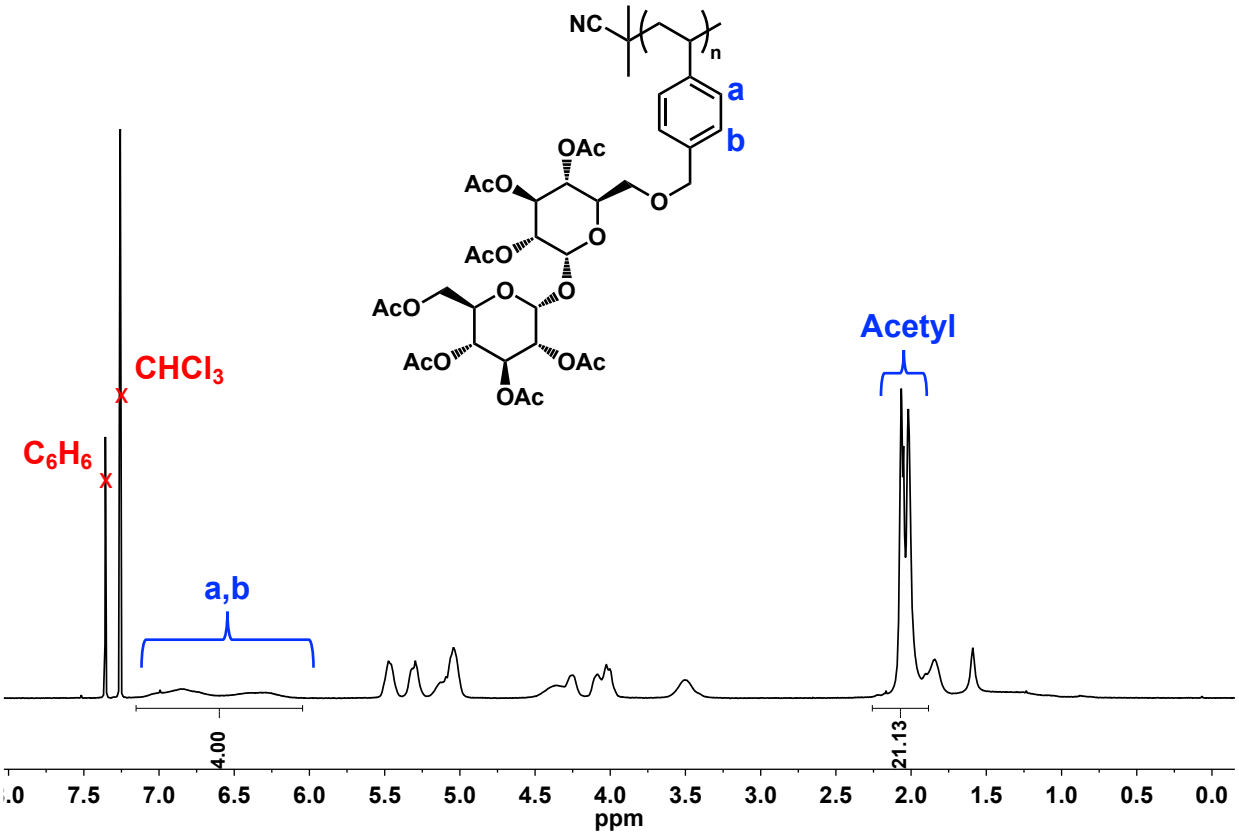

Figure A31. ^{1}H NMR spectrum of acetylated **P6-OAc** in $CDCl_3$ at 298 K.

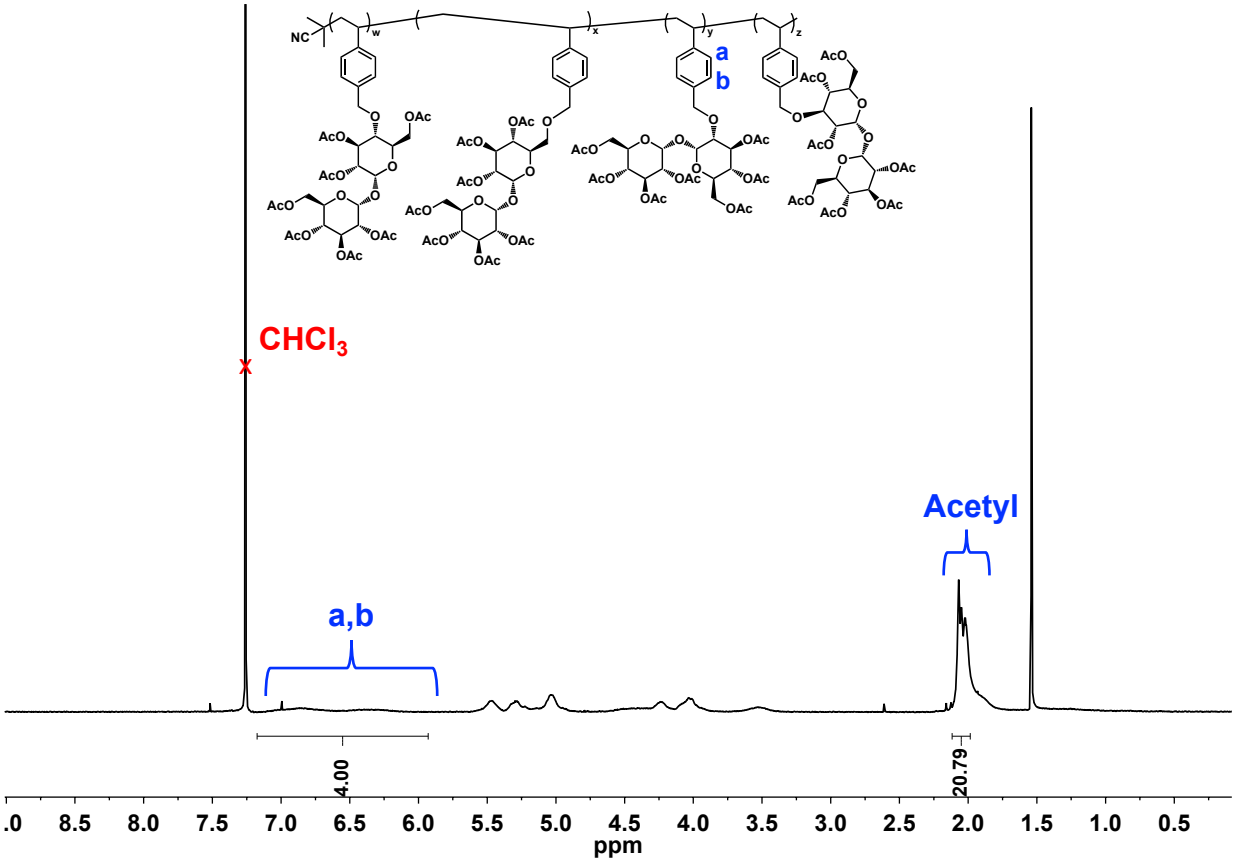

Figure A32. ^{1}H NMR spectrum of acetylated **PA-OAc** in $CDCl_3$ at 298 K.

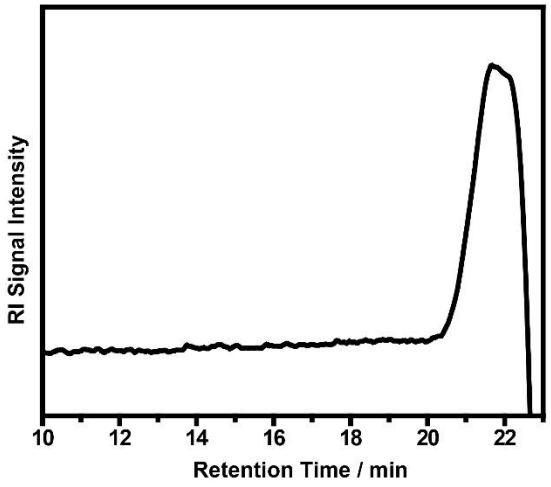

Figure A33. GPC trace of **P2**. M_n= 1.9 kDa; M_w= 2.1 kDa; $Đ$= 1.09.

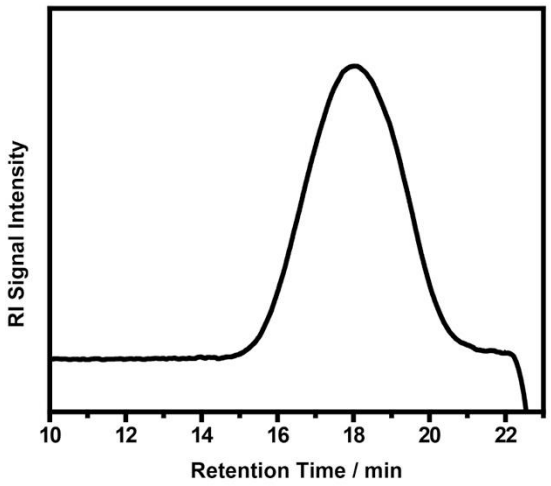

Figure A34. GPC trace of **P2-OAc**. M_n= 15.7 kDa; M_w= 25.0 kDa; $Đ$= 1.59.

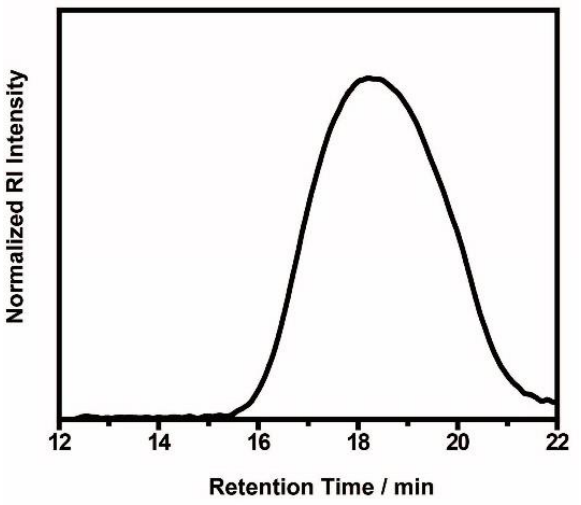

Figure A35. GPC trace of **P4**. M_n= 14.8 kDa; M_w= 23.2 kDa; $Đ$= 1.56.

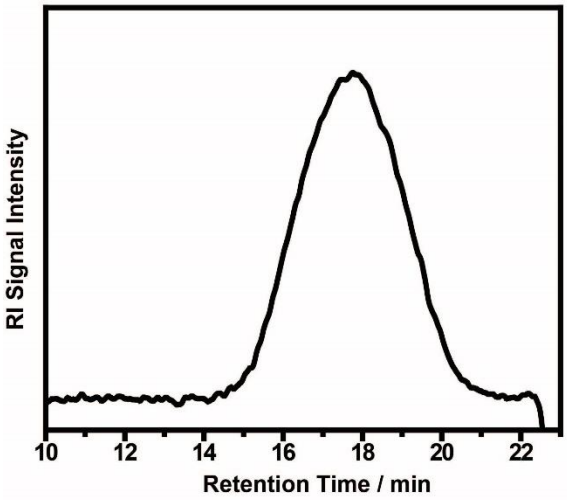

Figure A36. GPC trace of **P4-OAc**. M_n=19.6 kDa; M_w= 31.7 kDa; $Đ$= 1.62.

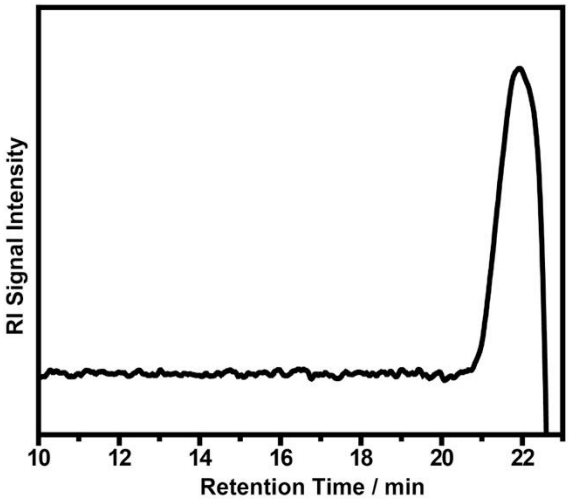

Figure A37. GPC trace of **P6**. M_n=1.8 kDa; M_w= 1.9 kDa; $Đ$= 1.05.

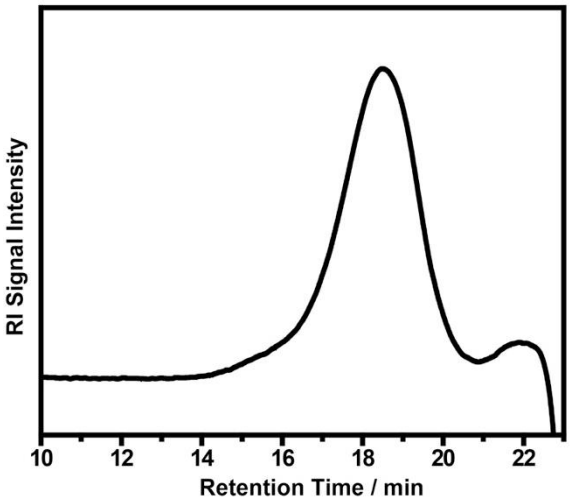

Figure A38. GPC trace of **P6-OAc**. M_n=15.4 kDa; M_w= 21.2 kDa; $Đ$= 1.37.

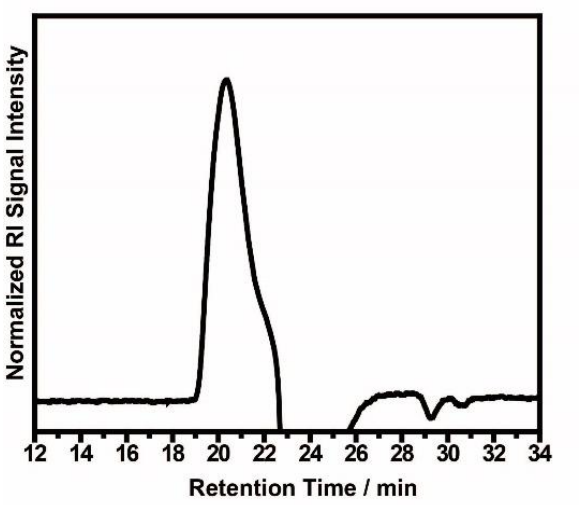

Figure A39. GPC trace of **PA**. M_n=4.4 kDa; M_w= 5.4 kDa; $Đ$= 1.21.

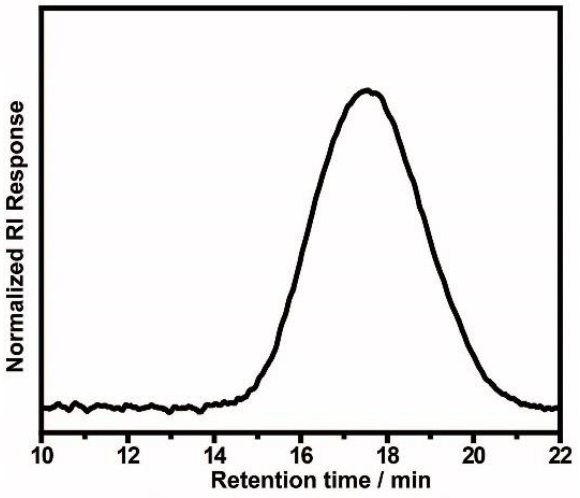

Figure A40. GPC trace of **PA-OAc**. M_n=19.6 kDa; M_w= 35.0 kDa; $Đ$= 1.62.

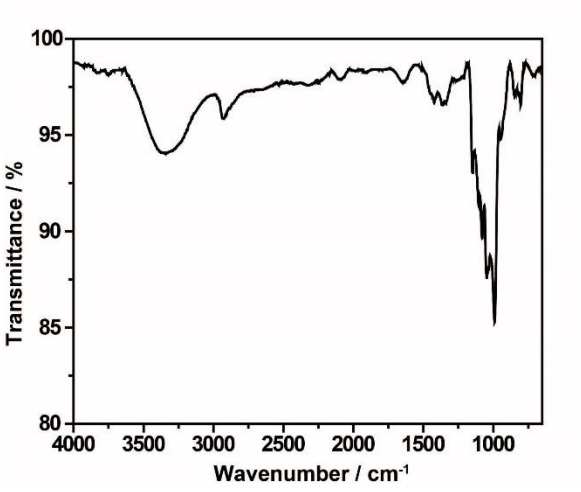

Figure A41. IR spectrum of **P2**.

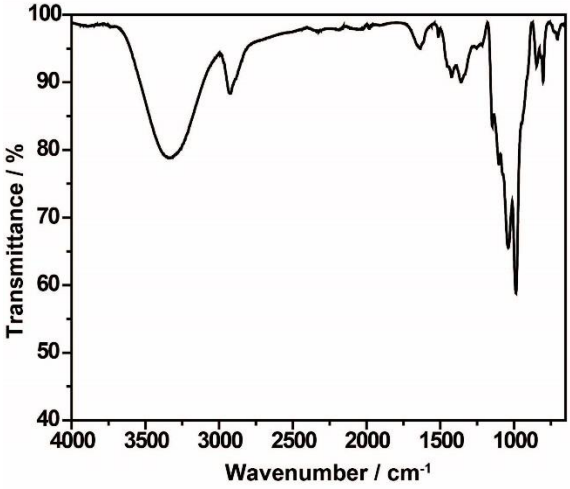

Figure A42. IR spectrum of **P4**.

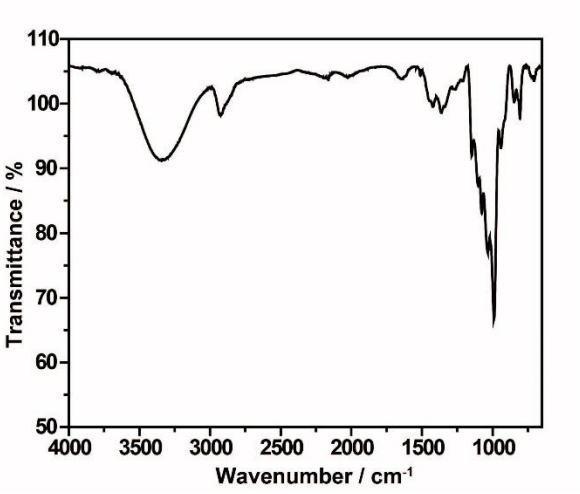

Figure A43. IR spectrum of **P6**.

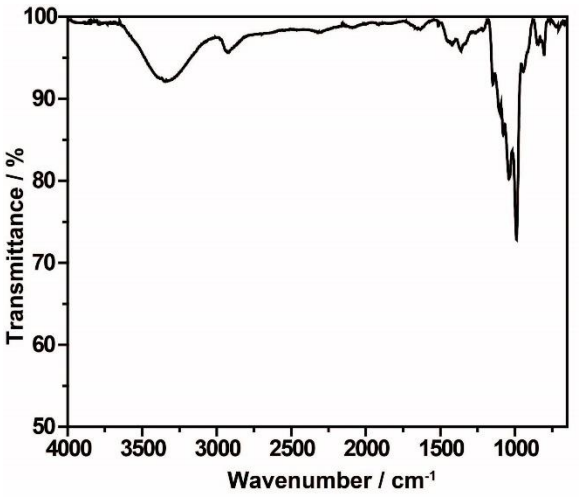

Figure A44. IR spectrum of **PA**.

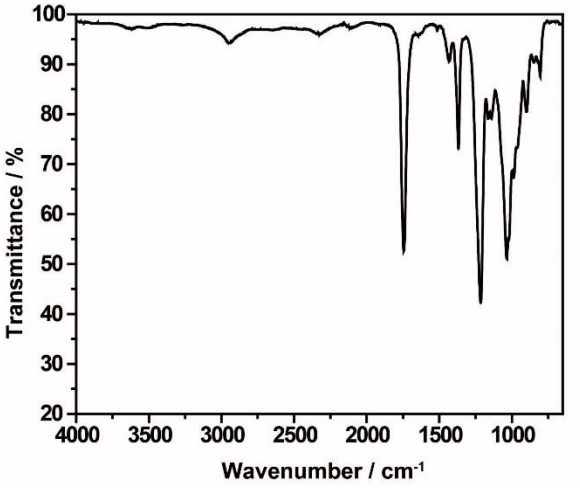

Figure A45. IR spectrum of **PA-OAc**.

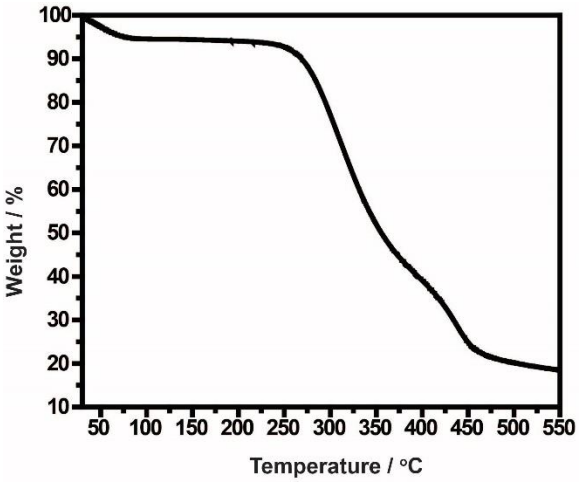

Figure A46. TGA of **P2**.

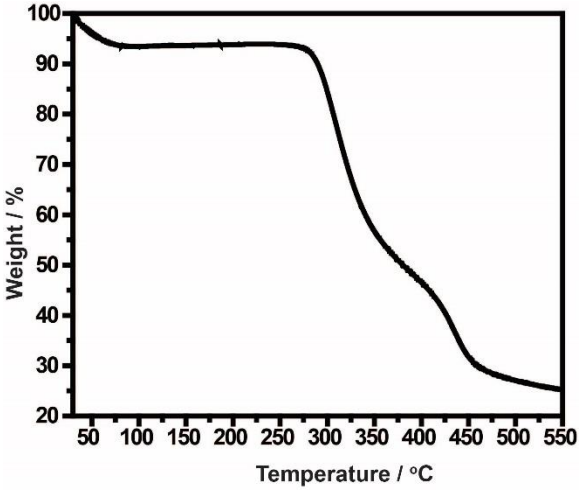

Figure A47. TGA of **P4**.

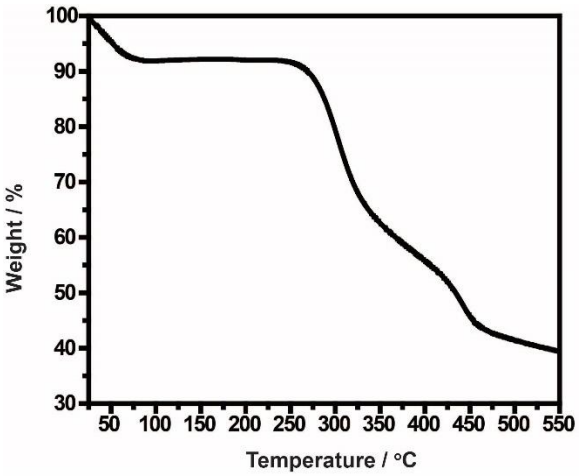

Figure A48. TGA of **P6**.

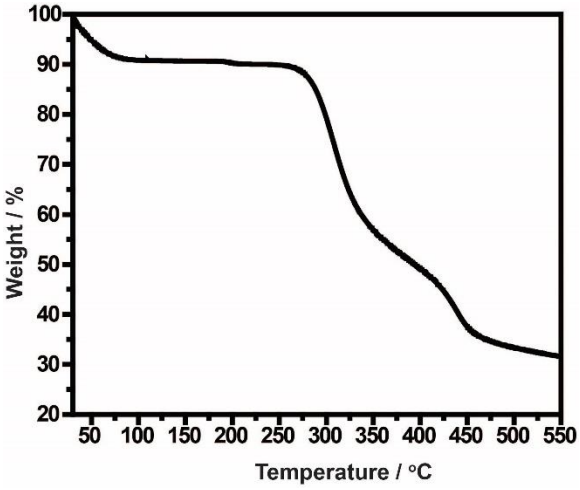

Figure A49. TGA of **PA**.

2.5.8.8 Insulin Assay Data

Figure A50. Non-aggregated (left) and aggregated (right) insulin samples.

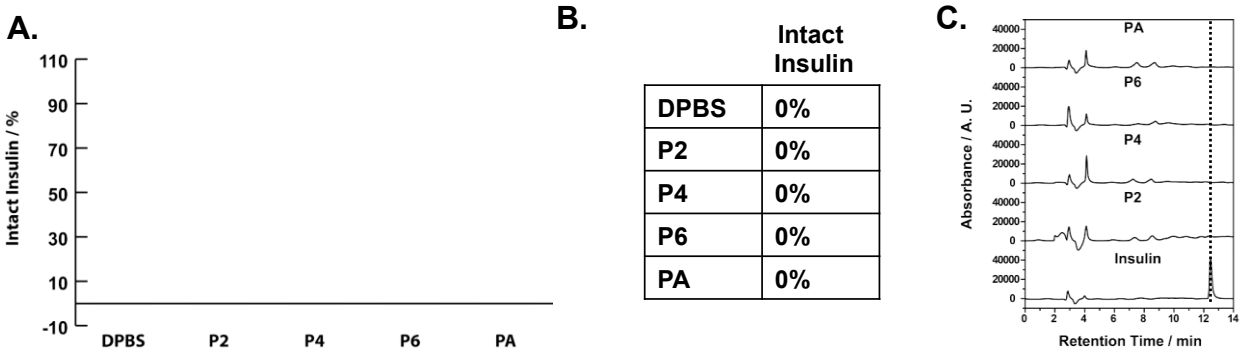

Figure A51. A) Insulin agitation assay using 1 wt. equiv. of polymer shows no stabilization. Samples were heated to 37 °C with 250 rpm agitation for 3 hours. B) Table of insulin agitation assay results using 1 wt. equiv. of polymer shows no intact insulin. C) Intact insulin quantified by HPLC, representative traces for 1 wt equiv polymer assay shown. Insulin data on bottom panel is an unstressed insulin stock solution with the protein eluting at 12 minutes. (n=3)

2.5.8.9 Computational Methods

Conformers for regioisomer **O2**, **O4**, and **O6** were searched by using Maestro 9.4. with OPLS_2015 force field in implicit water. For each regioisomer, the ensemble of conformers consist of those whose energies are within 10 kcal/mol from the lowest one. This ensemble typically include ~400 structures. The structures were then clustered to 25 representatives for **O2**, 33 for **O4**, and 42 for **O6** using the chemical informatics tool in Maestro 9.4. These structures were then optimized using B3LYP/6-31g(d) with SMD water model in Gaussian 09.

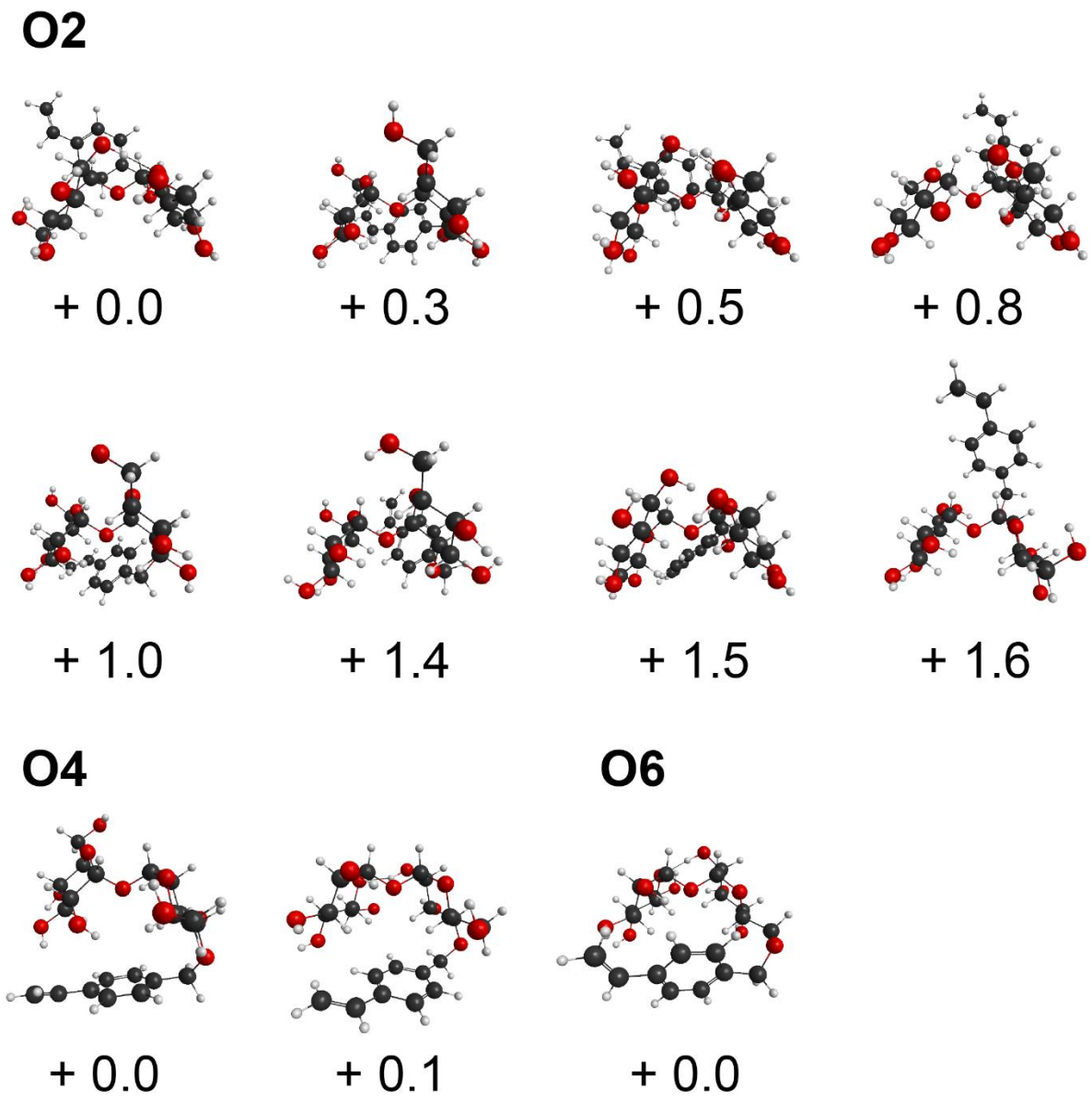

Figure A52. Conformers for the regioisomers within 2 kcal/mol of the most stable conformer (energy difference in kcal/mol shown below the structures).

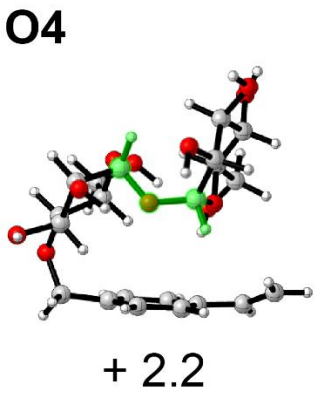

Figure A53. Example of conformer with disrupted clam shell conformation (O4 conformer with 2.2 kcal/mol higher energy than the most stable conformation).

Chapter 3

Visible-Light-Induced Olefin Activation Using 3D Aromatic Boron-Rich Cluster Photooxidants

3.1 Introduction

We report a discovery that perfunctionalized icosahedral dodecaborate clusters of the type $B_{12}(OCH_2Ar)_{12}$ (Ar = Ph or C_6F_5) can undergo photo- excitation with visible light, leading to a new class of metal-free photooxidants. Excitation in these species occurs as a result of the charge transfer between low-lying orbitals located on the benzyl substituents and an unoccupied orbital delocalized throughout the boron cluster core. Here we show how these species, photo-excited with a benchtop blue LED source, can exhibit excited-state reduction potentials as high as 3 V and can participate in electron- transfer processes with a broad range of styrene monomers, initiating their polymerization. Initiation is observed in cases of both electron-rich and electron- deficient styrene monomers at cluster loadings as low as 0.005 mol%. Furthermore, photo-excitation of $B_{12}(OCH_2\text{-}C_6F_5)_{12}$ in the presence of a less activated olefin such as isobutylene results in the production of highly branched poly(isobutylene). This work introduces a new class of air- stable, metal-free photo-redox reagents capable of mediating chemical transformations.

Photoredox processes are ubiquitous in chemistry and require a chromophore to absorb a photon, triggering the formation of an excited state with a redox potential dramatically different than that of the parent ground state. Well-defined molecular chromophores typically possess functional groups that are capable of absorbing light, upon which an electron is promoted into a higher energy molecular orbital; in many of these cases, these photoexcited species can behave as photooxidants or photoreductants. There exist two broad classes of molecular-based chromophores capable of undergoing photoredox processes: metal-based complexes and organic dyes.[1] Metal-based chromophores possess excited states with highly tunable lifetimes, as they are able to reach triplet states and are also able to delocalize electrons over a number of molecular orbitals.[2] On the

other hand, the majority of organic chromophores possess relatively short-lived excited states featuring π→π* electronic excitations with radicals centered primarily within *s* or *p* orbitals.[3] (Figure 3-1). Both classes have been utilized to harness energy from visible light, enabling the formation of new chemical bonds in the context of building complex and diverse molecular architectures.[4]

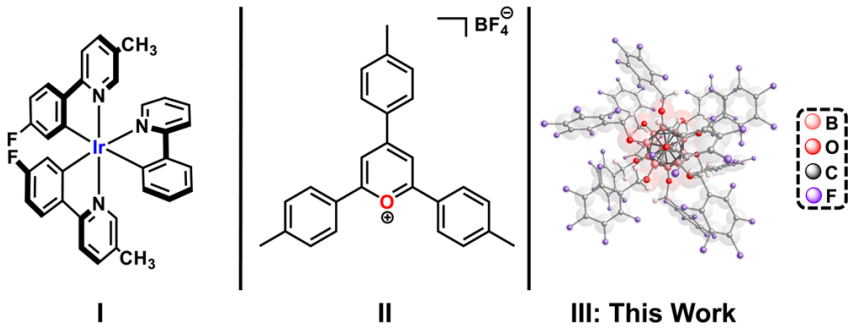

Figure 3-1. Molecular chromophores with photoredox activity include transition-metal complexes (e.g., **I**[5]) and organic dyes (e.g., pyrylium[6] **II**). This work reports $B_{12}(OR)_{12}$ clusters as a new class of photoredox-active molecular chromophores (**III**).

Boron-rich clusters are a class of molecules that can contain characteristics of both metal complexes and organic molecules.[7-10] Many polyhedral boron clusters are robust and kinetically stable, and can undergo facile functionalization chemistry.[9-11] In particular, dodecaborate clusters feature a unique, 3D aromatic bonding situation in which the skeletal electrons are delocalized in three dimensions.[11,12] Importantly, unfunctionalized boron-rich clusters containing B–H bonds do not absorb light in the visible region and also cannot undergo well-defined redox processes.[13] However, researchers previously demonstrated that several classes of perfunctionalized polyhedral boron clusters are capable of undergoing reversible redox processes.[11,a,b,f,14-17] For example, colorless ether-functionalized $[B_{12}(OR)_{12}]^{2-}$ clusters can undergo two sequential quasi-reversible

one-electron redox processes, leading to $[B_{12}(OR)_{12}]$- and neutral $B_{12}(OR)_{12}$, respectively, both of which exhibit strong visible light absorption bands (Figure 3-2 A−C).[15-17] We hypothesized that this light absorption can be used to generate reactive photoexcited species, though up to this point no such behavior has been realized for this class of boron-rich clusters.[18] Here we demonstrate the visible light photoredox behavior of $B_{12}(OR)_{12}$ clusters which interact with olefinic species and subsequently initiate their polymerization. Specifically, we show that this process occurs across a wide array of both electron-rich and electron-deficient styrene monomers as well as isobutylene. The latter process represents the first visible-light-induced metal-free polymerization leading to highly branched poly(isobutylene).

3.2 Results and Discussion

We recently developed an improved synthetic method which affords perfunctionalized $B_{12}(OR)_{12}$ clusters with tunable electrochemical properties (Figure 3-2).[17] During the course of our synthetic investigations, we discovered that, upon leaving cluster species **1a** in the presence of 4-methoxystyrene (**2a**) in a dichloromethane (CH_2Cl_2) solution, a viscous mixture resulted, indicating polymerization of **2a** (see Appendix B). Interestingly, the same reaction did not produce any polymer when left in the dark, suggesting that this process is likely photodriven. We decided to investigate this interesting behavior more closely via controlled irradiation of a 2 M solution of **2a** in CH_2Cl_2 at room temperature under an N_2 atmosphere with 0.5 mol% **1a** ($\lambda_{max,abs}$ = 470 nm) illuminated under blue LED light (450 nm). After 4 h of irradiation, the reaction produced polymer in <10% yield (Table 3-1). During the course of our investigations, Nicewicz reported an elegant pyrilium-catalyzed (**II**, Figure 3-1), photomediated polymerization protocol of **2a** and suggested that the mechanism of the polymerization likely occurs through a cationic route.[19] We

hypothesized that a similar process might be in operation with the $B_{12}(OBn)_{12}$ system and, if so, a cluster functionalized with more electron-withdrawing substituents would increase the oxidation potential of the photoinitiator, thereby providing greater photooxidizing power of these species. Therefore, $B_{12}(OCH_2C_6F_5)_{12}$ (**1b**) was synthesized in a manner analogous to that of **1a** and was isolated as a yellow solid in 63% yield (Figure 3-2 D). UV-vis absorption shows that **1a** and **1b** exhibit similar λ_{max} wavelengths (470 and 454 nm, respectively; Figure 3-2 C), and, notably, cyclic voltammetry experiments show a 500 mV increase in the -1/0 redox couple of **1b** compared to **1a** (Figure 3-2 B).

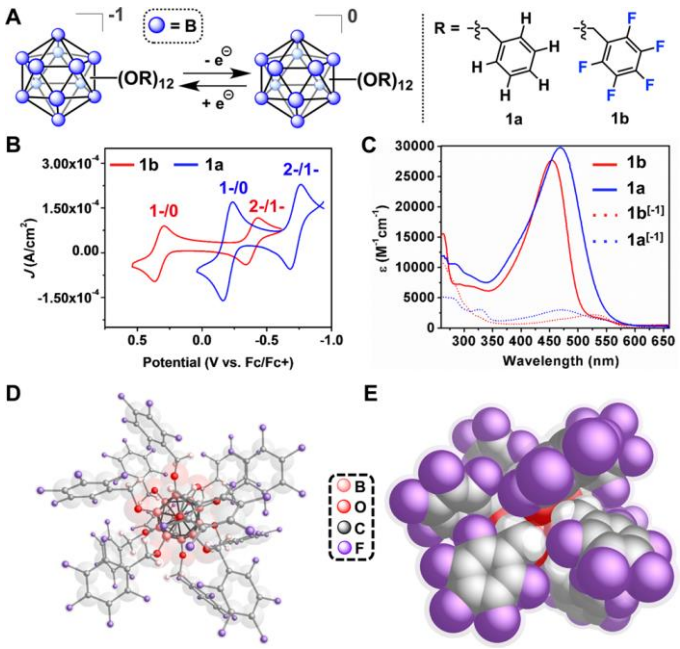

Figure 3-2. (A) Reversible oxidation/reduction of substituted boron-rich clusters (0/-1 is shown). (B) Cyclic voltammogram of **1a** and **1b**. (C) UV/vis spectrum of photooxidants 1a and **1b** in their fully oxidized states and mono-anionic states. (D,E) Ball-and-stick and space-filling representations of the X-ray crystal structure of **1b**.

Addition of 0.1 mol% **1b** to a 2 M CH_2Cl_2 solution of **2a** under ambient lighting resulted in the instantaneous formation of a polymer gel with a high dispersity (see Appendix B and Table 3-1). Surprisingly, reducing the loading of **1b** to 0.005 mol% still resulted in immediate gelation upon addition to **2a**. Under optimized conditions, irradiation of 0.05 mol% **1b** in a 0.2 M CH_2Cl_2 solution of **2a** with 450 nm light for 6 h produced 198 kDa polymer in 97% yield (Table 3-1).

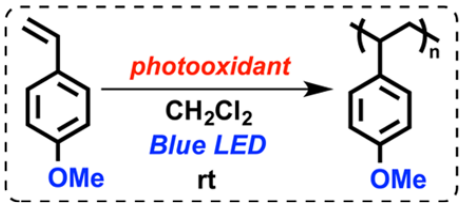

Oxidant (mol%)	Conc.	$Đ$	M_n (kDa)	Time	Yield
1a (0.5)	2 M	1.3	13.8	4 h	< 10%
1b (0.1)	2 M	15.2	255	< 1m	81%
1b (0.005)	2 M	1.7	198	< 1m	90%
1b (0.05)	0.2 M	1.7	198	6 h	97%

Table 3-1. Polymerization of **2a**: number-average molecular weight (M_n) and dispersity ($Đ$) determined by GPC. Reported data are average of two runs.

To understand the observed photoinitiation, we performed TD-DFT studies on **1a** and **1b**. This work reveals the existence of a favorable charge-transfer (aryl to boron cluster) excitation pathway leading to an excited species with a redox potential roughly matching the one-electron oxidation potential of styrene (Figure 3-3). This is consistent with the previous computational work of Schleid on $B_{12}(OH)_{12}^{-}$ monoradical species.[20] Our proposed mechanism involves the generation of a potent photooxidant by visible light promotion of an electron from a low-lying occupied orbital on aryl rings to the cluster-based LUMO. The resulting excited species initiates polymerization via a single-electron oxidation of styrene (or styrene derivative), producing a cluster-based radical anion the stabilities of which are documented[12,17c] and a monomer-based radical cation.

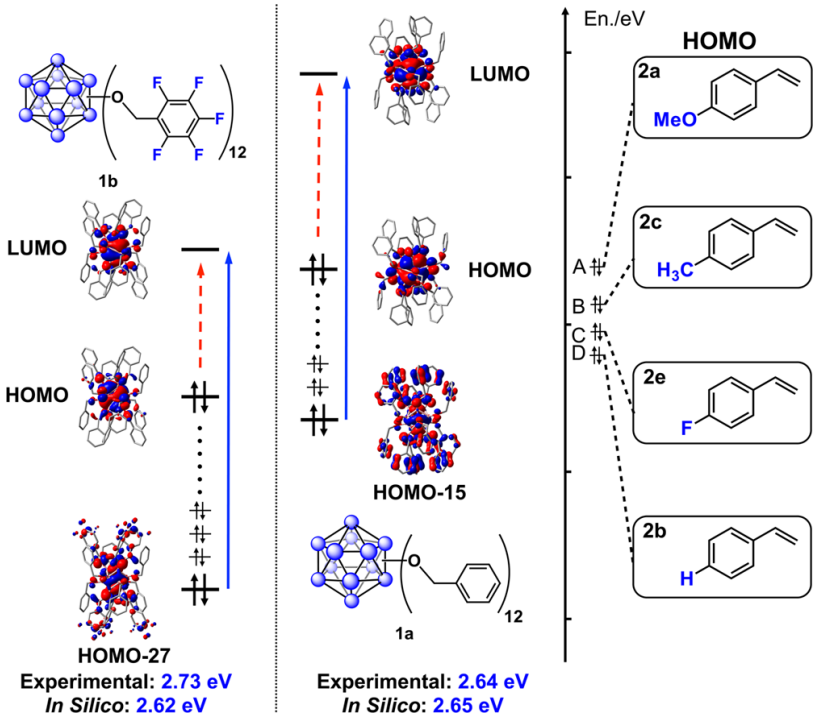

Figure 3-3. TD-DFT studies indicating charge-transfer excitation pathway in **1a**/**1b**. Also shown are the relative energies of the HOMO levels of monomers **2a**–**c**,**e**.

Fluorescence decay measurements were employed to bench-mark the photoexcited properties of **1b**. The excited-state lifetime of **1b**, measured from the 600 nm emission maximum, was found to be ~380 ps (Figure B50). From these data and the known ground-state reduction potential (-1/0 couple), an excited-state reduction potential value of ~2.98 V (vs SCE) was estimated for **1b** (Appendix B, section 2.5.11). This value is consistent with the ability of **1b** to initiate the polymerization of **2a**. The photoinduced oxidative behavior of these persubstituted clusters is unprecedented and stands as a new contribution to the field of molecular photoredox chemistry. Furthermore, the kinetic stability of both the neutral and mono-anionic clusters due to the 3D delocalization of valence electrons within the cluster core provides an opportunity for implementation in systems amenable to photochemistry involving a diversity of functional groups

and reactive radical species. Notably, the polymerization of **2a** initiated by **1b** also proceeds under ambient conditions, affording a polymer of similar quality as that generated from a reaction set up under inert gas conditions. Given this successful polymerization, we were interested in further exploring the reactivity and electron-transfer processes of **1b**. We set out to expand our substrate scope by employing styrene monomers **2b**−**2i**, which possess a range of electronic and steric profiles. Polymerization of styrene (**2b**) with 0.1 mol% **1b** produced polystyrene in yields averaging 96% in 4 h without incorporation of 1a in the polymer (Appendix B, Figures B22 and B23). Varying the cluster loading did not have an effect on the molecular weight or dispersity of poly-**2b** (Appendix B, Figure B15). Furthermore, propagation proceeds in the absence of light, indicating that formation of the radical anion on **1b** is irreversible (Appendix B, Figure B46).

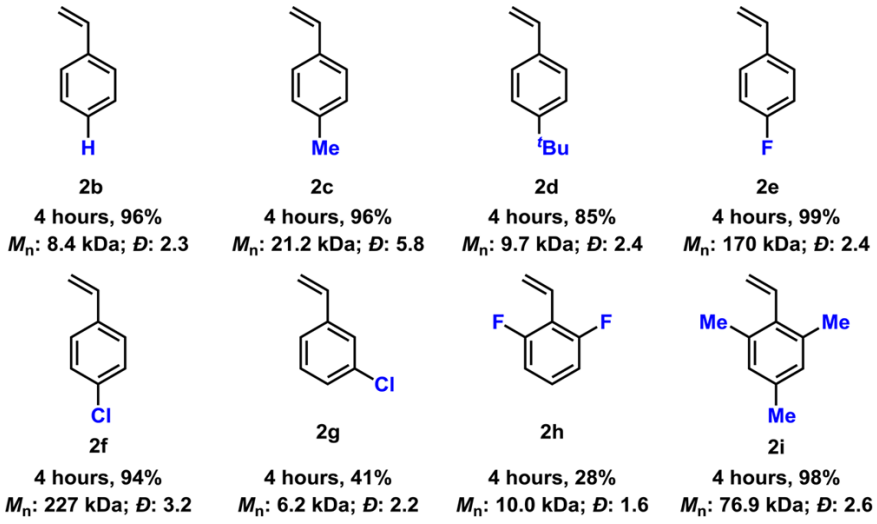

Table 3-2. Substrate scope for polymerization using **1b**. General reaction conditions: monomer (50 μL, 0.2−2.0 M CH_2Cl_2 solution), **1b** (0.1 mol%), 4−24 h. Isolated yields after precipitation.

Notably, the pyrilium-based catalyst utilized by Nicewicz does not produce polymer, which is consistent with the stronger photooxiding power of **1b** compared to **II**. Polymers of other

electron-rich styrenes are generated in the presence of **1b** within hours in good yield (Table 3-2: **2c−e,i**); more electron-poor substrates can also be polymerized (Table 3-2: **2f−h**), albeit with somewhat diminished efficiency, consistent with our mechanistic hypothesis. The perfluorinated nature of **1b** led us to wonder whether the successful polymerization of such a wide range of styrene monomers in comparison to either **1a** or **II** (Figure 3-1) may be due, in part, to specific interactions between the fluorinated rings of the initiator and the monomer. Such intermolecular π–π-type interactions are well-recognized.[21] We therefore subjected styrene (**2b**) to the optimized polymerization conditions in the presence of 1b employing benzene as solvent. Polymerization of **2b** produced polystyrene in 96% yield in 4 h, though M_w values observed for polystyrene produced in benzene are slightly smaller than those of polymers produced in CH_2Cl_2. Given the likelihood of competitive association of solvent with the fluorinated aryl rings of **1b**, one would expect a reduction in polymer yield when using aromatic solvents if these π–π-type interactions are essential to polymerization. Therefore, this experiment suggests that, if π-type interactions between the initiator and the monomer exist, they are not critical for the polymerization overall.

We were further interested to see if **1b**, in light of its high excited-state reduction potential (vide supra), might coax reactivity out of more challenging substrates. Cationic polymerization of isobutylene, a less activated vinyl substrate than styrene, typically utilizes metal catalysts or harsh conditions.[22] Irradiation (450 nm) of a 2 mM solution of **1b** in CH_2Cl_2 at isobutylene pressures as low as 1 psi for 4 h at room temperature produced polymeric material. Neither irradiation of isobutylene in the absence of **1b** nor stirring **1b** in the presence of isobutylene in the dark, under reaction conditions otherwise identical to those described above, afforded polymer. Interestingly, ^1H and ^{13}C NMR spectra of the formed polymer material closely resembles those of the polymer obtained previously by Michl and are consistent with the formation of a highly branched

poly(isobutylene) (see Figure 3-4 and Appendix B).[23] This represents the first example of a visible light-activated polymerization of isobutylene under metal-free conditions.

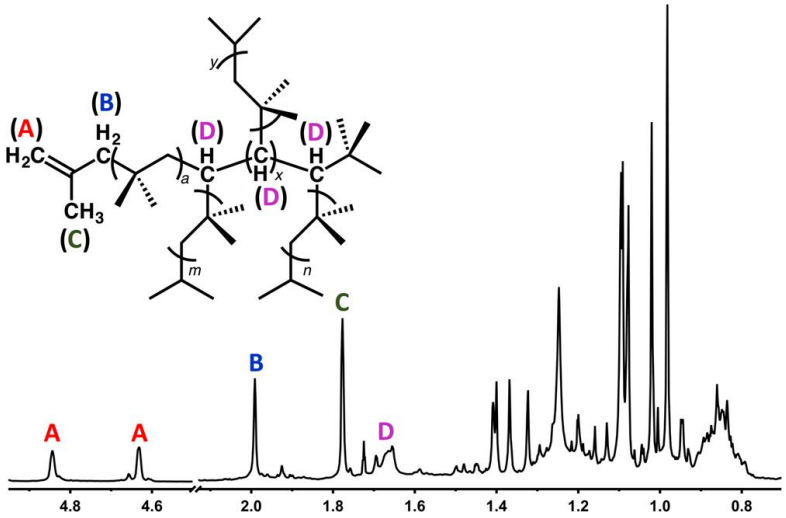

Figure 3-4. ^{1}H NMR spectrum of poly(isobutylene) produced from irradiation of **1b** with 450 nm light under 4 psi isobutylene. Label A indicates protons of the olefinic chain end; B/C, allylic protons of the chain end; D, methine protons.

3.3 Conclusions

In conclusion, we have demonstrated for the first time that icosahedral dodecaborate clusters of the type $B_{12}(OR)_{12}$, where R is a benzyl derivative, can undergo photoexcitation with visible light and activate styrene derivatives toward polymerization. Increasing the electron-withdrawing power of the benzyl substituents results in increased activity, and that allowed us to develop the first example of a metal-free visible light photooxidant capable of polymerizing isobutylene. DFT calculations suggest that photoexcitation in these species occurs through the promotion of an electron from a low-lying, aryl-based orbital on the cluster substituent to an unoccupied cage-based orbital by visible(~450nm) light. Overall, our work indicates that B_{12}-

based clusters can behave as powerful yet air-stable photoredox reagents. This work also expands on an exciting untapped potential of molecular main-group systems as unique photoactive components.[11,24] Current efforts in our group are focused on underpinning the mechanism of the discovered photoexcitation and the further tuning of the disclosed system.[25]

Acknowledgements

A.M.S. thanks the UCLA Department of Chemistry and Biochemistry for start-up funds and 3M for a Non-Tenured Faculty Award. M.S.M. thanks the NSF for the Bridge-to- Doctorate and the Predoctoral (GRFP) Fellowships. H.B.G. and O.S.S. acknowledge funding from the NIH (R01DK019038) and the Arnold and Mabel Beckman Foundation. A.N.A. thanks the NSF for CAREER Award CHE-1351968. Y.W. thanks the CSST Scholarship. H.D.M. thanks the NSF (CHE-1507735) for funding. B.M.U. thanks UCLA for a Dissertation Year Fellow- ship. The authors thank Mr. Daniel Hatfield (UCLA) for assistance with computational studies and Prof. Andrea Kasko (UCLA) for generously allowing access to her GPC instrument.

3.4 References

(1) (a) Prier, C. K.; Rankic, D. A.; MacMillan, D. W. C. *Chem. Rev.* **2013**, *113*, 5322. (b) Fagnoni, M.; Dondi, D.; Ravelli, D.; Albini, A. *Chem. Rev.* **2007**, *107*, 2725. (c) Narayanam, J. M. R.; Stephenson, C. R. J. *Chem. Soc. Rev.* **2011**, *40*, 102. (d)Nicewicz,D.A.; Nguyen,T.M. *ACS Catal.* **2014**, *4*, 355. (e) Theriot, J. C.; Lim, C.-H; Yang, H.; Ryan, M. D.; Musgrave, C. B.; Miyake, G. M. *Science* **2016**, DOI: 10.1126/ science.aaf3935.

(2) (a) Kalyanasundaram, K. *Coord. Chem. Rev.* **1982**, *46*, 159. (b) Fox, L. S.; Kozik, M.; Winkler, J. R.; Gray, H. B. *Science* **1990**, *247*, 1069. (c) Juris, A.; Balzani, V.; Barigelletti, F.; Campagna, S.; Belser, P.; von Zelewsky, A. *Coord. Chem. Rev.* **1988**, *84*, 85. (d) Lumpkin, R. S.; Kober, E. M.; Worl, L. A.; Murtaza, Z.; Meyer, T. J. *J. Phys. Chem.* **1990**, *94*, 239. (e) Li, J.; Djurovich, P. I.; Alleyne, B. D.; Yousufuddin, M.; Ho, N. N.; Thomas, J. C.; Peters, J. C.; Bau, R.; Thompson, M. E. *Inorg. Chem.* **2005**, *44*, 1713.

(3) Marin, M. L.; Santos-Juanes, L.; Arques, A.; Amat, A. M.; Miranda, M. A. *Chem. Rev.* **2012**, *112*, 1710.

(4) (a) Wilger, D. J.; Grandjean, J.-M. M.; Lammert, T. R.; Nicewicz, D. A. *Nat. Chem.* 2014, *6*, 720. (b) Yoon, T. P.; Ischay, M. A.; Du, J. *Nat. Chem.* **2010**, *2*, 527. (c) Xu, J.; Jung, K.; Atme, A.; Shanmugam, S.; Boyer, C. *J. Am. Chem. Soc.* **2014**, *136*, 5508. (d) Yagči, Y.; Reetz,I. *Prog. Polym. Sci.* **1998**, *23*, 1485. (e) Chen, M.; MacLeod, M. J.; Johnson, J. A. *ACS Macro Lett.* **2015**, *4*, 566. (f) Dadashi-Silab, S.; Doran, S.; Yagči, Y. *Chem. Rev.* **2016**, DOI: 10.1021/acs.chemrev.5b00586.

(5) Demissie, T. B.; Ruud, K.; Hansen, J. H. *Organometallics* **2015**, *34*, 4218.

(6) Miranda, M. A.; García, H. *Chem. Rev.* **1994**, *94*, 1063.

(7) Boron Hydride Chemistry; Mutterties, E. L., Ed.; Academic Press Inc.: New York, 1975.

(8) Grimes, R. N. *J. Chem. Educ.* **2004**, *81*, 657. (9) Hawthorne, M. F. *J. Chem. Educ.* **2009**, *86*, 1131. (10) Spokoyny, A. M. *Pure Appl. Chem.* **2013**, *85*, 903. (11) (a) Kaim, W.; Hosmane, N. S.; Zaĺis; ˇMaguire, J. A.; Lipscomb, W. N. *Angew. Chem., Int. Ed.* **2009**, *48*, 5082. (b) Power, P. P. *Chem. Rev.* **2003**, *103*, 789. (c) Aihara, J. *J. Am. Chem. Soc.* **1978**, *100*, 3339. (d) King, R. B. *Chem. Rev.* **2001**, *101*, 1119. (e) Wright, J. H.; Kefalidis, C. E.; Tham, F. S.; Maron, L.; Lavallo, V. *Inorg. Chem.* **2013**, *52*, 6223. (f) Malischewski, M.; Bukovsky, E. V.; Strauss, S. H.; Seppelt, K. *Inorg. Chem.* **2015**, *54*, 11563.

(12) Lorenzen, V.; Preetz, W.; Baumann, F.; Kaim, W. *Inorg. Chem.* **1998**, *37*, 4011.

(13) Sivaev, I. B.; Bregadze, V. I.; Sjöberg, S. *Collect. Czech. Chem. Commun.* **2002**, *67*, 679. Pitochelli, A. R.; Hawthorne, M. F. *J. Am. Chem. Soc.* **1960**, *82*, 3228.

(14) King, B. T.; Noll, B. C.; McKinley, A. J.; Michl, J. *J. Am. Chem. Soc.* **1996**, *118*, 10902.

(15) Lee, M. W.; Farha, O. K.; Hawthorne, M. F.; Hansch, C. H. *Angew. Chem., Int. Ed.* **2007**, *46*, 3018.

(16) Peymann, T.; Knobler, C. B.; Khan, S. I.; Hawthorne, M. F. *Angew. Chem., Int. Ed.* **2001**, *40*, 1664.

(17) (a) Maderna, A.; Knobler, C. B.; Hawthorne, M. F. *Angew. Chem., Int. Ed.* **2001**, *40*, 1661. (b) Farha, O. K.; Julius, R. L.; Lee, M. W.; Huertas, R. E.; Knobler, C. B.; Hawthorne, M. F. *J.*

Am. Chem. Soc. 2005, *127*, 18243. (c) Wixtrom, A. I.; Shao, Y.; Jung, D.; Machan, C. W.; Kevork, S. N.; Qian, E. A.; Axtell, J. C.; Khan, S. I.; Kubiak, C. P.; Spokoyny, A. M. *Inorg. Chem. Front.* **2016**, *3*, 711.

(18) (a) Mukherjee, S.; Thilagar, P. *Chem. Commun.* **2016**, *52*, 1070. (b) Cerdań, L.; Braborec, J.; Garcia-Moreno, I.; Costela, A.; Londesborough, M. G. S. *Nat. Commun.* **2015**, *6*, 5958.

(19) Perkowski, A. J.; You, W.; Nicewicz, D. A. *J. Am. Chem. Soc.* **2015**, *137*, 7580.

(20) Van, N.; Tiritiris, I.; Winter, R. F.; Sarkar, B.; Singh, P.; Duboc, C.; Muñoz-Castro, A.; Arratia-Peŕez, R. ; Kaim, W.; Schleid, T. *Chem.-Eur.J.* **2010**, *16*, 11242.

(21) (a) Martinez, C. R.; Iverson, B. L. *Chem. Sci.* **2012**, *3*, 2191. (b) Cozzi, F.; Ponzini, F.; Annunziata, R.; Cinquini, M.; Siegel, J. S. *Angew. Chem., Int. Ed. Engl.* **1995**, *34*, 1019. (c) Zhao, Y.; Beuchat, C.; Domoto, Y.; Gajewy, J.; Wilson, A.; Mareda, J.; Sakai, N.; Matile, S. *J. Am. Chem. Soc.* **2014**, *136*, 2101. (d) Coates, G. W.; Dunn, A. R.; Henling, L. M.; Dougherty, D. A.; Grubbs, R. H. *Angew. Chem., Int. Ed. Engl.* **1997**, *36*, 248.

(22) Kostjuk, S. V. *RSC Adv.* **2015**, *5*, 13125.

(23) Li^+-catalyzed polymerization of isobutylene supported by a weakly coordinated mono-anionic carborane: (a) Merna, J.; Vlček, P.; Volkis, V.; Michl, J. *Chem. Rev.* **2016**, *116*, 771. (b) Volkis, V.; Shoemaker, R. K.; Michl, J. *Macromolecules* **2012**, *45*, 9250. (c) Volkis, V.; Mei, H.; Shoemaker, R. K.; Michl, J. *J. Am. Chem. Soc.* **2009**, *131*, 3132. (d) Vyakaranam, K.; Barbour, J. B.; Michl, J. *J. Am. Chem. Soc.* **2006**, *128*, 5610.

(24) Recent representative examples: (a) Calitree, B.; Donnelly, D. J.; Holt, J. J.; Gannon, M. K.;

Nygren, C. L.; Sukumaran, D. K.; Autschbach, J.; Detty, M. R. *Organometallics* **2007**, *26*, 6248. (b) Carrera, E. I.; Seferos, D. S. *Dalton Trans.* **2015**, *44*, 2092. (c) Lin, T.-P.; Gabbaï, F. P. *J. Am. Chem. Soc.* **2012**, *134*, 12230. (d) Hirai, H.; Nakajima, K.; Nakatsuka, S.; Shiren, K.; Ni, J.; Nomura, S.; Ikuta, T.; Hatakeyama, T. *Angew. Chem., Int. Ed.* **2015**, *54*, 13581. (e) Leitao, E. M.; Jurca, T.; Manners, I. *Nat. Chem.* **2013**, *5*, 817. (f) Loudet, A.; Burgess, K. *Chem. Rev.* **2007**, *107*, 4891.

(25) Chen, M.; Zhong, M.; Johnson, J. A. *Chem. Rev.* **2016**, *116*, 10167-10211.

3.5 Appendix B

3.5.1 Reagent Information

All commercially available chemicals were used as received unless otherwise stated. All polymerizations were prepared in the glovebox under nitrogen atmosphere unless otherwise stated. All solvents were purified via a solvent purification system and kept in the glovebox. All monomers were degassed and stored with 4Å molecular sieves. 4-Vinylanisole (97%), 4-methylstyrene (96%), styrene (≥99%), 4-fluorostyrene (99%), 4-*tert*-butylstyrene (93%), 4-chlorostyrene (97%), 3-chlorostyrene (98%), and 2,6-difluorostyrene (99%) were purchased from Sigma-Aldrich. *Closo*-dodecahydrododecaborate ($[NEt_3H]_2[B_{12}H_{12}]$) was purchased from Boron Specialties (USA). Ethanol (200 proof) was purchased from Decon Labs and used as received. Iron(III) chloride hexahydrate (≥97%), cesium hydroxide monohydrate (≥99.5%), hydrogen peroxide (30% in H_2O), tetrabutylammonium hydroxide (40% in H_2O), acetonitrile (≥99.9%), dichloromethane (≥99.5%), ethyl acetate (≥99.5%), hexanes (≥98.5%), methanol (≥99.8%), N,N-diisopropylethylamine (≥99%), and tetrabutylammonium hexafluorophosphate (≥99.0%, electrochemical grade), 2-methylpropene (99%) were purchased from Sigma-Aldrich. Tetrabutylammonium hexafluorophosphate was further purified by recrystallization from ethanol and drying under vacuum at 90 °C and benzyl bromide (99%) was purchased from Alfa Aesar. Tetramethylammonium tetrafluoroborate (>98%) was purchased from TCI.

3.5.2 General Analytical Information

NMR spectra were recorded using spectrometers at 400 or 500 MHz (^{1}H), 125 MHz (^{13}C), 80 MHz (^{11}B), and 282 MHz (^{19}F) reported in δ (parts per million) relative to tetramethylsilane (^{1}H, ^{13}C), $BF_3{\cdot}Et_2O$ (^{11}B) or C_6H_5F (^{19}F), respectively, and referenced to residual ^{1}H/^{13}C signals of the deuterated solvent (^{1}H (δ) $CDCl_3$ 7.26; ^{13}C (δ) $CDCl_3$ 77.16; ^{11}B (δ) $BF_3{\cdot}Et_2O$ 0.00 ppm; ^{19}F (δ)

C_6H_5F -113.15 ppm). Deuterated solvents (Cambridge Isotope Laboratories) for NMR spectroscopic analyses were stored over 4Å molecular sieves. ^1H NMR spectra were acquired with a relaxation of 2 s for small molecules and 30 s for polymers. Gel permeation chromatography (GPC) for all polymers was conducted on a Jasco system equipped with a refractive index detector, a UV detector, one Waters Styragel guard column, and four Waters HR Styragel 5 μm columns (100-5K, 500-30K, 50-100K, 5-600 K) using tetrahydrofuran (THF) at 30 °C and a flow rate of 1.0 mL/min. Calibration was performed using near-monodisperse polystyrene standards from Jordi Laboratories and chromatograms were analyzed using ChromNAV chromatography software. GPC for poly-4-methoxystyrene was conducted on a Shimadzu high performance liquid chromatography (HPLC) system with a refractive index RID-10A, one Polymer Laboratories PLgel guard column, and two Polymer Laboratories PLgel 5 μm mixed D columns. Eluent was DMF with LiBr (0.1 M) at 40 °C (flow rate: 0.60 mL/min). Chromatograms from DMF GPC were analyzed using LabSolutions software. GPC was also conducted on a Shimadzu HPLC Prominence-i system equipped with a UV detector, Wyatt DAWN Heleos-II Light Scattering detector, Wyatt Optilab T-rEX RI detector, one MZ-Gel SDplus guard column, and two MZ-Gel SDplus 100 Å 5μm 300x8.0 mm columns. Eluent was $CHCl_3$ at 40 °C (flow rate: 0.70 mL/min). Chromatograms from $CHCl_3$ GPC were analyzed using Astra 6.0 software. Calibration was performed using near-monodisperse polystyrene standards from Polymer Laboratories. All GPC samples were dissolved in HPLC grade solvent at a concentration of 1-2 mg/mL and filtered through a 0.2 μm TFE filter. All reported molecular weight and dispersity data determined by GPC are the average of two runs unless otherwise noted. A Bruker EMX EPR spectrometer was used to acquire EPR spectra, with all spectra collected in CH_2Cl_2 at ambient temperature. Mass spectrometry data was acquired using a Thermo ScientificTM Q-ExactiveTM Plus instrument with

a quadrupole mass filter and Orbitrap mass analyzer. ICP-MS was performed on an Agilent 7500c quadrupole with hydrogen/helium octopole collision cell. Thermogravimetric analysis was performed on a Perkin Elmer Diamond TG/DTA instrument. UV-Vis spectra were recorded on a Hewlett-Packard 8453 diode array spectrometer. Extinction coefficients were determined through a series of 5 dilutions with a maximum absorption between 0.1 and 0.7.

3.5.3 Microwave Reactor Information

Microwave reactions were performed using a CEM Discover SP microwave synthesis reactor. Except where noted otherwise, all reactions were performed in glass 10 mL microwave reactor vials purchased from CEM with silicone/PTFE caps. Flea micro PTFE-coated stir bars were used in the vials with magnetic stirring set to high and 15 seconds of premixing prior to the temperature ramping. All microwave reactions were carried out at 140 °C with the pressure release limit set to 250 psi (no reactions exceeded this limit to trigger venting) and the maximum wattage set to 250W (the power applied was dynamically controlled by the microwave instrument and did not exceed this limit for any reactions). Column chromatography was performed using 2.0 - 2.25 cm inner diameter glass fritted chromatography columns with 20-30 cm of slurry-packed silica gel to ensure full separation of reagents and products. Unfiltered pressurized air was used to assist column chromatography.

3.5.4 LED Light Source

Irradiation of photochemical polymerizations were performed utilizing a 120V Blue LED Custom Rope Light Kit ½" 2 wire 3 foot cable purchased from Novelty Lights, Inc. (Eaglewood, CO).

3.5.5 Cyclic Voltammetry Information

Cyclic voltammetry was performed on using a BAS Epsilon potentiostat with a glassy carbon disc working electrode, platinum wire counter electrode, and Ag/Ag^{+} wire pseudoreference. All

experiments were conducted in 0.1 M $[NBu_4]PF_6/CH_2Cl_2$ with ~5 mM analyte concentrations. The CH_2Cl_2 was dried in house with a custom drying system running through two alumina columns prior to use. The solution was degassed by bubbling argon, and the cyclic voltammetry was performed under argon gas. A scan rate of 0.1 mV/s was used with Fc/Fc^+ as an external standard.

3.5.6 X-ray data collection and processing parameters

A single crystal of **1b** was mounted on a nylon loop using perfluoropolyether oil and cooled rapidly to 100 K with a stream of cold dinitrogen. Diffraction data were measured using a Bruker APEX-II CCD diffractometer using Mo-K_α radiation. The cell refinement and data reduction were carried out using Bruker SAINT and the structure was solved with SHELXS-97. All subsequent crystallographic calculations were performed using SHELXL-2013

3.5.7 Synthetic Procedures for cluster photoinitiators and polymers

3.5.7.1 Synthesis of $Cs_2B_{12}H_{12}$, $Cs_2B_{12}(OH)_{12}$, and $(NBu_4)_2B_{12}(OH)_{12}$

$CsOH{\cdot}H_2O$ (14.0g, 83.4 mmol) was dissolved in 130 mL methanol in a 300 mL round bottom flask. 13.4 g of triethylammonium dodecahydrododecaborate was added, the reaction was left to stir for 12-18 hours at ambient temperature (~20 ^{0}C). The solution mixture was then filtered through a 60 ml fritted glass funnel and washed with 20 mL methanol three times. The resulting white solid was dried under high vacuum at 50 ^{0}C for 12 hours and characterized by NMR to confirm complete conversion to Cs_2[*closo*-$B_{12}H_{12}$]. Cs_2[*closo*-$B_{12}H_{12}$] was per-hydroxylated to form Cs_2[*closo*-$B_{12}(OH)_{12}$] via previously described methods.[1] The resulting Cs_2[*closo*-$B_{12}(OH)_{12}$] was converted to $(TBA)_2$[*closo*-$B_{12}(OH)_{12}$] (**1**) via previously described methods.[1]

3.5.7.2 Synthesis of Dodeca(benzyloxy)-*hypercloso*-dodecaborane ($B_{12}(OCH_2Ph)_{12}$, 1a)

$(TBA)_2B_{12}(OH)_{12}$ (50.0 mg, 0.061 mmol) was transferred out of a nitrogen filled glovebox, opened to the air, and dissolved in 1 mL acetonitrile in a 10 mL glass microwave vial. *N*,*N*-

diisopropylethylamine (0.2 mL, 1.15 mmol) and benzyl bromide (1.74 mL, 14.7 mmol) were added along with a magnetic stir bar, the vial was sealed with a Teflon/silicone cap, and the reaction mixture was heated under microwave conditions at 140 ^{0}C with high stirring for 15 minutes. The volatiles were removed via rotary evaporation, and the excess reagent was eluted through a silica column with 65/35 hexanes/ethyl acetate, and the pink/purple product mixture was eluted with dichloromethane. The dichloromethane was removed *via* rotary evaporation, the remaining charged $^{-1/-2}$ product mixture was dissolved in ~5 ml 90/5/5 ethanol/acetonitrile/H_2O, $FeCl_3 \cdot 6H_2O$ (0.3 g, 1.11 mmol) was added and the mixture was left to stir for 12-24 hours. Following oxidation, the solvent mixture was removed via rotary evaporation, and an orange band containing the neutral product was separated from the $FeCl_3 \cdot 6H_2O$ through a silica column with dichloromethane. The dichloromethane was removed *via* rotary evaporation and the final neutral product **1a** was dried under high vacuum to obtain an isolated yield of 63%. Compound **1a** is an orange solid. ^{1}H NMR (500 MHz, $CDCl_3$): δ 7.08 - 7.19 (m, 60H, C_6H_5), 5.25 (s, 24H, O-CH_2). $^{13}C\{^{1}H\}$ NMR (125 MHz, $CDCl_3$): δ 140.8, 128.4, 127.3, 73.4. $^{11}B\{^{1}H\}$ NMR (128 MHz, $CDCl_3$): δ 41.8. HRMS (Orbitrap): m/z calculated for $C_{84}H_{84}B_{12}O_{12}$ (M-), 1414.72 Da; found, 1414.72 Da.

3.5.7.3 Synthesis of Dodeca(pentafluorobenzyloxy)-*hypercloso*-dodecaborane ($B_{12}(OCH_2C_6F_5)_{12}$, 1b)

$(TBA)_2B_{12}(OH)_{12}$ (300 mg, 0.366 mmol) was transferred out of a nitrogen filled glovebox, opened to the air, and dissolved in 4 mL acetonitrile in a 30 mL glass microwave vial. *N*,*N*-diisopropylethylamine (1.21 mL, 6.96 mmol) and 2,3,4,5,6-pentafluorobenzyl bromide (6.86 mL 45.4 mmol) were added along with a magnetic stir bar, the vial was sealed with a Teflon/silicone cap, and the reaction mixture was heated under microwave conditions at 140˚C with high stirring for 15 minutes. The volatiles were removed via rotary evaporation, and the excess reagent was

eluted through a silica column with 65/35 hexanes/ethyl acetate, and the pink/purple product mixture was eluted with acetone. The acetone was removed via rotary evaporation and the residue was dissolved in ~5 mL 90/5/5 ethanol/acetonitrile/H_2O. $FeCl_3 \cdot 6H_2O$ (1.88 g, 6.96 mmol) was added and the mixture was left to stir for 24 hours. The mixture was concentrated *in vacuo*. The residue (while still in the roundbottom flask) was rinsed three times with water. The residue was then taken up in toluene and extracted three times with water. The organic fractions were combined and dried under vacuum. The resulting solid was charged with hexane and isolated by filtration to afford an orange/yellow solid (574 mg, 63%). ^{1}H NMR (500 MHz, $CDCl_3$): δ 5.23 (s, 24H). ^{13}C NMR (125 MHz, $CDCl_3$): δ 60.1. ^{11}B NMR (160 MHz, $CDCl_3$): δ 40.9. HRMS (Orbitrap): *m/z* calculated for $C_{84}H_{84}B_{12}O_{12}$ (M^-), 2494.1499 Da; found, 2494.1631 Da.

3.5.7.4 General Procedure for Polymer Synthesis

Styrene (0.05 mL, 0.435 mmol) was passed through activated basic alumina and added to a dram vial equipped with a magnetic stir bar. $B_{12}(OCH_2C_6F_5)_{12}$ (**1b**) (1.1 mg, 0.1 mol%) was then added. This mixture was dissolved in 219 µL dichloromethane, affording a 2M solution of monomer. The dram vial was sealed with a polypropylene cap containing a Teflon coated septum and brought out of the glove box. The mixture was then irradiated with blue LED light (450 nm) (see picture of representative setup below) while stirring for 4 hours at room temperature. For all reactions, the reaction setup is covered with aluminum foil to keep out ambient light. Once the polymerization was complete, the reaction was diluted with ~500 µL dichloromethane and precipitated with cold methanol. The resulting suspension was transferred to a tared falcon tube and centrifuged for 5 minutes at 4,400 RPM. The supernatant was discarded, methanol was then added, stirred to solubilize any excess initiator, and centrifuged again. The supernatant was discarded and the polymer was dried under vacuum. **Polymer conversion experiments:** Polymerizations were set

up using optimized conditions (*vide supra*) along with the addition of an equimolar amount of hexamethyldisilane (as an internal reference) with respect to monomer. Aliquots (50 μL) of reaction mixture were taken at given time points and added into a mixture of trimethylamine (5 μL) and $CDCl_3$ (700 μL). Conversions were calculated by ^1H NMR spectroscopy by integration of unreacted monomer to hexamethyldisilane.

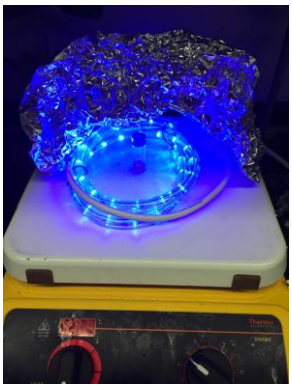

3.5.7.5 General Procedure for Polymerization of Isobutylene (1-4 psi of Isobutylene)

In the glovebox, **1b** (3.4mg, 1.36 μmol) was added to a Schlenk vessel, equipped with a teflon stopper, containing a magnetic stir bar. Dichloromethane (680 μL) was then added to provide a 2mM solution of **1b**. The vessel was sealed and brought out of the glovebox. The Schlenk vessel containing the mixture was connected to a vacuum transfer bridge; the other outlets were connected to a Schlenk manifold (for vacuum) and the isobutylene regulator (Airgas Part # Y11N570L510), which is connected directly to the isobutylene canister. The entire bridge was then put under vacuum. The mixture of **1b** was submerged in a dry ice bath until the solvent froze, opened to vacuum for ~5 minutes, and then closed to vacuum and allowed to thaw. This cycle was repeated two more times. The bridge was then closed off from vacuum. Once the mixture containing **1b** thawed, the headspace of the closed system was then backfilled with isobutylene, with the regulator dial set to the desired pressure; for higher amounts of resulting product, 4 psi was used.

The mixture of **1b** in CH_2Cl_2 in the isobutylene atmosphere was then irradiated with blue LED light for 4 hours at room temperature with stirring. After 4 hours, the isobutylene source was closed off, and the reaction vessel was carefully vented to let excess isobutylene escape. The mixture was then charged with ~4mL methanol and subsequently all volatiles were removed *in vacuo*. The resulting white residue was qualitatively characterized as highly branched isobutylene by ^{1}H and ^{13}C NMR spectroscopy, with reference to NMR spectra collected by Michl and co-workers (see Volkis, V.; Shoemaker, R. K.; Michl, J. *Macromolecules* **2012**, *45*, 9250-9257).

3.5.7.6 Electrochemical Bulk Electrolysis (Fe-free) Oxidation of 1b

Microwave synthesis of **1b** was carried out according to the general procedure, excluding the oxidation with $FeCl_3 \cdot 6H_2O$. $[N^nBu_4]_2B_{12}(OH)_{12}$ (99.0 mg, 0.121 mmol) was added to a 10 mL glass microwave vial and transferred out of a nitrogen filled glovebox, opened to air, and dissolved in 2 mL acetonitrile. *N*,*N*-diisopropylethylamine (0.4 mL, 2.30 mmol) and 2,3,4,5,6-pentafluorobenzyl bromide (1.70 mL, 11.3 mmol) were added along with a flea micro stir bar, the vial was sealed with a PTFE/silicone cap, and the mixture was heated at 140 °C with stirring under microwave conditions for 15 min. The volatiles were removed via rotary evaporation and the excess reagent was eluted through a slurry-packed silica gel column with 65/35 hexanes/ethyl acetate, and the pink/purple product mixture was eluted with CH_2Cl_2. The CH_2Cl_2 was removed via rotary evaporation, and the remaining 2-/1- product mixture was dissolved in 25 mL dichloromethane containing 50 mM tetramethylammonium tetrafluoroborate in a 50 mL beaker. Pt mesh was used as the working electrode, Pt wire inside of a 1 cm diameter glass fritted chamber as the counter electrode, and Ag wire as a pseudoreference electrode. A flea micro stir bar was added, and a potential of -1.3 V was applied for 1 h with stirring. The initially pink solution turned clear outside of the fritted inner chamber, and the solution in the chamber turned orange-red, progressing toward

a final yellow-orange color. The fritted chamber containing the yellow-orange solution was removed, the dichloromethane was removed via rotary evaporation, and the remaining yellow-orange solid was dried under high vacuum to yield pure **1b** (5.0 mg, 1.6%). NMR analysis of the product confirmed the complete oxidation of the fraction collected. *Note: This is a non-optimized experiment. The purpose of this procedure was to obtain a small amount of oxidized **1b** without contacting Fe for control experiment use.*

3.5.7.7 Synthesis of 2,4,6-tri(*p*-tolyl)pyrylium tetrafluoroborate.

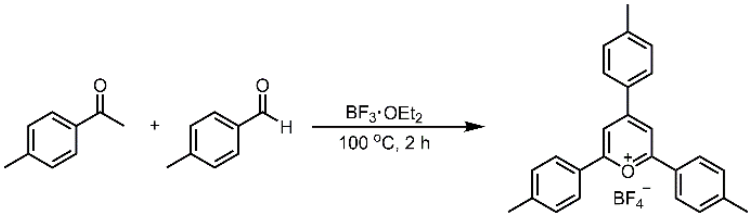

p-Methylacetophenone (5 mL, 5.095 g, 42.4 mmol) and *p*-tolualdehyde (11.32 mL, 11.38 g, 84.8 mmol) were allowed to stir. To this mixture boron trifluoride diethyl etherate (12.56 mL, 14.44 g, 101.8 mmol) was added dropwise. Reaction temperature was then raised to 100 °C and kept stirring for 2 hours. After two hours, reaction was cooled to room temperature and diethyl ether was removed under reduced pressure producing a black oil. To this oil, acetone was added and product was precipitated upon addition of diethyl ether. Product was then collected via filtration and recrystallized five times out of acetone.

3.5.8 Cluster Characterization

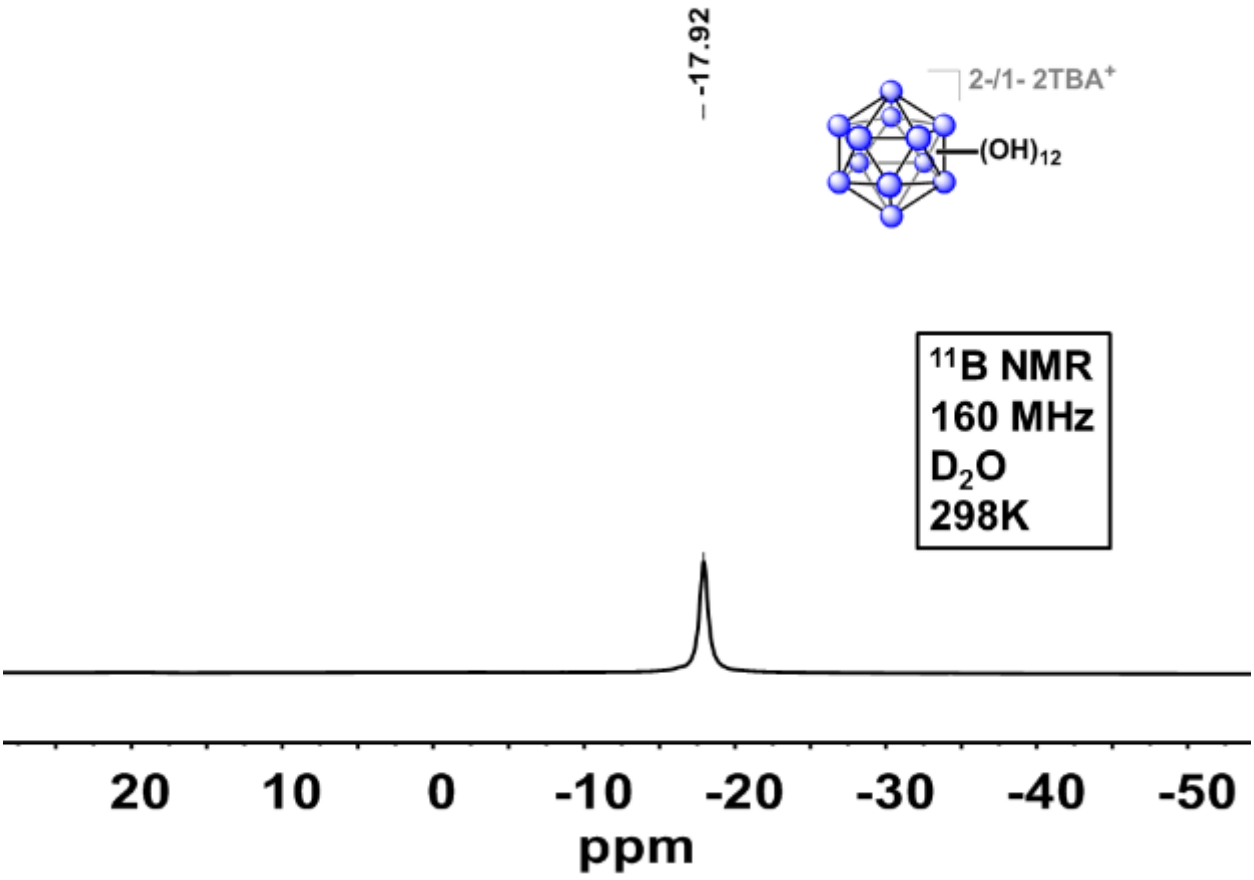

Figure B4. ^{11}B NMR spectrum of *closo*-$B_{12}(OH_{12})$ in D_2O at 298 K.

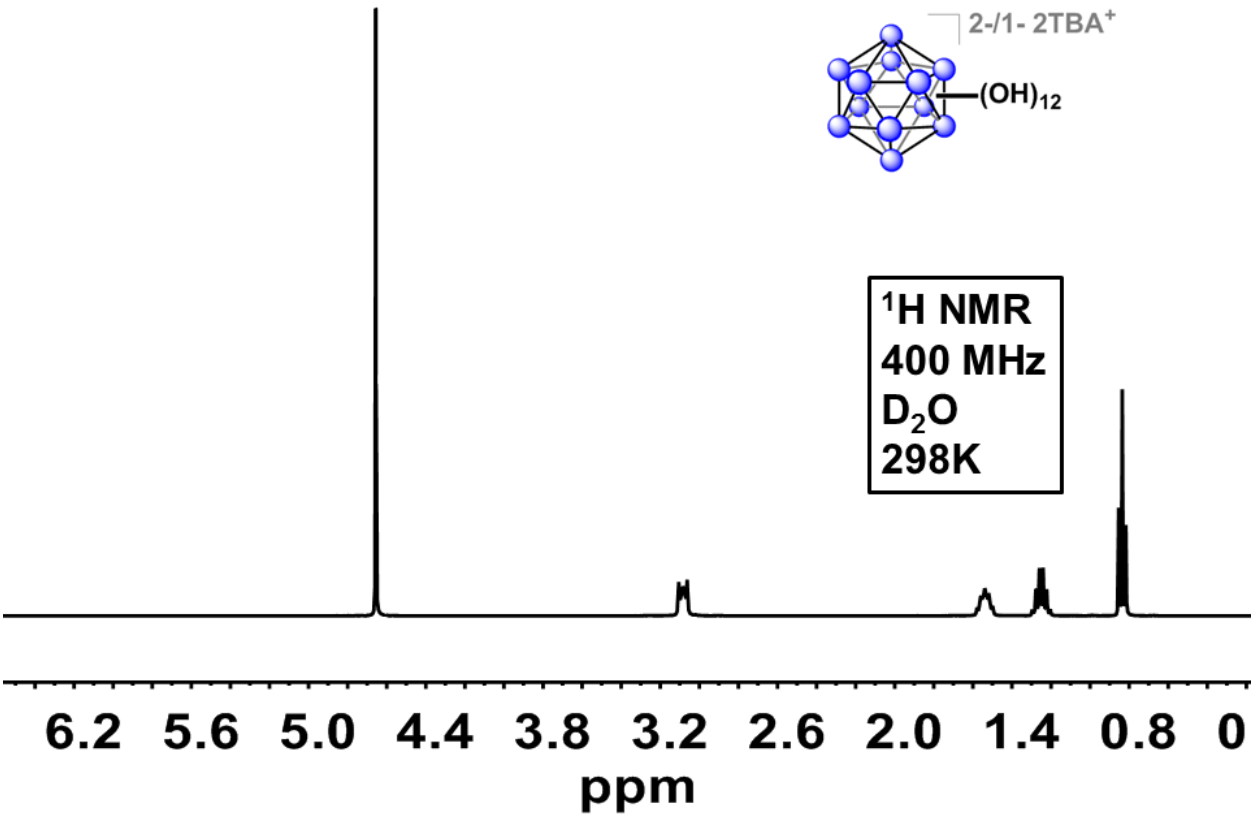

Figure B5. ^{1}H NMR spectrum of *closo*-$B_{12}(OH_{12})$ in D_2O at 298 K.

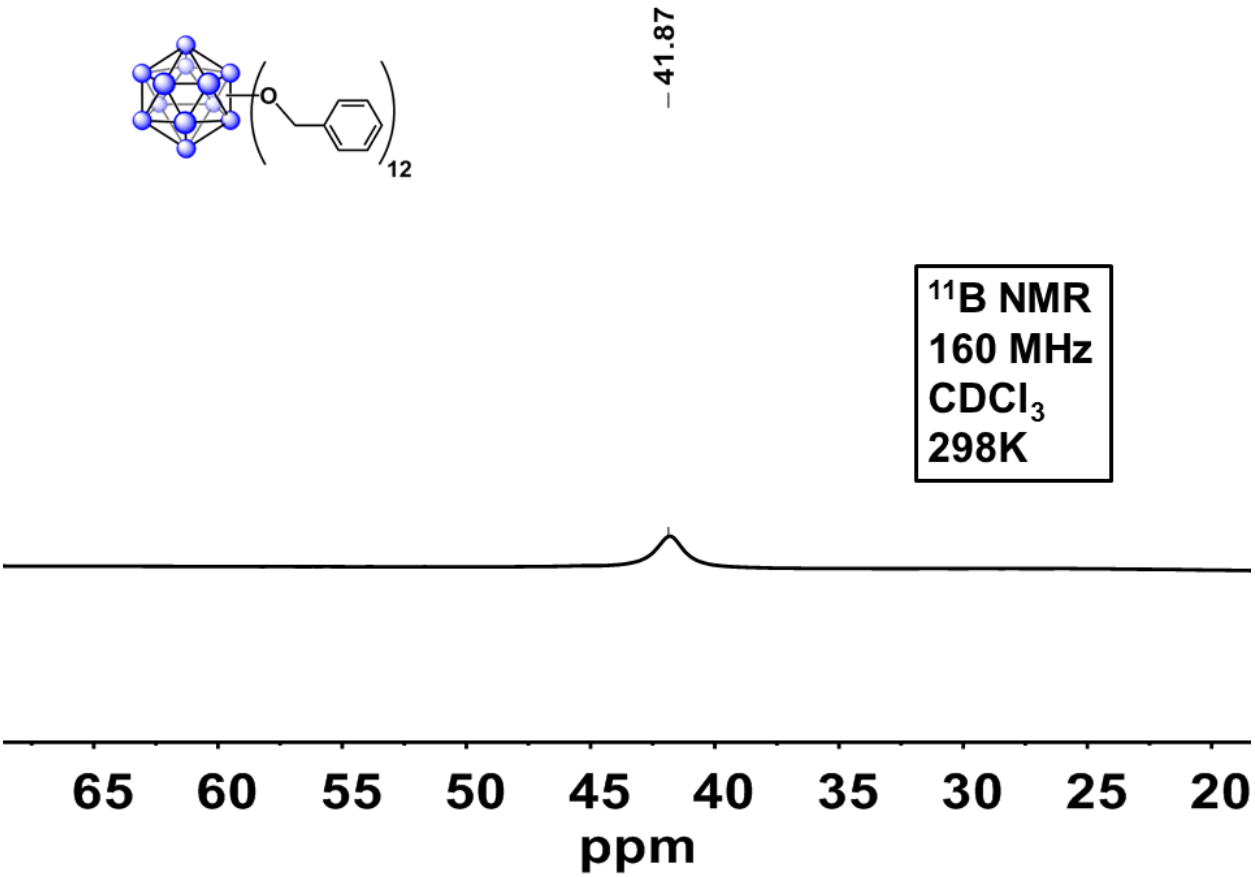

Figure B6. ^{11}B NMR spectrum of $B_{12}(OCH_2Ph)_{12}$ (**1a**) in $CDCl_3$ at 298 K.

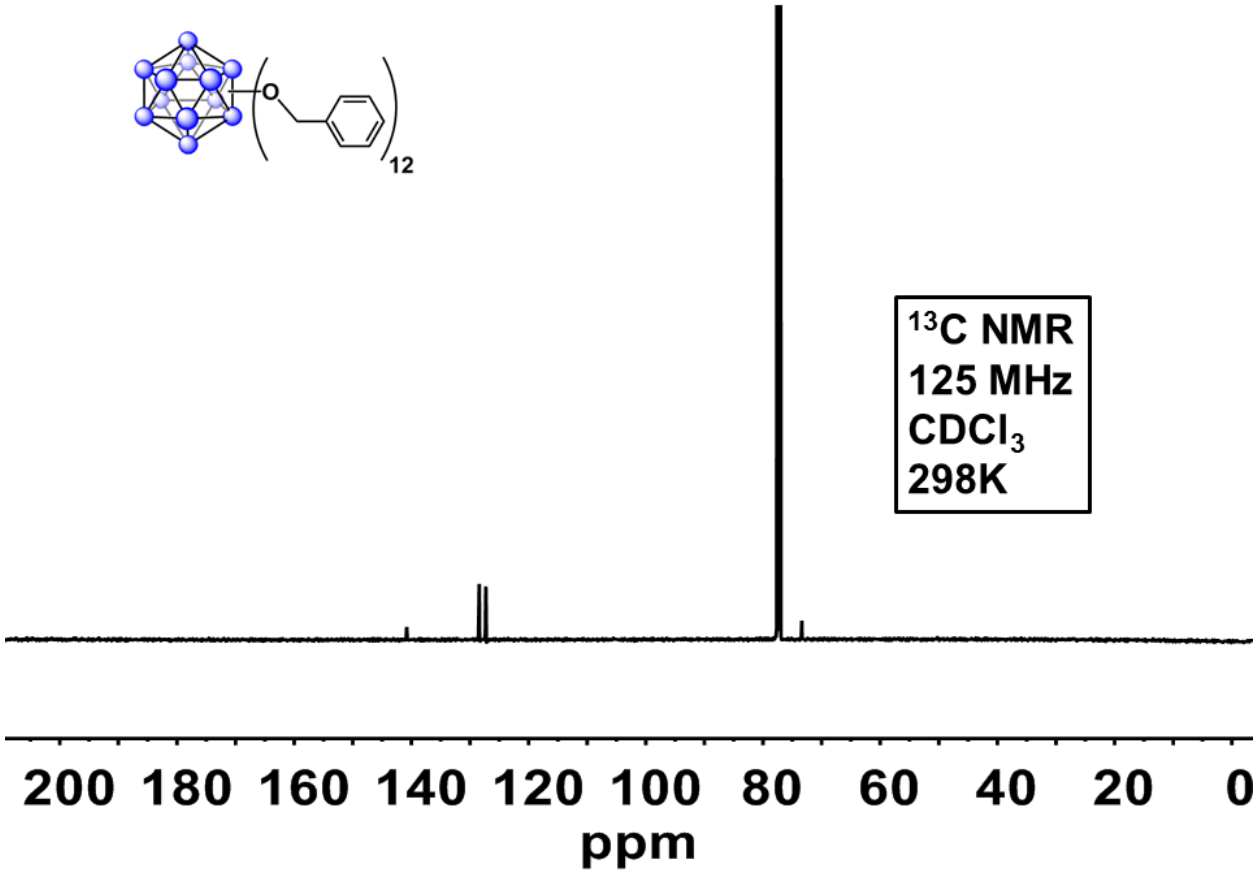

Figure B7. ^{13}C NMR spectrum of $B_{12}(OCH_2Ph)_{12}$ (**1a**) in $CDCl_3$ at 298 K.

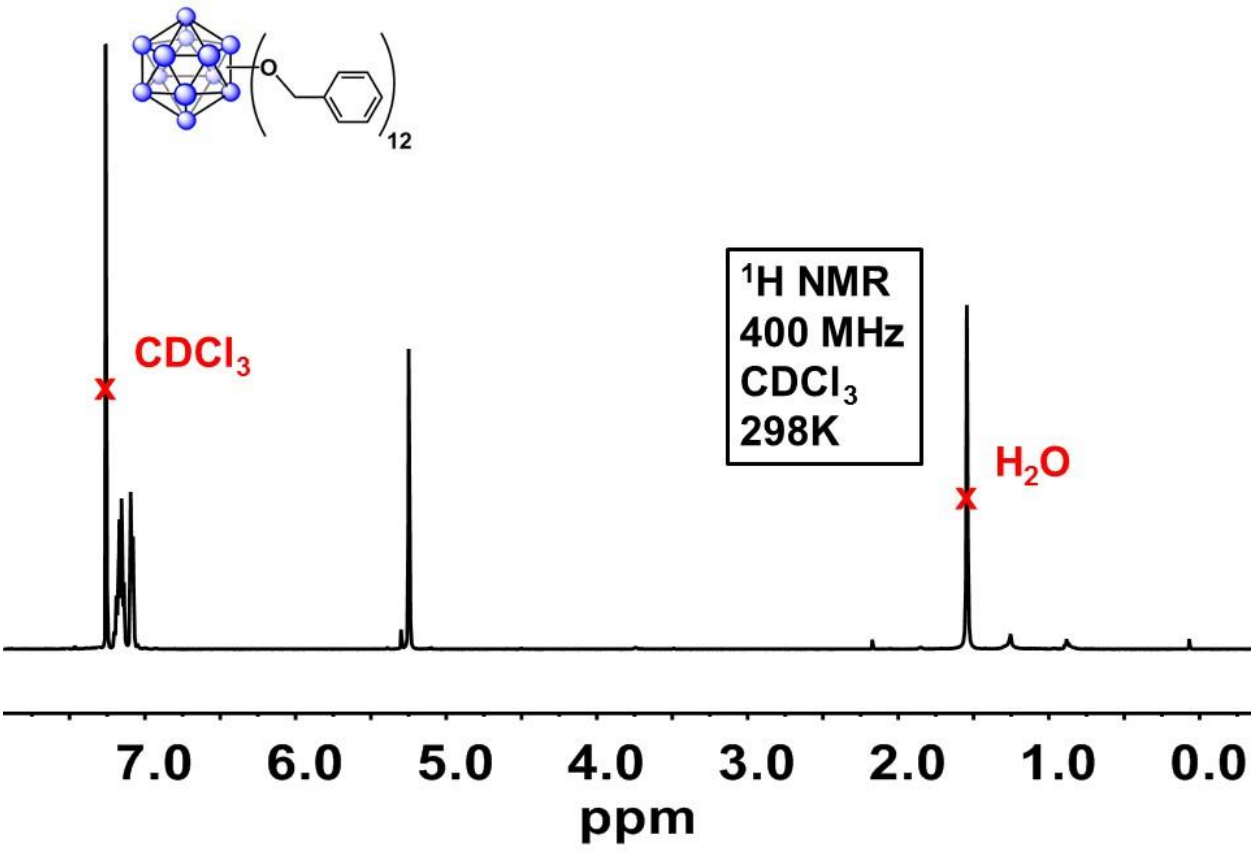

Figure B8. ^{1}H NMR spectrum of $B_{12}(OCH_2Ph)_{12}$ (**1a**) in $CDCl_3$ at 298 K.

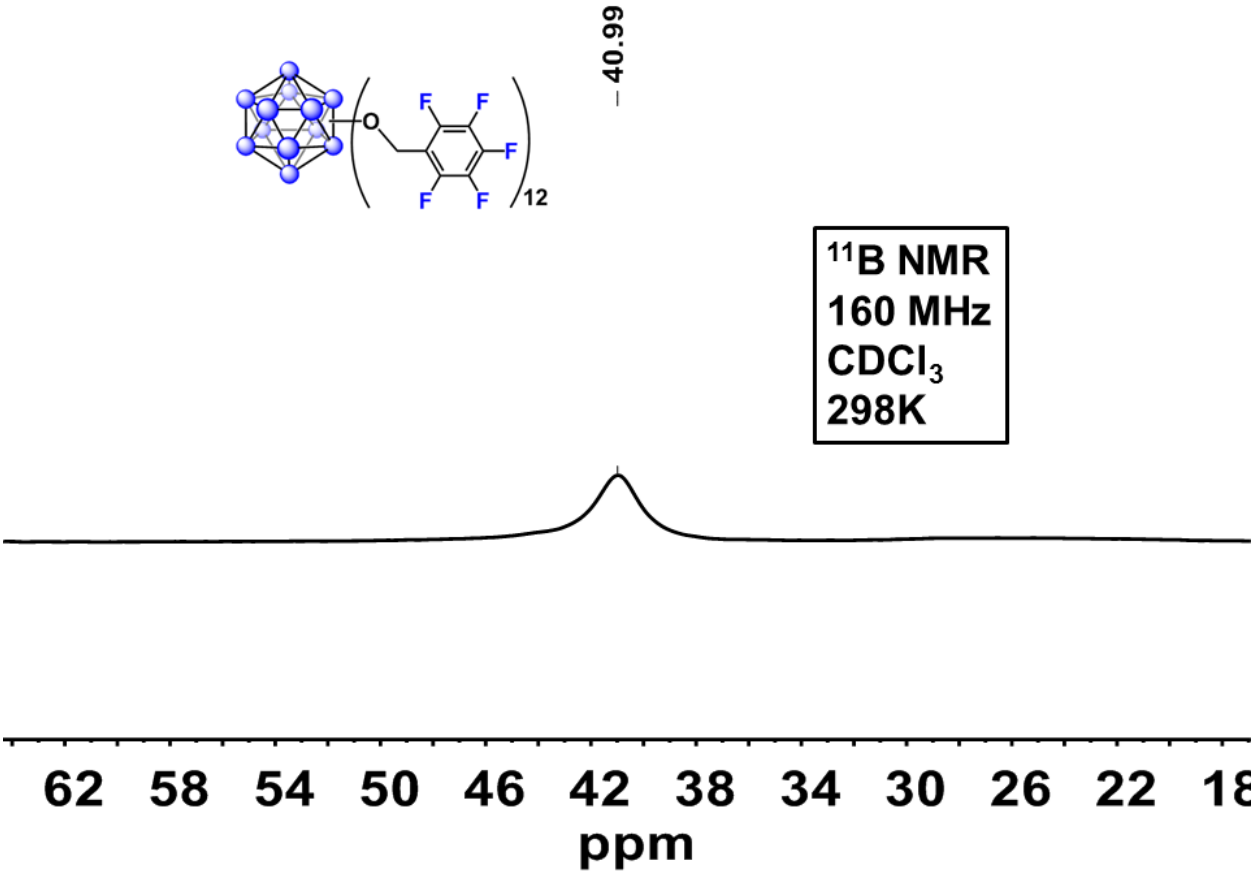

Figure B9. ^{11}B NMR spectrum of $B_{12}(OCH_2C_6F_5)_{12}$ (**1b**) in $CDCl_3$ at 298 K.

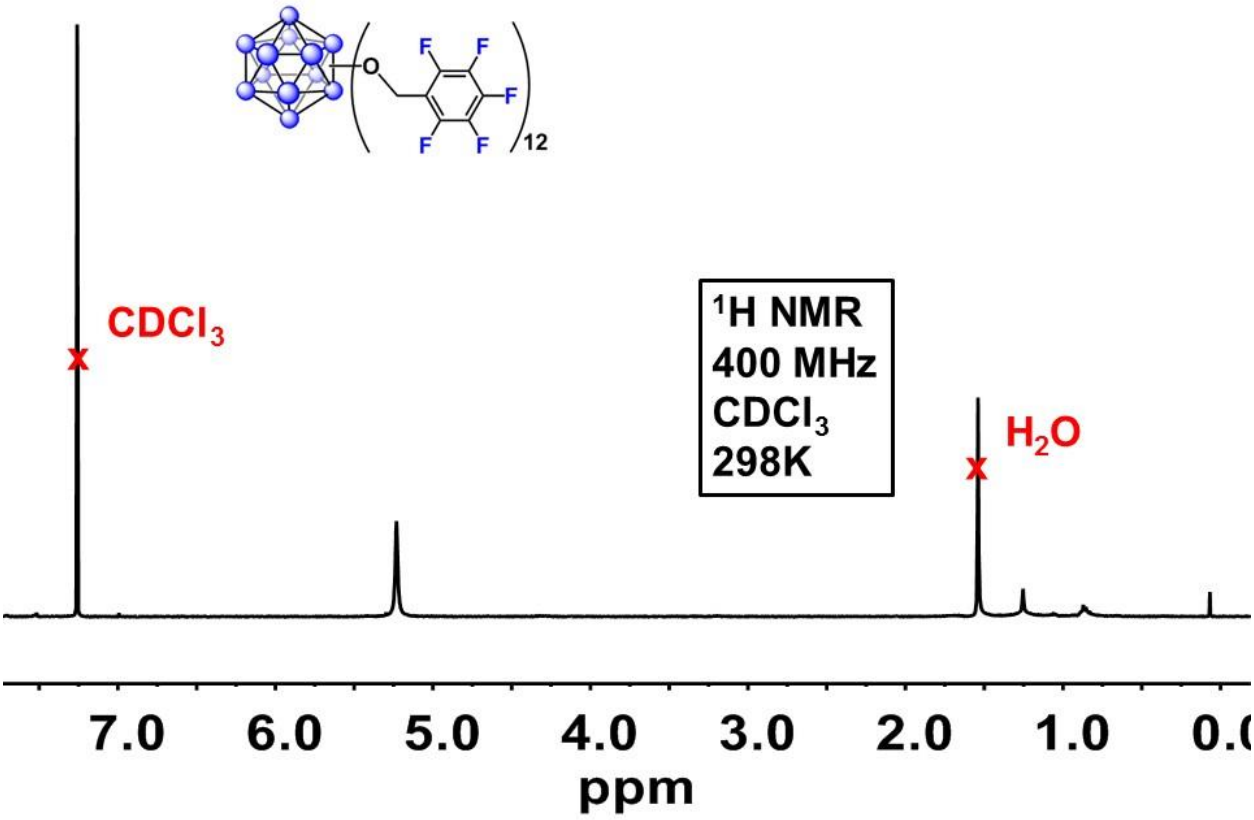

Figure B10. ^{1}H NMR spectrum of $B_{12}(OCH_2C_6F_5)_{12}$ (**1b**) in $CDCl_3$ at 298 K.

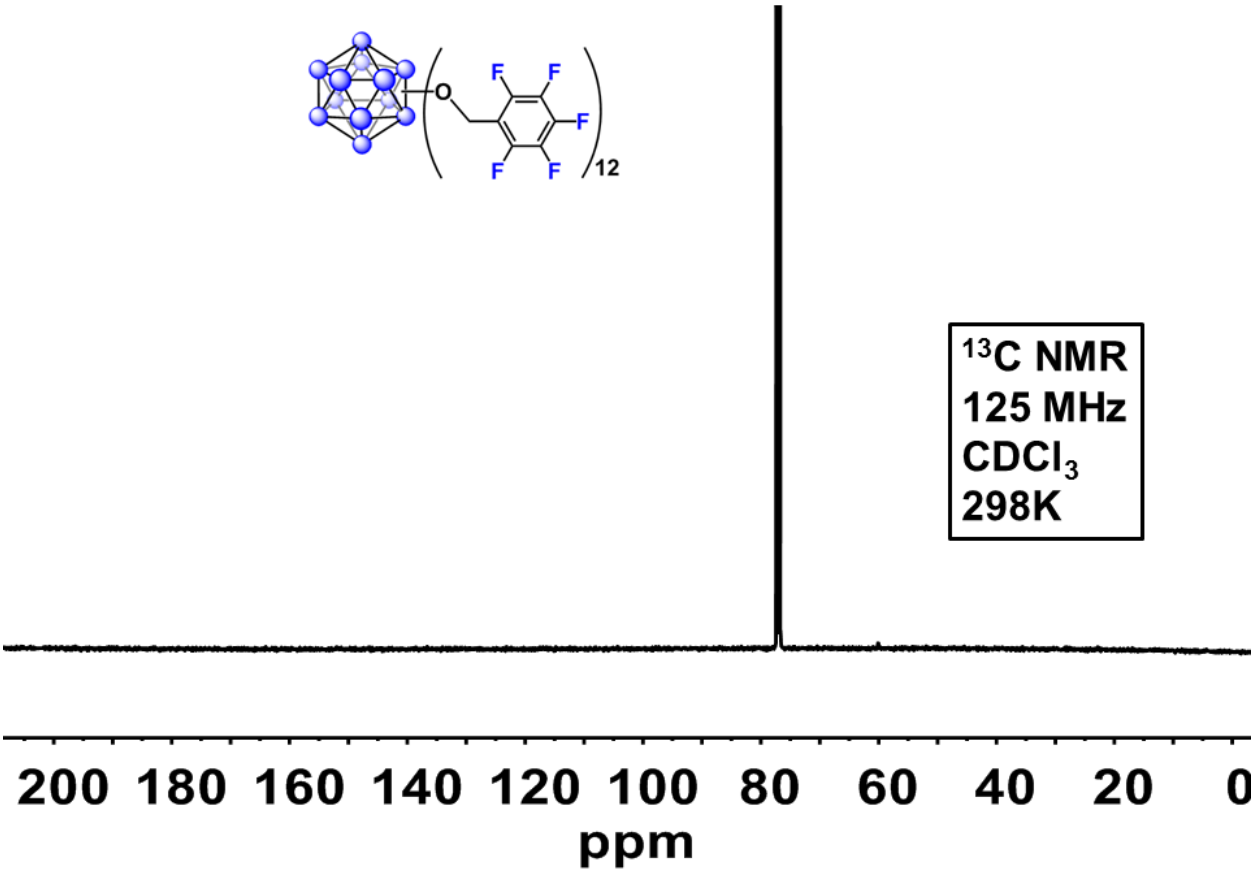

Figure B11. ^{13}C NMR spectrum of $B_{12}(OCH_2C_6F_5)_{12}$ (**1b**) in $CDCl_3$ at 298 K.

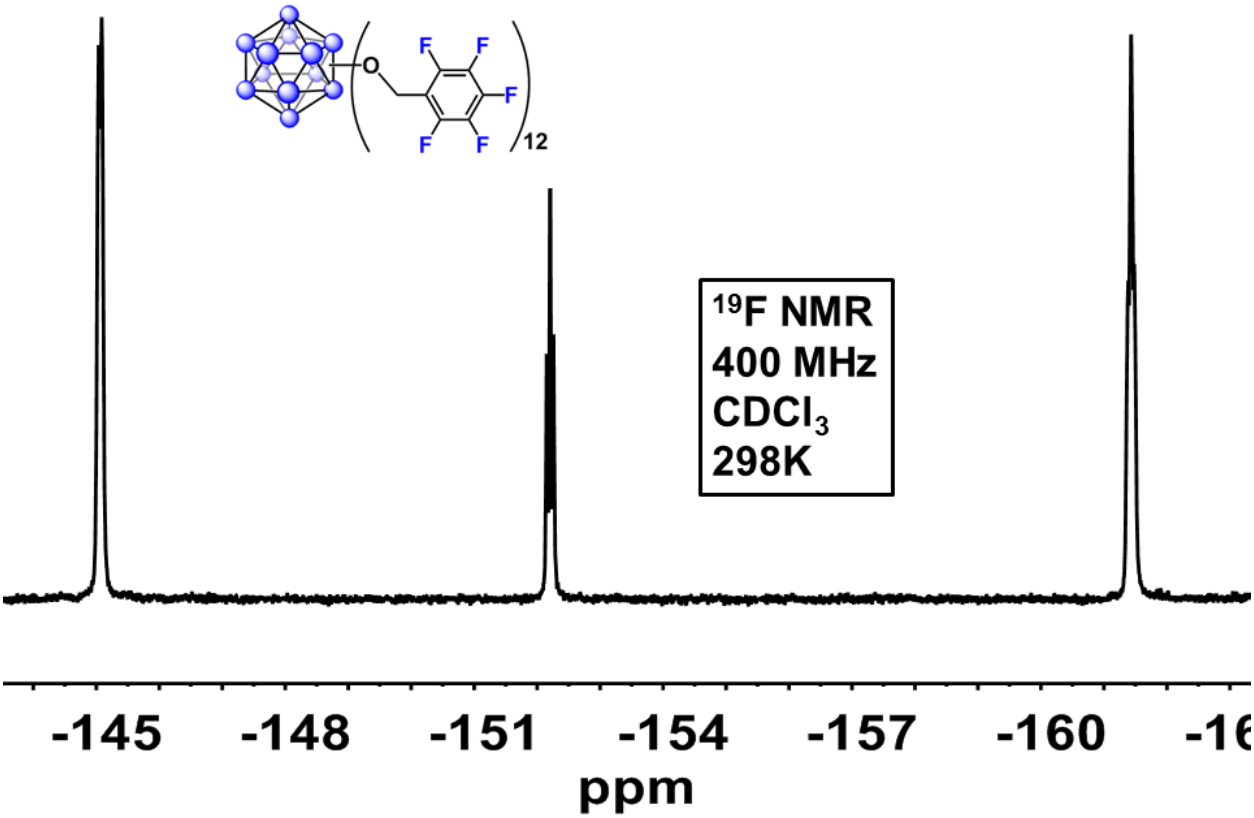

Figure B12. ^{19}F NMR spectrum of $B_{12}(OCH_2C_6F_5)_{12}$ (**1b**) in $CDCl_3$ at 298 K.

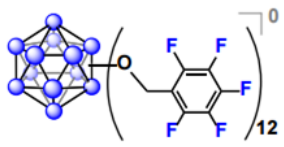

Q Exactive
High-Res Mass Spec

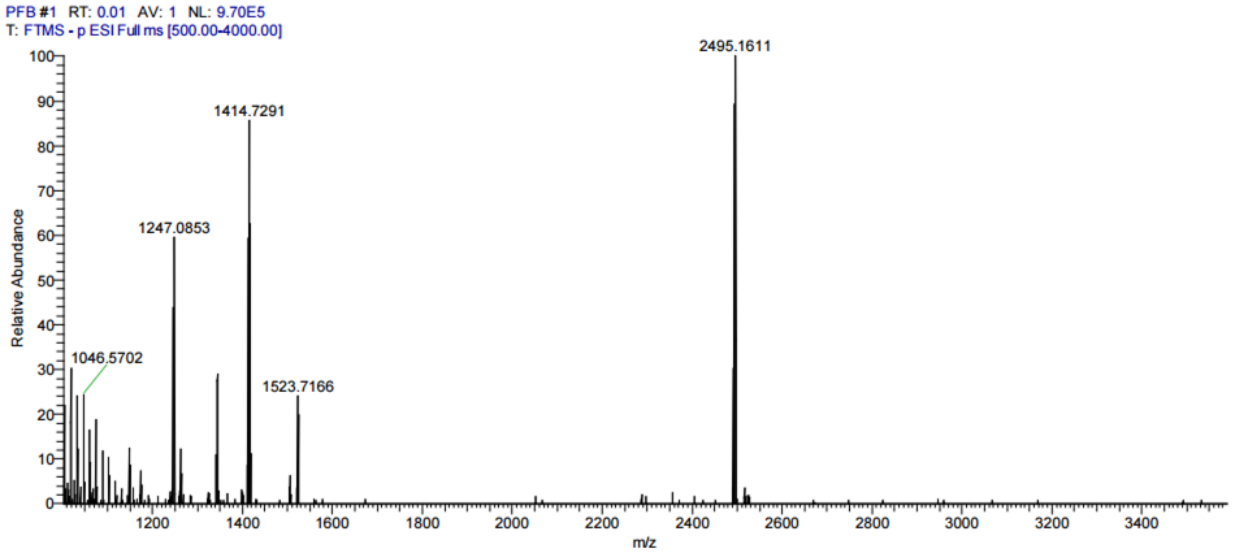

Figure B13. HRMS spectrum of $B_{12}(OCH_2C_6F_5)_{12}$ (**1b**).

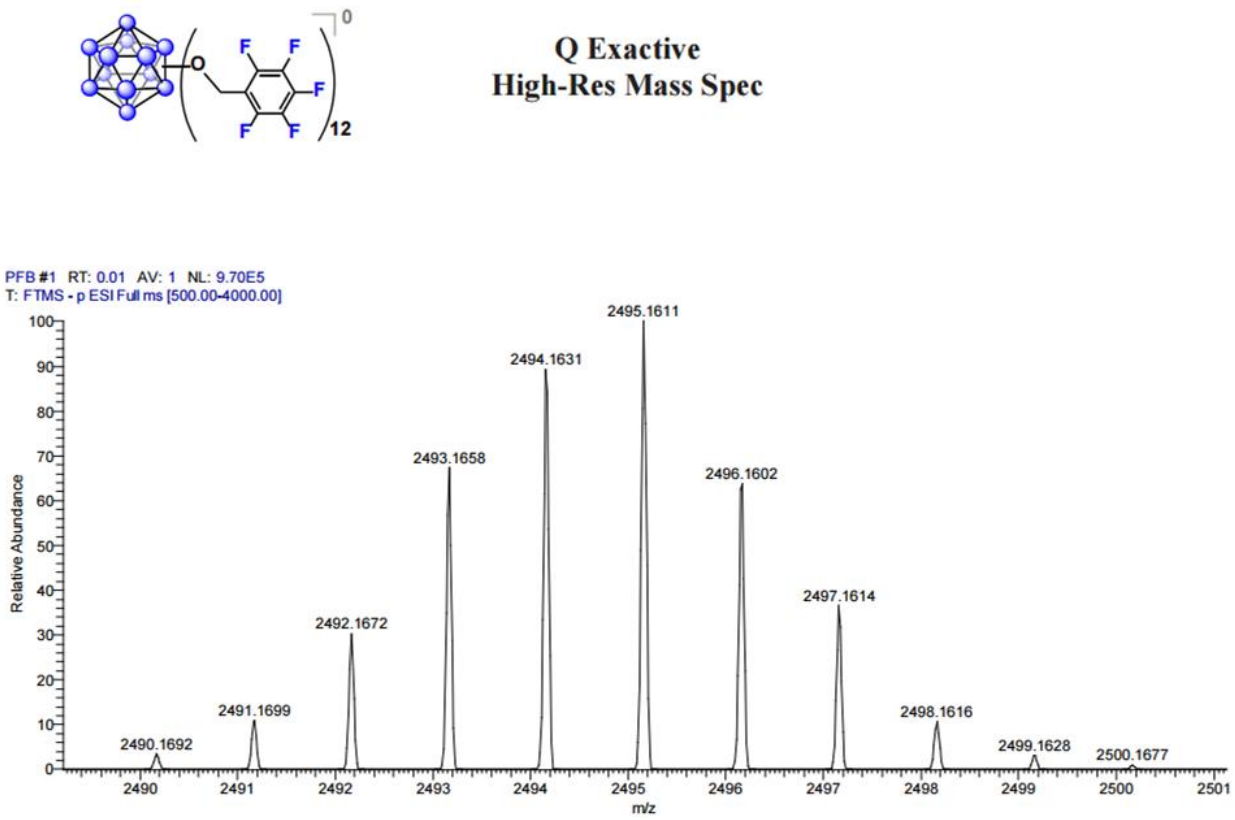

Figure B14. HRMS spectrum of $B_{12}(OCH_2C_6F_5)_{12}$ (**1b**).

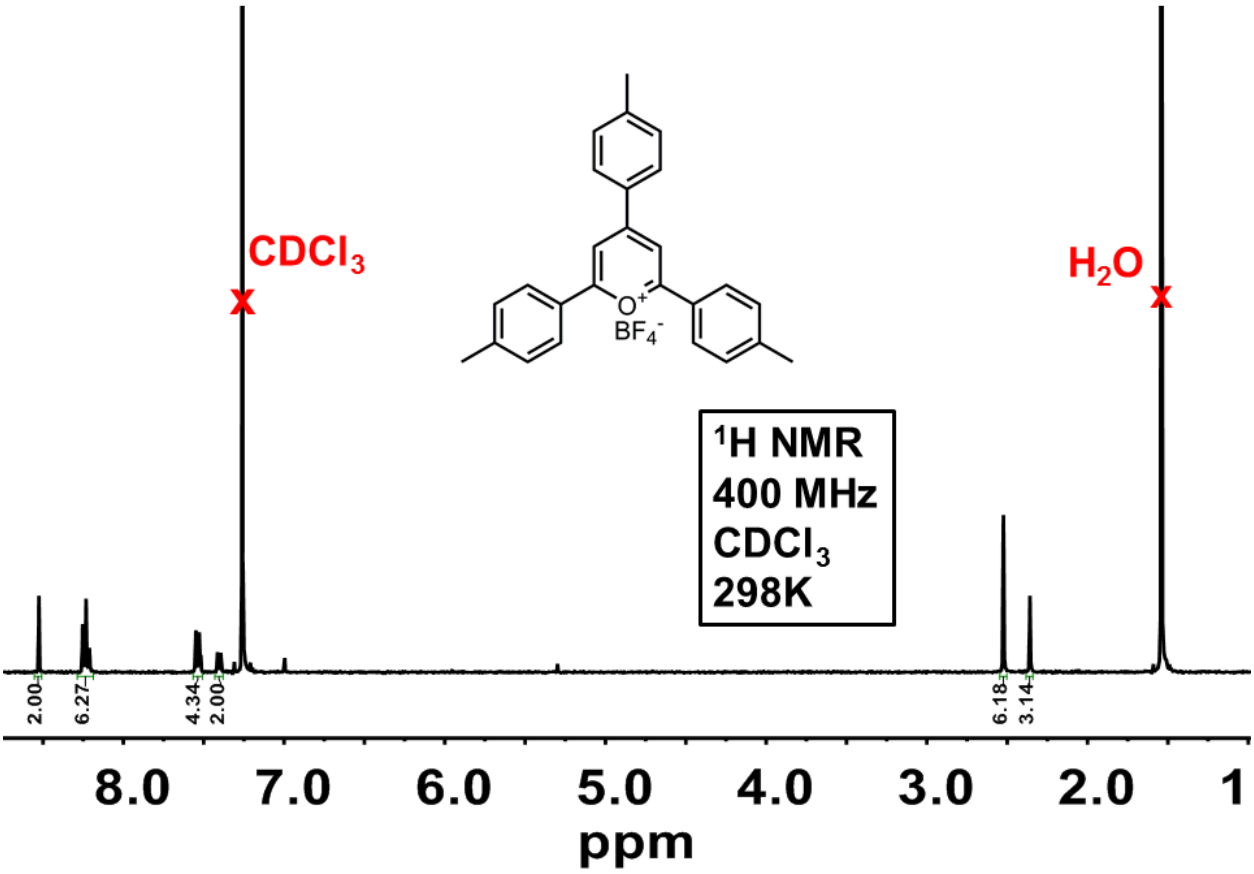

Figure B15. ^{1}H NMR spectrum of 2,4,6-tri(p-tolyl)pyrylium tetrafluoroborate in $CDCl_3$ at 298 K.

3.5.9 Polymer Characterization

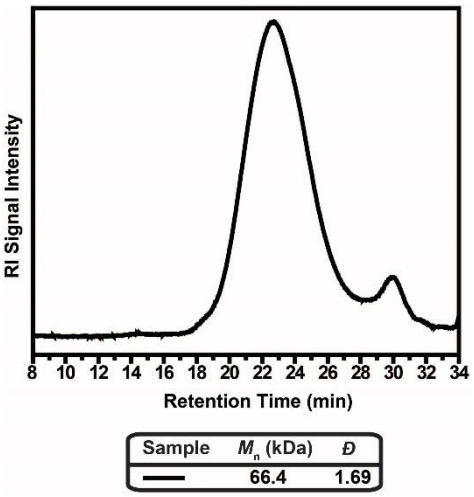

Figure B16. GPC trace from polymerization of **2a** treated with 0.5 mol% **1a** for two days. Calculated yield after precipitation is 71%. Smaller peak has a reported M_n value of 31.1 kDa and a dispersity of 1.1. GPC performed in chloroform.

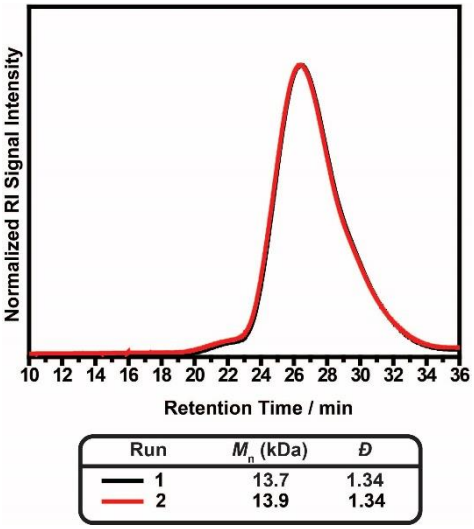

Figure B17. GPC trace overlay of a 2M solution of **2a** in CH_2Cl_2 treated with 0.5 mol% of **1a**. GPC performed in THF.

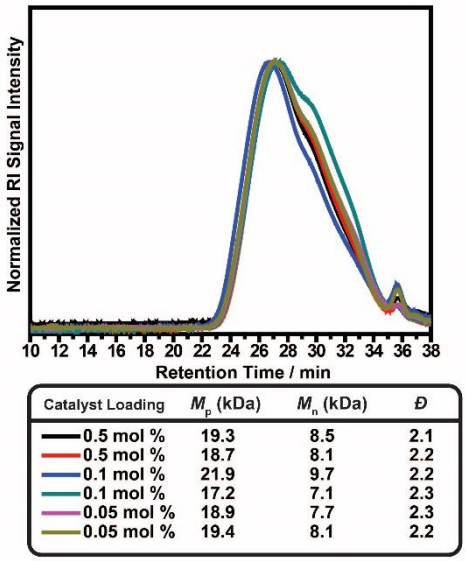

Catalyst Loading	M_p (kDa)	M_n (kDa)	Đ
0.5 mol %	19.3	8.5	2.1
0.5 mol %	18.7	8.1	2.2
0.1 mol %	21.9	9.7	2.2
0.1 mol %	17.2	7.1	2.3
0.05 mol %	18.9	7.7	2.3
0.05 mol %	19.4	8.1	2.2

Figure B18. GPC trace overlay of polystyrene from experiments treating styrene (**2b**) with varying concentrations of **1b**. GPC performed in THF.

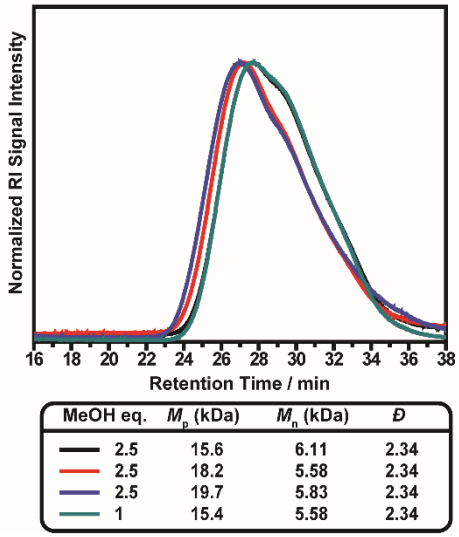

MeOH eq.	M_p (kDa)	M_n (kDa)	Đ
2.5	15.6	6.11	2.34
2.5	18.2	5.58	2.34
2.5	19.7	5.83	2.34
1	15.4	5.58	2.34

Figure B19. GPC trace overlay of styrene (**2b**) polymerization experiments varying concentrations of methanol to 1b under optimized conditions. GPC performed in THF.

3.5.9.1 Polymerization of 4-methoxystyrene (2a)

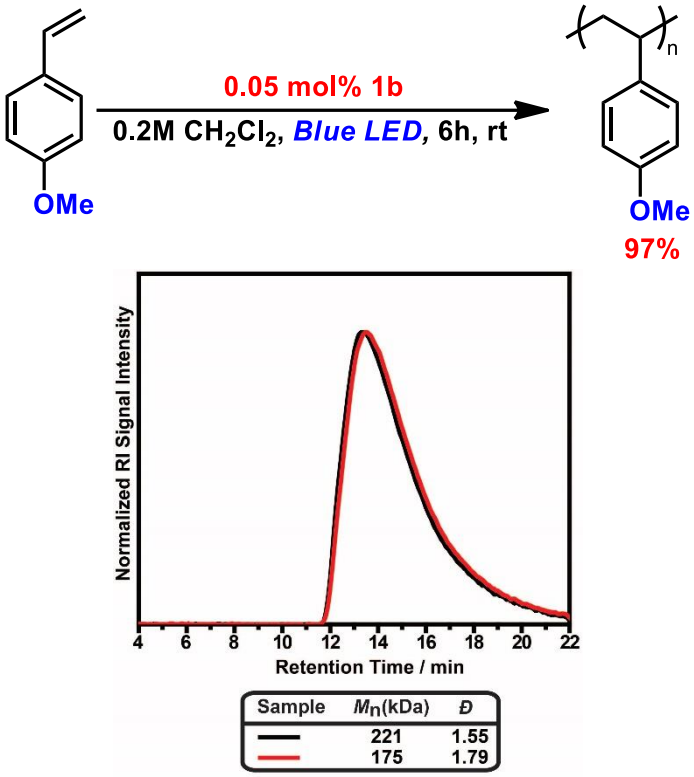

Figure B20. GPC trace overlay of poly-(4-methoxystyrene) generated using **1b** as initiator. GPC performed in DMF.

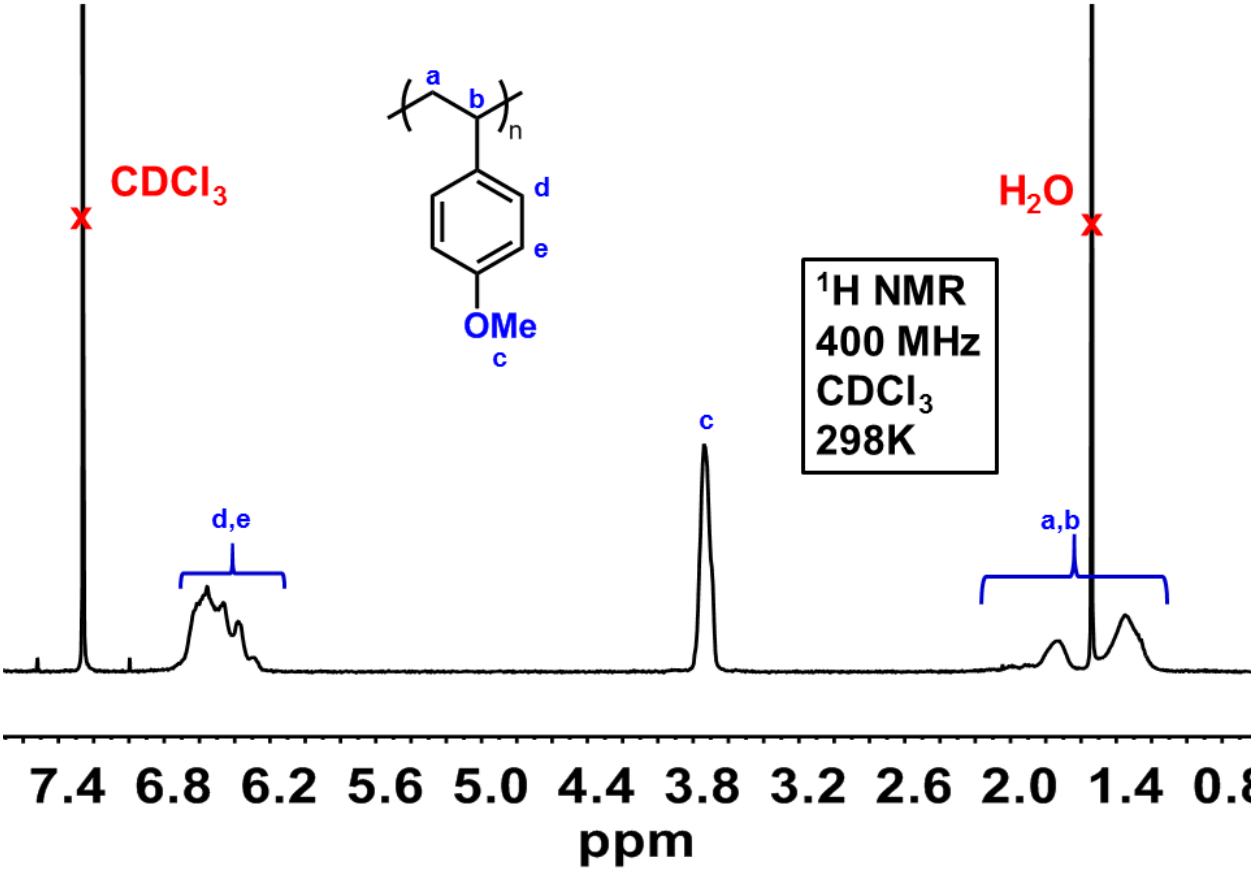

Figure B21. ^{1}H NMR spectrum of poly-(4-methoxystyrene) in $CDCl_3$ at 298 K.

3.5.9.2 Polymerization of styrene (2b)

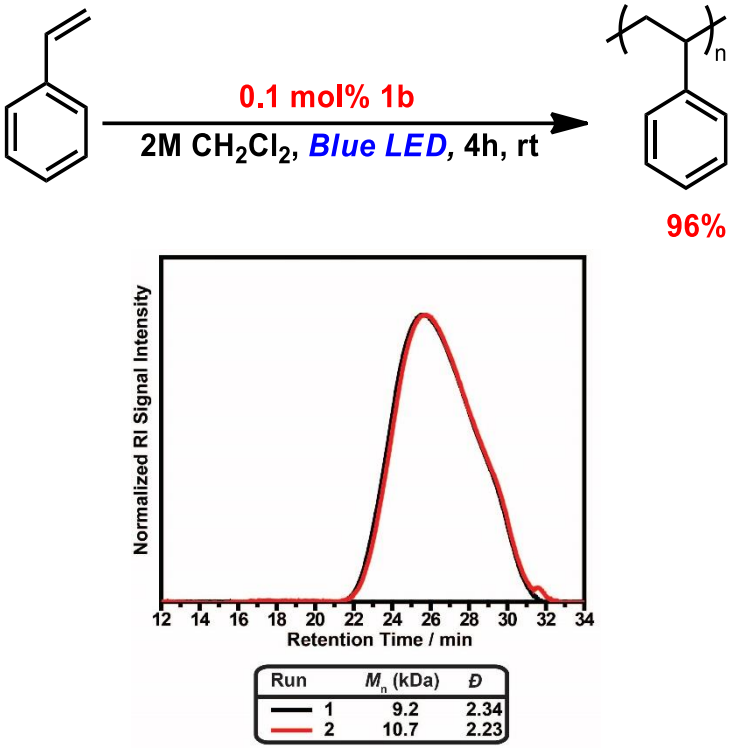

Figure B19. GPC trace overlay of polystyrene. GPC performed in $CHCl_3$.

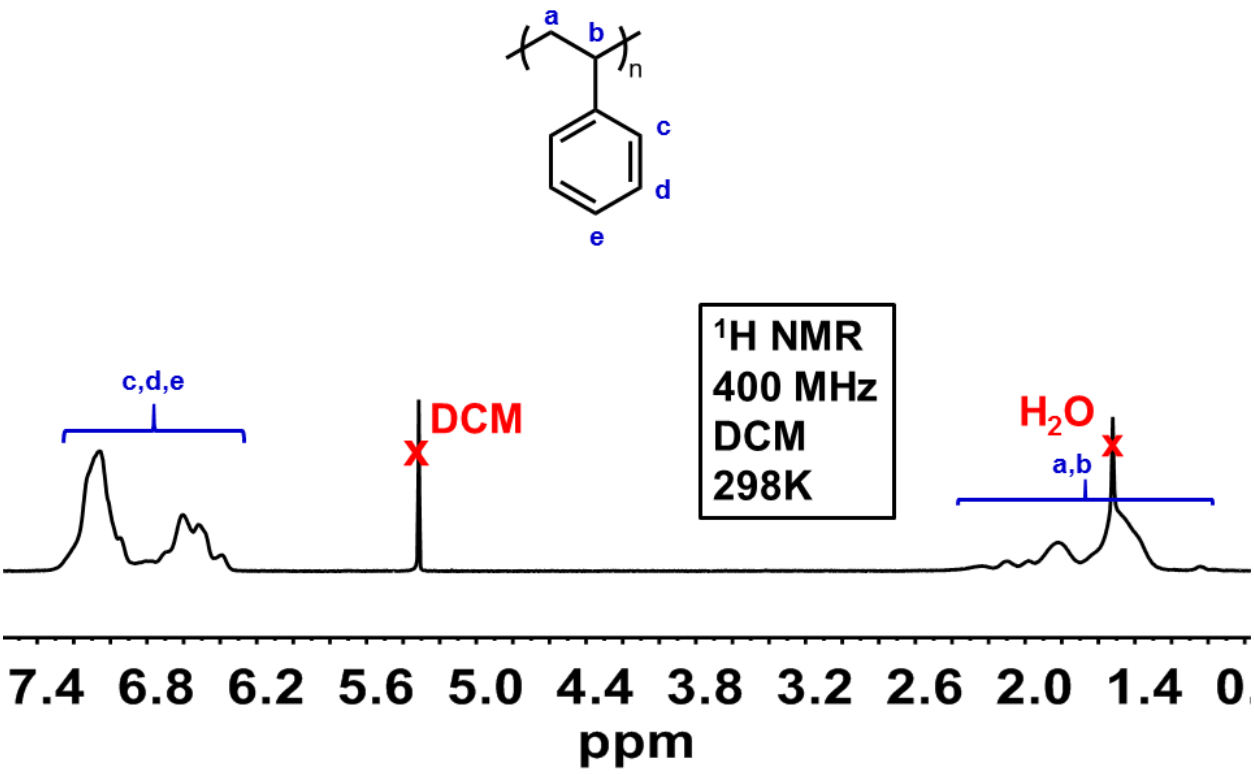

Figure B20. ^{1}H NMR spectrum of polystyrene in $CDCl_3$ at 298 K.

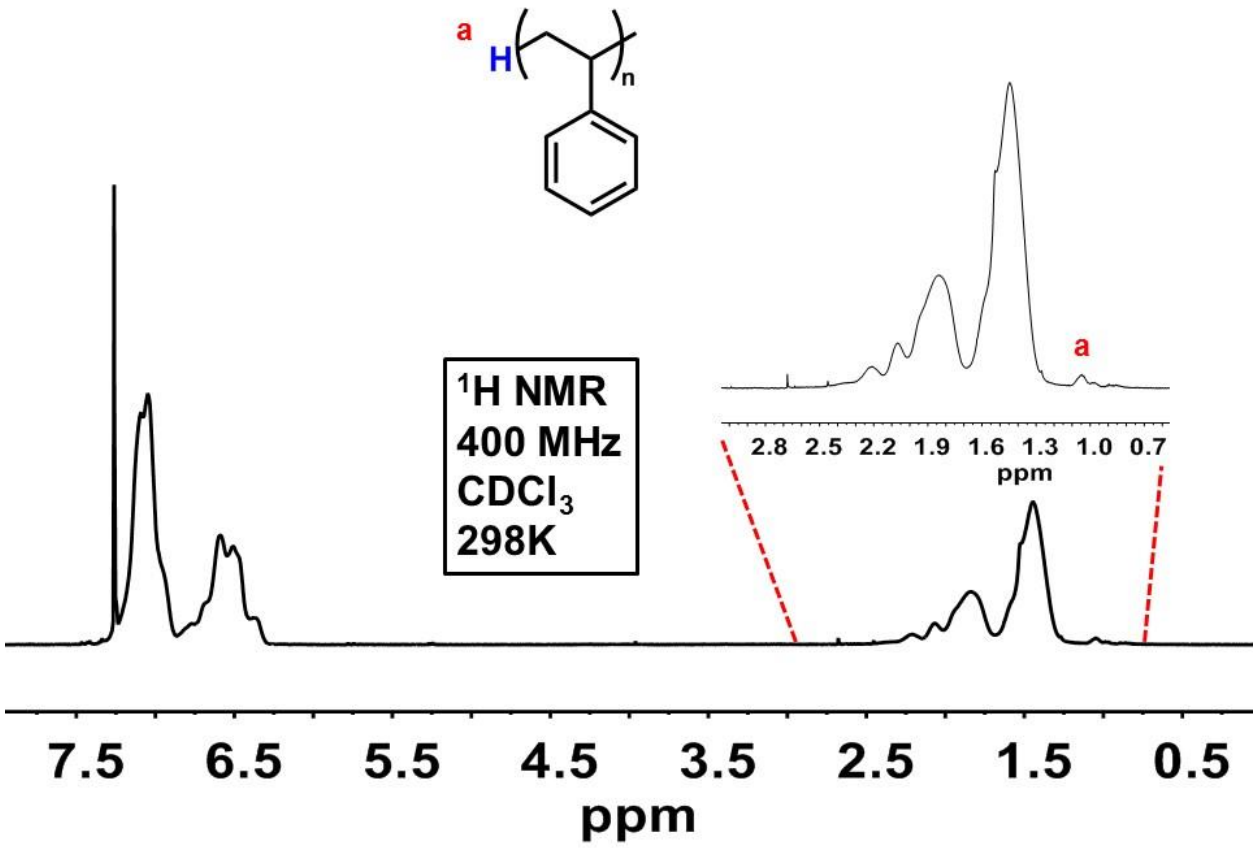

Figure B21. ^{1}H NMR spectrum of polystyrene in $CDCl_3$ at 298 K indicating the potential presence of a proton attached onto the end of the polymer.

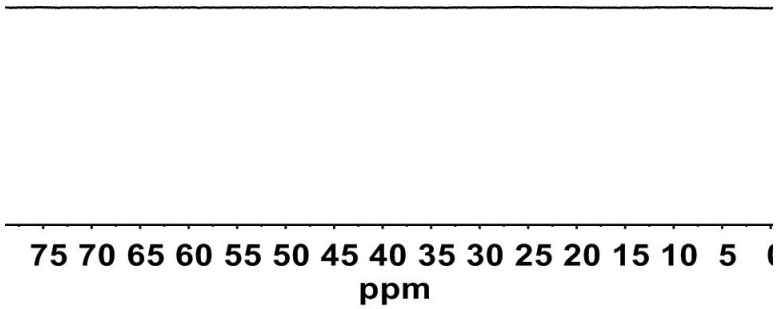

Figure B22. ^{11}B NMR spectrum of purified polystyrene synthesized utilizing optimized reaction conditions which shows that **1b** is not attaching to the polymer. Additional ICP-MS analysis on a polystyrene sample generated using **1b** determined that it contains 0.003% of boron by mass.

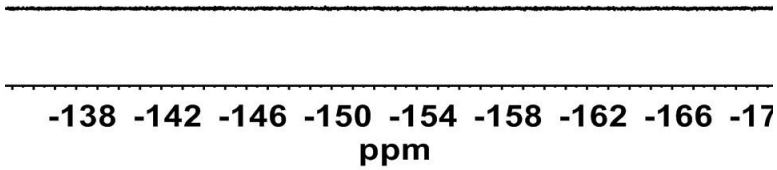

Figure B23. ^{19}F NMR spectrum of purified polystyrene synthesized utilizing optimized reaction conditions which shows that 1b is not attaching to the polymer.

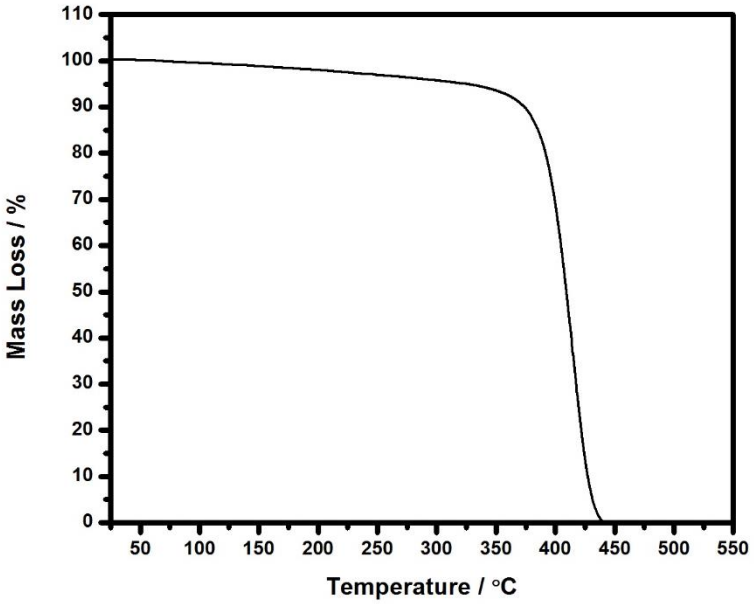

Figure B24. TGA analysis of 3.3 mg sample of polystyrene. Temperature ramping from 25 °C to 500 °C at 15 °C/min.

3.5.9.3 Polymerization of 4-methylstyrene (2c)

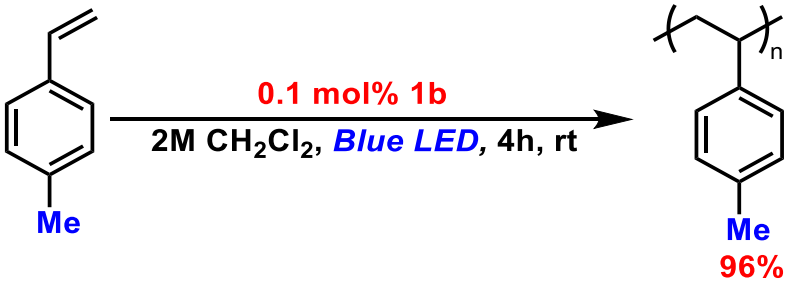

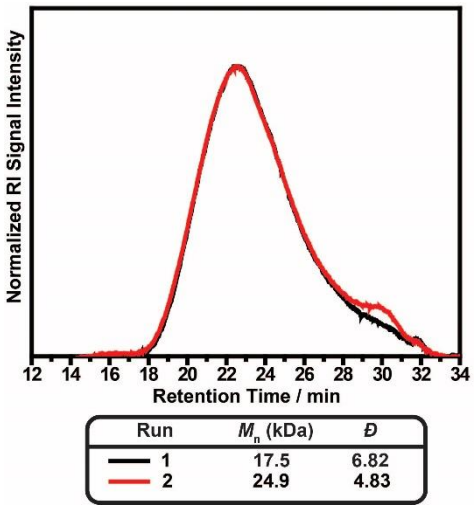

Figure B25. GPC trace overlay of poly-(4-methylstyrene).

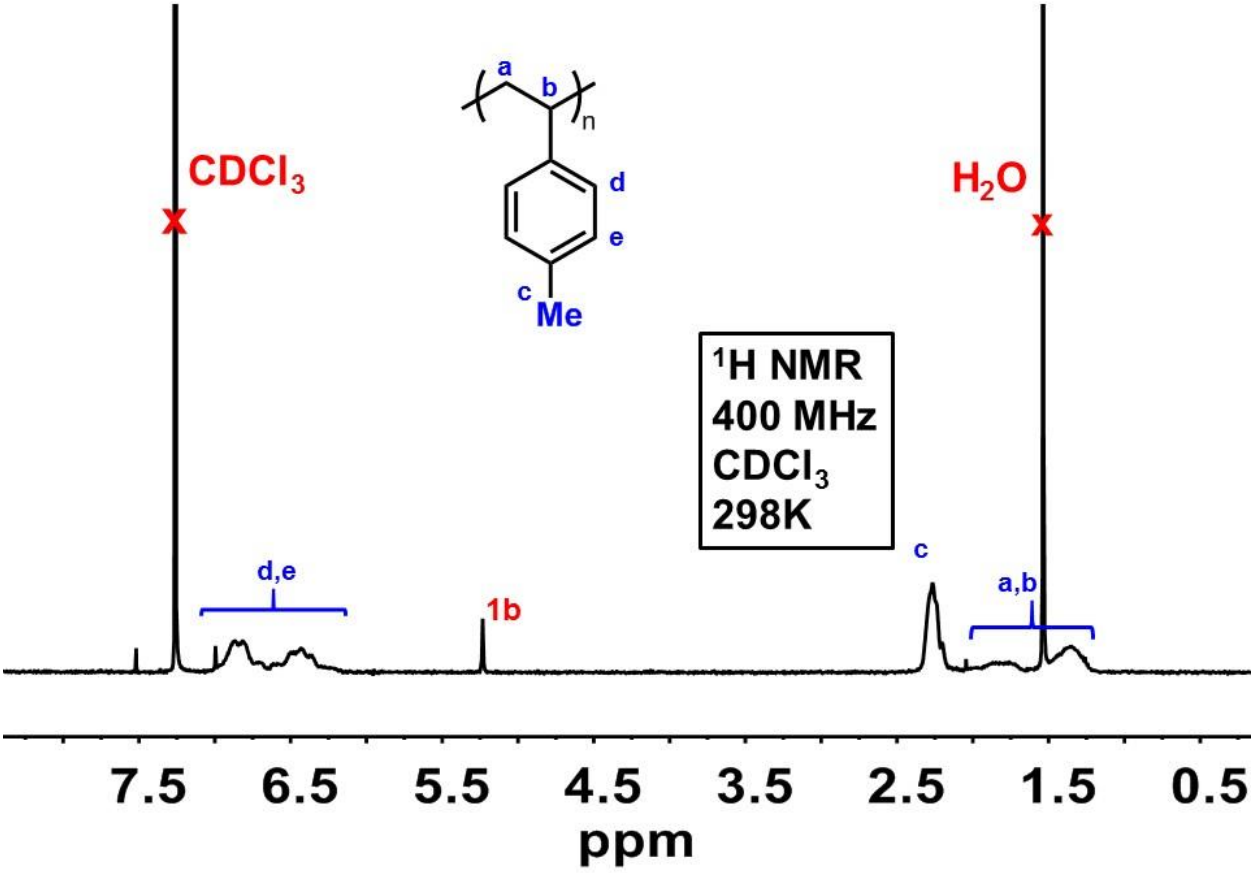

Figure B26. ^{1}H NMR spectrum of poly-(4-methylstyrene) in $CDCl_3$ at 298 K.

3.5.9.4 Polymerization of 4-*tert*-butylstyrene (2d)

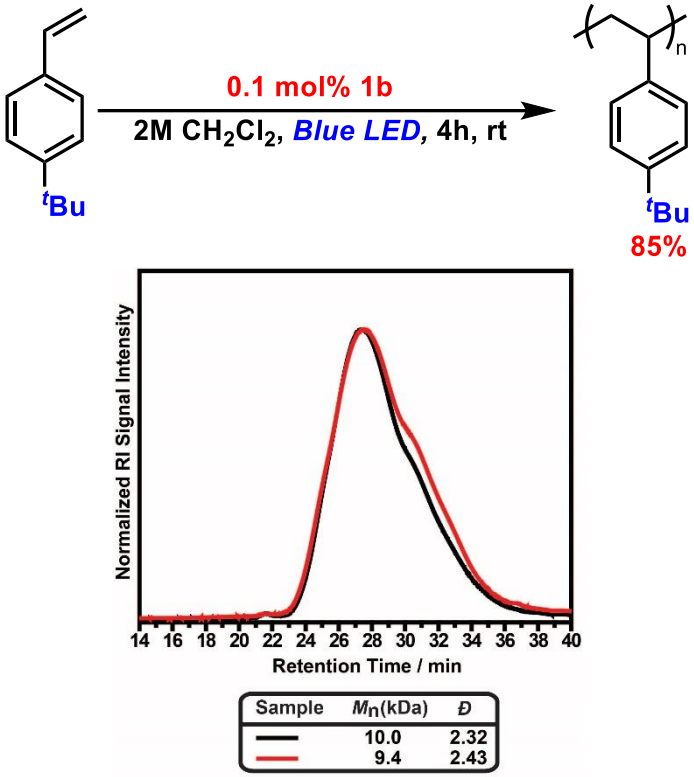

Figure B27. GPC trace of poly-(4-*tert*-butylstyrene). GPC performed in THF.

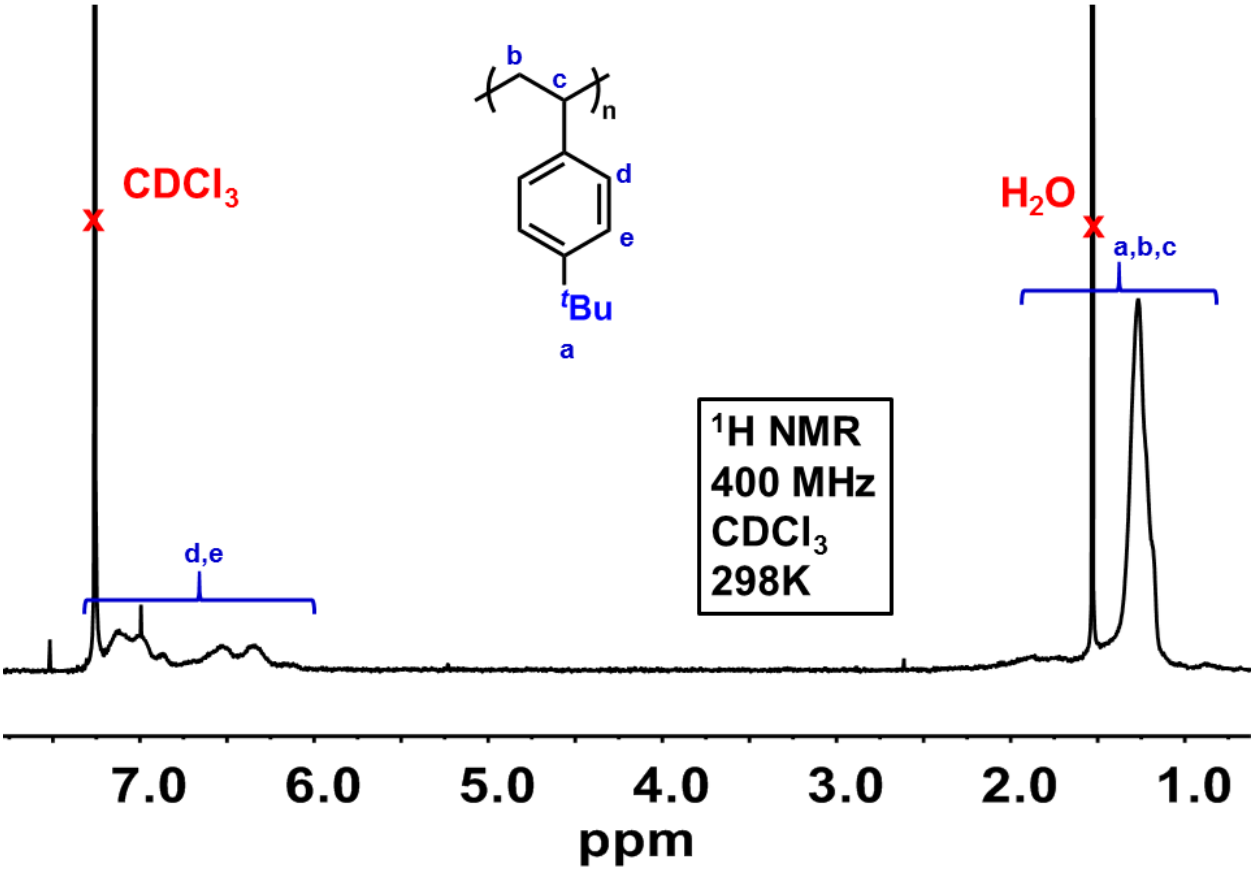

Figure B28. ^{1}H NMR spectrum of poly-(4-tert-butylstyrene) in $CDCl_3$ at 298 K.

3.5.9.5 Polymerization of 4-fluorostyrene (2e)

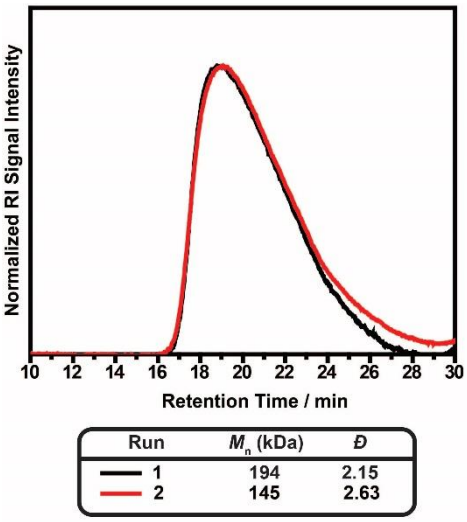

Figure B29. GPC trace overlay of poly-(4-fluorostyrene). GPC performed in $CHCl_3$.

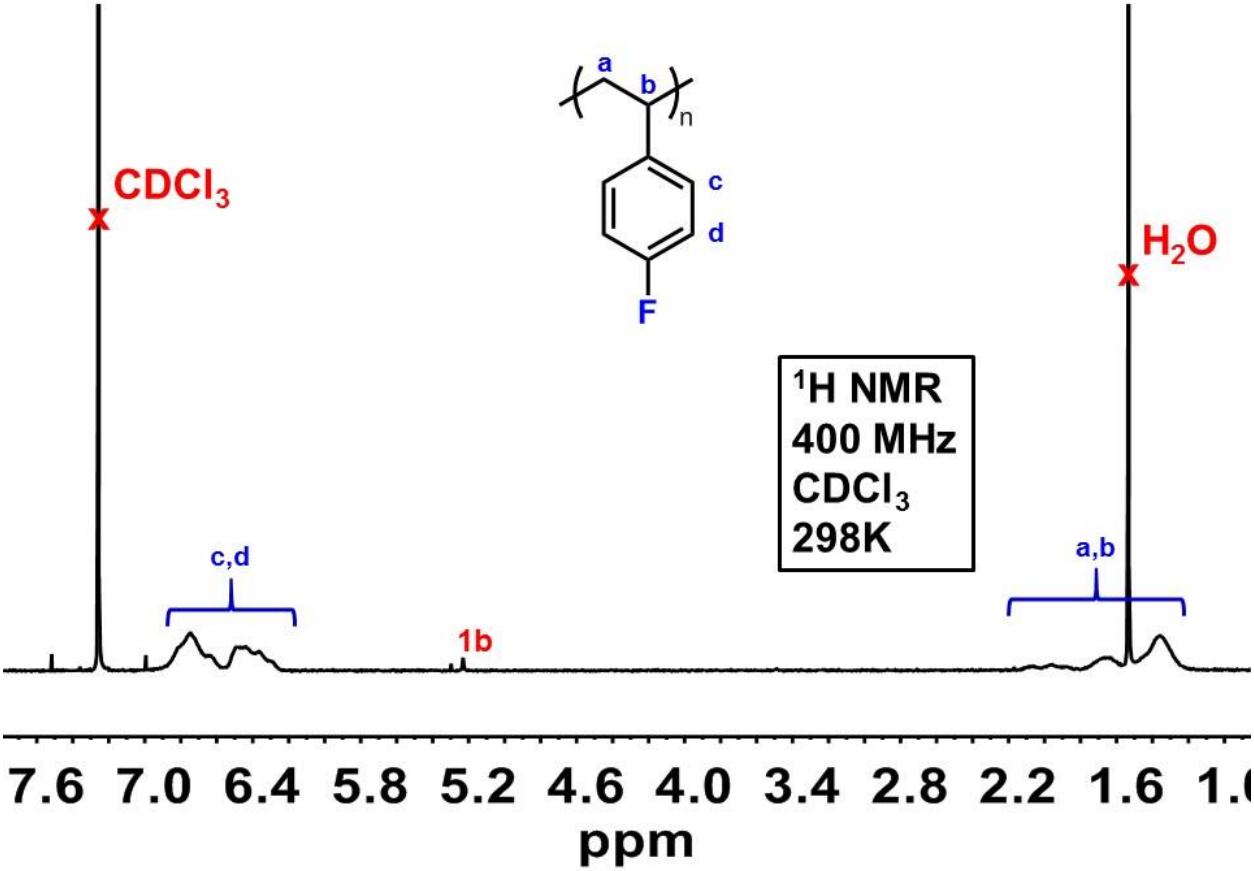

Figure B30. ^{1}H NMR spectrum of poly-(4-fluorostyrene) in $CDCl_3$ at 298 K.

3.5.9.6 Polymerization of 4-chlorostyrene (2f)

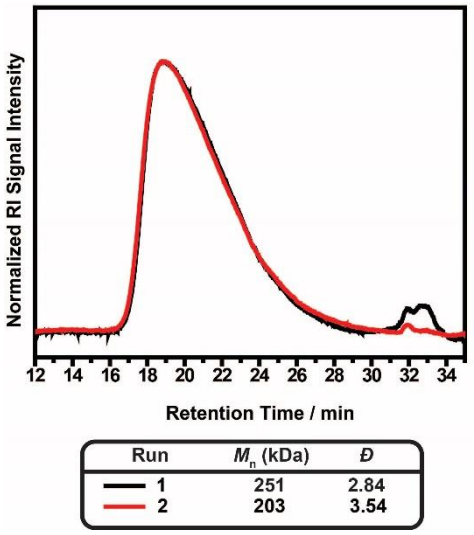

Figure B31. GPC trace overlay of poly-(4-chlorostyrene). GPC performed in $CHCl_3$.

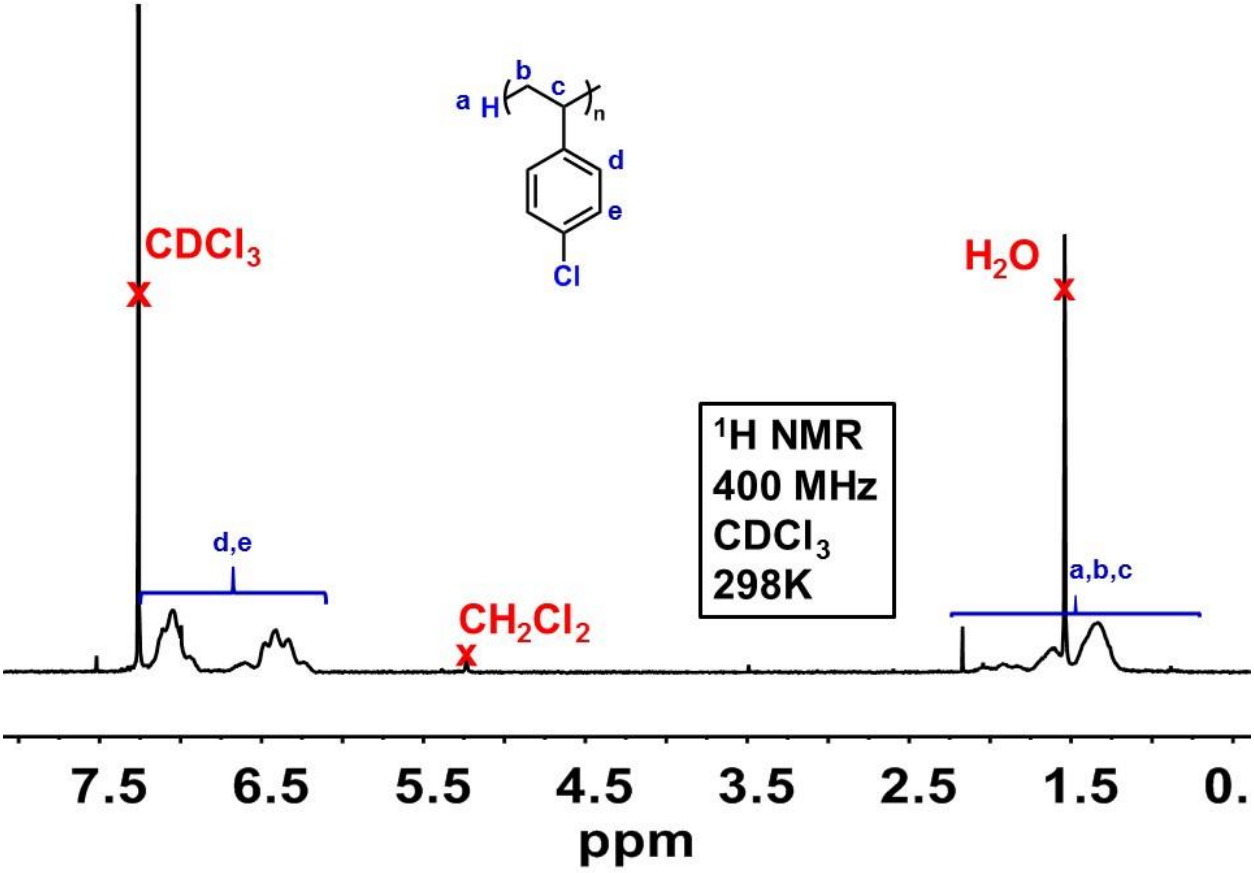

Figure B32. ^{1}H NMR spectrum of poly-(4-chlorostyrene) in $CDCl_3$ at 298 K.

3.5.9.7 Polymerization of 3-chlorostyrene (2g)

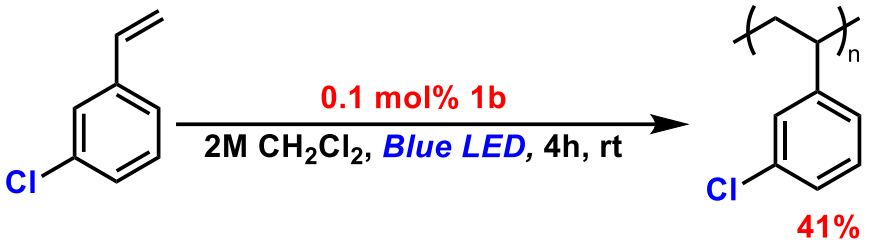

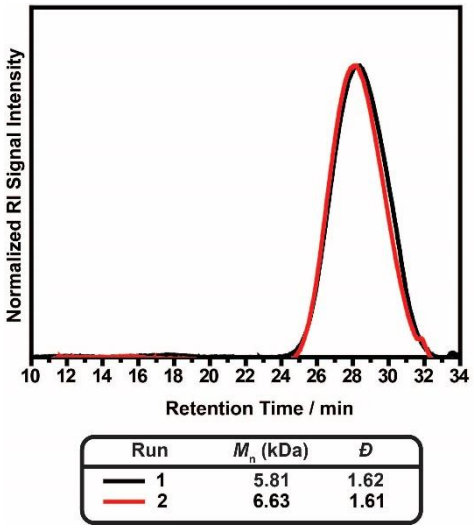

Figure B33. GPC trace overlay of poly-(3-chlorostyrene). GPC performed in $CHCl_3$.

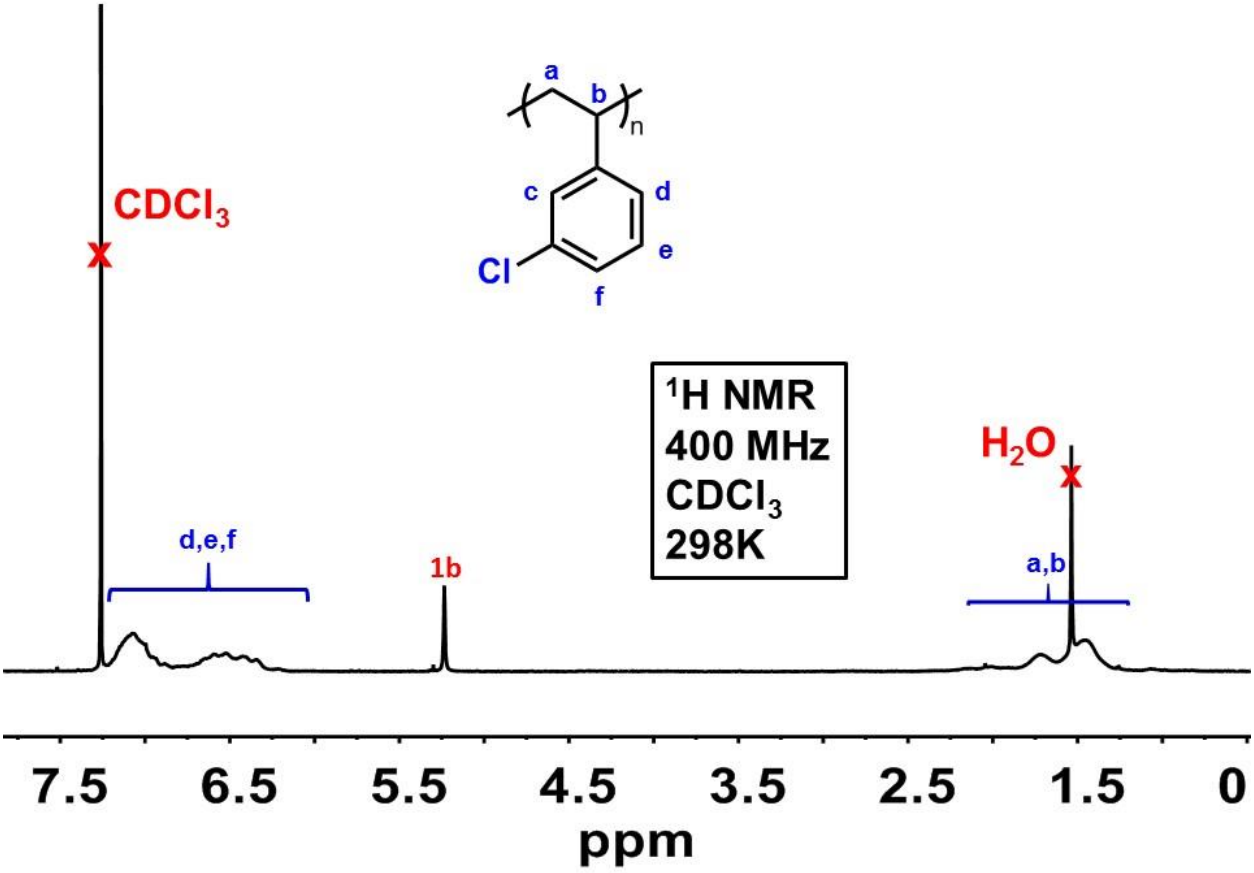

Figure B34. ^{1}H NMR spectrum of poly-(3-chlorostyrene) in $CDCl_3$ at 298 K.

3.5.9.8 Polymerization of 2,6-difluorostyrene (2h)

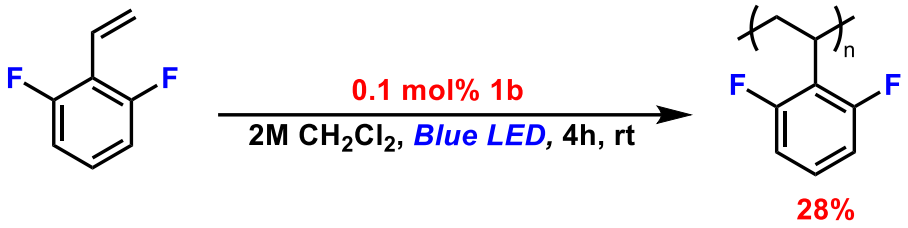

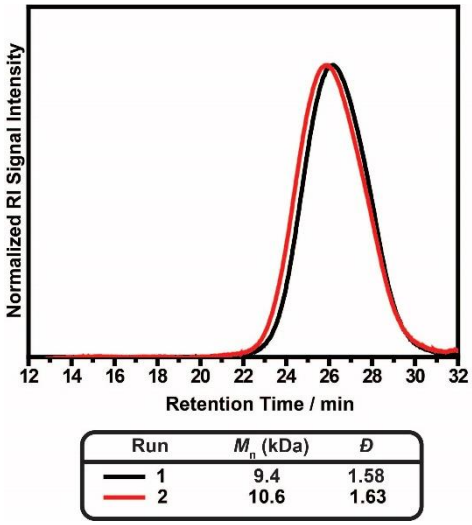

Figure B35. GPC trace overlay of poly-(2,6-difluorostyrene). GPC performed in $CHCl_3$.

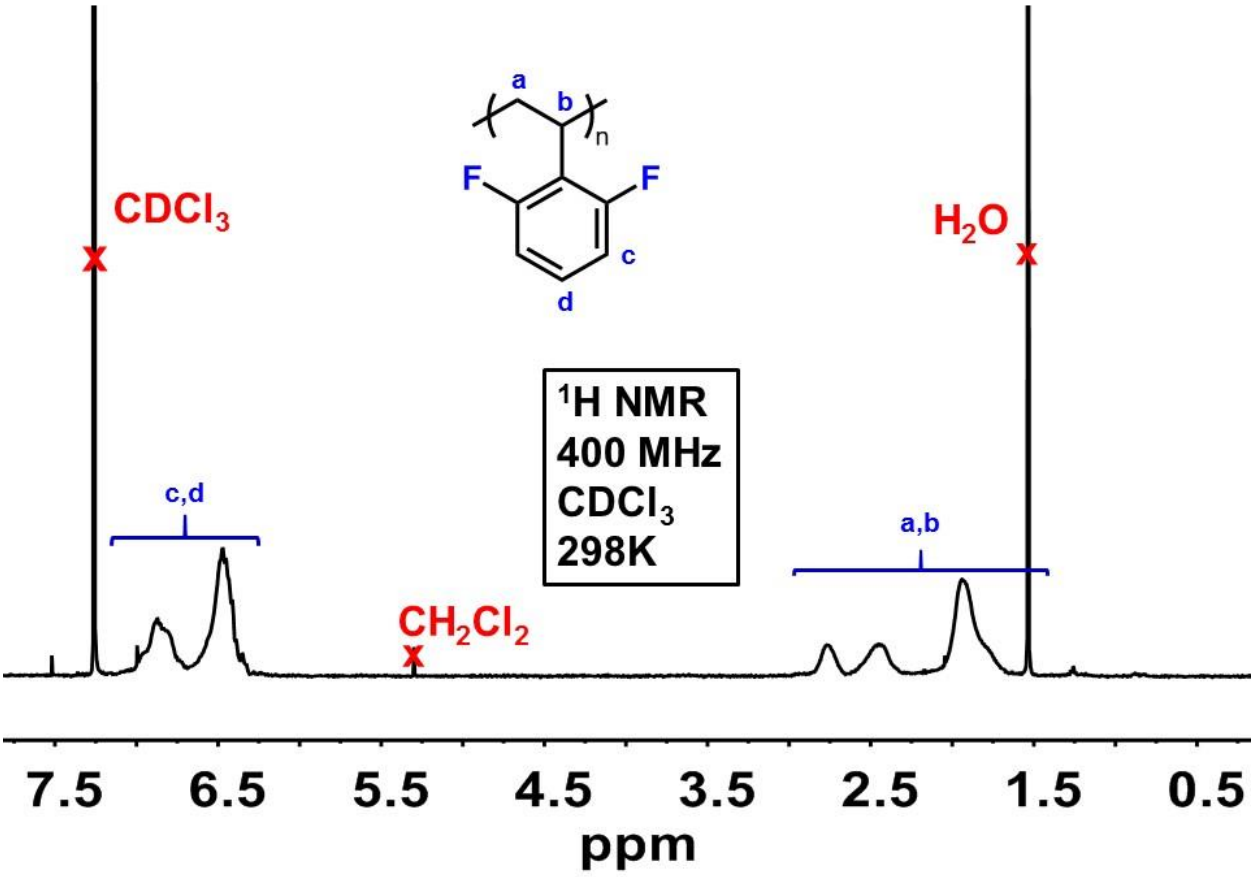

Figure B36. ^{1}H NMR spectrum of poly-(2,6-difluorostyrene) in $CDCl_3$ at 298 K.

3.5.9.9 Polymerization of 2,4,6-trimethylstyrene (2i)

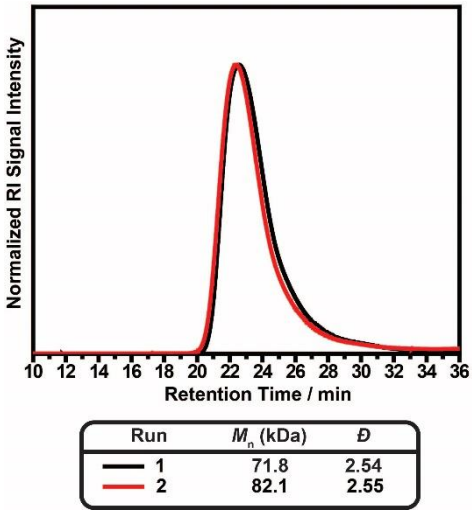

Figure B37. GPC trace overlay of poly-(2,4,6-trimethylstyrene). GPC performed in $CHCl_3$.

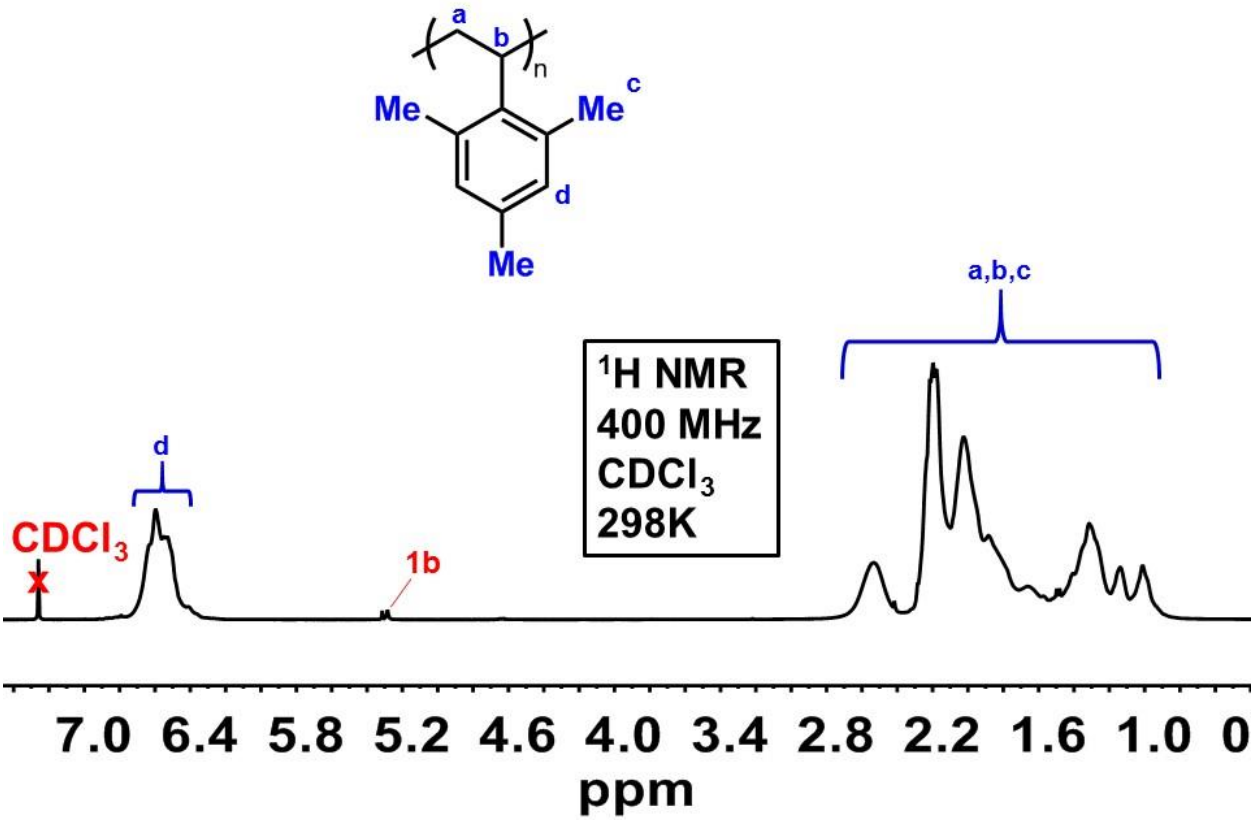

Figure B38. ^{1}H NMR spectrum of poly-(2,4,6-trimethylstyrene) in $CDCl_3$ at 298 K. Signal next to **1b** due to residual CH_2Cl_2.

3.5.9.10 Polymerization of isobutylene

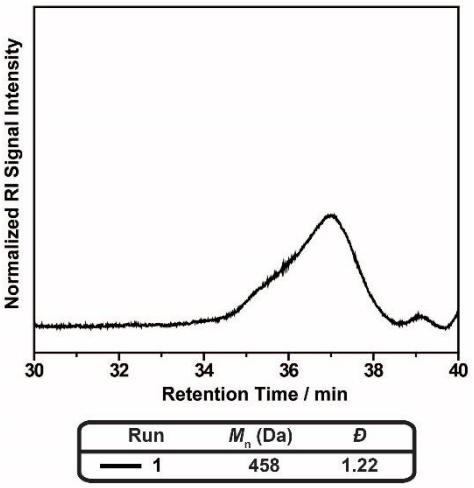

Figure B39. GPC trace of poly(isobutylene). GPC performed in THF.

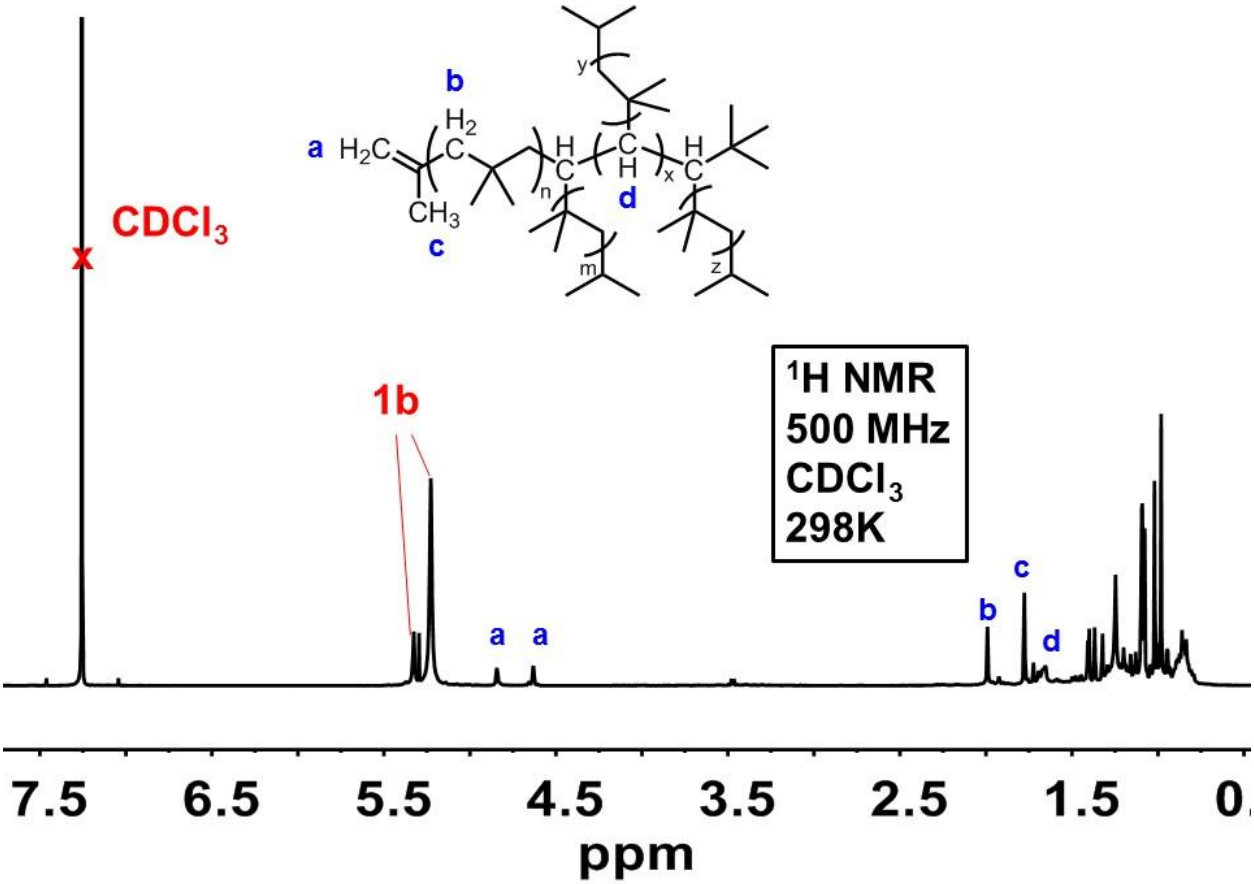

Figure B40. ^{1}H NMR spectrum of poly(isobutylene) in $CDCl_3$ at 298 K.

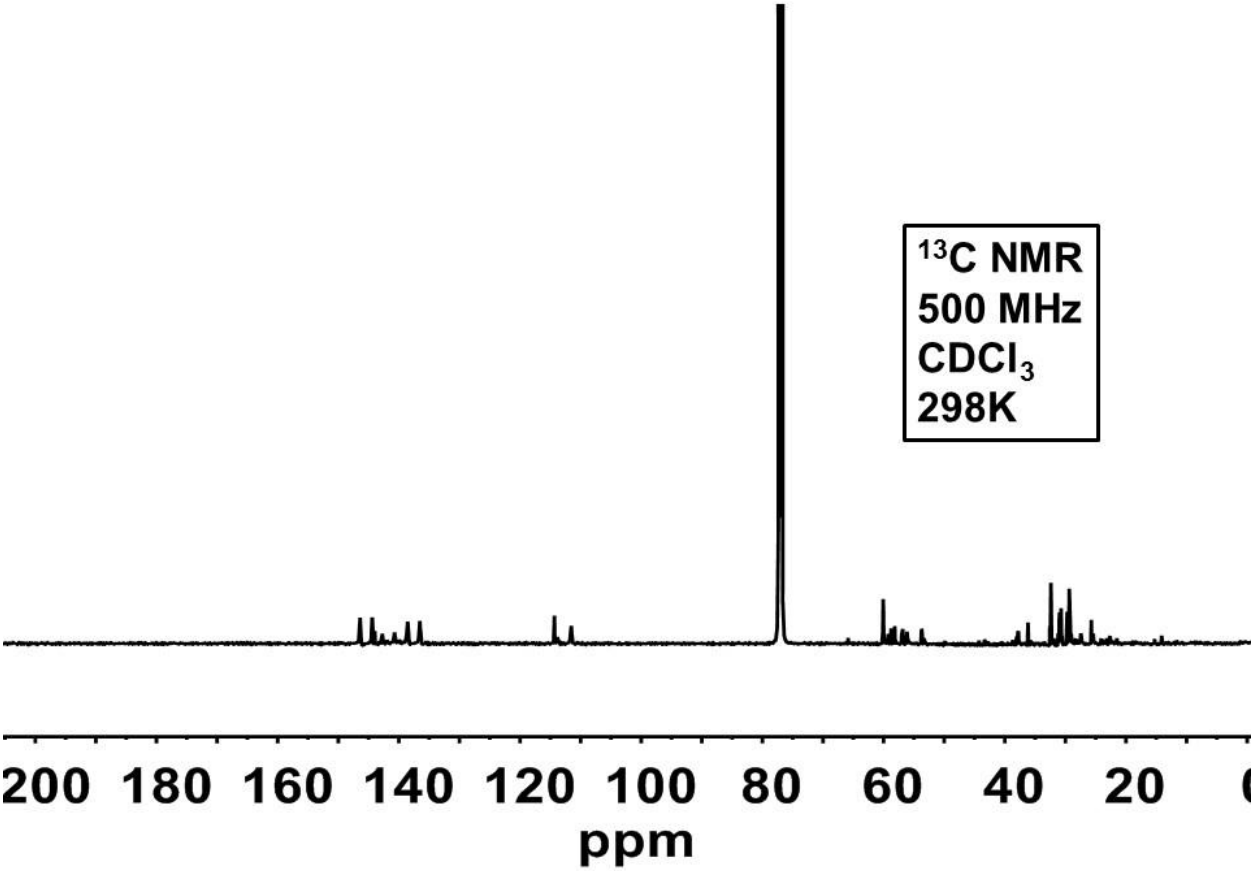

Figure B41. ^{13}C NMR of poly(isobutylene) in $CDCl_3$ at 298K.

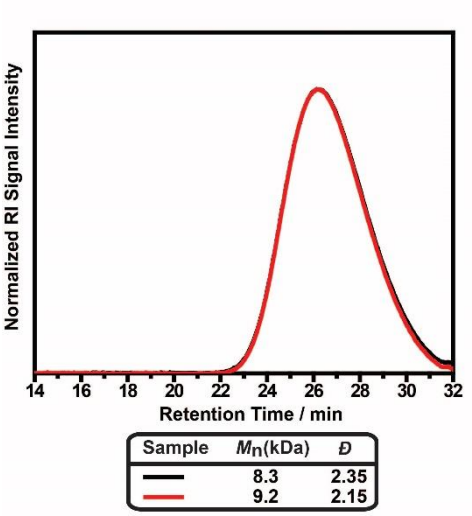

Figure B42. GPC trace overlay of optimized styrene reaction utilizing **1b** in benzene. GPC performed in $CHCl_3$.

Monomer	**Yield**	M_n **(kDa)**	$Đ$
4-methoxystyrene	97%	198	1.7
Styrene	96%	9.9	2.3
4-methylstyrene	96%	21.2	5.8
4-*tert*-butylstyrene	85%	9.7	2.4
4-fluorostyrene	99%	170	2.4
4-chlorostyrene	94%	227	3.2
3-chlorostyrene	41%	6.2	2.2
2,6-difluorostyrene	28%	10.0	1.6
2,4,6-trimethylstyrene	98%	79.6	2.6
Isobutylene	<10%	458 Da	1.2
4-fluorostyrene	21%	16.8	1.7
4-chlorostyrene	24%	9.7	1.7
4-methylstyrene	32%	31.7	2.1
Styrene	34%	5.3	1.7

Table B1. Polymer yields, M_n and $Đ$ (averaged over two runs) of polymerizations. Polymerizations of monomers in bold were prepared in ambient conditions utilizing optimized conditions (2M [monomer] in CH_2Cl_2 with 0.1 mol% **1b** and not passed through activated basic alumina.

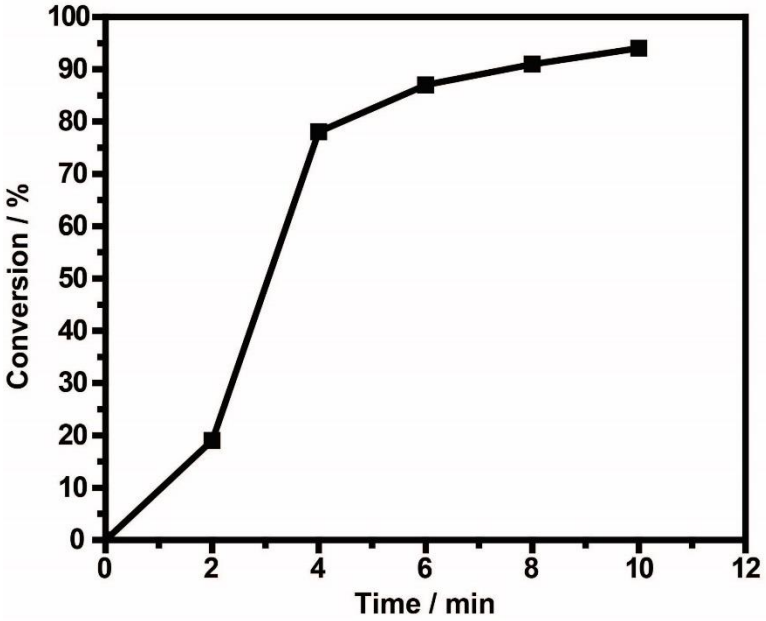

Figure B43. Conversion of optimized styrene polymerization utilizing **1b**. Time points taken every two minutes.

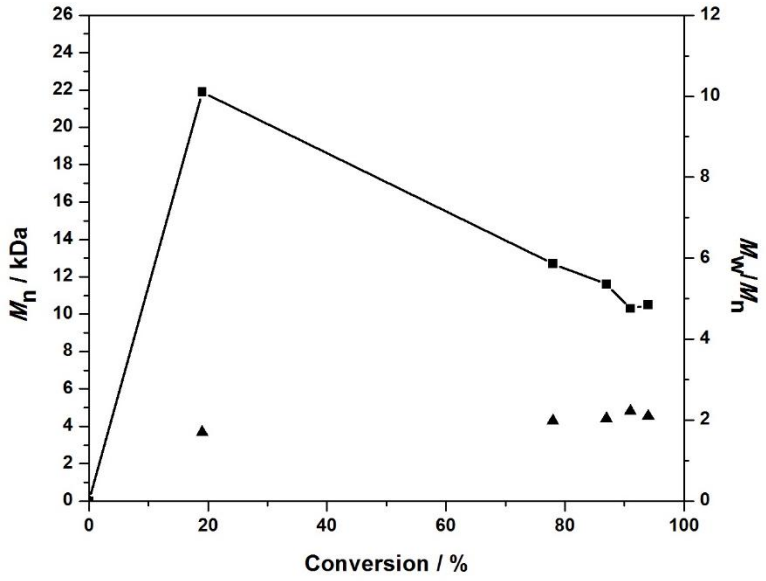

Figure B44. Conversion, M_n (Squares), and $Đ$ (Triangles) of optimized styrene polymerization utilizing **1b** (Same experiment as shown in **Figure B29**). The high M_n (21.9 kDa) at 20% conversion (2 minutes) followed by the drop in M_n at 80% conversion is unusual but can best be explained by the higher amount of termination events as conversion increases—there are a larger amount of shorter polymer chains as conversion increases.

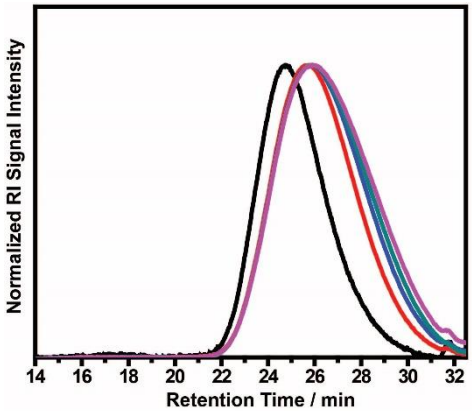

Time (min)	M_n (kDa)	M_w (kDa)	$Đ$
2	21.9	37.4	1.70
4	12.7	25.3	1.99
6	11.6	23.6	2.04
8	10.3	22.9	2.23
10	10.5	22.1	2.10

Figure B45. GPC trace overlay of optimized styrene polymerization utilizing **1b** with aliquots taken every two minutes (Same Experiment as **Figure B43** and **B44**).

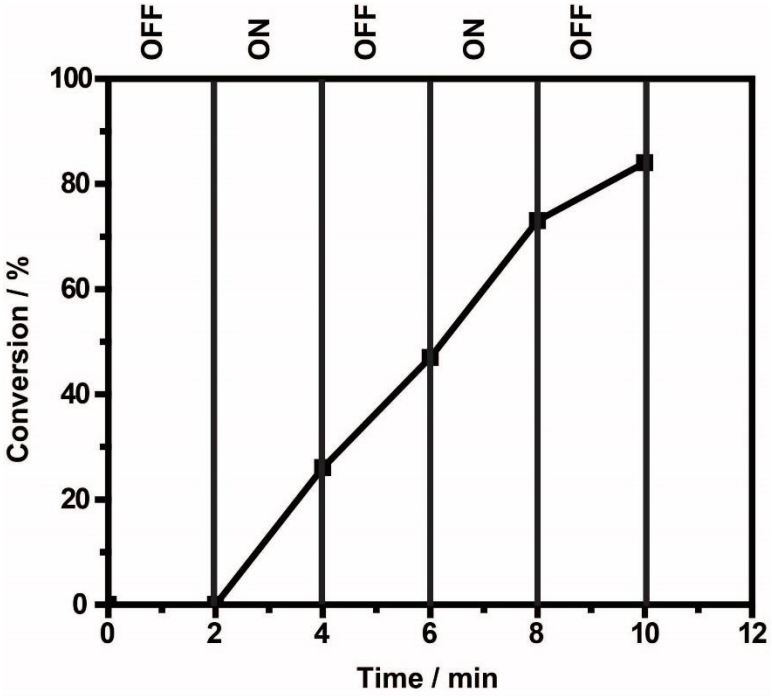

Figure B46. Polymerization of styrene under optimized conditions utilizing **1b** with light "on" and "off" cycling.

Solvent	Yield	Dispersity	M_n (kDa)	M_w (kDa)
C_6H_6	96%	2.3	8.8	19.7
$C_6H_5CF_3$	90%	3.2	5.2	16.8
1,2-$F_2C_6H_4$	92%	2.6	6.9	18.2
CH_3CN	< 5%	NA	NA	NA

Figure B47. Solvent screen (single run) for the polymerization of styrene (**2b**) in the presence of **1b** with accompanying yield, dispersity, and molecular weight data.

3.5.10 Theoretical Studies:

3.5.10.1 Methods

The geometry optimizations of the ground states of the neutral molecules were performed using *Turbomole*,[2] and the Density Functional Theory (DFT) B3LYP method,[3] with the def2-SVP[4,5] basis set. Initial coordinates were adopted from the single crystal X-ray structures of **1a** and **1b**. In order to access the energies of the unoccupied molecular orbitals (MOs) and to calculate the electronic absorption spectra, the time-dependent DFT (TD-DFT)[5,6] formalism was using with the same choice for the functional and basis set. Gaussian 09[7] was used for these calculations. GaussView[8] was used for visualization.

3.5.10.2 Computational results

Initiator structures. Figure 1 shows the optimized structures for **1a** and **1b**, and the MOs relevant to the discussion below. One may notice the oblong shapes of the optimized structures, deviating significantly from the I_h symmetry generally dictated by the B_{12} core.

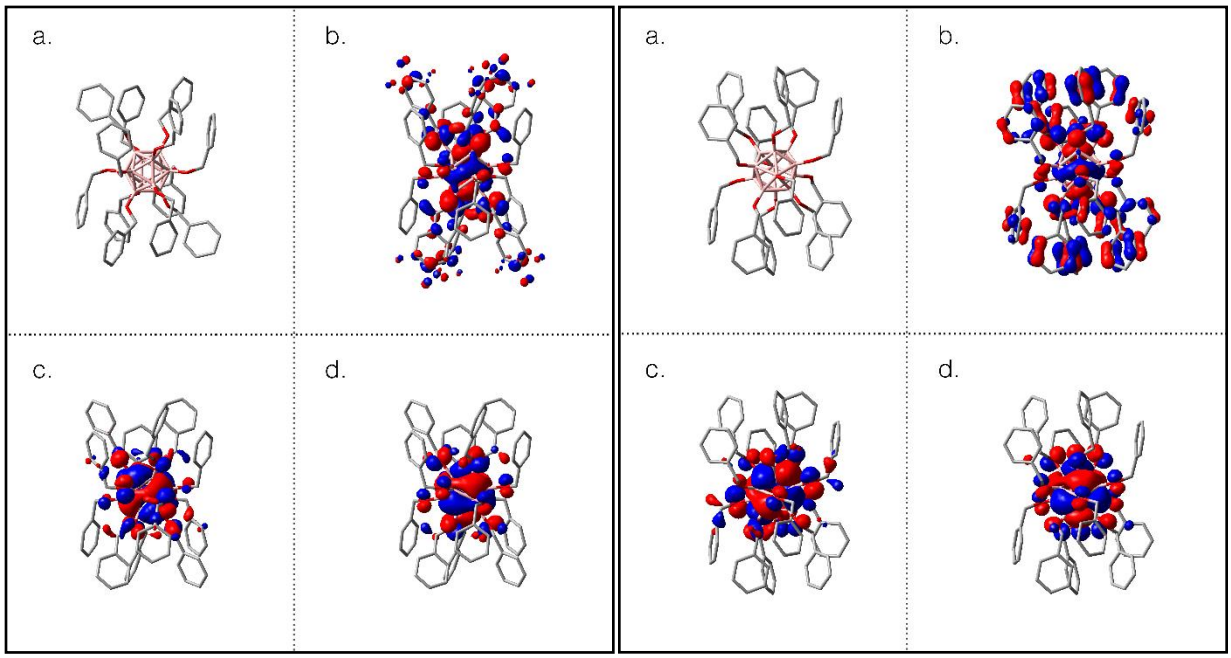

Figure B48. Optimized structures of the **1a** (left) and **1b** (right, fluorine atoms omitted for clarity) and the MOs relevant to the proposed photocatalytic mechanism. (Fig. 1, Left) a. Calculated structure, b. HOMO-15, c. HOMO, d. LUMO. (Fig1b) a. Calculated structure, b. HOMO-27, c. HOMO, d. LUMO.

Theoretical electronic spectra

The theoretical electronic spectra of **1a** and **1b** computed with TD-DFT, as described above, are shown in Tables B3 and B4, and the most relevant features are given in Tables B3-1 and B3-2 (see below). In both molecules, the HOMO to LUMO transition, and a few other transitions involving

the orbitals near the HOMO were found to have near-zero oscillator strengths (i.e. being loosely forbidden). There are very few bright transitions, which is surprising, considering the high density of states. For **1b**, the experimentally observed feature at 454 nm was assigned to the promotion of an electron from the HOMO-27 to the LUMO (both MOs are shown in Figure B40, right). The computed excitation energy was 474.07 nm (455.36 nm at M06), in a good agreement with the experiment. The HOMO-27 is the MO delocalized over the system and mainly localized on the pentafluorophenyl substituents and B-O bonds. The LUMO, on the other hand, is the MO belonging almost exclusively to the B_{12} core. Thus, the excitation corresponds to a pentafluorophenyl-to-boron cage charge transfer. For **1a**, the bright excitation involves electron transfer from the HOMO-15 to the LUMO (Figure B40, left). These MOs are very similar to those involved in the transition in **1b**. The process is again a ring-to-boron cage charge transfer. Interestingly, the calculated absorption maximum is hypsochromically shifted compared to **1b**. It is important to note that the donor orbital in **1a**, the HOMO-15, is significantly higher in energy than that of the HOMO-27 in **1b**. This is consistent with the reactivity of **1b** with a wider range of substrates than **1a**. Overall, computational characterization of the molecular and electronic structure of the photoinitiators agrees well with the experimental results, giving confidence in the performance of DFT calculations for these systems, and in theory-substantiated mechanism.

Table B3-1. TD-DFT results (at B3LYP/def2-SVP).

Initiator	Experimental Absorption (nm)	TD-DFT Absorption (nm)	Excitation Energy (eV)	Transition MOs	Energy of LUMO (eV)	Energy of Vacancy (eV)
1b	454	474.07	2.6153	HOMO-27→LUMO	-5.310	-7.925
1a	470	468.17	2.6482	HOMO-15→LUMO	-4.125	-6.773

Table B3-2. TD-DFT results (at M06/def2-SVP).

Initiator	Experimental Absorption (nm)	TD-DFT Absorption (nm)	Excitation Energy (eV)	Transition MOs	Energy of LUMO (eV)	Energy of Vacancy (eV)
1b	454	455.36	2.7228	HOMO-27→LUMO	-5.711	-8.434
1a	470	452.66	2.7390	HOMO-15→LUMO	-4.485	-7.224

Polymerization mechanism. Experimentally, the initiator is irradiated with blue LED light at 450 nm in the presence of monomer. In order to rule out the possibility of the styrene molecule undergoing the excitation at this wavelength, we calculated its absorption spectrum and found that the lowest energy bright excitation would occur at much higher energies, significantly blue-shifted from the 450 nm light source. Additionally, if styrene excitation initiated the polymerization, the reaction would proceed in the absence of **1a** or **1b**. This control experiment was performed and, as expected, no polymer was observed. Therefore, we hypothesize that the mechanism of initiation involves the electronic photo-excitation of the initiator **1a**/**1b**, resulting in the creation of a low-lying vacancy in the valence MO manifold. The hole then accepts an electron from the HOMO of the styrene monomer, producing the stable radical anion of **1a**/**1b**; the styrene radical-cation then propagates to form polymer. This oxidation process is energetically favorable, and contributes to the driving force behind electron transfer to the initiator.

Initiator tuning. Since the proposed mechanism involves hole generation in a low-lying ring-based orbital on the initiator, followed by electron transfer from the styrene monomer to that hole, the critical component of the catalytic functional is the proper positioning of the hole with respect to the HOMO of the monomer. Thus, the MO of the initiator from which the initial excitation occurs is the one to be tuned through the nature of the ligands in order to provide a good match for the HOMO of the monomer of interest. The nature and energy of the LUMO of the initiator is less

easily manipulated, since the LUMO is centered on the B_{12} core. Therefore, when the donor orbital is modulated in energy, the excitation energy will shift, possibly requiring a different light source to initiate the reaction.

Initiators **1a** and **1b**, as well as representative styrenes, were examined to further investigate this design opportunity. Four styrene derivatives were considered: 4-methoxystyrene (**2a**), styrene (**2b**), 4-methylstyrene (**2c**) and 4-fluorostyrene (**2e**). These molecules differ in the energies of the HOMO (Figure B41). All of the four styrene derivatives could be polymerized in the presence of **1b** under blue LED irradiation under the same conditions. With **1a**, under the same conditions, **2a** was polymerized, albeit in low yields. We compared the energy levels of the substrates and photoinitiators, and found a reasonable explanation: the HOMO energy of styrene and its derivatives decreases as follows: **2a** > **2c** > **2e** >**2b**, spreading over ca 0.5 eV, whereas the energy of vacancy site of **1b** and **1a** differ by ca. 1.2 eV. Therefore, the driving force for monomer oxidation should decrease in the order of **2a**, **2c**, **2e**, **2b**, and the electron affinity of the hole is higher in **1b** than in **1a**. Hence, only the monomer with the highest HOMO energy, **2a**, could

transfer an electron to vacancy site in **1a**, while for **1b** all four substrates are polymerized efficiently.

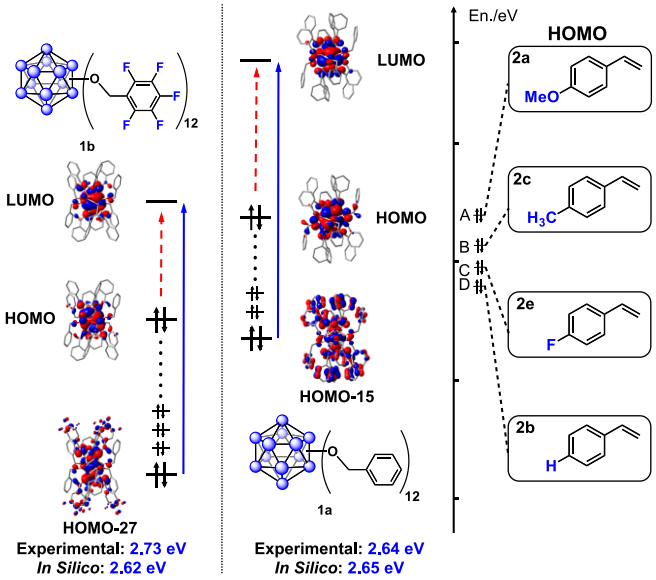

Figure B49. Depiction of the relative energy levels of initiators **1a** and **1b** with respect to the HOMO levels of monomers **2a**, **2b**, **2c**, **2e**. The schematic shows forbidden electronic transitions within the cluster core for both **1a** and **1b**, as well as the allowed (and experimentally measured) transitions (454nm and 470nm, **1b** and **1a**, respectively) from low-lying HOMO levels to a cluster-based LUMOs that give rise to monomer oxidation.

Energy calculations for relevant molecular orbitals in **1a**, **1b**, and monomers **2a**, **2b**, **2c**, and **2e** using both B3LYP/def2-SVP and M06/def2-SVP.

M06_1a

Ground State MO:

MO#357 eigenvalue = -.2654934 H = -7.224 eV

HOMO#372 eigenvalue = -.2255475 H = -6.137 eV

B3LYP_1a

Ground State MO:

MO#357 eigenvalue = -0.248912 H = -6.77324eV

HOMO#372 eigenvalue = -0.208523 H = -5.674 eV

M06_2a, 2b, 2c, 2e

Ground State MO:

2a HOMO: -0.223699 H = -6.087 eV

2b HOMO: -0.235116 H = -6.398 eV

2c HOMO: -0.241813 H = -6.580 eV

2e HOMO: -0.243277 H = -6.620 eV

B3LYP_2a, 2b, 2c, 2e

Ground State MO:

2a HOMO: -0.206900 H = -5.630 eV

2b HOMO: -0.219830 H = -5.982 eV

2c HOMO: -0.227429 H = -6.189 eV

2e HOMO: -0.227245 H = -6.184 eV

B3LYP_1b

Ground State MO:

MO#583 eigenvalue=-.3006032 H = -8.180eV

MO#584 eigenvalue=-.2993478 H = -8.146eV

MO#585 eigenvalue=-.2912243 H = -7.925eV

MO#586 eigenvalue=-.2901954 H = -7.897eV

HOMO#612 eigenvalue=-0.245620 H = -6.684 eV

M06_1b

Ground State MO:

MO#583 eigenvalue=-.3197782 H = -8.702 eV

MO#584 eigenvalue=-.3175671 H = -8.641 eV

MO#585 eigenvalue=-.3099336 H = -8.434 eV

MO#586 eigenvalue=-.3086511 H = -8.399 eV

HOMO#612 eigenvalue=-.2617867 H = -7.124 eV

Full Calculated Electronic Spectrum:

Two different computational analyses were performed to calculate additional probable transitions within initiators **1a** and **1b**. As shown above, the results using either B3LYP or M06 functionals with the def2-SVP basis set closely reproduced relevant excitations to monomer initiation.

Table B3. Probable electronic transitions within **1a** and **1b** using B3LYP/def2-SVP.

1a	**(B3LYP / def2-SVP)**		
	Excitation Energy / eV	**Absorption / nm**	**Transition Probability**
Excited State 4	2.2742	545.18	0.0138
Excited State 5	2.2754	544.9	0.0138
Excited State 10	2.4149	513.42	0.069
Excited State 16	2.5821	480.16	0.0428
Excited State 17	2.5825	480.09	0.0428
Excited State 18	2.6482	468.17	0.1275
Excited State 27	2.7279	454.5	0.0381
Excited State 28	2.7287	454.38	0.0382
Excited State 36	3.634	341.18	0.2726
Excited State 37	3.8708	320.3	0.0225
Excited State 38	3.872	320.21	0.0228

1b	**(B3LYP/ def2-SVP)**		
	Excitation Energy / eV	**Absorption / nm**	**Transition Probability**
Excited State 23	2.2506	550.89	0.0206
Excited State 26	2.4187	512.6	0.016
Excited State 28	2.5084	494.28	0.0986
Excited State 29	2.5713	482.18	0.0722

Excited State 30	2.6153	474.07	0.1576
Excited State 32	3.0214	410.36	0.0122
Excited State 34	3.361	368.89	0.0653
Excited State 35	3.3707	367.83	0.0844
Excited State 37	3.6992	335.17	0.0312
Excited State 38	3.7377	331.71	0.0485

Table B4. Probable transitions in **1a** and **1b** computed using M06/def2-SVP.

1a	**(M06 / def2-SVP)**		
	Excitation Energy / eV	**Absorption / nm**	**Transition Probability**
Excited State 4	2.3628	524.74	0.0131
Excited State 5	2.3649	524.26	0.013
Excited State 10	2.51	493.95	0.0851
Excited State 16	2.6625	465.67	0.0529
Excited State 17	2.6635	465.49	0.053
Excited State 18	2.739	452.66	0.1235
Excited State 26	2.8195	439.73	0.0248
Excited State 27	2.8201	439.65	0.0249
Excited State 36	3.7614	329.62	0.2485
Excited State 37	3.9588	313.19	0.0221
Excited State 38	3.9597	313.12	0.0221

1b	**(M06 / def2-SVP)**		
	Excitation Energy / eV	**Absorption / nm**	**Transition Probability**
Excited State 12	2.0612	601.5	0.0751
Excited State 18	2.2581	549.07	0.0456
Excited State 28	2.6378	470.03	0.0431

Excited State 29	2.6388	469.85	0.0434
Excited State 30	2.7228	455.36	0.1733
Excited State 36	3.5637	347.91	0.0158
Excited State 37	3.7697	328.9	0.0454
Excited State 38	3.7718	328.71	0.0454

3.5.11 Fluorescence Spectroscopy:

Steady-state fluorescence profiles were obtained with 457.9 nm excitation (Coherent Innova 70 argon-ion laser). Luminescence was collected using an optical fiber optic and directed to a Melles Griot 13 FOS 200 spectrometer. A 457.9 nm long-pass cutoff filter was used to reject excitation light.

Fluorescence decay measurements were performed as previously described.[9,10] Briefly, a mode-locked Nd:YAG laser (Vanguard 2000-HM532; Spectra-Physic) generated ~10ps pulses which were then regeneratively amplified (Continuum) and frequency tripled to produce 355 nm sample excitation. Fluorescence was collected with a single lens and focused tonto the entrance slit of a spectrograph (Acton Research Corp SpectraPro 275). A 355 nm dielectric mirror was placed before the slit of the spectrograph to reject scattered excitation light. We observed fluorescence in two different wavelength regions: spectrograph center wavelengths of 420 or 600 nm were chosen to characterize the decay kinetics of the two fluorophores. Fluorescence decays were collected using a streak camera (C5680; Hamamatsu Photonics) in photon counting mode over a 50 ns window.

Based on ^{1}H, ^{13}C, and ^{19}F NMR studies, **1b** is the only observable species in solution, so it is likely that both observed emissions are associated with neutral **1b**. The first (420 nm) emission likely arises from the excitation of the perfluoroaromatic rings situated on the periphery of the cluster; the strong emission and longer lifetime (~4ns) are consistent with that of fluorinated aromatic

systems.[11] The second, weaker emission at 600 nm, which exhibited solvent-dependent intensity and lifetime, may be associated with the cluster core.

The reduction potential of photo-excited **1b** was approximated[12] using in Eq. 1,

$$E^{*}_{red}{}^{0} = E_{red}{}^{0} + E_{0,0} \quad (1)$$

where $E_{red}{}^{0}$ represents the ground state 0/1- redox couple of **1b** and $E_{0,0}$ represents the wavelength of the onset of fluorescence (550 nm). Redox values are initially calculated based on the Fc/Fc^{+} reference and converted to SCE based on values reported by Connelly and Geiger,[13] where the formal potential of Fc/Fc^{+} referenced to SCE in CH_3CN with $[NBu_4][PF_6]$ as the supporting electrolyte is 0.40 V.

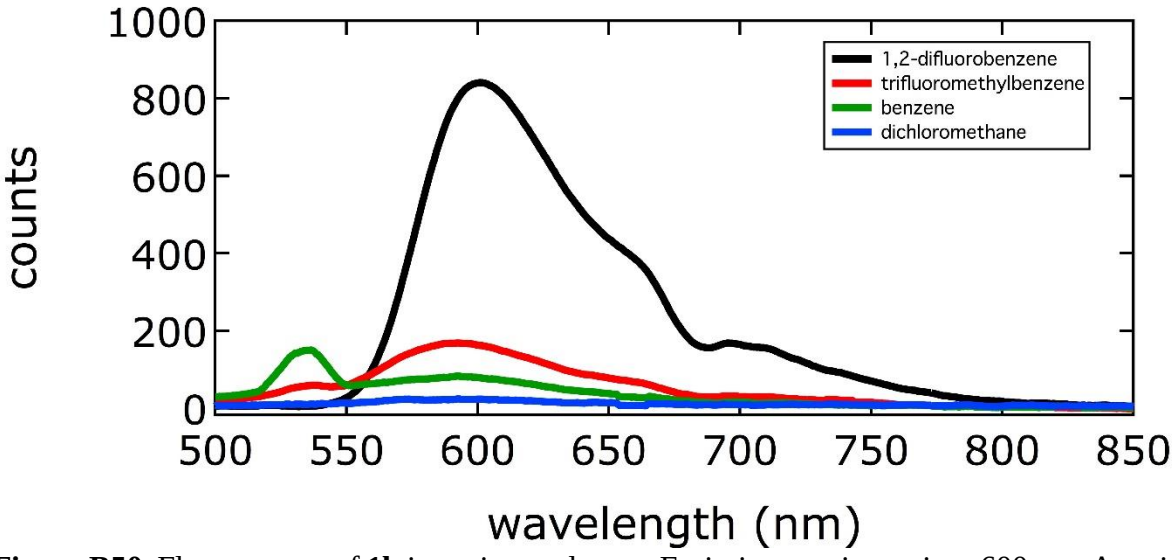

Figure B50. Fluorescence of **1b** in various solvents. Emission maximum is at 600 nm. Acquisition time was 1 s for 1,2-difluorobenzene and 2.5 s for all others.

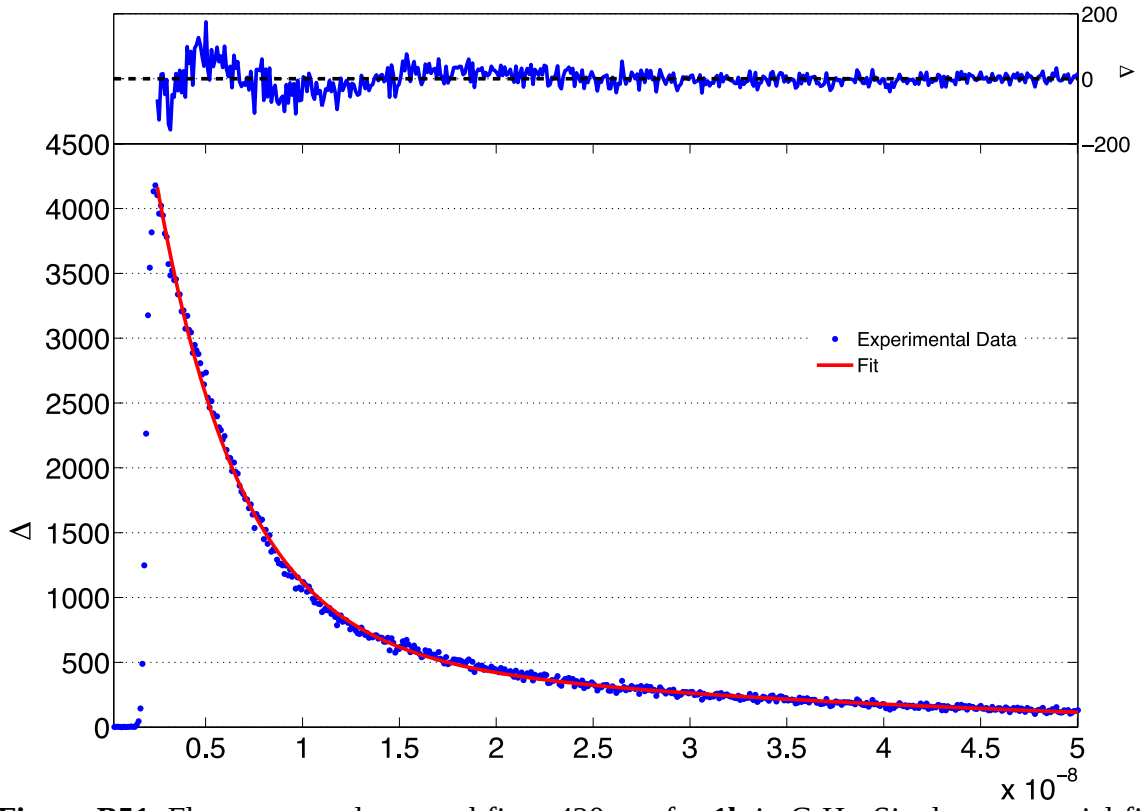

Figure B51. Fluorescence decay and fit at 420 nm for **1b** in C_6H_6. Single exponential fit gave a lifetime of 5 ns.

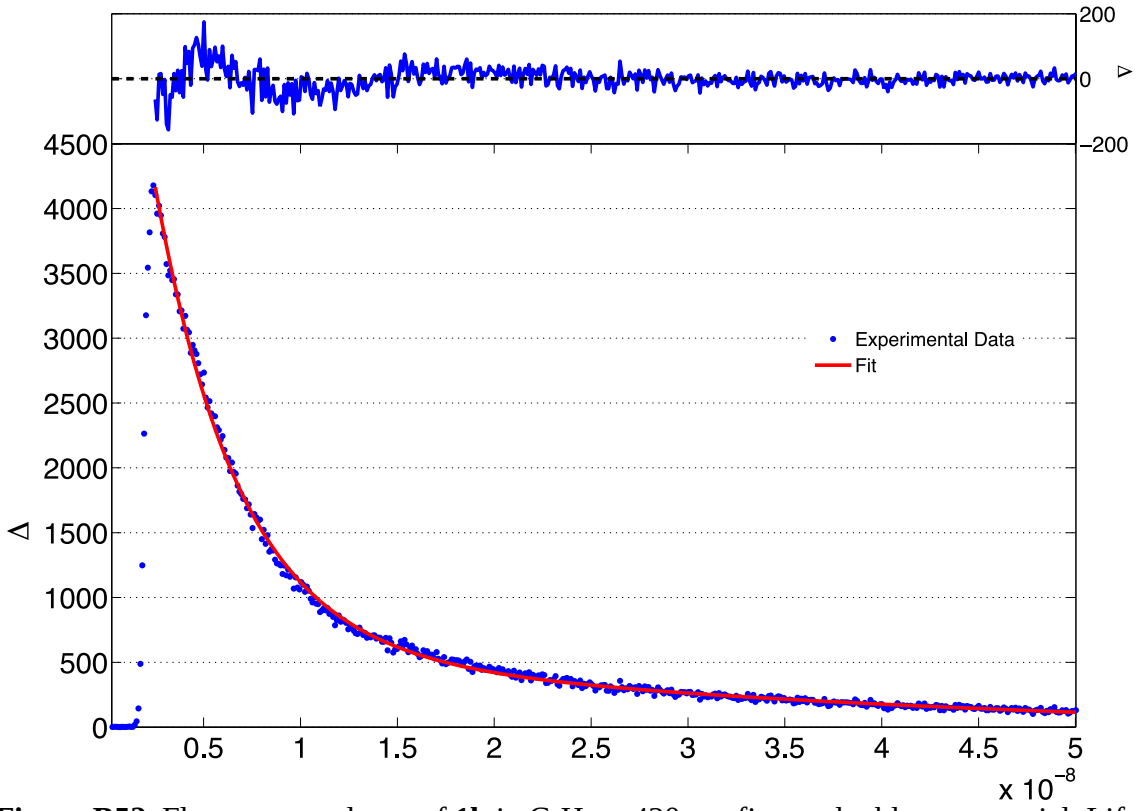

Figure B52. Fluorescence decay of **1b** in C_6H_6 at 420 nm fit to a double exponential. Lifetimes of the two species are 4 and 40 ns.

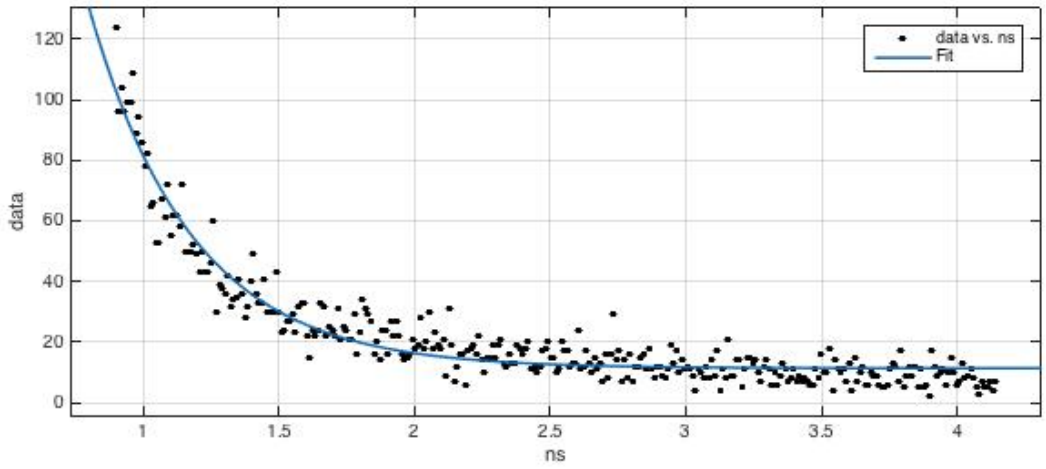

Figure B53. Fluorescence decay of **1b** in 1,2-dichlorobenzene at 600 nm. Single exponential fit gave a lifetime of 380 ps.

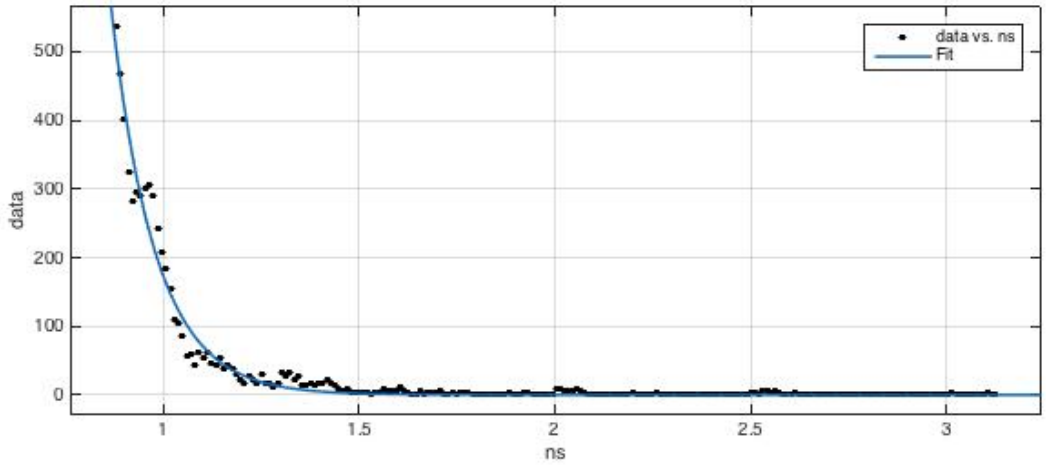

Figure B54. Fluorescence decay of **1b** in acetonitrile at 600 nm. Single exponential fit gave a lifetime of 110 ps.

3.5.12 Appendix B References

(1) a) Farha, O. K.; Julius, R. L.; Lee, M. W.; Huertas, R. E.; Knobler, C. B.; Hawthorne, M. F. *J. Am. Chem. Soc.* **2005**, *127*, 18243-18251; b) Bayer, M. J.; Hawthorne, M. F. *Inorg. Chem.* **2004**, *43*, 2018-2020.

(2) Turbomole, V6.3 2011, a development of University of Karlsruhe and Forschungszentrum Karlsruhe GmbH, 1989−2007, Turbomole GmbH, since 2007; http://www.turbomole.com.

(3) R.G. Parr, W. Yang, Density-Functional Theory of Atoms and Molecules, Oxford Univ. Press, Oxford (1989); A. D. Becke, J. Chem. Phys., 98, 1993, 5648.

(4) Weigend, F; Ahlrichs, R. *Phys. Chem. Chem. Phys.* **2005**, *7*, 3297-305.

(5) Weigend, F. *Phys. Chem. Chem. Phys.*, **2006**, *8*, 1057-65.

(6) Bauernschmitt, R.; Ahlrichs, R. *Chem. Phys. Lett.* **1996**, *256*, 454-64.

(7) Gaussian 09, Revision A.1, M. J. Frisch, G. W. Trucks, H. B. Schlegel, G. E. Scuseria, M. A. Robb, J. R. Cheeseman, G. Scalmani, V. Barone, B. Mennucci, G. A. Petersson, H. Nakatsuji, M. Caricato, X. Li, H. P. Hratchian, A. F. Izmaylov, J. Bloino, G. Zheng, J. L. Sonnenberg, M. Hada, M. Ehara, K. Toyota, R. Fukuda, J. Hasegawa, M. Ishida, T. Nakajima, Y. Honda, O. Kitao, H. Nakai, T. Vreven, J. A. Montgomery, Jr., J. E. Peralta, F. Ogliaro, M. Bearpark, J. J. Heyd, E. Brothers, K. N. Kudin, V. N. Staroverov, R. Kobayashi, J. Normand, K. Raghavachari, A. Rendell, J. C. Burant, S. S. Iyengar, J. Tomasi, M. Cossi, N. Rega, J. M. Millam, M. Klene, J. E. Knox, J. B. Cross, V. Bakken, C. Adamo, J. Jaramillo, R. Gomperts, R. E. Stratmann, O. Yazyev, A. J. Austin, R. Cammi, C. Pomelli, J. W. Ochterski, R. L. Martin, K. Morokuma, V. G. Zakrzewski, G. A. Voth, P. Salvador, J. J. Dannenberg, S. Dapprich, A. D. Daniels, O. Farkas, J. B.

Foresman, J. V. Ortiz, J. Cioslowski, and D. J. Fox, Gaussian, Inc., Wallingford CT, 2009.

(8) GaussView, Version 5, Roy Dennington, Todd Keith, and John Millam, Semichem Inc., Shawnee Mission, KS, 2009.

(9) Kimura, T.; Lee, J. C.; Gray, H. B.; Winkler, J. R. *Proc. Natl. Acad. Sci.* **2009**, *106* (19), 7834.

(10) Yamada, S.; Ford, N. D. B.; Keller, G. E.; Ford, W. C.; Gray, H. B.; Winkler, J. R. *Proc. Natl. Acad.Sci.* **2013**, *110* (5), 1606.

(11) Zhicheng, Z.; Ito, Y.; Washio, M.; Kobayashi, H.; Tagawa, S.; Tabata, Y. *Radiat. Phys. Chem.* **1986**, *28*, 65-68.

(12) Gray, H. B.; Maverick, A. W. *Science* **1981**, *214*, 1201-1205.

(13) Connelly, N. G.; Geiger, W. E. *Chem. Rev.* **1996**, *96*, 877-910.

Chapter 4

Carborane RAFT Agents as Tunable and Functional Molecular Probes for Polymer Materials

Reproduced with permission from: Messina, M. S.; Graefe, C. T.; Chong, P.; Ebrahim, O. M.; Pathuri, R. S.; Bernier, N. A.; Mills, H. A.; Rheingold, A. L.; Frontiera, R. R.; Maynard, H. D.; Spokoyny, A. M. "Carborane RAFT Agents as Tunable and Functional Molecular Probes for Polymer Materials" *Polym. Chem.* **2019**, *10*, *1660*-1667.

4.1 Introduction

There exist myriad molecular tools employed at the interface of polymer chemistry and biology to help elucidate the structure and/or functions of molecules. These tools come in the form of small molecule probes, affinity labels, and spectroscopic handles frequently applied to polymer chain ends.[1–10] Conjugation of such tools to polymer end groups is typically performed through rational design of polymer initiators or chain transfer agents, which are retained on the ends of polymers made from controlled polymerization processes.[11–19] Specifically, RAFT polymerization is a versatile method used to obtain polymers of uniform molecular weight.[20–23] This method has gained widespread attention due to its broad monomer scope, solvent compatibility, and ease of constructing well-defined macromolecular architectures, such as block co-polymers and brush polymers.[22,24] Key to this method is the use of the RAFT agent (Figure 4-1).[25–28]

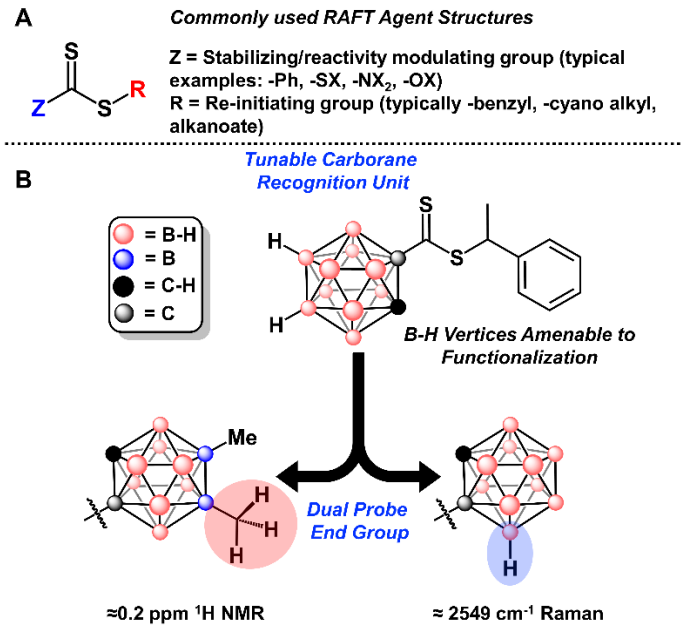

Figure 4-1. (A) Structures of frequently utilized chain transfer agents in RAFT polymerization. (B) Introduction of carborane RAFT agents as multi-purpose functional molecular probes and affinity label.

The RAFT agent confers control over polymerization processes through a reversible radical chain transfer reaction to and from the thiocarbonyl moiety. By greatly reducing the amount of active radicals capable of polymerization, thereby decreasing unwanted termination pathways, polymers with narrow molecular weight distributions are formed.[26,27] RAFT agents are comprised of thiocarbonylthio compounds, common classes of which include dithioesters, xanthates, trithiocarbonates, and dithiocarbamates (Figure 4-1 A).[26,27,29] The RAFT agent structure can be conceptually split into two parts wherein the "Z" group modulates the rates of addition and fragmentation during reversible chain transfer on the thiocarbonyl carbon and determines the stability of the intermediate radical, and the "R" group functions to re-initiate polymerization of another monomer upon homolytic cleavage from the RAFT agent structure (Figure 4-1 A).[26,30] Both the R and Z groups are incorporated on the polymer chain end upon termination. As a result, the structure of the RAFT agent is often tailored to serve as a functional handle and/or probe for characterization.[2,5,31,32] Some examples of functional handles include the use of carboxylic acid, succimidyl ester, azide, maleimide, aminooxy, or pyridyl disulfide functionalized RAFT agents, which serve as conjugation sites for molecular cargo such as fluorescence tags, affinity labels, and biomolecules.[2,7,14,15,33–42] Trimethylsilyl (TMS) substituted RAFT agents have also served as spectroscopic handles in the determination of polymer molecular weight via ^{1}H NMR spectroscopy.[5]

While these functional RAFT agents are able to perform one or two tasks, tunable and stable RAFT agents capable of performing multiple tasks simultaneously while retaining modularity are rare. We envisaged *ortho*-carborane functionalized RAFT agents as being ideally suited to interface many different applications through their ability to act as spectroscopic probes, easily modifiable molecular conjugation sites, and as affinity labels. Icosahedral carboranes ($C_2B_{10}H_{12}$) are boron-rich molecules which exhibit 3-dimensional (3D) electron delocalization non-uniformly due to the addition of carbon atoms within the cluster.[43,44] Carboranes are highly tunable, boasting multiple B–H vertices which are amenable to functionalization with a wide array of substituents through well-established methodology.[45–52] Due to the unique electronic character of *ortho*-carborane, substituents attached to boron at the vertices most distal to the carbon atoms experience a strong electronic shielding effect which results in a low chemical shift (methyl C–*H* $\approx$ 0.2 ppm) in the ^{1}H NMR spectrum (Figure 4-1 B).[52–54] The hydrophobic nature of carboranes allows them to bind into hydrophobic spaces within proteins and cell membranes, adding potential for their use as affinity labels.[55–58] Additionally, the B–H vibration resonates at ~2350–2600 cm^{-1}, a silent region in Raman spectra of biological milieu, and unique amongst other commonly used Raman tags, such as alkynes and nitriles, which vibrate at ~2000–2300 cm^{-1} (Figure 4-1 B).[59] Herein, we present a new class of functional RAFT agents containing an *ortho*-carborane scaffold. We demonstrate their ability to serve as tunable Raman active molecular probes (Figure 4-1 B), spectroscopic handles for determination of molecular weight via ^{1}H NMR spectroscopy, and as affinity labels through β-cyclodextrin binding as judged by isothermal titration calorimetry (ITC) studies.

4.2 Results and Discussion

4.2.1 Synthesis of RAFT Agents, Polymerization, and their use as 1H NMR Spectroscopy Handles

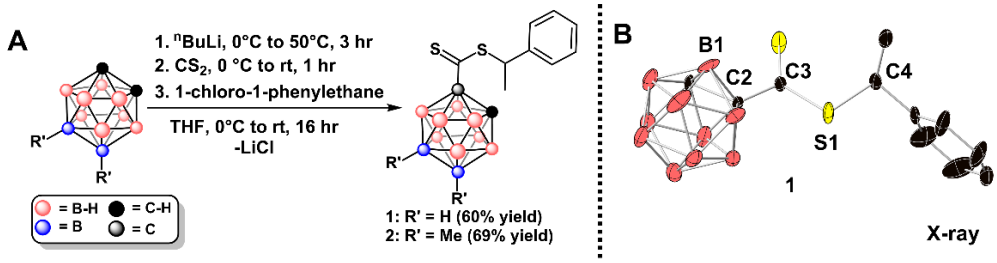

Figure 4-2. (A) Synthetic scheme for the preparation of carborane RAFT agents **1** and **2**. (B) Solid-state crystal structure of **1**, hydrogen atoms omitted for clarity.

We developed a facile and scalable synthetic method towards carborane-functionalized RAFT agents (Figure 4-2 A). Treatment of a lithiated *o*-carborane slurry in tetrahydrofuran (THF) with carbon disulfide (CS_2) at 0 °C resulted in the formation of a dark red mixture indicating the formation of a sulfide anion which was trapped upon addition of 1-chloro-1-phenylethane to form **1** (Figure 4-2 A). Following column chromatography and crystallization from a saturated solution of CH_2Cl_2 layered with pentane, **1** was isolated as an orange crystalline solid in 60% yield. Single crystals of **1** were grown and subjected to X-ray crystallographic analysis confirming the structural identity of this compound (Figure 4-2 B). We employed **1** in our preliminary polymerization attempts using styrene as the model substrate due to the monomer similarity with the R-group of **1** (Figure 4-3 A).[26]

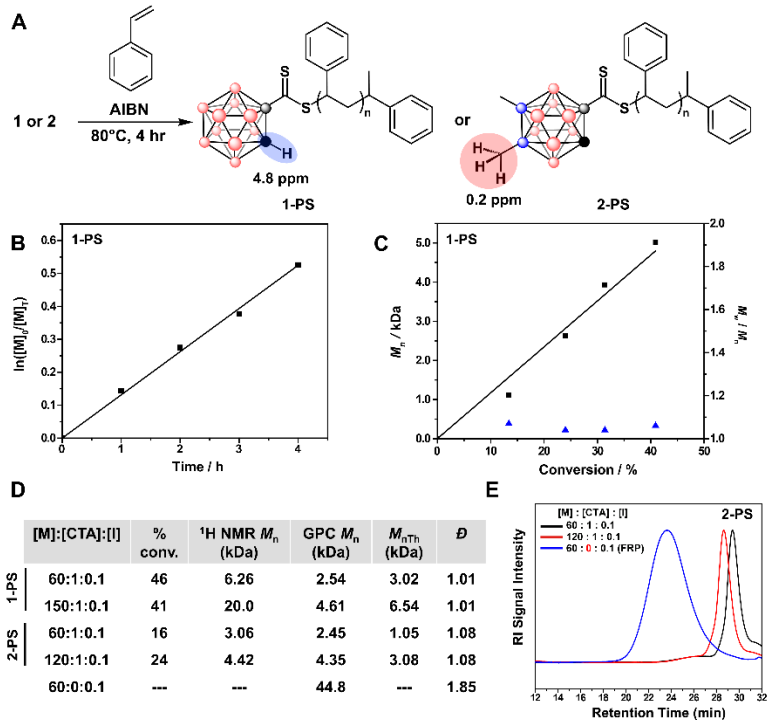

	[M]:[CTA]:[I]	% conv.	^{1}H NMR M_n (kDa)	GPC M_n (kDa)	M_{nTh} (kDa)	$Đ$
1-PS	60:1:0.1	46	6.26	2.54	3.02	1.01
1-PS	150:1:0.1	41	20.0	4.61	6.54	1.01
2-PS	60:1:0.1	16	3.06	2.45	1.05	1.08
2-PS	120:1:0.1	24	4.42	4.35	3.08	1.08
	60:0:0.1	---	---	44.8	---	1.85

Figure 4-3. (A) Thermal polymerization of styrene utilizing either **1** (produces polymer **1-PS**) or **2** (produces polymer **2-PS**) as the RAFT agent. (B) Kinetic analysis for **1-PS** polymerization exhibits first-order kinetics. (C) Evolution of M_n as a function of monomer conversion for **1-PS** polymerization. (D) Table comparing molecular weight determined by ^{1}H NMR spectroscopy and GPC of polymerizations using **1** as the RAFT agent to produce **1-PS** or **2** to produce **2-PS**. Polymerization performed in bulk styrene solution. (E) GPC curves of **2-PS** depicting experiments performed with different equivalents of monomer to CTA (red and black traces) as well as a control in which no CTA is added (blue trace). Polymerization was carried out in bulk styrene solution and stopped after 4 hours.

Polymerization of styrene using 2,2′-azobisisobutyronitrile (AIBN) as the thermal initiator and 1 resulted in nearly monodisperse ($Đ$ = 1.07–1.15) polystyrene (**1-PS**), as determined by gel permeation chromatography (GPC), the length of which was controlled by varying the loading of

1 (Figure 4-3 A, see Figure C11 for GPC traces). Polymerization using **1** exhibits first order kinetics and a linear evolution of number average molecular weight (M_n) versus conversion, highlighting the controlled nature of the polymerization and demonstrating the utility of carborane-based CTAs in RAFT processes (Figure 4-3 B and C). Control experiments in the absence of **1** resulted in highly disperse ($Đ$ = 3.00) polymers indicating loss of control over the polymerization process as expected (see Figure C11). The cage C–H proton of **1** exhibits a diagnostic chemical shift (~4.8 ppm, Figure 3 A) which does not overlap with any polystyrene ^{1}H NMR resonances. To investigate the potential usefulness of carboranes to act as spectroscopic probes to accurately determine M_n, we used this highly diagnostic resonance to determine the M_n via end-group analysis using ^{1}H NMR spectroscopy. Integration of the carborane C–H proton with the aryl protons of polystyrene resulted in M_n readings which deviated drastically with the M_n values determined by GPC with a multi-angle light scattering (MALS) detector (Figure 4-3 D, see Appendix C for dn/dc values). It is possible to lose the carborane due to its location at the Z group, which would also increase the apparent molecular weight by NMR. However we were unable to find appropriate synthetic conditions to place the carborane at the R group (data not shown). But more likely this deviation is due to the inherent broadness of the carborane cage C–H proton resonance which leads to a higher inaccuracy in M_n determination as the polymer length increases, as is typical for most end groups used for end-group analysis (Figure 4-3 D, **1-PS**; Figure C12). Additionally, the resonance at 4.8 ppm is not located in a generally silent region in most polymer samples, which would eliminate its use as a spectroscopic handle for other types of polymers.

To bypass these complications, we synthesized a carborane derivative bearing methyl groups on the B(9) and B(12) vertices (opposite to those of the carbon atoms) to take advantage of the electronic shielding effect of substituents attached on the B(9) and B(12) vertices, which results

in upfield chemical shifts of exohedral methyl proton resonances in ^{1}H NMR spectra and sharper signals.[52,53,60] Synthesis of **2** was carried out in a similar manner to that of **1** (Figure 2 A). Compound **2** was isolated as a dark orange oil in 69% yield after purification via column chromatography and removal of the benzyl chloride precursor by heating under reduced pressure (100 mTorr, 95 °C; Figure 4-2 A; see Appendix C for detailed synthetic procedures). Indeed, the proton signals of the B(9) and B(12) methyl substituents resonate in a characteristic region of the ^{1}H NMR spectrum (~0.2 ppm, see Appendix C). This provides a unique spectroscopic handle as the protons are sufficiently separated from resonances, which may overlap and make for inaccurate M_n determination via end-group analysis.

Polymerization of a bulk solution of styrene in the presence of **2** and AIBN produced well-defined ($Đ$ = 1.08, Figure 4-3 D and E) polystyrene (**2-PS**) bearing **2** on the chain end as determined by ^{1}H NMR after polymer purification via precipitation from a cold (0 °C) methanol solution (see Appendix C for characterization of all polymers). To test the accuracy of this method, we made polystyrene using different equivalents of **2** (2.45 and 4.35 kDa, Figure 4-3 D and E), determined their M_n values via end-group analysis using ^{1}H NMR spectroscopy, and compared the results with those of molecular weight readings measured via GPC. In all instances, the M_n values measured with GPC matched closely with the molecular weight determined by ^{1}H NMR spectroscopy (Figure 4-3 D, E, see Figure C14, C16, C19, and C22 for example of calculations).

We next sought to determine the applicability of **2** with a range of monomers. Matching the "R" and "Z" groups of the RAFT agent to the monomer is vital for controlled RAFT polymerization. As this is the first example of a carborane RAFT agent, we sought to match the R-group with the appropriate monomer classes. We tested *N*-isopropyl acrylamide, methyl acrylate, and 4-chlorostyrene monomers since the reactivity of the benzyl R-group on **2** matches

with those monomers.[26] Polymerization of 4-chlorostyrene and *N*-isopropyl acrylamide under thermal polymerization conditions in the presence of **2** and AIBN produced polymers with narrow molecular weight distributions, but with high molecular weight shoulders in the GPC spectra, indicating some polymer coupling (**2-pNIPAAm** and **2-(4-Cl)-PS**, Figure 4-4A and B).

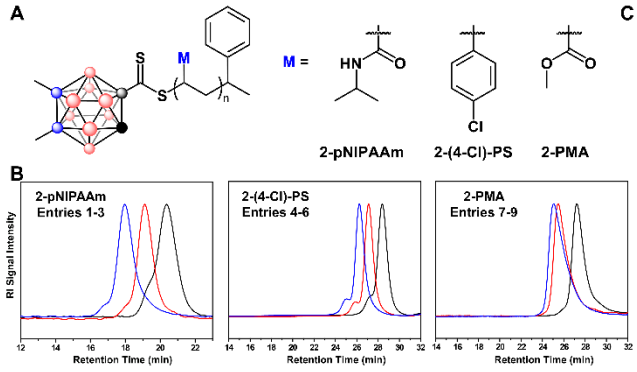

C

	Entry	[M]:[CTA]:[I]	Solvent[a]	% conv	^{1}H NMR M_n (kDa)	GPC M_n (kDa)	M_{nTh} (kDa)[b]	$Đ$
2-pNIPAAm	1	30:1:0.3	PhMe	96	5.84	5.92	3.60	1.10
	2	120:1:0.3	PhMe	93	12.5	11.5	12.9	1.06
	3	180:1:0.3	PhMe	98	20.6	21.3	20.4	1.09
2-(4-Cl)-PS	4	60:1:0.3	Bulk	81	10.7	9.97	7.07	1.08
	5	120:1:0.3	Bulk	56	19.9	18.4	9.67	1.07
	6	180:1:0.3	Bulk	47	27.9	26.6	12.1	1.08
2-PMA	7	60:1:0.3	Bulk	91	11.9	11.4	5.02	1.05
	8	180:1:0.3	Bulk	76	26.7	26.0	12.4	1.03
	9	240:1:0.3	Bulk	74	33.3	29.5	15.5	1.07
2-PS	10	60:1:0.3	EtOAc	33	3.34	3.05	2.18	1.12
	11	60:1:0.3	C_6H_6	43	3.52	3.49	2.83	1.19
	12	60:1:0.3	PhMe	46	4.45	3.52	3.04	1.21
2-PMA	13	60:1:0.3	EtOAc	82	4.95	6.35	4.53	1.13
	14	60:1:0.3	PhMe	82	6.25	5.60	4.53	1.20

Figure 4-4. (A) Polymerization of methyl acrylate, 4-chlorostyrene, and *N*-isopropylacrylamide. (B) GPC traces for **2-pNIPAAm**, **2-(4-Cl)-PS**, and **2-PMA** at different monomer to CTA ratios. (C) Table depicting results from polymerization experiments performed in bulk reaction conditions and in solvent. [a]Polymerizations were performed in 2 M solvent conditions. [b]Theoretical M_n values were calculated *via* ^{1}H NMR using tetralin as an internal standard.

Polymerization of methyl acrylate produced monodisperse polymers containing **2** on the polymer chain ends (**2-PMA**, Figure 4-4 A–C and Figure C25). The M_n determined by ^{1}H NMR spectroscopy matches closely with the M_n determined by GPC for a range of polymer sizes (Figure 4-4 B and C). Impressively, the methyl C–H protons on carborane are readily visible on the ^{1}H NMR spectrum and are competent spectroscopic handles to accurately determine M_n even at polymer molecular weights up to 30 kDa (Figure 4-4 C, entry 9, and Figure C21). It should be noted that we observe a significant disagreement between the theoretical and observed polymer

M_n values for **2-(4-Cl)-PS** and **2-PMA** when polymerized in bulk reaction conditions (Figure 4-4 C, entries 4–9), yet the dispersities remain narrow. This is also apparent in bulk polymer kinetic experiments, which indicate a loss of control over the course of the polymerization (Figure C32). The disagreement between theoretical and observed M_n values with maintenance of low molecular weight dispersity has been observed in previous reports detailing the RAFT polymerization of acrylamides.[61,62] However, we find that polymerization in solvent (2 M) leads to better agreement between both theoretical and observed M_n values for **2-PMA** (Figure 4-4, entries 10–14). Control is also maintained over the course of polymerization in solvent in the kinetic plots (Figure C34 and C35). This demonstrates that for these monomers the polymerization should be conducted in solution rather than the bulk phase.

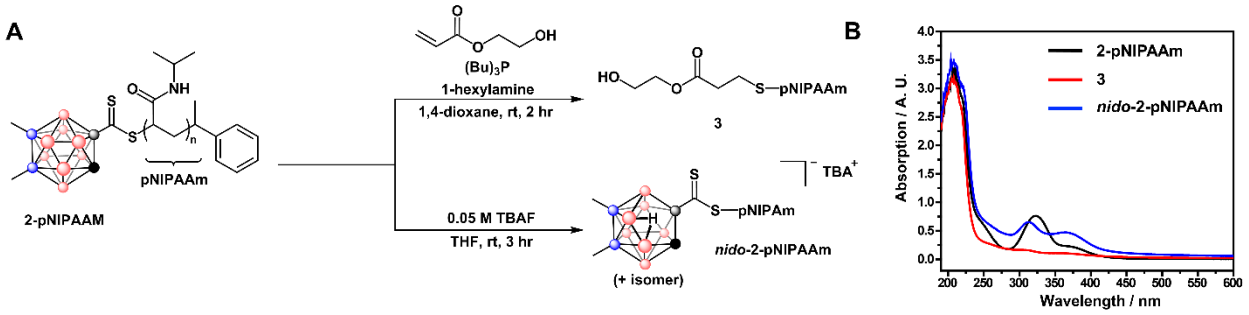

Figure 4-5. (A) Modification of carborane dithioester end-group of **pNIPAAm**. The end-group can either be removed *via* aminolysis and end-capping or the formation of *nido*-carborane can be achieved via deboronation of carborane using a 0.05 M solution of TBAF in THF. (B) The end-group modification can be followed by UV-Vis spectroscopy. The disappearance of the absorption band at 319 nm indicates the loss of the dithioester. Formation of an absorption band at 375 nm along with a shift in the absorption of the dithioester indicates deboronation of carborane.

The dithioester carborane end-group allows for a high degree of end-group functionality and tunability and can be easily removed or modified after polymerization.[32,63,64] We prepared **pNIPAAm** derivatives in which the carborane end-group was removed or deboronated (vide infra) to serve as controls for binding studies and to also investigate the properties invoked by having a *nido*-carborane terminated polymer. The carborane end-group of **2-pNIPAAm** was removed via aminolysis, thereby leaving an exposed thiol at the polymer end.[63] Despite our use of tributylphosphine to eliminate disulfide formation over the course of the deprotection reaction, we observed polymer coupling by GPC analysis (Figure C36).[65] In order to avoid disulfide formation, we introduced 2-hydroxyethylacrylate which undergoes Michael addition with the exposed thiol thereby attaching onto the end of the polymer and preventing polymer coupling (Figure 4-5 A).[66] The deprotection reaction was monitored via UV-Vis spectroscopy by the disappearance of the dithioester absorption band at ~319 nm (Figure 4-5 B). Complete removal of the carborane end-group could also be visualized by ^{1}H NMR spectroscopy after polymer purification by the disappearance of the carborane methyl proton signals at 0.2 ppm.

Deboronation is the partial degradation of the carborane cage where one of the cage boron atoms is stripped away through the use of a strong base. This leads to the formation of an anionic *nido*-carborane species $[7,8\text{-}C_2B_9H_{12}]^-$.[67] Having the monoanionic *nido*-carborane at the polymer end lends potential to interesting self-assembly properties as the polymer is rendered amphiphilic. Additionally, *nido*-carborane is used frequently to bind metal ions thereby forming metallacarboranes.[68,69] One can envisage the binding of metal ions in this system to synthesize block co-polymers and other higher order macromolecular architectures.[70] Preparation of *nido*-carborane terminated **pNIPAAm** (***nido*-2-pNIPAAm**) was carried out by stirring **2-pNIPAAm** in a solution of 0.05 M tetrabutylammonium fluoride (TBAF) in THF (Figure 4-5 A).[71] We were

unable to follow deboronation by ^{11}B NMR or ^{13}C NMR due to the large size of the polymer relative to the carborane endgroup. However, over the course of the reaction we noticed a diagnostic resonance corresponding to the formed hydride in the ^{1}H NMR spectrum at -2.1 ppm (Figure C38). We also followed deboronation by the appearance of a new UV band at ~375 nm as well as a shift of the dithioester absorption band (Figure 4-5 B).

4.2.2 Binding studies with polymers terminated with functional carborane handles

Affinity tags such as biotin are frequently exploited within the chemical biology community in purification and detection strategies such as in tandem orthogonal proteolysis-activity based protein profiling (TOP-ABPP) and enzyme-linked immunosorbent assay (ELISA).[72,73] To probe the ability of carborane appended onto a polymer chain to act as an affinity tag, we investigated the binding of **2-pNIPAAm**, ***nido*-2- pNIPAAm**, and **3** to β-cyclodextrin, a cyclic molecule composed of seven α-D-glucopyranoside units. The hydrophobic inner cavity of β-cyclodextrin is well-suited for the incorporation of hydrophobic guests thereby forming host–guest inclusion complexes through non-covalent bonding interactions. Carboranes are known to form 1:1 and 2:1 inclusion complexes with β-cyclodextrin exhibiting association constants (K_a) as strong as $\approx 10^6$ M^{-1}.[74–78] Previous studies have shown this interaction as a means to solubilize carborane scaffolds in aqueous solutions and for the immobilization of biomolecules on surfaces.[79,80]

We measured binding of **2-pNIPAAm** to β-cyclodextrin via isothermal titration calorimetry (ITC) in MilliQ water. A solution of a known concentration of β-cyclodextrin was titrated into a solution of **2-pNIPAAm**. Based on the titration curve, we calculated a K_a of 9.37×10^4 M^{-1} which agrees with previous literature reports of free carborane binding in the hydrophobic

pocket of β-cyclodextrin (Figure 4-6 A). An N = 0.5 value was also calculated, which is indicative of a 2:1 binding of carborane to β-cyclodextrin. While the binding of two carborane groups into β-cyclodextrin has not been reported, it is possible that the substituents on the carborane end-group of **2-pNIPAAm** block full incorporation of one carborane unit into β-cyclodextrin thereby allowing room for a second unit to partially bind. We were unable to perform the reverse titration due a lack of solubility of **2-pNIPAAm** in water at high concentrations.

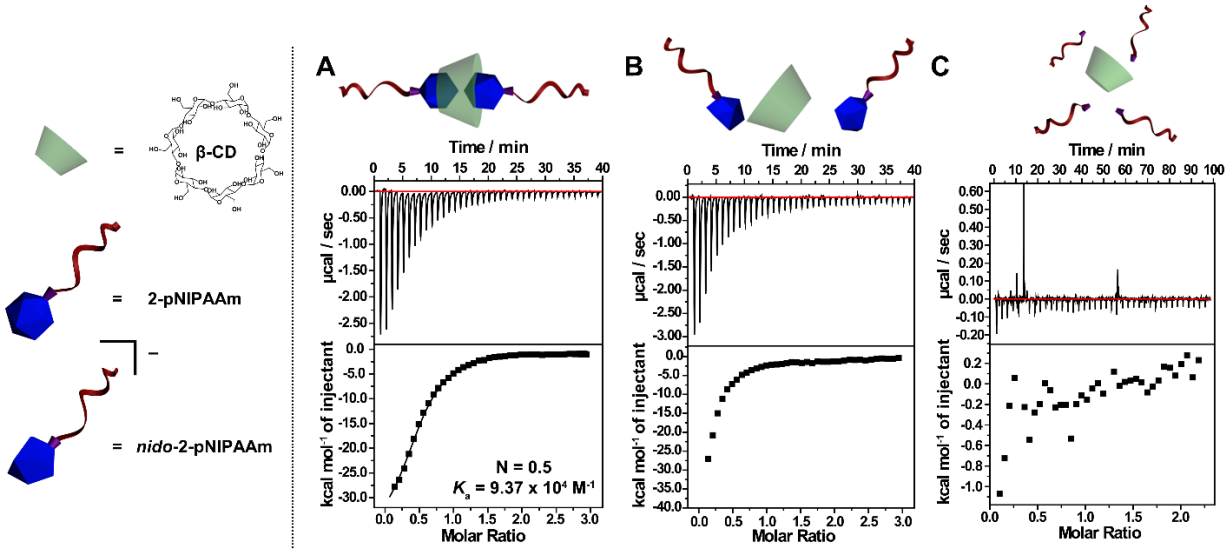

Figure 4-6. (A) ITC curve of a 0.1 mM solution of **2-pNIPAAm** titrated into a 1.06 mM β-cyclodextrin solution shows 2:1 binding (N=0.5). (B) ITC curve of ***nido*-2-pNIPAAm** shows only minimal binding (N=0.06) which can be attributed to small amounts of **2-pNIPAAm** still present in solution. The inability of ***nido*-2-pNIPAAm** to bind to β-cyclodextrin can possibly be attributed to the bulkiness of the TBA^+ counterion present on the polymer chain end. (C) ITC curve of 3 and β-cyclodextrin shows no observable binding.

We observed a negligible amount of binding (N = 0.06) when we carried out similar ITC studies with ***nido*-2-pNIPAAm** (Figure 4-6 B). While the binding of *nido*-carboranes to β-

cyclodextrin has not been studied, *nido*-carborane drug derivatives were shown to bind in the hydrophobic subpockets of the proteins carbonic anhydrase (CA) and cyclooxygenase-2 (COX-2).[81,82] It is likely that in this instance, the bulkiness of the TBA^+ counterion does not allow for binding of ***nido*-2-pNIPAAm** in the hydrophobic β-cyclodextrin pocket. Likewise, compound **3** does not exhibit any detectable binding, highlighting that only polymer samples terminated with carborane end-groups can undergo self-assembly processes thereby emphasizing their potential application in affinity labeling (Figure 4-6 C).

4.2.3 Carborane CTA for use in Raman spectroscopy and self-assembly processes

Raman spectroscopy, especially stimulated Raman spectroscopy (SRS), is emerging as a powerful technique for use in bioimaging.[83] Although fluorescence techniques still remain ubiquitous, there are many inherent limitations which include photobleaching of small molecule dyes, which shortens their lifetimes, and the need to use external chemical or photophysical stimuli which could damage biological samples.[83] Raman spectroscopy bypasses these limitations by relying on the inherent molecular vibrations in samples. Label-free Raman spectroscopy has been utilized in the analysis of biological samples, primarily investigating bond vibrational signals in the fingerprint (500–1700 cm^{-1}) region as well as higher regions (2800–3200 cm^{-1}).[83] However, there is a need to develop Raman active labels as a way to overcome limitations with label-free analysis which include difficulty in differentiating signals within biological media, weak signal-to-noise ratios, and the inability to track molecules within samples. Because the B–H vibrational signal (~2350–2600 cm^{-1}) of carborane compounds appear in silent regions within the Raman spectra of biological samples (~1740–2800 cm^{-1}), they are ideally suited to serve as bioorthogonal molecular probes for Raman applications.[59,83]

We first analyzed the polymers via infrared spectroscopy and found that despite the carborane only accounting for 144 Da of polymers ranging 2000 to 6000 Da, we still observed the B–H vibrational signal (Figure C39 and C40). To demonstrate the potential utility of carborane terminated polymers to act as probes for Raman imaging, a thin film of **1-pNIPAAm** on a glass substrate was scanned using spontaneous Raman scattering. The B–H vibration occurs at a unique frequency (2549 cm^{-1}) which is in a Raman-silent region of biological samples (Figure 4-7 A). We also drop-cast a thin-film of **1-pNIPAAm** on a quartz substrate and performed a Raman scan at the edge of the film. A significant Raman amplitude at 2549 cm^{-1} is observed only in areas where the thin film is present, the amplitude quickly drops off when scanning over areas where the **1-pNIPAAm** film is absent (Figure 4-7 B). The intensity of the B–H Raman vibration is also worthy to note in this application, with an estimated cross section per bond that is **3** times that of a typical C–H stretching mode cross section (Appendix C). This experiment therefore demonstrates the potential utility of the B–H vibrational stretches inherent to carboranes for Raman imaging in polymer materials made via controlled polymerization.

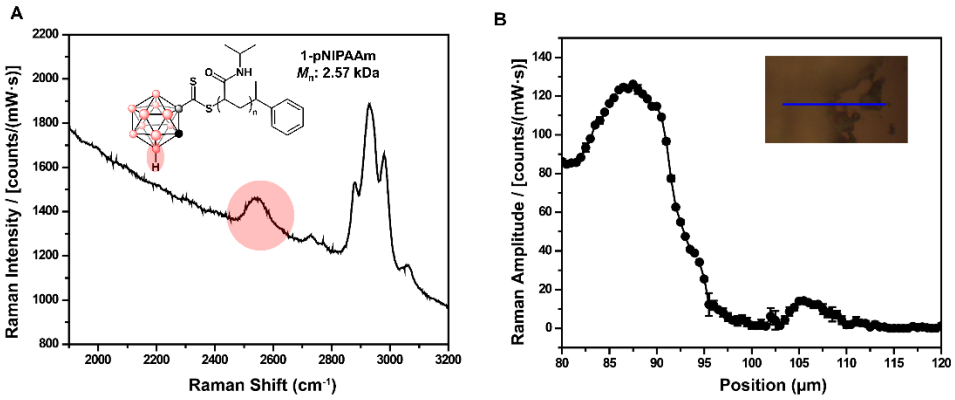

Figure 4-7. (A) Representative Raman spectrum of **1-pNIPAAm** thin film indicating B-H Raman signal at 2549 cm^{-1}. (B) Film-edge Raman scan of a **1-pNIPAAm** thin film showing Raman

activity only in areas where the polymer is present. Inset: optical image of the thin film analyzed, the blue line denotes the region scanned.

4.3 Conclusions

In summary, we present the utilization of tunable carborane functionalized RAFT agents. We investigated their ability to control polymerization processes of multiple monomer classes, and to serve as universal ^{1}H NMR spectroscopic handles, affinity labels, and Raman active molecular probes. We were able to accurately determine polymer molecular weight via end-group analysis using ^{1}H NMR spectroscopy. ITC studies of carborane terminated **pNIPAAm** samples showed a 2:1 (carborane : β-cyclodextrin) binding with a K_a value of 9.37×10^4 M^{-1}. Similar studies using *nido*-carborane terminated **pNIPAAm** and **pNIPAAm** samples without carborane end-groups showed no binding to β-cyclodextrin. Additionally, the B–H bonds on carborane are able to act as a Raman active spectroscopic probes with a vibrational signal (2350–2600 cm^{-1}), a Raman silent region of biological samples. This new class of RAFT agents adds to the expanding chemical toolbox available to biologists, chemists, and materials scientists while providing a new avenue of study at the intersection of main-group chemistry and polymer materials.[84–89]

Acknowledgements

A.M.S. thanks UCLA Department of Chemistry and Biochemistry for start-up funds and 3M for a Non-Tenured Faculty Award. M.S.M. thanks the NSF for the Bridge-to-Doctorate (HRD-1400789) and the Predoctoral (GRFP) (DGE-0707424) Fellowships and UCLA for the Christopher S. Foote Fellowship. O.M.E. thanks the Raymond and Dorothy Wilson Fellowship. H.D.M. thanks the NSF (CHE-1507735) for funding. C.T.G. and R.R.F. thank the NSF (CHE-1552849) for funding. P. C. thanks the Gold Family Foundation and the

SPE Foundation for funding. The authors would like to thank the UCLA-DOE and Biochemistry Instrumentation Facility for providing access to the ITC instrument and for helpful discussions relating to the data acquisition.

4.4 References

1. H. Gao and K. Matyjaszewski, *Prog. Polym. Sci.*, 2009, **34**, 317-350.

2. M. Bathfield, F. D'Agosto, R. Spitz, M.-T. Charreyre and T. Delair, *J. Am. Chem. Soc.*, 2006, **128**, 2546-2547.

3. B. R. Elling and Y. Xia, *ACS Macro Lett.*, 2018, **7**, 656-661.

4. C. A. Figg, A. N. Bartley, T. Kubo, B. S. Tucker, R. K. Castellano and B. S. Sumerlin, *Polym. Chem.*, 2017, **8**, 2457-2461.

5. M. Päch, D. Zehm, M. Lange, I. Dambowsky, J. Weiss and A. Laschewsky, *J. Am. Chem. Soc.*, 2010, **132**, 8757-8765.

6. D. Vinciguerra, J. Tran and J. Nicolas, *Chem. Commun.*, 2018, **54**, 228-240.

7. Y. Bao, E. Guégain, V. Nicolas and J. Nicolas, *Chem. Commun.*, 2017, **53**, 4489-4492.

8. S. Liu, Y. Cheng, H. Zhang, Z. Qiu, R. T. Kwok, J. W. Lam and B. Z. Tang, *Angew. Chem. Int. Ed.*, 2018, **57**, 6274-6278.

9. B. S. Tucker, J. D. Stewart, J. I. Aguirre, L. S. Holliday, C. A. Figg, J. G. Messer and B. S. Sumerlin, *Biomacromolecules*, 2015, **16**, 2374-2381.

10. C. P. Ryan, M. E. Smith, F. F. Schumacher, D. Grohmann, D. Papaioannou, G. Waksman, F. Werner, J. R. Baker and S. Caddick, *Chem. Commun.*, 2011, **47**, 5452-5454.

11. V. Coessens, T. Pintauer and K. Matyjaszewski, *Prog. Polym. Sci.*, 2001, **26**, 337-377.

12. Y. Bao, E. Guégain, J. Mougin and J. Nicolas, *Polym. Chem.*, 2018.

13. K. Matyjaszewski and N. V. Tsarevsky, *Nat. Chem.*, 2009, **1**, 276.

14. B. Le Droumaguet and J. Nicolas, *Polym. Chem.*, 2010, **1**, 563-598.

15. F. Lecolley, L. Tao, G. Mantovani, I. Durkin, S. Lautru and D. M. Haddleton, *Chem. Commun.*, 2004, 2026-2027.

16. W. Agut, D. Taton and S. Lecommandoux, *Macromolecules*, 2007, **40**, 5653-5661.

17. K. Matyjaszewski, *Macromolecules*, 2012, **45**, 4015-4039.

18. C.-Y. Hong and C.-Y. Pan, *Macromolecules*, 2006, **39**, 3517-3524.

19. S. Martens, F. Driessen, S. Wallyn, O. u. Türünç, F. E. Du Prez and P. Espeel, *ACS Macro Lett.*, 2016, **5**, 942-945.

20. J. Chiefari, Y. Chong, F. Ercole, J. Krstina, J. Jeffery, T. P. Le, R. T. Mayadunne, G. F. Meijs, C. L. Moad and G. Moad, *Macromolecules*, 1998, **31**, 5559-5562.

21. C. Boyer, V. Bulmus, T. P. Davis, V. Ladmiral, J. Liu and S. Perrier, *Chem. Rev.*, 2009, **109**, 5402-5436.

22. G. Moad, E. Rizzardo and S. H. Thang, *Aust. J. Chem.*, 2012, **65**, 985-1076.

23. G. Moad, E. Rizzardo and S. H. Thang, *Chem. Asian J.*, 2013, **8**, 1634-1644.

24. J. Bernard, X. Hao, T. P. Davis, C. Barner-Kowollik and M. H. Stenzel, *Biomacromolecules*, 2006, **7**, 232-238.

25. S. b. Perrier, *Macromolecules*, 2017, **50**, 7433-7447.

26. G. Moad, E. Rizzardo and S. H. Thang, *Acc. Chem. Res.*, 2008, **41**, 1133-1142.

27. D. J. Keddie, G. Moad, E. Rizzardo and S. H. Thang, *Macromolecules*, 2012, **45**, 5321-5342.

28. M. J. Monteiro, *J. Polym. Sci. A: Polym. Chem.*, 2005, **43**, 3189-3204.

29. J. Skey and R. K. O'Reilly, *Chem. Commun.*, 2008, 4183-4185.

30. J. Chiefari, R. T. Mayadunne, C. L. Moad, G. Moad, E. Rizzardo, A. Postma, M. A. Skidmore and S. H. Thang, *Macromolecules*, 2003, **36**, 2273-2283.

31. D. Estupinan, T. Gegenhuber, J. P. Blinco, C. Barner-Kowollik and L. Barner, *ACS Macro Lett.*, 2017, **6**, 229-234.

32. G. Moad, E. Rizzardo and S. H. Thang, *Polym. Int.*, 2011, **60**, 9-25.

33. C. Boyer, V. Bulmus, P. Priyanto, W. Y. Teoh, R. Amal and T. P. Davis, *J. Mater. Chem.*, 2009, **19**, 111-123.

34. V. Vázquez-Dorbatt, Z. P. Tolstyka and H. D. Maynard, *Macromolecules*, 2009, **42**, 7650-7656.

35. S. J. Paluck and H. D. Maynard, *Polym. Chem.*, 2017, **8**, 4548-4556.

36. J. Xu, C. Boyer, V. Bulmus and T. P. Davis, *J. Polym. Sci. A: Polym. Chem.*, 2009, **47**, 4302-4313.

37. M. Li, P. De, S. R. Gondi and B. S. Sumerlin, *Macromol. Rapid Commun.*, 2008, **29**, 1172-1176.

38. M. P. Robin, M. W. Jones, D. M. Haddleton and R. K. O'Reilly, *ACS Macro Lett.*, 2011, **1**, 222-226.

39. M. M. Lorenzo, C. G. Decker, M. U. Kahveci, S. J. Paluck and H. D. Maynard, *Macromolecules*, 2015, **49**, 30-37.

40. L. McDowall, G. Chen and M. H. Stenzel, *Macromol. Rapid Commun.*, 2008, **29**, 1666-1671.

41. C. Boyer, V. Bulmus, J. Liu, T. P. Davis, M. H. Stenzel and C. Barner-Kowollik, *J. Am. Chem. Soc.*, 2007, **129**, 7145-7154.

42. J. T. Lai, D. Filla and R. Shea, *Macromolecules*, 2002, **35**, 6754-6756.

43. R. N. Grimes, *Carboranes*, Academic Press, 2016.

44. A. M. Spokoyny, *Pure Appl. Chem.*, 2013, **85**, 903-919.

45. Z. Qiu, *Tetrahedron Lett.*, 2015, **56**, 963-971.

46. R. M. Dziedzic, J. L. Martin, J. C. Axtell, L. M. Saleh, T.-C. Ong, Y.-F. Yang, M. S. Messina, A. L. Rheingold, K. N. Houk and A. M. Spokoyny, *J. Am. Chem. Soc.*, 2017, **139**, 7729-7732.

47. R. M. Dziedzic, L. M. Saleh, J. C. Axtell, J. L. Martin, S. L. Stevens, A. T. Royappa, A. L. Rheingold and A. M. Spokoyny, *J. Am. Chem. Soc.*, 2016, **138**, 9081-9084.

48. A. M. Spokoyny, C. W. Machan, D. J. Clingerman, M. S. Rosen, M. J. Wiester, R. D. Kennedy, C. L. Stern, A. A. Sarjeant and C. A. Mirkin, *Nat. Chem.*, 2011, **3**, 590-596.

49. R. Cheng, Z. Qiu and Z. Xie, *Nat. Commun.*, 2017, **8**, 14827.

50. Z. Qiu, Y. Quan and Z. Xie, *J. Am. Chem. Soc.*, 2013, **135**, 12192-12195.

51. W.-B. Yu, P.-F. Cui, W.-X. Gao and G.-X. Jin, *Coord. Chem. Rev.*, 2017, **350**, 300-319.

52. Z. Zheng, W. Jiang, A. A. Zinn, C. B. Knobler and M. F. Hawthorne, *Inorg. Chem.*, 1995, **34**, 2095-2100.

53. F. Teixidor, G. Barberà, A. Vaca, R. Kivekäs, R. Sillanpää, J. Oliva and C. Viñas, *J. Am. Chem. Soc.*, 2005, **127**, 10158-10159.

54. A. M. Spokoyny, C. D. Lewis, G. Teverovskiy and S. L. Buchwald, *Organometallics*, 2012, **31**, 8478-8481.

55. M. P. Grzelczak, S. P. Danks, R. C. Klipp, D. Belic, A. Zaulet, C. Kunstmann-Olsen, D. F. Bradley, T. Tsukuda, C. Viñas and F. Teixidor, *ACS Nano*, 2017, **11**, 12492-12499.

56. A. F. Armstrong and J. F. Valliant, *Dalton Trans.*, 2007, 4240-4251.

57. D. Gabel, *Pure Appl. Chem.*, 2015, **87**, 173-179.

58. J. F. Valliant, K. J. Guenther, A. S. King, P. Morel, P. Schaffer, O. O. Sogbein and K. A. Stephenson, *Coord. Chem. Rev.*, 2002, **232**, 173-230.

59. D. C. Kennedy, D. R. Duguay, L.-L. Tay, D. S. Richeson and J. P. Pezacki, *Chem. Commun.*, 2009, 6750-6752.

60. A. Siedle, G. Bodner, A. Garber, D. Beer and L. Todd, *Inorg. Chem.*, 1974, **13**, 2321-2324.

61. M. S. Donovan, A. B. Lowe, B. S. Sumerlin and C. L. McCormick, *Macromolecules*, 2002, **35**, 4123-4132.

62. D. B. Thomas, A. J. Convertine, L. J. Myrick, C. W. Scales, A. E. Smith, A. B. Lowe, Y. A. Vasilieva, N. Ayres and C. L. McCormick, *Macromolecules*, 2004, **37**, 8941-8950.

63. H. Willcock and R. K. O'Reilly, *Polym. Chem.*, 2010, **1**, 149-157.

64. H. Golf, R. O'Shea, C. Braybrook, O. E. Hutt, D. W. Lupton and J. Hooper, *Chem. Sci.*, 2018, **9**, 7370-7375.

65. M. Li, P. De, S. R. Gondi and B. S. Sumerlin, *J. Polym. Sci. A: Polym. Chem.*, 2008, **46**, 5093-5100.

66. J. M. Spruell, B. A. Levy, A. Sutherland, W. R. Dichtel, J. Y. Cheng, J. F. Stoddart and A. Nelson, *J. Polym. Sci. A: Polym. Chem.*, 2009, **47**, 346-356.

67. M. F. Hawthorne, D. C. Young, P. M. Garrett, D. A. Owen, S. G. Schwerin, F. N. Tebbe and P. A. Wegner, *J. Am. Chem. Soc.*, 1968, **90**, 862-868.

68. M. F. Hawthorne, D. C. Young and P. A. Wegner, *J. Am. Chem. Soc.*, 1965, **87**, 1818-1819.

69. R. N. Grimes, *Coord. Chem. Rev.*, 2000, **200**, 773-811.

70. A. V. Safronov, Y. V. Sevryugina, K. R. Pichaandi, S. S. Jalisatgi and M. F. Hawthorne, *Dalton Trans.*, 2014, **43**, 4969-4977.

71. M. Fox, W. Gill, P. Herbertson, J. MacBride, K. Wade and H. Colquhoun, *Polyhedron*, 1996, **15**, 565-571.

72. E. Weerapana, A. E. Speers and B. F. Cravatt, *Nat. Protoc.*, 2007, **2**, 1414.

73. C. Kendall, I. Ionescu-Matiu and G. R. Dreesman, *J. Immunomol. Methods*, 1983, **56**, 329-339.

74. K. Ohta, S. Konno and Y. Endo, *Tetrahedron Lett.*, 2008, **49**, 6525-6528.

75. R. Vaitkus and S. Sjöberg, *J. Incl. Phenom. Macrocycl. Chem.*, 2011, **69**, 393-395.

76. K. Sadrerafi, E. E. Moore and M. W. Lee, *J. Incl. Phenom. Macrocycl. Chem.*, 2015, **83**, 159-166.

77. A. Harada and S. Takahashi, *J. Chem. Soc., Chem. Commun.*, 1988, 1352-1353.

78. J. Nekvinda, B. Grüner, D. Gabel, W. Nau and K. Assaf, *Chem. Eur. J.*, 2018, **24**, 12970-12975.

79. H. Xiong, D. Zhou, X. Zheng, Y. Qi, Y. Wang, X. Jing and Y. Huang, *Chem. Commun.*, 2017, **53**, 3422-3425.

80. P. Neirynck, J. Schimer, P. Jonkheijm, L.-G. Milroy, P. Cigler and L. Brunsveld, *J. Mater. Chem. B*, 2015, **3**, 539-545.

81. W. Neumann, S. Xu, M. B. Sárosi, M. S. Scholz, B. C. Crews, K. Ghebreselasie, S. Banerjee, L. J. Marnett and E. Hey-Hawkins, *ChemMedChem*, 2016, **11**, 175-178.

82. J. Brynda, P. Mader, V. Šícha, M. Fábry, K. Poncová, M. Bakardiev, B. Grüner, P. Cígler and P. Řezáčová, *Angew. Chem.*, 2013, **125**, 14005-14008.

83. L. Wei, F. Hu, Z. Chen, Y. Shen, L. Zhang and W. Min, *Acc. Chem. Res.*, 2016, **49**, 1494-1502.

84. T. Dellermann, N. E. Stubbs, D. A. Resendiz-Lara, G. R. Whittell and I. Manners, *Chem. Sci.*, 2018, **9**, 3360-3366.

85. G. M. Adams, A. L. Colebatch, J. T. Skornia, A. I. McKay, H. C. Johnson, G. C. Lloyd− Jones, S. A. Macgregor, N. A. Beattie and A. S. Weller, *J. Am. Chem. Soc.*, 2018, **140**, 1481-1495.

86. S. N. Mendis, T. Zhou and R. S. Klausen, *Macromolecules*, 2018, **51**, 6859-6864.

87. Y. Adachi, Y. Ooyama, Y. Ren, X. Yin, F. Jäkle and J. Ohshita, *Polym. Chem.*, 2018, **9**, 291-299.

88. S. Ye, M. Steube, E. I. Carrera and D. S. Seferos, *Macromolecules*, 2016, **49**, 1704-1711.

89. F. Jäkle and F. Vidal, *Angew. Chem. Int. Ed.*, 2019, DOI: 10.1002/anie.201810611.

4.5 Appendix C

4.5.1 Reagent Information

All commercially available chemicals were used as received unless otherwise stated. All polymerizations were prepared in the glovebox under nitrogen atmosphere unless otherwise stated. Benzene, diethyl ether, and tetrahydrofuran were purified *via* a solvent purification system and kept in the glovebox over 4 Å molecular sieves. Toluene (Fisher) and ethyl acetate (Fisher) were degassed and stored over 4 Å molecular sieves. Dichloromethane (Fisher), hexanes (Fisher), pentane (Sigma-Aldrich), and 1,4-dioxane (Sigma-Aldrich) were used as received. All monomers were degassed and stored with 4Å molecular sieves. Styrene (≥99%), 4-chlorostyrene (97%), methyl acrylate (99%), *N*-isopropylacrylamide (97%), tributylphosphine (97%), 1-hexylamine (99%), 2-hydroxyethyl acrylate (96%), dithranol (>90%), silver trifluoroacetate (98%), *n*-butyllithium (2.5 M solution in hexanes), and carbon disulfide (99%) were purchased from Sigma-Aldrich. *O*-carborane was purchased from Boron Specialties (USA). Tetrabutylammonium fluoride hydrate (TBAF) (97%) was purchased from Oakwood Chemicals. 1-chloro-1-phenylethane (97%) was purchased from Acros Organics. 2,2′-Azobis(2-methylpropionitrile) was purchased from Sigma-Aldrich and recrystallized from methanol. 1,2,3,4-tetrahydronapthalene (tetralin) was purchased from TCI.

4.5.2 General Analytical Information

NMR spectra were recorded on DRX 400, DRX 500, and AVIII 500 spectrometers at 500 MHz (^{1}H), 125 MHz (^{13}C), and 80 MHz (^{11}B) reported in δ (parts per million) relative to tetramethylsilane (^{1}H, ^{13}C) or $BF_3 \cdot Et_2O$ (^{11}B), and referenced to residual ^{1}H/^{13}C signals of the

deuterated solvent (^{1}H (δ) $CDCl_3$ 7.26; ^{13}C (δ) $CDCl_3$ 77.16; ^{1}H (δ) $(CD_3)_2CO$ 2.05; ^{1}H (δ) CD_3CN 1.94; ^{11}B (δ) $BF_3 \cdot Et_2O$ 0.00 ppm). Deuterated solvents (Cambridge Isotope Laboratories) for NMR spectroscopic analyses were stored over 4Å molecular sieves. Gel permeation chromatography (GPC) was conducted on a Shimadzu HPLC Prominence-I system equipped with a UV detector, Wyatt DAWN Heleos-II Light Scattering detector, Wyatt Optilab T-rEX RI detector, one MZ-Gel SDplus guard column, and two MZ-Gel SDplus 100 Å 5μm 300x8.0 mm columns. Eluent was THF at 40 °C (flow rate: 0.70 mL/min). Chromatograms from THF GPC were analyzed using Astra 6.0 software using dn/dc values of 0.1828 for polystyrenes and 0.048 for poly(methyl acrylate) at 664 nm. Polymer analysis of poly(NIPAAm) was performed on a Shimadzu high performance liquid chromatography (HPLC) system with a refractive index RID-10A, one Polymer Laboratories PLgel guard column, and two Polymer Laboratories PLgel 5 μm mixed D columns in DMF eluent with LiBr (0.1 M) at 40 °C (flow rate: 0.80 mL/min). Calibration was performed using near-monodisperse pMMA standards from Polymer Laboratories. Chromatograms from DMF GPC were analyzed using LabSolutions software. All GPC samples were dissolved in HPLC grade solvent at a concentration of 4-5 mg/mL and filtered through a 0.2 μm TFE filter. UV-Vis spectroscopy was performed on an Agilent / HP 8453 spectrophotometer with an Agilent 89090A Peltier temperature controller. Thin-layer chromatography (TLC) samples for carborane-containing compounds were stained with 1 wt. % $PdCl_2$ in 6M HCl and were developed with heat. Mass spectrometry was performed on a Q Exactive™ Plus Hybrid Quadrupole-Orbitrap™ Mass Spectrometer with Dionex UltiMate 3000 RSLCnano Systems.

4.5.3 Isothermal Titration Calorimetry

Isothermal Titration Calorimetry (ITC) data were recorded on a MicroCal^{TM} iTC$_{200}$ System (GE Healthcare Life Sciences) housed in the University of California, Los Angeles (UCLA) Department of Energy (DOE) Biochemistry Instrumentation Core Technology Center. All titrations were recorded at 25 ºC in neat water. Syringe concentration was typically 10-20 times larger than the cell concentration. The syringe volume is approximately 39 µL and the cell volume is approximately 250 µL. The first data point (a 0.4µL injection) was removed before data processing using MicroCal Analysis Software and Origin Software. Heats of dilution were determined by titrating the titrant of interest into neat water at the same injection volume used for each experiment. Heats of dilution were subtracted from the data prior to curve fitting. Exact concentrations, number of injections, and volume of injection are reported for each experiment.

4.5.4 Raman Experimental Details

Samples for Raman imaging were prepared by dissolving 4.44 mg of **1-pNIPAAm** in 0.888 mL of water and drop casting the solution onto a quartz coverslip. A sharp edge was created by scraping some of the **1-pNIPAAm** off of the coverslip with a razor blade.

Imaging was completed using a 633 nm HeNe continuous wave laser (Thorlabs). A 20x objective with a numerical aperture of 0.40 was used to focus the laser onto the sample. The sample was mounted on a 3D nano-positioning stage (Mad City Labs Nano-3D200 Stage). The laser power at the sample was 1.09 mW. Raman scattering was collected in a backscatter orientation, focused into a spectrograph, and dispersed by a 600 gr/mm grating blazed at 750 nm. The signal was then detected with a PIXIS 400BR CCD array detector (Princeton Instruments) with 100 rows binned. Three exposures of 12 s were averaged together at each postion.

The relative Raman cross section for the B-H vibration can be approximated by comparing the number of B-H bonds to the number of C-H bonds in an average-sized **1-pNIPAAm** polymer and the relative intensities of their Raman peaks. The efficiency of the detector at the wavelength of the vibration must also be considered. For a given Raman peak,

$$I \propto QnR \qquad (1)$$

$$R \propto \frac{I}{Qn} \qquad (2)$$

where I is the area under the peak, Q is the quantum efficiency of the detector at the center wavelength of the peak, n is the number of bonds in the polymer undergoing the particular vibration, and R is the Raman cross section for that vibration. By dividing equation (2) for B-H by equation (2) for C-H, an equation for the ratio of the Raman cross sections is obtained.

$$\frac{R_{BH}}{R_{CH}} = \frac{Q_{CH} n_{CH} I_{BH}}{Q_{BH} n_{BH} I_{CH}} \quad (3)$$

Q_{CH} and Q_{BH} are 0.95 and 0.94 respectively The average **1-pNIPAAm** polymer was composed of 20 NIPAm subunits and one **1**. This results in 210 C-H bonds and 10 B-H bonds per molecule. Signal intensities for I_{CH} and I_{BH} were calculated to be 73900 and 10500 respectively by fitting the spectrum using a multipeak Gaussian fit with a linear baseline. By entering these values into equation (3), we can determine $R_{BH} \approx 3R_{CH}$. As C-H stretches are frequently used for Raman imaging, this relationship demonstrates carborane's exciting potential as a Raman probe.

4.5.5 Small Molecule Synthesis and Characterization

4.5.5.1 Purification of *o*-carborane purchased from Boron Specialties

O-carborane (15g, 10.4 mmol) was charged to a round bottom flask with MeOH (150 mL). 12 M HCl (50 mL) was added slowly to the reaction vessel, and the resulting mixture was heated to 50 ˚C and stirred for 16 hours. The solution was then cooled, charged with H_2O (200 mL) and the resulting white solid was isolated by vacuum filtration, washed with water, and air dried. The solid was then dissolved in CH_2Cl_2, dried over $MgSO_4$, and filtered through Celite. The solution was dried *in vacuo* to afford a white powder. The powder was then sublimed at 60 ˚C under dynamic vacuum. After sublimation away from the yellow residue, the white crystals were taken up in $C_2H_4Cl_2$, charged with activated carbon/charcoal, and stirred for 2-3 hours at 75˚C. The suspension was then filtered and the filtrate was evaporated under vacuum. The resulting white solid was again sublimed at 60˚C to produce white crystals.

4.5.5.2 Synthesis of 1

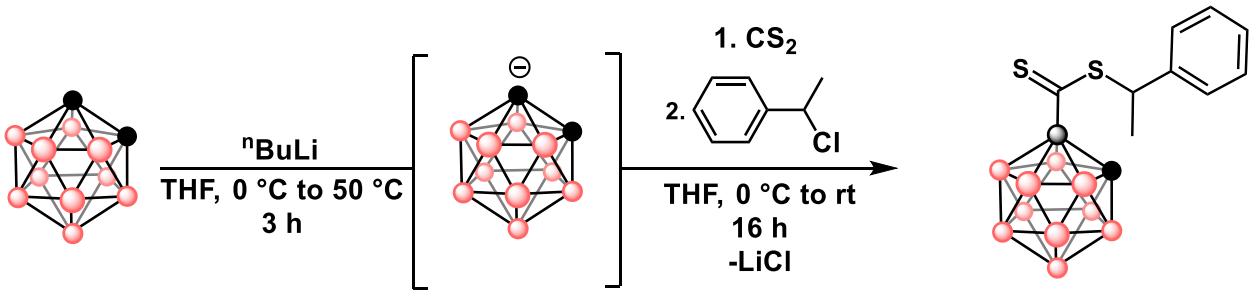

O-carborane (324 mg, 2.24 mmol, 1.0 eq.) was dissolved in dry THF (3 mL) in a dry and degassed round-bottom flask equipped with magnetic stir bar. The reaction temperature was lowered to 0 °C at which point ^{n}BuLi (2.5 M in hexanes, 988.0 µL, 2.47 mmol, 1.1 equiv) was added dropwise slowly, the immediate formation of white precipitate was observed. The reaction temperature was

raised to 50 °C and stirred for 3 h. After 3 h, the reaction was cooled to 0 °C at which point carbon disulfide (148.0 µL, 2.47 mmol, 1.1 equiv) was added slowly dropwise, an immediate red color change was observed. The reaction was stirred at room temperature for 1 h. After 1 h, the reaction temperature was lowered to 0 °C and 1-chloro-1-phenylethane (328.0 µL, 2.47 mmol, 1.1 equiv) was then added dropwise slowly. An immediate dark purple color change was observed. The reaction was stirred at room temperature for 16 h at which point the solvent was removed under reduced pressure to afford the crude material as a dark orange oil. The product was purified *via* column chromatography using (90:10 hexanes: CH_2Cl_2). Product was further purified via crystallization from dichloromethane layered with pentane at -30 °C to remove excess 1-chloro-1-phenylethane. Pure product is a bench-stable crystalline orange solid. Yield: 60%.

Single crystals suitable for x-ray crystallographic analysis were obtained from a concentrated solution of dichloromethane layered with pentane at -20 °C.

Rf = 0.67 (90:10 hexanes : CH_2Cl_2; $PdCl_2$ stain)

^{1}H NMR (500MHz, Chloroform-*d*, 298K): δ 7.37-7.25 (m, 5H, H_{Ar}), 4.91 (q, *J* = 7.1 Hz, 1H, -C*H*), 4.81 (s, 1H, cage-C*H*), 3.30-1.60 (bm, 10H, cage-B*H*), 1.72 (d, *J* = 7.1 Hz, 3H, -CH_3).

^{13}C{^{1}H} NMR (125MHz, Chloroform-*d*, 298K): δ 217.40, 139.56, 129.00, 128.41, 127.92, 82.31, 60.74, 53.28, 20.45.

^{11}B{^{1}H} NMR (128 MHz, Chloroform-*d*, 298K) δ -3.24, -8.76, -10.93, -11.37, -13.43.

IR: $\tilde{\nu}$ (cm^{-1}): 3053, 2972, 2926, 2572, 1493, 1445, 1371, 1195, 1126, 1087, 1038, 1013, 931, 766, 719, 694.

HRMS (Q-Exactive Plus) [M-H]$^{1-}$: 323.19 (calc'd for $C_{11}H_{20}B_{10}S_2$ 323.19) m/z

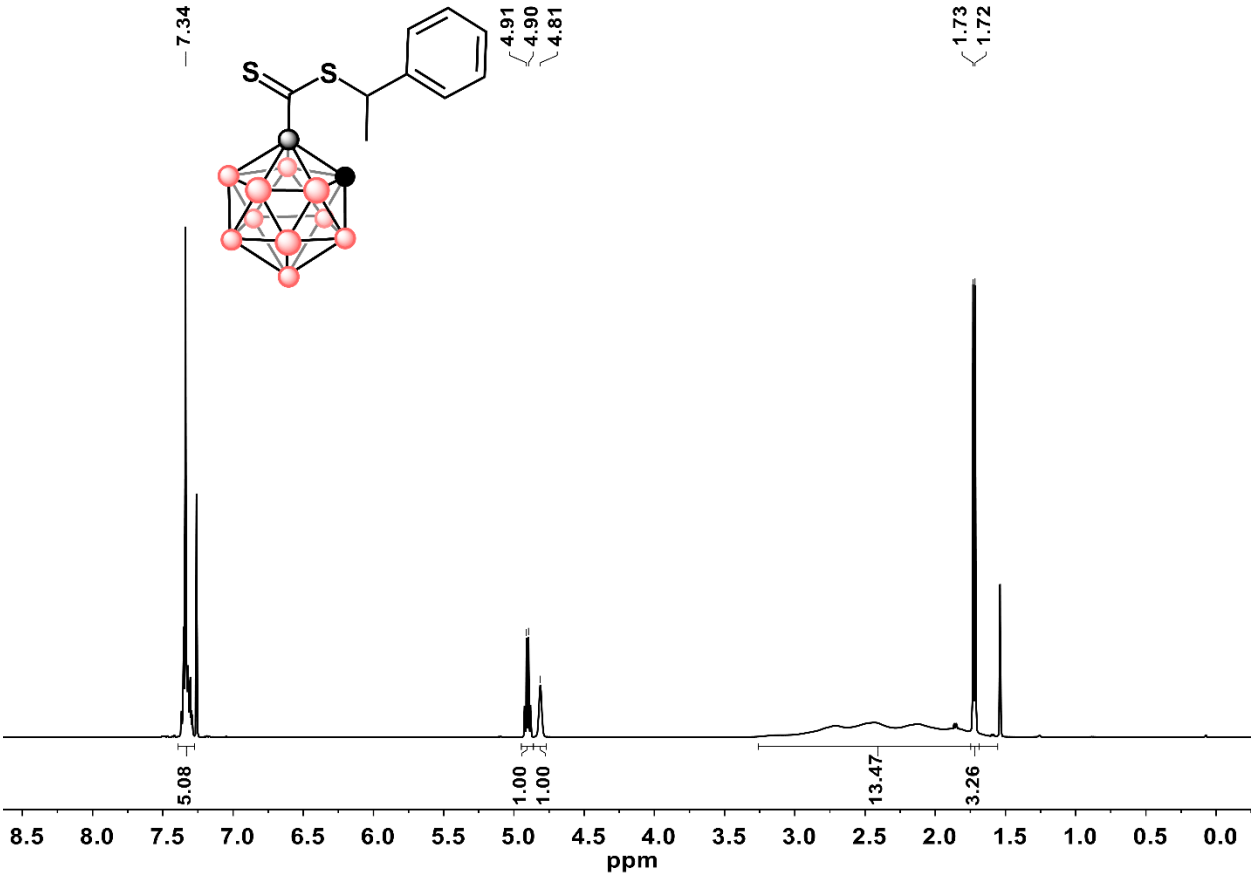

Figure C1. ^{1}H NMR spectrum of **1** in chloroform-*d* at 298 K.

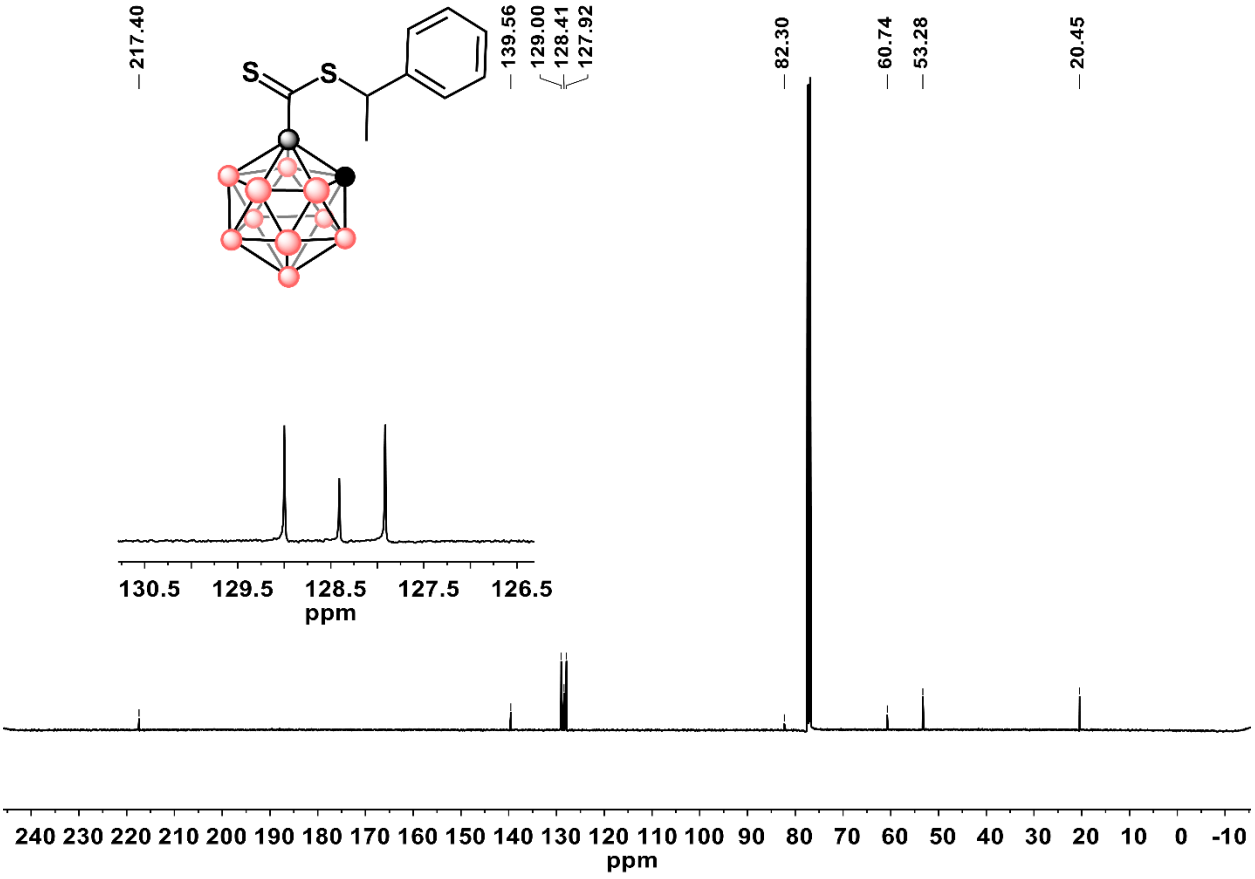

Figure C2. ^{13}C NMR spectrum of **1** in chloroform-*d* at 298 K.

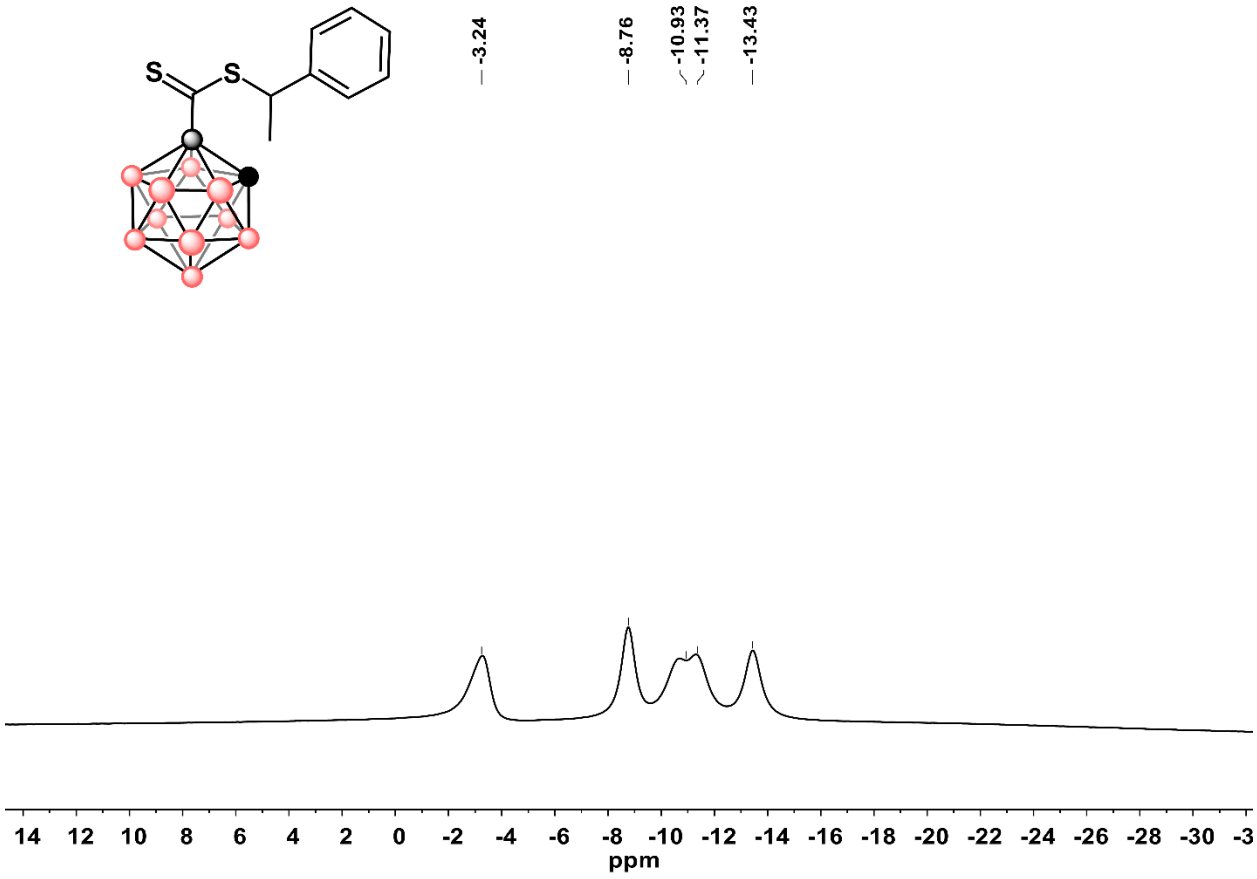

Figure C3. ^{11}B NMR spectrum of **1** in chloroform-*d* at 298 K.

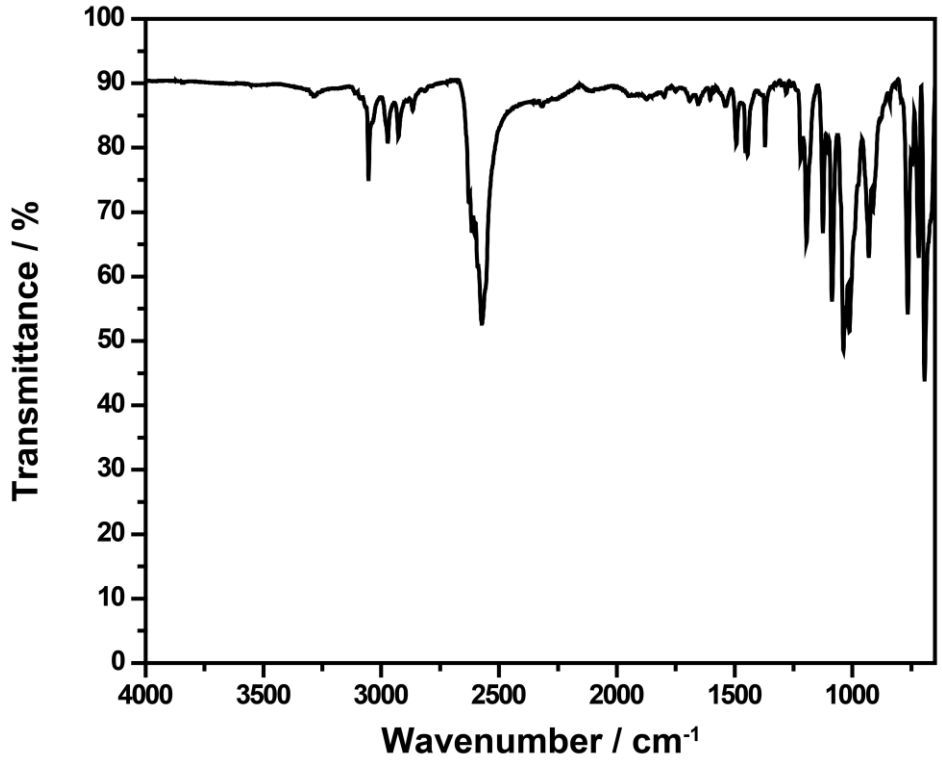

Figure C4. Infrared spectrum of **1**.

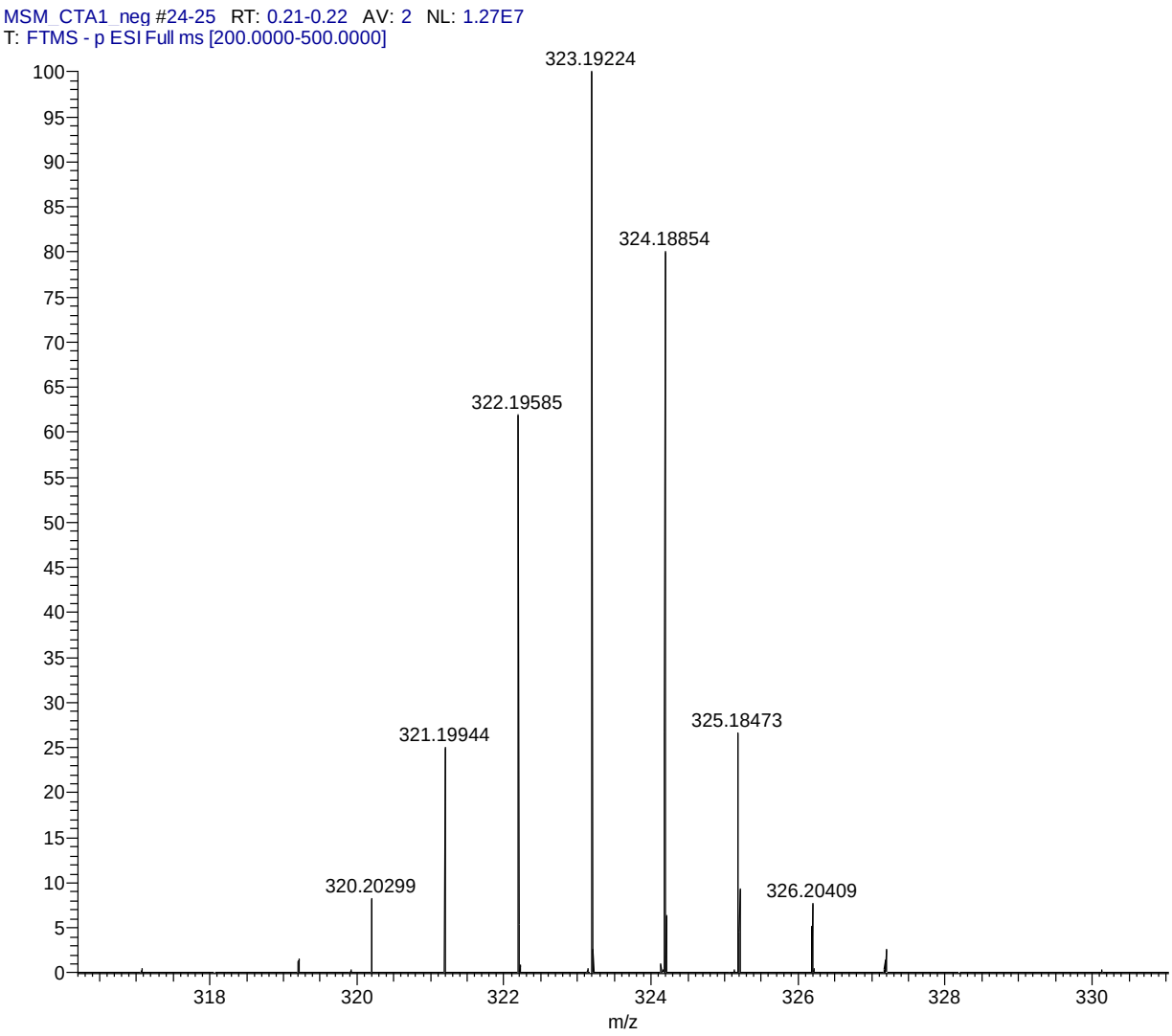

Figure C5. HRMS of **1**.

4.5.5.3 Synthesis of 9,12-diiodo-*o*-carborane

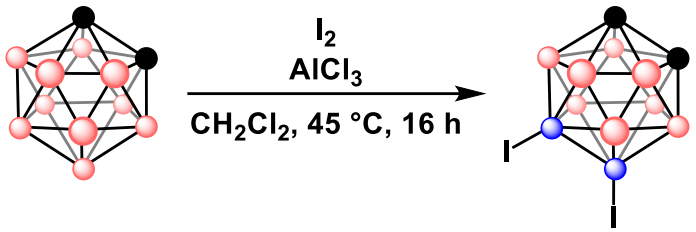

Ortho-$C_2B_{10}H_{12}$ (1.44 g, 10.0 mmol), was added to an oven-dried Schlenk flask capped with a rubber septum and evacuated/backfilled with N_2 three times. I_2 (2.54 g, 10.0 mmol) was added under a positive N_2 flow before the addition of dry CH_2Cl_2 (50 mL) via cannula. $AlCl_3$ (0.266 g, 20 mol%) was added to the stirring solution under a positive N_2 flow before the rubber septum was replaced with a greased glass stopper. The reaction mixture was subsequently refluxed (~37 °C) until the color faded to pale yellow (~4 h). A second equivalent of I_2 (2.54 g, 10.0 mmol) and $AlCl_3$ (0.133 g, 10 mol%) were added and the reaction was stirred at 37 °C overnight. The dark brown reaction mixture was diluted with deionized H_2O (25 mL), and unreacted I_2 was quenched by the dropwise addition of a saturated aqueous $Na_2S_2O_3$ solution until the solution was no longer colored. The opaque organic layer was collected and the aqueous layer was extracted with CH_2Cl_2 (2 x 15 mL). The organic portions were combined and dried with $MgSO_4$ resulting in a clear, colorless solution. The solution was then filtered through a pad of Celite on a fritted funnel and the CH_2Cl_2 was removed under reduced pressure to yield an off-white solid that was further purified by sublimation at 130 °C to produce the title compound as a white solid. Spectral data matches that previously reported in the literature (see: Kirlikovali, K. O.; Axtell, J. C.; Gonzalez, A.; Phung, A. C.; Khan, S. I.; Spokoyny, A. M. *Chem. Sci.* **2016**, *7*, 5132-5138).

4.5.5.4 Synthesis of 9,12-dimethyl-*o*-carborane

9,12-dimethyl-*o*-carborane was prepared from 9,12-diiodo-*o*-carborane according to the procedure reported in the following manuscript: Li, J.; Logan, C. F.; Jones, M. *Inorg. Chem.* **1991**, *30* (25), 4866-4868.

4.5.5.5 Synthesis of 2

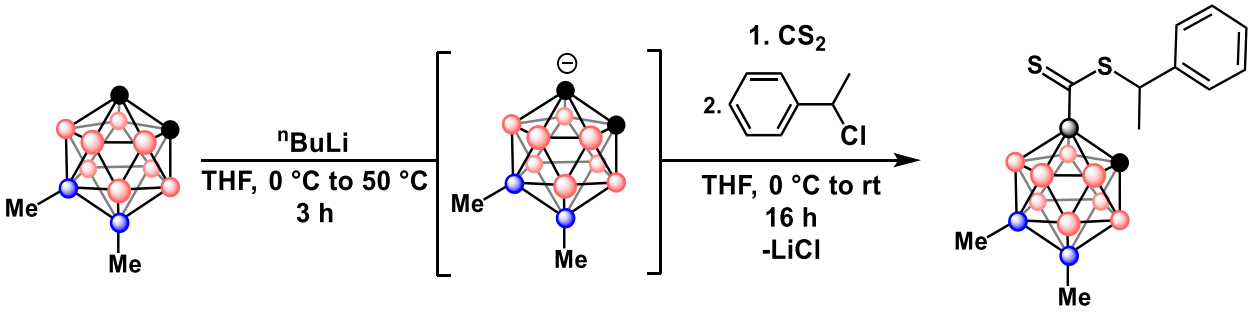

9,12-dimethyl-*o*-carborane (770.6 mg, 4.48 mmol, 1.0 equiv) was dissolved in dry THF (6 mL) in a dry and degassed round-bottom flask equipped with magnetic stir bar. The reaction temperature was lowered to 0 °C at which point ^{n}BuLi (2.5 M in hexanes, 1.98 mL, 4.94 mmol, 1.1 equiv) was added dropwise slowly, the immediate formation of white precipitate was observed. The reaction temperature was raised to 50 °C and left stirring for 3 hours. After 3 hours, the reaction was cooled to 0 °C at which point carbon disulfide (296.0 µL, 4.94 mmol, 1.1 equiv) was added dropwise slowly, an immediate red color change was observed. The reaction was stirred at room temperature for 1 hour. After 1 hour, the reaction temperature was lowered to 0 °C and 1-chloro-1-phenylethane (656.0 µL, 4.94 mmol, 1.1 equiv) was then added dropwise slowly. The reaction was stirred at room temperature for 16 hours at which point the solvent was removed under reduced pressure. The product was purified *via* column chromatography (95:5 hexanes:acetone) to remove residual

carborane. Excess 1-chloro-1-phenylethane was removed under dynamic vacuum and heating (100 mTorr at 95 °C). Pure product is a bench-stable dark orange oil. Yield: 69%.

Rf = 0.8 (95:5 hexanes:acetone; $PdCl_2$ stain)

^{1}H NMR (500MHz, Chloroform-*d*, 298K): δ 7.36 – 7.30 (m, 5H, H_{Ar}), 4.90 (q, *J* = 7.0 Hz, 1H, -C*H*), 4.61 (s, 1H, cage-C*H*), 3.12 – 1.59 (bm, 10H, cage-B*H*), 1.72 (d, *J* = 7.2 Hz, 3H, -CH_3), 0.23 (s, 3H, -BCH_3), 0.20 (s, 3H, -BCH_3).

^{13}C{^{1}H} NMR (125MHz, Chloroform-*d*, 298K): δ 218.32, 139.70, 128.96, 128.33, 127.92, 76.36, 54.44, 53.13, 20.42.

^{11}B{^{1}H} NMR (161 MHz, Chloroform-*d*, 298K) δ 6.95, 6.37, -7.00, -11.56, -12.18, -13.78.

IR: $\tilde{\nu}$ (cm^{-1}): 3059, 2906, 2591, 1493, 1452, 1314, 1199, 1094, 1071, 1022, 990, 912, 761, 738, 695.

HRMS (Q-Exactive Plus) [M-H]$^{1-}$: 351.22 (calc'd for $C_{13}H_{24}B_{10}S_2$ 351.22) m/z

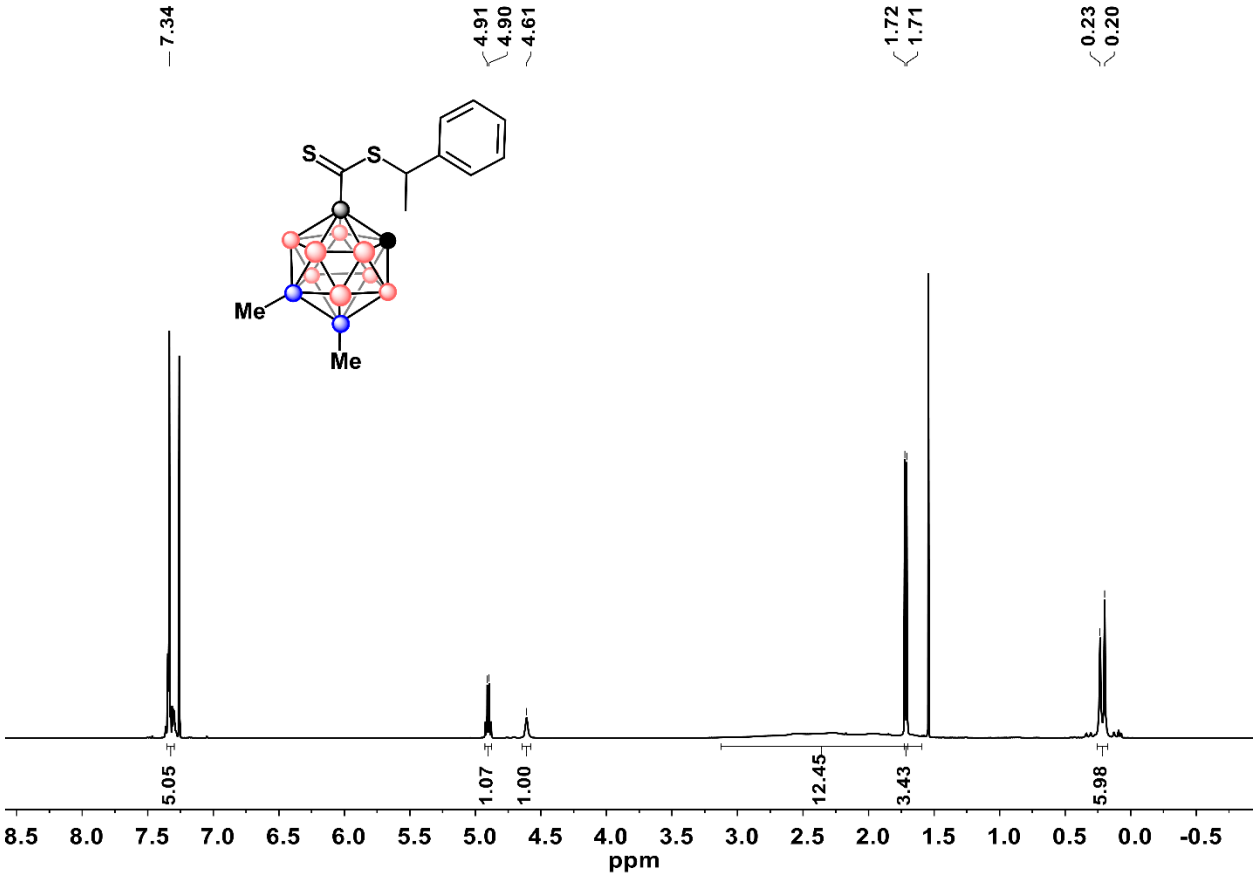

Figure C6. ^{1}H NMR spectrum of **1** in chloroform-*d* at 298 K.

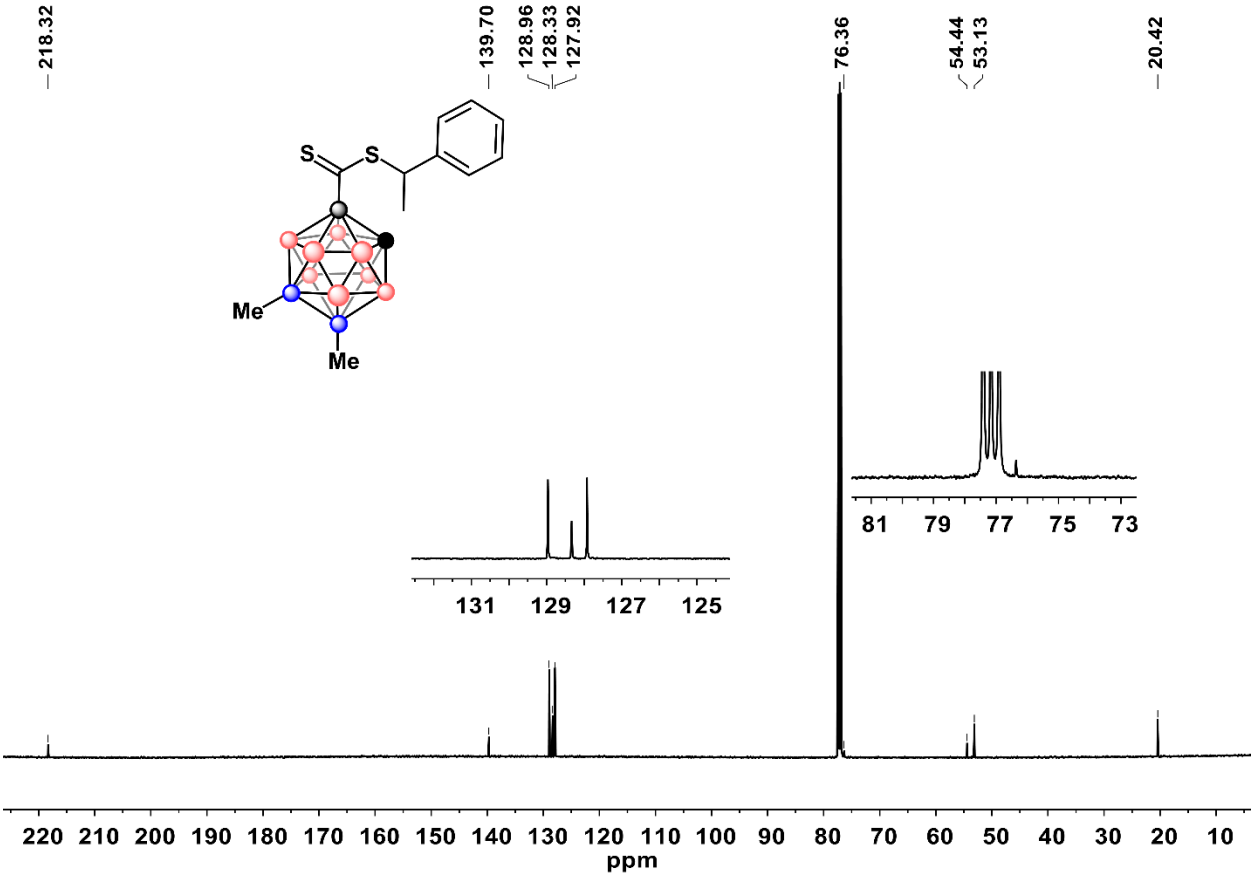

Figure C7. ^{13}C NMR spectrum of **1** in chloroform-*d* at 298 K.

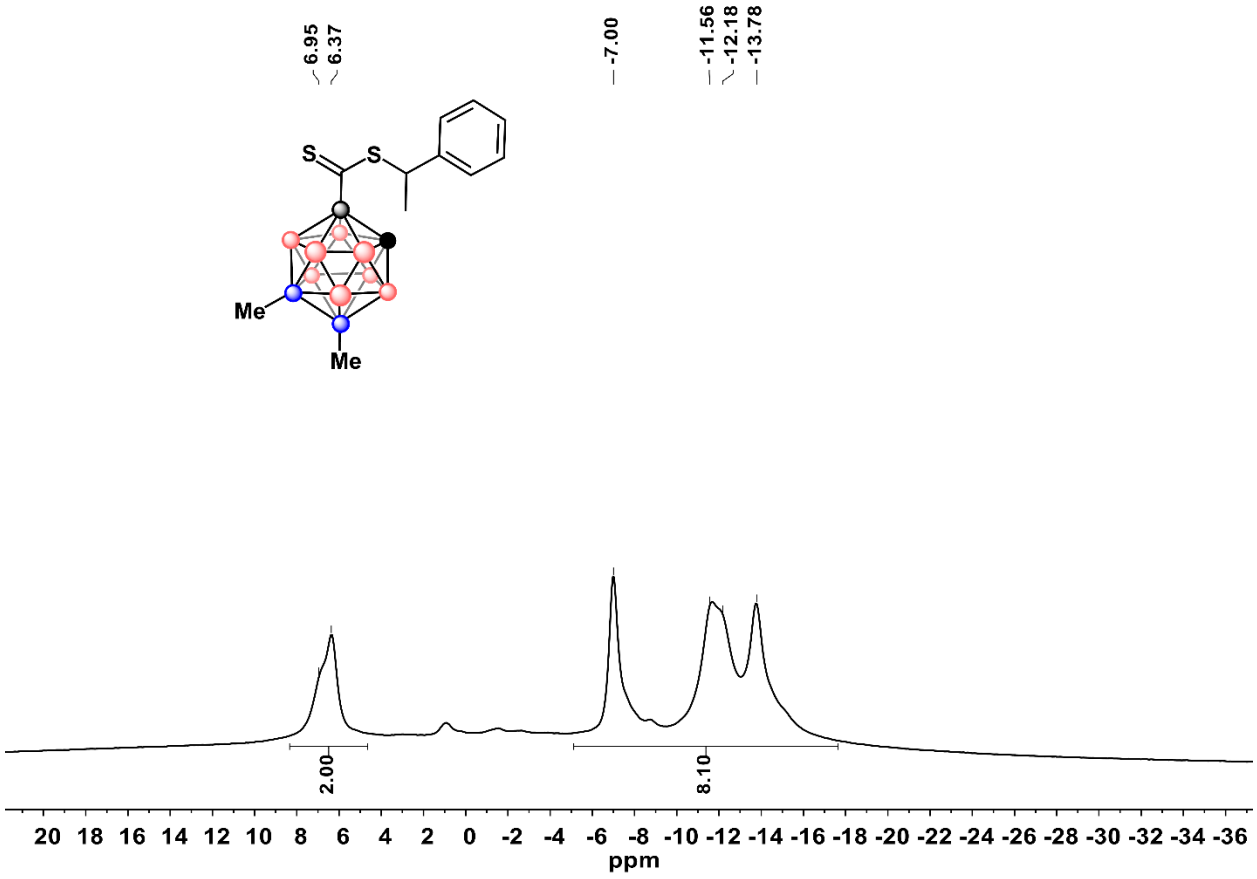

Figure C8. ^{11}B NMR spectrum of **1** in chloroform-*d* at 298 K.

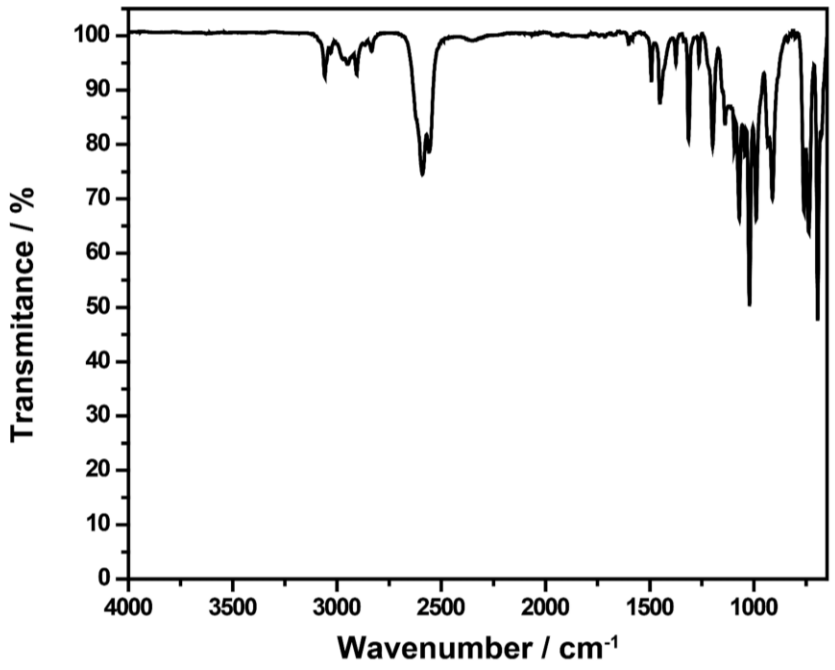

Figure C9. Infrared spectrum of **1**.

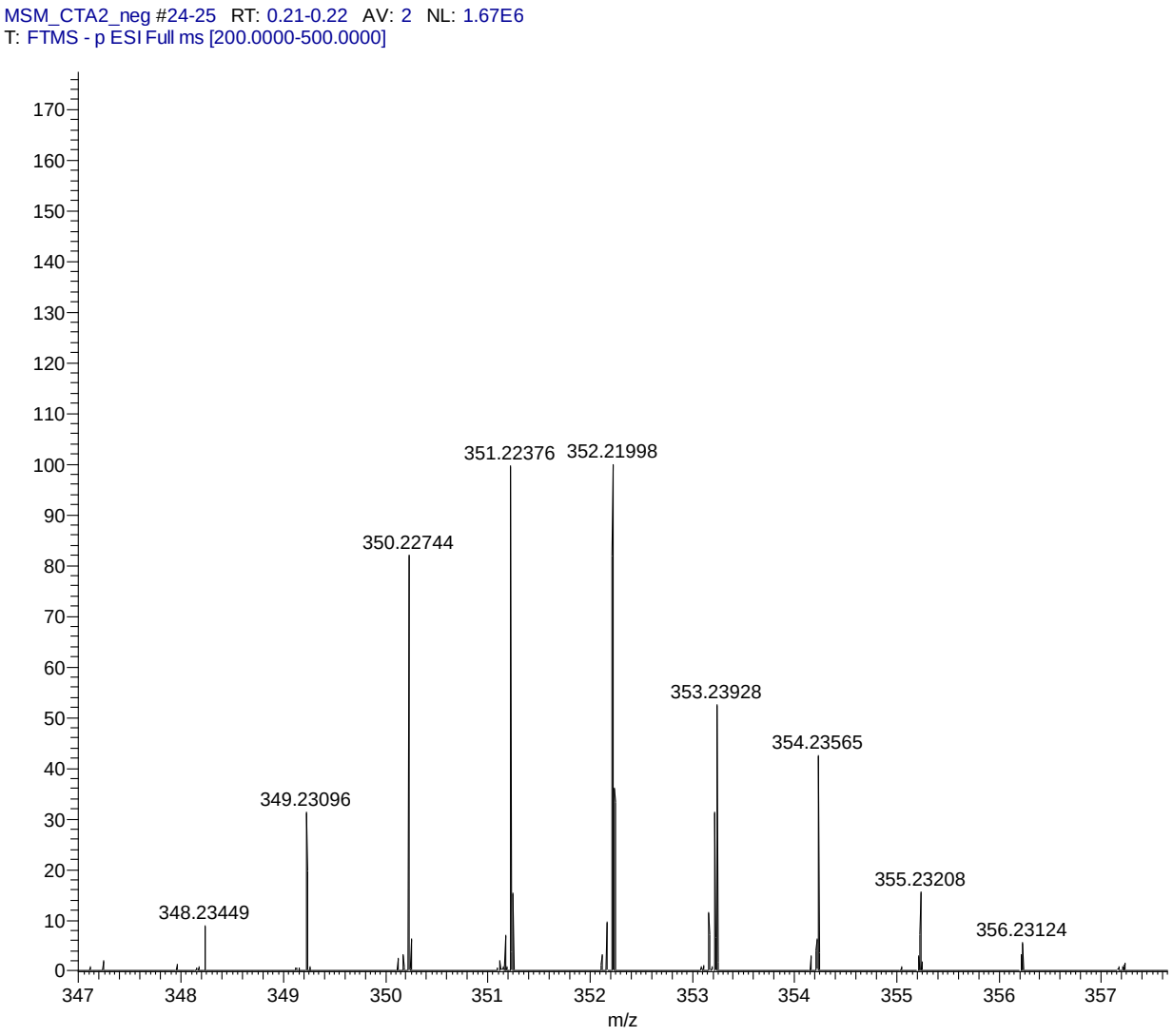

Figure C10. HRMS of **2**.

4.5.6 Polymer Synthesis, Characterization, and End-group Modification

4.5.6.1 General Polymerization Procedure for Liquid Monomers (Methyl Acrylate, Styrene, 4-chlorostyrene)

Polymerizations were prepared in the glovebox under nitrogen atmosphere. Methyl acrylate (0.20 mL, 2.20 mmol, 60 equiv.) was passed through dry activated basic alumina and added to a dram vial equipped with a magnetic stir bar. CTA **2** (12.7 mg, 0.036 mmol, 1 equiv.) and AIBN (1.8 mg, 0.011 mol, 0.3 equiv.) were dissolved in a minimal amount of EtOAc (~70 µL) and transferred to the dram vial containing the monomer. Tetralin (20 µL) was then added to the solution. The solution was stirred for 1 minute before collecting a 50 µL aliquot (t=0 min). The dram vial was then sealed with a polypropylene cap containing a Teflon coated septum and brought out of the glove box. The polymerization was initiated by immersing the dram vial in an 80 ˚C oil bath. Aliquots (50 µL) of the reaction mixture were collected at pre-determined time intervals and added into 700 µL of $CDCl_3$ to determine monomer conversion via ^1H NMR spectroscopy. The reaction was quenched by opening the dram vial to the atmosphere and the polymer was purified *via* precipitation from cold methanol.

4.5.6.2 General Polymerization Procedure for NIPAAm

All reactions were prepared in a glovebox under nitrogen atmosphere. *N*-isopropylacrylamide (500.0 mg, 4.42 mmol, 60 equiv), **2** (25.9 mg, 7.31×10^{-5} mol, 1 equiv), and AIBN (6.05 mg, 3.68×10^{-5} mol, 0.3 equiv) were added to a dram vial equipped with a magnetic stir bar. The reagents were dissolved in 2.2 mL toluene making a 2 M solution. The dram vial was sealed with a polypropylene cap containing a Teflon coated septum and brought out of the glove box. The polymerization was started by immersing the dram vial in an 80 ˚C oil bath. The reaction was

quenched by the opening dram vial to atmosphere and the polymer was purified *via* precipitation from cold methanol or diethyl ether.

4.5.6.3 Polymer conversion experiments

The reactions were prepared using optimized conditions (*vide supra*) along with the addition of an internal standard (≈20 μL tetralin). Aliquots (50 μL) of the reaction mixture were collected at predetermined time intervals and added into $CDCl_3$ (700 μL) for analysis *via* ^1H NMR spectroscopy. Monomer conversion was calculated by ^1H NMR spectroscopy by integration of unreacted vinyl monomer signal to the tetralin proton resonance at ~2.75-2.8 ppm.

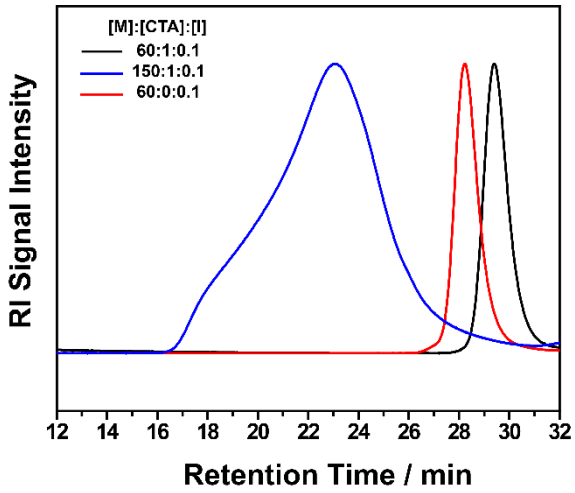

Figure C11. GPC overlay of **1-PS**.

4.5.6.4 Polymer Characterization

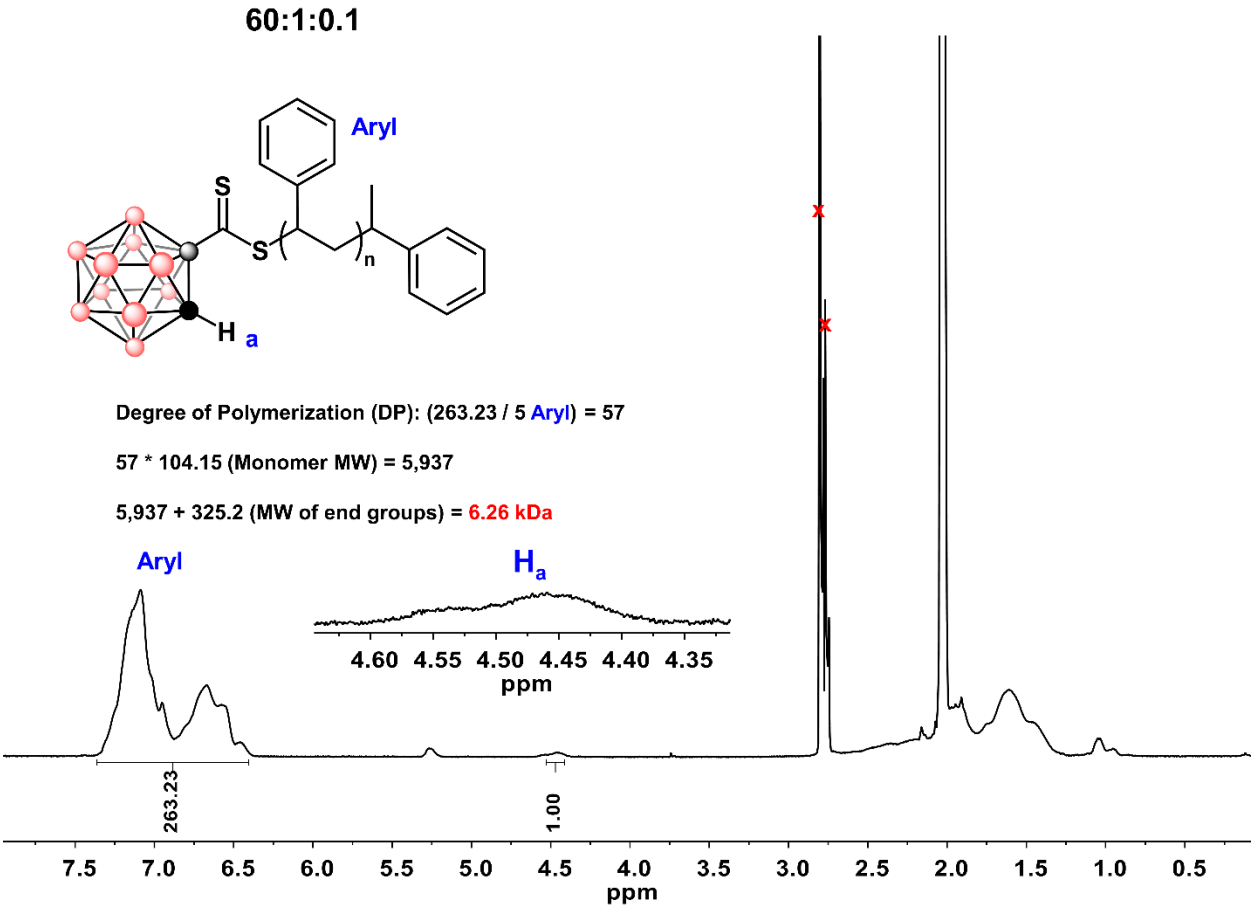

Figure C12. ^{1}H NMR spectrum of **1-PS** in acetonitrile-d_3 at 298 K and sample calculation of polymer molecular weight.

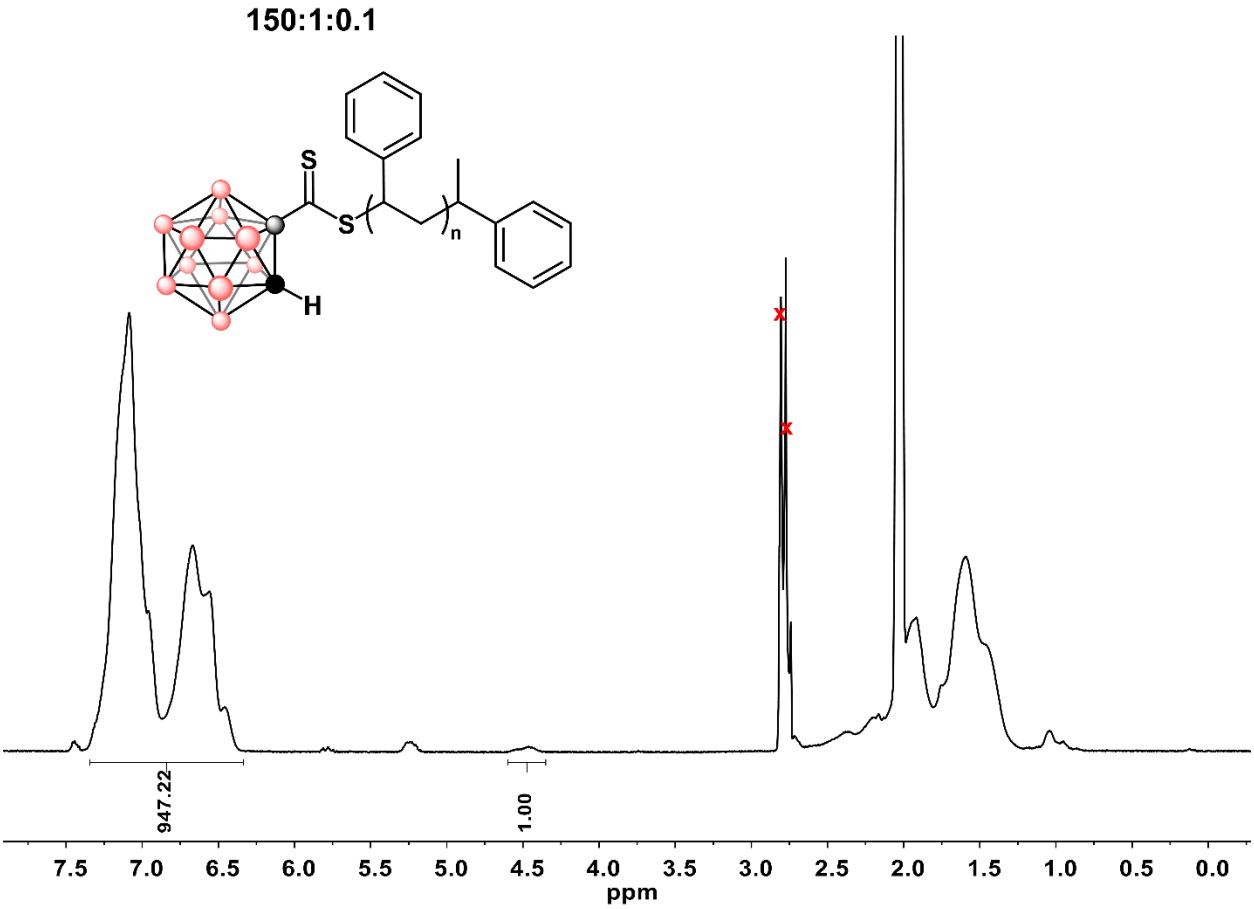

Figure C13. ^{1}H NMR spectrum of **1-PS** in acetonitrile-d_3 at 298 K and sample calculation of polymer molecular weight.

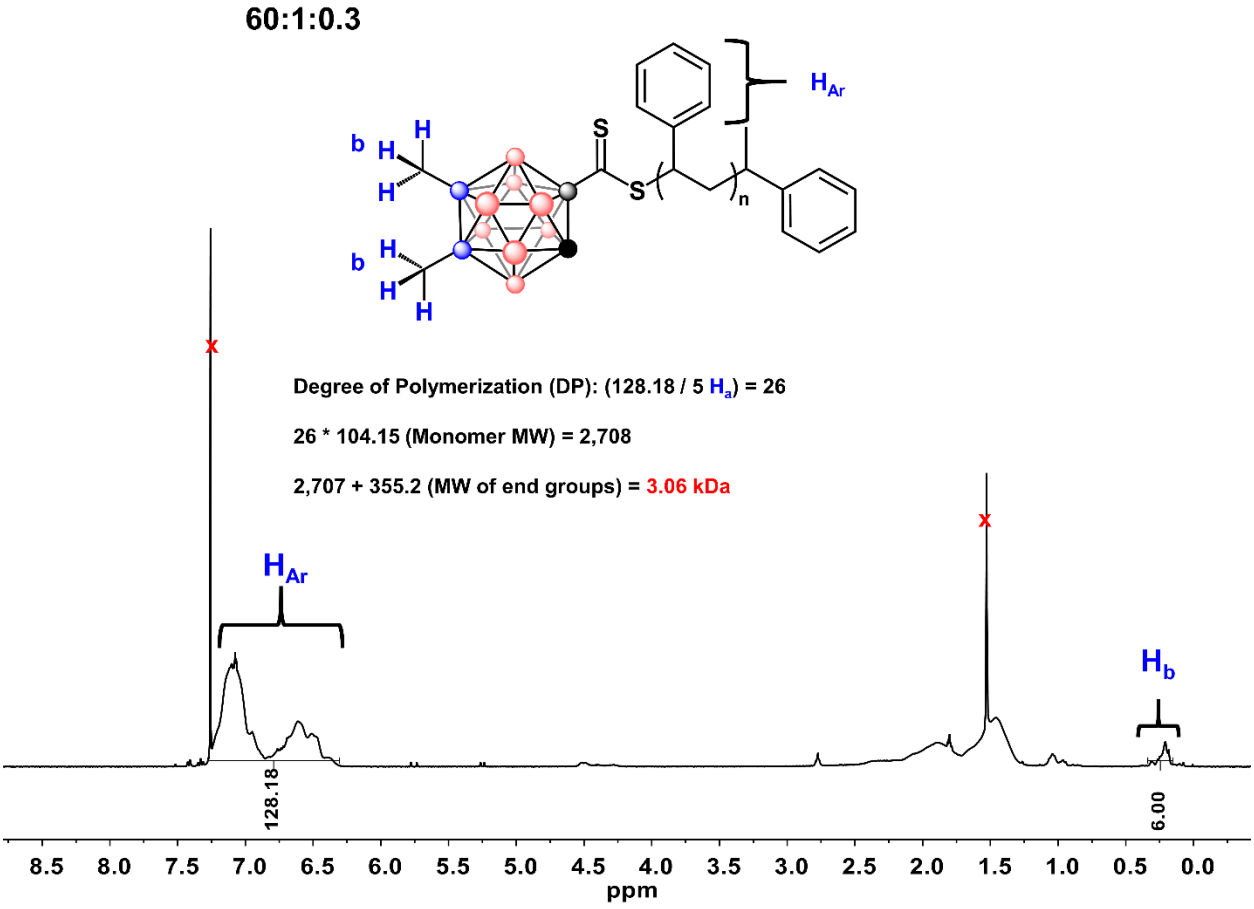

Figure C14. ^{1}H NMR spectrum of **2-PS** in chloroform-*d* at 298 K and sample calculation of polymer molecular weight.

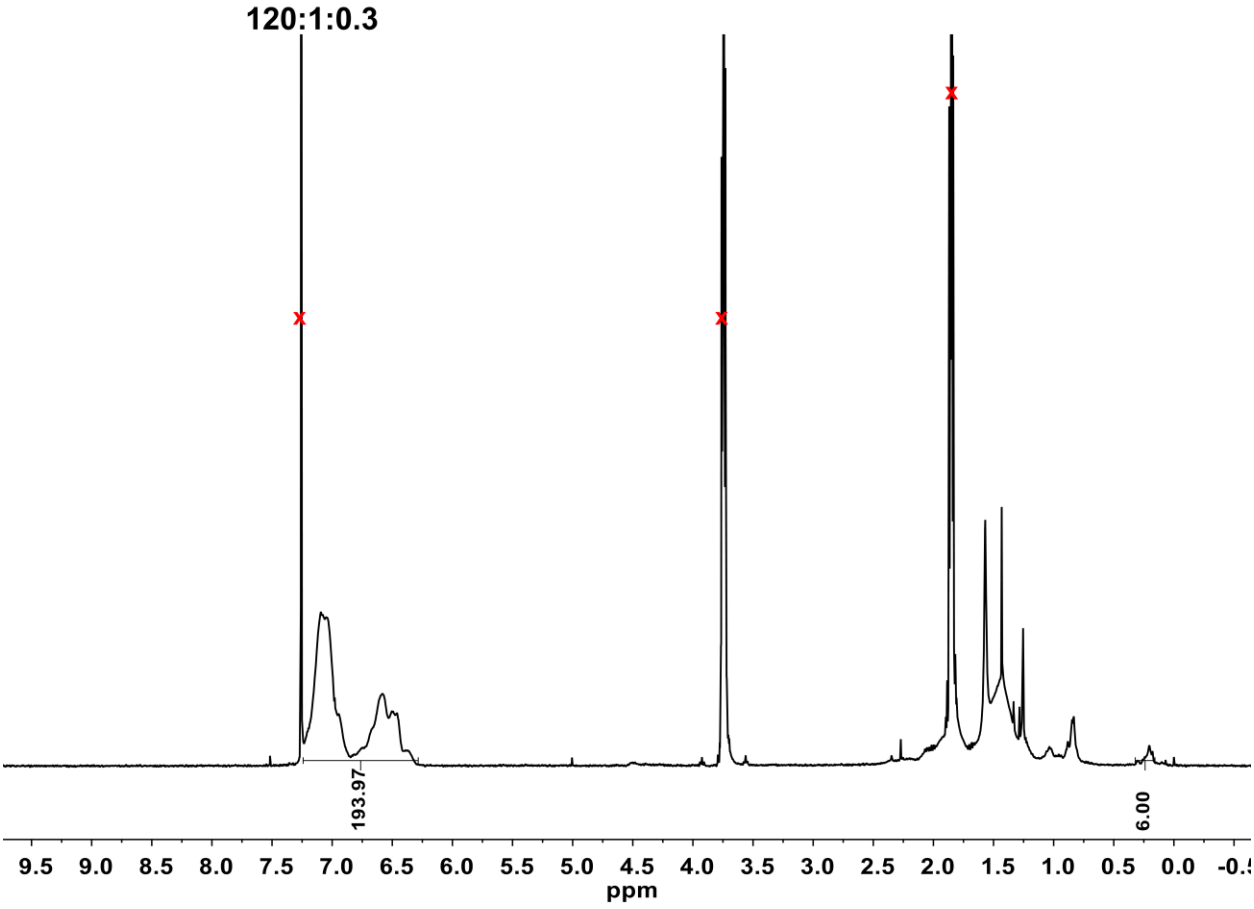

Figure C15. ^{1}H NMR spectrum of **2-PS** in chloroform-*d* at 298 K.

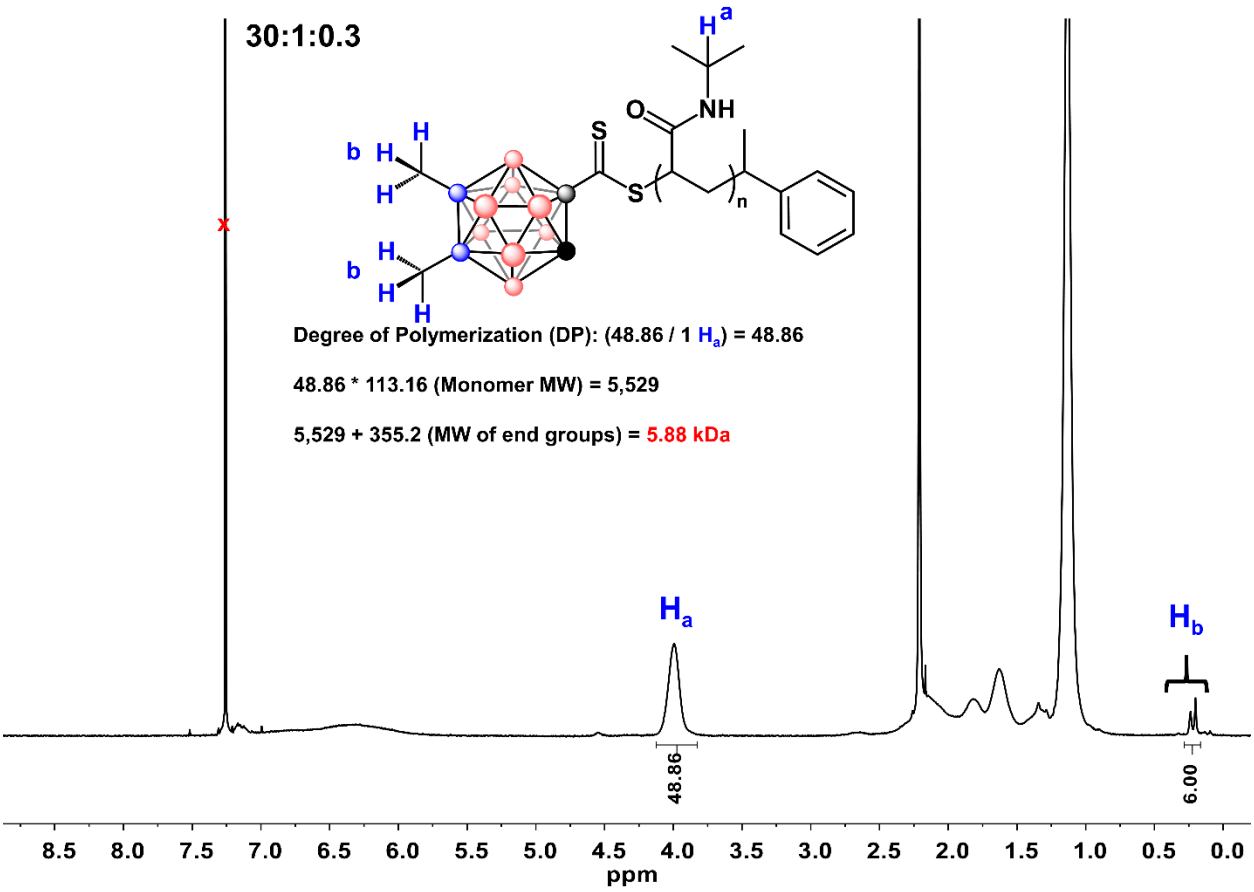

Figure C16. ^{1}H NMR spectrum of **2-pNIPAAm** in chloroform-*d* at 298 K and sample calculation of polymer molecular weight.

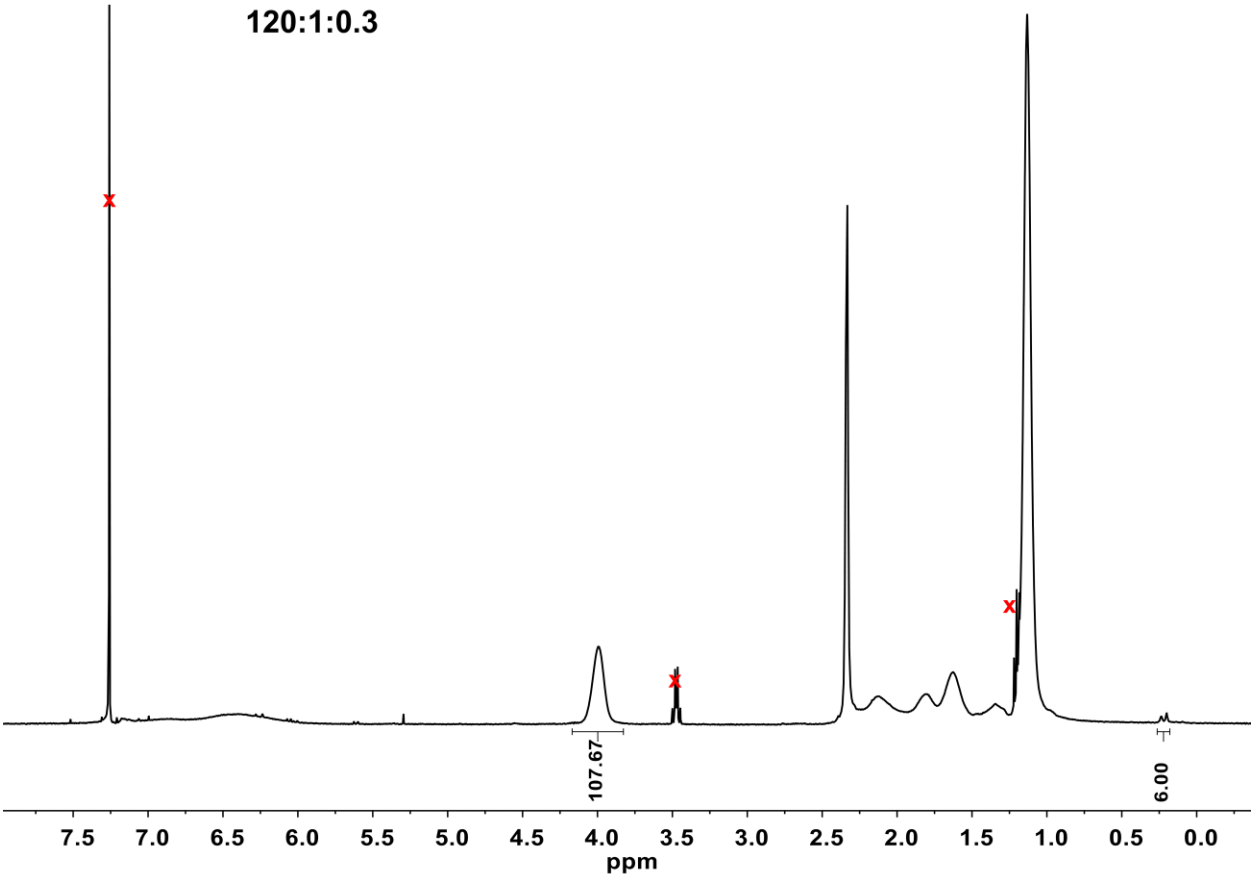

Figure C17. ^{1}H NMR spectrum of **2-pNIPAAm** in chloroform-*d* at 298 K.

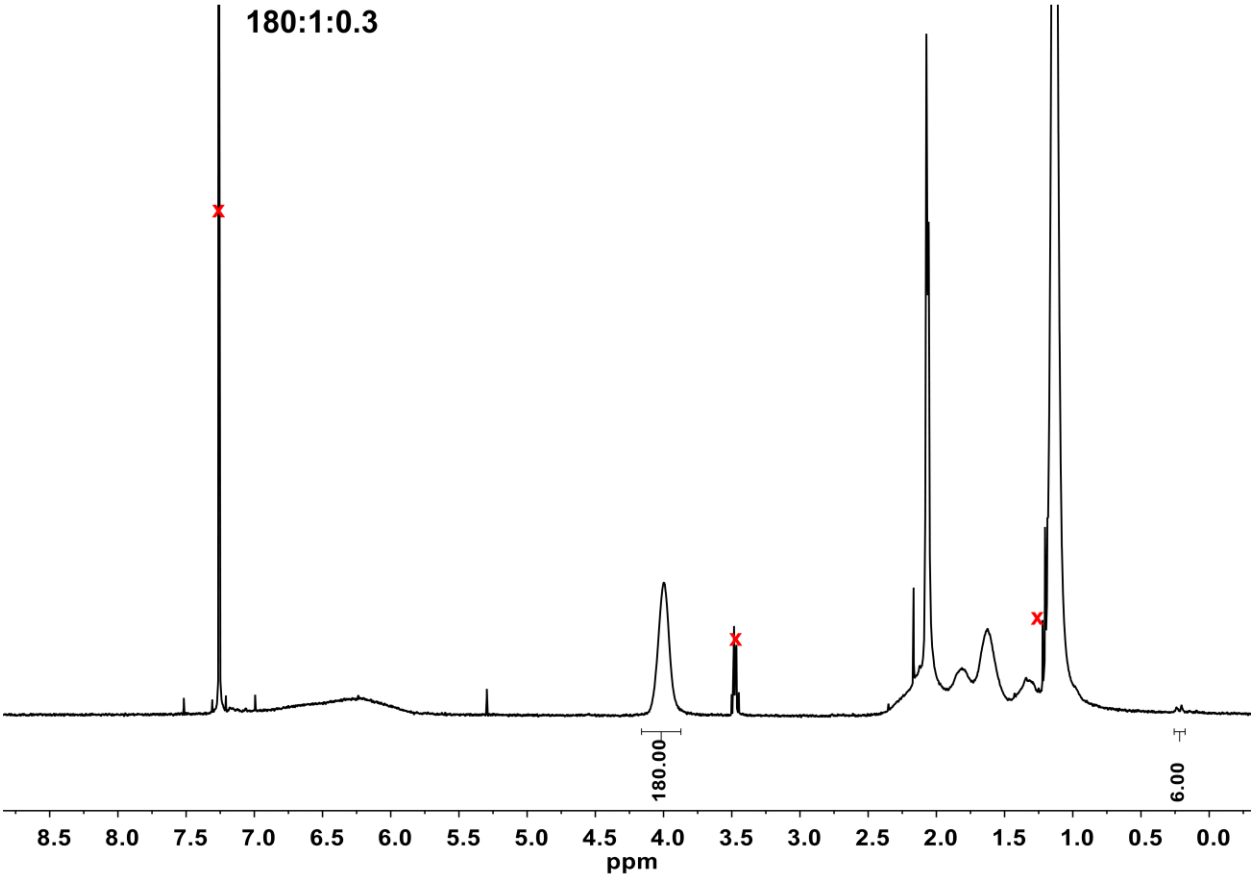

Figure C18. ^{1}H NMR spectrum of **2-pNIPAAm** in chloroform-*d* at 298 K.

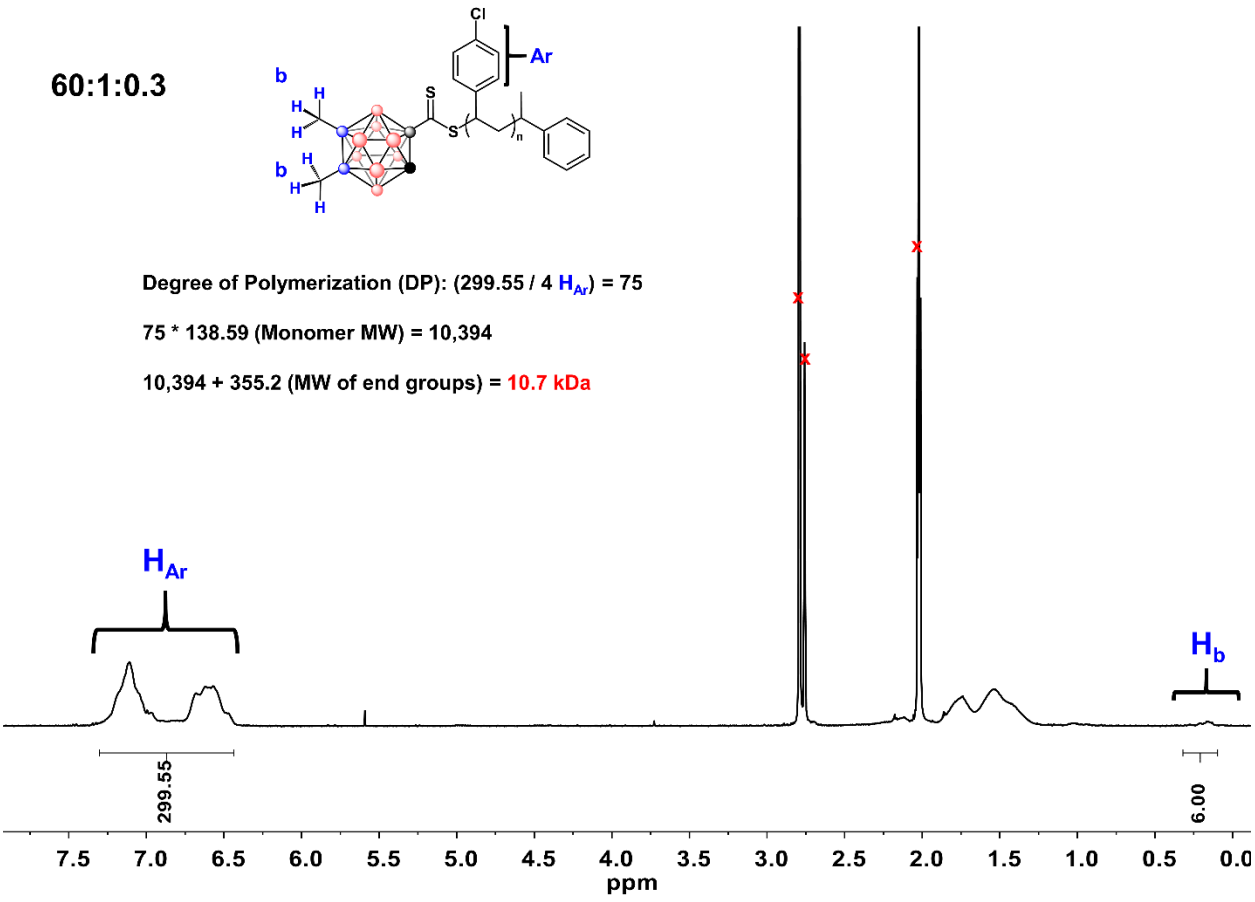

Figure C19. ^{1}H NMR spectrum of **2-(4-Cl)-PS** in acetone-d_6 at 298 K and sample calculation of polymer molecular weight.

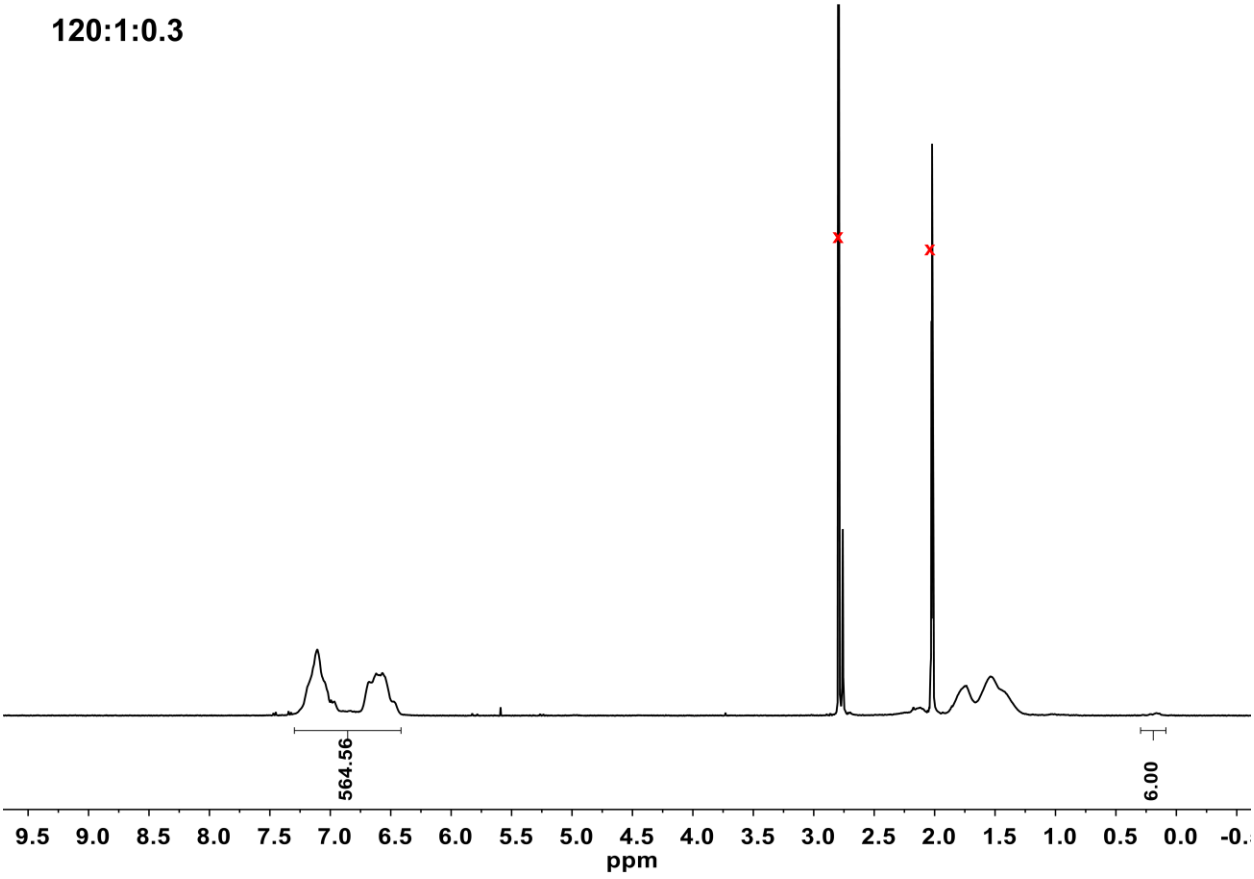

Figure C20. ^{1}H NMR spectrum of **2-(4-Cl)-PS** in in acetone-d_6 at 298 K.

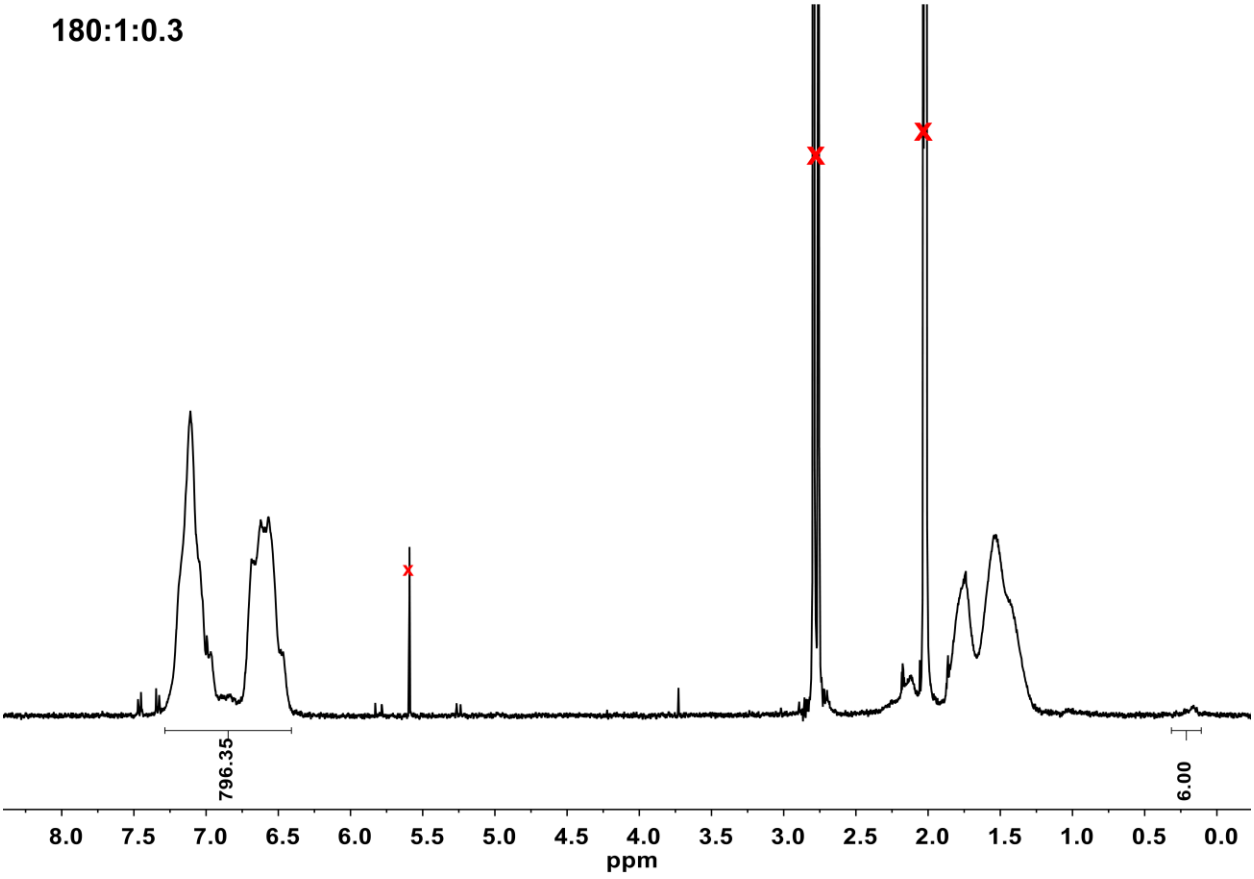

Figure C21. ^{1}H NMR spectrum of **2-(4-Cl)-PS** in in acetone-d_6 at 298 K.

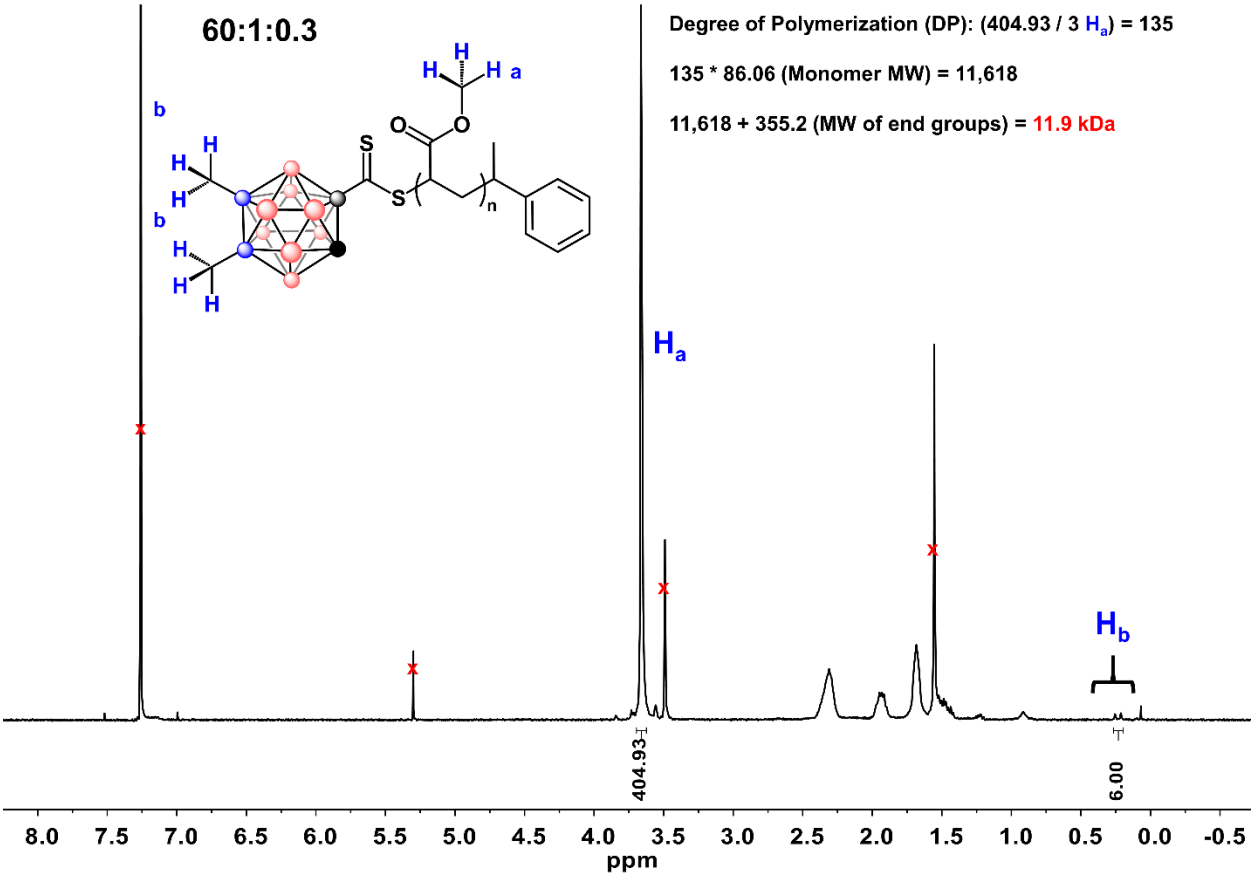

Figure C22. ^{1}H NMR spectrum of **2-PMA** in chloroform-*d* at 298 K and sample calculation of polymer molecular weight.

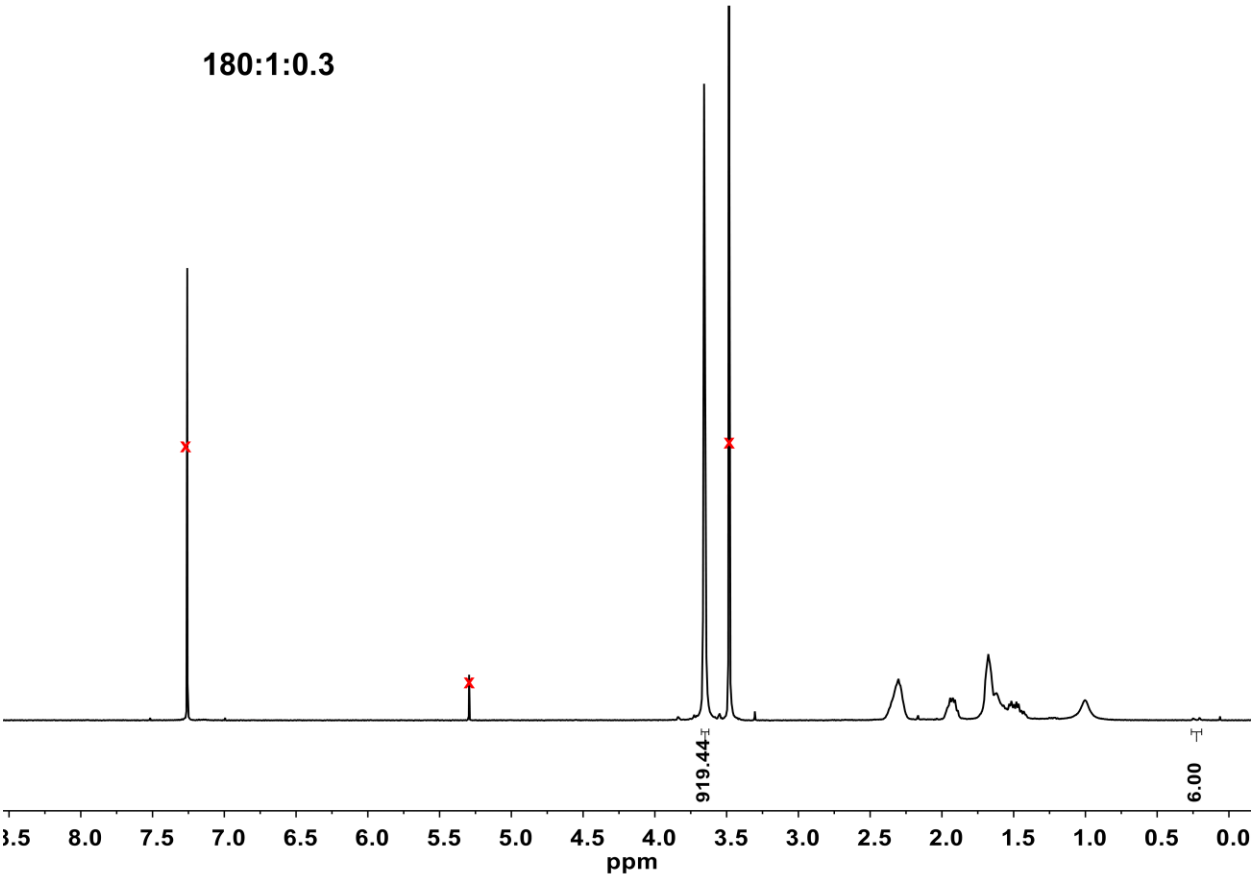

Figure C23. ^{1}H NMR spectrum of **2-PMA** in chloroform-*d* at 298 K.

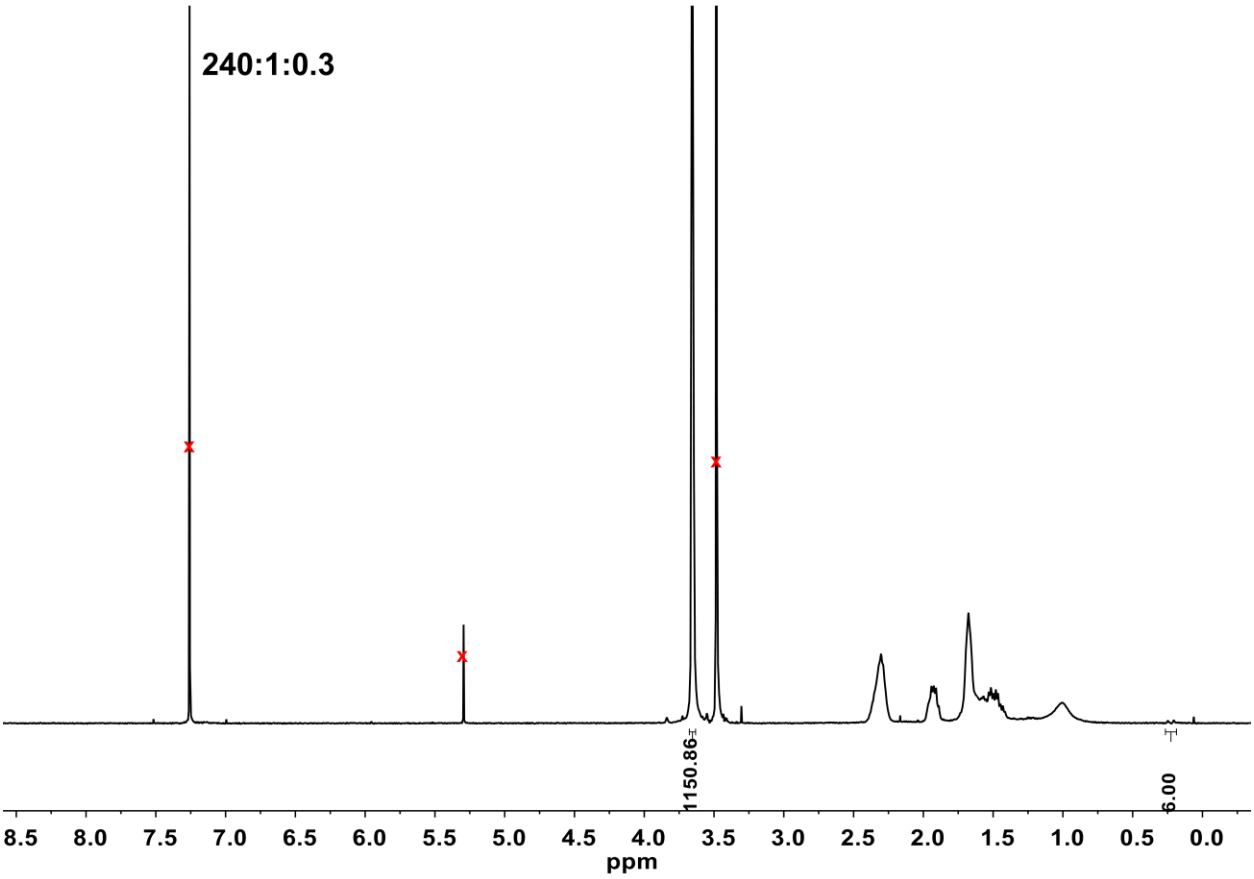

Figure C24. ^{1}H NMR spectrum of **2-PMA** in chloroform-*d* at 298 K.

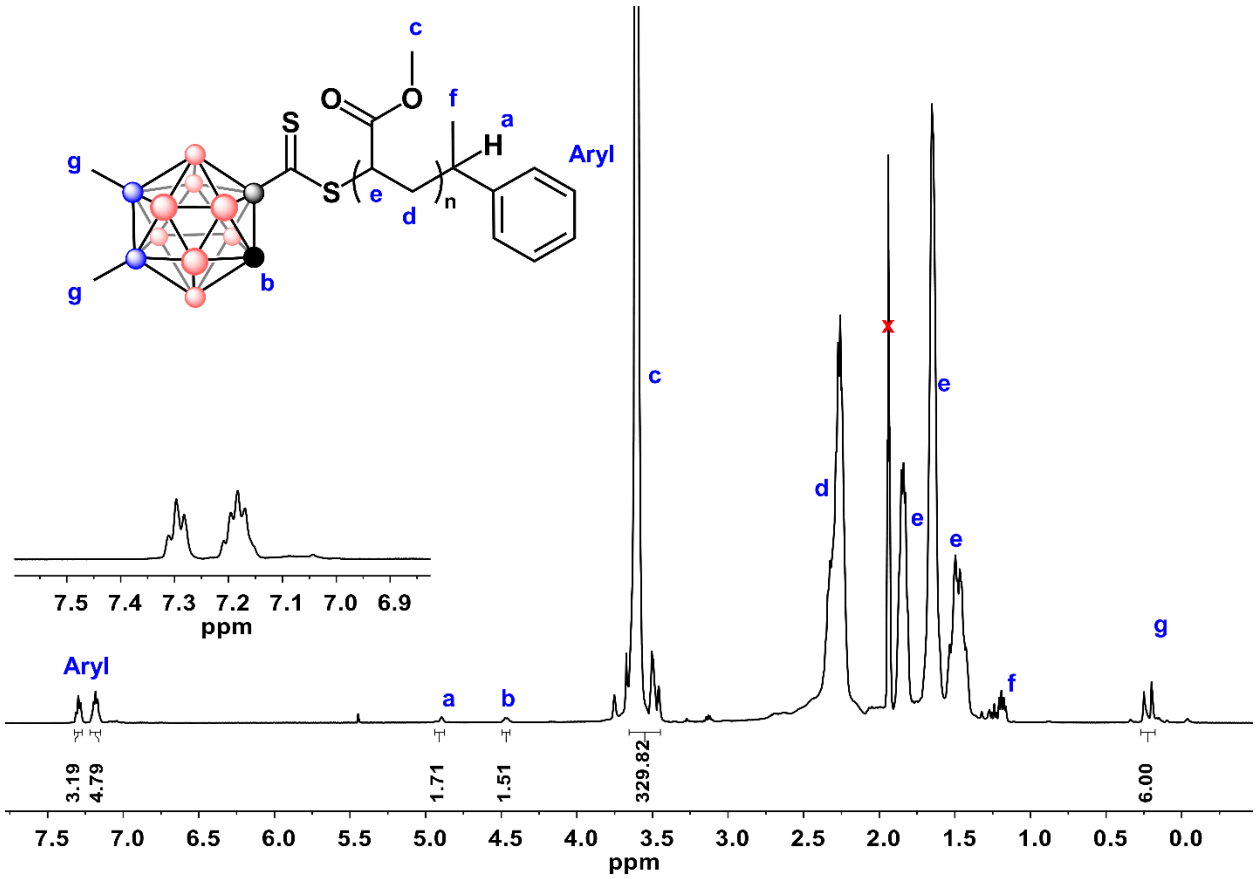

Figure C25. ^{1}H NMR spectrum of **2-PMA** in acetonitrile-d_3 at 298 K.

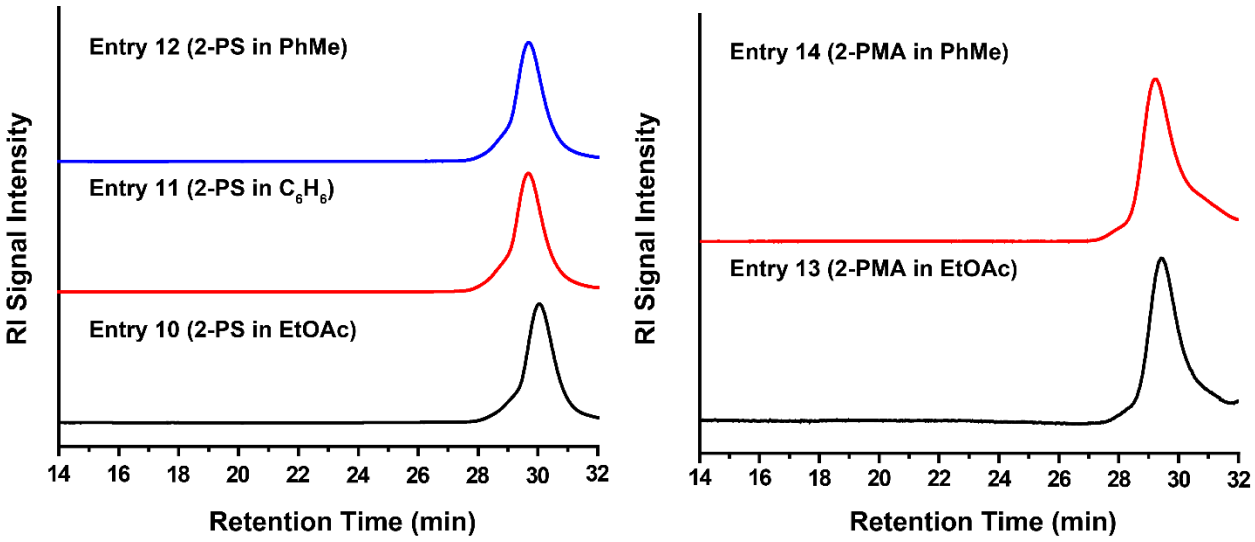

Figure C26. GPC traces of styrene and methyl acrylate in various solvents. GPC acquired using THF as the eluent.

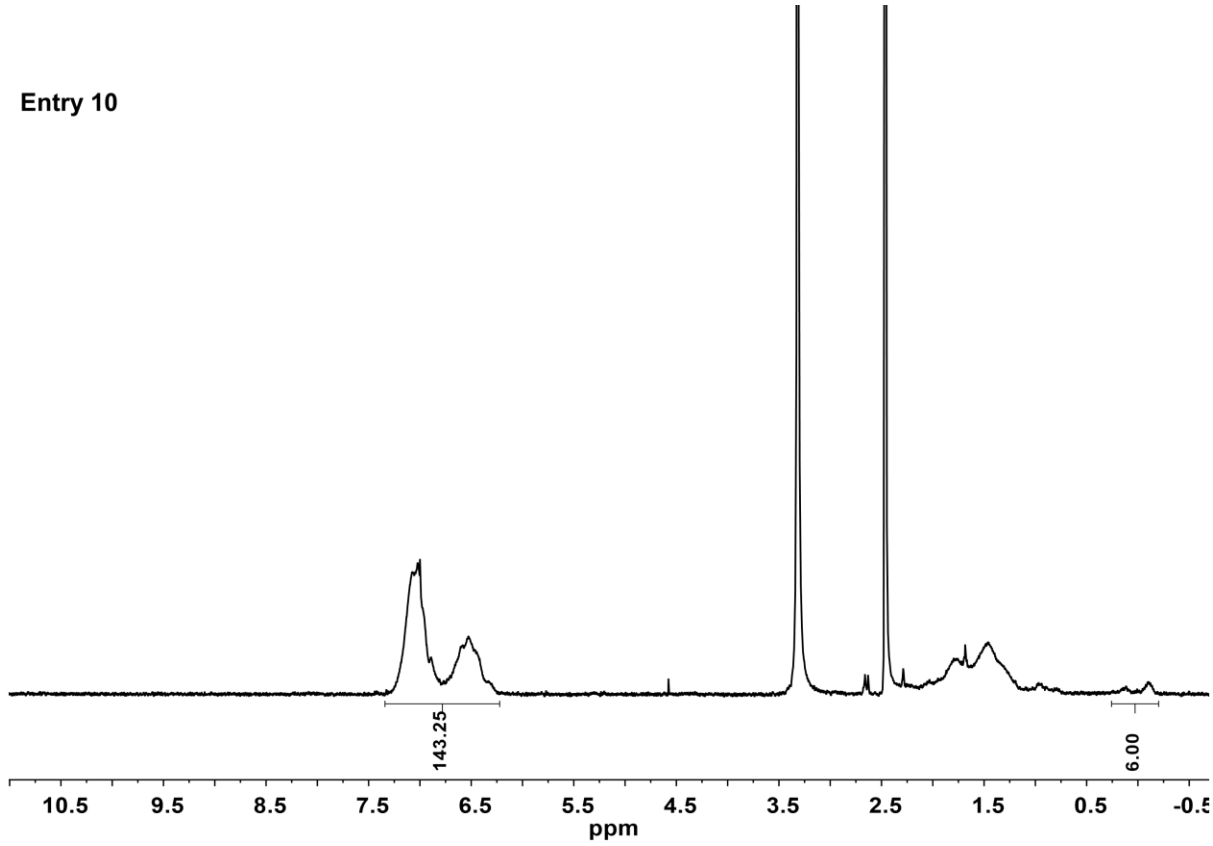

Figure C27. ^{1}H NMR spectrum of **2-PS** in acetone-d_6 at 298 K, related to entry 10, **Figure C19**.

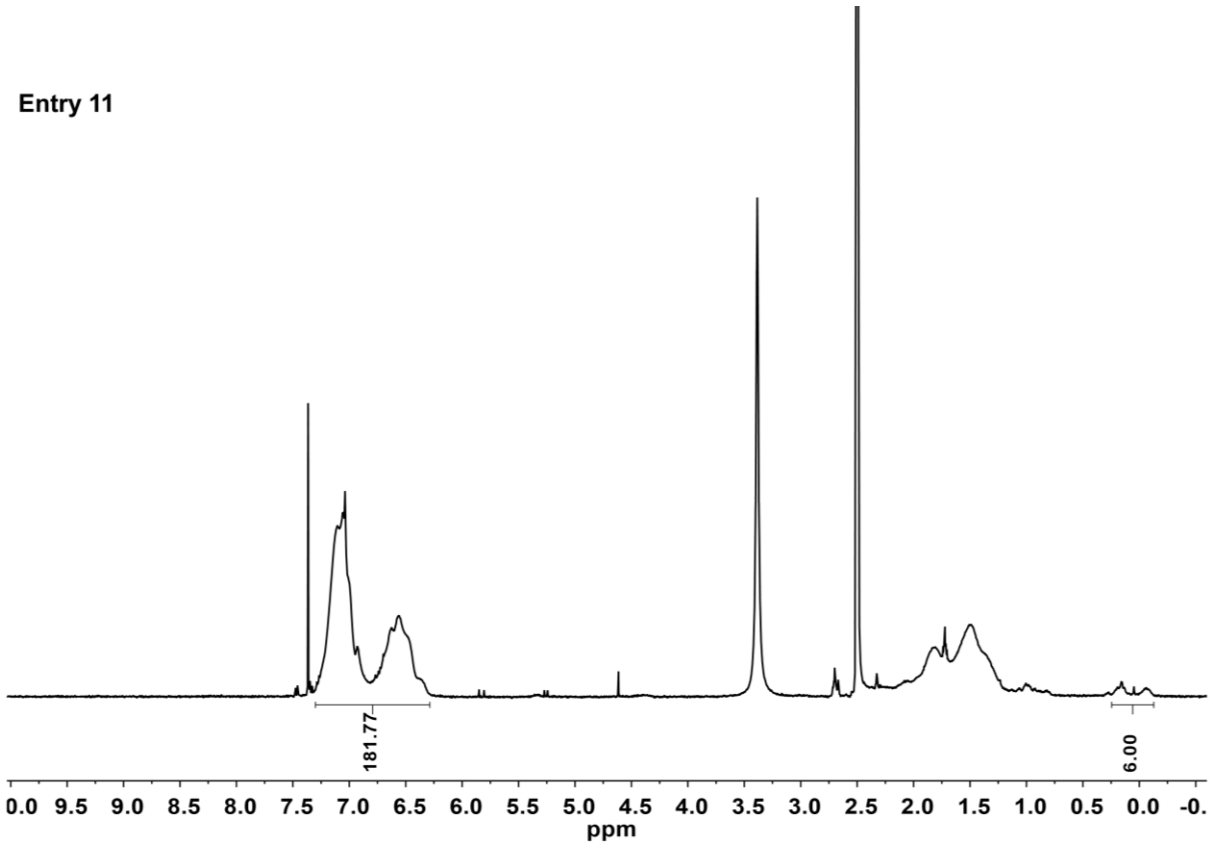

Figure C28. ^{1}H NMR spectrum of **2-PS** in chloroform-*d* at 298 K, related to entry 11, **Figure C19**.

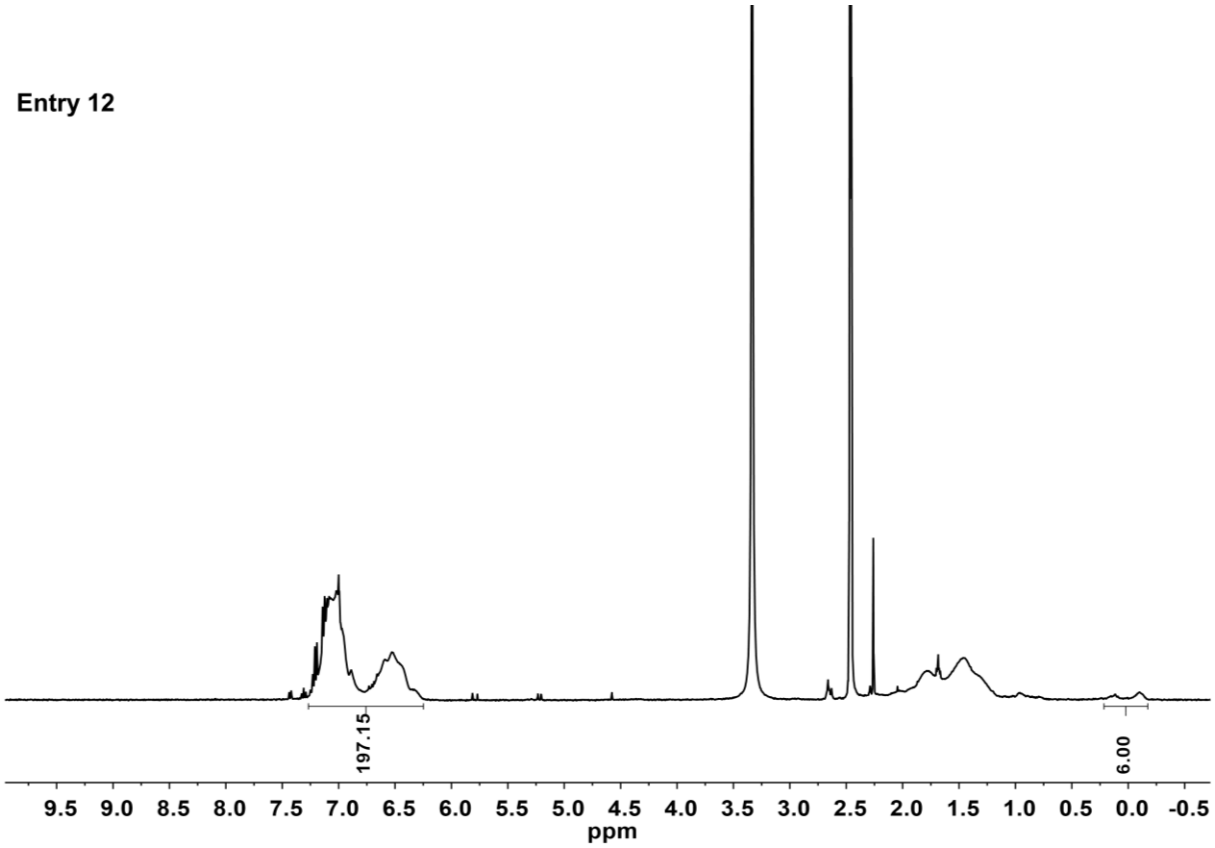

Figure C29. ^{1}H NMR spectrum of **2-PS** in acetone-d_6 at 298 K, related to entry 12, **Figure C19**.

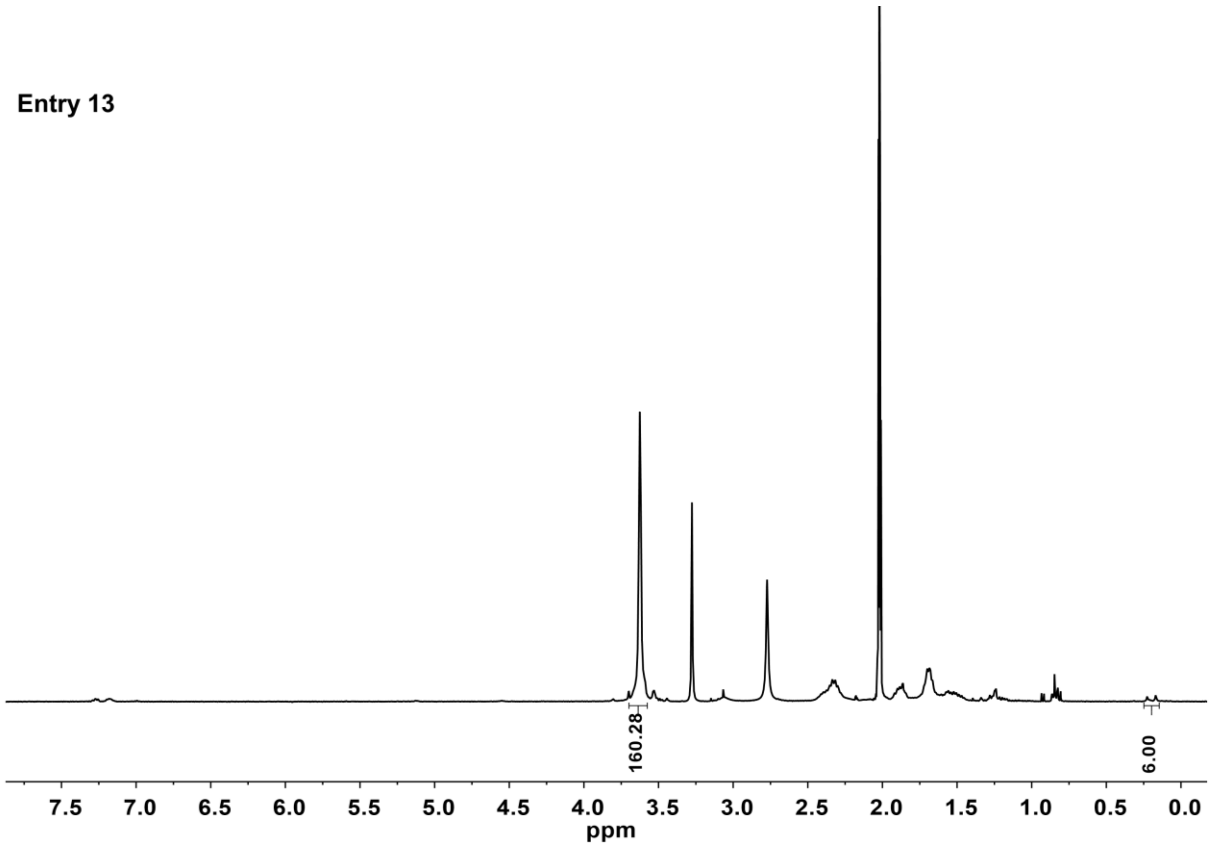

Figure C30. ^{1}H NMR spectrum of **2-PMA** in acetonitrile-d_3 at 298 K, related to Entry 13, **Figure C19**.

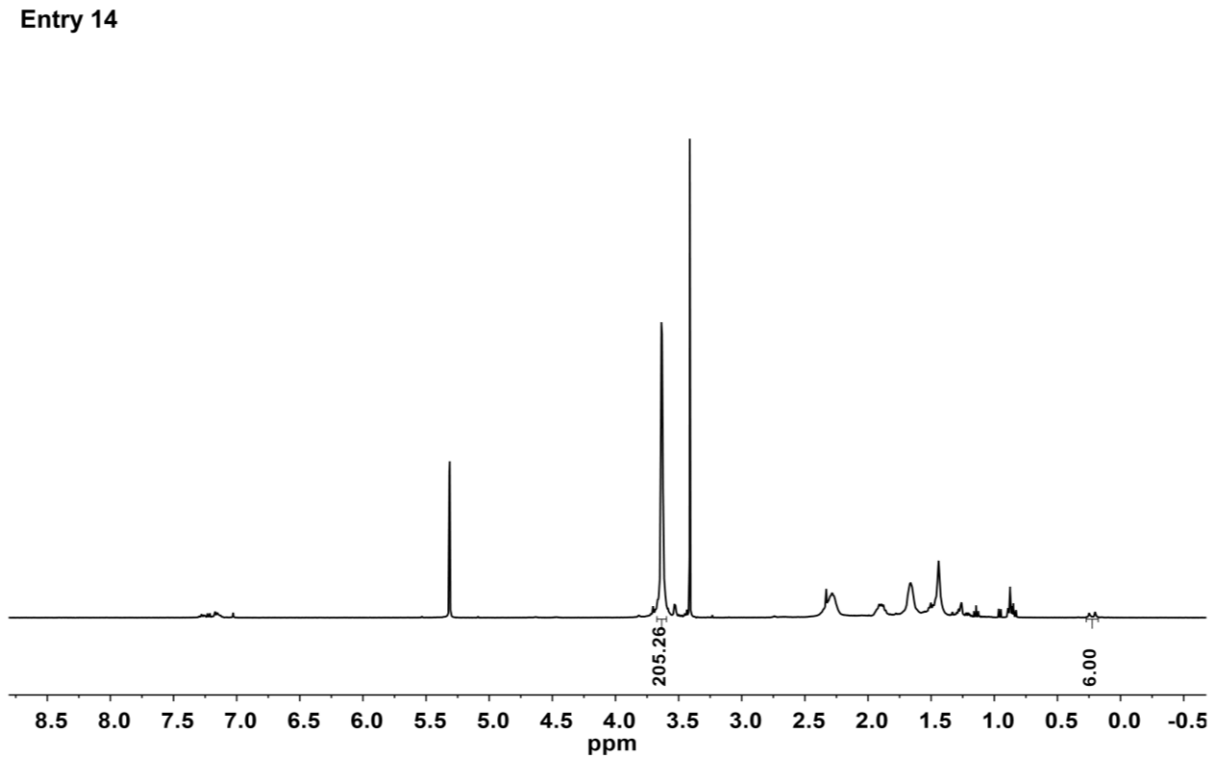

Figure C31. ^{1}H NMR spectrum of **2-PMA** in acetonitrile-d_3 at 298 K, related to Entry 14, **Figure C19**.

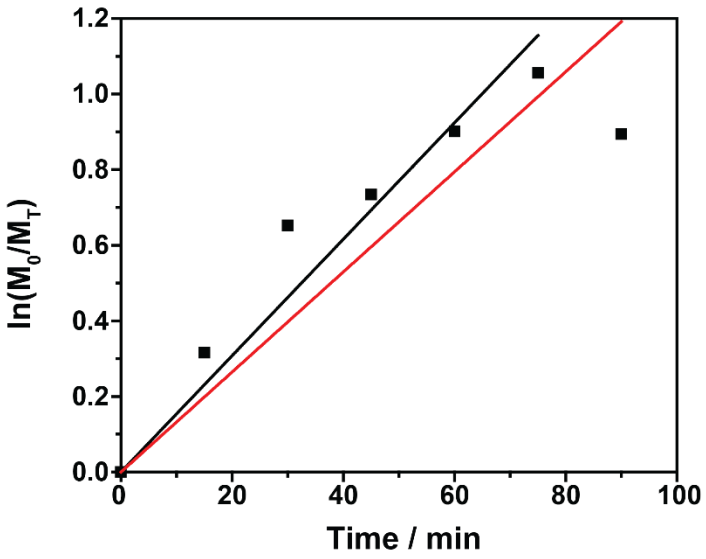

Figure C32. Polymer kinetic plot of polymerization of a bulk methyl acrylate solution. Black line indicates fitting without 90 minute time aliquot included ($R^2 = 0.97$). Red line indicates fitting with 90 minute time aliquot included ($R^2 = 0.93$). Experiment performed by making separate reaction aliquots in dram vials with Teflon coated caps from a stock solution of the monomer, initiator, and CTA. Aliquots were quenched at pre-determined time intervals by exposing the reaction mixture to air. It is possible that the final 90 minute aliquot losing linearity is due to minor pipetting error or due to the viscosity of the bulk solution.

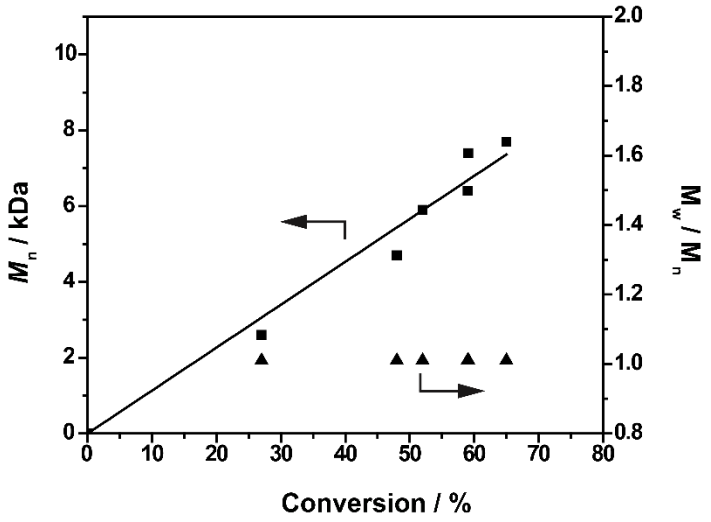

Figure C33. Evolution of M_n as a function of monomer conversion from the experiment in **Figure C32**.

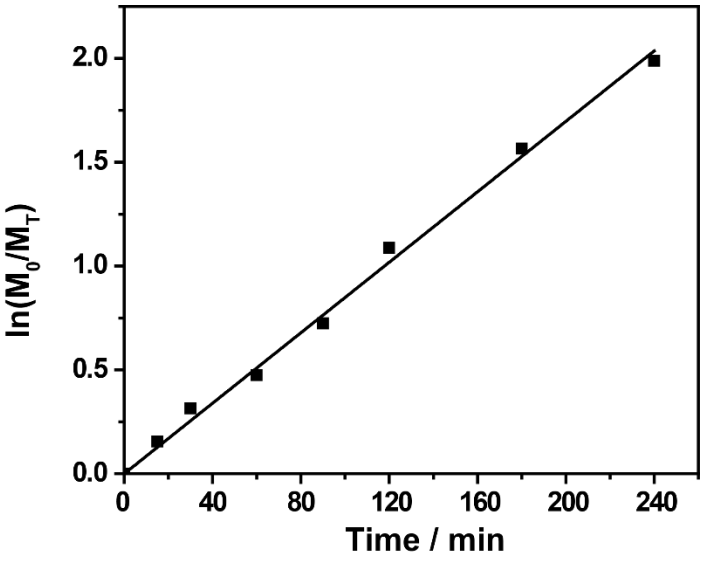

Figure C34. Polymer kinetic plot of polymerization of a 2M solution of methyl acrylate in PhMe ($R^2 = 0.99$).

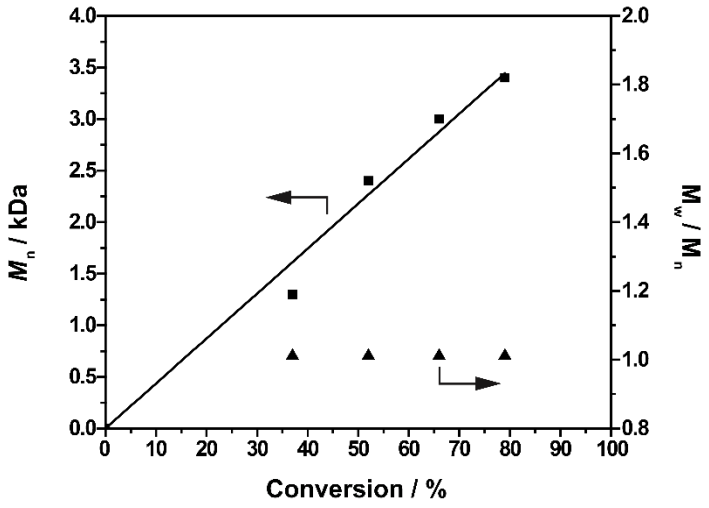

Figure C35. Evolution of M_n as a function of monomer conversion from the experiment in **Figure C34**.

4.5.6.5 Polymer end-group modification

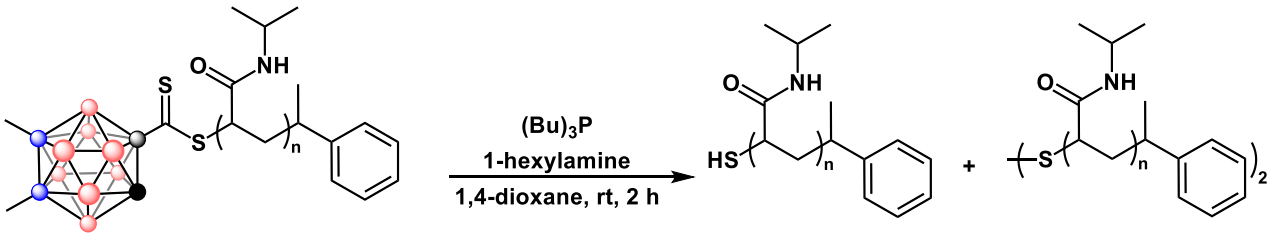

2-pNIPAAm (370.0 mg mg, 2.66x10^{-5} mol, 1 equiv) was added to a dry and degassed 4-mL dram vial sealed with a Teflon coated septum cap and equipped with a magnetic stir bar. Tributylphosphine (66.4 uL, 0.27 mmol, 10 equiv) dissolved in 1,4-dioxane (5 mL) and added to the vial containing 2-pNIPAAm. The solution was sparged with argon for 10 minutes. After sparging, 1-hexylamine (176.0 uL, 1.33 mmol, 50 equiv) was added and the solution was stirred at room temperature for 16 hours. Precipitation of the polymer from cold methanol afforded both deprotected and coupled polymer products.

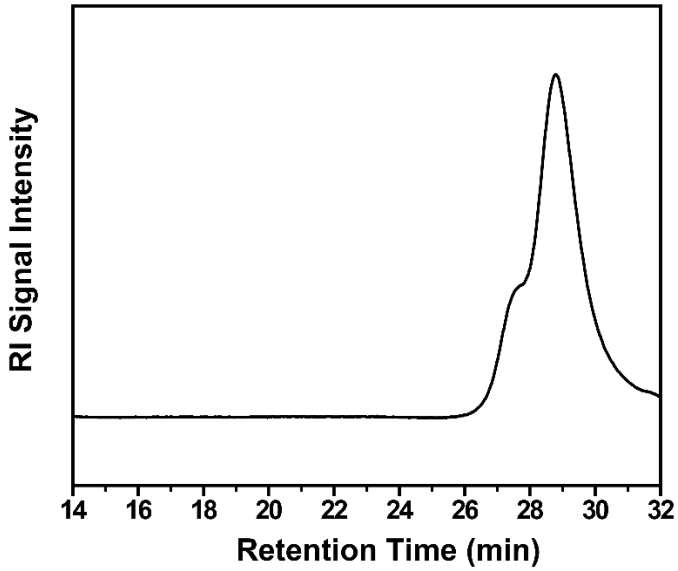

Figure C36. GPC spectrum of carborane deprotection reaction, which shows a high degree of polymer coupling over the course of the reaction. GPC acquired using DMF with 0.1 M LiBr as the eluent.

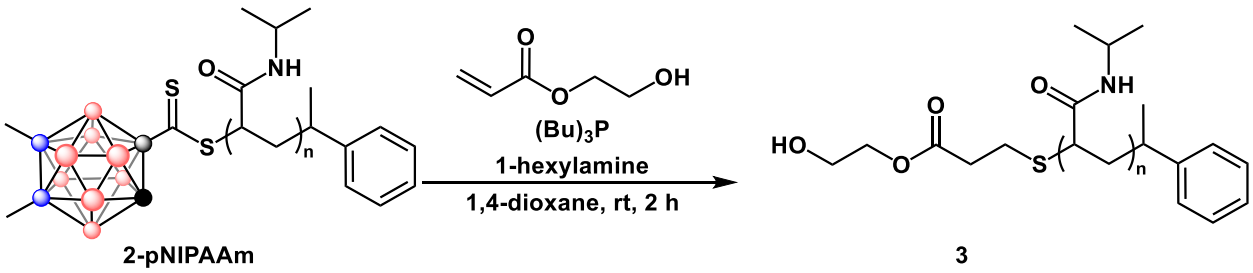

2-pNIPAAm (20.0 mg, 8.37x10^{-6} mol, 1 equiv) was added to a dry and degassed 4-mL dram vial sealed with a Teflon coated septum cap and equipped with a magnetic stir bar. Tributylphosphine (41.3 uL, 0.17 mmol, 20 equiv) and 2-hydroxyethyl acrylate (96.0 uL, 0.84 mmol, 100 equiv) were dissolved in 1,4-dioxane (1 mL) and added to the vial containing 2-pNIPAm. The solution was sparged with argon for 10 minutes. After sparging, 1-hexylamine (22.1 uL, 0.17 mmol, 20 equiv)

was added and the solution was stirred at room temperature for 16 hours. Precipitation of the polymer from cold methanol afforded pure product as a light yellow solid.

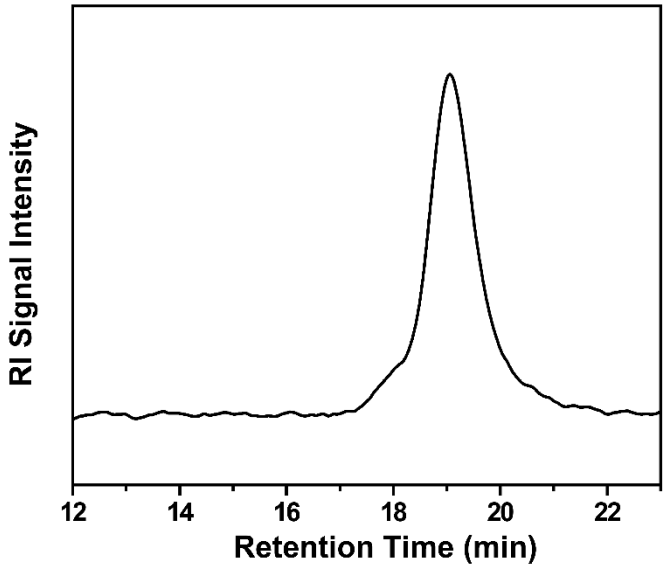

Figure C37. GPC spectrum of **3**. GPC acquired using DMF with 0.1 M LiBr as the eluent.

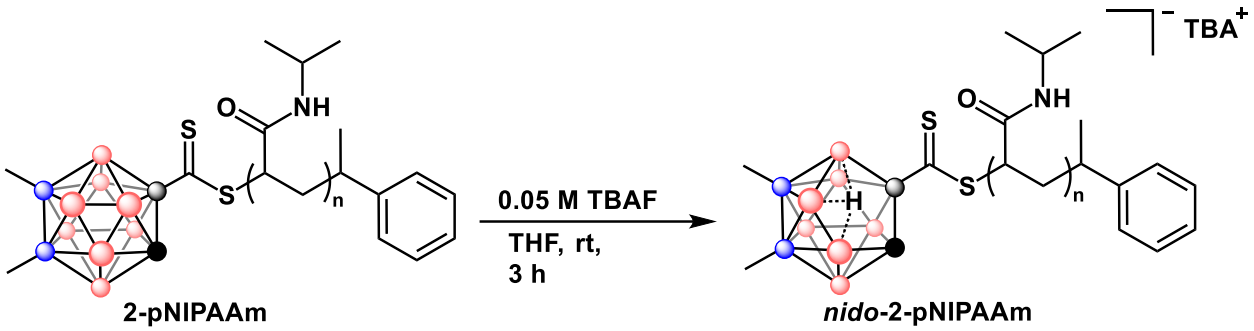

2-pNIPAAm (26.1 mg, 2.0×10^{-6} mol, 1 equiv) and TBAF (2.6 mg, 1.0×10^{-5} mol, 5 equiv) were added to a 4 mL scintillation vial equipped with a magnetic stir bar and dissolved in THF (200 µL). The reaction was left stirring at room temperature for 3 hours at which point the solution was diluted in water (2 mL) and purified *via* dialysis (MWCO = 3500 Da) against water for 2 days. The water was removed *via* lyophilization to produce the pure product as a yellow solid.

^{1}H NMR (500MHz, acetonitrile-d_3, 298K): δ 6.57 (bs, -N*H*), 3.94 (s, -C*H*(CH_3)$_2$), 2.43 (bs, -C*H*), 2.05 (bs, -CH_2), 1.67 (bs, -CH_2), 1.51 – 1.10 (bs, -CH(CH_3)$_2$), 0.23 (bs, -BCH_3), 0.16 (bs, -BCH_3), -2.1 (bs, $H_{Hydride}$).

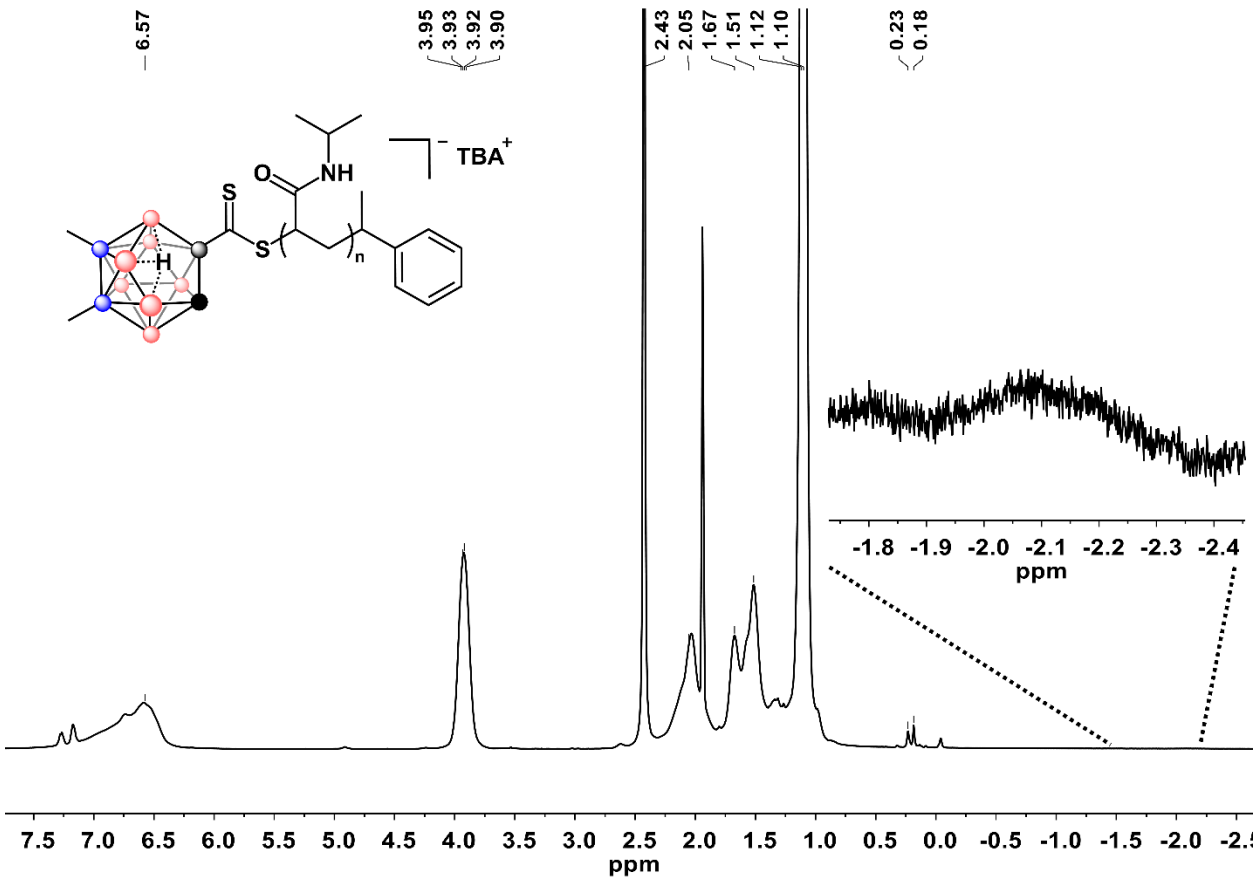

Figure C38. ^{1}H NMR spectrum of ***nido*-2-pNIPAAm** in acetonitrile-d_3 at 298 K.

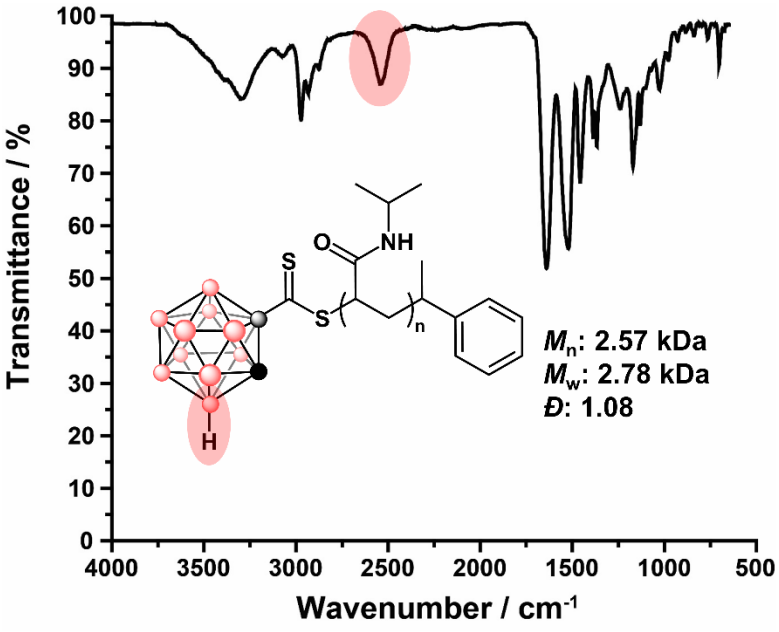

Figure C39. IR spectrum of **1-pNIPAAm**.

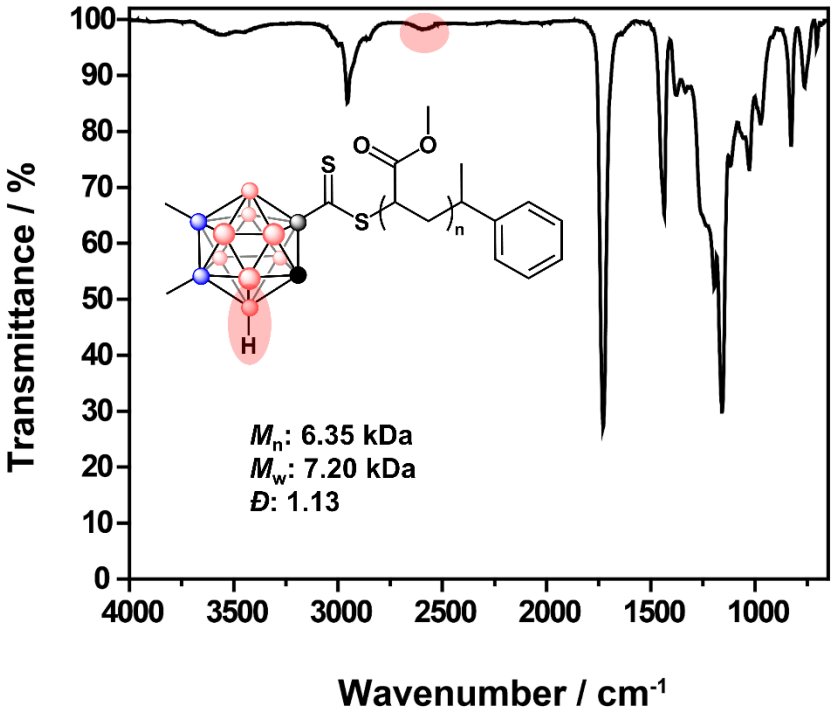

Figure C40. IR spectrum of **2-PMA**.

4.5.7 Crystallographic Characterization

Identification code	PC18	
Empirical formula	C11 H20 B10 S2	
Formula weight	324.49	
Temperature	150.0 K	
Wavelength	0.71073 Å	
Crystal system	Monoclinic	
Space group	P 21/c	
Unit cell dimensions	a = 12.427(2) Å	□= 90°.
	b = 12.068(3) Å	□= 92.622(9)°.
	c = 11.6342(17) Å	□ = 90°.
Volume	1742.9(6) $Å^3$	
Z	4	
Density (calculated)	1.237 Mg/m^3	
Absorption coefficient	0.291 mm^{-1}	
F(000)	672	
Crystal size	0.98 x 0.28 x 0.26 mm^3	
Theta range for data collection	2.354 to 26.391°.	
Index ranges	-11<=h<=15, -15<=k<=9, -14<=l<=13	
Reflections collected	8343	
Independent reflections	3449 [R(int) = 0.0581]	
Completeness to theta = 25.242°	97.4 %	

Absorption correction	Semi-empirical from equivalents
Max. and min. transmission	0.7454 and 0.5007
Refinement method	Full-matrix least-squares on F^2
Data / restraints / parameters	3449 / 2 / 209
Goodness-of-fit on F^2	1.049
Final R indices [I>2sigma(I)]	R1 = 0.0868, wR2 = 0.2110
R indices (all data)	R1 = 0.1578, wR2 = 0.2405
Extinction coefficient	n/a
Largest diff. peak and hole	0.454 and -0.546 e.$Å^{-3}$

Atomic coordinates (x 10^4) and equivalent isotropic displacement parameters ($Å^2$x 10^3) for **1**. U(eq) is defined as one third of the trace of the orthogonalized U^{ij} tensor.

	x	y	z	U(eq)
S(1)	6670(1)	3636(2)	6609(1)	46(1)
S(2)	6367(1)	3491(2)	9154(1)	54(1)
C(2)	4718(3)	3759(5)	7501(3)	26(1)
C(6)	8734(3)	3121(5)	6248(3)	29(2)
C(1)	3881(3)	3648(5)	8541(3)	26(1)
C(4)	8068(4)	3620(6)	7190(4)	34(2)
C(5)	8417(4)	4763(7)	7591(4)	48(2)
C(3)	5911(4)	3636(6)	7825(4)	34(2)
B(10)	4154(4)	3263(6)	6241(4)	30(2)
B(7)	3951(4)	2579(7)	7579(4)	33(2)
B(3)	2709(5)	3030(7)	8097(5)	33(2)
B(9)	3027(4)	4126(7)	5935(4)	31(2)
B(2)	2794(5)	4480(7)	8342(4)	34(2)
B(8)	2834(5)	2792(7)	6596(5)	35(2)
B(1)	4107(5)	4943(7)	7986(4)	37(2)
B(6)	4245(5)	4688(7)	6490(4)	38(2)
B(4)	2130(5)	3985(7)	7070(5)	40(2)
B(5)	3000(6)	5160(8)	7013(5)	48(2)

C(9)	9953(4)	2202(8)	4554(5)	54(2)
C(11)	9022(6)	2040(7)	6296(5)	59(2)
C(10)	9618(7)	1568(7)	5441(5)	68(2)
C(8)	9686(5)	3280(7)	4504(5)	59(2)
C(7)	9075(4)	3779(5)	5343(4)	49(2)

Chapter 5

Organometallic Gold(III) Reagents for Cysteine Arylation

5.1 Introduction

Cysteine bioconjugation is a powerful tool that allows for the introduction of a diverse array of substrates to biomolecules via the formation of covalent linkages.[1–5] Transition-metal-mediated reactions have emerged recently as attractive methods for the modification of complex biomolecules due to the high functional group tolerance, chemoselectivity, and rapid reaction kinetics associated with these metal-based transformations.[6–13] Additionally, the rational choice of transition-metal ion and ligand platform can provide the ability to design organometallic-based bioconjugation reagents with highly tailored reactivity, solubility, and stability properties. This concept is embodied by the versatile and efficient palladium-mediated cysteine arylation methods reported by Buchwald, Pentelute, et al. in the past three years that enable access to a broad range of bioconjugates under mild reaction conditions (Scheme 1).[9–13]

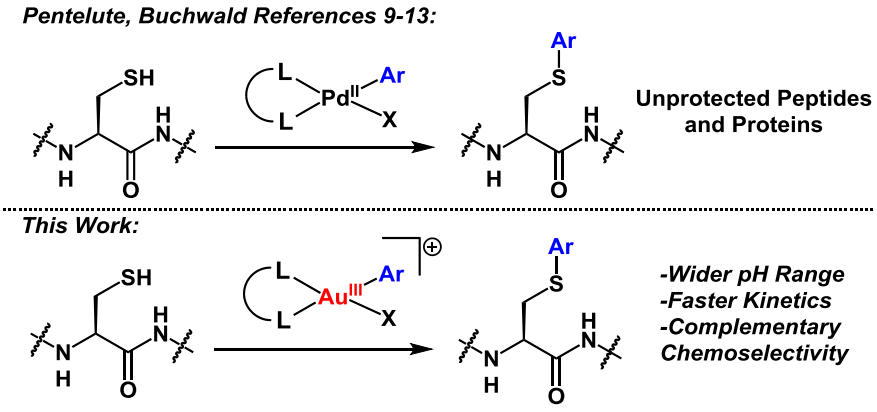

Scheme 5-1. Previous work utilizing Pd^{II} reagents (references 9–13) and this work detailing Au^{III}-mediated cysteine *S*-arylation of biomolecules.

Herein, we expand the scope, generality, and utility of transition-metal-mediated cysteine arylation via a C–S bond forming, reductive elimination process occurring from a class of robust organometallic Au(III) complexes. The reluctance of Au(I) to undergo oxidative addition[14–19] potentially provides gold-based species with high functional-group tolerance, minimizing the

propensity for background reactivity with the variety of functional groups present in complex biomolecules. Furthermore, the thiophilic nature of gold renders Au(III)- based complexes prime candidates for reduction by cysteine thiols, engendering such systems as potential reagents for bioconjugation.[20,21] Surprisingly, there are currently no auxiliary-free methods using gold-based complexes for cysteine arylation.[22] Here we introduce such a methodology using easily accessed, air-stable Au(III)-aryl complexes. The resulting methodology provides rapid access to a diverse array of protein and peptide bioconjugates with high conversion under mild reaction conditions. The broad scope and utility of the described method are highlighted by the variety of well-defined, air-stable, crystalline Au(III)-based arylation reagents that were prepared in one synthetic step from commercial reagents. The present strategy is positioned at the interface of organometallic and bioconjugation chemistry and aims to provide new and efficient tools for biomolecule modification.

5.2 Results and Discussion

Bourissou et al. recently described an elegant approach to enhance the reactivity of Au(I) species toward oxidative addition by using pre-organized ligand architectures that support the square planar geometry of the ensuing Au(III) products.[14,23,24] These systems appeared ideal to us to accommodate the elementary steps of oxidative addition, trans-metalation, and reductive elimination[17,19,25–27] required for C−S bond formation in cysteine arylation processes (Scheme 1).

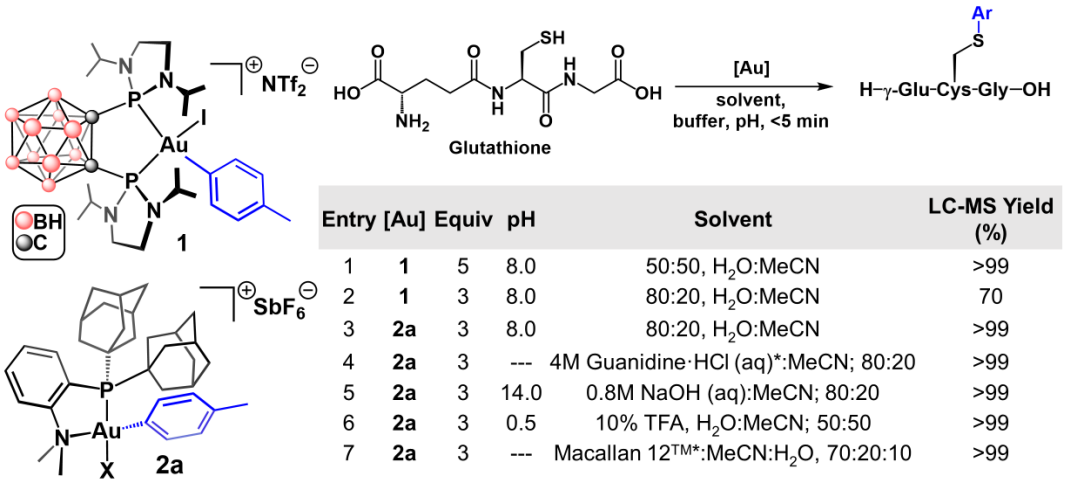

Entry	[Au]	Equiv	pH	Solvent	LC-MS Yield (%)
1	**1**	5	8.0	50:50, H_2O:MeCN	>99
2	**1**	3	8.0	80:20, H_2O:MeCN	70
3	**2a**	3	8.0	80:20, H_2O:MeCN	>99
4	**2a**	3	---	4M Guanidine·HCl (aq)*:MeCN; 80:20	>99
5	**2a**	3	14.0	0.8M NaOH (aq):MeCN; 80:20	>99
6	**2a**	3	0.5	10% TFA, H_2O:MeCN; 50:50	>99
7	**2a**	3	---	Macallan 12™*:MeCN:H_2O, 70:20:10	>99

Figure 5-1. Gold(III) reagents **1** and **2a** (X = Cl/I), and glutathione arylation scheme with reaction optimization parameters.

Optimization of cysteine arylation reaction conditions with **1** were carried out using L-glutathione (GSH) as the model peptide substrate (Figure 5-1). Full conversion to the *S*-tolyl GSH-conjugate was observed in GSH-conjugate <5 min upon treatment of GSH with **1** (5 equiv) at 25 °C in the presence of Tris buffer (pH 8) as determined by LC-MS analysis of the crude reaction mixture. Reaction solutions containing up to 80% H_2O in H_2O/MeCN mixtures were tolerated (Figure 5-1), whereas higher ratios of H_2O led to reduced reaction conversion. This limited efficiency led us to seek another Au(III)-based system that would exhibit improved compatibility in biologically relevant reaction media.

We prepared the Au(III)-tolyl oxidative addition complex, [(Me-DalPhos)Au(tolyl)Cl][SbF_6] ([**2a**][SbF_6], Me-DalPhos = ($Ad_2P(o\text{-}C_6H_4)NMe_2$) [28,29]),[24] isolated as a crystalline, airstable solid. We next evaluated the suitability of **2a** to serve as a cysteine arylation reagent under a variety of reaction conditions. Quantitative conversion of GSH to the corresponding *S*-tolyl conjugate was observed in minutes (<5 min) at 25 °C in a 80:20 H_2O:MeCN (v/v) mixture, as assayed by LC-MS analysis of the crude reaction mixture. The optimized reaction

conditions provided significant improvements upon those employing complex 1, such as lower reagent loading (3 vs 5 equiv), and a reduced percentage of organic solvent required (20% vs 50%, see Figure 5-1). Notably, the **2a**-mediated cysteine arylation reactions proceeded to completion within a large pH range (0.5−14) and in the presence of several common buffers (Tris, HEPES, Na_2CO_3). The bioconjugation reactions were also compatible with the disulfide reducing agent, TCEP (tris(2-carboxyethyl)phosphine, 1 equiv), protein denaturing agent, guanidine·HCl (4 M) and several other unconventional solvents (SI Figure D79).

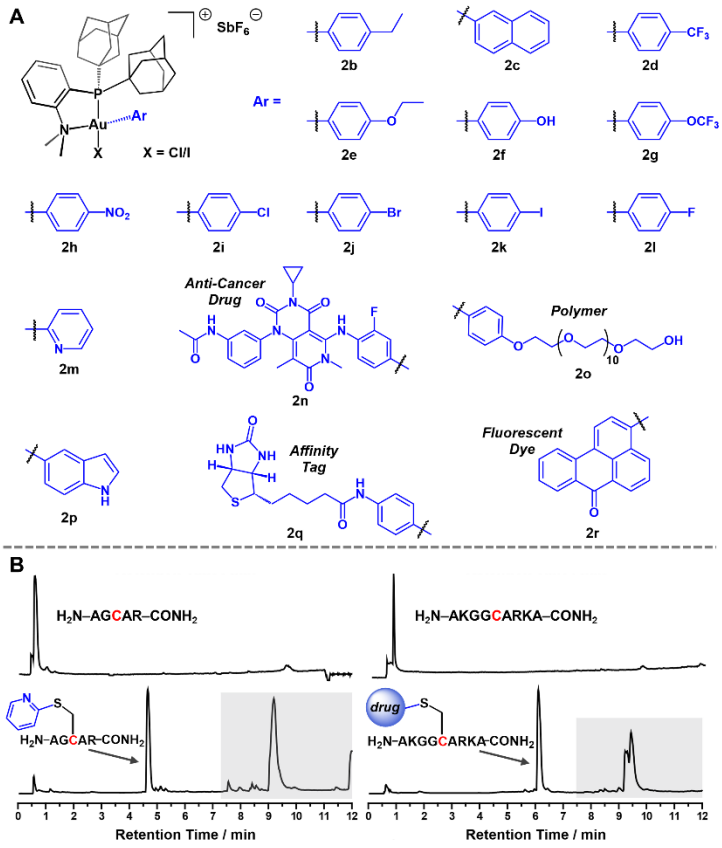

Figure 5-2. A: Scope of [(Me-DalPhos)AuArCl][SbF_6] bioconjugation reagents. B: LC traces of cysteine arylation reaction mixtures with two peptides using reagents **2m** (left) and **2n** (right). Gold-based species are highlighted in grey. See Appendix D for further experimental details.

We further prepared a library of [(Me-DalPhos)AuArCl][SbF_6] oxidative addition complexes (Figure 5-2A) bearing various biorelevant groups including heterocycles (**2m**, **2p**), an affinity label (**2q**), fluorescent tag (**2r**), complex drug molecule (**2n**), and a poly(ethylene glycol) (PEG) polymer (**2o**). Oxidative addition reactions to generate complexes 2a−2r proceeded rapidly and cleanly upon treatment of CH_2Cl_2 solutions of (Me-DalPhos)AuCl with the corresponding aryl iodide electrophile in the presence of the halide scavenger, $AgSbF_6$.[24] After removal of the liberated AgI byproduct by filtration, the [(Me-DalPhos)AuArCl][SbF_6] salts readily crystallized directly from the resulting solution upon standing at 25 °C. This purification procedure afforded X-ray diffraction quality single crystals of several complexes that enabled their structural determination (see Appendix D section 4.5.25 for crystallographic data). Notably, iodide to chloride exchange occurs at the gold center during the course of the oxidative addition reaction, as confirmed by X-ray diffraction analysis of several complexes that display Cl/I disorder with a 75−100% range of chloride occupancy (Appendix D section 4.5.25). This observation is in line with X-ray diffraction studies of closely related complexes prepared under similar conditions,[24] and is consistent with formation of the more stable gold(III) chloride derivative.[30]

Interestingly, despite the exclusion of oxygen and water from the reported preparation of **2a** and related complexes previously,[24] we found that the synthesis and purification of all [(Me-DalPhos)AuArCl][SbF_6] salts presented in this work proceeded cleanly even when performed under open atmosphere conditions using commercial, unpurified solvents. The salts exhibited excellent long-term air and water stability, and no observable degradation was detected after prolonged periods (>3 months) when the reagents were stored on the benchtop at 25 °C as assayed by ^{1}H and ^{31}P NMR spectroscopy. Complex **2o** displayed solubility in neat H_2O due to the hydrophilicity imparted by the PEG group. This species also demonstrated excellent water

stability, showing only limited degradation (ca. 20%) after a sample was allowed to stand for 4 days at 25 °C in H_2O as judged by 31P NMR spectroscopy (see Figure D69).

A comprehensive demonstration of the aryl scope was performed with GSH under the optimized bioconjugation conditions (25 °C, 3 equiv Au complex, 80:20 H_2O:MeCN, 0.1 M Tris buffer, pH 8.0). Quantitative conversion to the GSH *S*-aryl conjugates was observed in <5 min for all 17 substrates displayed in Figure 5-2A (b−r). Notably, the reaction does not inherently necessitate organic cosolvent when the organometallic reagent is soluble in water (**2o**, see Appendix D Figure D93). As a representative example, the S-(C6H4-p-Cl) conjugate was easily separated from small-molecule byproducts and Au-based species by reversed-phase HPLC, and ICP-AES analysis of the purified peptide indicated more than 99.9% of gold was removed using this purification procedure (see Appendix D section 4.5.20).

The chemoselectivity of oxidative addition was probed through treatment of (Me-DalPhos)AuCl with *p*-chloro- and *p*-bromoiodobenzene electrophiles in the presence of $AgSbF_6$ (see Appendix D). For both substrates, oxidative addition occurs exclusively across the Ar−I bond, resulting in the formation of complexes **2i** and **2j** (Figure 5-2A), respectively. Furthermore, treatment of GSH with **2i** and **2j** generated the *p*-Cl-C_6H_4 and *p*-Br-C_6H_4 tagged peptides as the sole products, without any evidence for iodoaryl-based conjugates as judged by LC-MS analyses. The high chemoselectivity of the (MeDalPhos)Au system is in stark contrast to that observed for reported Pd-based platforms that readily react with all Ar−X (X = Cl, Br, I) species with limited selectivity.[9] Thus, the functional group tolerance coupled with the high selectivity of the reported Au-based system may provide complementary advantages to the previously developed Pd-based reagents for transferring aryl groups of various complexities to biomolecules.

To further establish the versatility and utility of this methodology, we applied our bioconjugation strategy to more complex peptide substrates. Cysteine arylation of two different peptide sequences was observed in nearly quantitative conversion for a variety of aryl substrates (see Appendix D; representative examples shown in Figure 5-2B). No reaction was observed using a control peptide where the cysteine residue was mutated to serine, highlighting the chemoselectivity of the Au(III)-mediated bioconjugation method. Additionally, trypsin digest and MS/MS analyses of a (*p*-Cl-C_6H_4)−peptide conjugate support modification at the cysteine residue exclusively (see Appendix D section 4.5.24 for experimental details).

We next extended the scope of Au(III)-mediated cysteine bioconjugation to the modification of proteins. Cysteine arylation of DARPin (designed ankyrin repeat protein) was observed using complex **2a** within 30 min at 25 °C, as verified by LC-MS analysis of the reaction mixture (Figure 5-3A). The presence of a small amount of DMF cosolvent (5%) was required for efficient bioconjugation due to the inherent solubility constraints of **2a**. However, treatment of fibroblast growth factor 2 (FGF2)[31] with water-soluble **2o** (15 equiv) in aqueous buffer only resulted in complete conversion to the PEGylated conjugate as confirmed by the deconvoluted mass spectrum from LC-MS analysis of the reaction mixture (see Appendix D Figure D102). The rapid and efficient protein bioconjugation reactions demonstrate the potential generality and suitability of the described Au(III)-mediated methodology for the modification of complex proteins under mild, biologically relevant conditions and at low micromolar concentration of protein (36 μM).

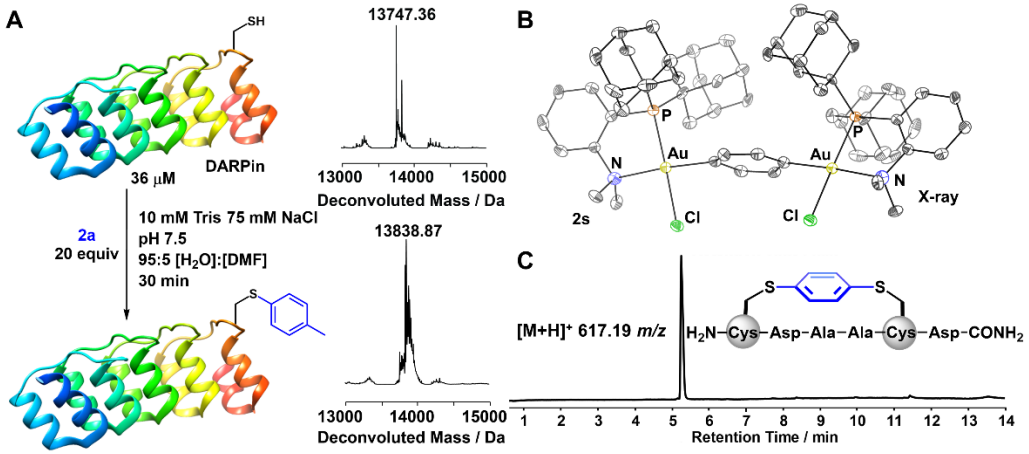

Figure 5-3. A: DARPin modification using **2a**, and deconvoluted mass spectra of the protein before and after conjugation. B: Solid-state structure of peptide stapling reagent, $[((Me\text{-}DalPhos)AuCl)_2(\mu_2\text{-}1,4\text{-}C_6H_4)]^{2+}$ (**2s**), with thermal ellipsoids rendered at the 50% probability level and with hydrogen atoms and two SbF_6^- anions removed for clarity. C: LC-MS trace of the purified phenylene-stapled peptide. $[M+H]^+$: 670.1965 (calc'd, 670.1968) *m/z*.

With a protocol for Au-mediated cysteine arylation, we envisaged the same route could furnish a stapled peptide through the construction of an intramolecular cysteine–cysteine linkage. There has been significant interest in the development of stapled peptides as therapeutic agents; however, there is still a growing need for easily accessible peptide macrocyclization methods that allow for modular tuning of cross-linking units.[32–36] The straightforward and efficient Au(III)-mediated bioconjugation procedures together with the use of commercially available (Me-DalPhos)AuCl and diiodoaryl reagents provide a versatile and systematic approach to peptide stapling that is complementary to existing state-of-the-art methods.[4,10,34–37] The *o*-phenylene-bridged digold(III) stapling reagent, **2s**, was prepared in a single synthetic step through treatment of (Me-DalPhos)AuCl (2 equiv) with 1,4- diiodobenzene (1 equiv) in the presence of $AgSbF_6$ (2 equiv), and isolated as a crystalline solid in 64% yield. A single-crystal X-ray diffraction study

confirmed the solid-state structure of [**2s**][SbF_6]$_2$ (Figure 5-3B). Peptide stapling was observed under optimized conditions (30 min, 50:50 H_2O:MeCN, 25 °C, 0.1 M Tris, pH 8) using a 2-fold excess of the **2s** macrocyclization reagent for a peptide containing cysteine residues at the *i*, *i*+4 positions (Figure 5-3C). The *o*-phenylene *i*, *i*+4 stapled peptide was isolated away from gold-based impurities after purification by reversed-phase HPLC.

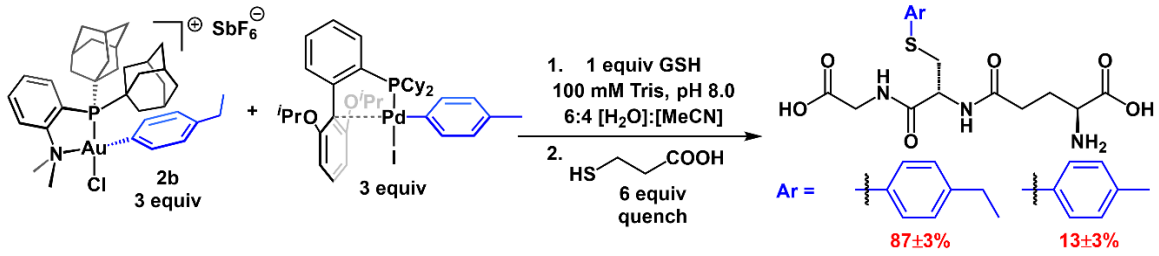

Scheme 5-2. Competition experiment between (RuPhos)Pd(tolyl)I and [**2b**][SbF_6] with GSH.

The apparent exceptionally rapid kinetics of Au(III)- mediated bioconjugation were benchmarked by performing a comparative study against a closely related Pd(II)-based analogue. The (RuPhos)Pd(tolyl)Cl complex reported previously[9] was ideally suited for comparison with the [(MeDalPhos)Au(*p*-ethylbenzene)Cl]$^+$ complex **2b** on account of its performance as a cysteine arylation reagent and the similar electronic and steric properties of the aryl substituents on both complexes. Treatment of GSH with equimolar amounts of **2b** and (RuPhos)Pd(tolyl)Cl (Scheme 2) under conditions compatible with both systems resulted in 92 ±1% conversion to the ethylbenzene conjugate, indicating that the Au-mediated conjugation outperformed the Pd-based arylation in over 9:1 kinetic ratio. These data suggest that the kinetics for Au-mediated bioconjugation are on the order of, or faster than those estimated for the Pd-based systems (10^3 -10^4 M^{-1} s^{-1}).[9]

5.3 Conclusions

In summary, we present a general protocol for cysteine *S*-arylation of unprotected peptides and proteins using robust, Au(III) oxidative addition complexes bearing a diverse array of aryl substituents. The reported method operates in a large pH range under mild reaction conditions and displays rapid reaction kinetics, high chemoselectivity, and excellent functional group tolerance. With this work, we expand the scope of biomolecule modification[3,5,38–40] by providing tools that interface bond-forming processes characteristic of organometallic complexes[18,25,41–46] with bioconjugation. The straightforward synthetic procedures and commercially available or otherwise easily accessible reagents presented should expand the bioconjugation space well beyond the substrates and peptides reported in this study. This work also expands on a relatively under-represented class of organometallic reagents containing metal−carbon bonds capable of withstanding relatively harsh environmental conditions.[47]

Acknowledgements

A.M.S. thanks UCLA Department of Chemistry and Biochemistry for start-up funds, 3M for a Non-Tenured Faculty Award, Alfred P. Sloan Foundation for a Fellowship in Chemistry and the National Institutes of Health (NIH) for a Maximizing Investigators Research Award (MIRA, R35GM124746). H.D.M thanks the National Science Foundation (NSF, CHE-1507735) for funding. M.S.M thanks the NSF for the Bridge-to-Doctorate (HRD-1400789) and the Predoctoral (GRFP) (DGE-0707424) Fellowships and UCLA for the Christopher S. Foote Fellowship. Dr. Jacquelin Kammeyer (UCLA) is acknowledged for helpful discussions and Mr. Nicholas Bernier (UCLA) is thanked for assistance with ICP-AES measurements. The authors thank Dr. Chi Zhang and Prof. Bradley L. Pentelute (MIT) for generously sharing the plasmid used for DARPin

expression and the UCLA-DOE Institute Protein Expression Technology Center (PETC) for expression of DARPin and Dr. Yu Chen (UCLA) for help with mass spectrometry.

5.4 References

(1) Kalia, J.; Raines, R. T. *Curr Org Chem.* **2010**, *14*, 138–147.

(2) Boutureira, O.; Bernardes, G. J. L. *Chem. Rev.* **2015**, *115*, 2174–2195.

(3) Chalker, J. M.; Bernardes, G. J. L.; Lin, Y. A.; Davis, B. G. *Chem. - An Asian J.* **2009**, *4*, 630–640.

(4) Spokoyny, A. M.; Zou, Y.; Ling, J. J.; Yu, H.; Lin, Y. S.; Pentelute, B. L. *J. Am. Chem. Soc.* **2013**, *135*, 5946–5949.

(5) DeGruyter, J. N.; Malins, L. R.; Baran, P. S. *Biochemistry* **2017**, *56*, 3863–3873.

(6) Vinogradova, E. V. *Pure Appl. Chem.* **2017**, *89*, 1619–1640.

(7) Jbara, M.; Maity, S. K.; Brik, A. *Angew. Chem. - Int. Ed.* **2017**, *56*, 10644–10655.

(8) Vara, B. A.; Li, X.; Berritt, S.; Walters, C. R.; Petersson, E. J.; Molander, G. A. *Chem. Sci.* **2018**, *9*, 336–344.

(9) Vinogradova, E. V; Zhang, C.; Spokoyny, A. M.; Pentelute, B. L.; Buchwald, S. L. *Nature* **2015**, *526*, 687–691.

(10) Rojas, A. J.; Zhang, C.; Vinogradova, E. V.; Buchwald, N. H.; Reilly, J.; Pentelute, B. L.; Buchwald, S. L. *Chem. Sci.* **2017**, *8*, 4257–4263.

(11) Lee, H. G.; Lautrette, G.; Pentelute, B. L.; Buchwald, S. L. *Angew. Chem. - Int. Ed.* **2017**, *56*, 3177–3181.

(12) Rojas, A. J.; Pentelute, B. L.; Buchwald, S. L. *Org. Lett.* **2017**, *19*, 4263–4266.

(13) Kubota, K.; Dai, P.; Pentelute, B. L.; Buchwald, S. L. *J. Am. Chem. Soc.* **2018**, *140*, 3128–3133.

(14) Joost, M.; Amgoune, A.; Bourissou, D. *Angew. Chem. - Int. Ed.* **2015**, *54*, 15022–15045.

(15) Harper, M. J.; Arthur, C. J.; Crosby, J.; Emmett, E. J.; Falconer, R. L.; Fensham-Smith, A.

J.; Gates, P. J.; Leman, T.; Mcgrady, J. E.; Bower, J. F.; Russell, C. A. *J. Am. Chem. Soc.* **2018**, *140*, 4440–4445.

(16) Livendahl, M.; Goehry, C.; Maseras, F.; Echavarren, A. M. *Chem. Commun.* **2014**, *50*, 1533–1536.

(17) Scott, V. J.; Labinger, J. A.; Bercaw, J. E. *Organometallics* **2010**, *29*, 4090–4096.

(18) Hopkinson, M. N.; Gee, A. D.; Gouverneur, V. *Chem. - A Eur. J.* **2011**, *17*, 8248–8262.

(19) Wegner, H. A.; Auzias, M. *Angew. Chem. - Int. Ed.* **2011**, *50*, 8236–8247.

(20) On-Yee Chan, A.; Lui-Lui Tsai, J.; Kar-Yan Lo, V.; Li, G.-L.; Wong, M.-K.; Che, C.-M. *Chem. Commun.* **2013**, *49*, 1428–1430.

(21) Zou, T.; Lum, C. T.; Lok, C.-N.; Zhang, J.-J.; Che, C.-M. *Chem. Soc. Rev.* **2015**, *44*, 8786–8801.

(22) Kung, K. K.-Y.; Ko, H.-M.; Cui, J.-F.; Chong, H.-C.; Leung, Y.-C.; Wong, M.-K. *Chem. Commun.* **2014**, *50*, 11899–11902.

(23) Joost, M.; Zeineddine, A.; Estévez, L.; Mallet-Ladeira, S.; Miqueu, K.; Amgoune, A.; Bourissou, D. *J. Am. Chem. Soc.* **2014**, *136*, 14654–14657.

(24) Zeineddine, A.; Estévez, L.; Mallet-Ladeira, S.; Miqueu, K.; Amgoune, A.; Bourissou, D. *Nat. Commun.* **2017**, *8* (1).

(25) Wolf, W. J.; Winston, M. S.; Toste, F. D. *Nat. Chem.* **2014**, *6*, 159–164.

(26) Kang, K.; Liu, S.; Xu, T.; Wang, D.; Leng, X.; Bai, R.; Lan, Y.; Shen, Q. *Organometallics* **2017**, *36*, 4727–4740.

(27) Bachman, R. E.; Bodolosky-Bettis, S. A.; Pyle, C. J.; Gray, M. A. *J. Am. Chem. Soc.* **2008**, *130*, 14303–14310.

(28) Hesp, K. D.; Stradiotto, M. *J. Am. Chem. Soc.* **2010**, *132*, 18026–18029.

(29) Lundgren, R. J.; Sappong-Kumankumah, A.; Stradiotto, M. *Chem. - A Eur. J.* **2010**, *16*, 1983–1991.

(30) Winston, M. S.; Wolf, W. J.; Toste, F. D. *J. Am. Chem. Soc.* **2015**, *137*, 7921–7928.

(31) Itoh, N.; Ornitz, D. M. *J. Biochem.* **2011**, *149*, 121–130.

(32) Yudin, A. K. *Chem. Sci.* **2015**, *6*, 30–49.

(33) Kaspar, A. A.; Reichert, J. M. *Drug Discov. Today* **2013**, *18*, 807–817.

(34) White, C. J.; Yudin, A. K. *Nat. Chem.* **2011**, *3*, 509–524.

(35) Blackwell, H. E.; Grubbs, R. H. *Angew. Chem. - Int. Ed.* **1998**, *37*, 3281–3284.

(36) Verdine, G. L.; Hilinski, G. J. *Stapled peptides for intracellular drug targets*, 1st ed.; Elsevier Inc., 2012; Vol. 503.

(37) Lau, Y. H.; de Andrade, P.; Wu, Y.; Spring, D. R. *Chem. Soc. Rev.* **2015**, *44*, 91–102.

(38) Lin, S.; Yang, X.; Jia, S.; Weeks, A. M.; Hornsby, M.; Lee, P. S.; Nichiporuk, R. V.; Iavarone, A. T.; Wells, J. A.; Toste, F. D.; Chang, C. J. *Science* **2017**, *355*, 597–602.

(39) Stephanopoulos, N.; Francis, M. B. *Nat. Chem. Biol.* **2011**, *7*, 876–884.

(40) Cal, P. M. S. D.; Bernardes, G. J. L.; Gois, P. M. P. *Angew. Chem. Int. Ed.* **2014**, *53*, 10585–10587.

(41) Fors, B. P.; Watson, D. A.; Biscoe, M. R.; Buchwald, S. L. *J. Am. Chem. Soc.* **2008**, *3*, 3–5.

(42) Wu, C. Y.; Horibe, T.; Jacobsen, C. B.; Toste, F. D. *Nature* **2015**, *517*, 449–454.

(43) Mankad, N. P.; Toste, F. D. *J. Am. Chem. Soc.* **2010**, *2*, 5–7.

(44) Tellis, J. C.; Primer, D. N.; Molander, G. A. *Science* **2014**, *345*, 433–436.

(45) Biffis, A.; Centomo, P.; Del Zotto, A.; Zecca, M. *Chem. Rev.* **2018**, *118*, 2249–2295.

(46) Stahl, S. S.; Labinger, J. A.; Bercaw, J. E. *Angew. Chem. - Int. Ed.* **1998**, *37*, 2180–2192.

(47) For selected examples see: (a) Crabtree, R. H. *Organomet. Chem. Transit. Met.* **2005**, 491–520. For selected example see: (b) Hull, J. F.; Balcells, D.; Blakemore, J. D.; Incarvito, C. D.; Brudvig, G. W.; Crabtree, R. H.; Haven, N. *J. Am. Chem. Soc.* **2009**, *131*, 8730–8731. (c) Breno, K. L.; Ahmed, T. J.; Pluth, M. D.; Balzarek, C.; Tyler, D. R. *Coord. Chem. Rev.* **2006**, *250*, 1141–1151. (d) Therrien, B. In *Chemistry of Nanocontainers*; 2012; Vol. 319, pp 35–56. (e) Allardyce, C. S.; Dorcier, A.; Scolaro, C.; Dyson, P. J. *Appl. Organomet. Chem.* **2005**, *19*, 1–10. (f) Mohr, F.; Cerrada, E.; Laguna, M. *Organometallics* **2006**, *25*, 644–648.

5.5 Appendix D

5.5.1 Methods and Materials

All commercially available chemicals were used as received unless otherwise stated. The Au(THT)Cl and (RuPhos)Pd(tolyl)I complexes were prepared according to literature procedures.[1,2] Dry solvents were obtained from Grubbs columns with activated alumina and copper catalysts and stored in a Vacuum Atmospheres glovebox over 4Å molecular sieves. *O*-carborane was purchased from Boron Specialties (USA). Phosphorus trichloride (98%), *N,N'*-diisopropylethylenediamine (97%), chlorobis(3,5-dimethylphenyl)phosphine (90%), and silver bis(trifluoromethanesulfonyl)imide ($AgNTf_2$) were purchased from Alfa Aesar. *N,N'*-Di-*tert*-butylethylenediamine (98%), chloro[di(1-adamantyl)-2-dimethylaminophenylphosphine]gold(I), 2-iodonaphthalene (99%), 4-iodotoluene (99%), and L-glutathione reduced (BioXtra grade) were purchased from Sigma-Aldrich. Silver hexafluoroantimonate ($AgSbF_6$) (98%), silver tetrafluoroborate ($AgBF_4$) (98%), 4-iodobenzotrifluoride (98%), 1-fluoro-4-iodo-benzene (99%), 1-bromo-4-iodobenzene (99%), 4-iodophenol (98%), 2-iodopyridine (98%), 4-iodoaniline (98%) and 4-(trifluoromethoxy)iodobenzene (97%) were purchased from Oakwood Chemical. Trametinib (GSK1120212, 99%), and 1-ethyl-4-iodobenzene (98%) were purchased from Fisher Scientific. Monodisperse PEG_{12} was purchased form JenKem Technology USA. 1-Hydroxy-7-azabenzotriazole solution (HOAt, 0.6 M in DMF), 1-[Bis(dimethylamino)methylene]-1H-1,2,3-triazolo[4,5-b]pyridinium 3-oxid hexafluorophosphate (HATU), *N,N,N',N'*-Tetramethyl-*O*-(1*H*-benzotriazol-1-yl)uronium hexafluorophosphate (HBTU), D-Biotin, Fmoc-Rink amide linker, Fmoc-L-Arg(Pbf)-OH, Fmoc-L-Ala-OH, Fmoc-L-Cys(Trt)-OH, Fmoc-L-Gly-OH, Fmoc-L-Asp(OtBu)-OH, Fmoc-L-Ser(tBu)-OH, Fmoc-L-Lys(Boc)-OH were purchased from Chem-Impex International.

5.5.2 General Analytical Information:

NMR spectra were recorded on DRX 400, DRX 500, and AVIII 500 Bruker spectrometers at 400 or 500 MHz (^{1}H), 125 MHz (^{13}C), 282 MHz (^{19}F), 80 MHz (^{11}B), and 121 MHz (^{31}P). Spectra are reported in δ (parts per million) relative to residual protio-solvent signals for ^{1}H and ^{13}C, C_6H_5F - (δ -113.15 ppm) for ^{19}F, $BF_3{\cdot}Et_2O$ (δ 0.00 ppm) for ^{11}B, and H_3PO_4 (δ 0.00 ppm) for ^{31}P. Deuterated solvents (Cambridge Isotope Laboratories) used for NMR spectroscopic analyses were stored over 4Å molecular sieves. Electrospray ionization mass spectra of small molecules and Au-based complexes (ESI-MS(+)) were collected on a Waters LCT premier mass spectrometer. Samples were prepared in MeCN at concentrations <1 µM, and the data were processed using the program mMass Version 5.4.1.0.

5.5.3 Peptide Purification and LC-MS Analysis:

Peptide purification was carried out on an Agilent Technologies 1260 Infinity II HPLC system equipped with an Agilent ZORBAX 300SB-C18 column (5 µm, 9.4 × 250 mm) using 0.1% TFA in water and 0.1% TFA in acetonitrile as the eluent. Data were processed using Agilent Mass Hunter software. Deconvoluted mass spectra of proteins were gathered using maximum entropy setting. Peptide modification yield was calculated *s* integrations of the peptide and modified peptide peaks in the TIC spectra using the following formula: $(I_{[MP]}/I_{[MP+SP]})\times100$ where $I_{[MP]}$ is the integration of the modified peptide peak and $I_{[MP+SP]}$ is the sum of integrations of the modified peptide peak and the starting peptide peak.

5.5.3.1 Peptide Purification Method Information: Column temperature: 23 °C. Flow rate: 3 mL/min. Gradient: 95-60% water (0.1% TFA) over 22 min.

LC-MS analysis was carried out using an Agilent 6530 ESI-Q-TOF. Peptide and DARPin analyses were carried out using an Agilent ZORBAX 300SB C18 column (5 µm, 2.1 × 500 mm). Analysis

of FGF2 was carried out using an Agilent ZORBAX 300SB C3 column (3.5 µm, 3.0 × 150 mm) using 0.1% TFA in water and 0.1% TFA in acetonitrile as the eluent.

5.5.3.2 LC-MS Method Information:

Method used for peptides: Column temperature: 23 °C. Flow rate: 0.8 mL/min. Gradient: 99% water (0.1% formic acid (FA)) for 2 minutes; 99%-91% water (0.1% FA) 2-11 minutes; 5% water (0.1% FA) from 12-15 min.

Method used for proteins: Column temperature: 23 °C. Flow rate: 0.8 mL/min. Gradient: 99% water (0.1% formic acid (FA)) for 2 minutes; 99%-9% water (0.1% FA) 2-11 minutes; 5% water (0.1% FA) from 11-12 min.

MS/MS analysis was performed using a 30 eV collision energy and fragment analysis was carried out using ProSight Lite software.

5.5.4 ICP-AES Measurements

Gold ICP-AES analyses were conducted using a Shimadzu ICPE-9000 inductively coupled plasma atomic emission spectrometer (ICP-AES). Solutions of standard concentrations were used for calibration purposes and were prepared from a gold standard solution purchased from Sigma Aldrich, designated suitable for ICP analysis. Standard solutions were prepared with concentrations of 50, 100, 300, and 600 ppb in 2% OmniTrace HCl diluted with Milli-Q H_2O, and analyses were run at $\lambda = 242.795$ nm.

5.5.5 Synthetic Procedures

5.5.5.1 Synthesis of 1,3-diisopropyl-2-chloro-1,3,2-diazaphospholidine

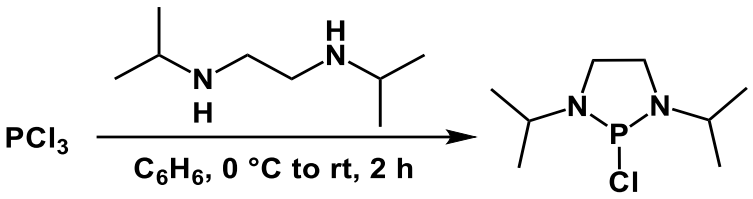

Phosphorus trichloride (483 μL, 5.55 mmol, 1.00 equiv) was added to C_6H_6 (7 mL), and the solution was cooled to 0 °C. Once at 0 °C, a solution of *N,N'*-diisopropylethylenediamine (1.0 mL, 5.6 mmol, 1.0 equiv) and triethylamine (787 μL, 5.55 mmol, 1.00 equiv) in C_6H_6 (8 mL) cooled to 0 °C, was added dropwise slowly to the solution containing phosphorus trichloride. White precipitate formed immediately upon addition. The suspension was then stirred at room temperature for 2 h. After 2 h, the precipitate was filtered off and the filtrate was concentrated under reduced pressure to afford the pure product as a yellow oil in quantitative yield.

The product is unstable in open atmosphere, and a degradation product was observed by ^{31}P NMR spectroscopy (δ ~7 ppm in CH_2Cl_2) within minutes of exposure to air. All manipulations with this product were conducted in a glovebox under an atmosphere of purified N_2 and with dried and degassed reagents and solvents.

^{1}H NMR (400 MHz, CD_2Cl_2, 298 K): δ 3.48-3.42 (m, 2H, C*H*), 3.32 (s, 2H, C*H*2), 3.31 (s, 2H, CH_2), 1.30 (d, 12H, CH_3, J = 6.6 Hz) ppm.

^{13}C{^{1}H} NMR (125 MHz, CD_2Cl_2, 298 K): δ 48.90 (*C*H), 47.25 (*C*H_2), 22.20 (*C*H_3) ppm.

^{31}P{^{1}H} NMR (121 MHz, CD_2Cl_2, 298 K): δ 168.0 ppm.

5.5.5.2 Synthesis of 1,2-bis(diaminophosphino)-1,2-dicarba-*closo*-dodecaborane

Syntheses and full characterization for 1,2-Bis(diaminophosphino)-1,2-dicarba-closo-dodecaborane compounds shown below can be found in the literature.[3] *Adapted syntheses are included here for convenience.*

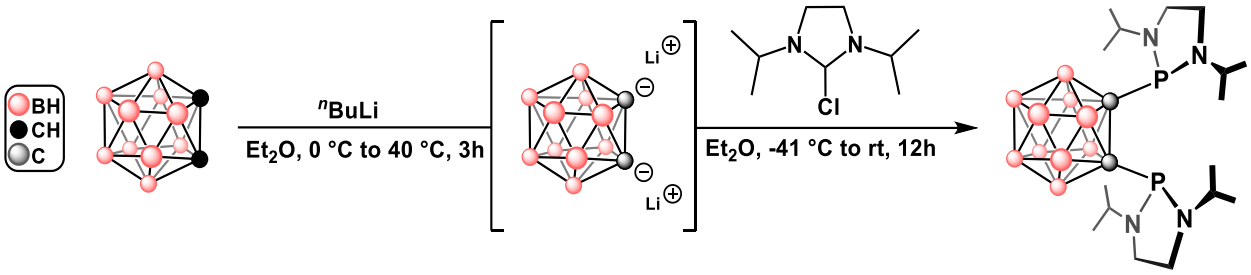

A round bottom flask was charged with a solution of *o*-carborane (318 mg, 2.20 mmol, 1.00 equiv) in Et_2O (5 mL) under an atmosphere of N_2, and the temperature of the solution was lowered to 0 °C. Once at 0 °C, ^{n}BuLi (2.5 M in hexane, 1.85 mL, 4.63 mmol, 2.10 equiv) was added dropwise, resulting in the formation of white precipitate. After complete addition, the mixture was refluxed at 40 °C for 3 h. After 3 h, the reaction temperature was lowered to -41 °C, at which point a solution of 1,3-diisopropyl-2-chloro-1,3,2-diazaphospholidine (1.15 g, 2.20 mmol, 2.50 equiv) in Et_2O (12 mL) was added via cannula transfer. The formation of an off-white precipitate was observed upon complete addition, at which point the reaction was allowed to warm to room temperature, and then stirred for 12 h. After 12 h, complete consumption of the starting materials was confirmed by TLC, and the solvent was evaporated under reduced pressure to yield an off-white solid. This solid was subjected to flash chromatography in a hexane and acetone (95:5) mixture to yield the pure product as a white solid (Rf = 0.77). The product was further purified *via* crystallization in dichloromethane layered with *n*-pentane at -30 °C.

The product was isolated as a white and crystalline solid and is stable for months when stored in the solid state under an N_2 atmosphere at -30 °C.

$^{31}P\{^{1}H\}$ NMR (121 MHz, $CDCl_3$, 298 K): δ 112.6 ppm.

5.5.5.3 Synthesis of (DPCb)AuCl ((1,2-bis(1,3-diisopropyl-1,3,2-diazaphospholidin-2-yl)-1,2-dicarba-*closo*-dodecaborane)AuCl)

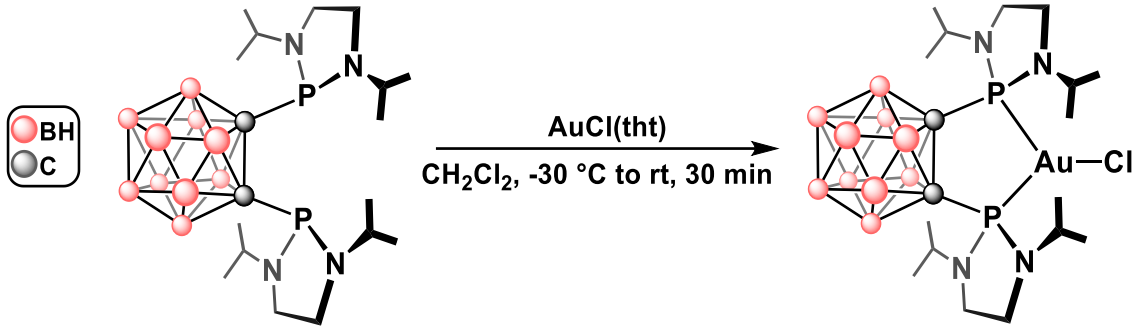

In the glovebox, a solution of 1,2-bis(1,3-diisopropyl-1,3,2-diazaphospholidin-2-yl)-1,2-dicarba-*closo*-dodecaborane (DPCb, 65 mg, 0.13 mmol, 1.0 equiv) in CH_2Cl_2 (4 mL) was cooled to -30 °C. This solution was then added dropwise to a cooled solution (-30 °C) of AuCl(tht) (43 mg, 0.13 mmol, 1.0 equiv) in CH_2Cl_2 (4 mL) over the course of 5 min. After stirring at room temperature for 30 min, the solution was concentrated *in vacuo* to afford the crude (DPCb)AuCl complex as a white solid. The crude material was purified *via* crystallization from a concentrated solution of CH_2Cl_2 layered with *n*-pentane at -30 °C. The pure product was isolated as a white crystalline solid that is yellow in solution, and the product is stable for months when stored in the solid state under an N_2 atmosphere at -30 °C.

$^{31}P\{^{1}H\}$ NMR (121 MHz, $CDCl_3$, 298 K): δ 116.6 ppm.

5.5.5.4 Synthesis of (DPCb)AuNTf$_2$

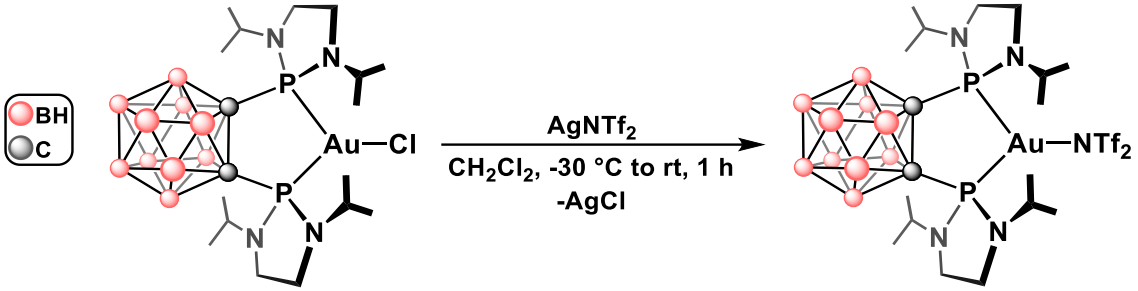

In the glovebox, a CH_2Cl_2 (7 mL) solution of (DPCb)AuCl (91 mg, 0.12 mmol, 1.0 equiv) was cooled to -30 °C. This solution was then added dropwise to a cooled suspension (-30 °C) of $AgNTf_2$ (49 mg, 0.12 mmol, 1.0 equiv) in CH_2Cl_2 (8 mL) over 5 min under protection from light. The reaction mixture was allowed to warm to room temperature, and after 1 h of stirring, the suspension was filtered through a pad of Celite and the filtrate was concentrated *in vacuo* to afford the (DPCb)AuNTf$_2$ product as a yellow solid. The product was used without further purification and is stable for months when stored in the solid state under an N_2 atmosphere at -30 °C.

^{31}P{^{1}H} NMR (121 MHz, $CDCl_3$, 298 K): δ 138.3 ppm.

5.5.5.5 Synthesis of 1

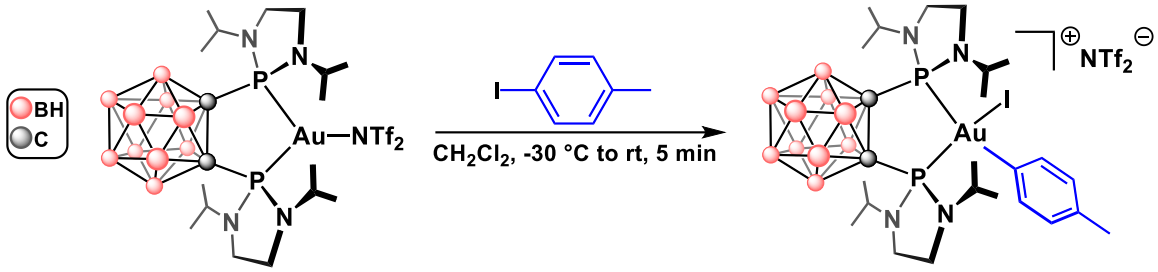

In the glovebox, a solution of (DPCb)AuNTf$_2$ (10 mg, 0.010 mmol, 1.0 equiv) in CH_2Cl_2 (350 μL) was cooled to -30 °C. To this cold solution was added a cooled (-30 °C) solution of 4-iodotoluene (12 mg, 0.053 mmol, 5.0 equiv) in CH_2Cl_2 (350 μL). The reaction was allowed to warm to room temperature for 5 min, during which time a color change to dark yellow was observed. The yellow solution was concentrated *in vacuo* to afford the product as a yellow solid. The isolated material was used for bioconjugation studies without further purification.

$^{31}P\{^1H\}$ NMR (121 MHz, CH_2Cl_2, 298 K): δ 132.09 (d, *J* = 22.7 Hz), 124.01 (d, *J* = 22.8 Hz) ppm.

5.5.5.6 Synthesis of Biotin Aryl-I

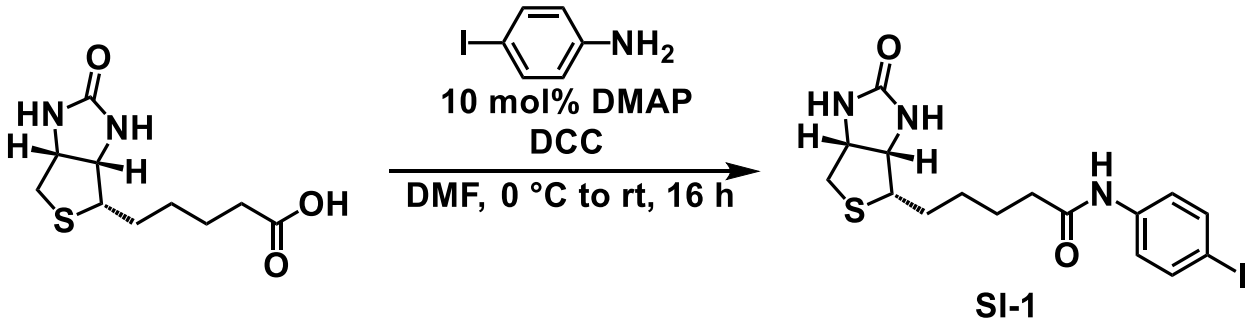

Aryl iodide substituted biotin (**Biotin Aryl-I**) was synthesized following Steglich esterification conditions.[4]

A 2-neck round bottom flask was charged with a solution biotin (217 mg, 0.890 mmol, 1.00 equiv) in dry DMF (5 mL) under an atmosphere of Ar. To this solution was added DMAP (11 mg, 0.080

mmol, 10 mol%) and 4-iodoaniline (778 mg, 3.55 mmol, 4.00 equiv) under stirring. The temperature of the reaction mixture was lowered to 0 ˚C, at which point a solution of DCC (202 mg, 0.980 mmol, 1.10 equiv) in DMF (5 mL) was added dropwise under stirring. The reaction mixture was allowed to warm to room temperature and then stirred for an additional 16 h. After 16 h, the solution was concentrated under reduced pressure, and CH_2Cl_2 (25 mL) was added, resulting in the precipitation of colorless solids that were isolated by filtration, washed with CH_2Cl_2 (2 × 25 mL) and then methanol (2 × 25 mL) to afford the product as a white solid.

^{1}H NMR (400 MHz, DMSO-d_6): δ 9.96 (s, 1H, -N*H*), 7.61 (d, 2H, *J* = 8.8 Hz, H_{Ar}), 7.43 (d, 2H, *J* = 8.8, H_{Ar}), 6.42 (s, 1H, -N*H*), 6.35 (s, 1H, -N*H*), 4.30 (m, 1H), 4.22–4.08 (m, 1H), 3.17–3.08 (m, 1H, -CH_2SCHCH_2-), 2.82 (dd, 1H, *J* = 12.4 Hz, 5.1 Hz, -CH_2SCHCH_2-), 2.57 (d, 1H, *J* = 12.4 Hz, -CH_2SCHCH_2-), 2.30 (t, 2H, *J* = 7.4 Hz, -CH_2CONH-), 1.70–1.53 (m, 2H, -CH_2), 1.55–1.48 (m, 2H, -CH_2), 1.36 (m, 2H, -CH_2) ppm.

^{13}C NMR (125 MHz, DMSO-d_6): δ 174.48, 171.36, 162.71, 139.13, 137.29, 121.23, 61.04, 59.20, 55.39, 36.26, 33.36, 28.22, 28.09, 25.02 ppm.

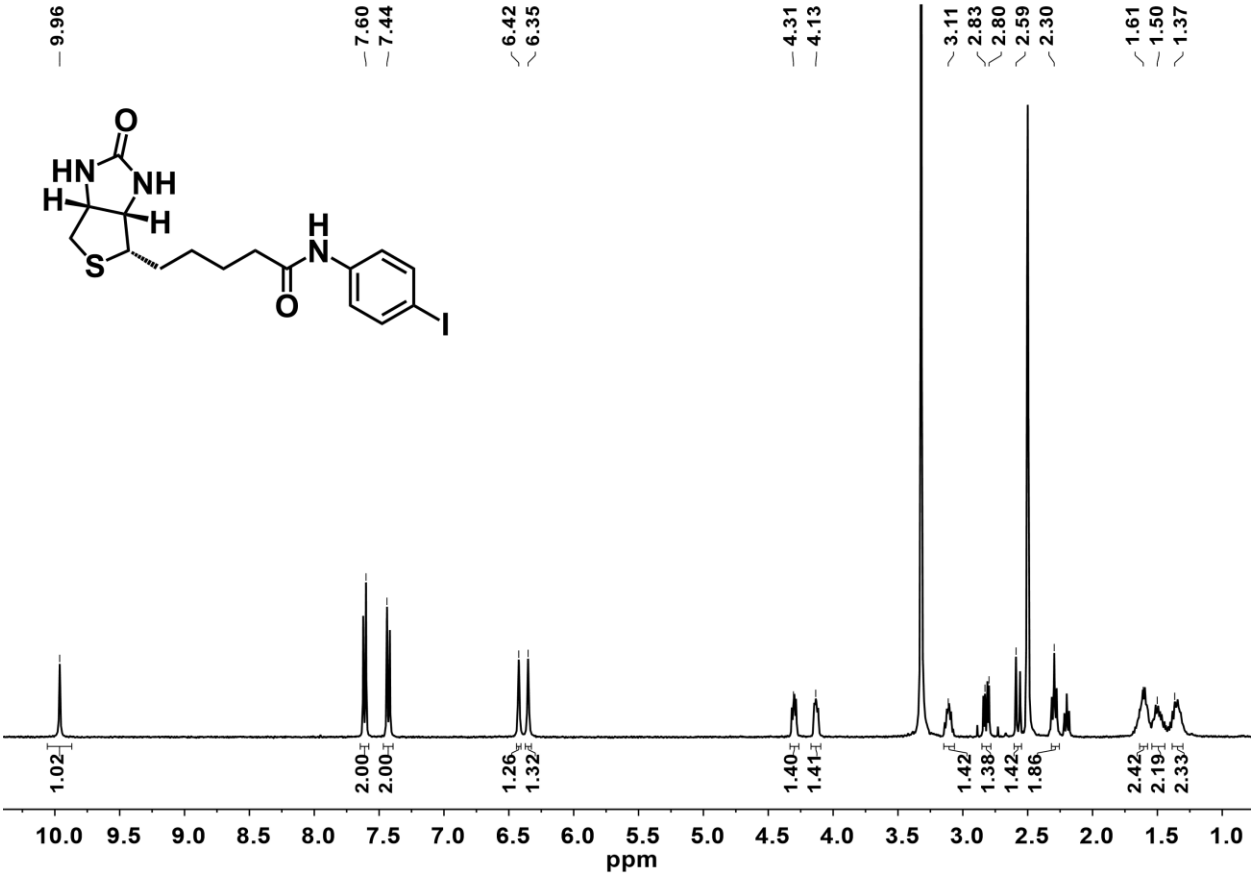

Figure D22. ^{1}H NMR spectrum of **Biotin Aryl-I** in DMSO-d_6 at 298 K.

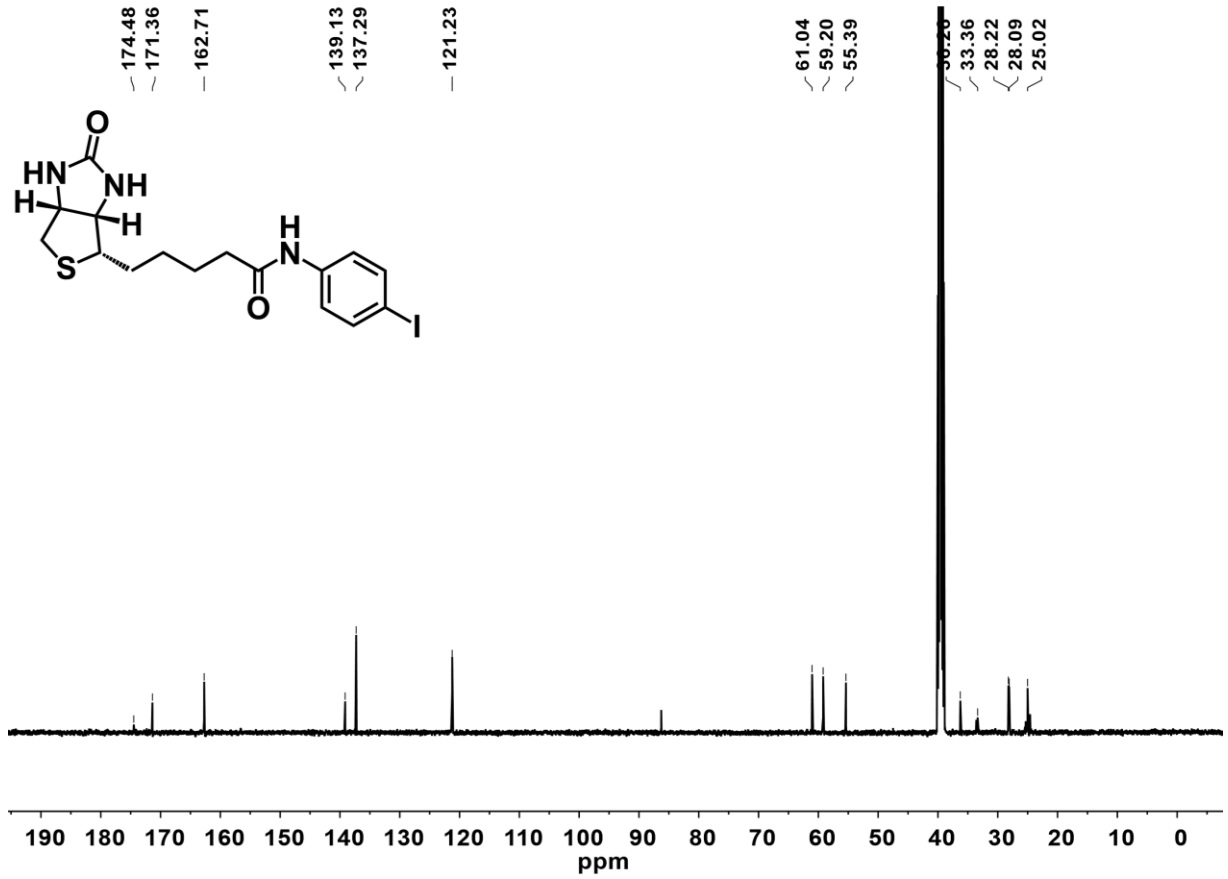

Figure D23. ^{13}C NMR spectrum of **Biotin Aryl-I** in DMSO-d_6 at 298 K.

5.5.5.7 Synthesis of PEG-Tosyl

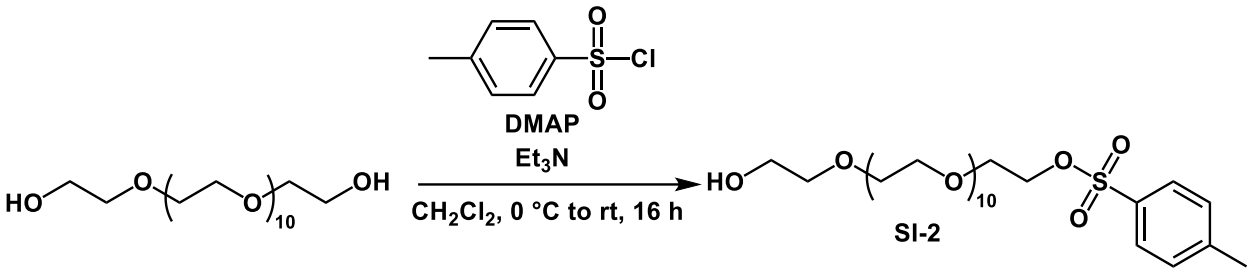

A 2-neck round bottom flask was charged with a solution of poly(ethylene glycol) (577 mg, 1.05 mmol, 1.00 equiv) in dry CH_2Cl_2 (5 mL) under an atmosphere of Ar. To this solution was added 4-dimethylaminopyridine (26 mg, 0.21 mmol, 0.20 equiv) under stirring, and then the temperature of the reaction mixture was lowered to 0 ˚C. A solution of tosyl chloride (141 mg, 0.740 mmol, 0.700 equiv) in CH_2Cl_2 (15 mL) was added dropwise to this solution, followed by dropwise addition of triethylamine (177 µL, 1.26 mmol, 1.20 equiv). The reaction mixture was allowed to warm to room temperature, and then stirred for an additional 16 h, at which point the reaction was diluted with water and the product was extracted three times with CH_2Cl_2. The organic layers were collected, dried over $MgSO_4$, and the solvent was removed under reduced pressure to afford the product as a yellow oil.

^{1}H NMR (400 MHz, $CDCl_3$): δ 7.80 (d, 1H, *J* = 8.3 Hz, H_{Ar}), 7.34 (d, 1H, *J* = 8.3 Hz, H_{Ar}), 4.19–4.10 (m, 2H), 3.70–3.62 (m, 44H), 3.00 (s, 2H), 2.45 (s, 3H) ppm.

^{13}C NMR (125 MHz, $CDCl_3$): δ 144.78, 133.01, 129.82, 127.99, 72.52, 70.57, 69.24, 68.69, 61.76, 21.66 ppm.

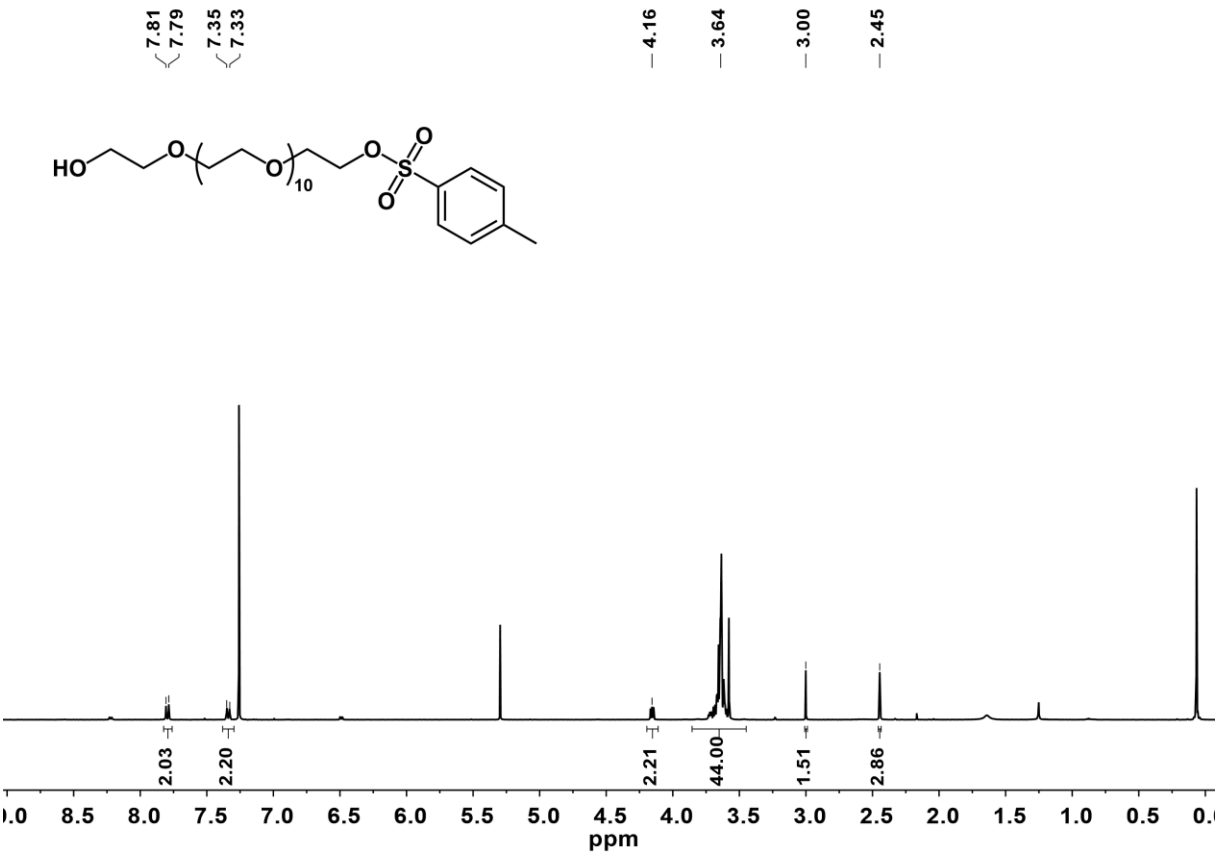

Figure D24. ^{1}H NMR spectrum of **PEG-Tosyl** in $CDCl_3$ at 298 K.

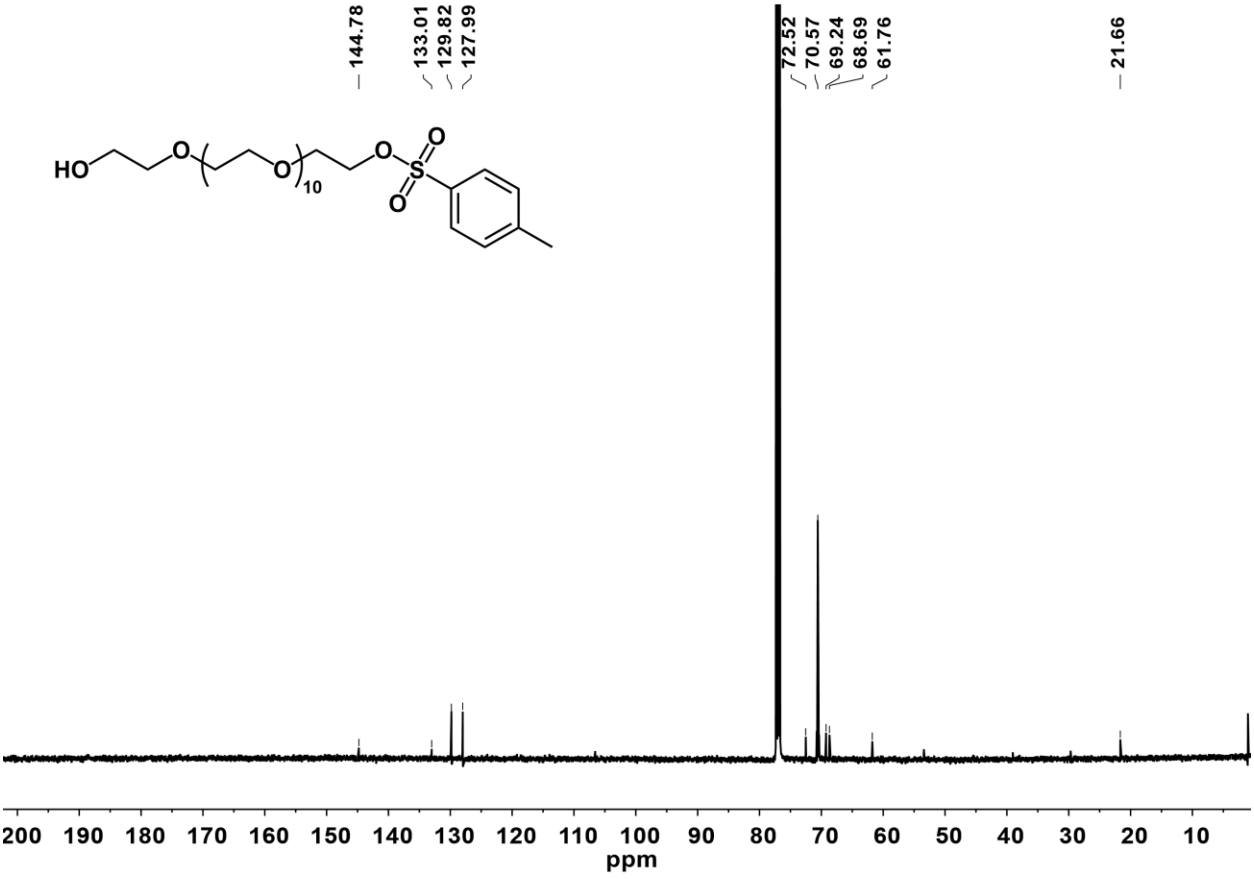

Figure D25. ^{13}C NMR spectrum of **PEG-Tosyl** in $CDCl_3$ at 298 K.

5.5.5.8 Synthesis of PEG-Aryl-I

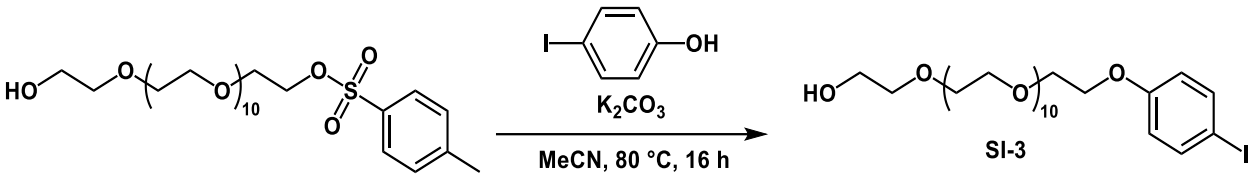

A 2-neck round bottom flask was charged with a solution of **SI-2** (395 mg, 0.520 mmol, 1.00 equiv) and 4-iodophenol (164 mg, 0.750 mmol, 1.45 equiv) in dry MeCN (20 mL). To this solution was added potassium carbonate (427 mg, 3.09 mmol, 6.00 equiv) under stirring. The reaction mixture was stirred at 80 °C for 16 h, at which point the solvent was removed under reduced pressure to afford colorless solids, which were dissolved in ethyl acetate and washed with water. The organic layer was collected, dried over $MgSO_4$, and the solvent was removed under reduced pressure. The crude product was purified *via* column chromatography (90:10 $CHCl_3$:MeOH) to afford pure **PEG-Aryl-I** as a yellow oil.

^{1}H NMR (400 MHz, $CDCl_3$): δ 7.54 (d, 2H, *J* = 9.0 Hz, H_{Ar}), 6.69 (d, 2H, *J* = 9.0 Hz, H_{Ar}), 4.10–4.05 (m, 2H), 3.88–3.79 (m, 2H), 3.74–3.60 (m, 44H), 2.60 (t, 1H, t, *J* = 6.2 Hz) ppm.

^{13}C NMR (125 MHz, $CDCl_3$): δ 158.79, 138.27, 117.18, 83.02, 72.81, 70.65, 69.70, 67.65, 61.78 ppm.

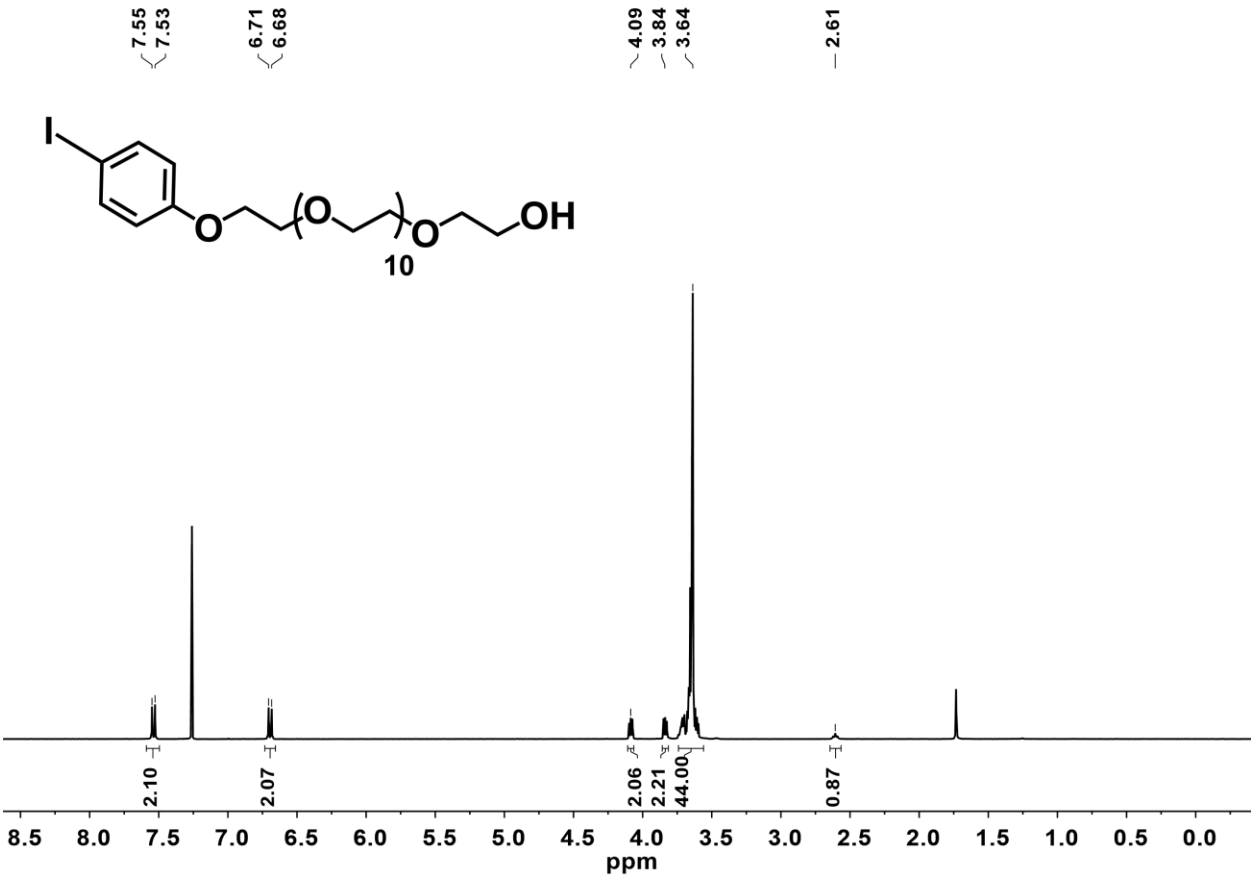

Figure D26. ^{1}H NMR spectrum of **PEG-Aryl-I** in $CDCl_3$ at 298 K.

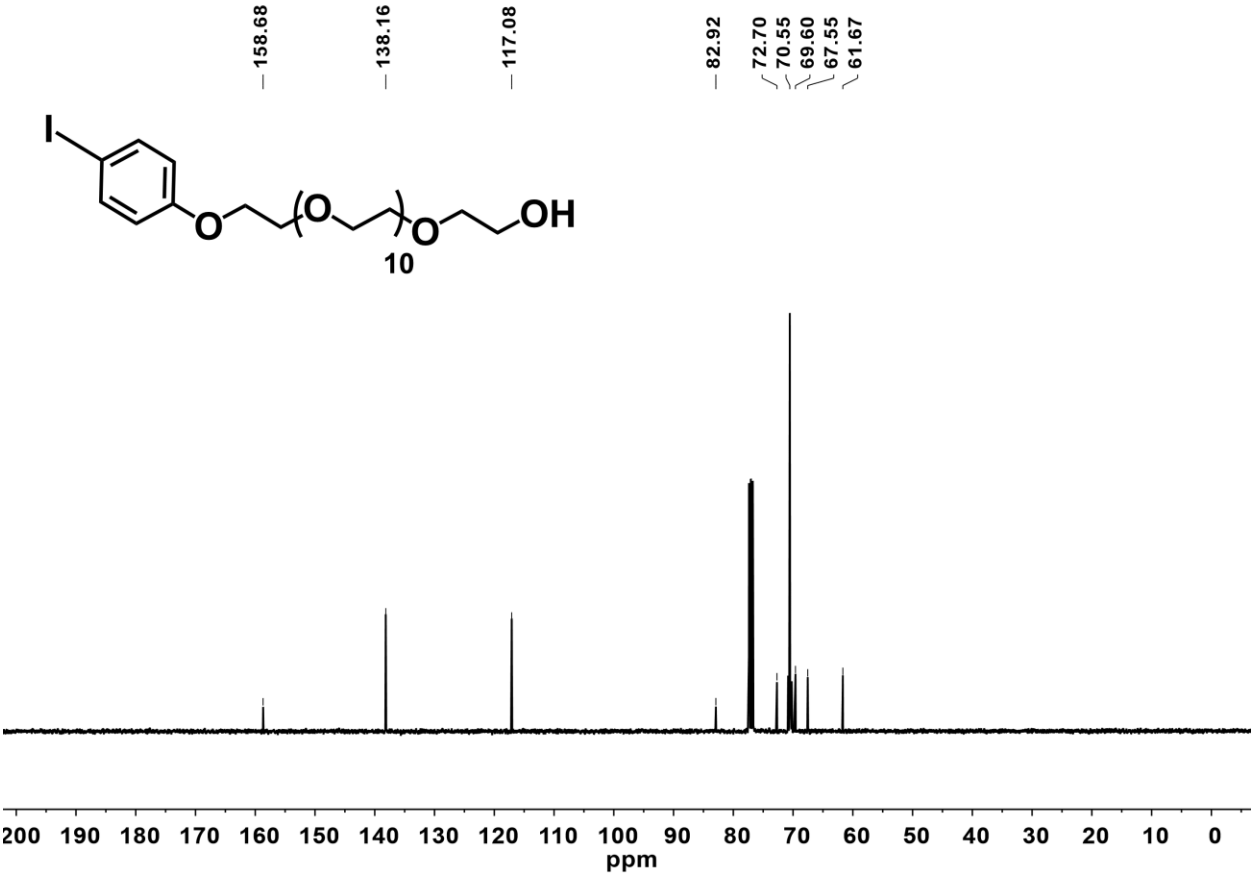

Figure D27. ^{13}C NMR spectrum of **PEG-Aryl-I** in $CDCl_3$ at 298 K.

5.5.6 General synthetic procedure for the preparation of [(Me-DalPhos)AuArX][SbF_6] oxidative addition complexes (X = Cl/I)

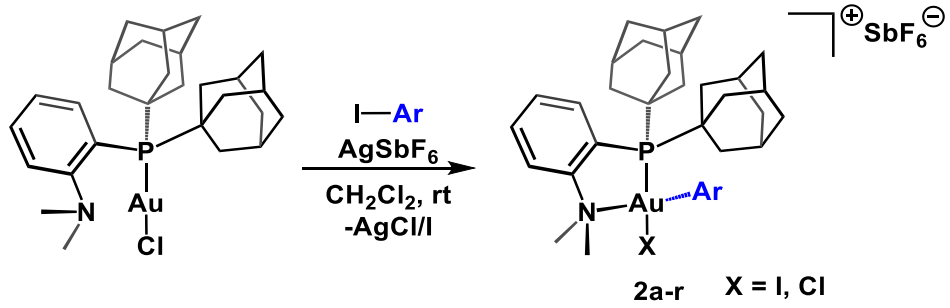

The $AgSbF_6$ and (Me-DalPhos)AuCl reagents were stored in the glovebox under an atmosphere of N_2 and then removed for use.

In the fume hood, $AgSbF_6$ was dissolved in DCM (2 mL) under protection from light, and the colorless solution was cooled to -20 °C. A DCM solution (2 mL) containing the aryliodide and (Me-DalPhos)AuCl reagents was prepared and also cooled to -20 °C. While both solutions were cold, the colorless aryliodide and (Me-DalPhos)AuCl solution was added in one portion to the solution of $AgSbF_6$, resulting in an immediate color change to bright yellow concomitant with precipitation of pale yellow solids. The reaction mixture was filtered through a pad of Celite to remove liberated AgX (X = Cl, I). Slow evaporation of solvent from the yellow filtrate over the course of 48 h at 25 °C resulted in saturation of the solution and the formation of yellow crystals. The supernatant was removed and the crystals were washed with C_6H_6 (2 × 3 mL), followed by *n*-pentane (2 × 3 mL), and then dried under reduced pressure to afford the [(Me-DalPhos)AuArCl][SbF_6] product as a yellow crystalline solid.

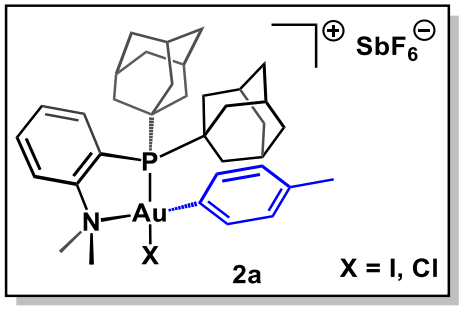

Following the general procedure, (Me-DalPhos)AuCl (43 mg, 0.066 mmol, 1.0 equiv), $AgSbF_6$ (23 mg, 0.066 mmol, 1.0 equiv) and 4-iodotoluene (43 mg, 0.20 mmol, 3.0 equiv) were used. The [**2a**][SbF_6] salt was isolated as a yellow crystalline solid in 72% yield (47 mg, 0.045 mmol). This complex has been previously reported.[5]

^{1}H NMR (400 MHz, CD_3CN): δ 8.03 (m, 1H, H_{Ar}), 8.01–7.88 (m, 2H, H_{Ar}), 7.68 (m, 1H, H_{Ar}), 7.43 (d, 2H, *J* = 8.4 Hz, H_{Ar}), 7.14 (d, 2H, *J* = 8.4 Hz, H_{Ar}), 3.45 (s, 6H, $N(CH_3)_2$), 2.34 (s, 3H, Tolyl-CH_3), 2.33–2.25 (m, 6H, H_{Ad}), 2.03–1.98 (m, 12H, H_{Ad}), 1.80–1.66 (m, 12H, H_{Ad}) ppm.

^{31}P{^{1}H} NMR (162 MHz, CD_3CN): δ 75.0 ppm.

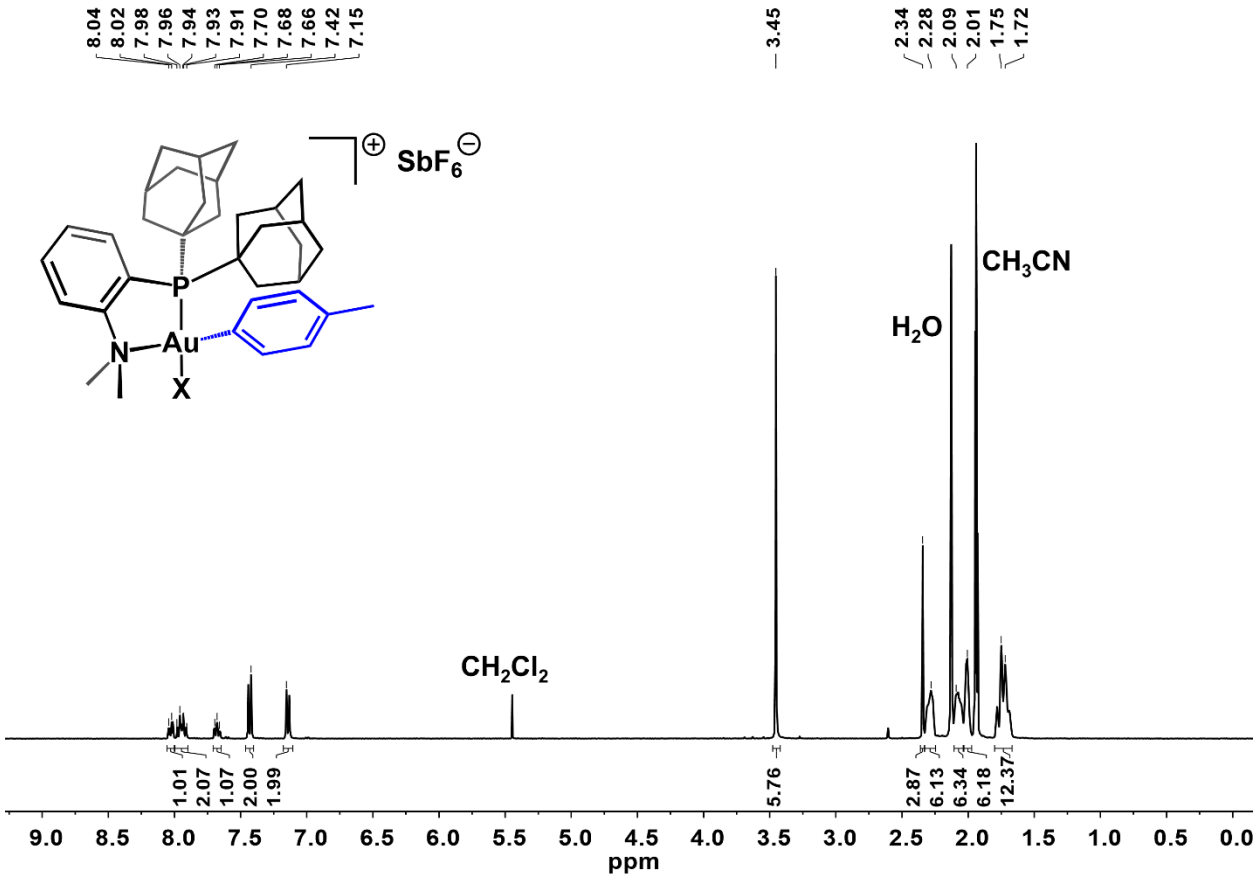

Figure D28. ^{1}H NMR spectrum of [**2a**][SbF_6] in CD_3CN at 298 K.

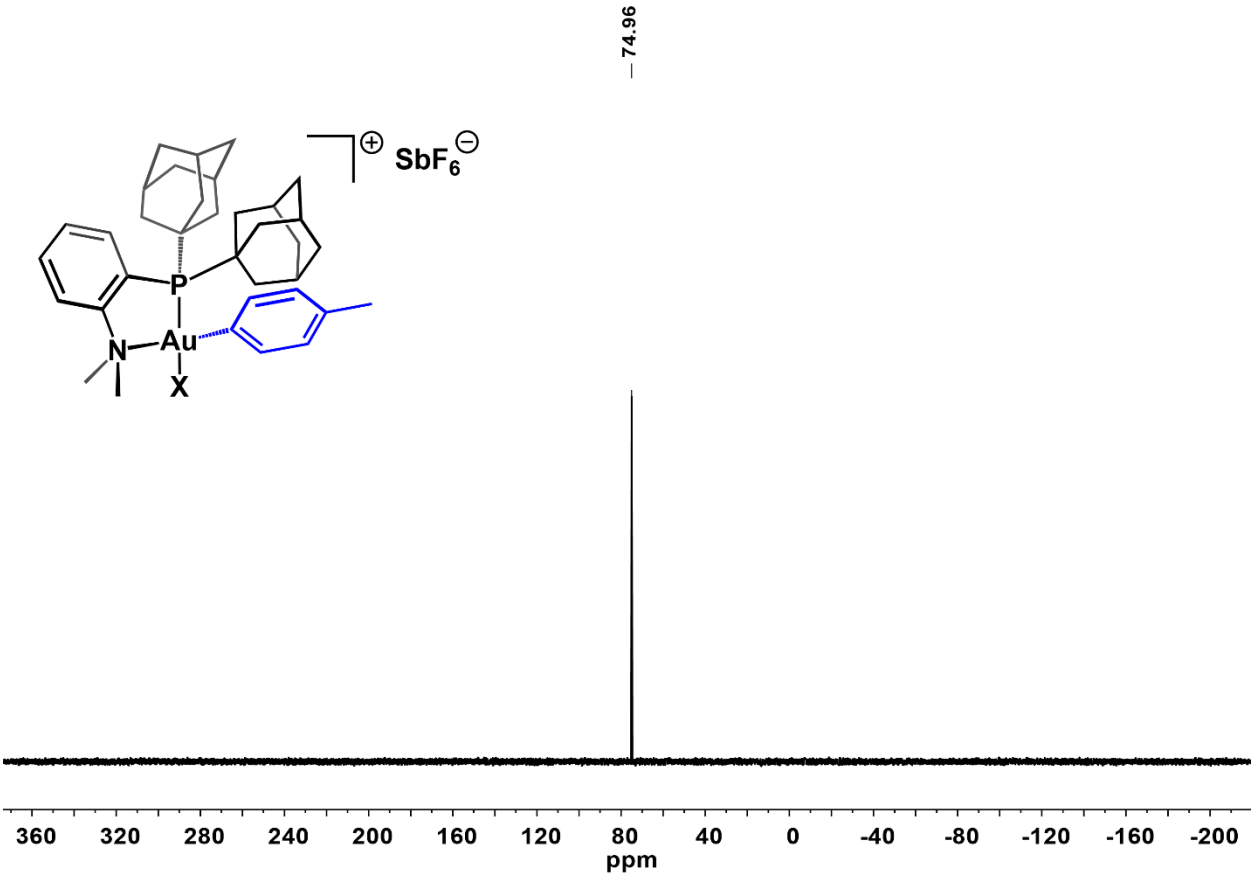

Figure D29. $^{31}P\{^{1}H\}$ NMR spectrum of [**2a**][SbF_6] in CD_3CN at 298 K.

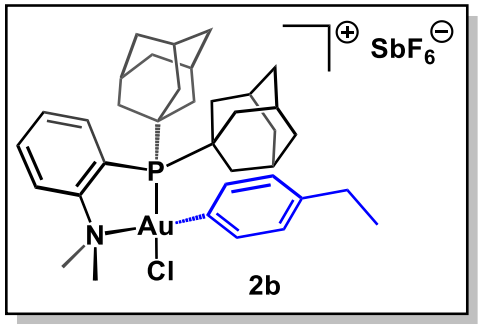

Following the general procedure, (Me-DalPhos)AuCl (30 mg, 0.046 mmol, 1.0 equiv), $AgSbF_6$ (16 mg, 0.046 mmol, 1.0 equiv) and 4-ethyliodobenzene (20 µL, 0.14 mmol, 3.0 equiv) were used. The [**2b**][SbF_6] salt was isolated as a yellow crystalline solid in 59% yield (27 mg, 0.027 mmol). A single crystal of suitable quality for an X-ray diffraction study was obtained using this procedure. The X-ray crystallographic analysis indicates 100% Cl occupancy (see section V for crystallographic details).

^{1}H NMR (400 MHz, CD_3CN): δ 8.03 (m, 1H, H_{Ar} 8.00–7.89 (m, 2H, H_{Ar}), 7.69 (m, 1H, H_{Ar}), 7.46 (d, 2H, *J* = 8.4, H_{Ar}), 7.17 (d, 2H, *J* = 8.2, H_{Ar}), 3.45 (s, 6H, $N(CH_3)_2$), 2.65 (q, 2H, *J* = 7.6 Hz, -CH_2CH_3), 2.28 (m, 6H, H_{Ad}), 2.11–2.08 (s, 6H, H_{Ad}) 2.04–1.99 (s, 6H, H_{Ad}), 1.73 (m, 12H, H_{Ad}), 1.23 (t, 3H, *J* = 7.6, -CH_2CH_3) ppm.

^{31}P{^{1}H} NMR (162 MHz, CD_3CN): δ 74.9 ppm.

ESI-MS(+): 768.33 (calc'd 768.33) *m/z*.

Note this sample was run in the presence of formic acid, and as a result, the [(Me-DalPhos)Au(*p*-ethylbenzene)OCHO]$^+$ ion is observed ($C_{37}H_{50}NO_2PAu$).

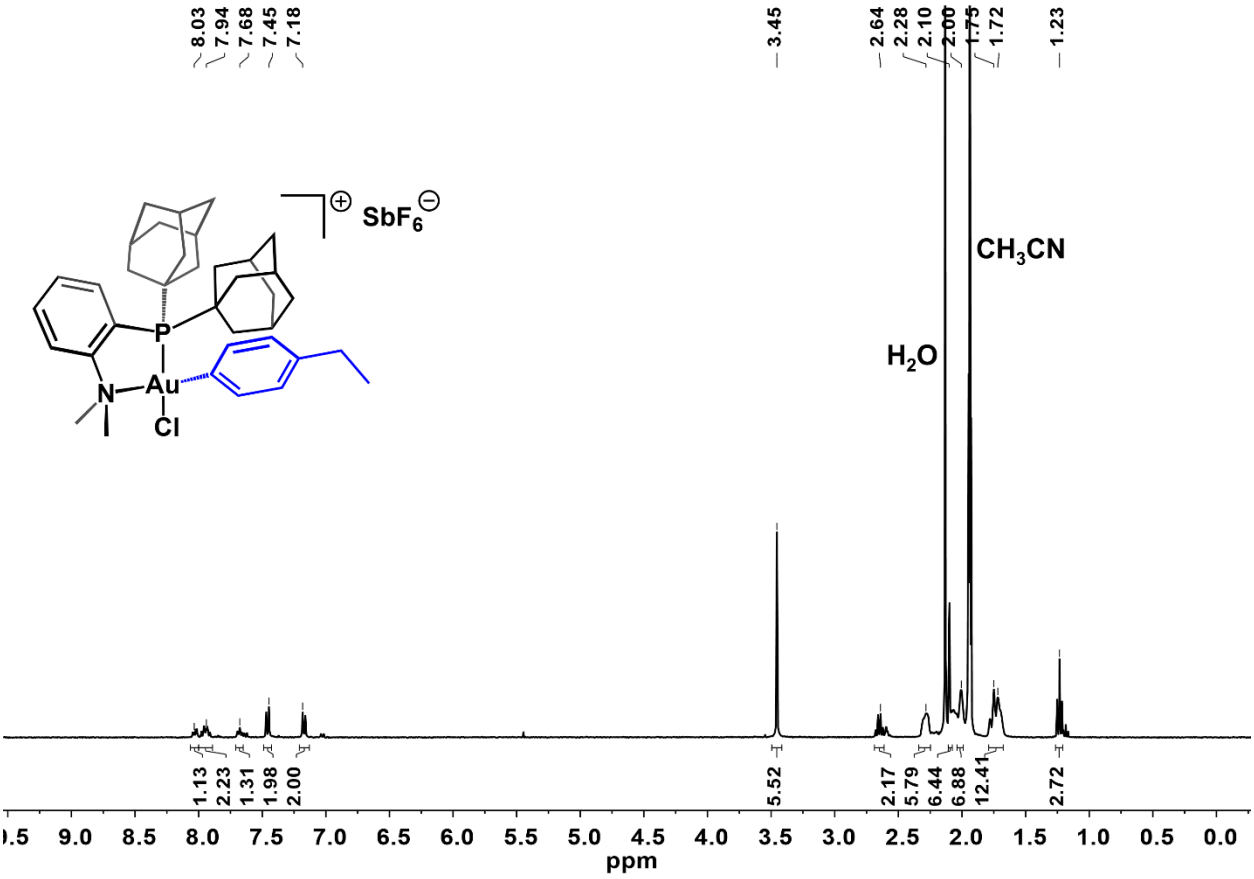

Figure D9. ^{1}H NMR spectrum of [**2b**][SbF_6] in CD_3CN at 298 K.

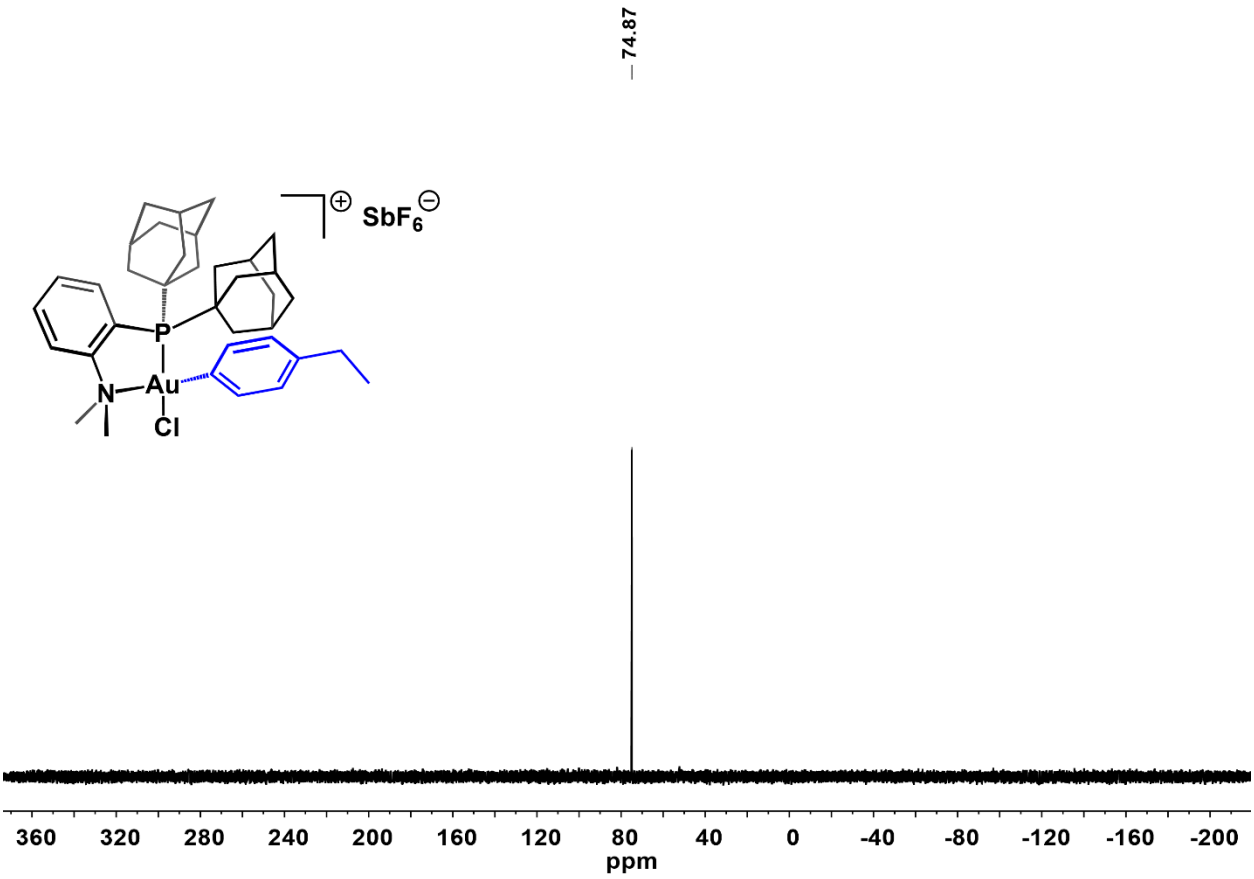

Figure D10. $^{31}P\{^{1}H\}$ NMR spectrum of [**2b**][SbF_6] in CD_3CN at 298 K.

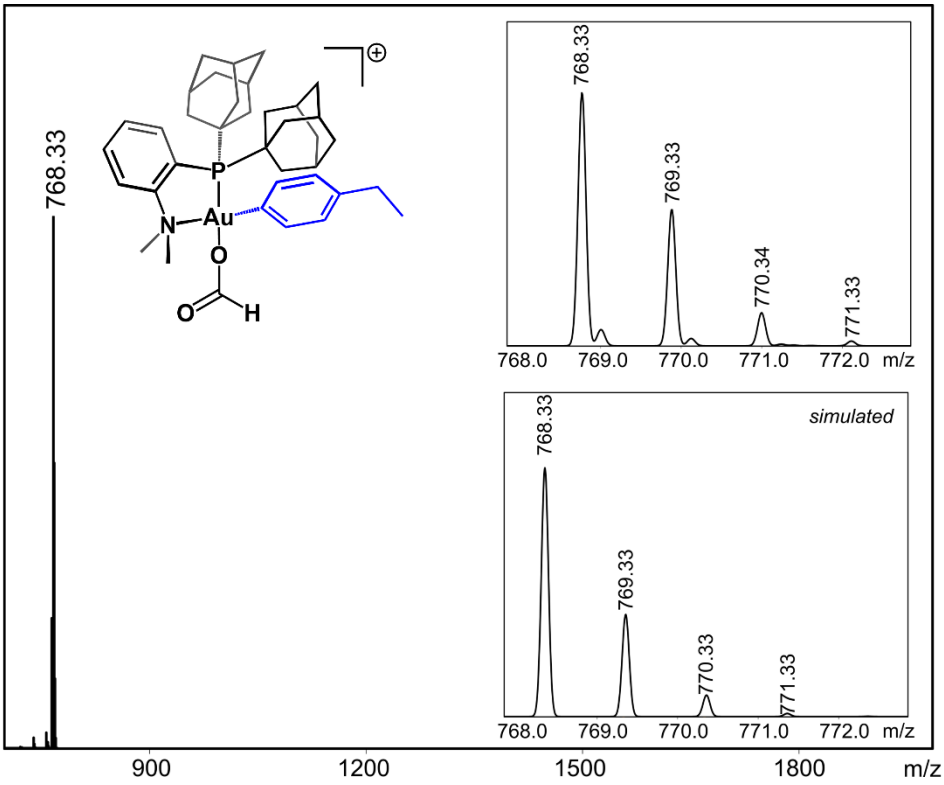

Figure D11. ESI-MS(+) of **2b**. Note this sample was run in the presence of formic acid, resulting in Cl^-/$OCHO^-$ exchange.

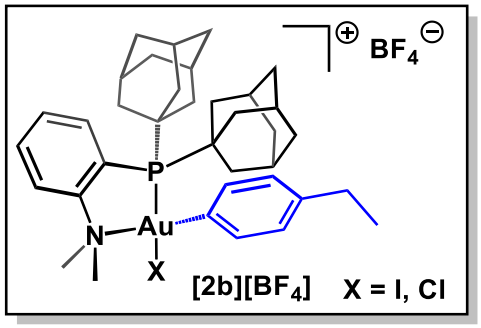

In the fume hood, a solution of $AgBF_4$ (9 mg, 0.05 mmol, 1 equiv) in DCM (2 mL) was prepared under protection from light, and then cooled to -20 °C. A DCM solution (2 mL) containing 4-ethyliodobenzene (20 µL, 0.14 mmol, 3.0 equiv) and (Me-DalPhos)AuCl (30 mg, 0.046 mmol, 1.0 equiv) reagents was prepared and also cooled to -20 °C. While both solutions were cold, the colorless 4-ethyliodobenzene and (Me-DalPhos)AuCl solution was added in one portion to the solution of $AgBF_4$, and the reaction mixture was sonicated for 2 min, during which time the solution became yellow concomitant with the precipitation of pale yellow precipitate. The resulting suspension was filtered through a pad of Celite, and the filtrate was dried *in vacuo* to give a pale-yellow powder. The solids were washed with C_6H_6 (2 × 3 mL), followed by *n*-pentane (2 × 3 mL), and then dried under reduced pressure to afford [**2b**][BF_4] as a pale yellow powder in 86% yield (36 mg, 0.043 mmol).

^{1}H NMR (400 MHz, CD_3CN): δ 8.05–8.01 (m, 1H, H_{Ar}), 7.99–7.92 (m, 2H, H_{Ar}), 7.73–7.67 (m, 1H), 7.46 (d, 2H, d, *J* = 8.4 Hz), 7.17 (d, 2H, *J* = 8.2 Hz), 3.45 (s, 6H, N(CH_3)$_2$), 2.65 (q, 2H, *J* = 7.7 Hz, -$CH_2$$CH_3$), 2.29 (s, 6H, H_{Ad}), 2.10 (s, 6H, H_{Ad}), 2.01 (s, 6H, H_{Ad}), 1.75 (s, 12H, H_{Ad}), 1.23 (t, 3H, *J* = 7.6 Hz, -$CH_2$$CH_3$) ppm.

^{31}P{^{1}H} NMR (162 MHz, CD_3CN): δ 75.7 ppm.

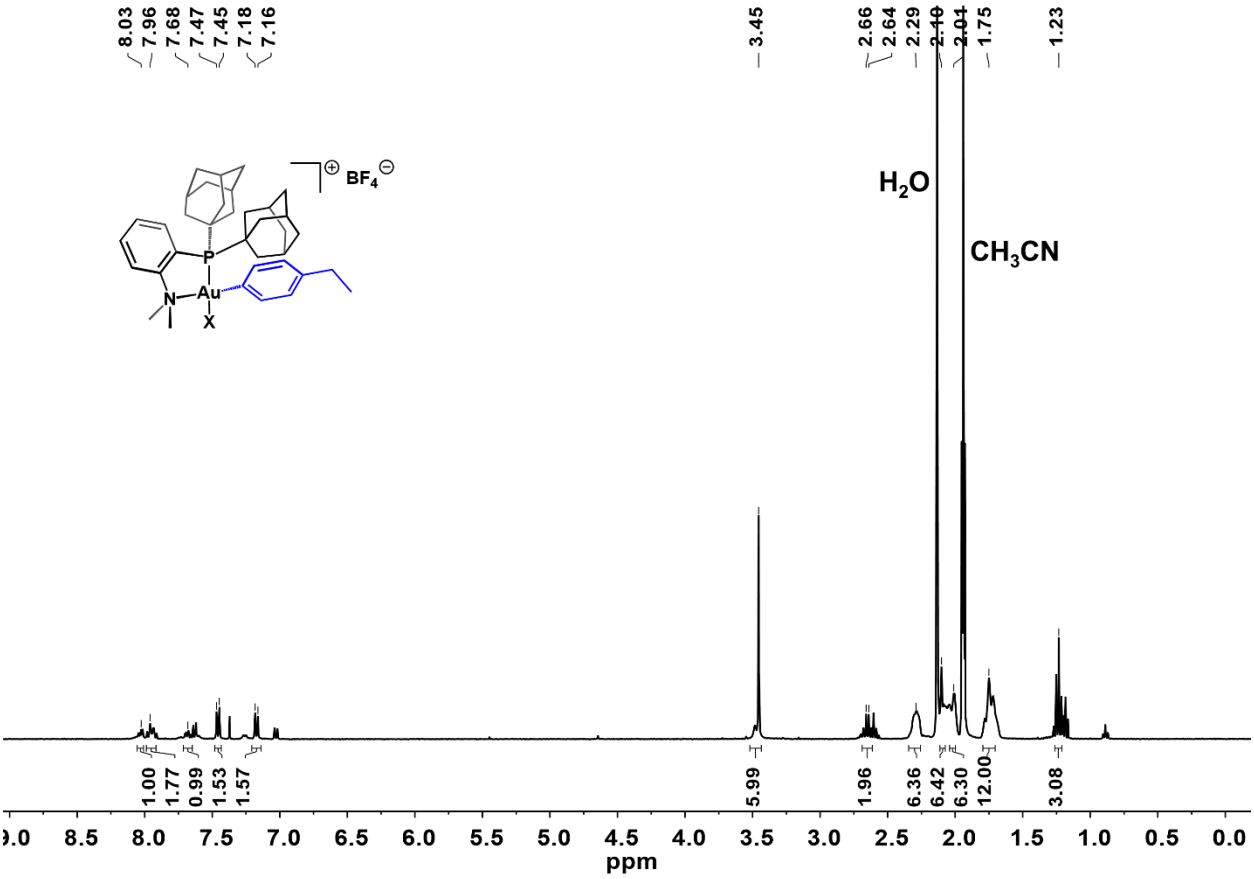

Figure D12. ^{1}H NMR spectrum of [**2b**][BF_4] in CD_3CN at 298 K.

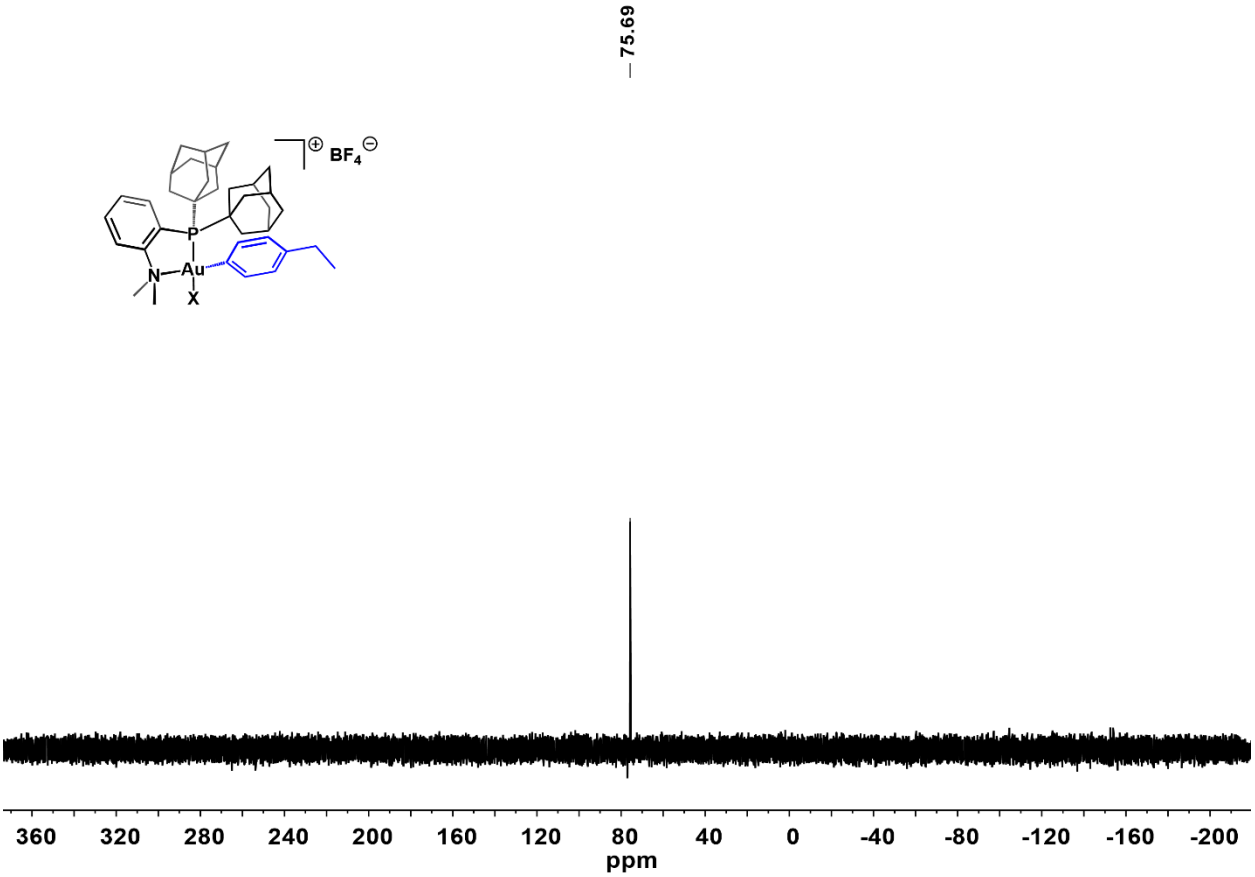

Figure D13. $^{31}P\{^{1}H\}$ NMR spectrum of [**2b**][BF_4] in CD_3CN at 298 K.

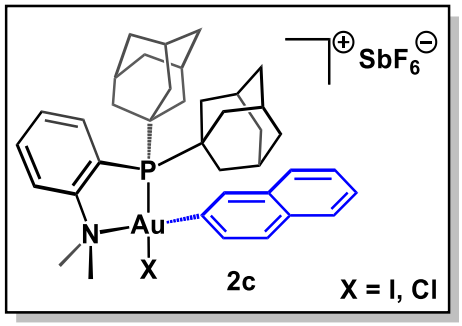

Following the general procedure, (Me-DalPhos)AuCl (30 mg, 0.046 mmol, 1.0 equiv), $AgSbF_6$ (16 mg, 0.046 mmol, 1.0 equiv) and 2-iodonaphthalene (35 µL, 0.14 mmol, 3.0 equiv) were used. The [**2c**][SbF_6] salt was isolated as a yellow crystalline solid in 64% yield (30 mg, 0.029 mmol). A single crystal of suitable quality for an X-ray diffraction study was obtained using this procedure (see section V for crystallographic details).

^{1}H NMR (400 MHz, CD_3CN): δ 8.10 (m, 1H, H_{Ar}), 8.06 (m, 1H, H_{Ar}), 8.01–7.89 (m, 3H, H_{Ar}), 7.84 (m, 2H, H_{Ar}), 7.75–7.66 (m, 2H, H_{Ar}), 7.57 (m, 2H, H_{Ar}), 3.51 (s, 6H, N(CH_3)$_2$), 2.35 (m, 3H, H_{Ad}), 2.29–2.25 (m, 3H, H_{Ad}), 2.15 (m, 3H, H_{Ad}), 2.02 (m, 10H, H_{Ad}), 1.84–1.61 (m, 14H, H_{Ad}) ppm.

^{31}P{^{1}H} NMR (162 MHz, CD_3CN): δ 76.1 ppm.

ESI-MS(+): 780.21 (calc'd 780.28) *m/z* ($C_{38}H_{47}ClNPAu$).

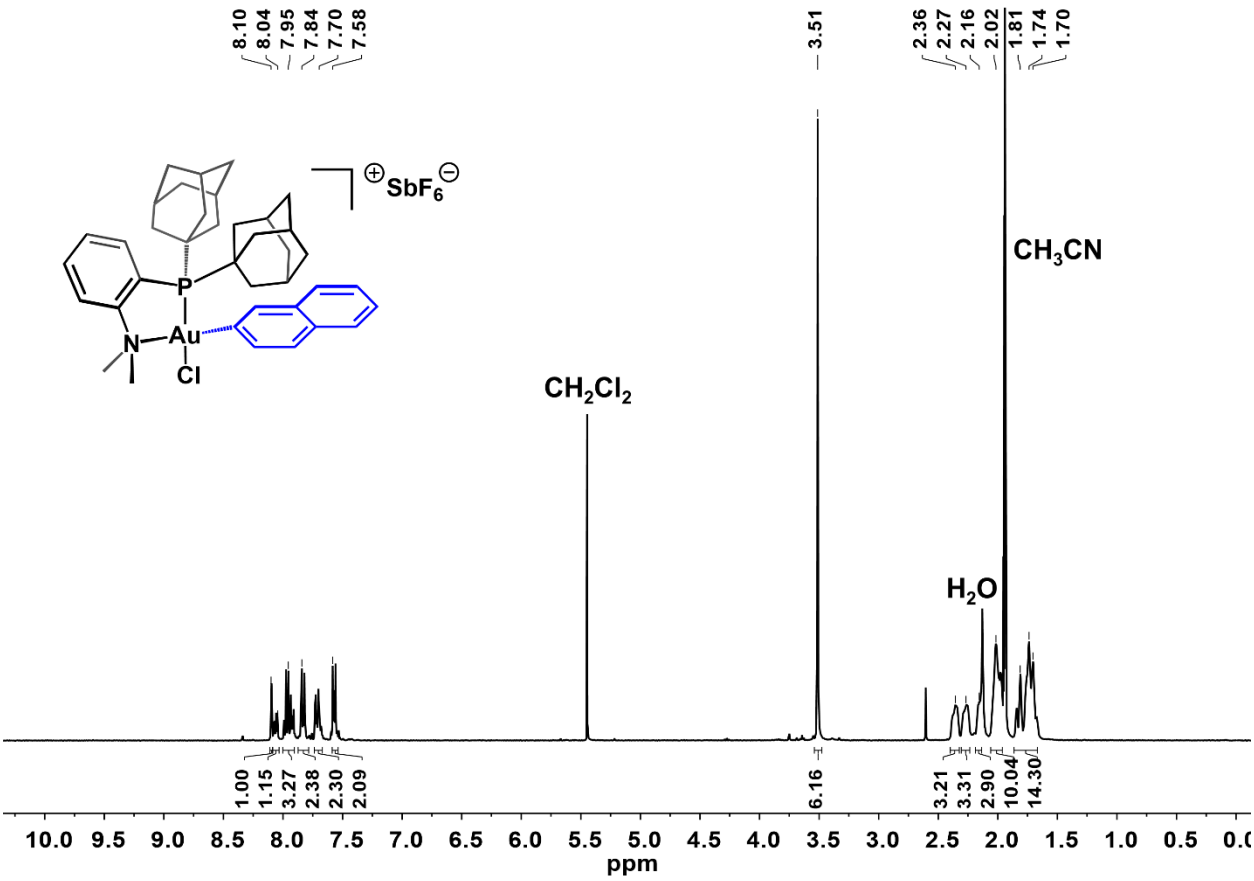

Figure D14. ^{1}H NMR spectrum of **2c** in CD_3CN at 298 K.

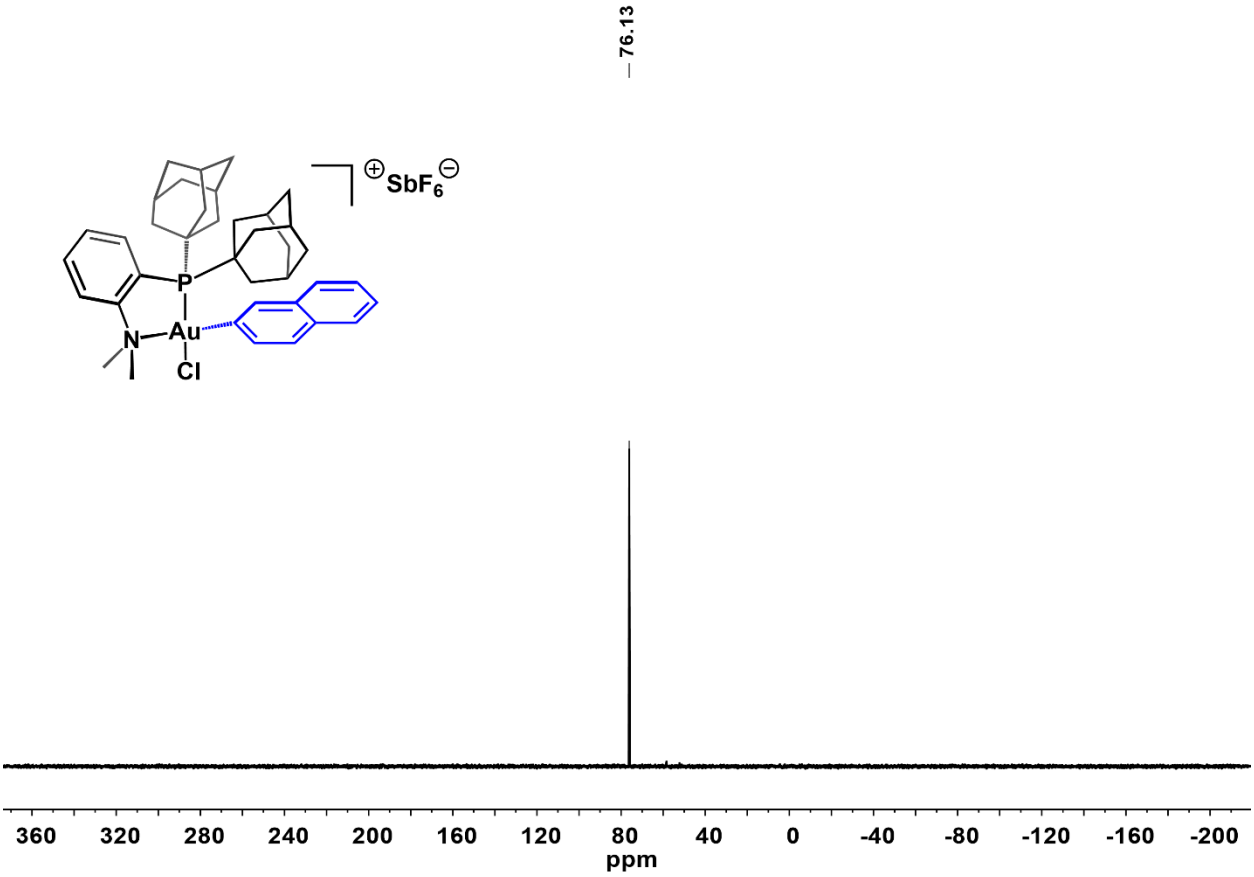

Figure D15. $^{31}P\{^{1}H\}$ NMR spectrum of **2c** in CD_3CN at 298 K.

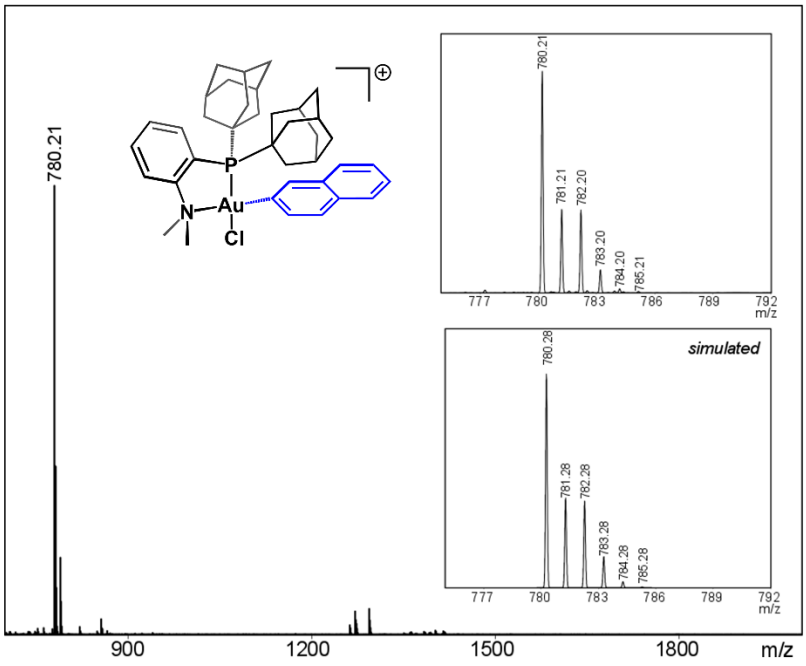

Figure D16. ESI-MS(+) of **2c**.

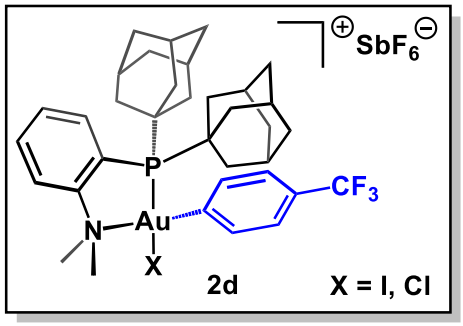

Following the general procedure, (Me-DalPhos)AuCl (22 mg, 0.034 mmol, 1.0 equiv), $AgSbF_6$ (12 mg, 0.034 mmol, 1.0 equiv) and 4-iodobenzotrifluoride (25 µL, 0.17 mmol, 5.0 equiv) were used. The [**2d**][SbF_6] salt was isolated as a yellow crystalline solid in 60% yield (21 mg, 0.020 mmol). A single crystal of suitable quality for an X-ray diffraction study was obtained using this procedure (see section V for crystallographic details).

^{1}H NMR (400 MHz, CD_3CN): δ 8.08–8.01 (m, 1H, H_{Ar}), 8.00–7.90 (m, 2H, H_{Ar}), 7.82 (d, *J* = 8.3 Hz, 2H, H_{Ar}), 7.74–7.66 (m, 1H, H_{Ar}), 7.64 (d, *J* = 8.3 Hz, 2H, H_{Ar}), 3.50 (s, 6H, $N(CH_3)_2$), 2.36–2.25 (m, 6H, H_{Ad}), 2.02 (m, 11H, H_{Ad}), 1.74 (m, 13H, H_{Ad}) ppm.

^{19}F NMR (376 MHz, CD_3CN): δ -63.0 ppm.

^{31}P{^{1}H} NMR (162 MHz, CD_3CN): δ 77.6 ppm.

ESI-MS(+): 798.17 (calc'd 798.25) *m/z* ($C_{35}H_{44}ClF_3NPAu$).

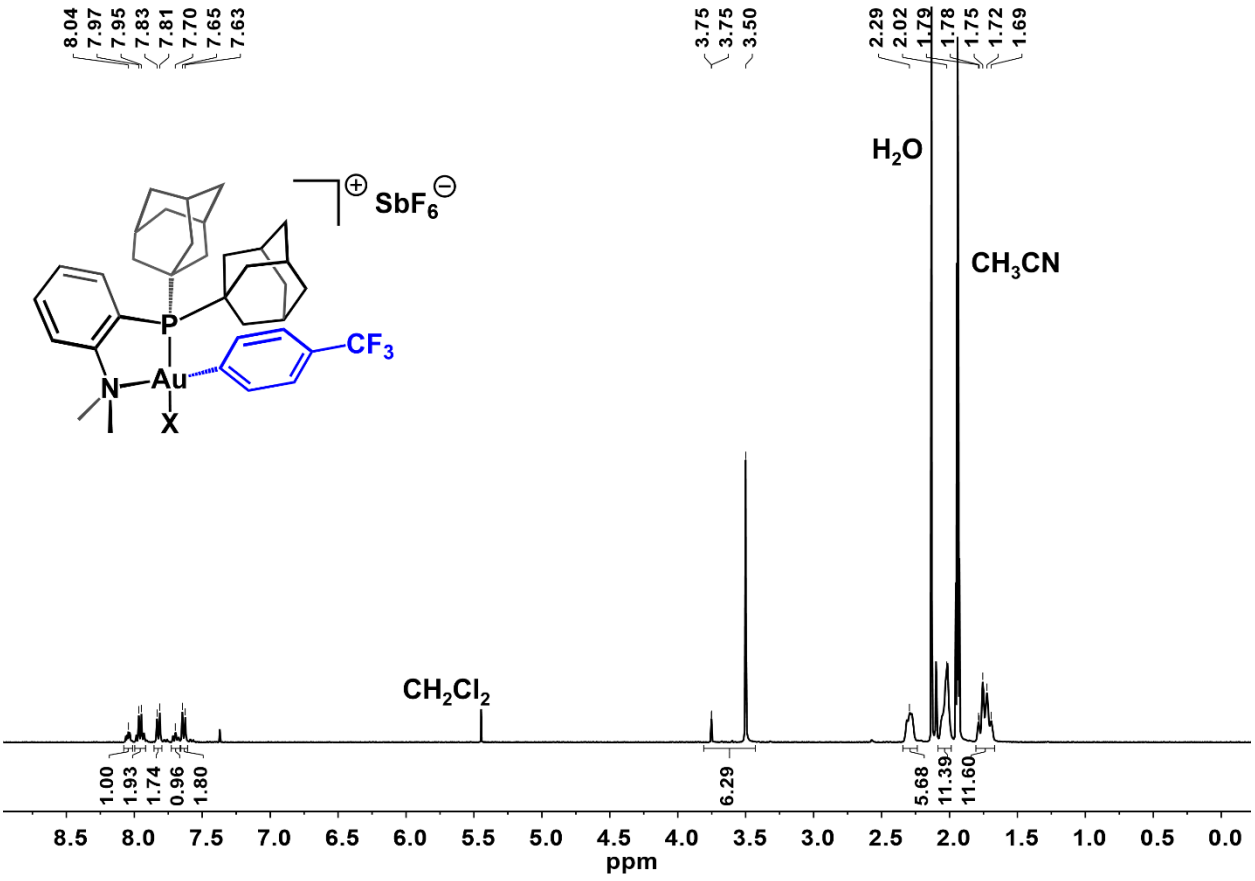

Figure D17. ^{1}H NMR spectrum of [**2d**][SbF_6] in CD_3CN at 298 K.

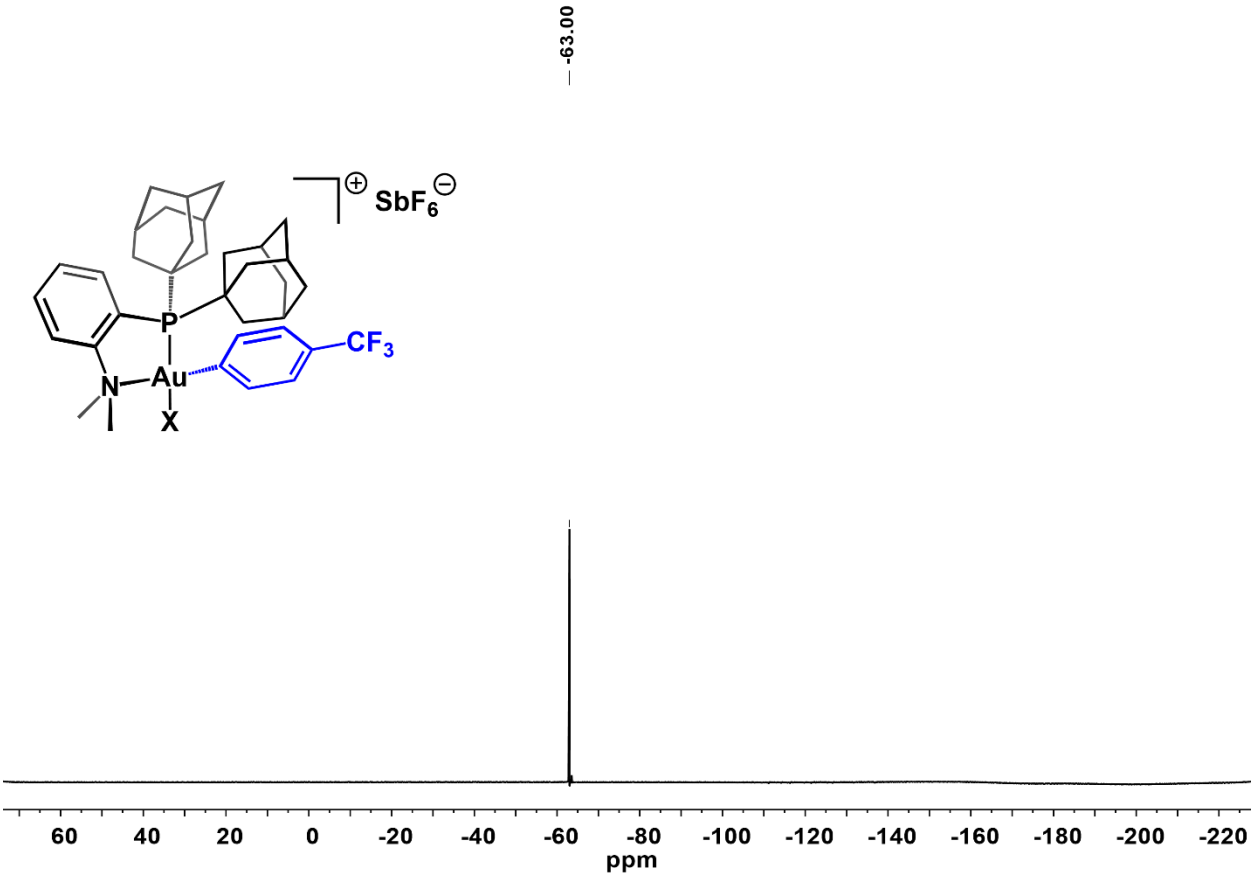

Figure D18. ^{19}F NMR spectrum of [**2d**][SbF_6] in CD_3CN at 298 K.

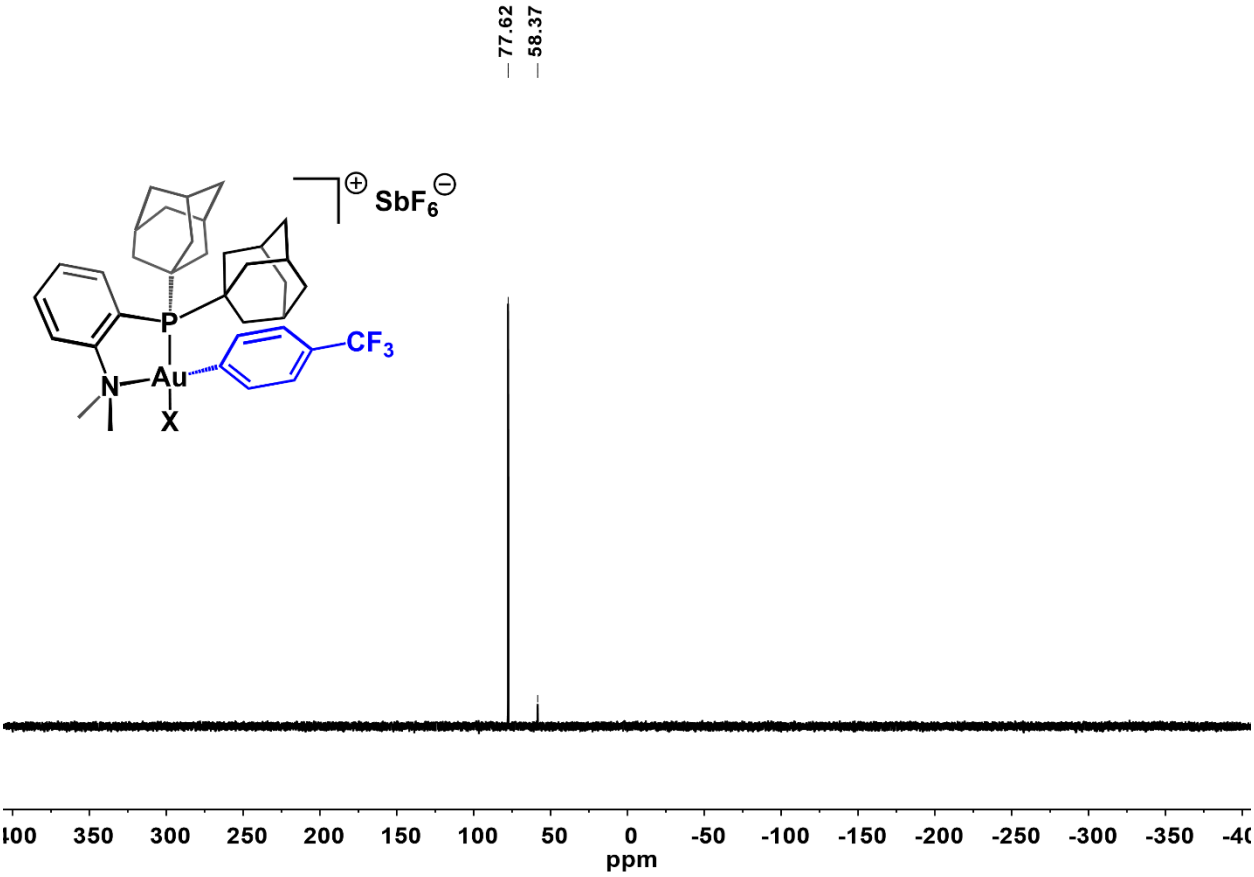

Figure D19. $^{31}P\{^{1}H\}$ NMR spectrum of [**2d**][SbF_6] in CD_3CN at 298 K. The signal at 58.3 ppm corresponds to the starting (Me-DalPhos)AuCl compound.

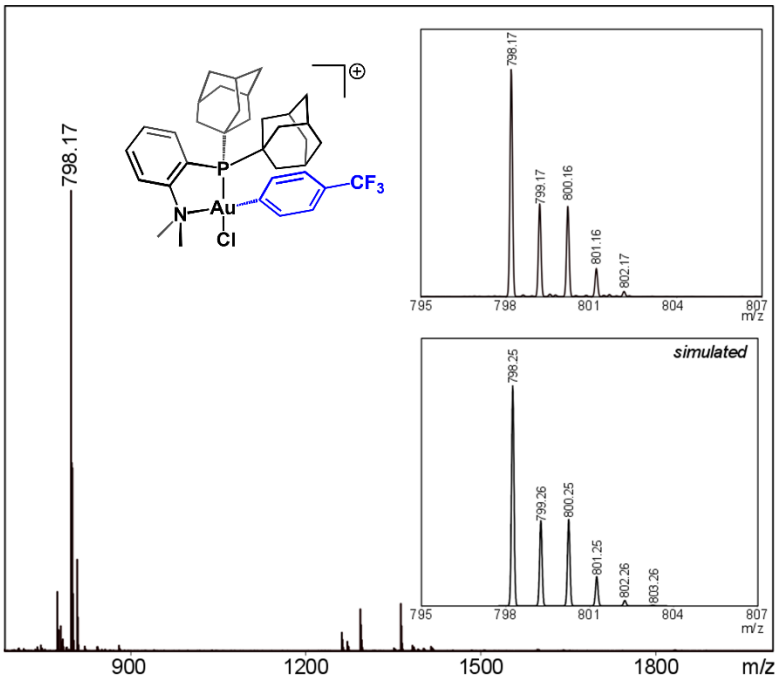

Figure D20. ESI-MS(+) of **2d**.

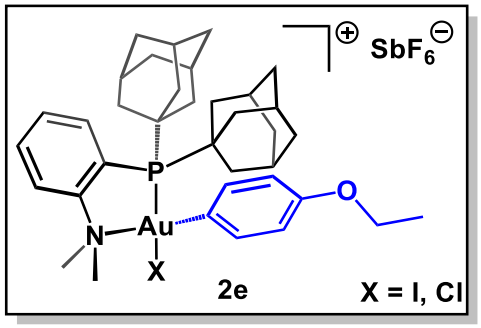

In the fume hood, a solution of $AgSbF_6$ (12 mg, 0.034 mmol, 1.0 equiv) in DCM (2 mL) was prepared under protection from light, and then cooled to -20 °C. A DCM solution (2 mL) containing 4-iodophenetole (34 mg, 0.14 mmol, 3.0 equiv) and (Me-DalPhos)AuCl (30 mg, 0.046 mmol, 1.0 equiv) reagents was prepared and also cooled to -20 °C. While both solutions were cold, the colorless 4-iodophenetole and (Me-DalPhos)AuCl solution was added in one portion to the solution of $AgSbF_6$, at which point an immediate color change to yellow occurred concomitant with the precipitation of pale yellow precipitate. The resulting suspension was filtered through a pad of Celite, and the filtrate was dried *in vacuo* to give a pale-yellow powder. The solids were washed with C_6H_6 (2 x 3 mL), followed by *n*-pentane (2 x 3 mL), and then dried under reduced pressure to afford [**2e**][SbF_6] as a pale yellow powder in 85% yield (29 mg, 0.029 mmol).

^{1}H NMR (400 MHz, CD_3CN): δ 8.02 (m, 1H, H_{Ar}), 7.95 (m, 2H, H_{Ar}), 7.72–7.64 (m, 1H, H_{Ar}), 7.43 (d, 2H, *J* = 9.0 Hz), 6.92 (d, 2H, *J* = 8.9 Hz), 4.04 (q, 2H, *J* = 7.0 Hz, -C*H*$_2$C*H*$_3$), 3.46 (s, 6H, N(C*H*$_3$)$_2$), 2.29 (m, 6H, H_{Ad}), 2.12–1.98 (m, 12H, H_{Ad}), 1.73 (m, 12H, H_{Ad}), 1.37 (t, 3H, *J* = 7.0 Hz) ppm.

^{31}P{^{1}H} NMR (162 MHz, CD_3CN): δ 75.1 ppm.

ESI-MS(+): 774.23 (calc'd 774.29) *m/z* ($C_{36}H_{49}ClNOPAu$).

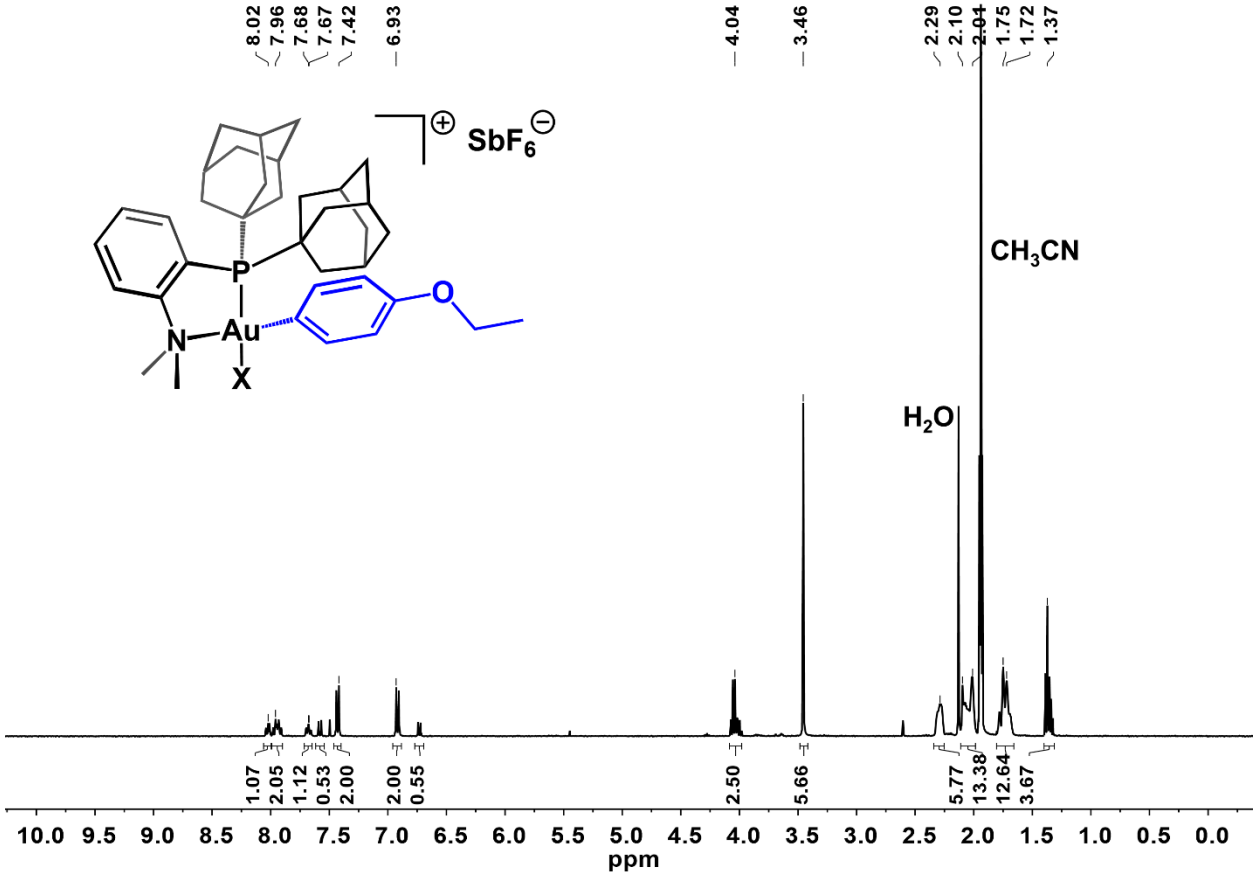

Figure D21. ^{1}H NMR spectrum of [**2e**][SbF_6] in CD_3CN at 298 K.

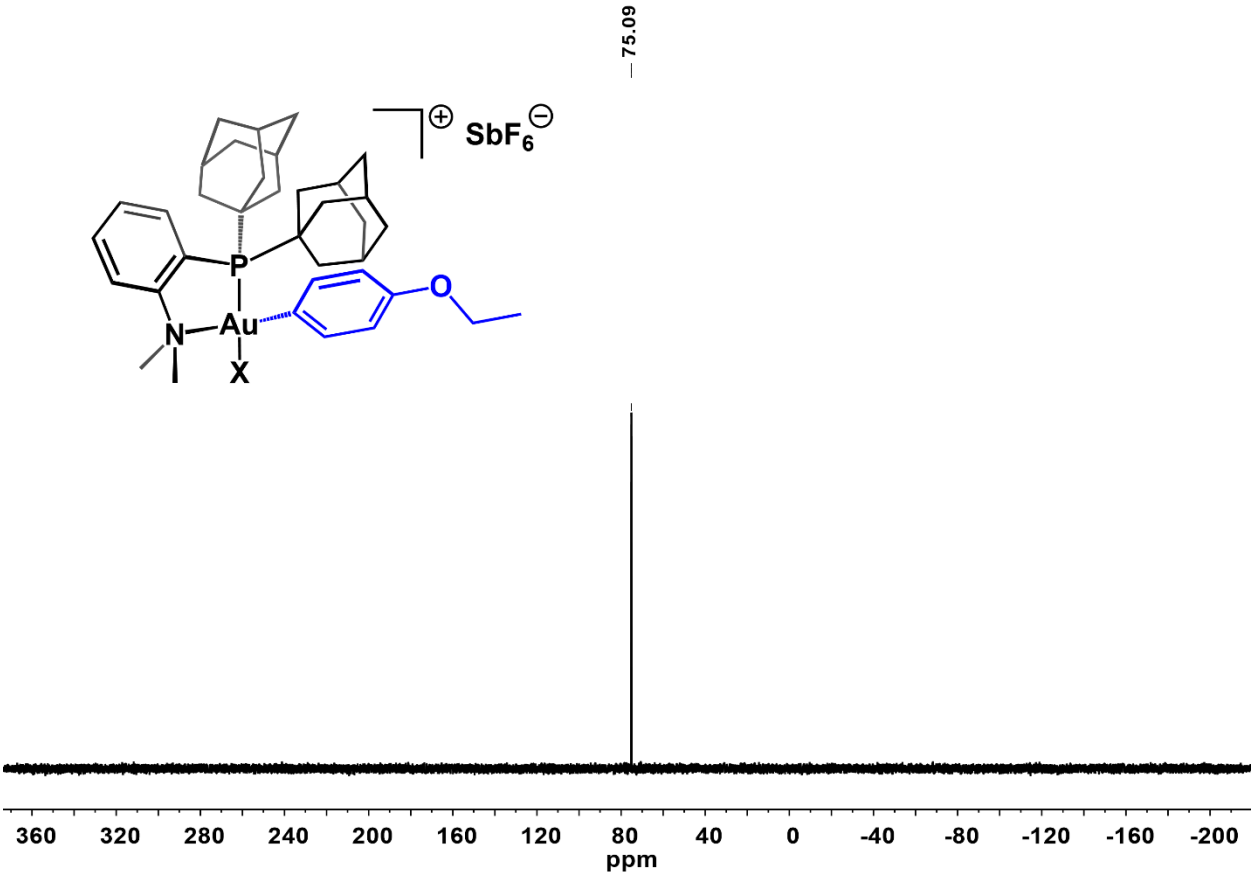

Figure D22. $^{31}P\{^{1}H\}$ NMR spectrum of [**2e**][SbF_6] in CD_3CN at 298 K.

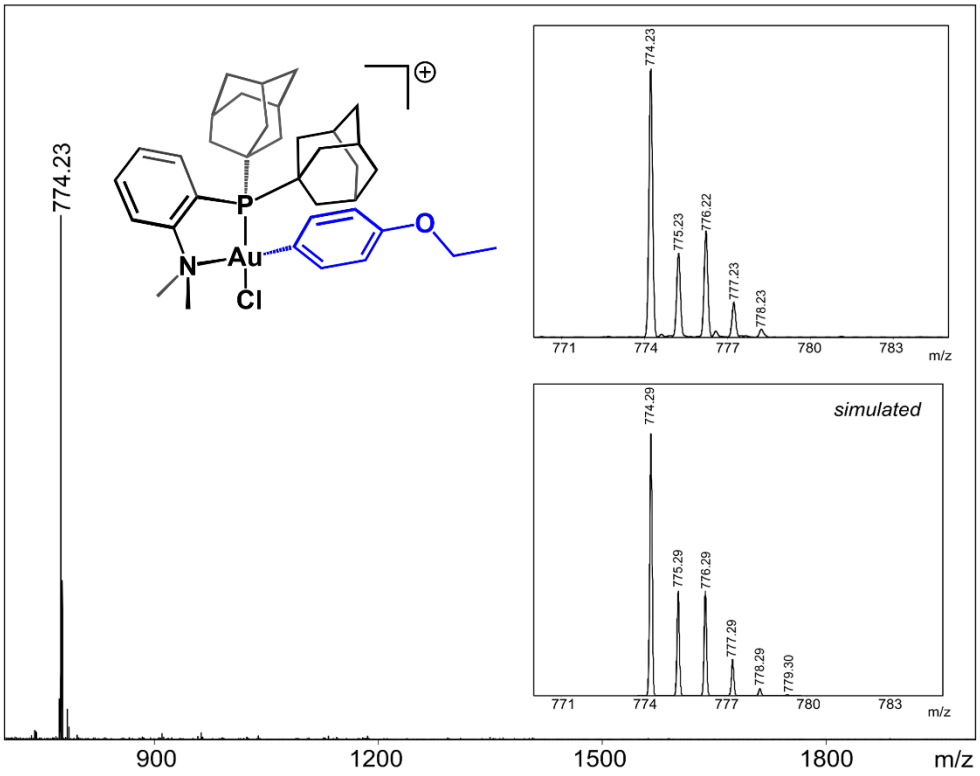

Figure D23. ESI-MS(+) of **2e**.

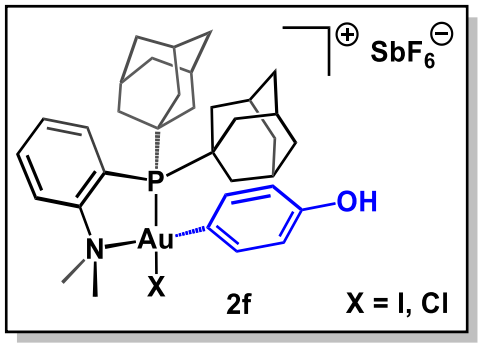

Following the general procedure, (Me-DalPhos)AuCl (30 mg, 0.046 mmol, 1.0 equiv), $AgSbF_6$ (16 mg, 0.046 mmol, 1.0 equiv) and 4-iodophenol (31 mg, 0.14 mmol, 3.0 equiv) were used. The [**2f**][SbF_6] salt was isolated as an orange crystalline solid in 65% yield (29 mg, 0.030 mmol). A single crystal of suitable quality for an X-ray diffraction study was obtained using this workup (See section V for crystallographic details). Elem. Anal. (Calc'd) for [**2f**][SbF_6]·H_2O, $C_{34}H_{47}AuClF_6NO_2PSb$: C, 40.64 (40.78); H, 4.51 (4.73); N, 1.39 (1.40). Crystallographic analysis displays one co-crystallized water molecule for each [**2f**][SbF_6] salt complex (see section V).

^{1}H NMR (400 MHz, CD_3CN): δ 8.02 (m, 1H, H_{Ar}), 8.01–7.88 (m, 2H, H_{Ar}), 7.67 (m, 1H, H_{Ar}), 7.35 (d, 2H, *J* = 8.9 Hz, H_{Ar}), 6.83 (d, 1H, *J* = 8.7 Hz, H_{Ar}), 3.45 (s, 6H, $N(CH_3)_2$), 2.28 (m, 6H, H_{Ad}), 2.11–2.01 (m, 12H, H_{Ad}), 1.75 (m, 12H, H_{Ad}) ppm.

^{31}P{^{1}H} NMR (162 MHz, CD_3CN): δ 75.6 ppm.

ESI-MS(+): 746.15 (746.26) *m/z* ($C_{34}H_{44}Cl_2NPAu$).

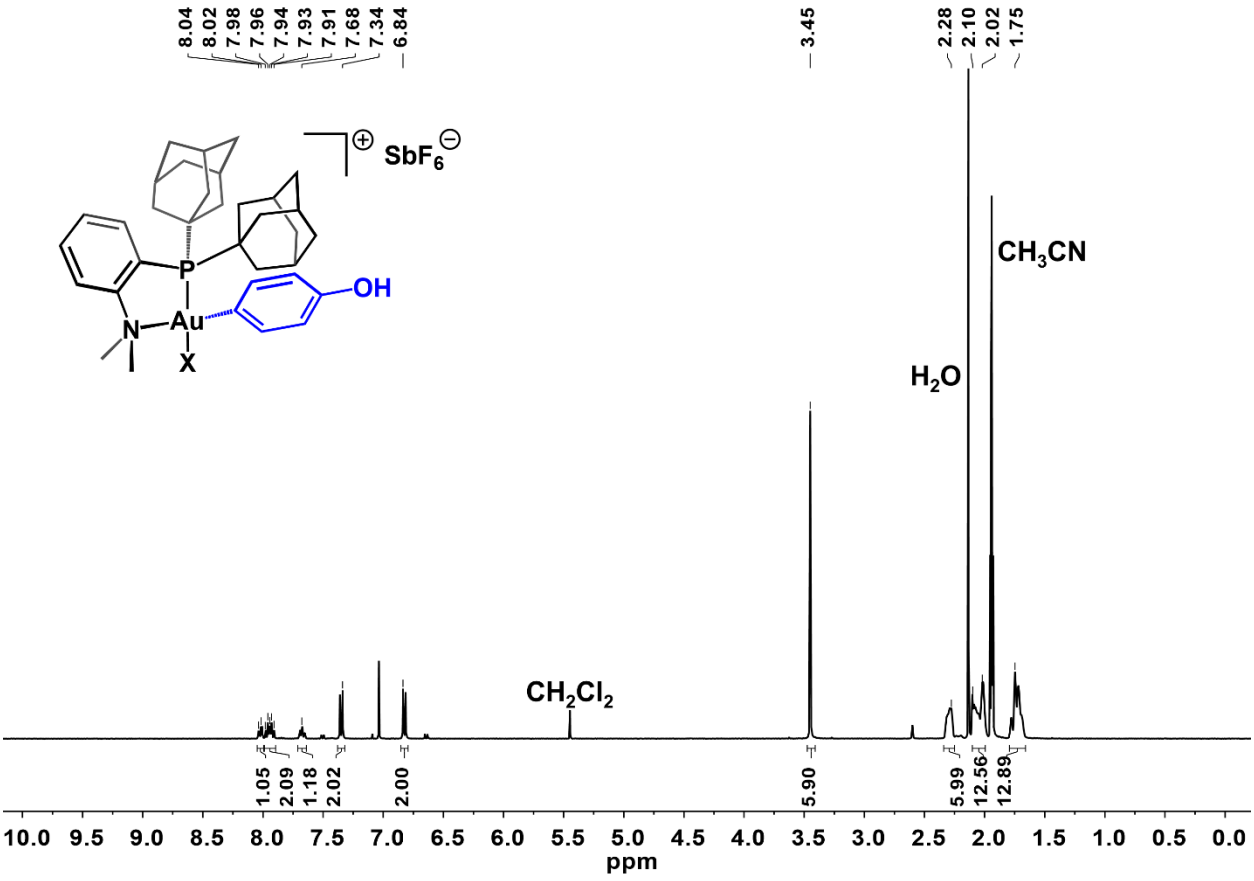

Figure D24. ^{1}H NMR spectrum of [**2f**][SbF_6] in CD_3CN at 298 K.

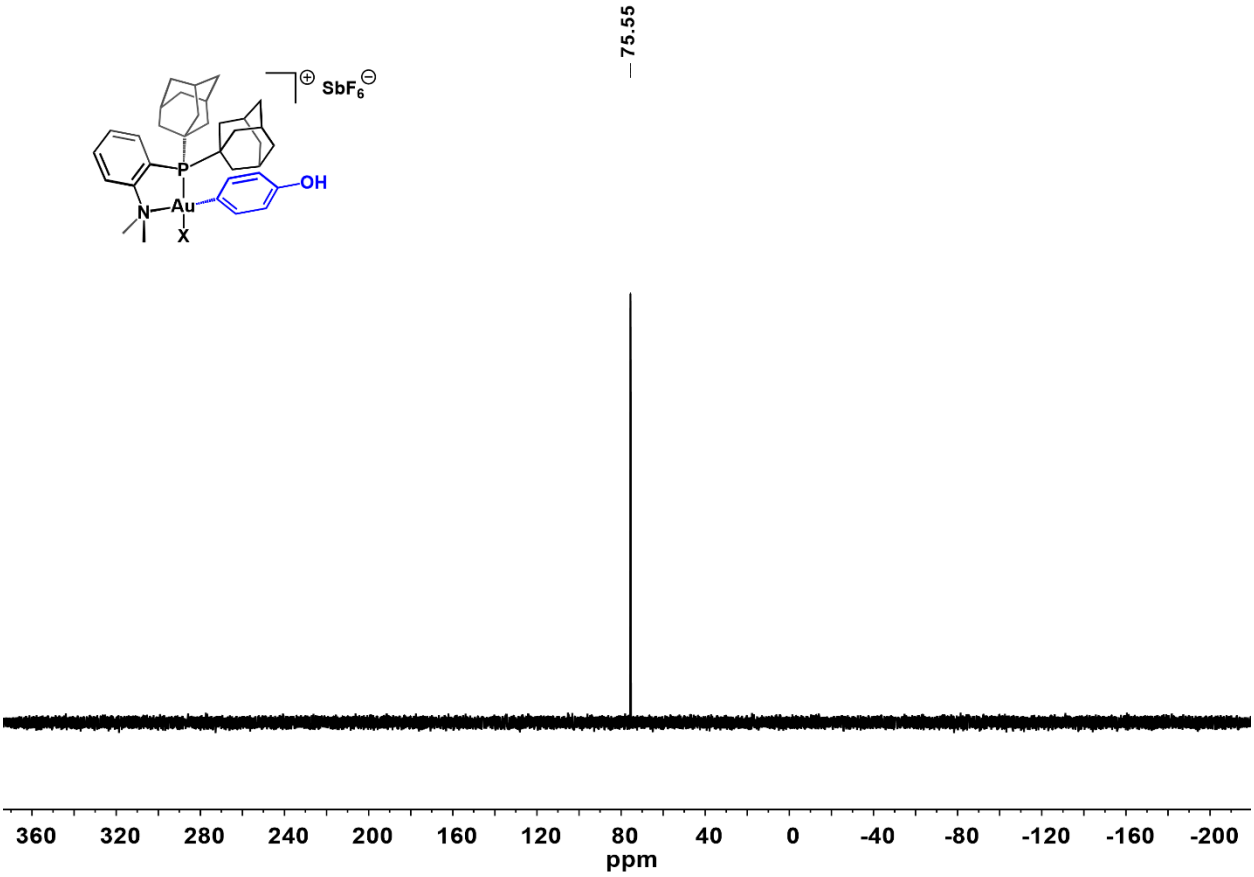

Figure D25. $^{31}P\{^{1}H\}$ NMR spectrum of [**2f**][SbF_6] in CD_3CN at 298K.

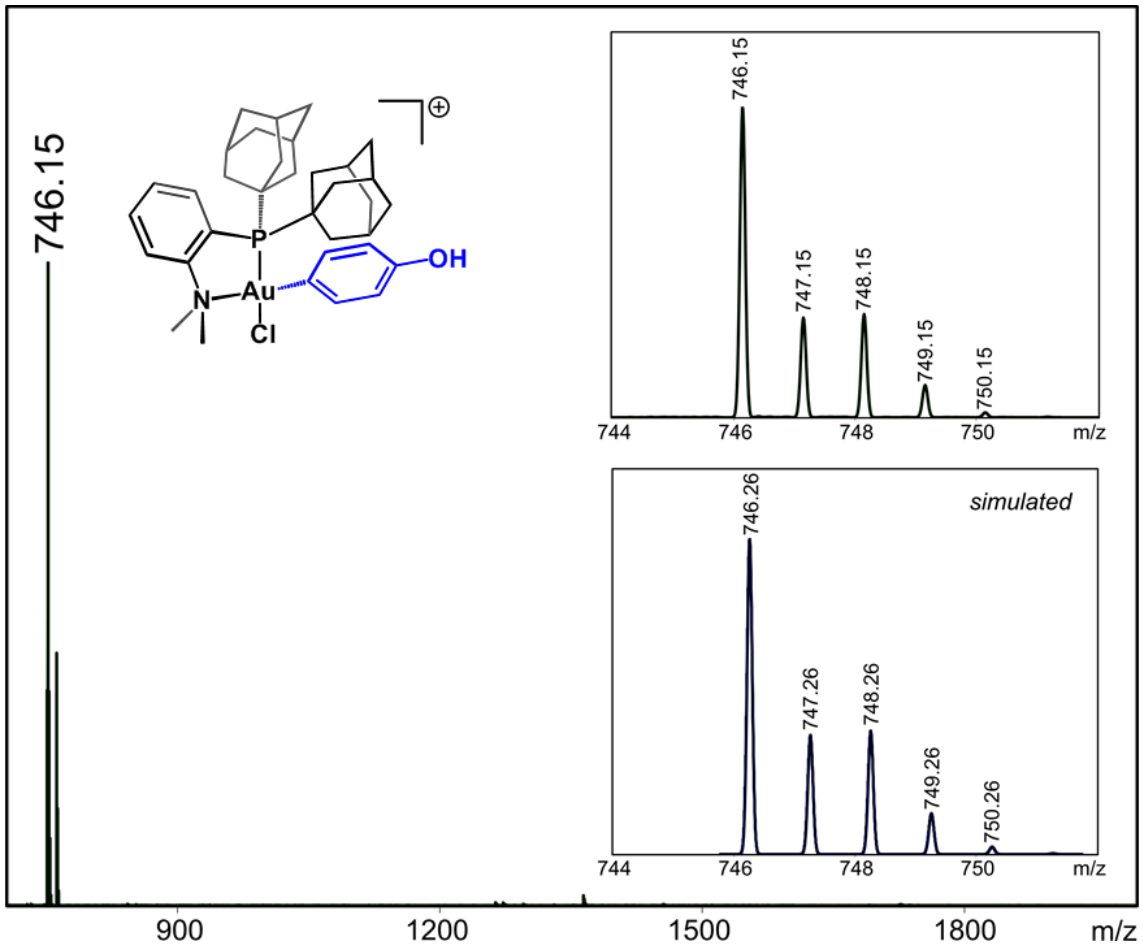

Figure D26. ESI-MS(+) of **2f**.

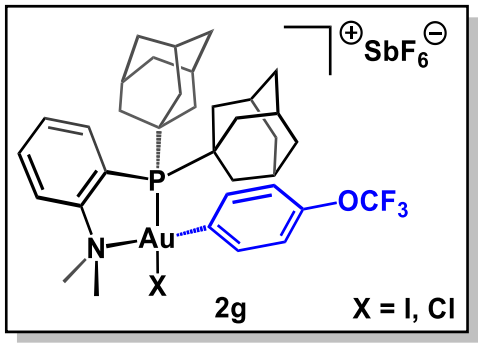

Following the general procedure, (Me-DalPhos)AuCl (22 mg, 0.034 mmol, 1.0 equiv), $AgSbF_6$ (12 mg, 0.034 mmol, 1.0 equiv) and 4-(trifluoromethoxy)iodobenzene (27 µL, 0.17 mmol, 5.0 equiv) were used. The [**2g**][SbF_6] salt was isolated as a yellow crystalline solid in 51% yield (18 mg, 0.017 mmol). A single crystal of suitable quality for an X-ray diffraction study was obtained using this procedure (See section V for crystallographic details).

^{1}H NMR (400 MHz, CD_3CN): δ 8.04 (dd, *J* = 8.3, 3.9 Hz, 1H, H_{Ar}), 7.95 (m, 2H, H_{Ar}), 7.79–7.56 (m, 3H, H_{Ar}), 7.30 (d, *J* = 8.4 Hz, 2H, H_{Ar}), 3.49 (s, 6H, $N(CH_3)_2$), 2.36–2.24 (m, 6H, H_{Ad}), 2.02 (m, 11H, H_{Ad}), 1.73 (m, 13H, H_{Ad}) ppm.

^{19}F NMR (376 MHz, CD_3CN): δ -58.7 ppm.

^{31}P{^{1}H} NMR (162 MHz, CD_3CN): δ 76.8 ppm.

ESI-MS(+): 814.17 (calc'd 814.25) *m/z* ($C_{35}H_{44}ClOF_3NPAu$).

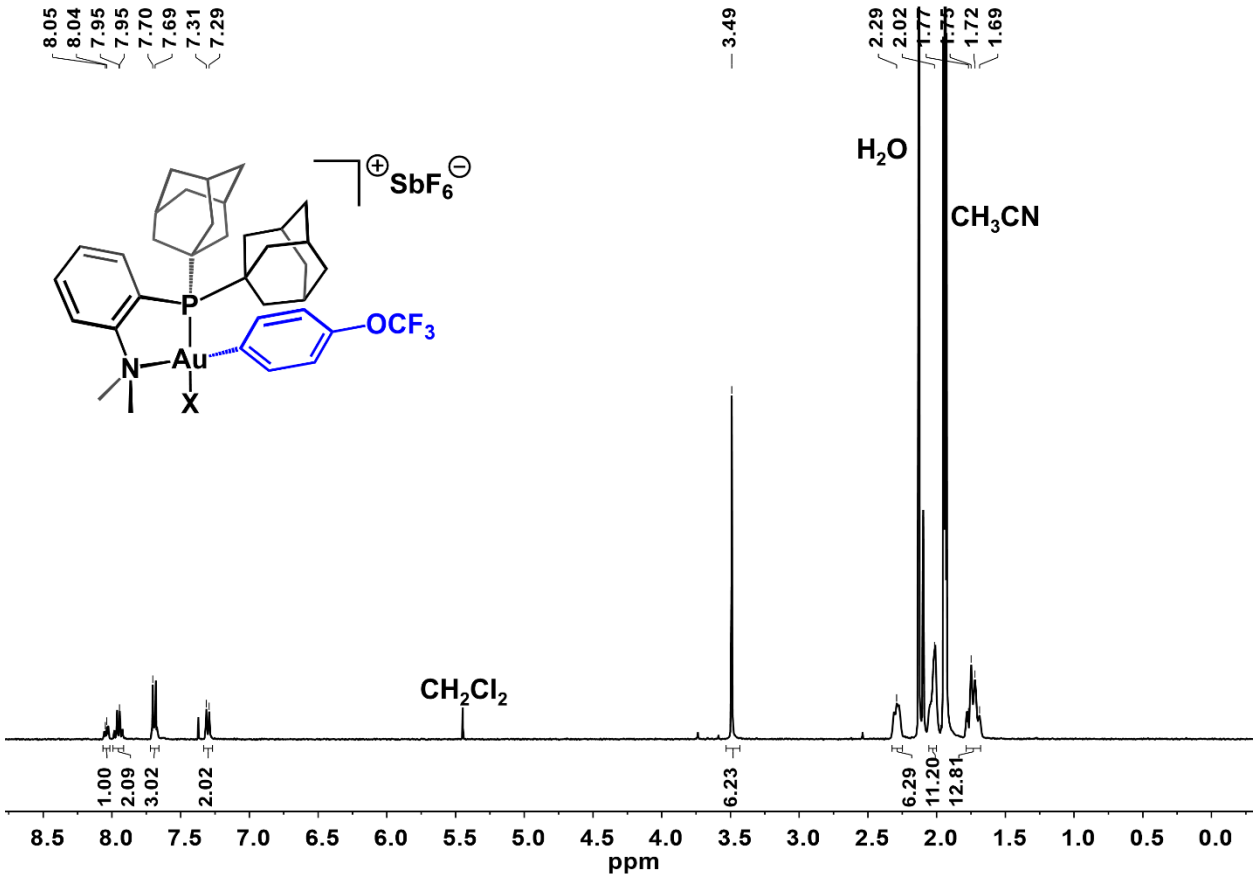

Figure D27. ^{1}H NMR spectrum of [**2g**][SbF_6] in CD_3CN at 298 K.

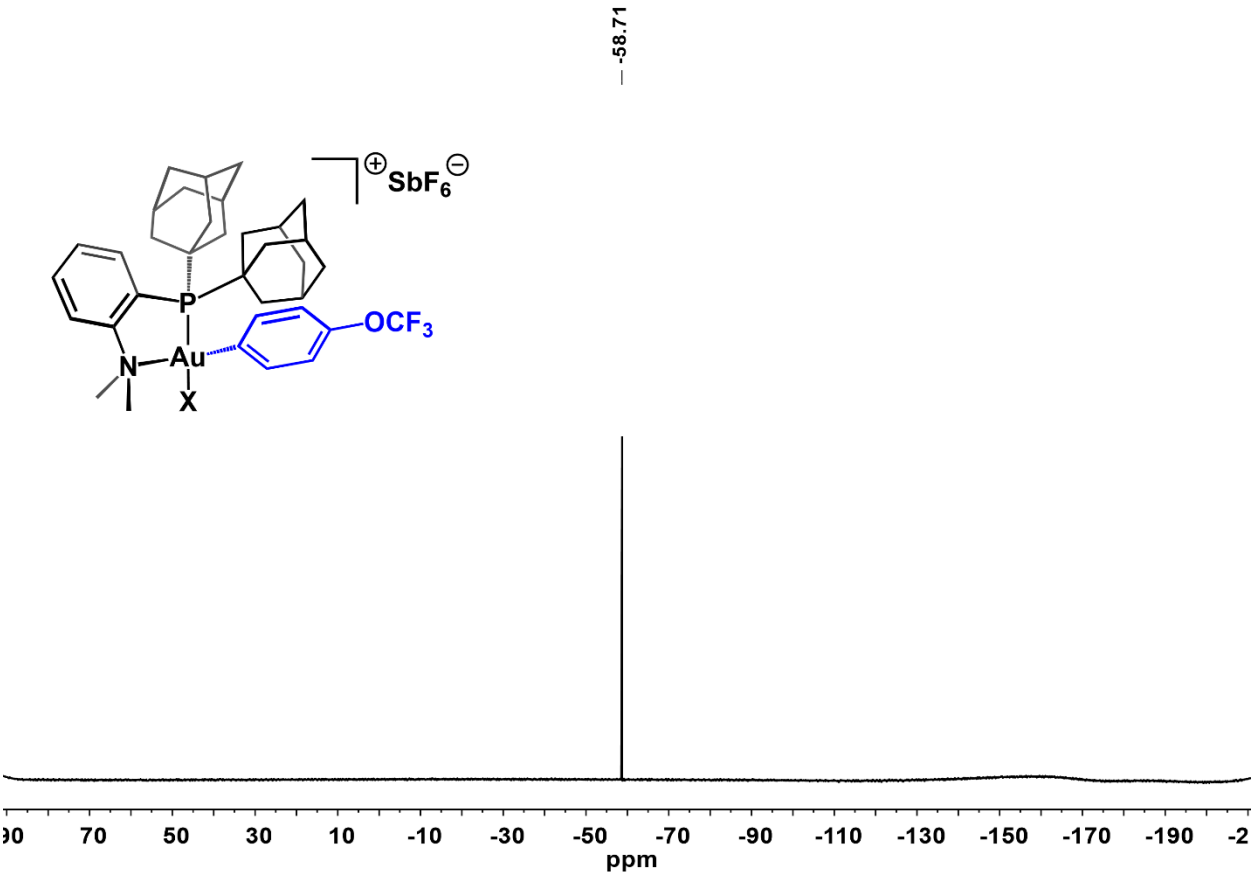

Figure D28. ^{19}F NMR spectrum of [**2g**][SbF_6] in CD_3CN at 298 K.

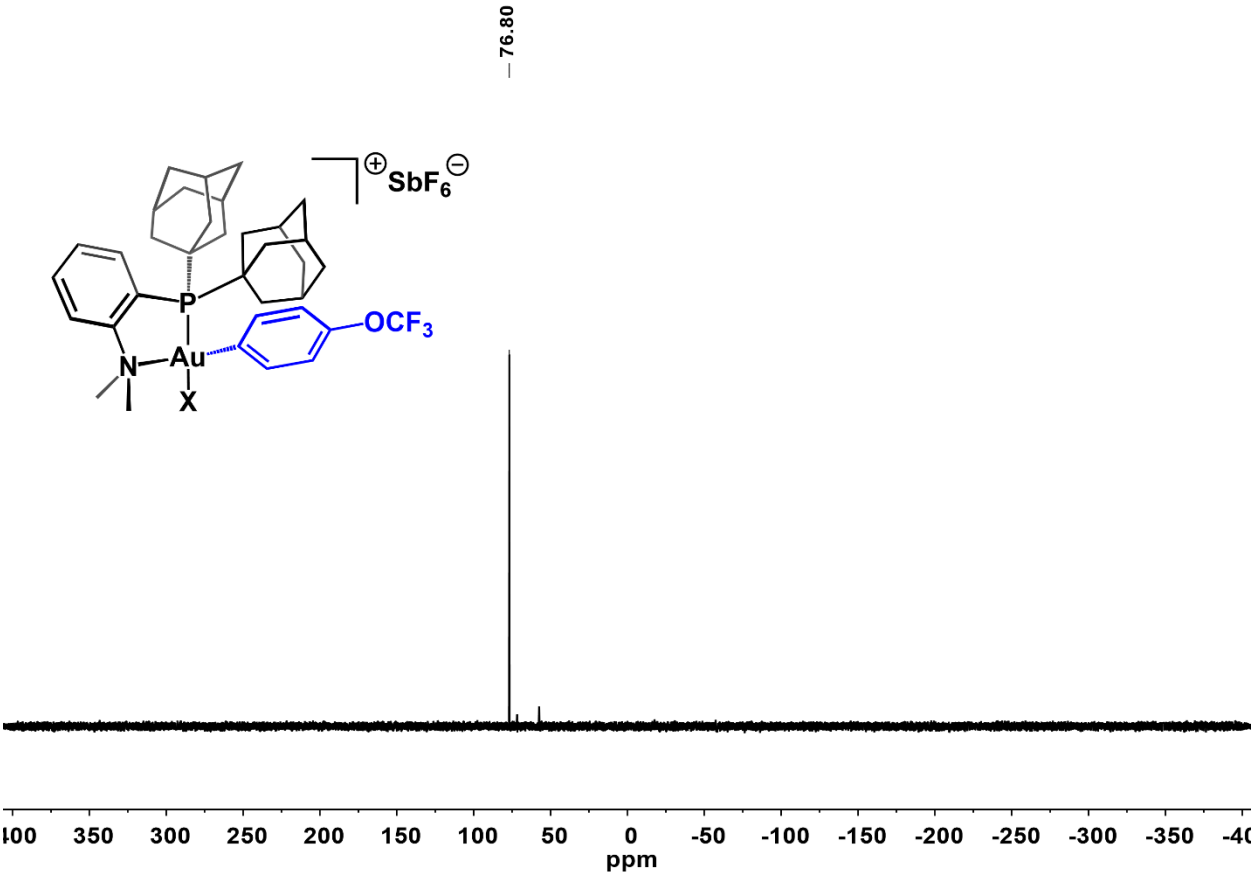

Figure D29. $^{31}P\{^{1}H\}$ NMR spectrum of [**2g**][SbF_6] in CD_3CN at 298 K.

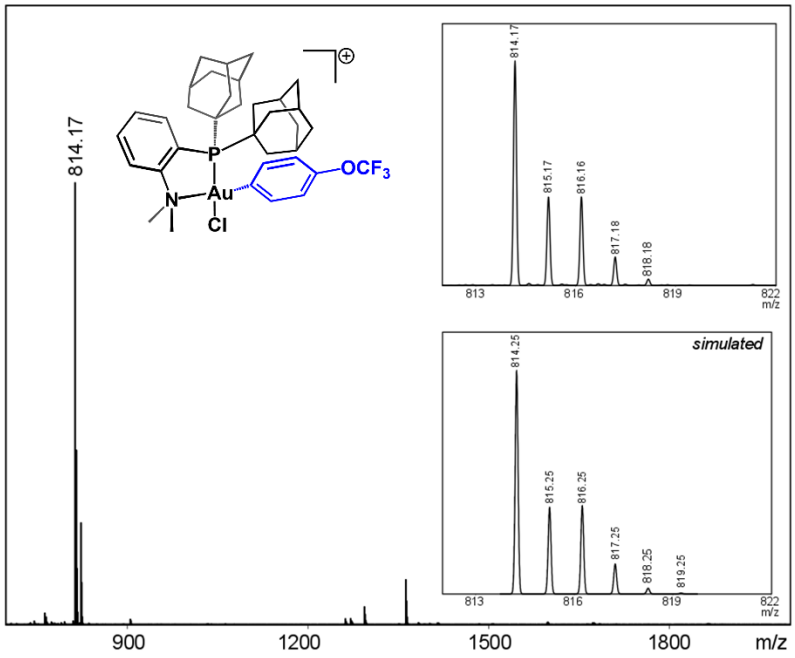

Figure D30. ESI-MS(+) of **2g**.

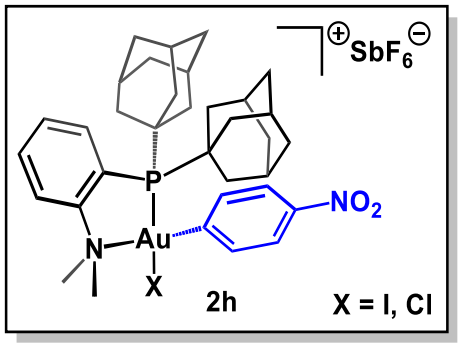

Following the general procedure, (Me-DalPhos)AuCl (30 mg, 0.046 mmol, 1.0 equiv), $AgSbF_6$ (16 mg, 0.046 mmol, 1.0 equiv) and 1-iodo-4-nitrobenzene (34 mg, 0.14 mmol, 3.0 equiv) were used. The [**2h**][SbF_6] salt was isolated as an orange crystalline solid in 75% yield (35 mg, 0.035 mmol). This complex has been previously reported.[3]

^{1}H NMR (400 MHz, CD_3CN): δ 8.16 (d, *J* = 9.0 Hz, 2H, H_{Ar}), 8.05 (m, 1H, H_{Ar}), 7.96 (m, 1H, H_{Ar}), 7.90 (d, *J* = 9.1 Hz, 2H, H_{Ar}), 7.70 (m, 1H, H_{Ar}), 3.52 (s, 6H, $N(CH_3)_2$), 2.41–2.22 (m, 6H, H_{Ad}), 2.07–1.99 (m, 12H, H_{Ad}), 1.74 (m, 12H, H_{Ad}) ppm.

^{31}P{^{1}H} NMR (162 MHz, CD_3CN): δ 79.9 ppm.

ESI-MS(+): 775.19 (calc'd 775.25) *m/z* ($C_{34}H_{44}ClN_2O_2PAu$).

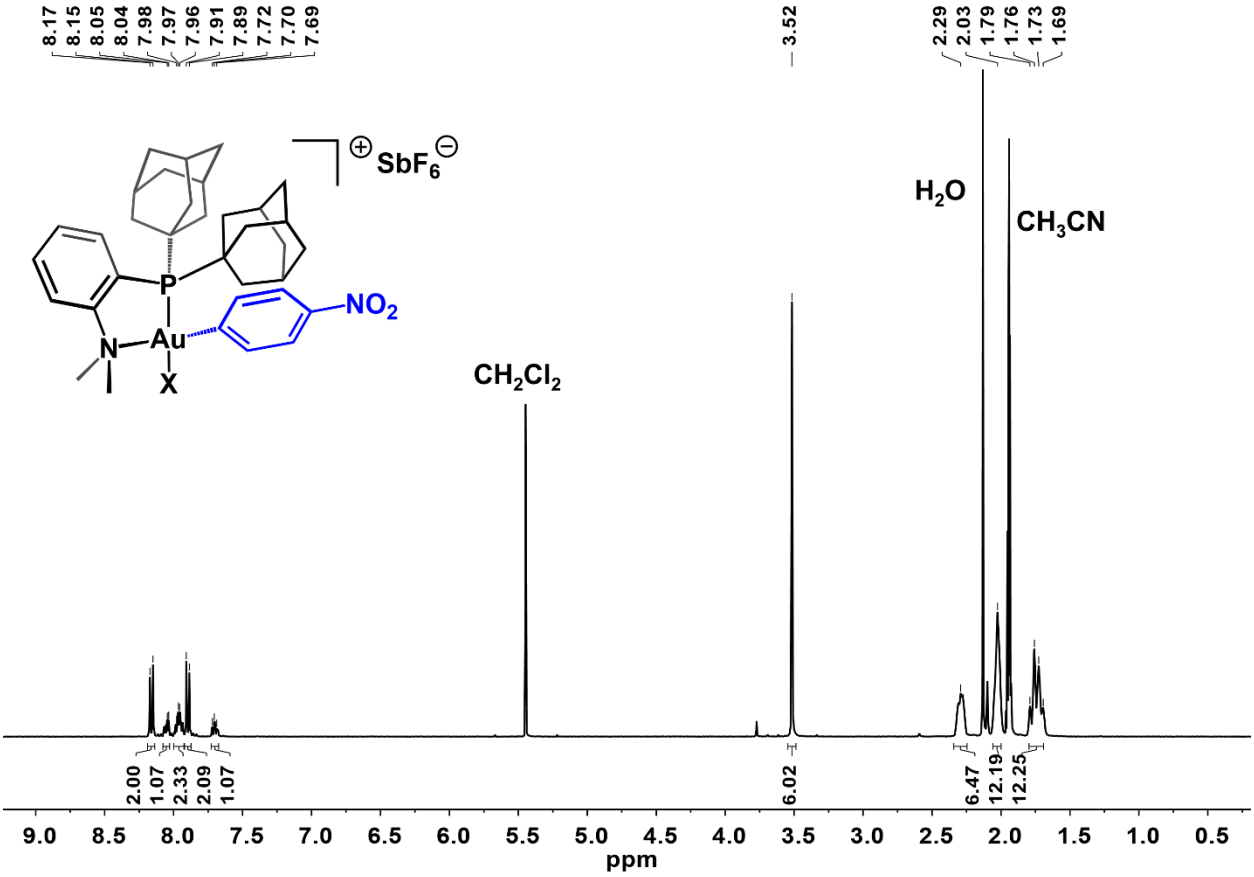

Figure D31. ^{1}H NMR spectrum of [**2h**][SbF_6] in CD_3CN at 298 K.

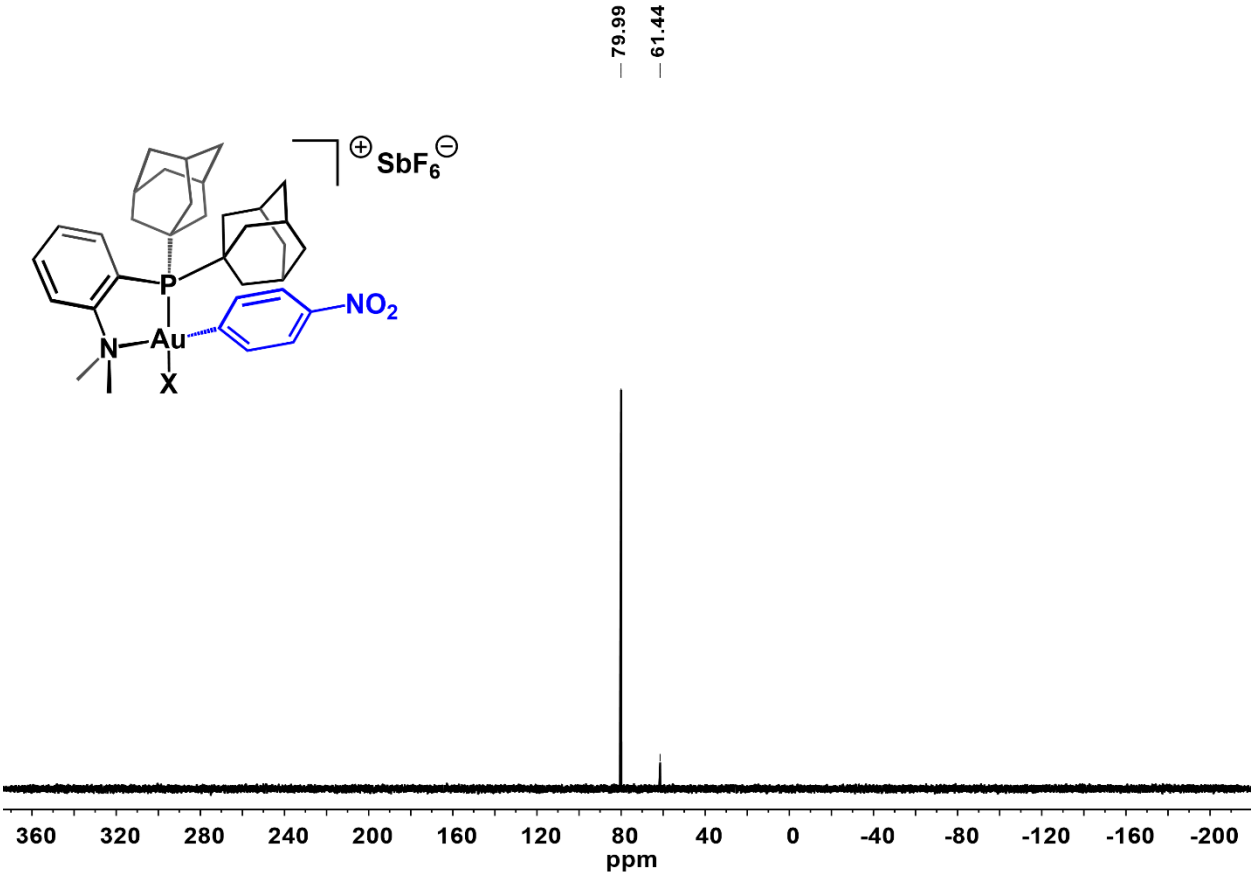

Figure D32. $^{31}P\{^{1}H\}$ NMR spectrum of [**2h**][SbF_6] in CD_3CN at 298 K.

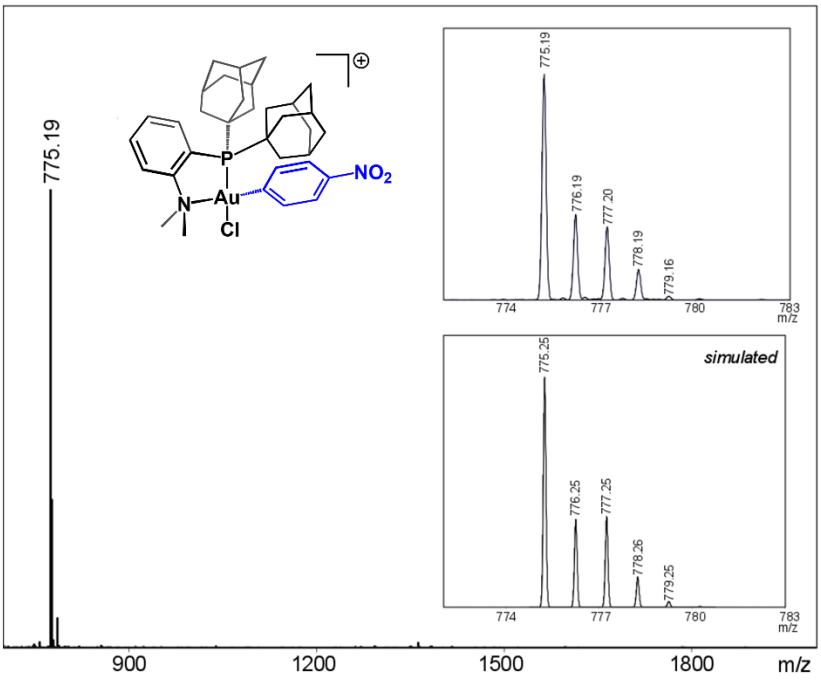

Figure D33. ESI-MS(+)of **2h**.

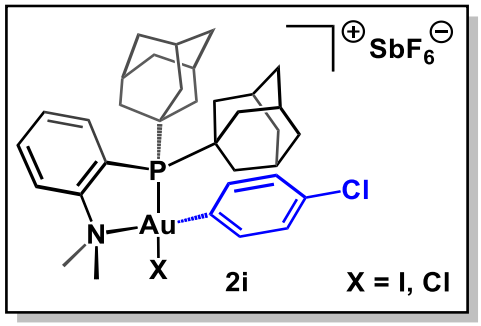

Following the general procedure, (Me-DalPhos)AuCl (66 mg, 0.10 mmol, 1.0 equiv), $AgSbF_6$ (34 mg, 0.10 mmol, 1.0 equiv) and 1-chloro-4-iodobenzene (120 mg, 0.50 mmol, 5.0 equiv) were used. The [**2i**][SbF_6] salt was isolated as a yellow crystalline solid in 87% yield (87 mg, 0.087 mmol). A single crystal of suitable quality for an X-ray diffraction study was obtained using this procedure (see section V for crystallographic details).

^{1}H NMR (400 MHz, CD_3CN): δ 8.04 (dd, *J* = 8.2, 4.0 Hz, 1H, H_{Ar}), 8.00–7.91 (m, 2H, H_{Ar}), 7.73–7.65 (m, 1H, H_{Ar}), 7.58 (d, *J* = 8.7 Hz, 1H, H_{Ar}), 7.37 (d, *J* = 8.6 Hz, 1H, H_{Ar}), 3.48 (s, 6H, $N(CH_3)_2$), 2.29 (m, 6H, H_{Ad}), 2.02 (s, 11H, H_{Ad}), 1.74 (m, 13H, H_{Ad}) ppm.

^{31}P{^{1}H} NMR (162 MHz, CD_3CN): δ 77.6 ppm.

ESI-MS(+): 764.15 (calc'd 764.23) *m/z* ($C_{34}H_{44}Cl_2NPAu$).

Elem. Anal. (Calc'd) for $C_{34}H_{44}AuCl_2F_6NPSb$: C, 40.50 (40.76); H, 4.24 (4.43); N, 1.37 (1.40).

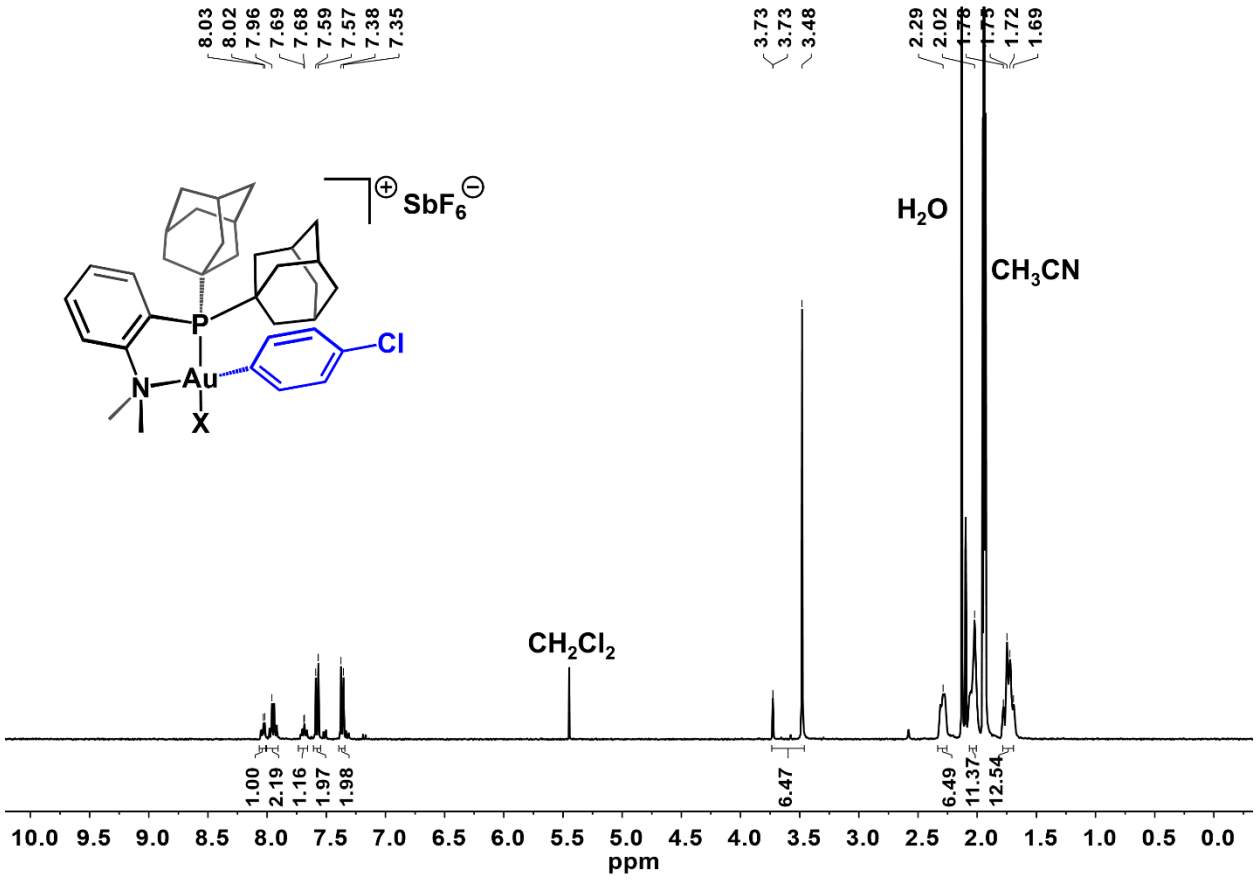

Figure D34. ^{1}H NMR spectrum of [**2i**][SbF_6] in CD_3CN at 298 K.

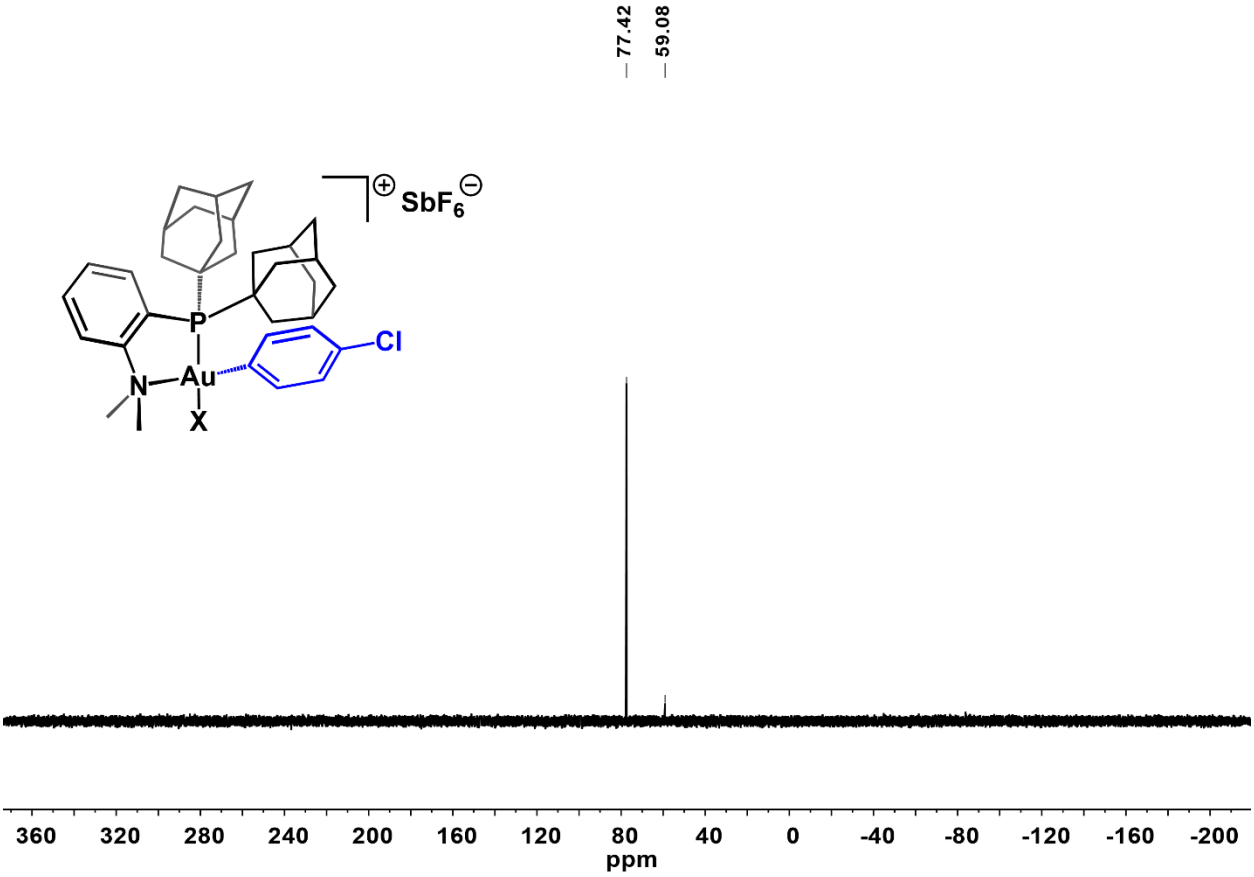

Figure D35. $^{31}P\{^{1}H\}$ NMR spectrum of [**2i**][SbF_6] in CD_3CN at 298 K. The signal at 59.0 ppm corresponds to the starting (Me-DalPhos)AuCl compound.

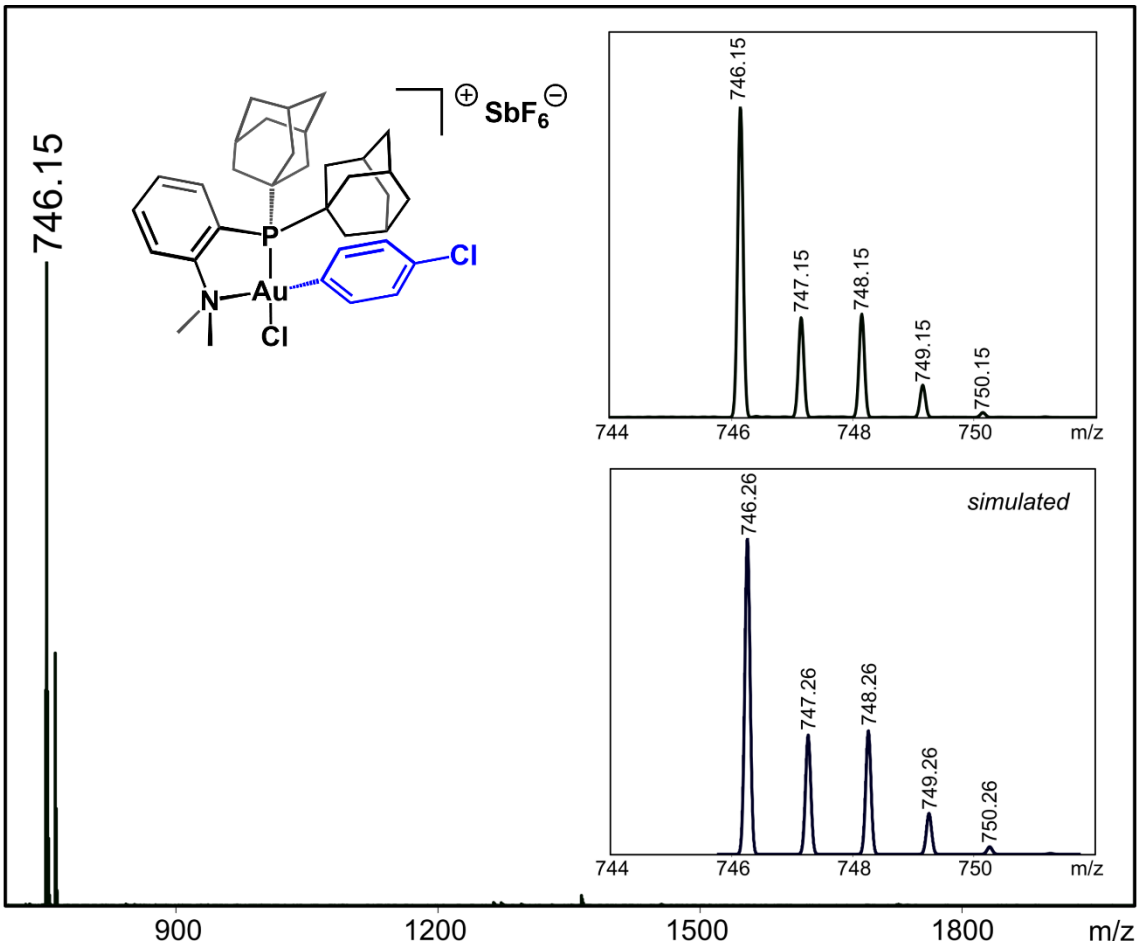

Figure D36. ESI-MS(+) of **2i**.

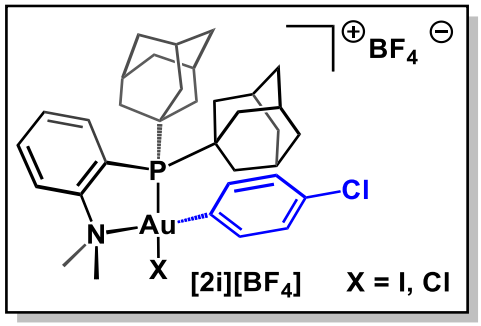

In the fume hood, a solution of $AgBF_4$ (9 mg, 0.05 mmol, 1 equiv) in DCM (2 mL) was prepared under protection from light, and then cooled to -20 °C. A DCM solution (2 mL) containing 4-chloroiodobenzene (55 mg, 0.23 mmol, 5.0 equiv) and (Me-DalPhos)AuCl (30 mg, 0.046 mmol, 1.0 equiv) reagents was prepared and also cooled to -20 °C. While both solutions were cold, the colorless 4-chloroliodobenzene and (Me-DalPhos)AuCl solution was added in one portion to the solution of $AgBF_4$, and the reaction mixture was sonicated for 2 min, during which time the solution became yellow concomitant with the precipitation of pale yellow precipitate. The resulting suspension was filtered through a pad of Celite. Slow evaporation of solvent from the yellow filtrate over the course of 48 h at 25 °C resulted in saturation of the solution and the formation of yellow crystals. The supernatant was removed and the crystals were washed with C_6H_6 (2 x 3 mL), followed by *n*-pentane (2 × 3 mL), and then dried under reduced pressure to afford [**2i**][BF_4] as a yellow crystalline solid in 61% yield (26 mg, 0.031 mmol).

^{1}H NMR (400 MHz, CD_3CN): δ 8.03 (m, 1H, H_{Ar}), 7.95 (m, 2H, H_{Ar}), 7.73–7.68 (m, 1H, H_{Ar}), 7.58 (d, 2H, *J* = 8.7 Hz, H_{Ar}), 7.37 (d, 2H, *J* = 8.7 Hz, H_{Ar}), 3.48 (s, 6H, N(CH_3)$_2$), 2.29 (s, 6H, H_{Ad}), 2.10 (s, 6H, H_{Ad}), 2.03 (s, 6H, H_{Ad}), 1.75 (s, 12H, H_{Ad}) ppm.

^{31}P{^{1}H} NMR (162 MHz, CD_3CN): δ 77.4 ppm.

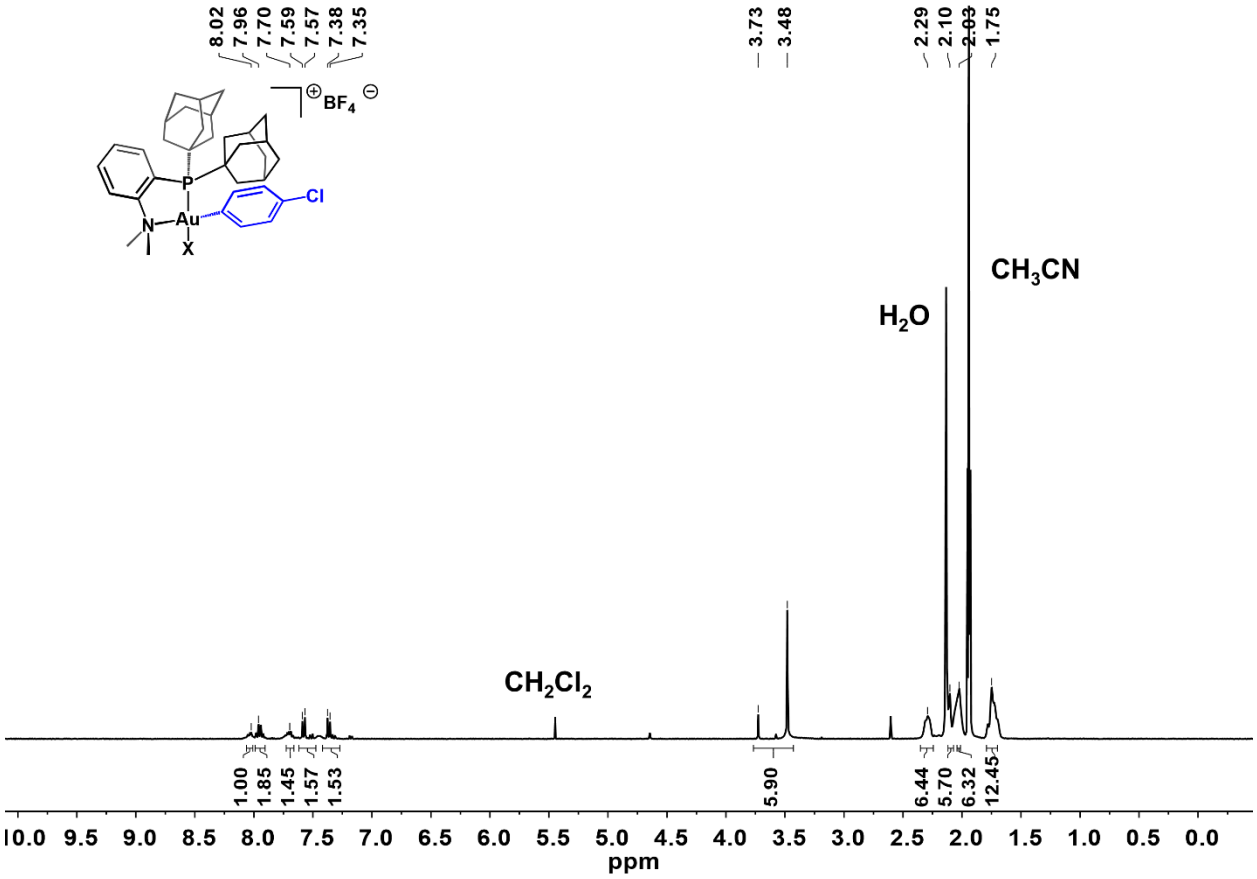

Figure D37. ^{1}H NMR spectrum of [**2i**][BF_4] in CD_3CN at 298 K.

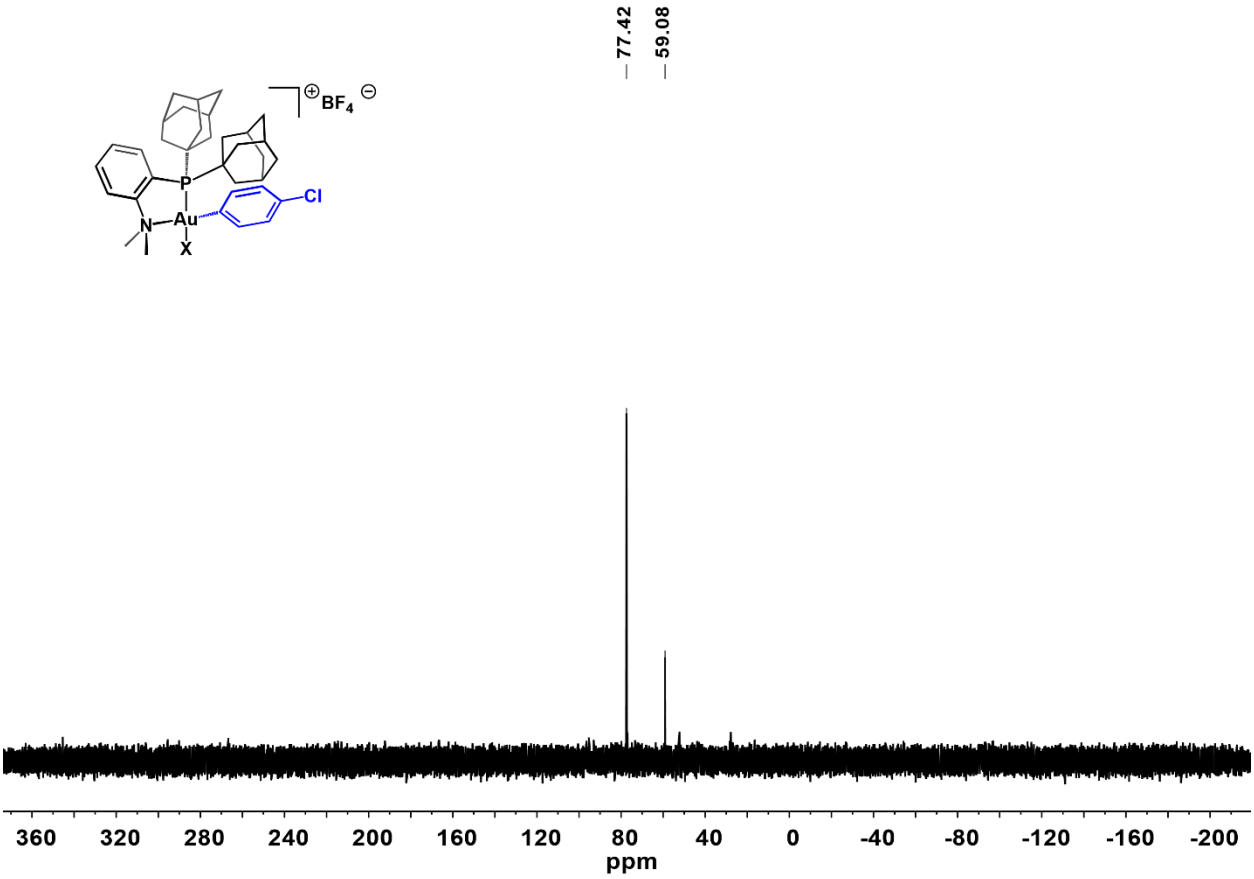

Figure D38. $^{31}P\{^{1}H\}$ NMR spectrum of [**2i**][BF_4] in CD_3CN at 298 K. The signal at 59.0 ppm corresponds to the starting (Me-DalPhos)AuCl compound.

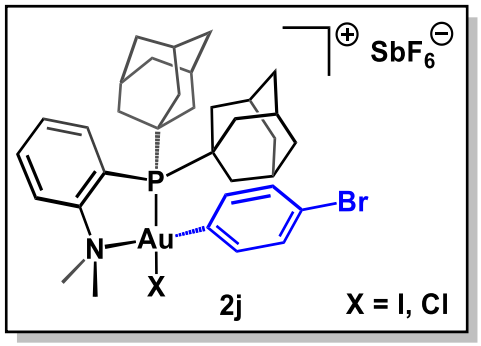

Following the general procedure, (Me-DalPhos)AuCl (30 mg, 0.046 mmol, 1.0 equiv), $AgSbF_6$ (16 mg, 0.046 mmol, 1.0 equiv) and 1-bromo-4-iodobenzene (65 mg, 0.23 mmol, 5.0 equiv) were used. The [**2j**][SbF_6] salt was isolated as a yellow crystalline solid in 82% yield (39 mg, 0.038 mmol). A single crystal of suitable quality for an X-ray diffraction study was obtained using this workup (See section V for crystallographic details). Elem. Anal. (Calc'd) for $C_{34}H_{44}AuBrClF_6NPSb$: C, 38.56 (39.03); H, 4.03 (4.24); N, 1.29 (1.34). The low value observed for carbon is likely due to crystallization of **2j** as a mixture of [(Me-DalPhos)Au(*p*-Br-C_6H_4)Cl]$^+$ and [(Me-DalPhos)Au(*p*-Br-C_6H_4)I]$^+$ species as confirmed by X-ray structural analysis of a single-crystal obtained from the described procedure. The X-ray structural analysis indicates 77% Cl and 23% I occupancy.

^{1}H NMR (400 MHz, CD_3CN): δ 8.02 (m, 1H, H_{Ar}), 7.99–7.88 (m, 2H, H_{Ar}), 7.72–7.62 (m, 1H, H_{Ar}), 7.49 (m, 4H, H_{Ar}), 3.46 (s, 6H, N(CH_3)$_2$), 2.27 (m, 6H, H_{Ad}), 2.04 (m, 12H, H_{Ad}), 1.72 (m, 12H, H_{Ad}) ppm.

^{31}P{^{1}H} NMR (162 MHz, CD_3CN): δ 77.6 ppm.

ESI-MS(+): 808.18 (calc'd 808.17) *m/z* ($C_{34}H_{44}ClBrNPAu$).

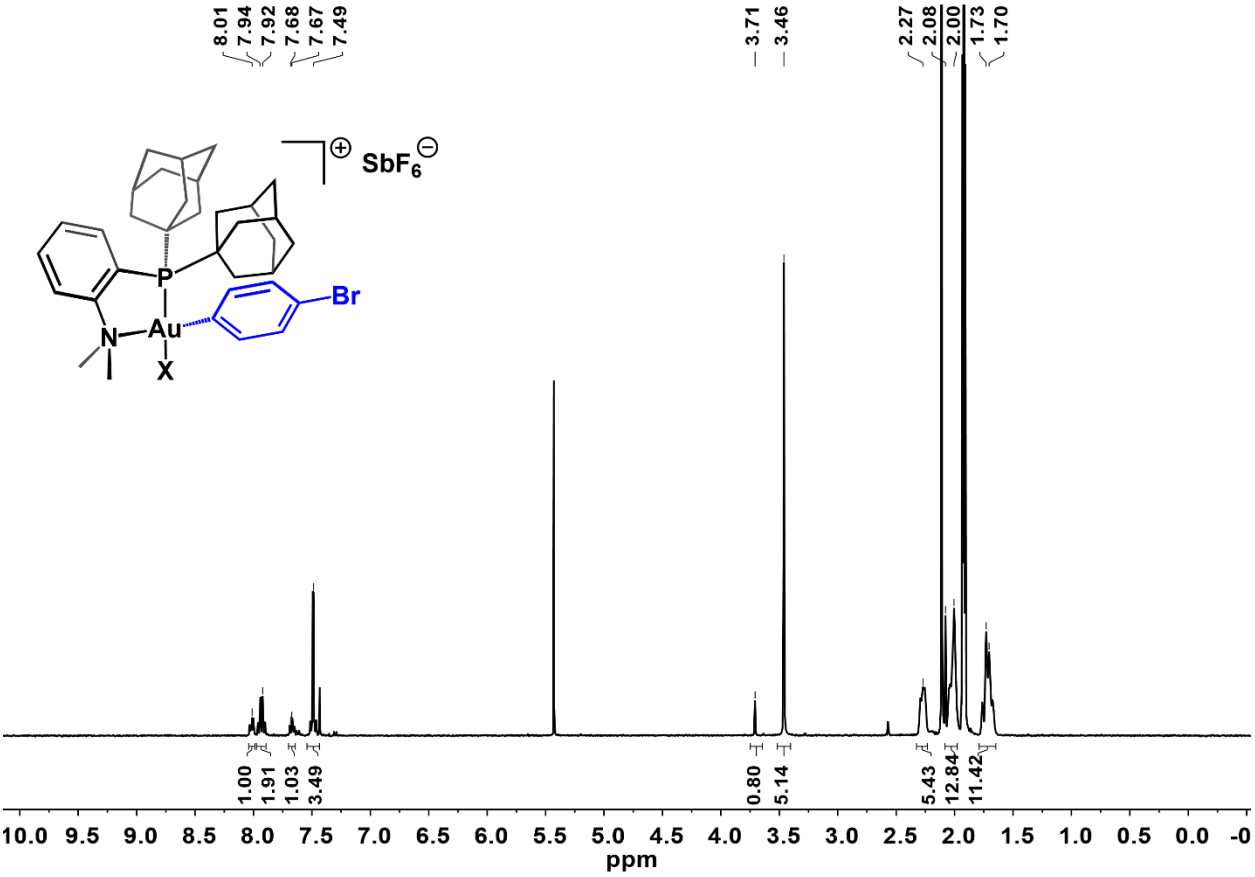

Figure D39. ^{1}H NMR spectrum of [**2j**][SbF_6] in CD_3CN at 298 K.

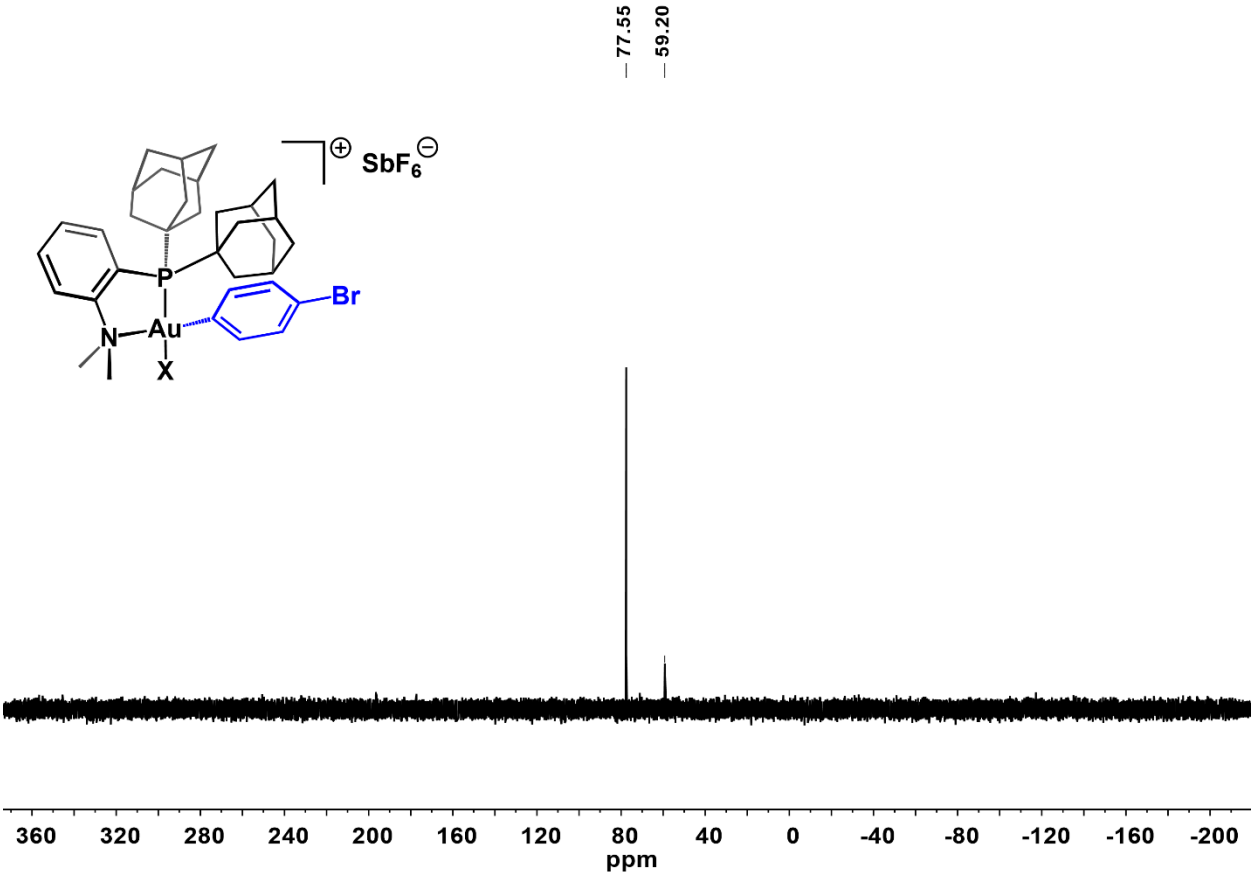

Figure D40. $^{31}P\{^{1}H\}$ NMR spectrum of [**2j**][SbF_6] in CD_3CN at 298 K. The signal at 59.2 ppm corresponds to the starting (Me-DalPhos)AuCl compound.

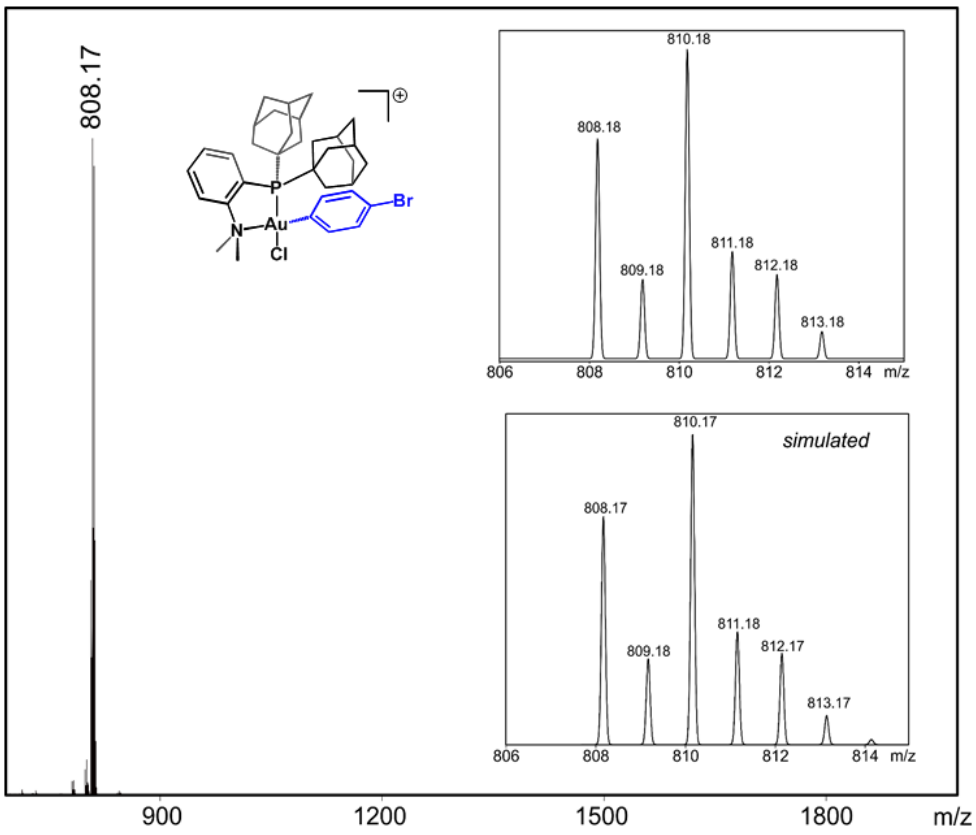

Figure D41. ESI-MS(+) of **2j**.

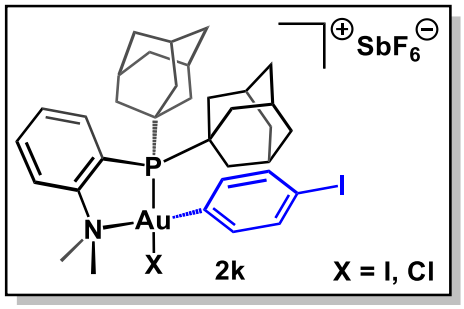

Following the general procedure, (Me-DalPhos)AuCl (30 mg, 0.046 mmol, 1.0 equiv), $AgSbF_6$ (16 mg, 0.046 mmol, 1.0 equiv) and 1,4-diiodobenzene (76 mg, 0.23 mmol, 5.0 equiv) were used. The [**2k**][SbF_6] salt was isolated as a yellow crystalline solid in 73% yield (37 mg, 0.034 mmol).

^{1}H NMR (400 MHz, CD_3CN): δ 8.03 (dd, *J* = 8.4, 4.0 Hz, 1H, H_{Ar}), 7.99–7.90 (m, 2H, H_{Ar}), 7.72–7.67 (m, 1H, H_{Ar}), 7.66 (d, *J* = 8.4 Hz, 2H, H_{Ar}), 7.38 (d, *J* = 8.5 Hz, 2H, H_{Ar}), 3.47 (s, 6H, $N(CH_3)_2$), 2.36–2.22 (m, 6H, H_{Ad}), 2.04 (d, *J* = 16.7 Hz, 13H, H_{Ad}), 1.73 (d, *J* = 10.4 Hz, 11H, H_{Ad}) ppm.

^{31}P{^{1}H} NMR (162 MHz, CD_3CN): δ 77.6 ppm.

ESI-MS(+): 856.08 (calc'd 856.16) *m/z* ($C_{34}H_{44}ClINPAu$).

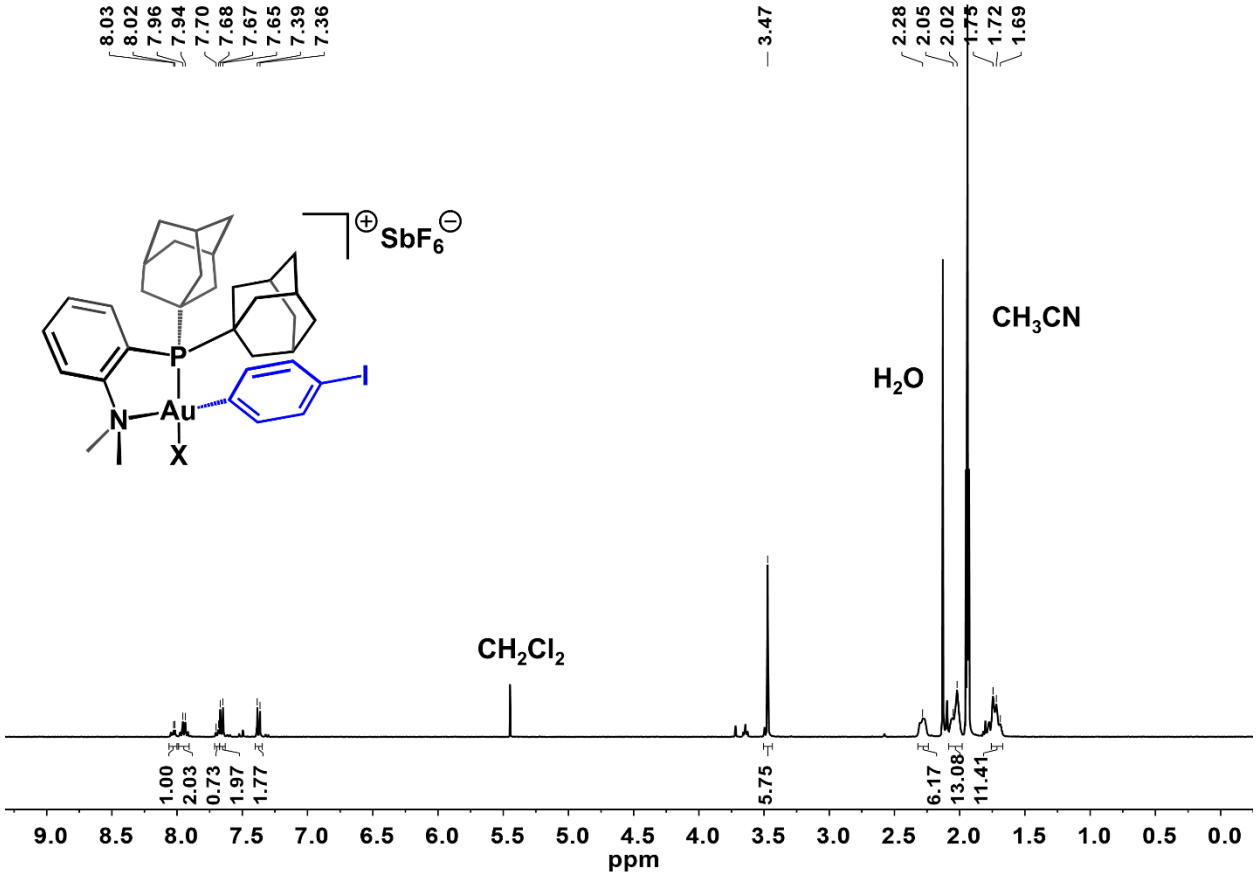

Figure D42. ^{1}H NMR spectrum of [**2k**][SbF_6] in CD_3CN at 298 K.

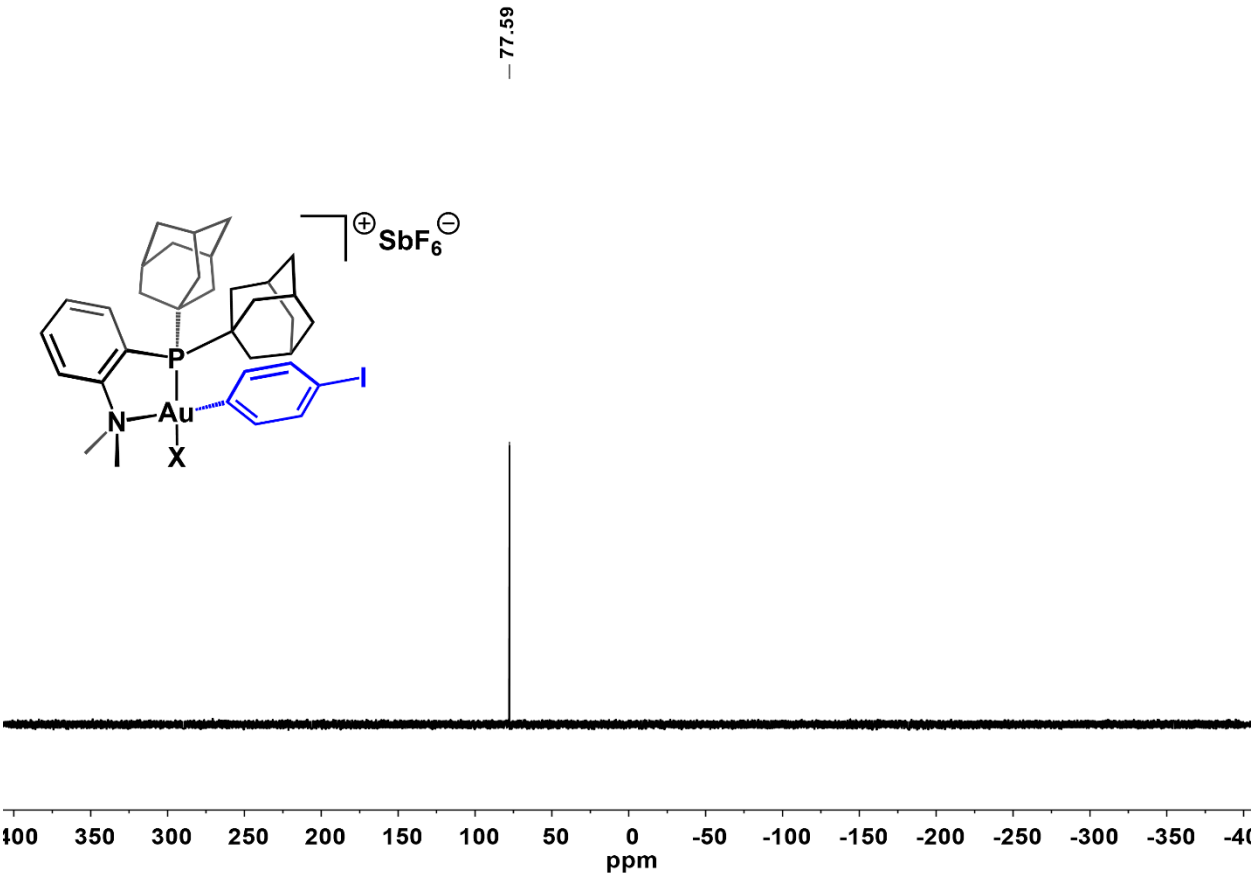

Figure D43. $^{31}P\{^{1}H\}$ NMR spectrum of [**2k**][SbF_6] in CD_3CN at 298 K.

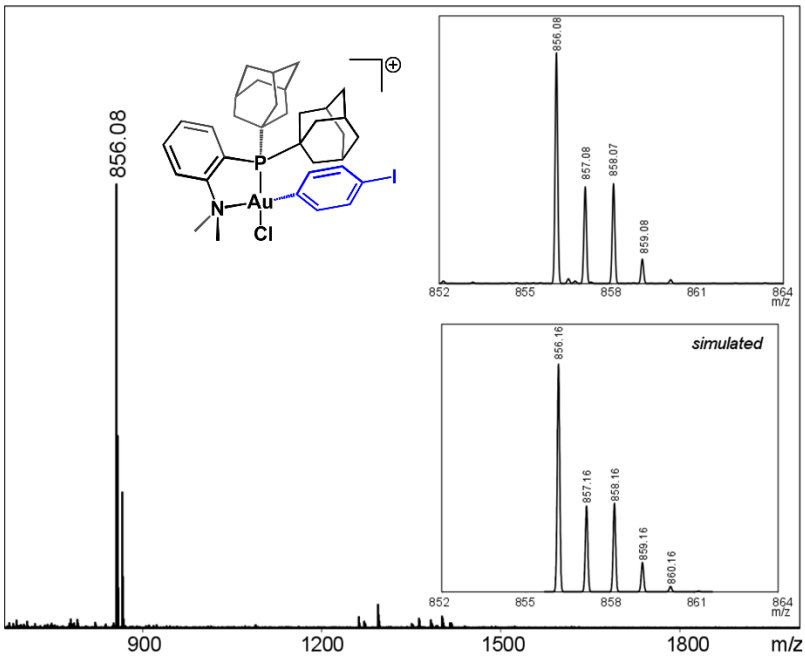

Figure D44. ESI-MS(+) of **2k**.

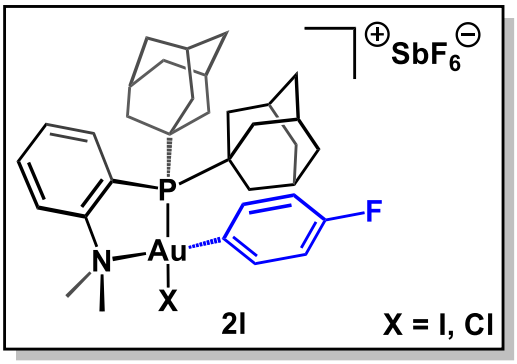

Following the general procedure, (Me-DalPhos)AuCl (30 mg, 0.046 mmol, 1.0 equiv), $AgSbF_6$ (16 mg, 0.046 mmol, 1.0 equiv) and 4-fluoroiodobenzene (16 µL, 0.14 mmol, 3.0 equiv) were used. The [**2l**][SbF_6] salt was isolated as a yellow crystalline solid in 74% yield (34 mg, 0.034 mmol). The spectroscopic features of the isolated material matched those reported in the literature for this salt. [5]

$^{31}P\{^1H\}$ NMR (162 MHz, CH_2Cl_2): δ 76.2 ppm.

ESI-MS(+): 748.25 (calc'd 748.20) *m/z* ($C_{34}H_{44}ClN_2PFAu$).

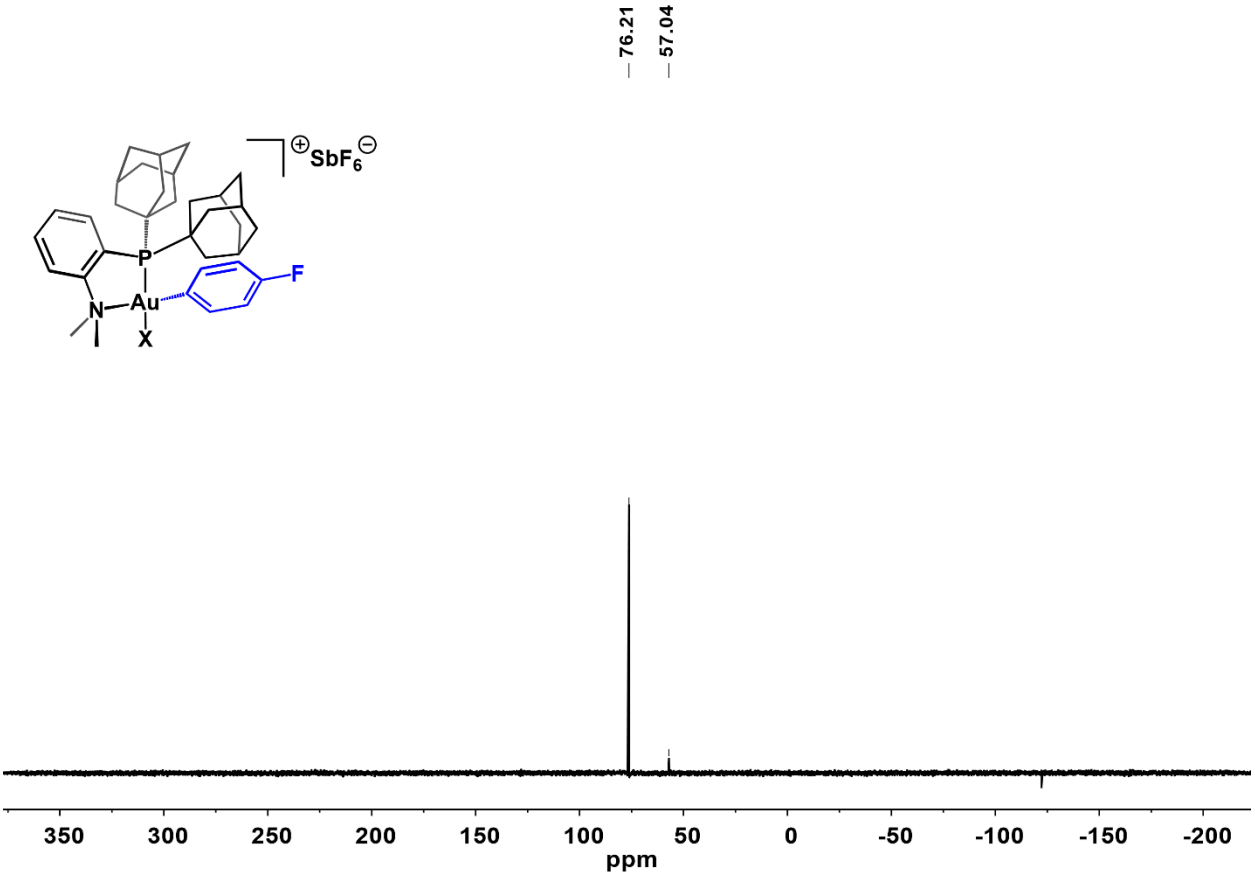

Figure D45. $^{31}P\{^{1}H\}$ NMR spectrum of [**2l**][SbF_6] in CH_2Cl_2 at 298 K.

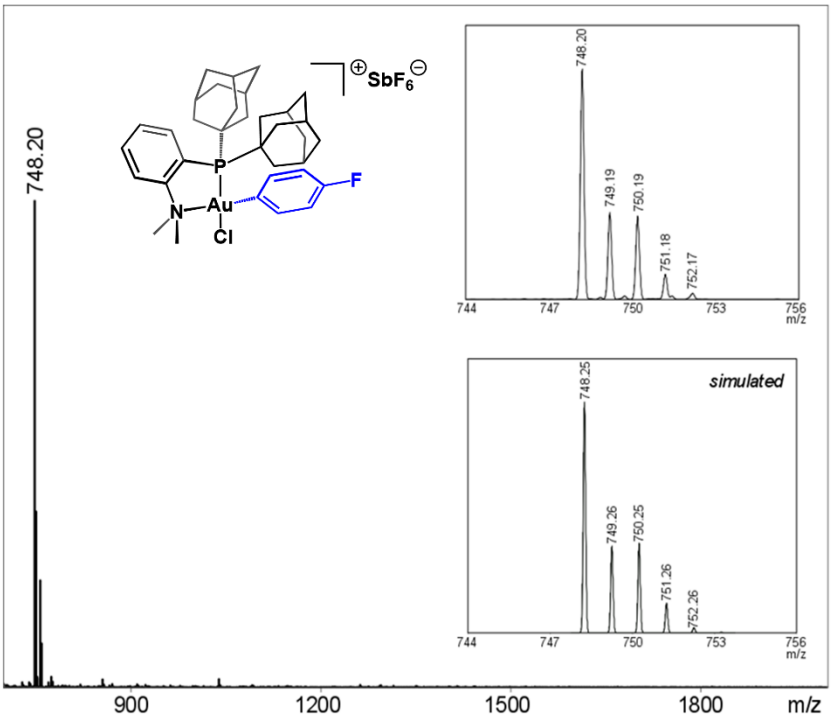

Figure D46. ESI-MS(+) of **2l**.

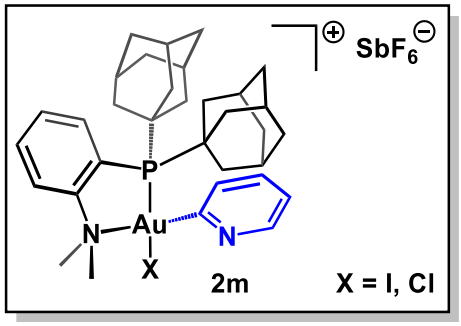

In the fume hood, $AgSbF_6$ (9 mg, 0.03 mmol, 1 equiv) was dissolved in DCM (2 mL) under protection from light, and the colorless solution was cooled to -20 °C. A DCM solution (2 mL) containing 2-iodopyridine (20 µL, 0.17 mmol, 6.0 equiv) and (Me-DalPhos)AuCl (18 mg, 0.028 mmol, 1.0 equiv) reagents was prepared and also cooled to -20 °C. While both solutions were cold, the pale yellow 2-iodopyridine and (Me-DalPhos)AuCl solution was added in one portion to the solution of $AgSbF_6$. The solution was allowed to stand at 25 °C for 24 h, during which time pale yellow solids precipitated out of solution. The reaction mixture was filtered through a pad of Celite, and the resulting pale-yellow filtrate was dried under reduced pressure. The pale-yellow residue was washed with C_6H_6 (2 x 3 mL), followed by *n*-pentane (2 x 3 mL), and then dried under reduced pressure to afford [**2m**][SbF_6] as a pale yellow powder in 77% yield (22 mg, 0.023 mmol).

^{1}H NMR (400 MHz, CD_3CN): δ 8.50–8.46 (m, 1H, H_{Ar}), 8.02 (m, 1H, H_{Ar}), 8.00–7.88 (m, 3H, H_{Ar}), 7.74–7.55 (m, 3H, H_{Ar}), 7.22 (m, 1H, H_{Ar}), 3.42 (s, 6H, N(CH_3)$_2$), 2.36 (m, 6H, H_{Ad}), 2.00 (m, 12H, H_{Ad}), 1.84–1.64 (m, 12H, H_{Ad}) ppm.

^{31}P{^{1}H} NMR (162 MHz, CD_3CN): δ 70.4 ppm.

ESI-MS(+): 731.25 (calc'd 731.26) *m/z* ($C_{33}H_{44}ClN_2PAu$).

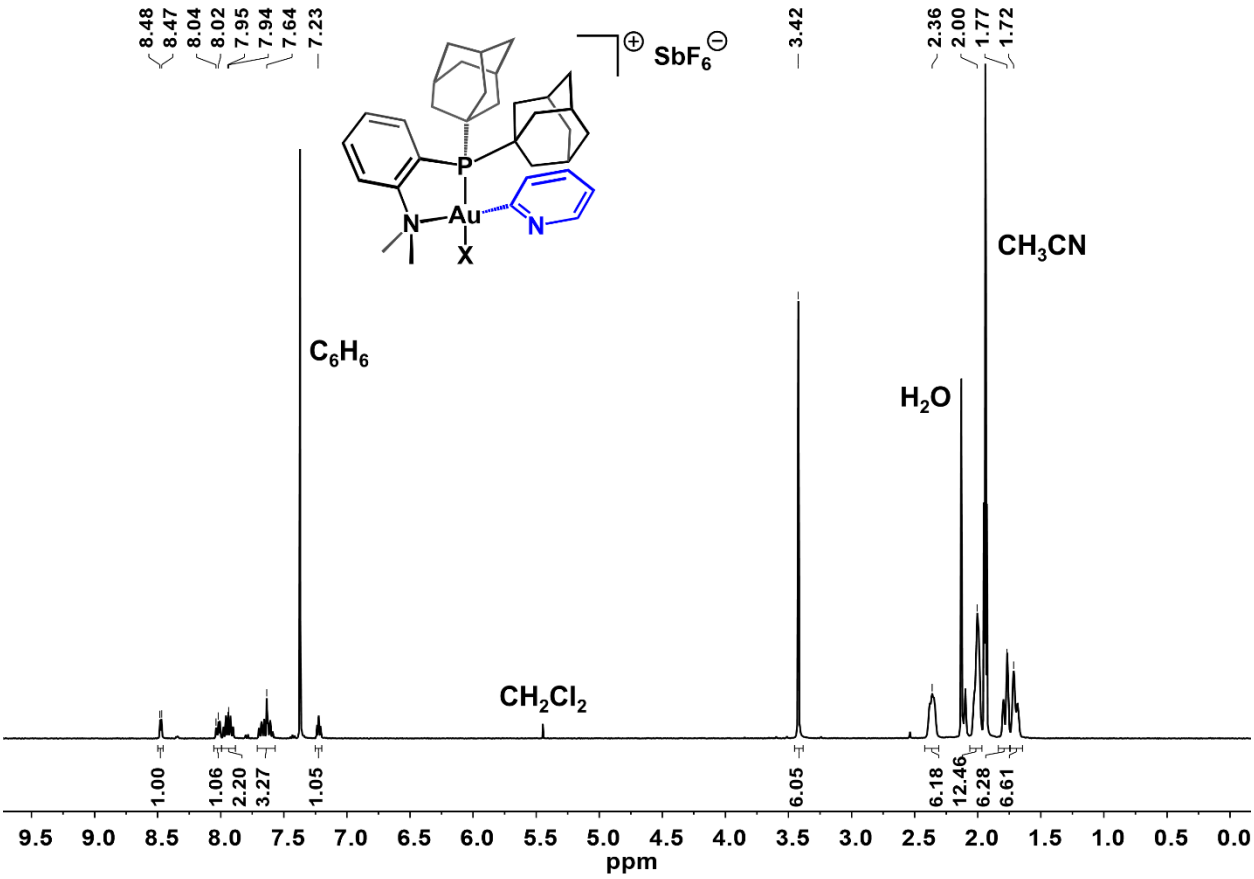

Figure D47. ^{1}H NMR spectrum of [**2m**][SbF_6] in CD_3CN at 298 K.

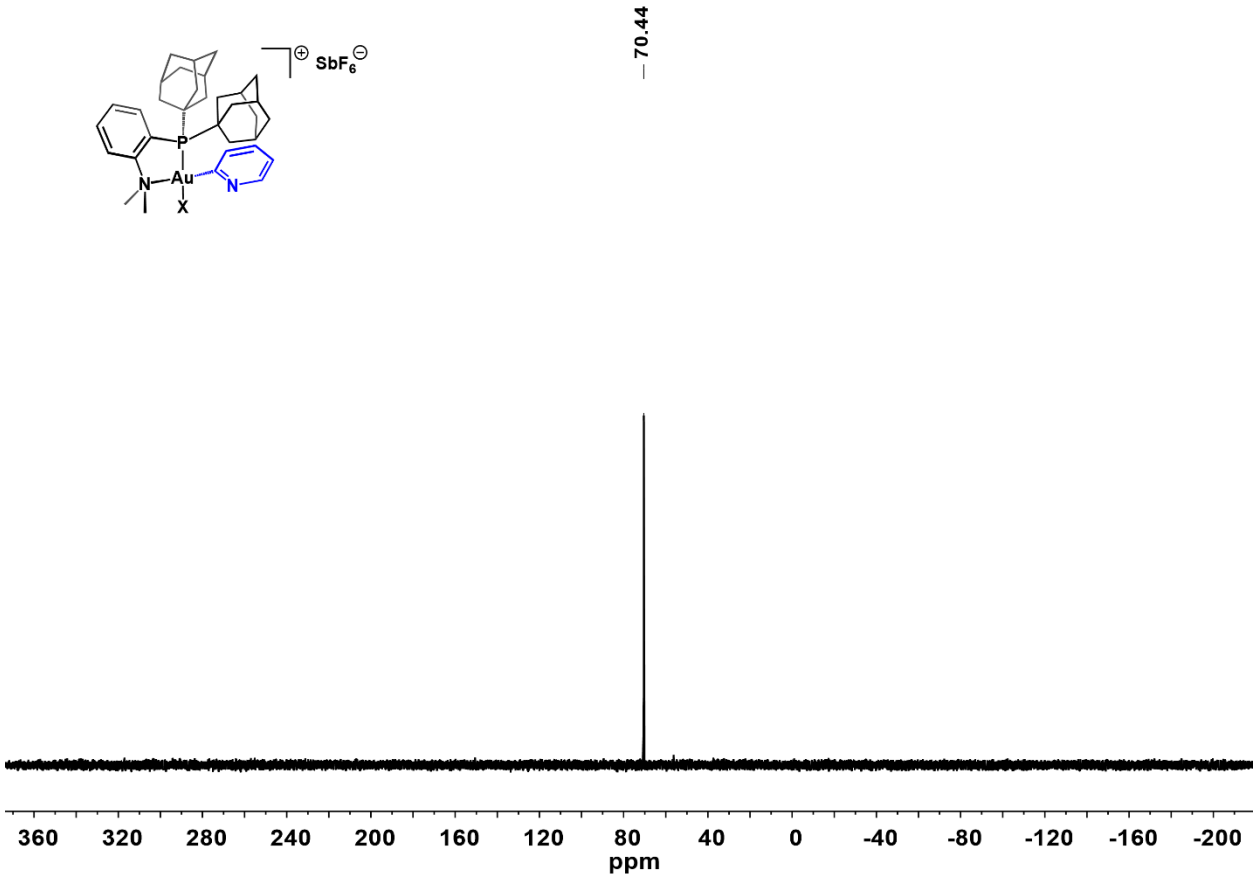

Figure D48. $^{31}P\{^{1}H\}$ NMR spectrum of [**2m**][SbF_6] in CD_3CN at 298 K.

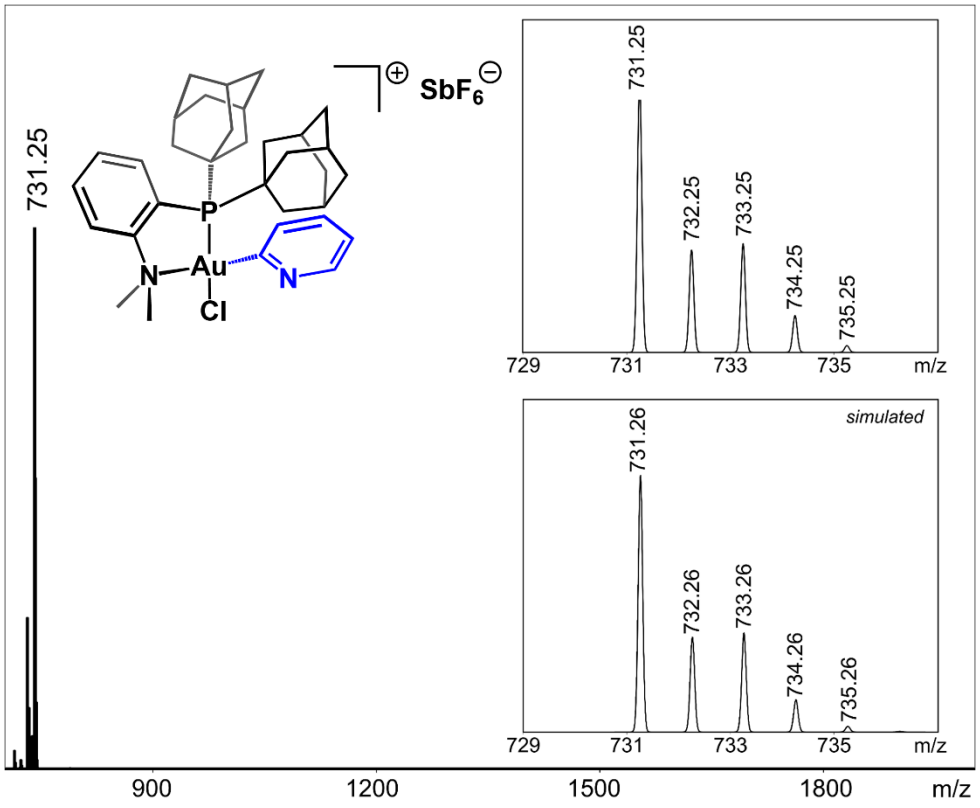

Figure D49. ESI-MS(+) of **2m**.

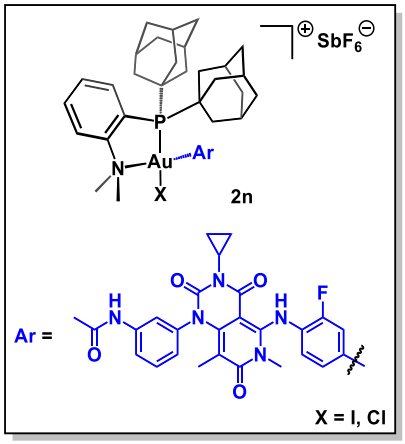

Following the general procedure, (Me-DalPhos)AuCl (4.23 mg, 0.006 mmol, 1.0 equiv), $AgSbF_6$ (2.22 mg, 0.006 mmol, 1.0 equiv) and Trametinib (19.9 mg, 0.032 mmol, 5.0 equiv) were used. Dichloromethane was removed under reduced pressure after filtration through a pad of Celite to afford a yellow solid. This material was used without further purification.

$^{31}P\{^1H\}$ NMR (162 MHz, CD_3CN): δ 79.7 ppm.

ESI-MS(+): 1141.41 (calc'd 1141.40) *m/z* ($C_{54}H_{63}ClFN_6O_4PAu$).

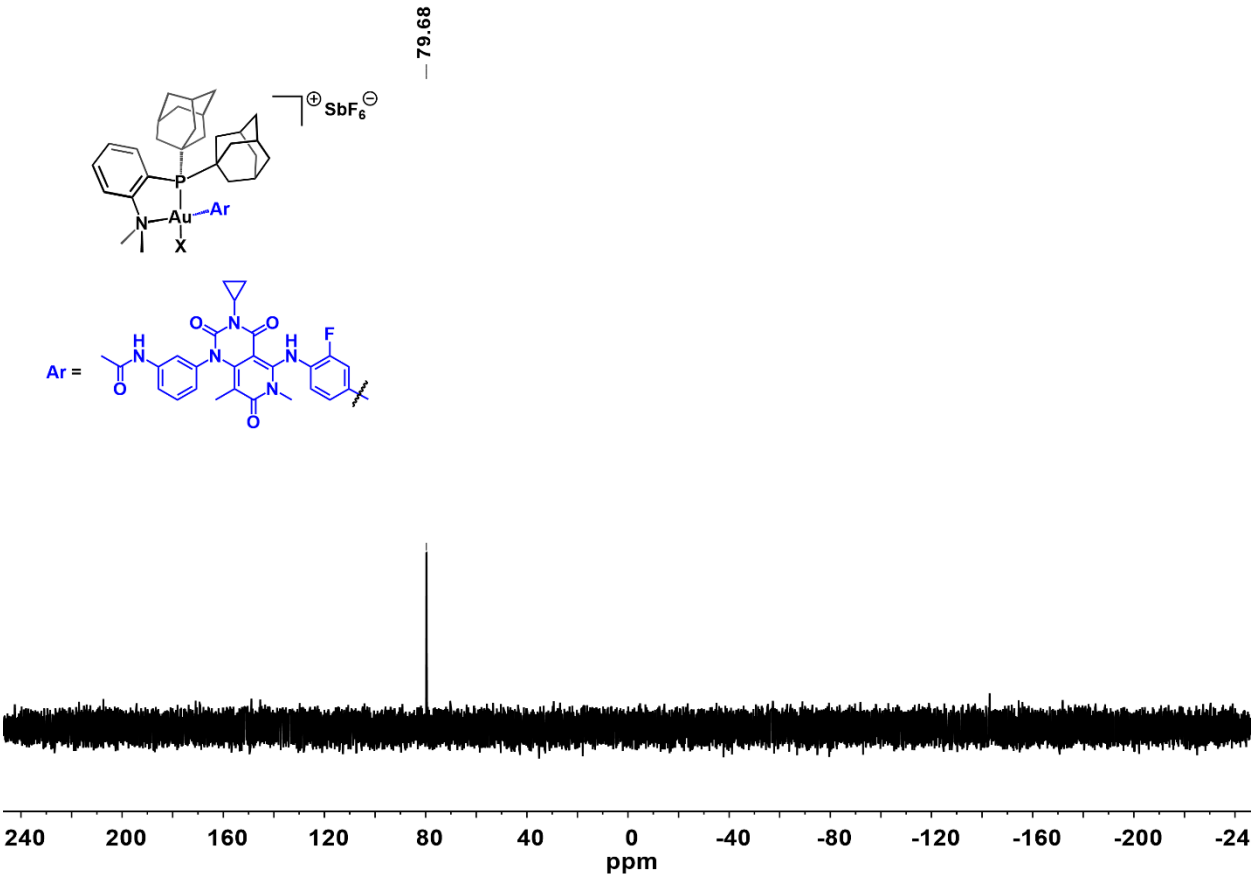

Figure D50. $^{31}P\{^{1}H\}$ NMR spectrum of [**2n**][SbF_6] in CD_3CN at 298 K.

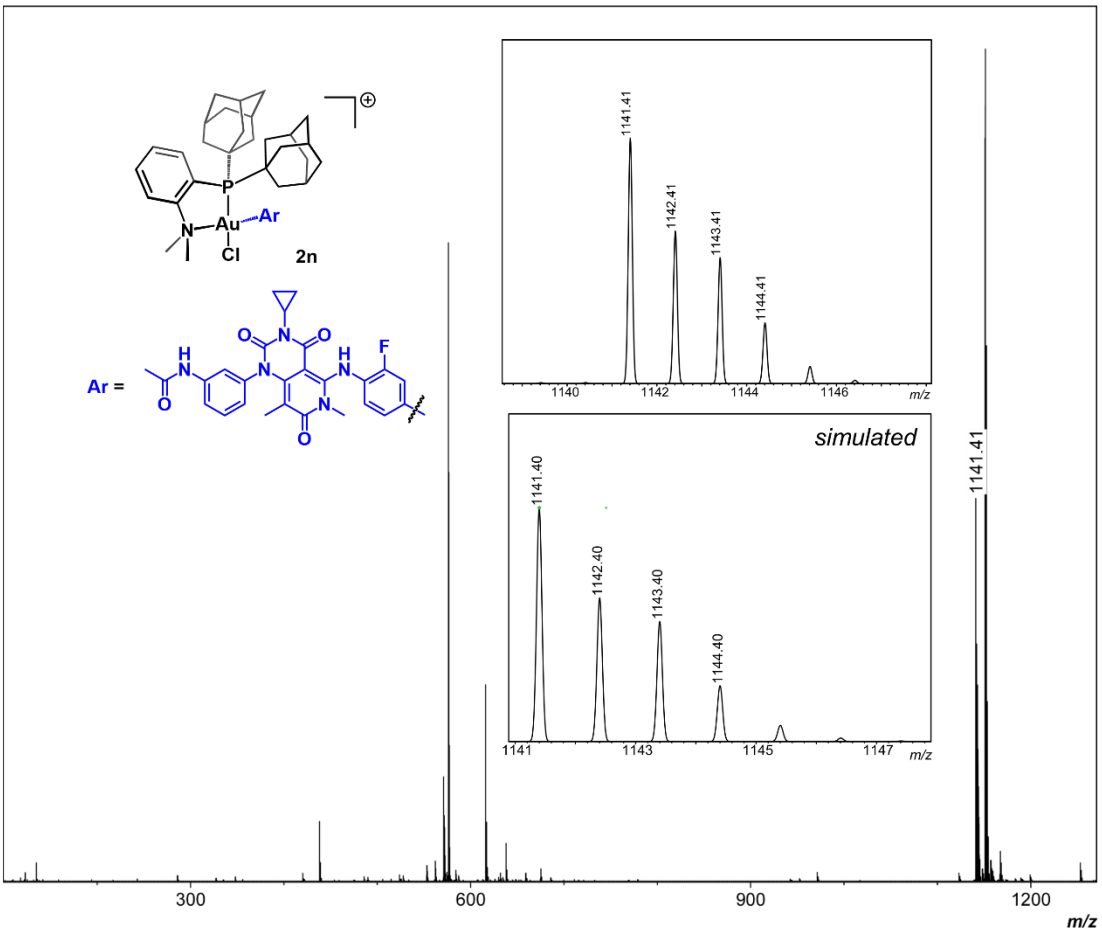

Figure D51. ESI-MS(+) of **2n**.

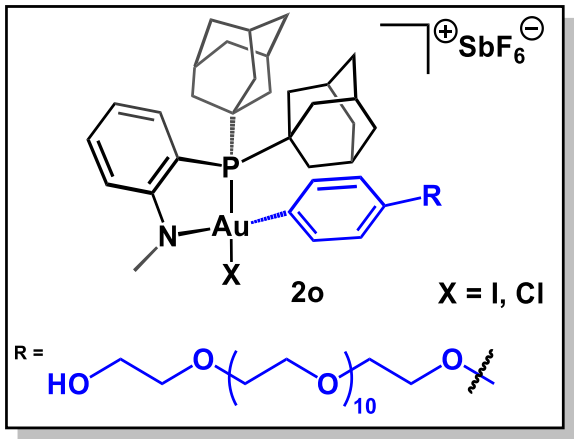

In the fume hood, $AgSbF_6$ (11 mg, 0.031 mmol, 1.0 equiv) was dissolved in DCM (2 mL) under protection from light, and the colorless solution was cooled to -20 °C. A DCM solution (2 mL) containing **SI-3** (52 mg, 0.078 mmol, 2.5 equiv) and (Me-DalPhos)AuCl (20 mg, 0.031 mmol, 1.0 equiv) reagents was prepared and also cooled to -20 °C. While both solutions were cold, the colorless **SI-3** and (Me-DalPhos)AuCl solution was added in one portion to the solution of $AgSbF_6$. The colorless solution was allowed to stand at 25 °C for 15 min, during which time pale yellow solids precipitated out of solution and a color change to pale yellow was observed. The reaction mixture was filtered through a pad of Celite, and the resulting pale-yellow filtrate was dried under reduced pressure. This material was used without further purification.

$^{31}P\{^{1}H\}$ NMR (162 MHz, CD_3CN): δ 74.3 ppm.

ESI-MS(+): 1262.42 (calc'd 1262.60) *m/z* $(C_{58}H_{93}ClNO_{13}PAu+Na)^+$.

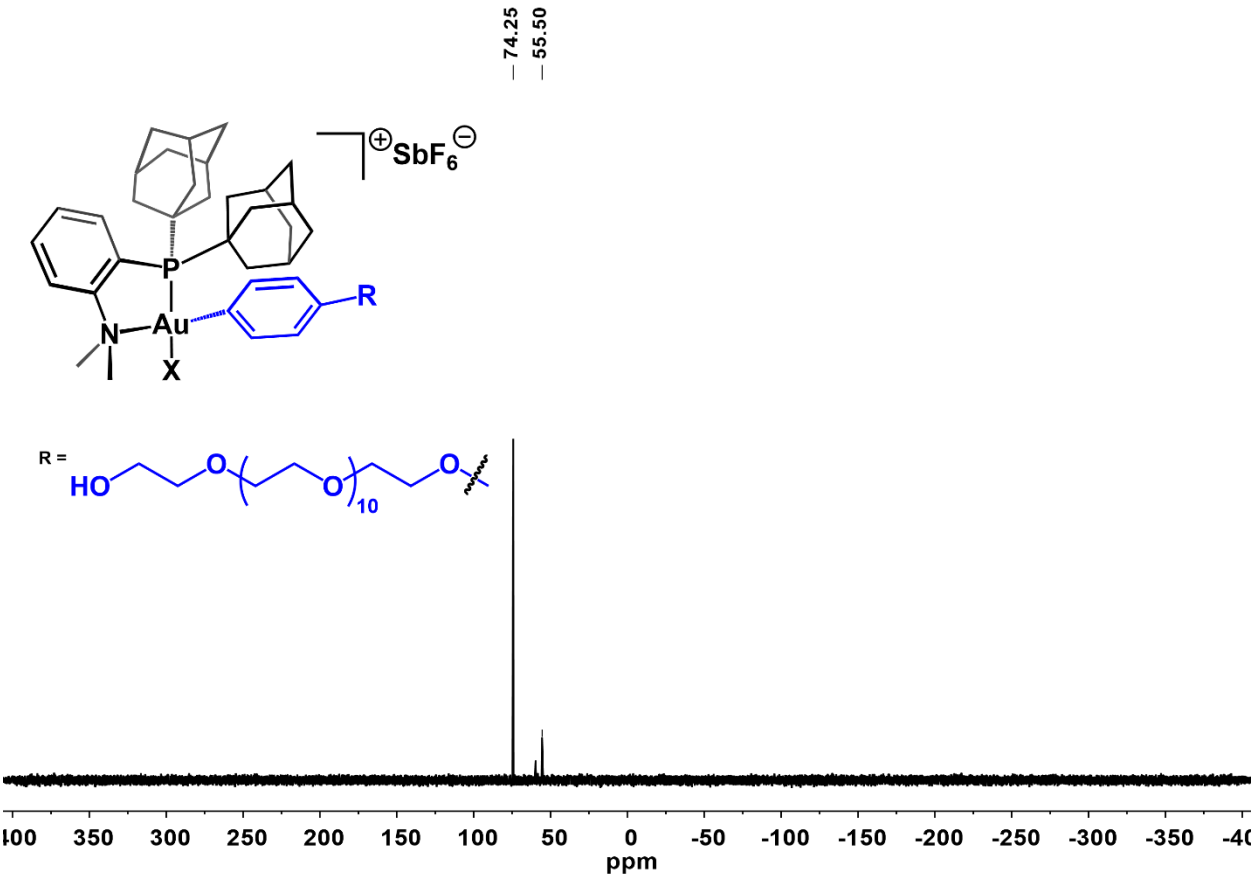

Figure D52. $^{31}P\{^{1}H\}$ NMR spectrum of [**2o**][SbF_6] in CD_3CN at 298 K.

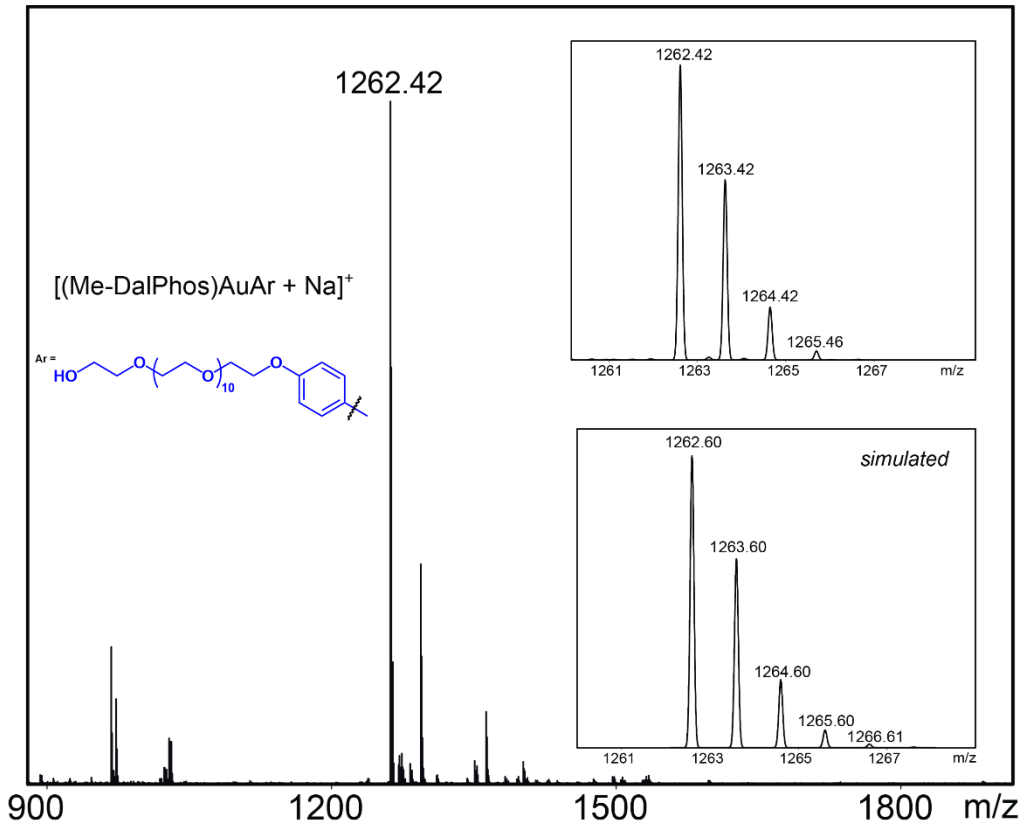

Figure D53. ESI-MS(+) of **2o**.

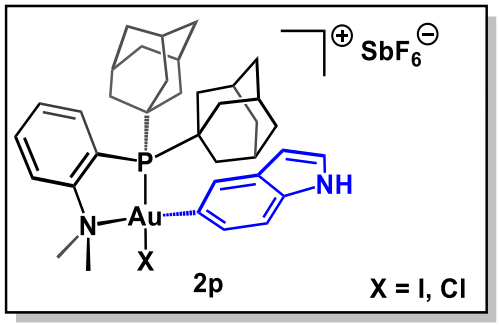

Following the general procedure, (Me-DalPhos)AuCl (30 mg, 0.046 mmol, 1.0 equiv), $AgSbF_6$ (16 mg, 0.046 mmol, 1.0 equiv) and 5-iodoindole (56 mg, 0.23 mmol, 5.0 equiv) were used. The [**2p**][SbF_6] salt was isolated as a red crystalline solid in 76% yield (35 mg, 0.035 mmol).

^{1}H NMR (400 MHz, CD_3CN): δ 9.61 (s, 1H, -N*H*), 8.07 (m, 1H, H_{Ar}), 8.03–7.92 (m, 2H, H_{Ar}), 7.69 (m, 1H, H_{Ar}), 7.48 (d, 1H, *J* = 7.6 Hz, H_{Ar}), 7.39 (d, 1H, *J* = 7.7 Hz, H_{Ar}), 7.02 (t, 1H, *J* = 7.7 Hz, -CHC*H*NH-), 6.52 (dd, 1H, *J* = 3.2 Hz, 2.0 Hz, -C*H*CHNH-), 3.58 (s, 3H, N(CH_3)$_2$), 3.52 (s, 3H, N(CH_3)$_2$), 2.36 (s, 4H, H_{Ad}), 2.24 (s, 4H, H_{Ad}), 2.00 (s, 3H, H_{Ad}), 1.84 (s, 4H, H_{Ad}), 1.70 (s, 10H, H_{Ad}), 1.54 (s, 5H, H_{Ad}) ppm.

^{31}P{^{1}H} NMR (162 MHz, CD_3CN): δ 80.7 ppm.

ESI-MS(+): 769.20 (calc'd 769.28) *m/z* ($C_{36}H_{46}ClN_2PAu$).

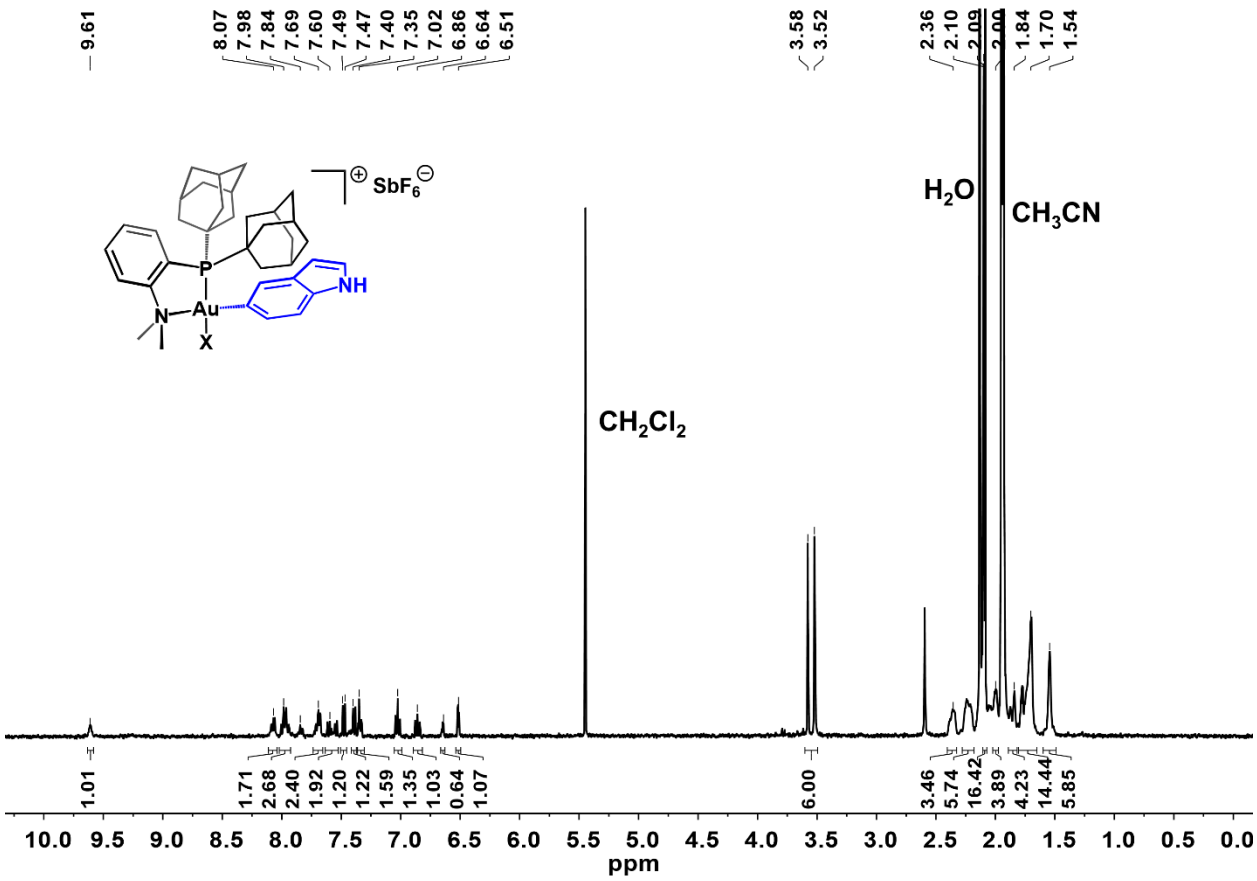

Figure D54. ^{1}H NMR spectrum of [**2p**][SbF_6] in CD_3CN at 298 K.

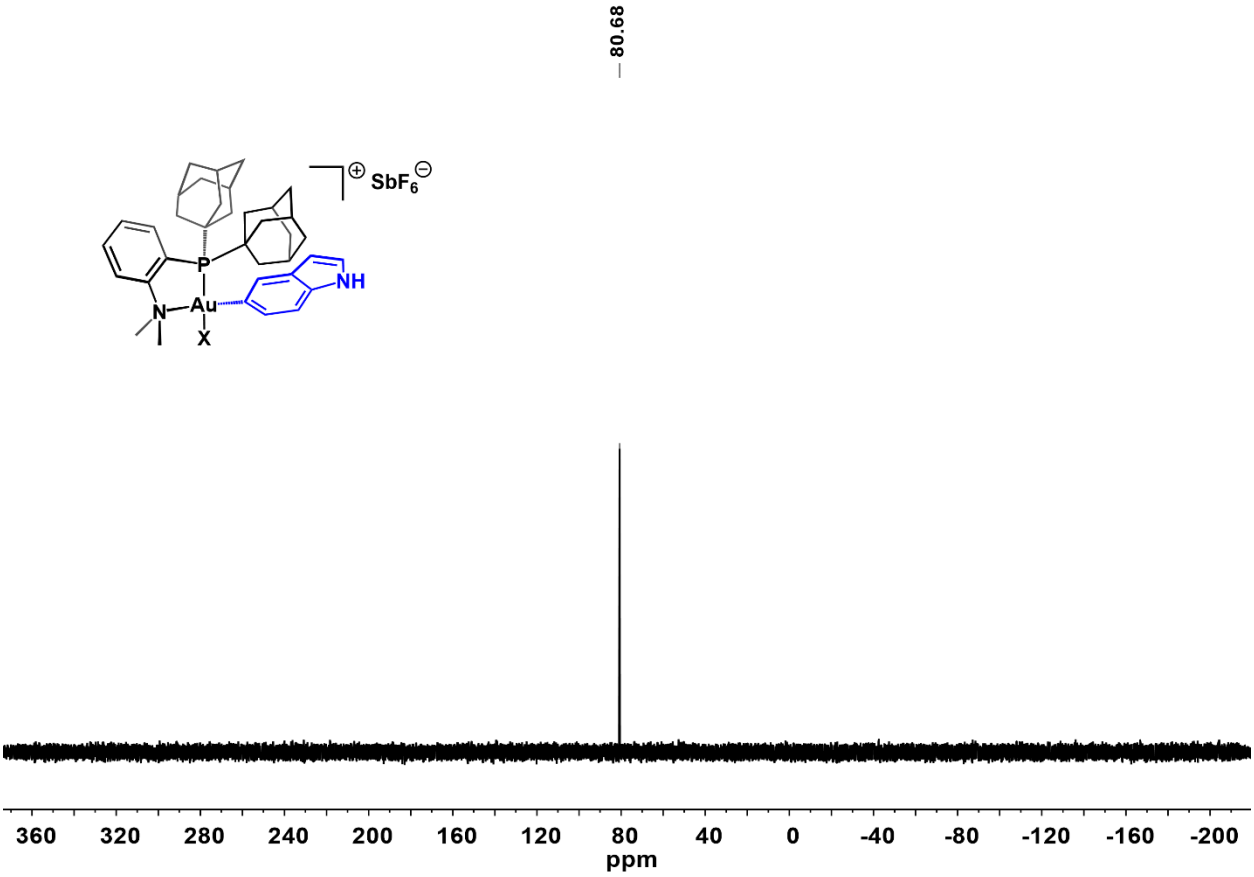

Figure D55. $^{31}P\{^{1}H\}$ NMR spectrum of [**2p**][SbF_6] in CD_3CN at 298 K.

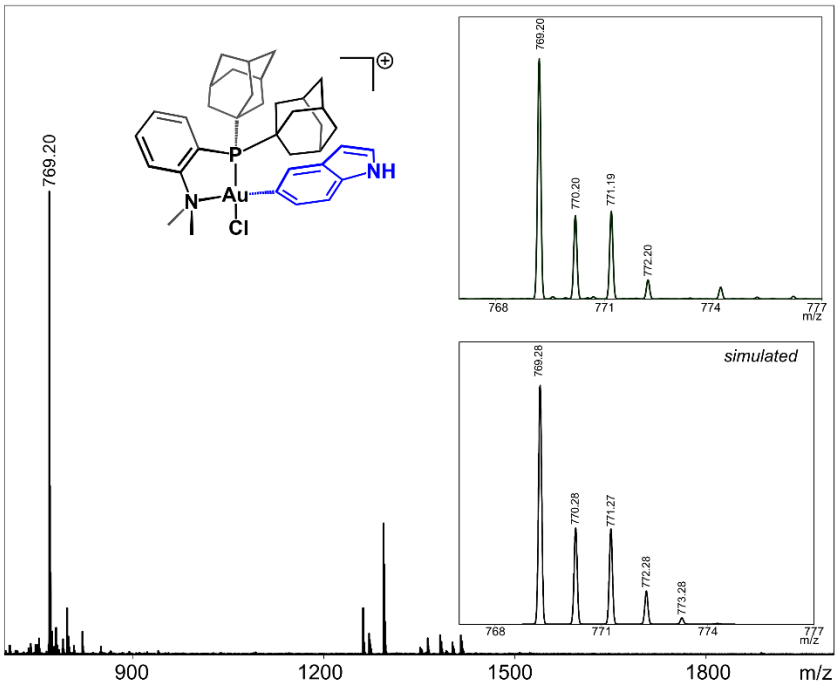

Figure D56. ESI-MS(+) of **2p**.

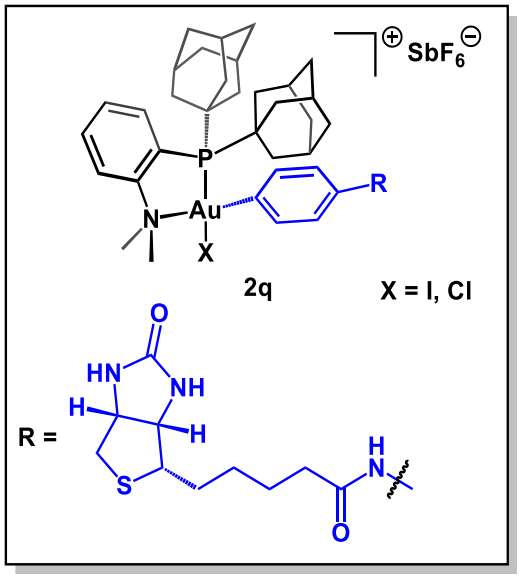

In the fume hood, $AgSbF_6$ (3 mg, 0.009 mmol, 1 equiv) was dissolved in DCM (2 mL) under protection from light, and the colorless solution was cooled to -20 °C. A DCM suspension (2 mL) containing **SI-1** (6 mg, 0.01 mmol, 1 equiv) and (Me-DalPhos)AuCl (6 mg, 0.009 mmol, 1 equiv) reagents was prepared and also cooled to -20 °C. While both solutions were cold, the colorless **SI-1** and (Me-DalPhos)AuCl suspension was added in one portion to the solution of $AgSbF_6$. The colorless suspension was sonicated for 1 min, and then the reaction mixture was filtered through a pad of Celite. The resulting pale-yellow filtrate was dried under reduced pressure. This material was used without further purification.

$^{31}P\{^1H\}$ NMR (162 MHz, CD_3CN): δ 74.7 ppm.

ESI-MS(+): 971.27 (calc'd 971.35) *m/z* ($C_{44}H_{60}ClN_4O_2PSAu$).

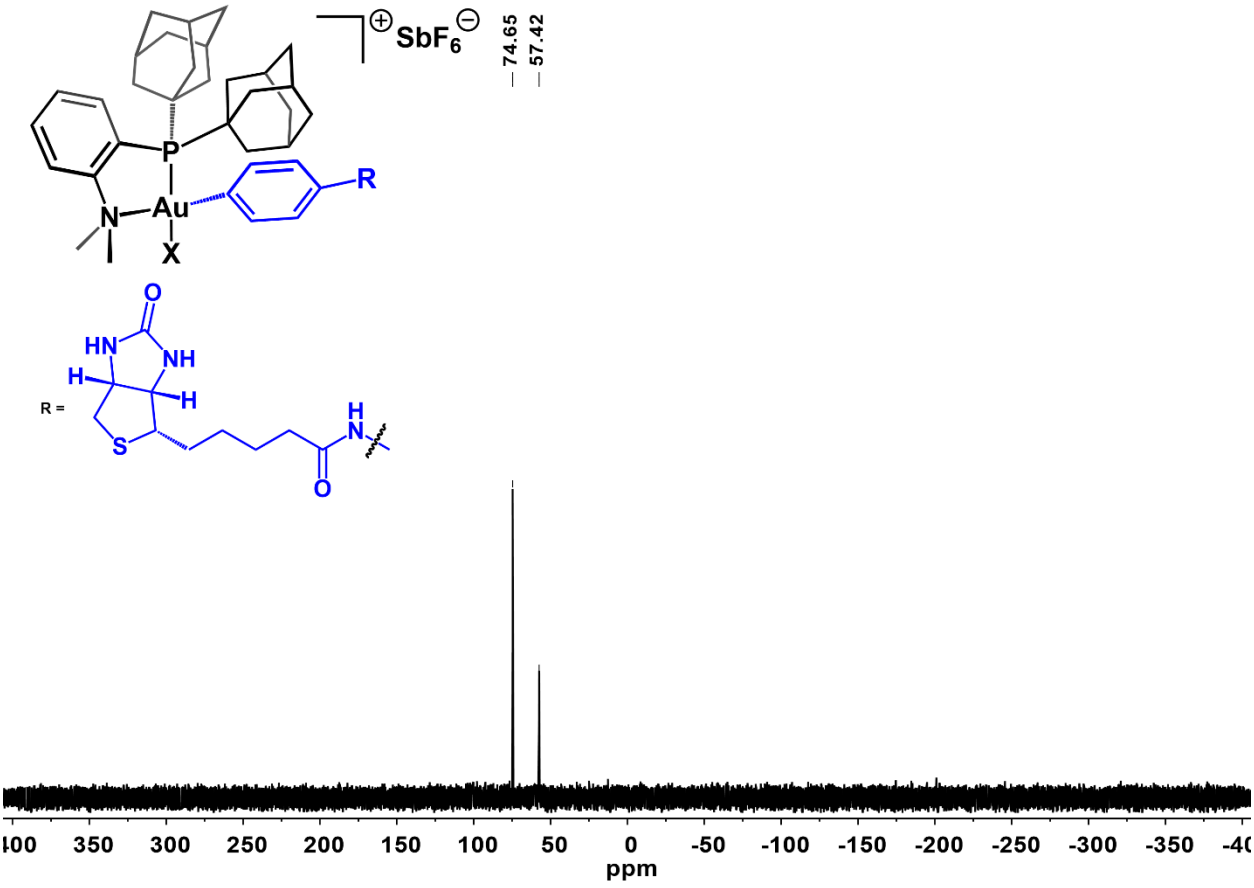

Figure D57. $^{31}P\{^{1}H\}$ NMR spectrum of [**2q**][SbF_6] in CD_3CN at 298 K. The signal at 57.4 ppm corresponds to the starting (Me-DalPhos)AuCl compound.

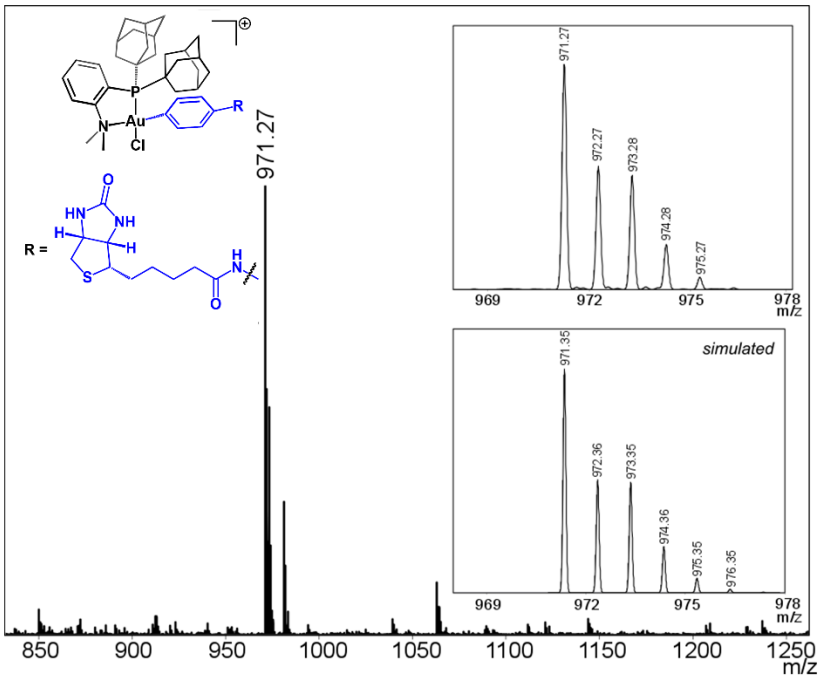

Figure D58. ESI-MS(+) of **2q**.

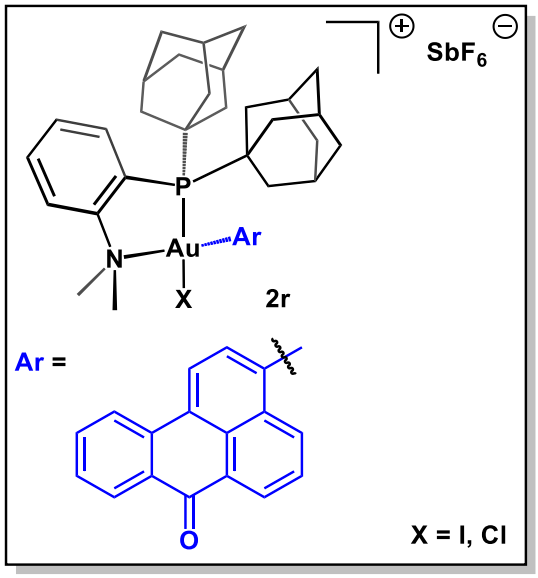

Following the general procedure, (Me-DalPhos)AuCl (16 mg, 0.024 mmol, 1.0 equiv), $AgSbF_6$ (8 mg, 0.02 mmol, 1 equiv) and 3-iodobenzanthrone (13 mg, 0.36 mmol, 1.5 equiv) were used. The [**2g**][SbF_6] salt was isolated as an orange crystalline solid in 31% yield (8 mg, 0.007). A single crystal of suitable quality for an X-ray diffraction study was obtained using this procedure (See section V for crystallographic details).

^{1}H NMR (400 MHz, CD_3CN): δ 8.79 (d, 1H, *J* = 7.2, H_{Ar}), 8.62 (t, 2H, *J* = 7.6 Hz, H_{Ar}), 8.55 (d, 1H, *J* = 8.0 Hz, H_{Ar}), 8.45 (dd, 1H, *J* = 7.9 Hz, 1.4 Hz, H_{Ar}), 8.22 (d, 1H, *J* = 8.2 Hz, H_{Ar}), 8.14 (m, 1H, H_{Ar}), 8.08 (m, 2H, H_{Ar}), 7.95 – 7.85 (m, 1H, H_{Ar}), 7.70 (t, 2H, *J* = 7.5 Hz, H_{Ar}), 3.67 (s, 3H, N(CH_3)$_2$), 3.64 (s, 3H, N(CH_3)$_2$), 2.49 (s, 4H, H_{Ad}), 2.34 (s, 4H, H_{Ad}), 2.20 (s, 3H, H_{Ad}), 1.86 (s, 4H, H_{Ad}), 1.77 (s, 4H, H_{Ad}), 1.70 (4H, s, H_{Ad}), 1.45 (s, 7H, H_{Ad}) ppm.

^{31}P{^{1}H} NMR (162 MHz, CD_3CN): δ 89.9 ppm.

ESI-MS(+): 892.31 (calc'd 892.33) *m/z*.

Note this sample was run in the presence of formic acid, and as a result, the [(Me-DalPhos)Au(benzanthrone)OCHO]$^+$ ion is observed ($C_{46}H_{50}NPO_3Au$).

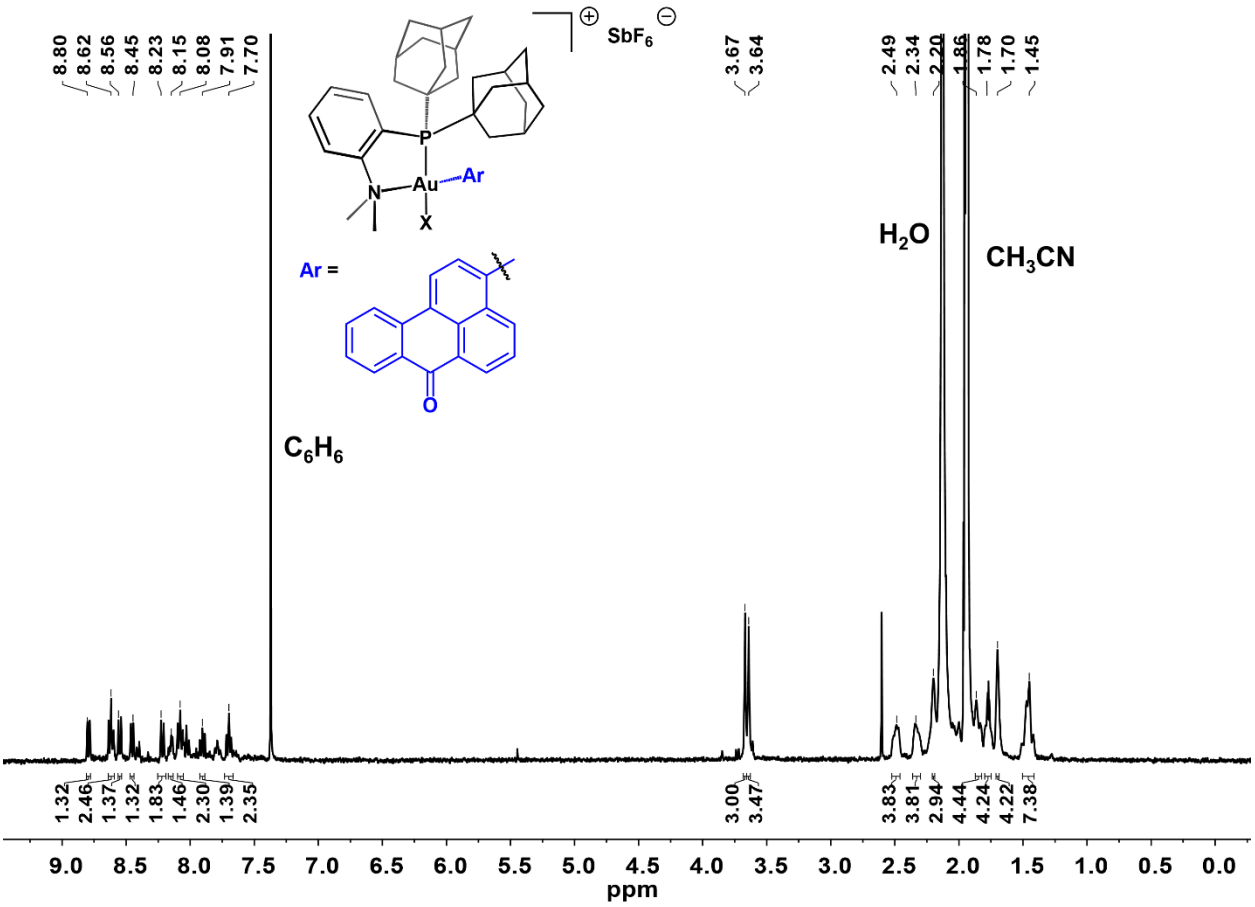

Figure D59. ^{31}P NMR spectrum of [**2r**][SbF_6] in CD_3CN at 298 K.

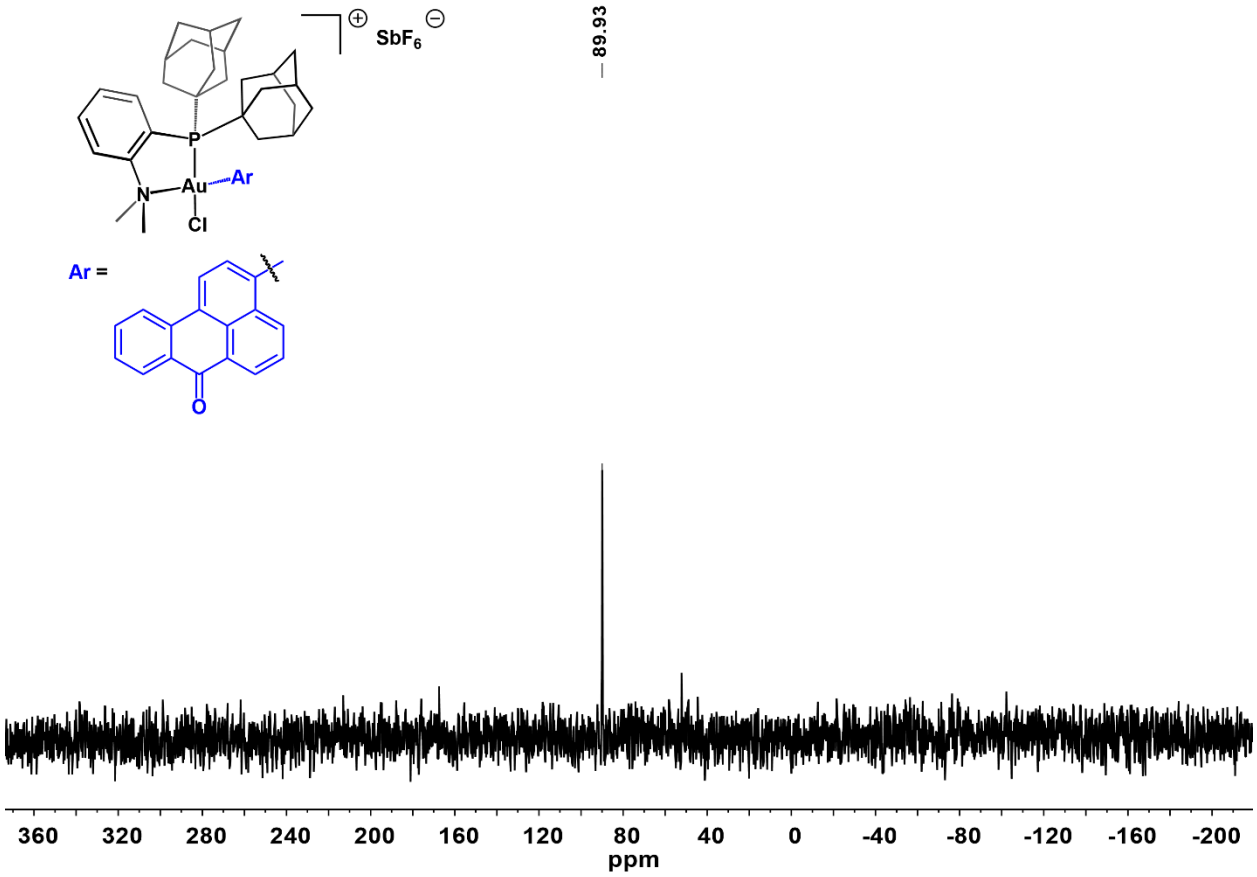

Figure D60. $^{31}P\{^{1}H\}$ NMR spectrum of [**2r**][SbF_6] in CD_3CN at 298 K.

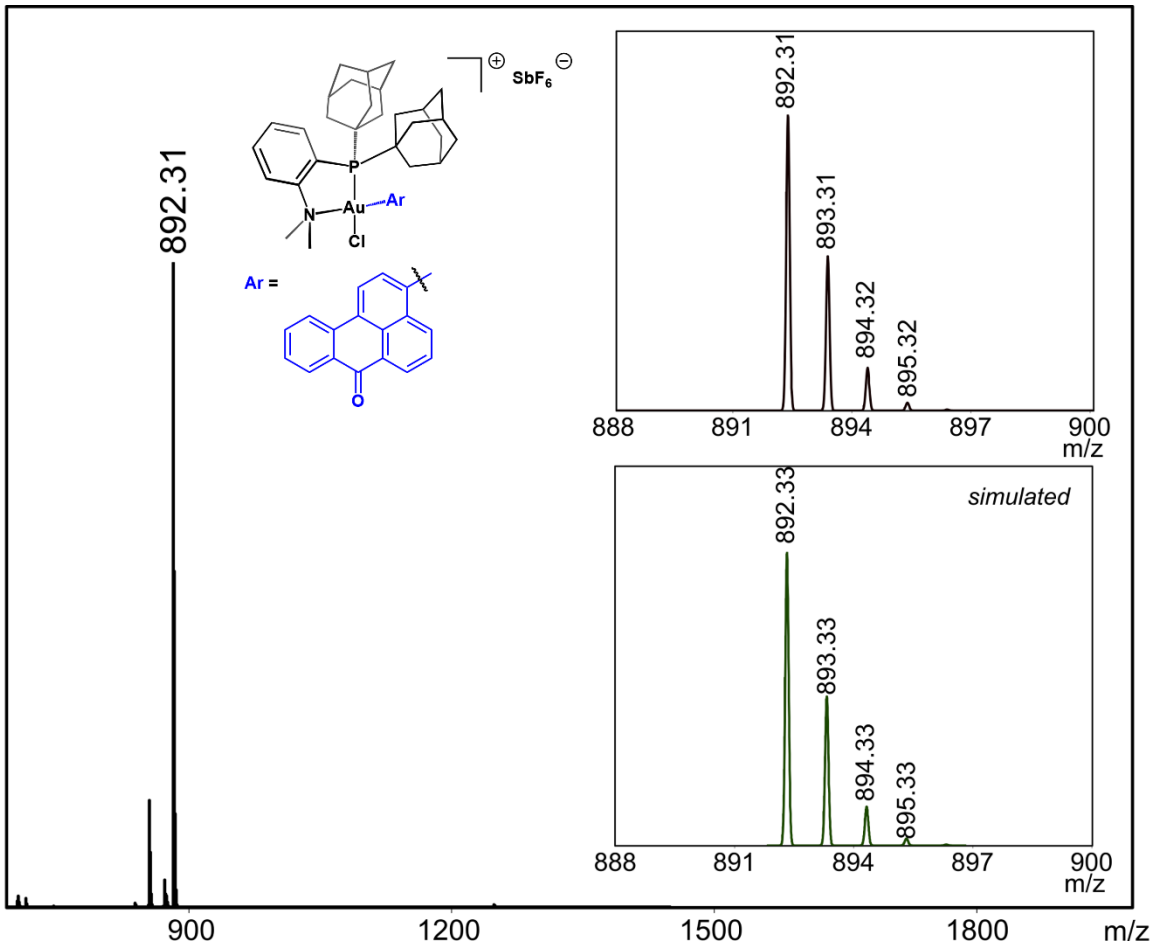

Figure D61. ESI-MS(+) of **2r**. Note this sample was run in the presence of formic acid.

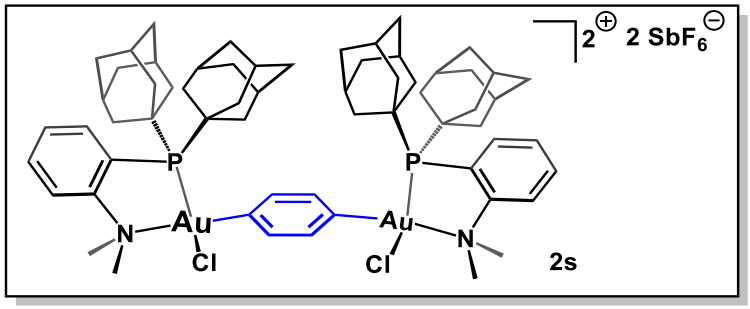

In the fume hood, $AgSbF_6$ (16 mg, 0.046 mmol, 2.2 equiv) was dissolved in DCM (2 mL) under protection from light, and the colorless solution was cooled to -20 °C. A DCM solution (2 mL) containing 1,4-diiodobenzene (7 mg, 0.02 mmol, 1 equiv) and (Me-DalPhos)AuCl (30 mg, 0.046 mmol, 2.2 equiv) reagents was prepared and also cooled to -20 °C. While both solutions were cold, the colorless 1,4-diiodobenzene and (Me-DalPhos)AuCl solution was added in one portion to the solution of $AgSbF_6$, resulting in an immediate color change to bright yellow concomitant with precipitation of pale yellow solids. The reaction mixture was filtered through a pad of Celite, and the resulting yellow filtrate was allowed to stand undisturbed at 25 °C for 48 h, during which time the [**2s**][SbF_6]$_2$ product crystallized from solution. The pale-yellow supernatant was decanted, and the yellow crystals were washed with C_6H_6 (3 × 2 mL). The crystals were then washed with *n*-pentane (3 mL) and dried under reduced pressure to afford [**2s**][SbF_6]$_2$ as a yellow crystalline solid in 67% yield (24 mg, 0.013 mmol). A crystal of suitable quality for an X-ray diffraction study was obtained using this procedure. The X-ray crystallographic analysis indicated **2s** crystallized with 100% Cl occupancy (see section V).

^{1}H NMR (400 MHz, CD_3CN): δ 8.08–8.04 (m, 2H, H_{Ar}), 8.02–7.91 (m, 4H, H_{Ar}), 7.70 (m, 2H, H_{Ar}), 7.53 (s, 4H, H_{Ar}), 3.50 (s, 12H, N(CH_3)$_2$), 2.28 (d, J = 8.8 Hz, 12H, H_{Ad}), 2.09 (s, 12H, H_{Ad}), 2.04–1.99 (m, 11H, H_{Ad}), 1.74 (m, 25H, H_{Ad}) ppm.

^{31}P{^{1}H} NMR (162 MHz, CD_3CN): δ 78.6 ppm.

ESI-MS: 691.17 (calc'd 691.24) *m/z* for $C_{62}H_{84}Cl_2N_2P_2Au_2$.

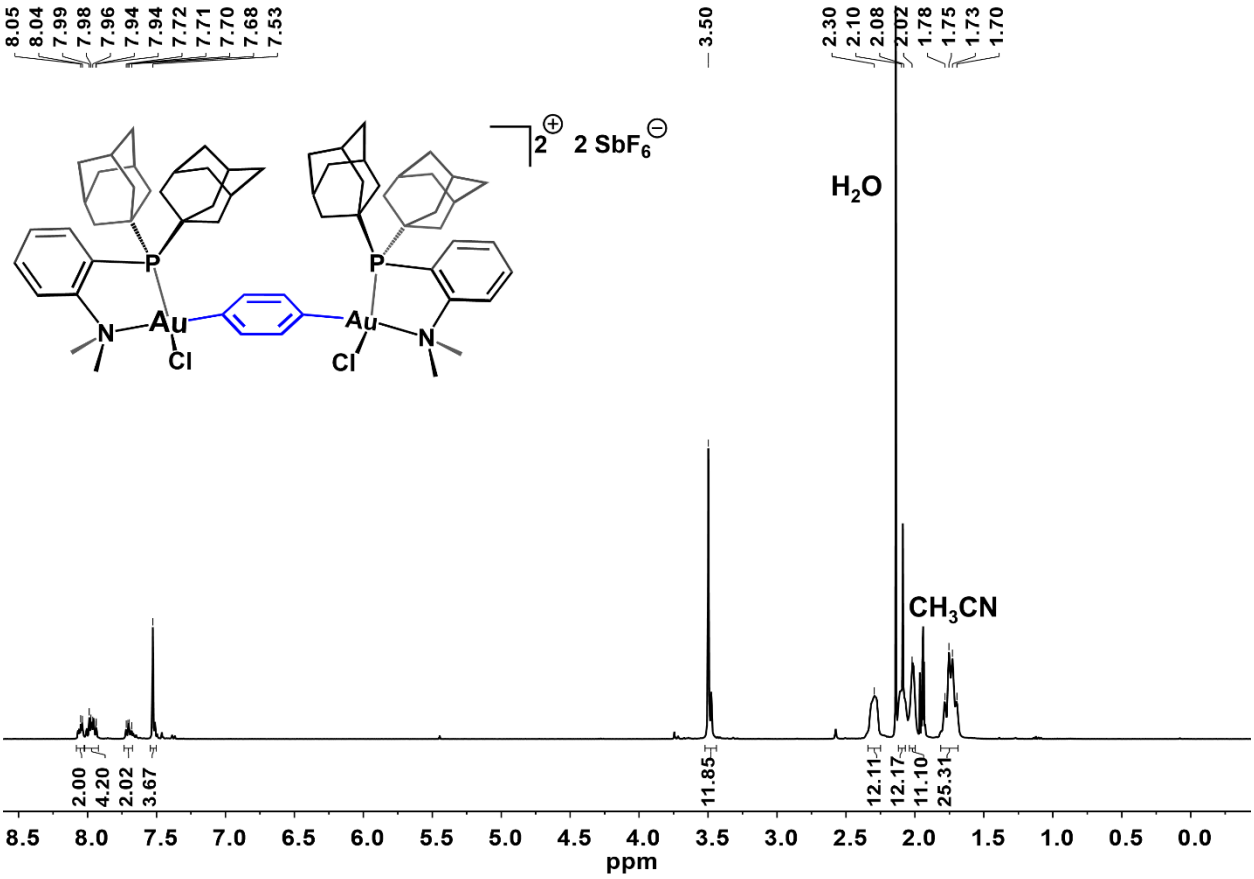

Figure D62. ^{1}H NMR spectrum of [**2s**][SbF_6]$_2$ in CD_3CN at 298 K.

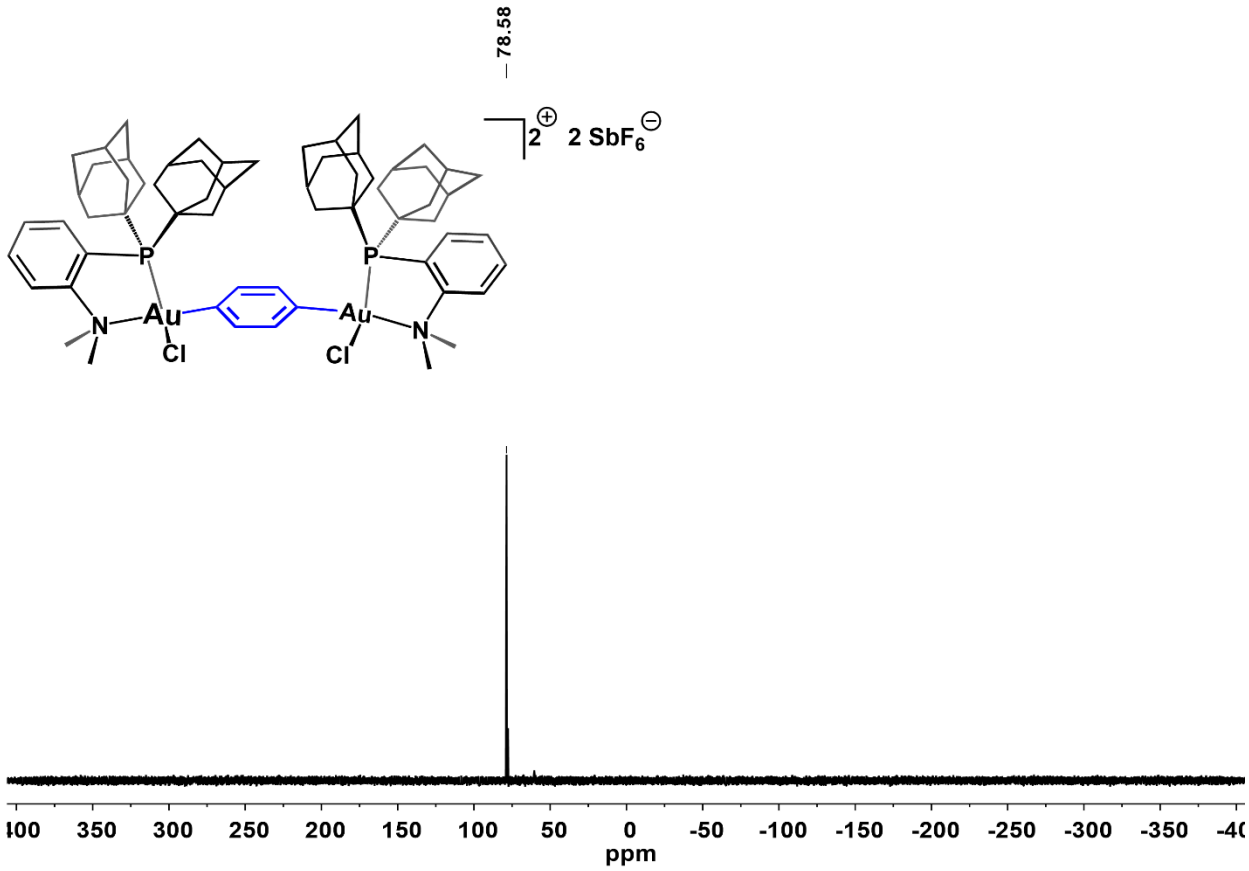

Figure D63. $^{31}P\{^{1}H\}$ NMR spectrum of [**2s**][SbF_6]$_2$ in CD_3CN at 298K.

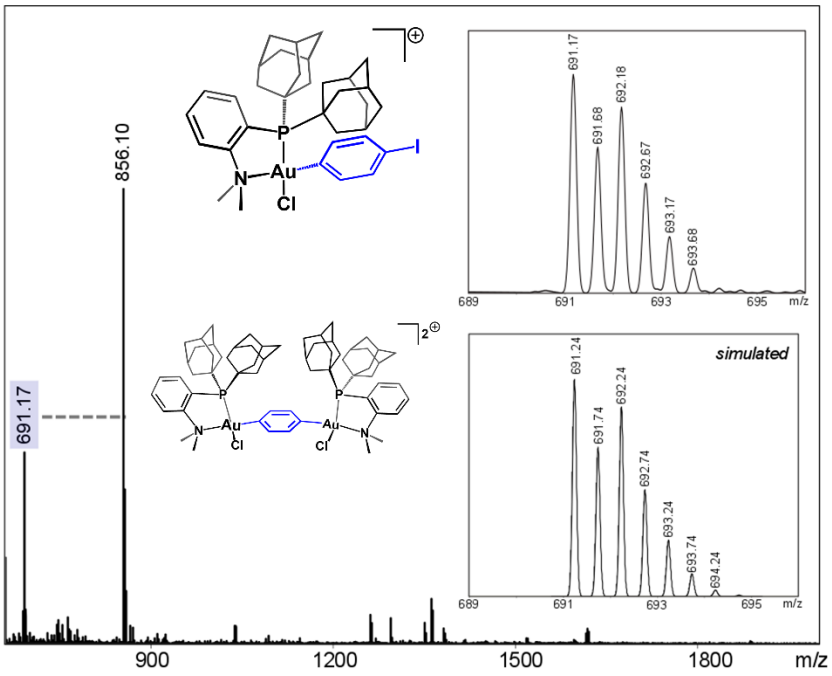

Figure D64. ESI-MS(+)of **2s**.

5.5.7 Stability studies of complexes [2a][SbF_6] and [2c][SbF_6].

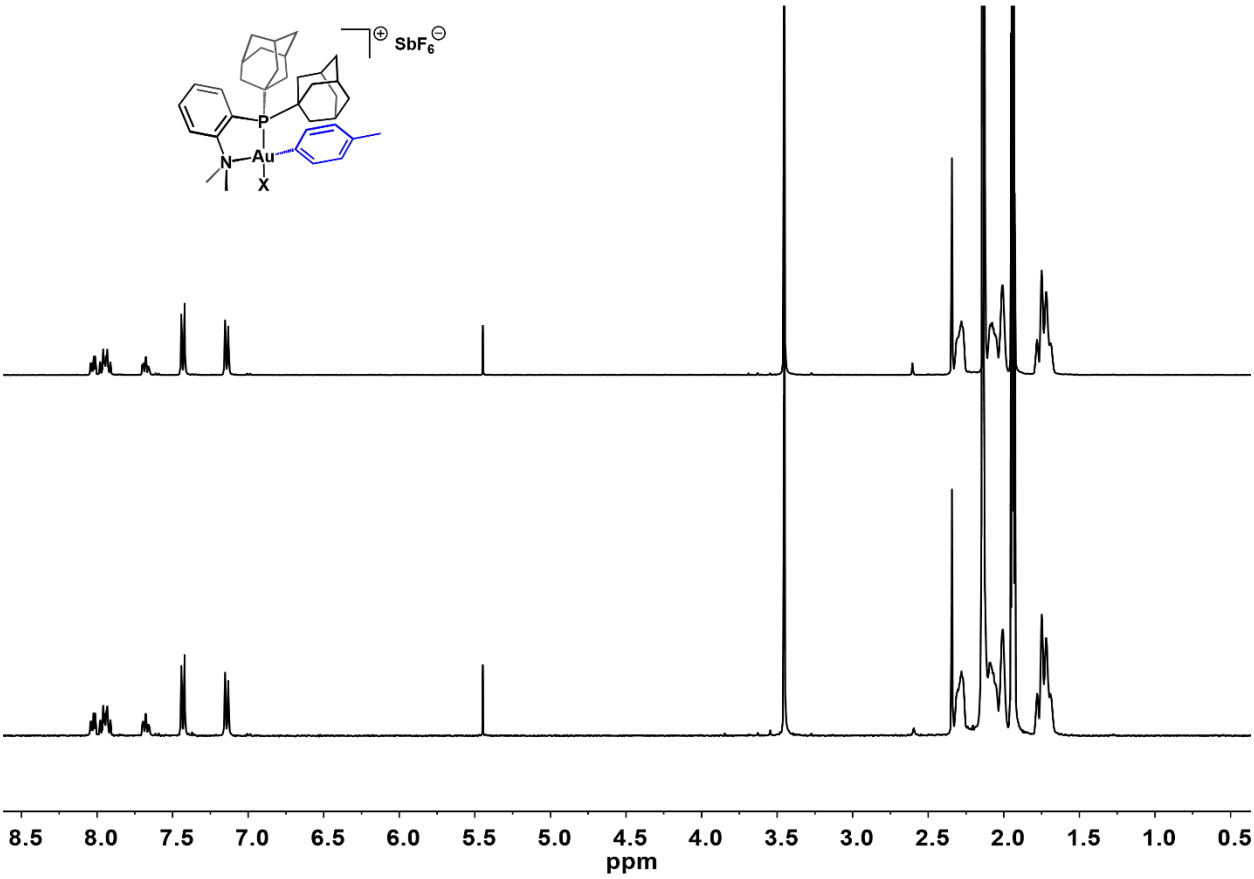

Figure D65. ^{1}H NMR spectrum of a newly prepared sample of [**2a**][SbF_6] (top) and spectrum of the same sample after storage as a solid for two months at 25 °C (bottom). Spectra collected in CD_3CN, 298 K.

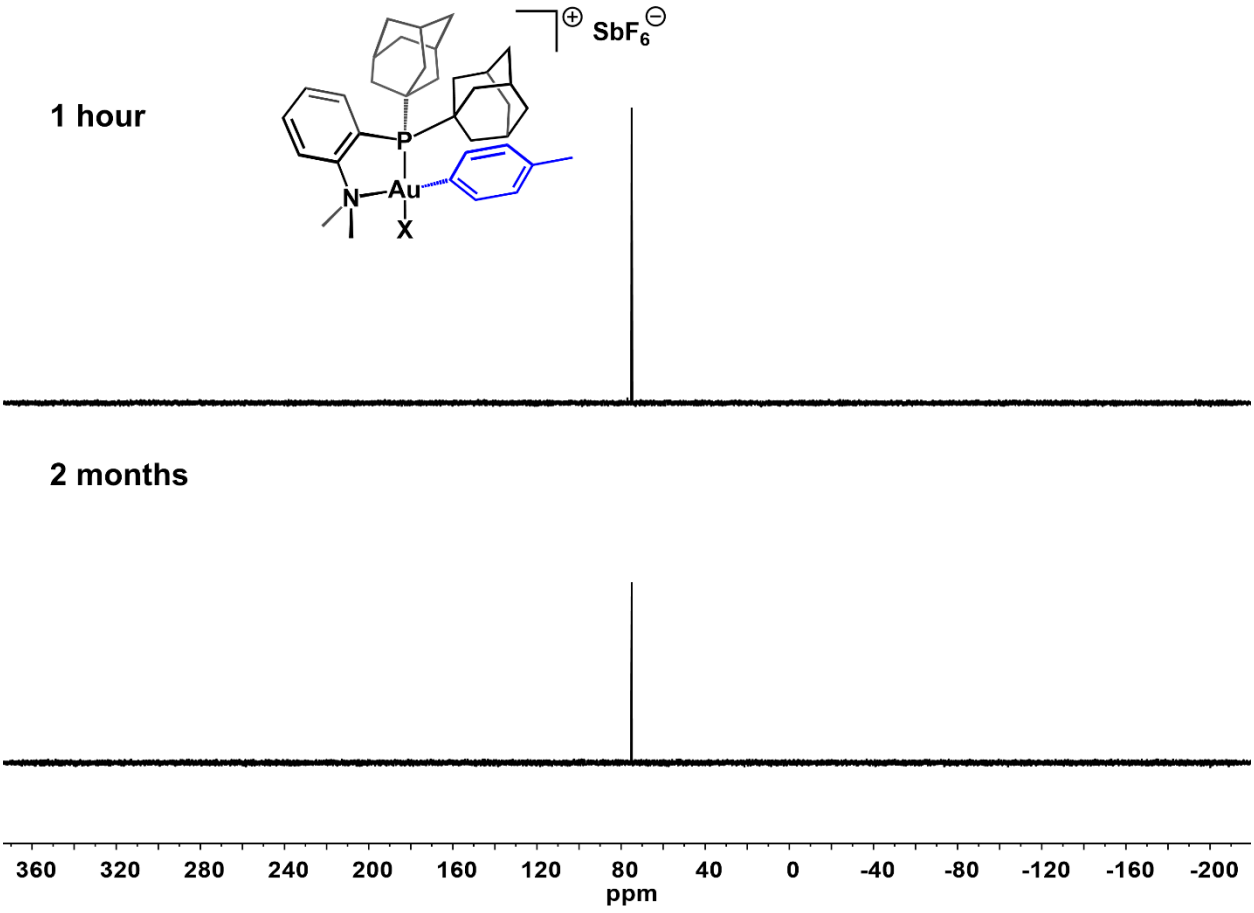

Figure D66. $^{31}P\{^{1}H\}$ NMR spectrum of a newly prepared sample of [**2a**][SbF_6] (top) and spectrum of the same sample after storage as a solid for two months at 25 °C (bottom). Spectra collected in CD_3CN, 298 K.

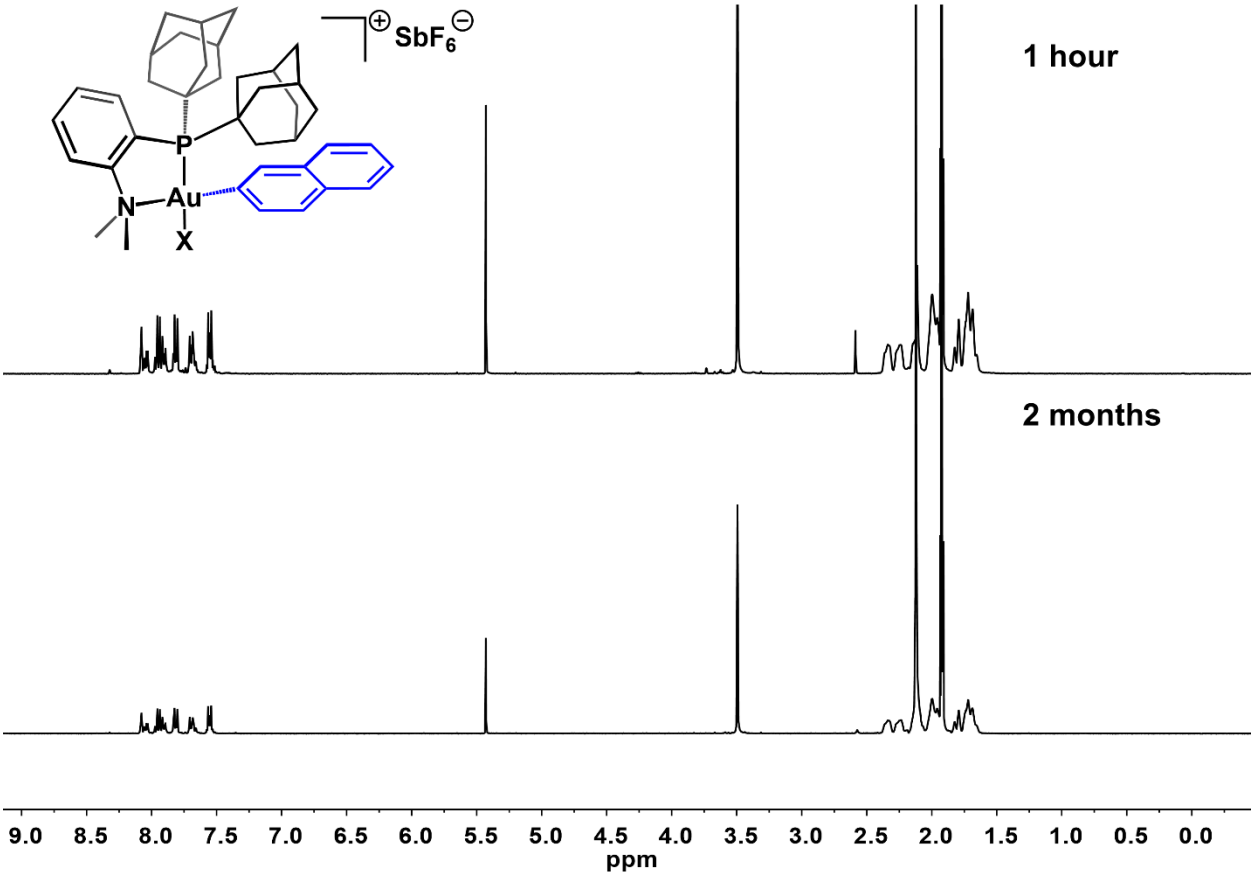

Figure D67. ^{1}H NMR spectrum of a newly prepared sample of [**2c**][SbF_6] (top) and spectrum of the same sample after storage as a solid for two months at 25 °C (bottom). Spectra collected in CD_3CN at 298 K.

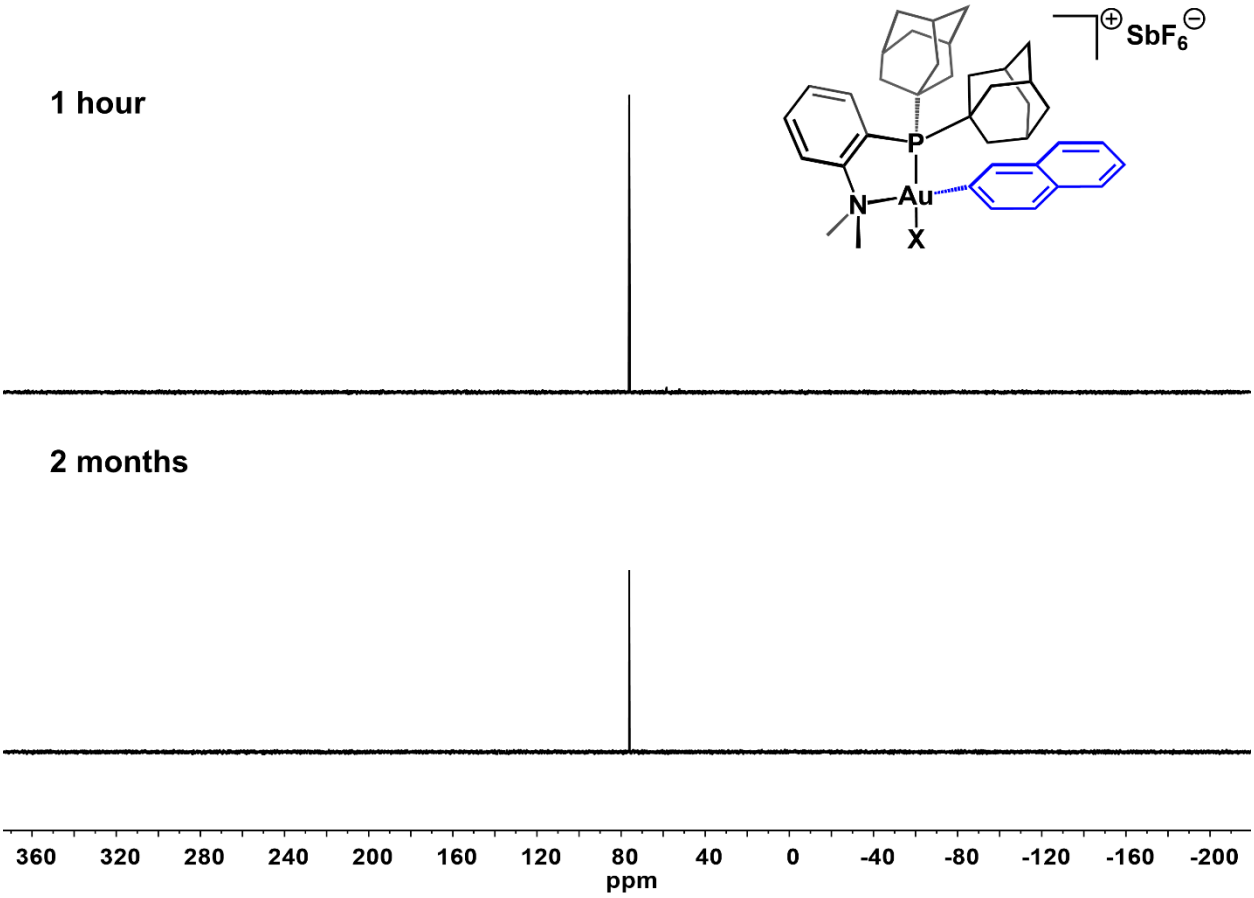

Figure D68. $^{31}P\{^{1}H\}$ NMR spectrum of a newly prepared sample of [**2c**][SbF_6] (top) and spectrum of the same sample after storage as a solid for two months at 25 °C (bottom). Spectra collected in CD_3CN at 298 K.

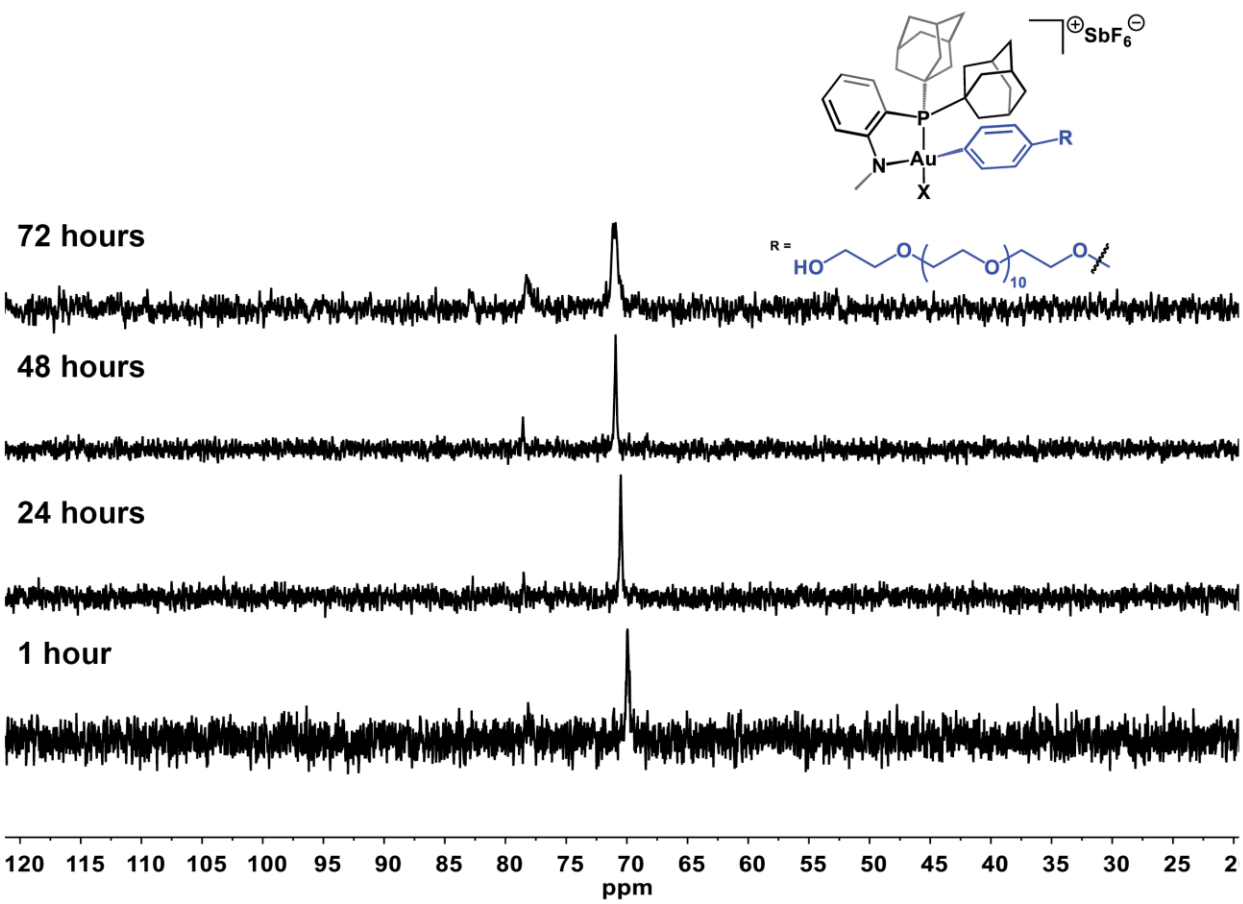

Figure D69. $^{31}P\{^{1}H\}$ NMR spectra of a newly prepared sample of [**2o**][SbF_6] in water (bottom) and after storage for up to 72 hours in water at 25 ˚C.

5.5.8 Peptide Synthesis and Protein Expression

The following general protocol was followed for all solid phase peptide syntheses:

Preparation of Resin:

Rink amide resin (1 g, 0.44 mmol/g) was weighed out and added to a 25 mL peptide synthesis vessel. Dimethylformamide (DMF; 10 mL) was added and the resin was shaken for a minimum of 1 h to swell. The resin was subsequently washed with DMF (3 × 10 mL), dichloromethane (3 × 10 mL), and DMF (3 × 10 mL).

First Deprotection:

A 20% solution of 4-methylpiperdine in DMF (10-15 mL/g of resin) was added and the vessel was shaken for 20 min. After shaking, the resin was washed once with DMF (10 mL). The 20% solution of 4-methylpiperdine in DMF (10-15 mL/g of resin) was added and the vessel was shaken for an additional 5 minutes. The resin was then washed three times with DMF (10 mL, 1 min washes) to ensure complete removal of 4-methylpiperdine.

Coupling of Amino Acids:

Amino acid (3 equiv to resin) and HBTU (2.9 equiv to resin) were weighed out and dissolved in DMF (10 mL). Once dissolved, DIPEA (6 equiv to resin) was added and the mixture stirred for 1 min. This mixture was then added to the resin and the resin was subjected to shaking for 45 min. After shaking, the resin was washed with DMF (3 × 10 mL, 1 min intervals) to ensure the complete removal of residual amino acid.

Coupling of Cysteine:

Coupling of Cysteine was performed using a procedure from: Han, Y. Albericio, F.; Barany, G. *J. Org. Chem.*, **1997**, *62*, 4307-4312.

Cysteine (3 equiv to resin), HATU (4 equiv to resin), and HOAt (0.6 M in DMF, 4 equiv to resin) were combined in DMF (6 mL) and CH_2Cl_2 (6 mL). Once dissolved, 2,4,6-trimethylpyridine (4 equiv to resin) was added and the mixture stirred quickly (1-2 seconds) and added to the resin. The mixture was shaken for 1 h. After shaking, the resin was washed with DMF (5 × 10 mL, 1 min intervals) to ensure the removal of residual amino acid. After the coupling of cysteine, the normal protocol was followed.

Deprotection of Amino Acids After Coupling:

A 20% solution of 4-methylpiperdine in DMF (10-15 mL/g of resin) was added and the vessel was shaken for 10 min. After shaking, the resin was washed once with DMF (10 mL). The 20% solution of 4-methylpiperdine in DMF (10-15 mL/g of resin) was added and the vessel was shaken for an additional 5 min. The resin was then washed three times with DMF (10 mL, 1 minute washes) to ensure the compete removal of 4-methylpiperdine.

Cleavage from Resin:

After the final deprotection, the resin was washed with DCM (3 × 10 mL). The dried resin was transferred to a 20 mL scintillation vial equipped with a magnetic stir bar and a septum. Argon gas was flowed over the resin for 5 minutes. A cleavage cocktail consisting of a 95:2.5:2.5 mixture of TFA:H_2O:TIPS (TIPS = triisopropylsilane) was prepared and added to the resin. The slurry was stirred for 3-4 hours under argon. Cleavage time depends on the amino acid composition of the peptide. Aliquots of the slurry were analyzed via LC-MS after filtration through a small pipette filter and dilution with water to determine full removal of peptide protecting groups. After 3-4 h, the cleavage cocktail was filtered and the filtrate was concentrated under a stream of argon until 1 mL remained. To this solution was added cold (-20 °C) diethyl ether, resulting in the precipitation

of the crude peptide. The suspension was centrifuged, the supernatant was decanted. This washing process was repeated twice more, and then the resulting solids were dried under reduced pressure. *It is important to use fresh TIPS solutions. TIPS stored longer than two months is less effective. All peptides were stored in sealed containers under argon at -20 °C.

The isolated crude peptides were purified by reversed-phase HPLC (retention time 5.5-6.6 min using procedure described in SI section I). The obtained pure fractions were combined, and lyophilized.

Protein Expression

DARPin-Cys protein expression and purification was performed following literature procedures.[4]

DARPin-Cys Sequence (Calculated Mass: 13747.3 Da):

GGCGGSDLGKKLLEAARAGQDDEVRILMANGADVNAYDDNGVTPLHLAAFLGHLEI
VEVLLKYGADVNAADSWGTTPLHLAATWGHLEIVEVLLKHGADVNAQDKFGKTAF
DISIDNGNEDLAEILQKLN

FGF2 was expressed and purified from plasmid pET29c (+)hFGF-2, provided by Professor Thomas Scheper from the Helmholtz Centre for Infection Research (Braunschweig, Germany) according to Chen *et al*.[6]

FGF2 Sequence (Calculated Mass: 17122.6 Da):

AAGSITTLPALPEDGGSGAFPPGHFKDPKRLYCKNGGFFLRIHPDGRVDGVREKSDPHIK
LQLQAEERGVVSIKGVCANRYLAMKEDGRLLASKCVTDECFFFERLESNNYNTYRSRK
YTSWYVALKRTGQYKLGSKTGPGQKAILFLPMSAKS

5.5.9 Peptide Traces and Masses:

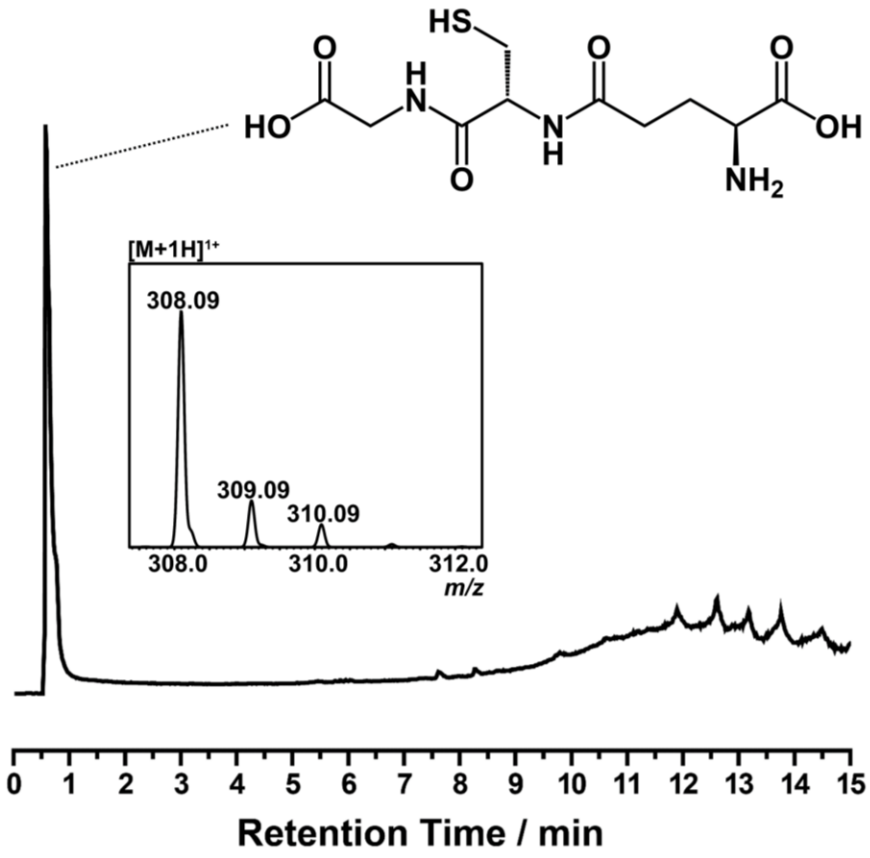

Figure D70. LC-MS trace for native GSH (BioXtra grade purchased from Sigma Aldrich). 308.0965 (calc'd 308.0911) *m/z* for $C_{10}H_{17}N_3O_6S$.

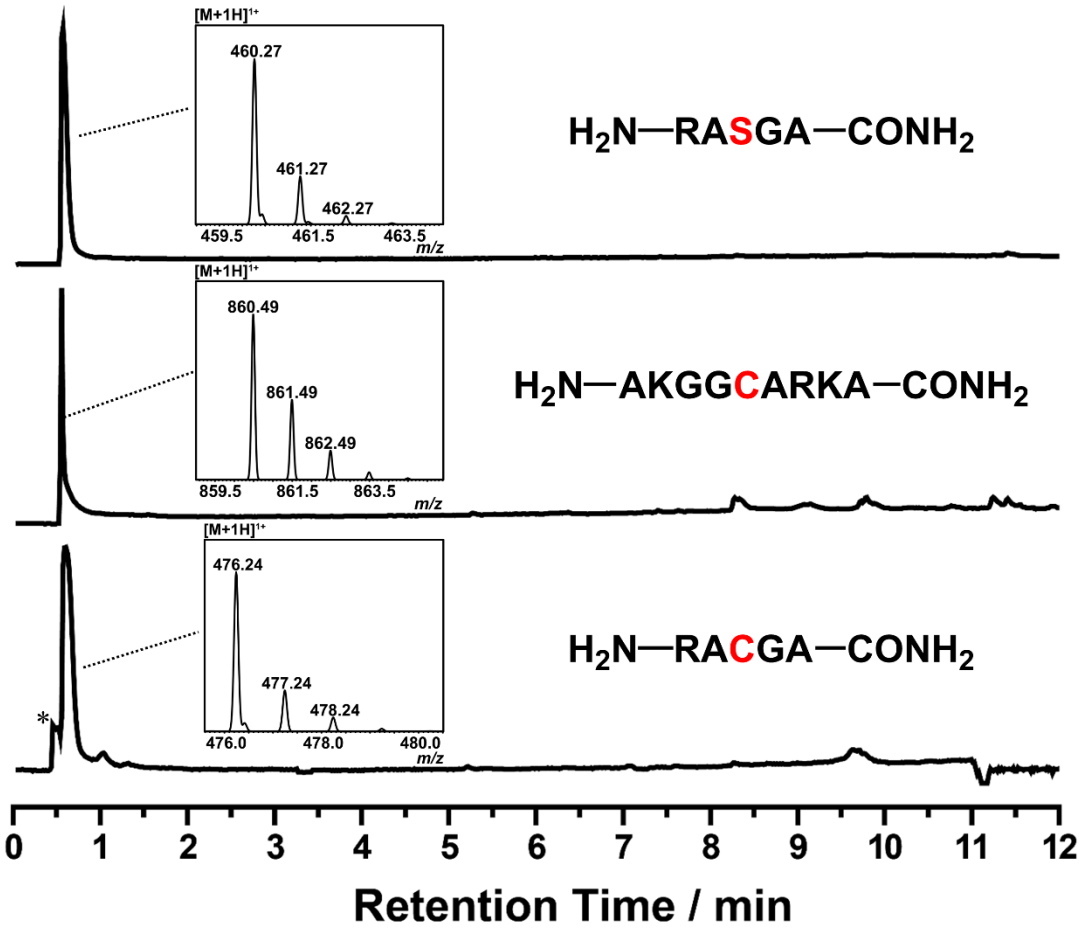

Figure D71. LC-MS traces for native peptides used in this study. (*) denotes Tris buffer (122 *m/z*). Top panel: 460.2605 (calc'd 460.2627) *m/z* for $C_{17}H_{33}N_9O_6$. Middle panel: 860.4908 (calc'd 860.4883) *m/z* for $C_{34}H_{65}N_{15}O_9S$. Bottom panel: 476.2416 (calc'd 476.2398) *m/z* for $C_{17}H_{33}N_9O_5S$.

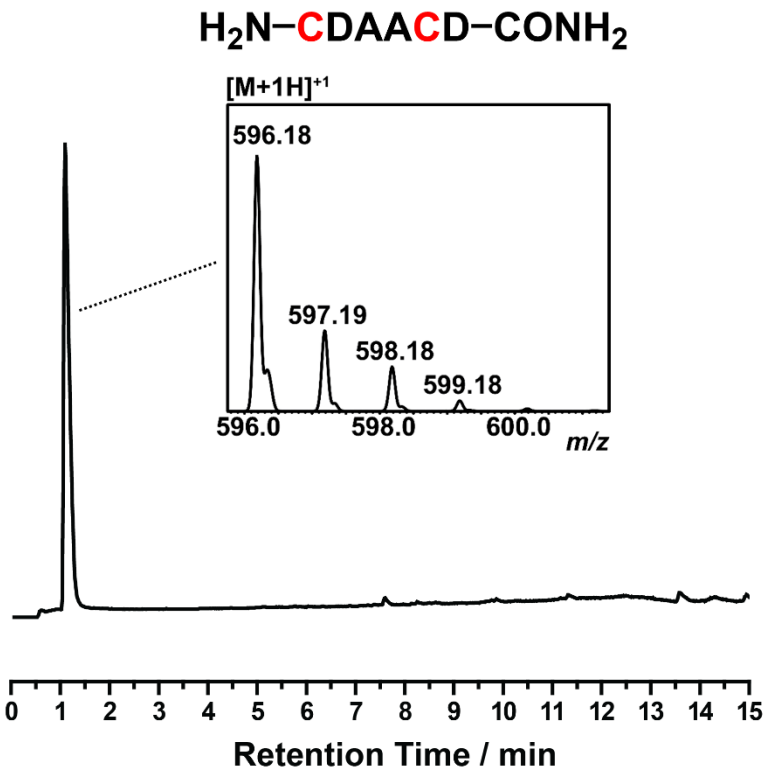

Figure D72. LC-MS trace for native dicysteine peptide. 596.1845 (calc'd 596.1803) *m/z* for $C_{20}H_{33}N_7O_{10}S_2$.

5.5.10 Procedures and Characterization for Cysteine Arylation

Procedure and Characterization Data for Peptide Arylation Studies Using Complex [1][NTf_2].

After the oxidative addition reaction of 4-iodotoluene with (DPCb)AuNTf_2 proceeded to quantitative conversion (>99%) as determined by ^{31}P NMR analysis, the reaction mixture was filtered through Celite and dichloromethane was removed from the filtrate under reduced pressure to produce a yellow solid. A 15 mM stock solution was prepared by dissolution of the obtained yellow solids in MeCN.

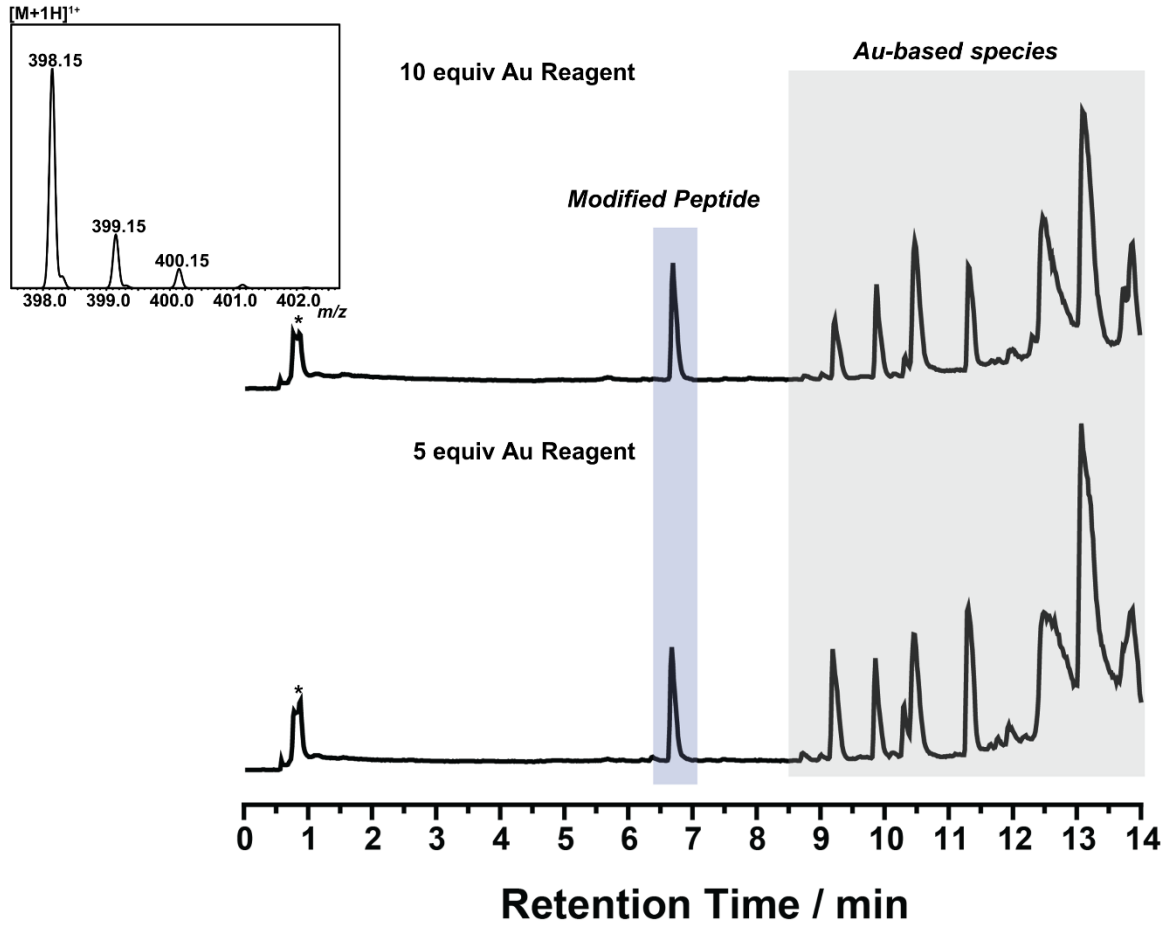

Figure D73. LC-MS traces for arylation of GSH using **1** at different reagent loadings. (*) denotes buffer. 398.1450 (calc'd 398.1380) *m/z* for $C_{17}H_{23}N_3O_6S$.

5.5.11 Procedure and Characterization Data for Water Equivalents Screen of Peptide Arylation Using [1][NTf_2].

After the oxidative addition reaction of 4-iodotoluene with (DPCb)AuNTf_2 proceeded to quantitative conversion (>99%), the solvent was removed under reduced pressure to produce a yellow solid. The yellow solid was dissolved in acetonitrile to prepare a 30 mM stock solution. Stock solutions of 15 mM and 10 mM were prepared from the initial 30 mM stock solution of the gold reagent in acetonitrile. A 2 mM solution of glutathione was prepared in 200 mM pH 8.0 Tris buffer. Reaction solutions were prepared in the following manner:

H_2O:MeCN	Gold Complex Stock Solution	Peptide Stock Solution	Water Added
90:10	10 μL of 30 mM	50 μL	40 μL
80:20	20 μL of 15 mM	50 μL	30 μL
70:30	30 μL of 10 mM	50 μL	20 μL

To a 2 mL Eppendorf tube was added 50 μL of the peptide stock solution and the appropriate amount of water (MilliQ). To this solution was added the appropriate amount of gold reagent stock solution, and the Eppendorf tube was vortexed (<5 seconds). After 1 min, a 20 μL aliquot was removed and diluted in a 100 μL solution of 1:1 H_2O:MeCN with 0.1% mol TFA. An aliquot from this solution was analyzed via LCMS.

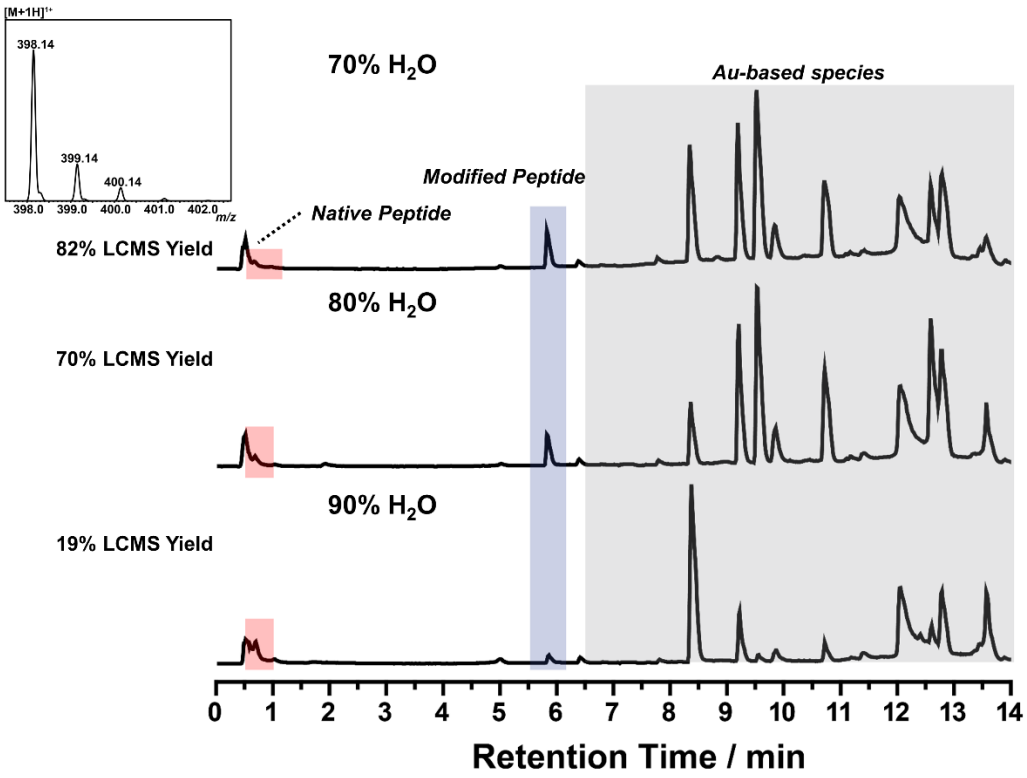

Figure D74. LC-MS traces for arylation of GSH using [**1**][NTf_2] in different water concentrations. 398.1433 (calc'd 398.1380) *m/z* for $C_{17}H_{23}N_3O_6S$.

5.5.12 Procedure and Characterization Data for Reagent Equivalents Screen of Peptide Arylation Using [2a][SbF_6].

Acetonitrile solutions of [**2a**][SbF_6] were prepared in 6, 4, and 2 mM concentrations. A 2 mM solution of glutathione was prepared in 200 mM pH 8.0 Tris buffer. In a 2 mL Eppendorf tube was added 20 µL of the peptide solution and 20 µL of the reagent solution, and the sample was then vortexed (<5 seconds). At one min, a 20 µL aliquot was removed from the reaction mixture and diluted in 100 µL of a solution of 1:1 H_2O:MeCN with 0.1% TFA. An aliquot from this solution was analyzed via LCMS.

Reagent:Peptide	Gold Complex Stock	Peptide Stock
3:1	20 μL of 6 mM	20 μL
2:1	20 μL of 4 mM	20 μL
1:1	20 μL of 2 mM	20 μL

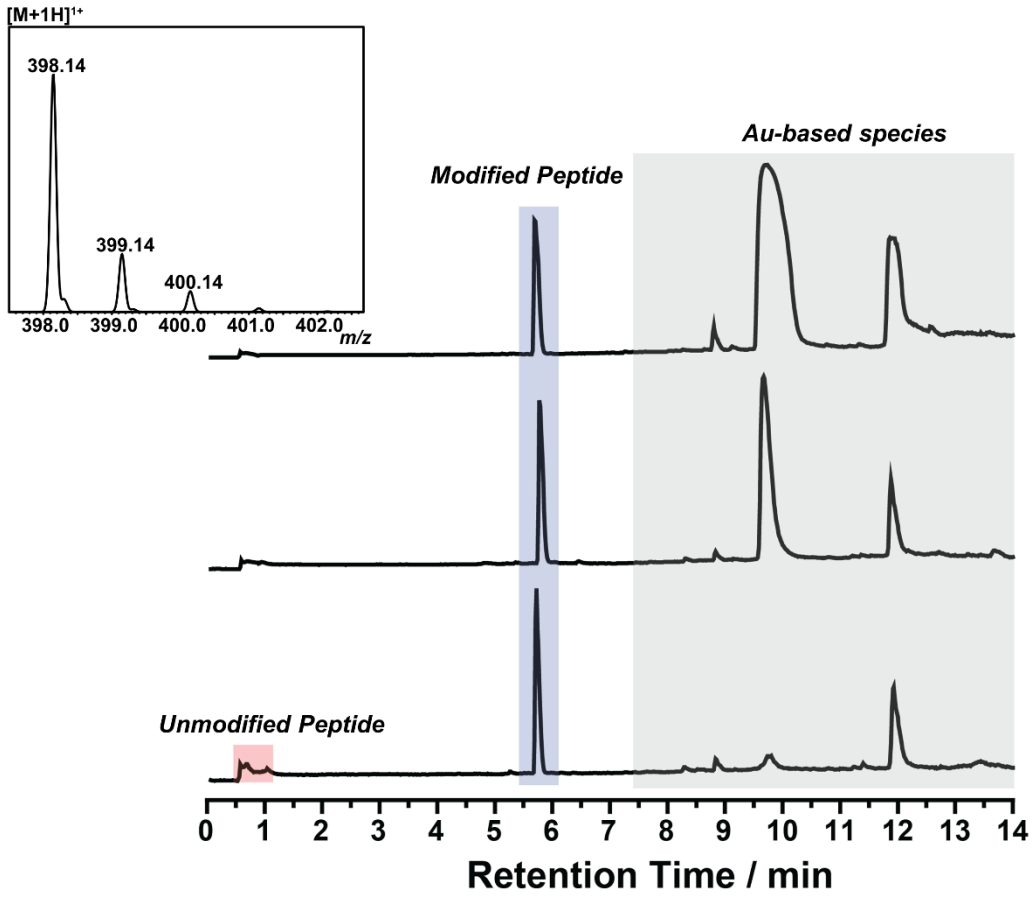

Figure D75. LC-MS traces for arylation of GSH using [**2a**][SbF_6] at different reagent loadings. 398.1417 (calc'd 398.1380) *m/z* for $C_{17}H_{23}N_3O_6S$.

5.5.13 Procedure and Characterization Data for Water Equivalents Screen of Peptide Arylation Using [2a][SbF_6]

Acetonitrile solutions of [**2a**][SbF_6] at 30, 15, and 10 mM concentrations were prepared. A 2 mM solution of glutathione was prepared in 200 mM pH 8.0 Tris buffer. Reaction solutions were prepared in the following manner:

H_2O:MeCN	Gold Complex Stock	Peptide Stock	Water Added
90:10	10 μL of 30 mM	50 μL	40 μL
80:20	20 μL of 15 mM	50 μL	30 μL
70:30	30 μL of 10 mM	50 μL	20 μL

To a 2 mL Eppendorf tube was added 50 μL of peptide stock solution and appropriate amount of water (MilliQ). To this solution was added the appropriate amount of gold reagent stock solution, and the Eppendorf tube was vortexed (<5 seconds). At one min, a 20 μL aliquot was removed and diluted in a 100 μL solution of 1:1 H_2O:MeCN with 0.1% mol TFA. An aliquot from this solution was analyzed *via* LCMS.

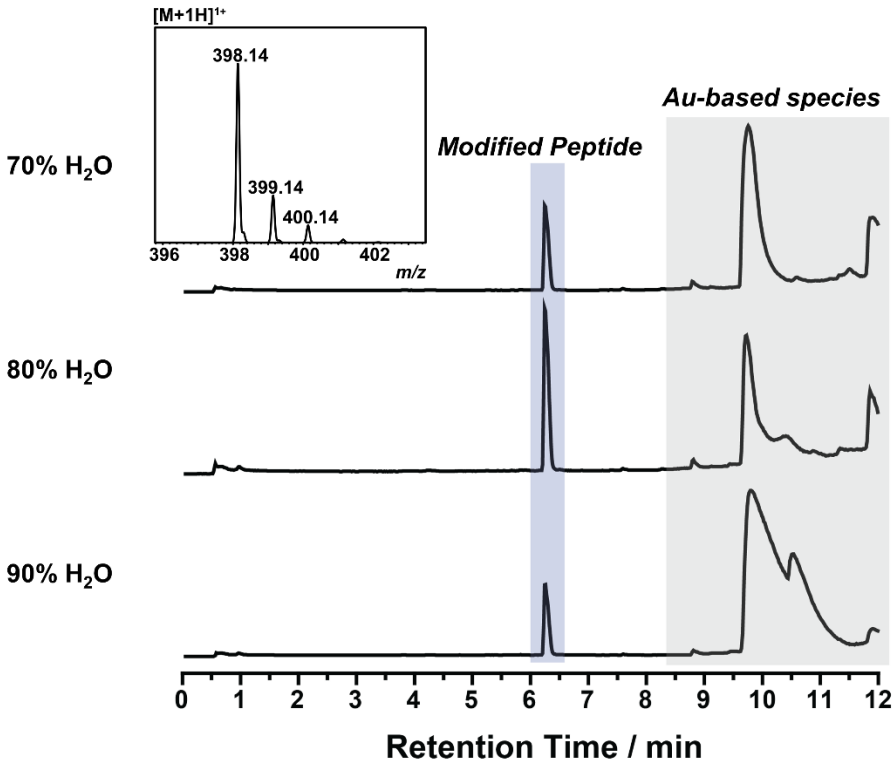

Figure D76. LC-MS traces for arylation of GSH using [**2a**][SbF_6] in different water concentrations. 398.1417 (calc'd 398.1380) *m/z* for $C_{17}H_{23}N_3O_6S$.

5.5.14 Procedure and Characterization Data for Buffer and pH Screen of Peptide Arylation Using [2a][SbF_6]

A 15 mM solution of [**2a**][SbF_6] in MeCN was prepared, and a 2 mM solution of glutathione was prepared in 1 M buffer.

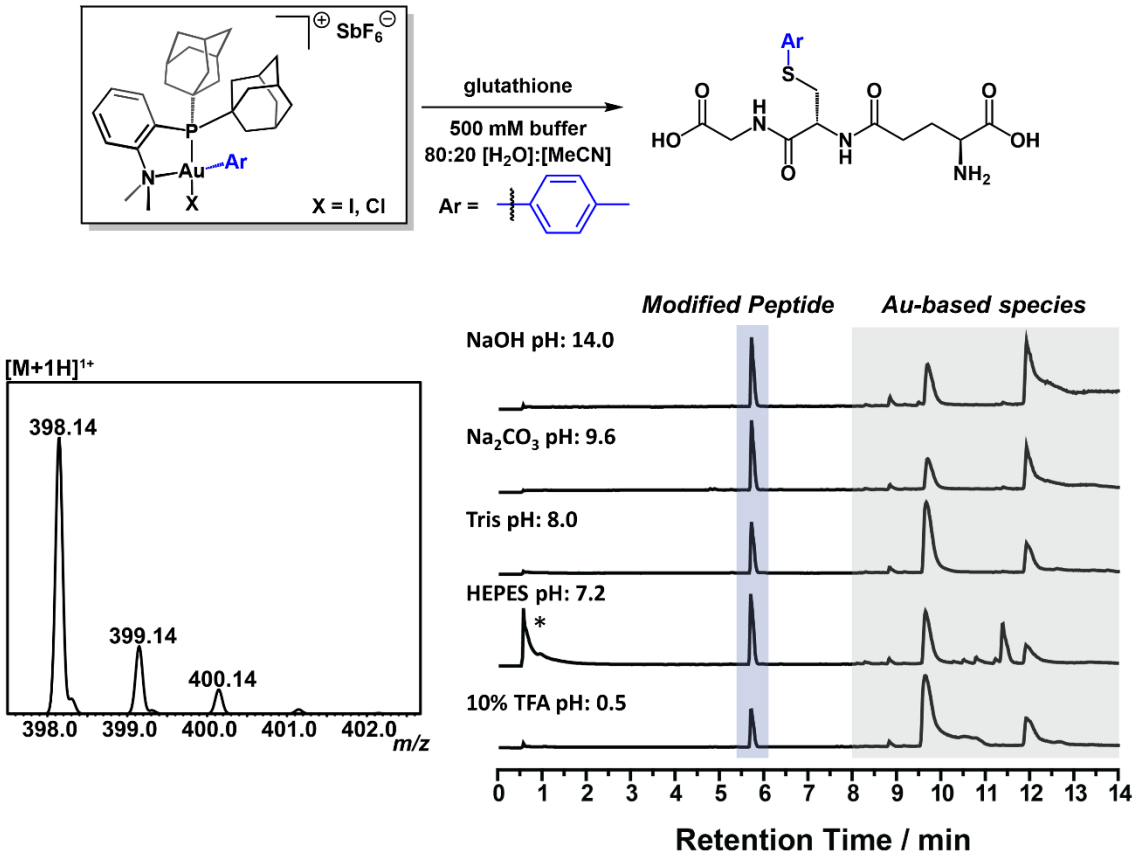

Figure D77. LC-MS traces for arylation of GSH using [**2a**][SbF_6] in different pH ranges. (*) denotes buffer. 398.1417 (calc'd 398.1380) *m/z* for $C_{17}H_{23}N_3O_6S$.

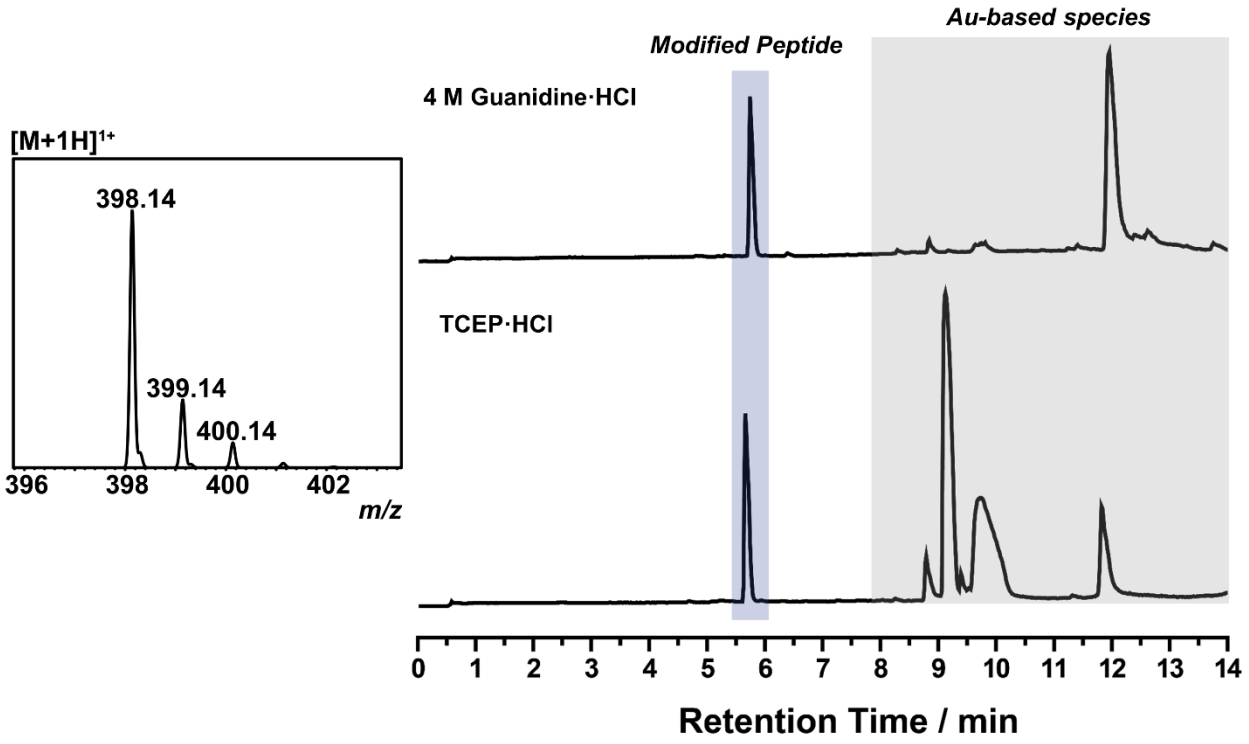

Figure D78. LC-MS traces for arylation of GSH using [**2a**][SbF_6] in the presence of 4 M guanidine·HCl (top) and TCEP·HCl. 398.1399 (calc'd 398.1380) *m/z* for $C_{17}H_{23}N_3O_6S$.

5.5.15 Cysteine Arylation in Unconventional Solvents

To a 2 mL Eppendorf tube was added 10 µL of peptide stock (20 mM) solution in 200 mM Tris pH 8.0 and 70 µL of solvent. To this solution was added 20 µL of the gold reagent stock solution (15 mM) in acetonitrile, and the Eppendorf tube was vortexed (<5 seconds). At one min, a 20 µL aliquot was removed and diluted in a 100 µL solution of 1:1 H_2O:MeCN with 0.1% mol TFA. An aliquot from this solution was analyzed *via* LCMS.

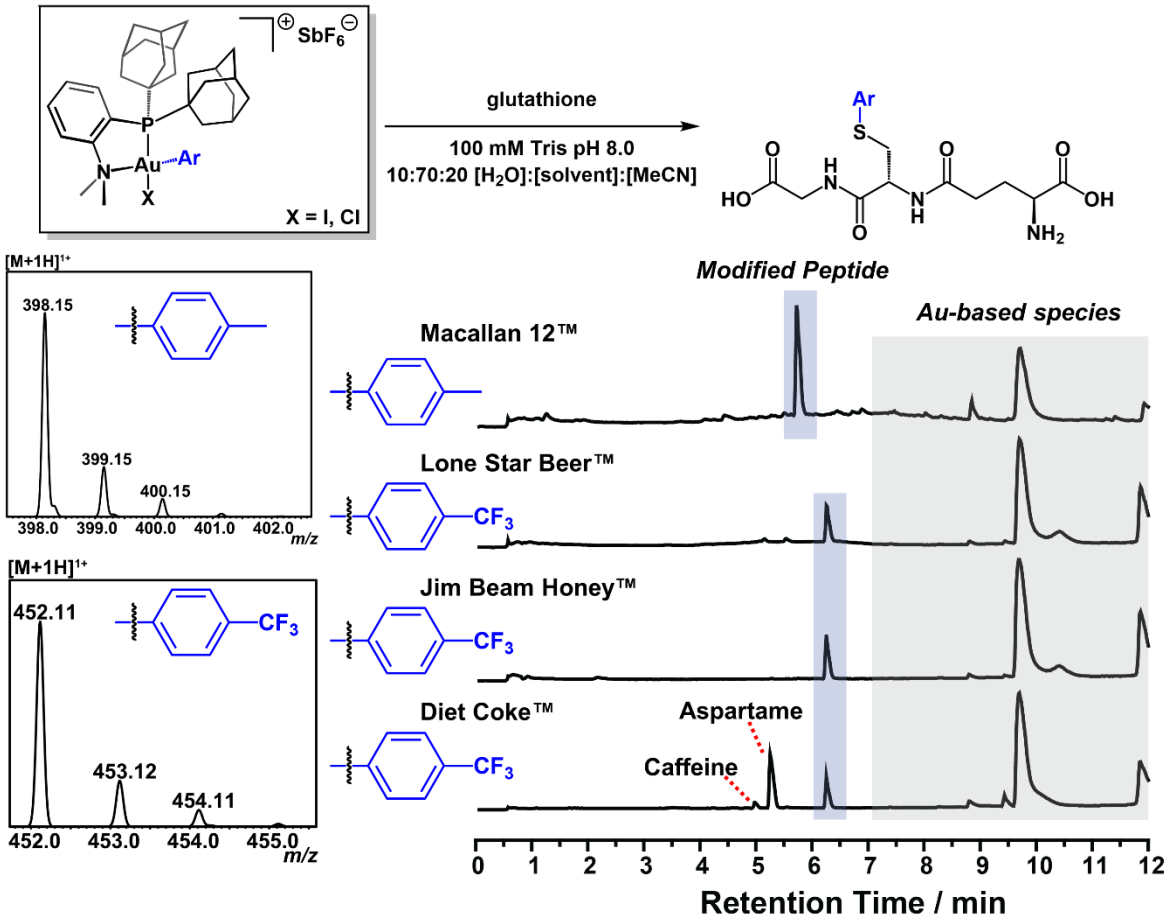

Figure D79. Arylation in unconventional solvents using [**2a**][SbF_6] and [**2b**][SbF_6]. Tolyl modified GSH: 398.1413 (calc'd 398.1380) *m/z* for $C_{17}H_{23}N_3O_6S$. *p*-CF_3 modified GSH: 452.1142 (calc'd 452.1098) *m/z* for $C_{17}H_{20}F_3N_3O_6S$.

5.5.16 Substrate Scope for Glutathione

To a 2 mL Eppendorf tube was added 50 µL of peptide stock solution in 1 M Tris pH 8.0 and 30 µL of water (MilliQ). To this solution was added 20 µL of a 15 mM gold reagent stock solution, and the Eppendorf tube was vortexed (<5 seconds). At one min, a 20 µL aliquot was removed and diluted in a 100 µL solution of 1:1 H_2O:MeCN with 0.1% mol TFA. An aliquot from this solution was analyzed *via* LCMS.

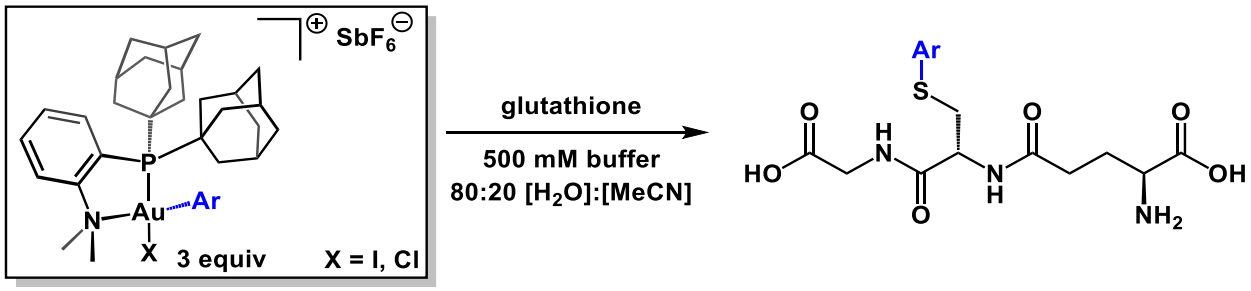

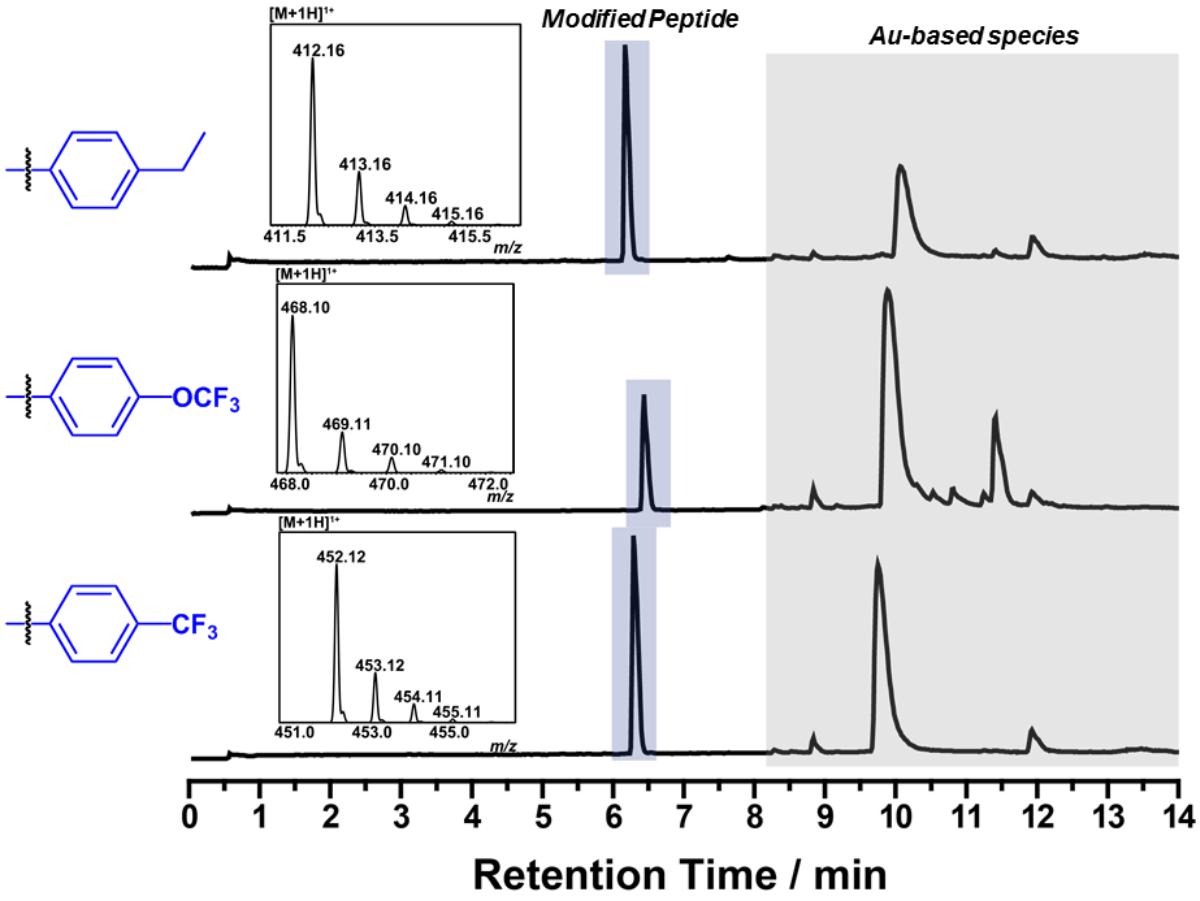

Figure D80. LC-MS traces for arylation of GSH using [**2b**][SbF_6], [**2g**][SbF_6], and [**2d**][SbF_6] with optimized conditions. Top panel: 412.1587 (calc'd 412.1537) *m/z* for $C_{18}H_{25}N_3O_6S$. Middle panel: 468.1099 (calc'd 468.1047) *m/z* for $C_{17}H_{20}F_3N_3O_7S$. Bottom panel: 452.1152 (calc'd 452.1098) *m/z* for $C_{17}H_{20}F_3N_3O_6S$.

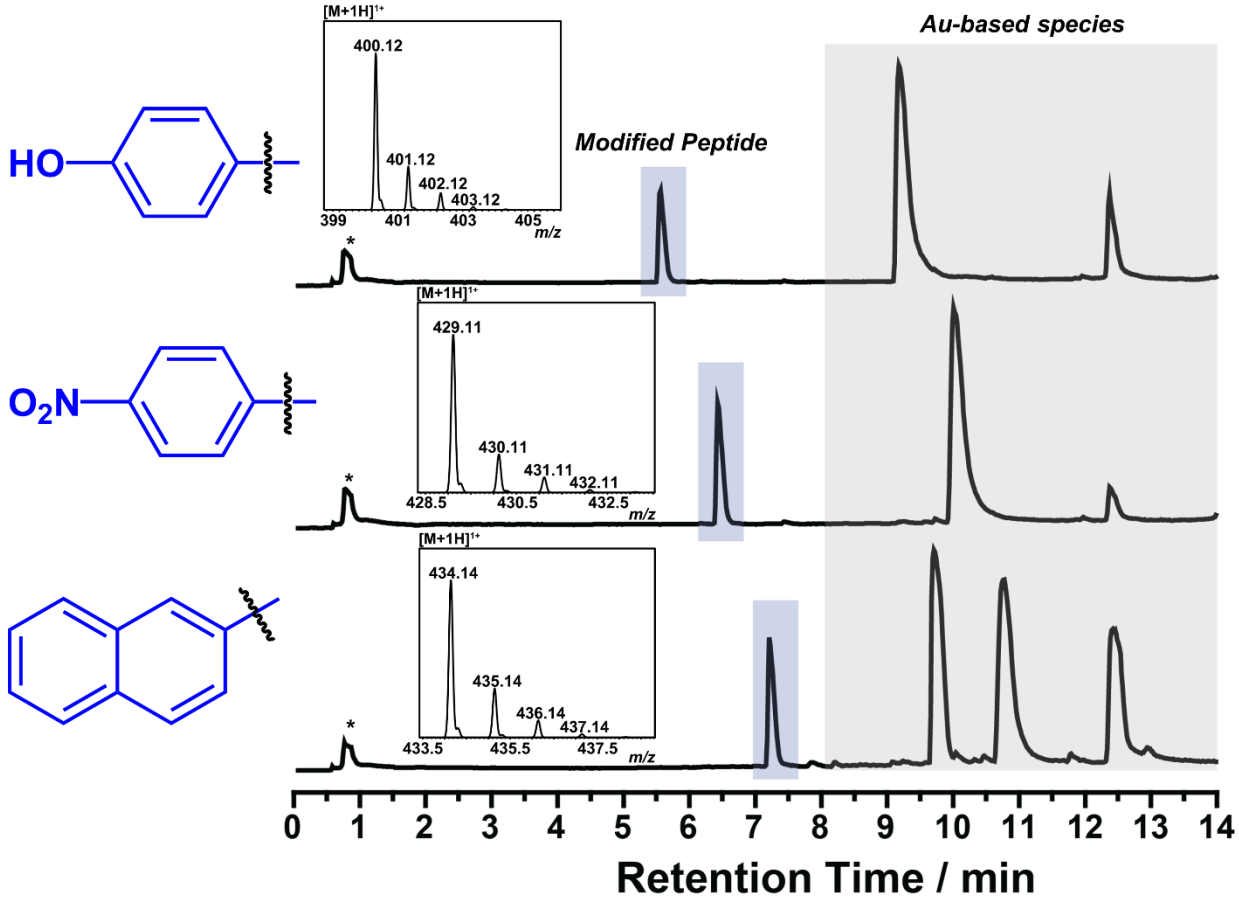

Figure D81. LC-MS traces for arylation of GSH using [**2f**][SbF_6], [**2h**][SbF_6], and [**2c**][SbF_6] with optimized conditions. (*) denotes Tris buffer (122 *m/z*). Top panel: 400.1200 (calc'd 400.1173) *m/z* for $C_{16}H_{21}N_3O_7S$. Middle panel: 429.1124 (calc'd 429.1075) *m/z* for $C_{16}H_{20}N_4O_8S$. Bottom panel: 434.1428 (calc'd 434.1380) *m/z* for $C_{20}H_{23}N_3O_6S$.

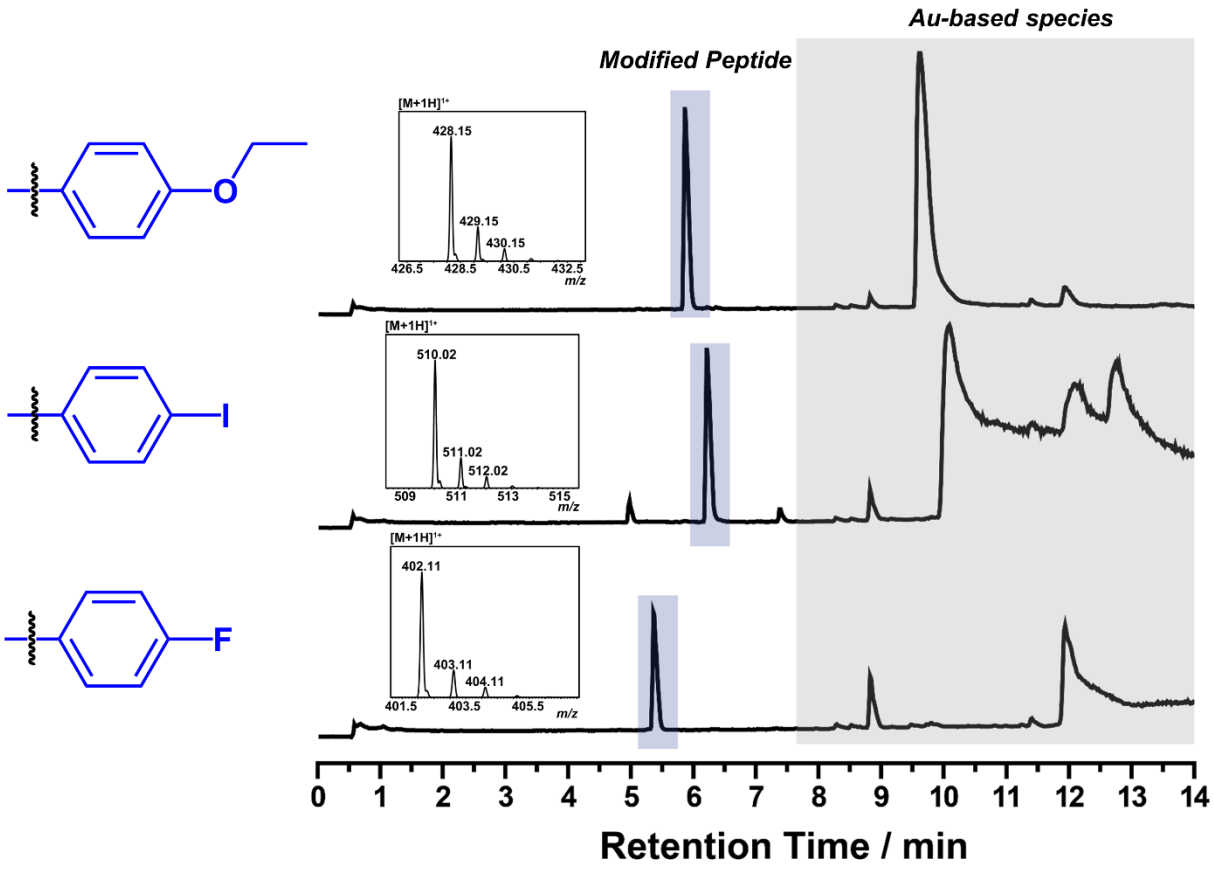

Figure D82. LC-MS traces for arylation of GSH using [**2e**][SbF_6], [**2k**][SbF_6], and [**2l**][SbF_6] with optimized conditions. Top panel: 428.1533 (calc'd 428.1486) *m/z* for $C_{18}H_{25}N_3O_7S$. Middle panel: 510.0217 (calc'd 510.0190) *m/z* for $C_{16}H_{20}N_3O_6IS$. Bottom panel: 402.1166 (calc'd 402.1130) *m/z* for $C_{16}H_{20}N_3O_6FS$.

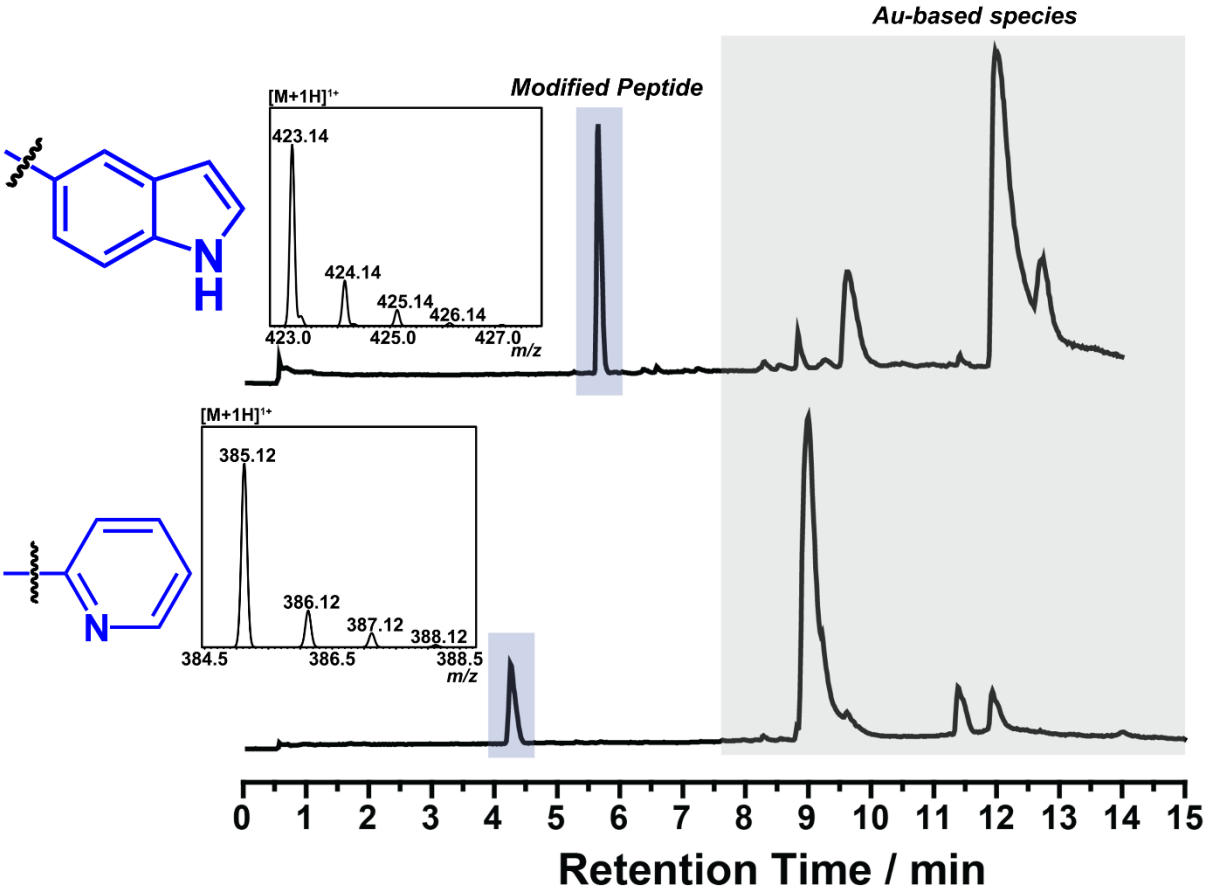

Figure D83. LC-MS traces for arylation of GSH using [**2p**][SbF_6] and [**2m**][SbF_6] with optimized conditions. Top panel: 423.1362 (calc'd 423.1333) *m/z* for $C_{18}H_{22}N_4O_6S$. Bottom panel: 385.1205 (calc'd 385.1176) *m/z* for $C_{15}H_{20}N_4O_6S$.

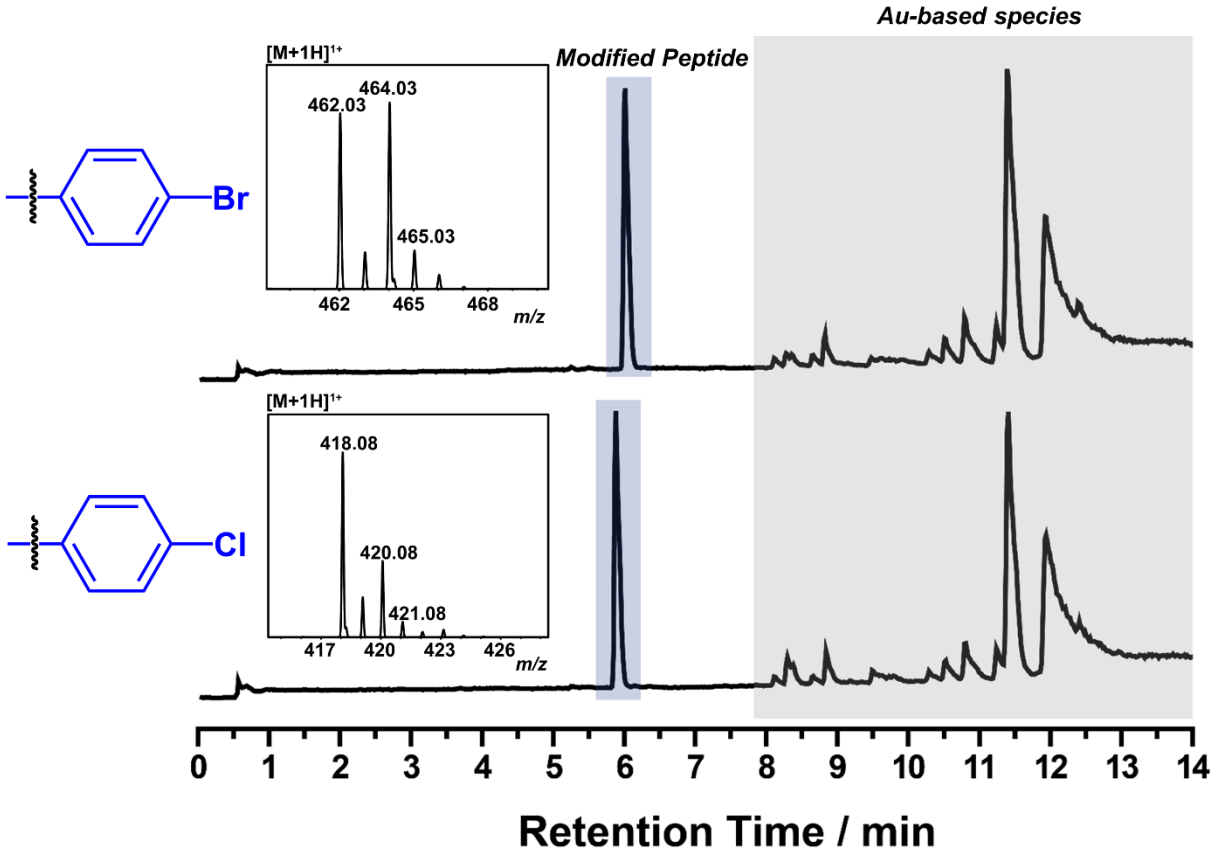

Figure D84. LC-MS traces for arylation of GSH using [**2j**][SbF_6] and [**2i**][SbF_6] with optimized conditions. Top panel: 462.0359 (calc'd 462.0329) *m/z* for $C_{16}H_{20}N_3O_6BrS$. Bottom panel: 418.0869 (calc'd 418.0834) *m/z* for $C_{16}H_{20}N_3O_6ClS$.

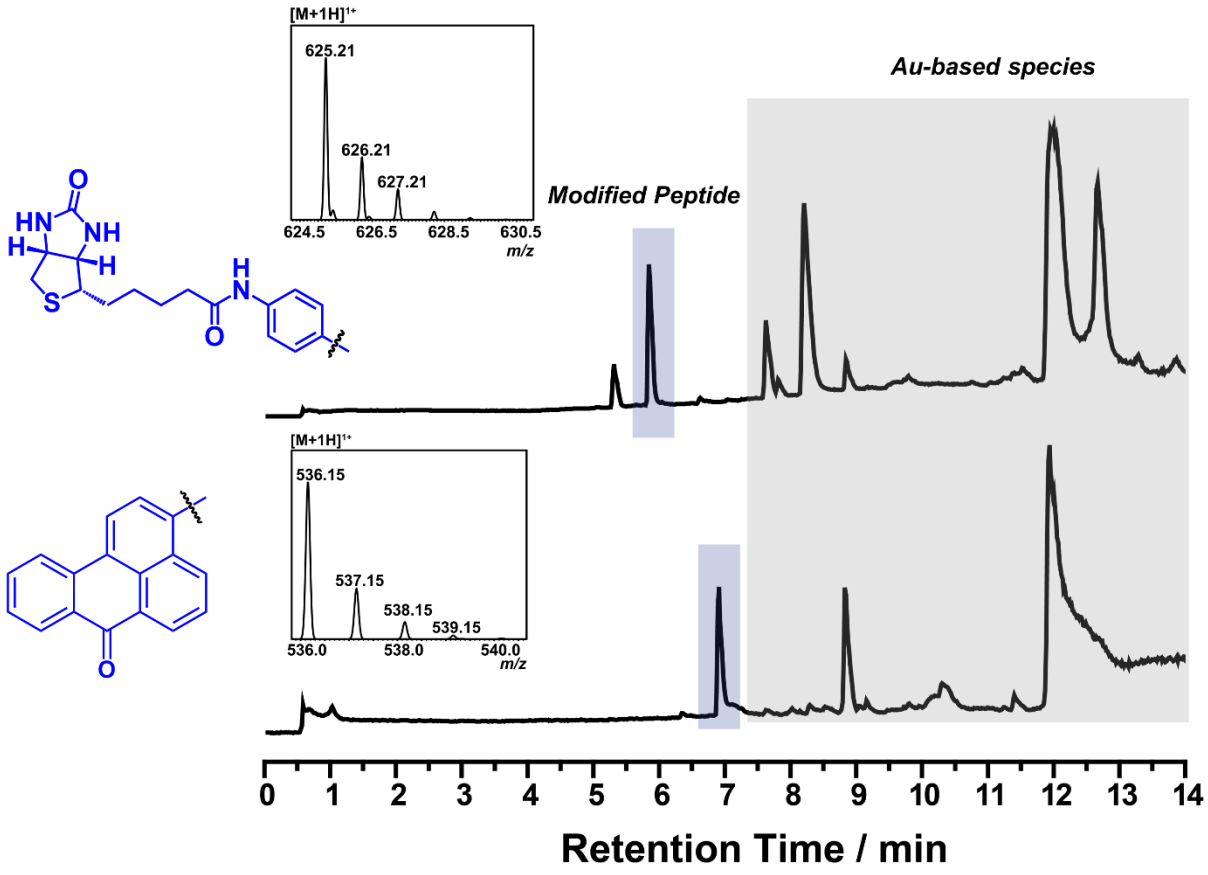

Figure D85. LC-MS traces for arylation of GSH using [**2q**][SbF_6] and [**2r**][SbF_6] with optimized conditions. Top panel: 625.2135 (calc'd 652.2109) *m/z* for $C_{26}H_{36}N_6O_8S_2$. Bottom panel: 536.1512 (calc'd 536.1486) *m/z* for $C_{27}H_{25}N_3O_7S$.

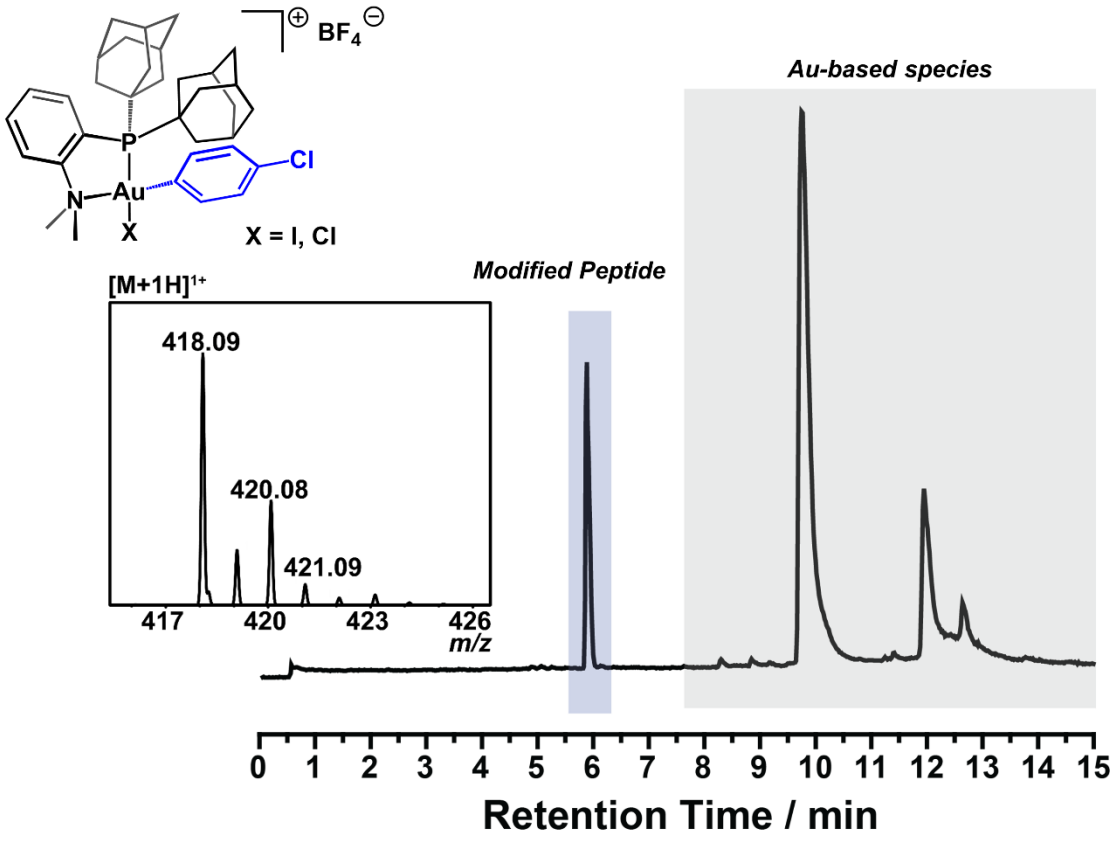

Figure D86. Modification of glutathione using [**2i**][BF_4] with optimized conditions. 418.0866 (calc'd 418.0834) *m/z* for $C_{16}H_{20}N_3O_6ClS$.

5.5.17 Au(III) and Pd(II) Competition Experiments with GSH

To 50 µL of a 2 mM GSH solution in 100 mM Tris buffer (pH 8.0) was added 20 µL of water followed by 45 µL of a mixture of [**2b**][SbF_6] (15 µL of a 10 mM MeCN solution) and (RuPhos)Pd(tolyl)I (30 µL of a 20 mM MeCN solution) in MeCN. The reaction mixture was vortexed for ca. 10 sec, and then allowed to stand at room temperature for 5 min. A 20 µL aliquot from the mixture was then diluted with a solution of thiopropionic acid (10 µL of a 0.3 M solution in H_2O) in a 1:1 H_2O:MeCN mixture with 0.1% TFA. An aliquot from this solution was analyzed by LCMS.

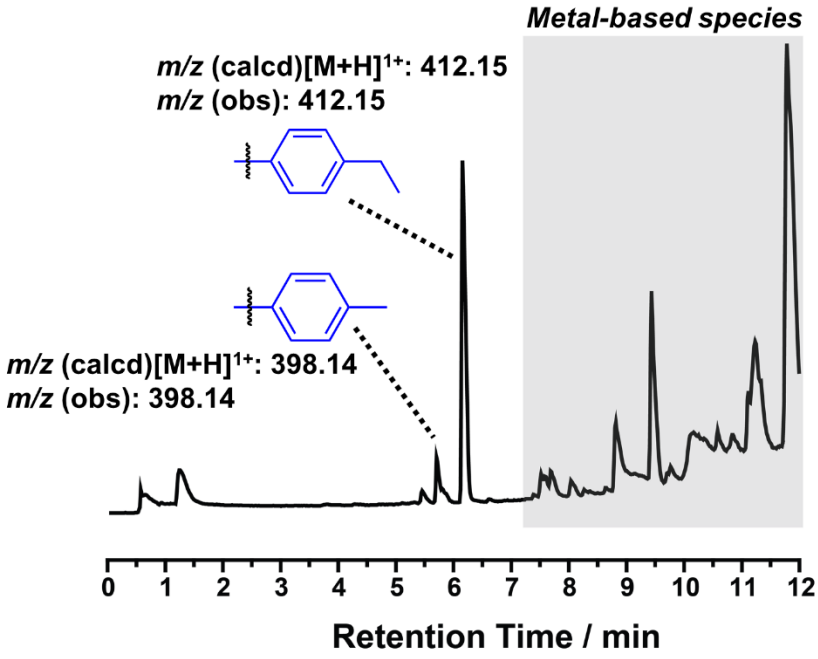

Figure D87. Representative LCMS trace for Au(III) and Pd(II) competition experiments. Ethylbenzene modified GSH: 412.1577 (calc'd 412.1537) *m/z* for $C_{18}H_{25}N_3O_6S$. Tolyl modified GSH: 398.1401 (calc'd 398.1380) *m/z* for $C_{17}H_{23}N_3O_6S$.

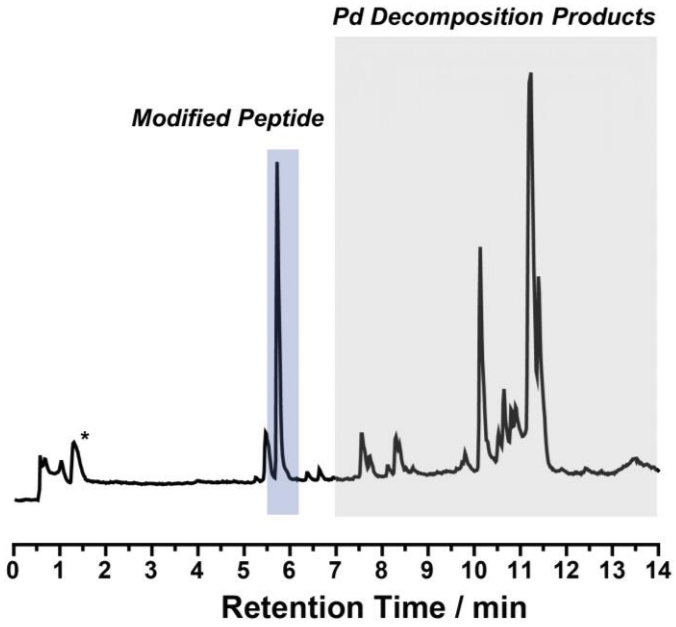

Figure D88. Modification of GSH using (RuPhos)Pd(tolyl)I in conditions replicating those used in Scheme 5-2 of the main text (100 mM Tris pH 8.0, 6:4 [H_2O]:[MeCN]).

5.5.18 Preparation of *S*-(*p*-Cl-C_6H_4) GSH conjugate

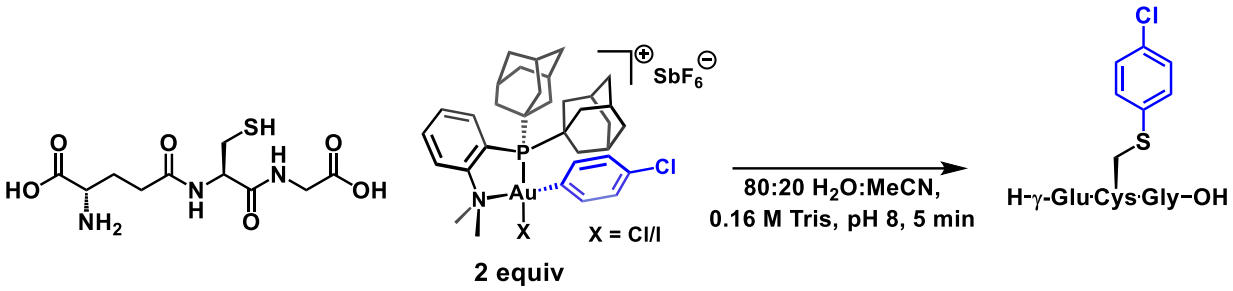

To a solution of GSH (16 mg, 0.052 mmol, 1.0 equiv) in H_2O (8 mL, 0.2 M Tris, pH 8) was added a suspension of [**2i**][SbF_6] (116 mg, 0.116 mmol, 2.23 equiv) in MeCN (2 mL). The resulting suspension was sonicated for 30 sec, and then allowed to stand at 25 °C for an additional 4.5 min. The reaction mixture was then diluted with a 50/50 mixture of MeCN/H_2O containing 0.1%TFA, and the resulting suspension was centrifuged for 2 min, at which point the supernatant was decanted and passed through a 0.45 μm filter. The filtrate was lyophilized and the obtained solid was dissolved in H_2O containing 0.1% TFA and purified by semi-preparative reversed-phase HPLC.

Solvent compositions for reversed-phase HPLC purification were: H_2O with 0.1% TFA (solvent A), MeCN with 0.1% TFA (solvent B). 0-5 min, 100% A; 5-60 min, linear gradient 100-60% A; 65-75 min, linear gradient 40-100% B. Flow rate: 3 mL/min. HPLC fractions containing the pure product were further confirmed by LC-MS, combined, and lyophilized.

ICP-AES was used to measure the remaining gold content in the purified *S*-(*p*-Cl-C_6H_4) GSH conjugate. Of the isolated material, 3.85 mg was dissolved in 10 mL of a 2% HCl (aq) solution (385 ppm concentration), and the material was filtered through a 0.45 μm filter. The resulting solution was analyzed by ICP-AES, and the concentration of gold in this sample was determined to be 55 ppb. This analysis indicates >99.9% efficiency for the removal of gold-containing species by the described purification procedure.

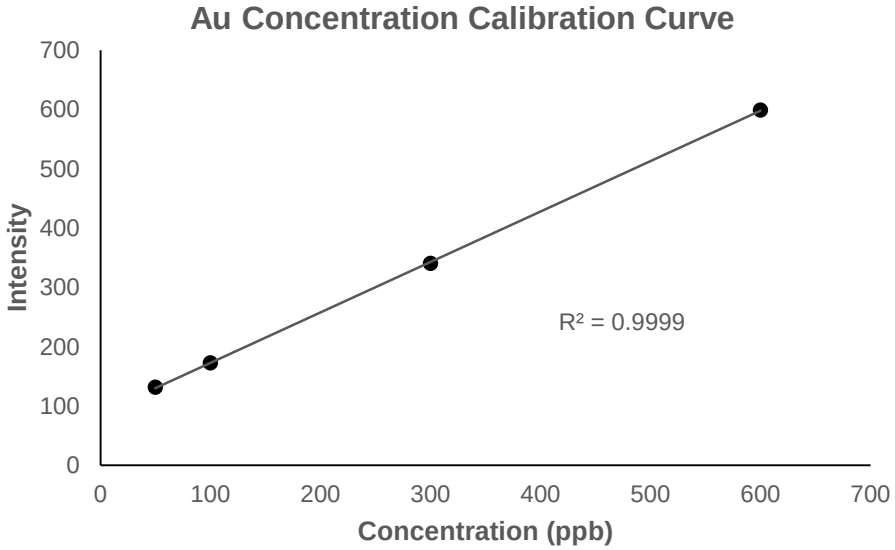

5.5.19 Substrate Scope for Larger Peptide Sequences

To a 2 mL Eppendorf tube was added 50 µL of peptide stock solution in 200 mM Tris pH 8.0 and 30 µL of water (MilliQ). To this solution was added 20 µL of a 15 mM gold reagent stock solution, and the Eppendorf tube was vortexed (<5 seconds). At one min, a 20 µL aliquot was removed and diluted in a 100 µL solution of 1:1 H_2O:MeCN with 0.1% mol TFA. An aliquot from this solution was analyzed *via* LCMS.

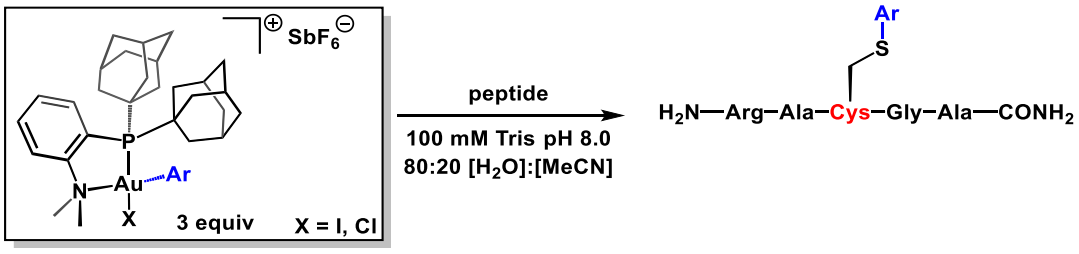

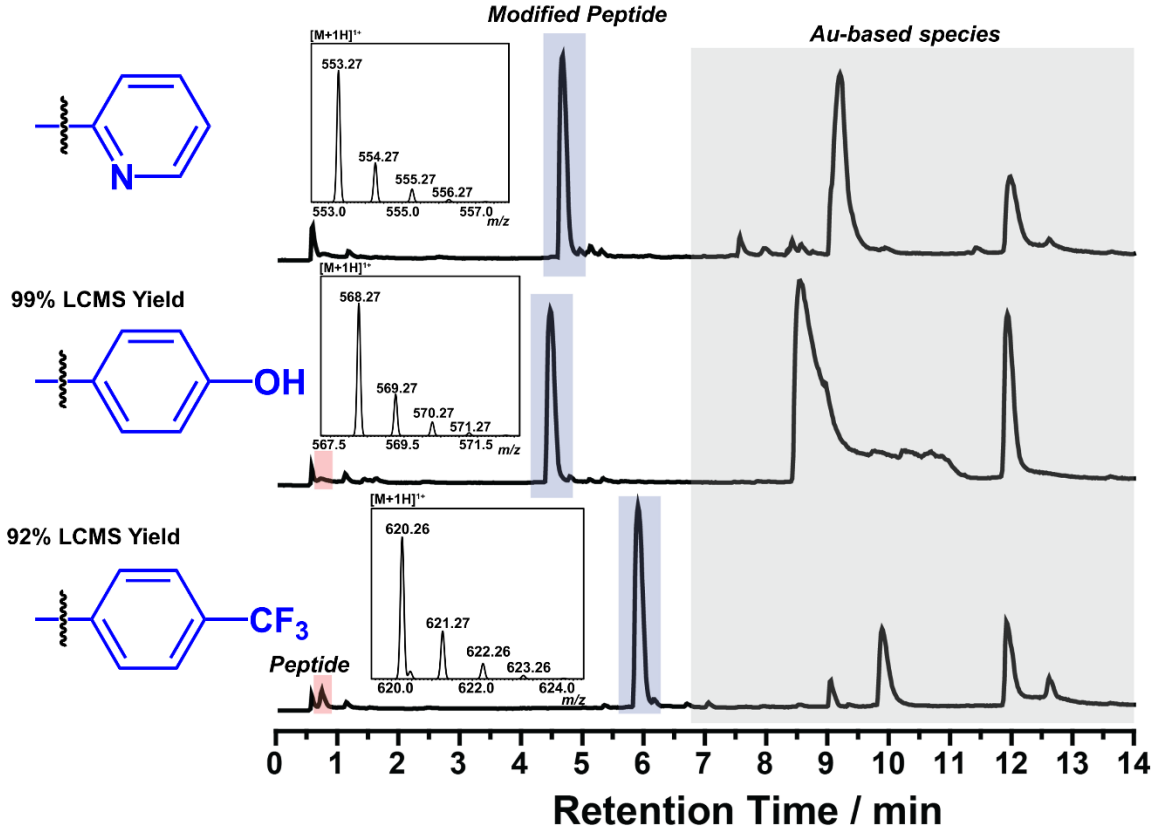

Figure D89. LC-MS traces for arylation of unprotected peptide using [**2m**][SbF_6], [**2f**][SbF_6], and [**2d**][SbF_6] with optimized conditions. Top panel: 553.2710 (calc'd 553.2664) *m/z* for $C_{22}H_{36}N_{10}O_5S$. Middle panel: 568.2700 (calc'd 568.2660) *m/z* for $C_{23}H_{37}N_9O_6S$. Bottom panel: 620.2639 (calc'd 620.2585) *m/z* for $C_{24}H_{36}F_3N_9O_5S$.

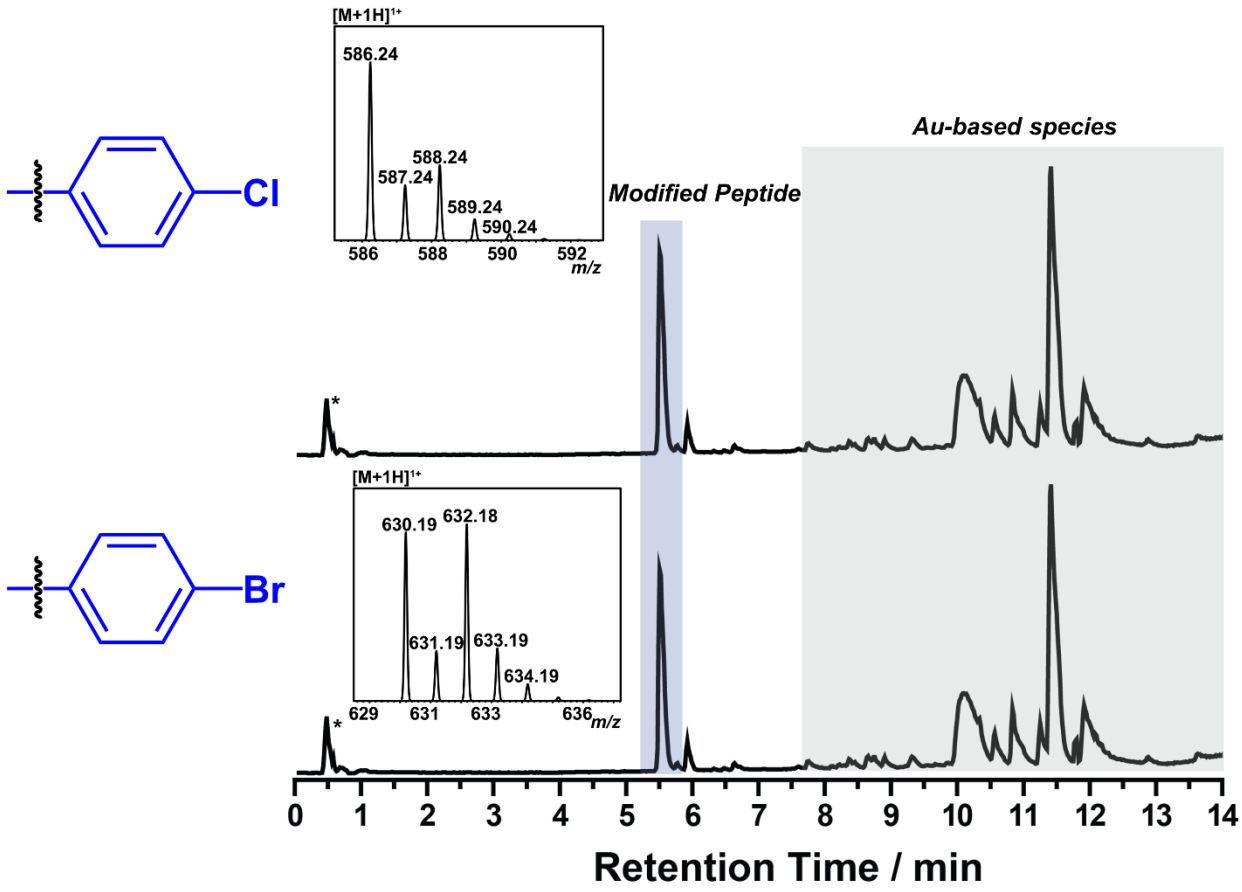

Figure D90. LC-MS traces for arylation of unprotected peptide using [**2i**][SbF_6] and [**2j**][SbF_6] with optimized conditions. (*) denotes Tris buffer (122 *m/z*). Top panel: 586.2371 (calc'd 586.2321) *m/z* for $C_{23}H_{36}ClN_9O_5S$. Bottom panel: 630.1864 (calc'd 630.1816) *m/z* for $C_{23}H_{36}BrN_9O_5S$.

To a 2 mL Eppendorf tube was added 50 µL of peptide stock solution in 1 M Tris pH 8.0. To this solution was added 50 µL of a 6 mM gold reagent stock solution, and the Eppendorf tube was vortexed (<5 seconds). At one min, a 20 µL aliquot was removed and diluted in a 100 µL solution of 1:1 H_2O:MeCN with 0.1% mol TFA. An aliquot from this solution was analyzed *via* LCMS.

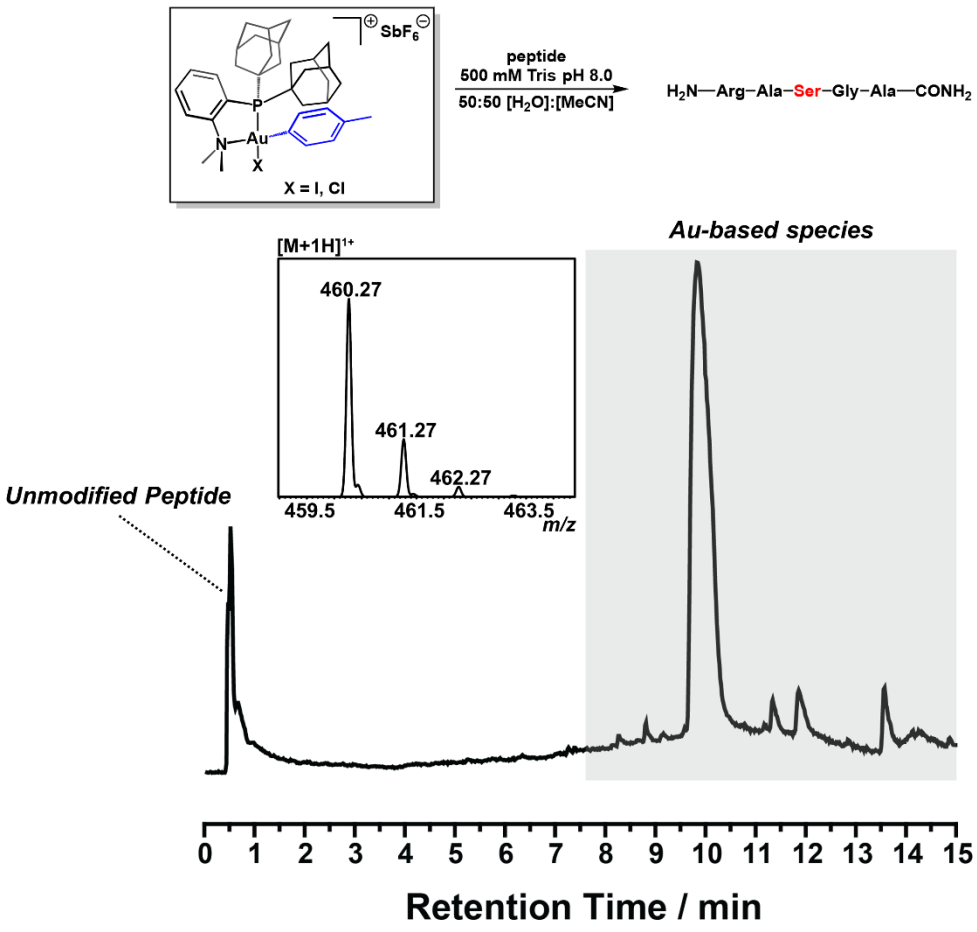

Figure D91. LC-MS trace of control reaction using serine substituted peptide. 460.2596 (calc'd 460.2627) *m/z* for $C_{17}H_{33}N_9O_6$.

To a 2 mL Eppendorf tube was added 50 µL of peptide stock solution in 200 mM Tris pH 8.0 and 30 µL of water (MilliQ). To this solution was added 20 µL of a 15 mM gold reagent stock solution in acetonitrile, and the Eppendorf tube was vortexed (<5 seconds). At one min, a 20 µL aliquot was removed and diluted in a 100 µL solution of 1:1 H_2O:MeCN with 0.1% mol TFA. An aliquot from this solution was analyzed *via* LCMS.

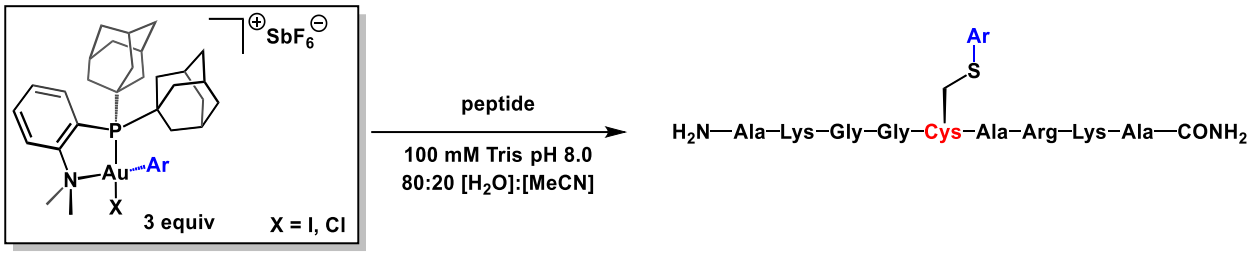

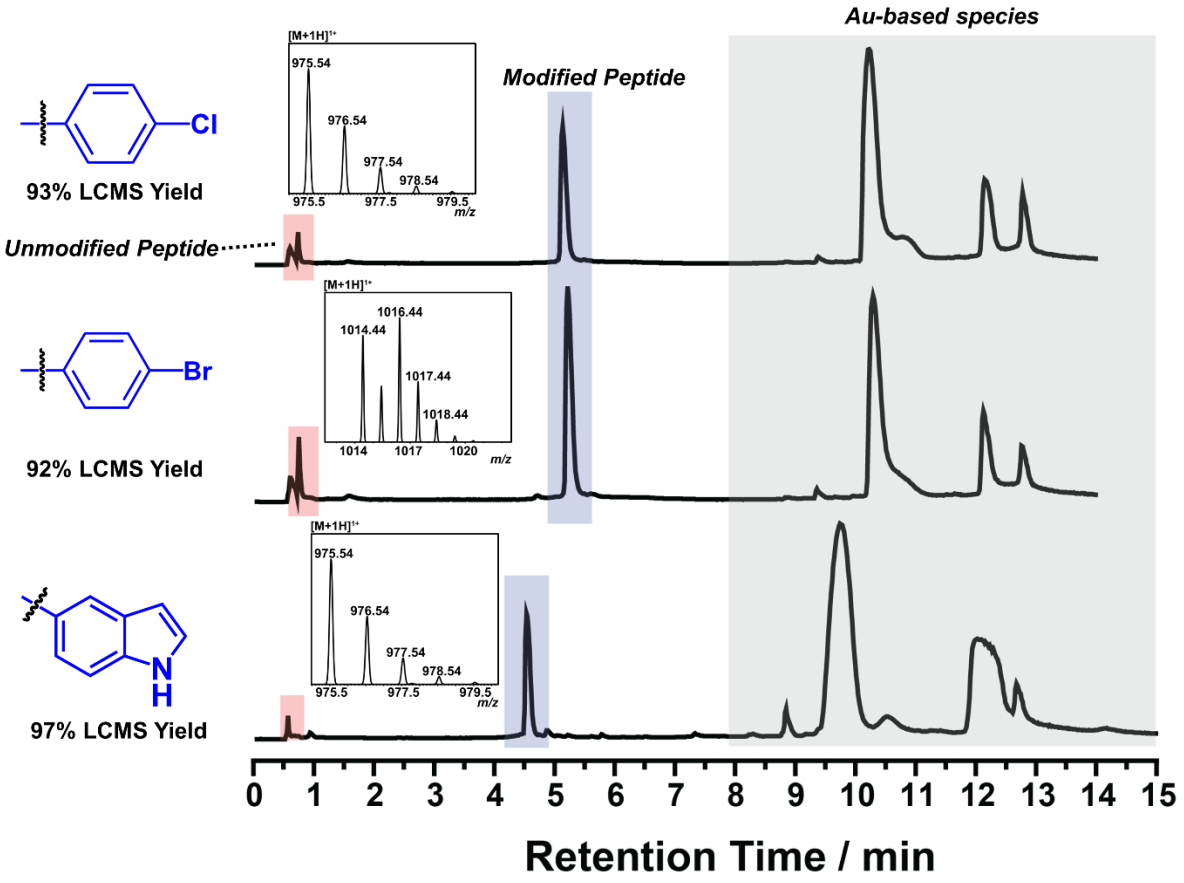

Figure D92. LC-MS traces for arylation of unprotected peptide using [**2i**][SbF_6], [**2j**][SbF_6], and [**2p**][SbF_6] with optimized conditions. Top panel: 970.4885 (calc'd 970.4806) *m/z* for $C_{40}H_{68}ClN_{15}O_9S$. Middle panel: 1014.4373 (calc'd 1014.4301) *m/z* for $C_{40}H_{68}BrN_{15}O_9S$. Bottom panel: 975.5369 (calc'd 975.5305) *m/z* for $C_{42}H_{70}N_{16}O_9S$.

Cysteine arylation using compound **2o**: To a 2 mL Eppendorf tube was added 50 µL of peptide stock solution in 200 mM Tris pH 8.0. To this solution was added 50 µL of a 6 mM gold reagent stock solution in water (MilliQ), and the Eppendorf tube was vortexed (<5 seconds). At one min, a 20 µL aliquot was removed and diluted in a 100 µL solution of 1:1 H_2O:MeCN with 0.1% mol TFA. An aliquot from this solution was analyzed *via* LCMS. Cysteine arylation using compound **2q** To a 2 mL Eppendorf tube was added 50 µL of peptide stock solution in 200 mM Tris pH 8.0

and 20 µL of water (MilliQ). To this solution was added 30 µL of a 10 mM gold reagent stock solution in acetonitrile, and the Eppendorf tube was vortexed (<5 seconds). At one min, a 20 µL aliquot was removed and diluted in a 100 µL solution of 1:1 H_2O:MeCN with 0.1% mol TFA. An aliquot from this solution was analyzed *via* LCMS.

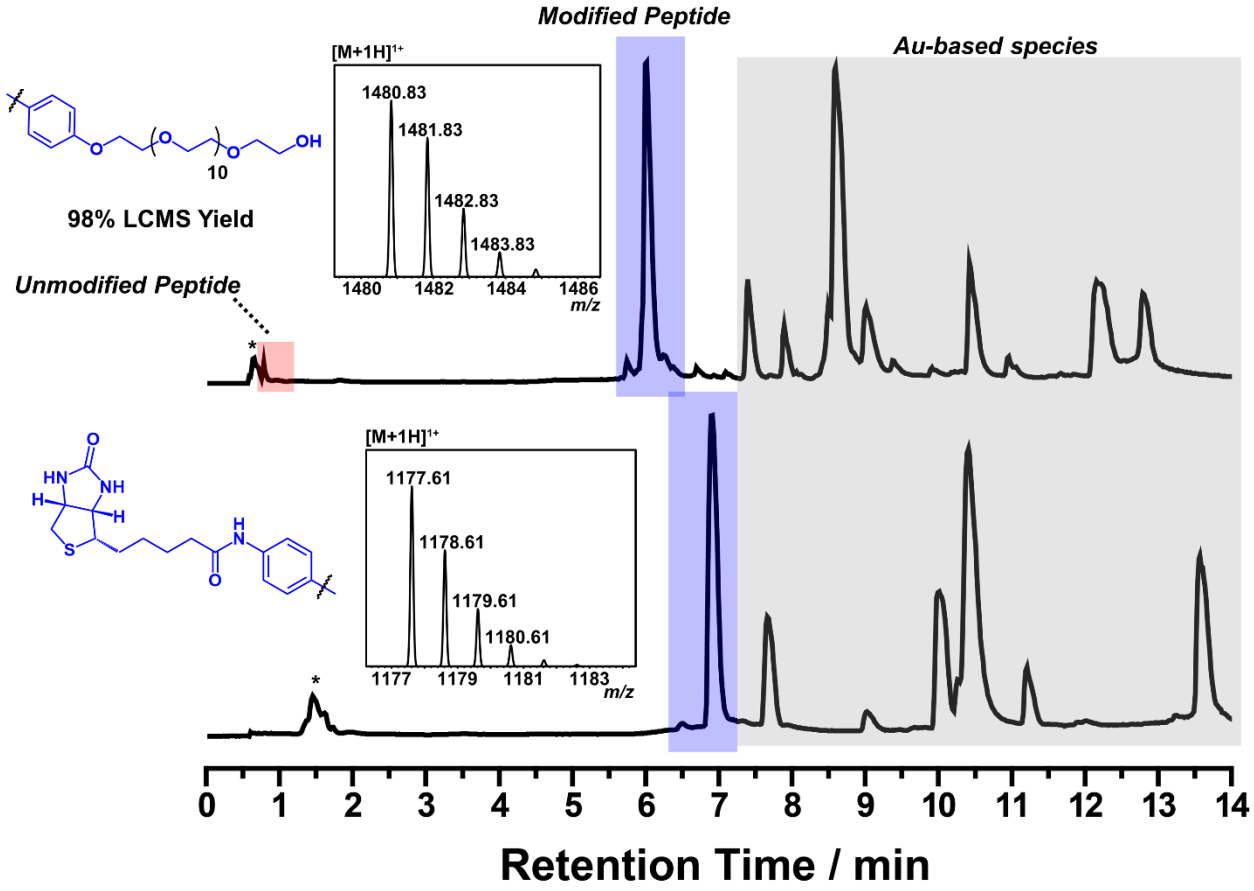

Figure D93. LC-MS traces for arylation of unprotected peptide using [**2o**][SbF_6] and [**2**q][SbF_6] with optimized conditions. (*) denotes Tris buffer (122 *m/z*). Top panel: 1480.8350 (calc'd 1480.8291) *m/z* for $C_{64}H_{117}N_{15}O_{22}S$. Bottom panel: 1177.6129 (calc'd 1177.6081) *m/z* for $C_{50}H_{84}N_{18}O_{11}S_2$.

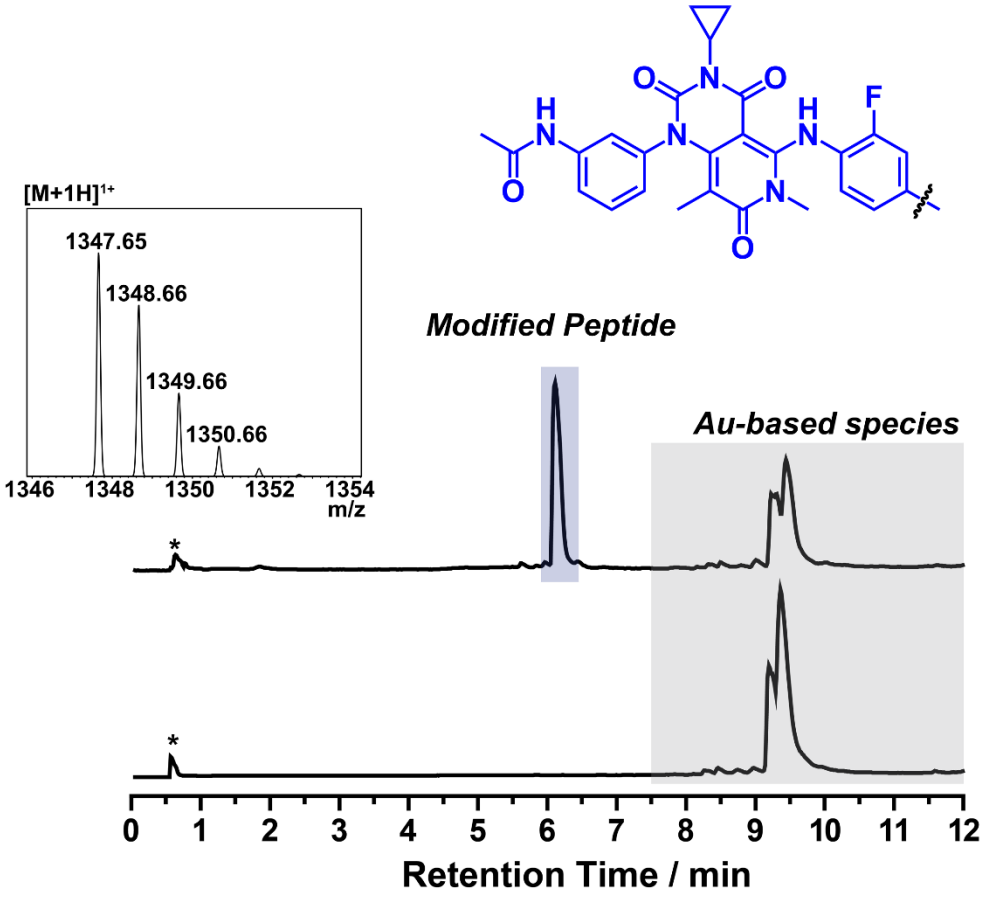

Figure D94. LC-MS trace of unprotected peptide modified with [**2n**][SbF_6] (top) as well as a control in which no peptide was added (bottom). (*) indicate Tris buffer (122 *m/z*). 1347.6594 (calc'd 1347.6539) *m/z* for $C_{60}H_{87}FN_{20}O_{13}S$.

5.5.20 Peptide Stapling Procedure

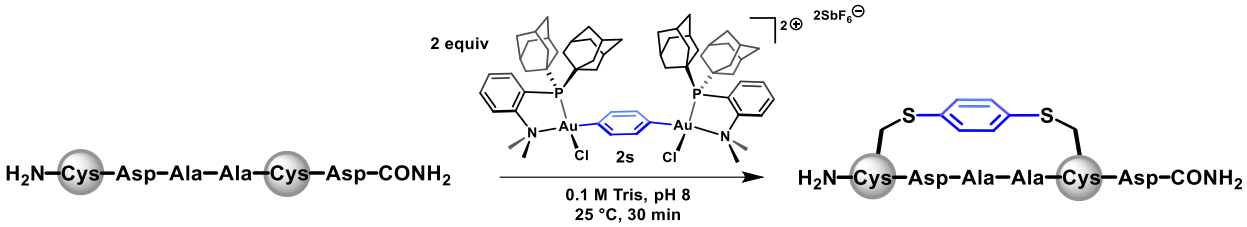

To a solution of the peptide (H_2N-CDAACD-$CONH_2$) in H_2O (2.8 mM, 5 mL, 0.2 M Tris, pH 8) was added a solution of [**2s**][SbF_6]$_2$ in MeCN (5.6 mM, 5 mL). The suspension was sonicated for 1 min, and then allowed to stand at 25 °C for a total of 30 min, at which point the reaction mixture was diluted with a 50/50 mixture of MeCN/H_2O containing 0.1%TFA, and the resulting suspension was centrifuged for 2 min. The supernatant was decanted and passed through a 0.45 μm filter. The filtrate was lyophilized and the obtained solid was dissolved in H_2O containing 0.1% TFA and purified by semi-preparative reversed-phase HPLC.

Solvent compositions for reversed-phase HPLC purification were: H_2O with 0.1% TFA (solvent A), MeCN with 0.1% TFA (solvent B). 0-5 min, 100% A; 5-60 min, linear gradient 100-60% A; 65-75 min, linear gradient 40-100% B. Flow rate: 3 mL/min. HPLC fractions containing the pure product were further confirmed by LC-MS, combined, and lyophilized.

5.5.21 Double Arylation of Dicysteine Peptide

To an Eppendorf tube containing 20 µL H_2O was added 50 µL (1.0 equiv) of a 2 mM solution of the peptide (H_2N-CDAACD-$CONH_2$) in H_2O (0.2 M Tris, pH 8). To this tube was added 40 µL (6.0 equiv) of a 15 mM solution of [**2m**][SbF_6] in MeCN. The reaction mixture was vortexed for 5 sec, and then allowed to stand for 5 min. A 20 µL aliquot of this solution was diluted with 100 µL of a 50/50 mixture of MeCN/H_2O containing 0.1%TFA, and the resulting solution was analyzed by LC-MS.

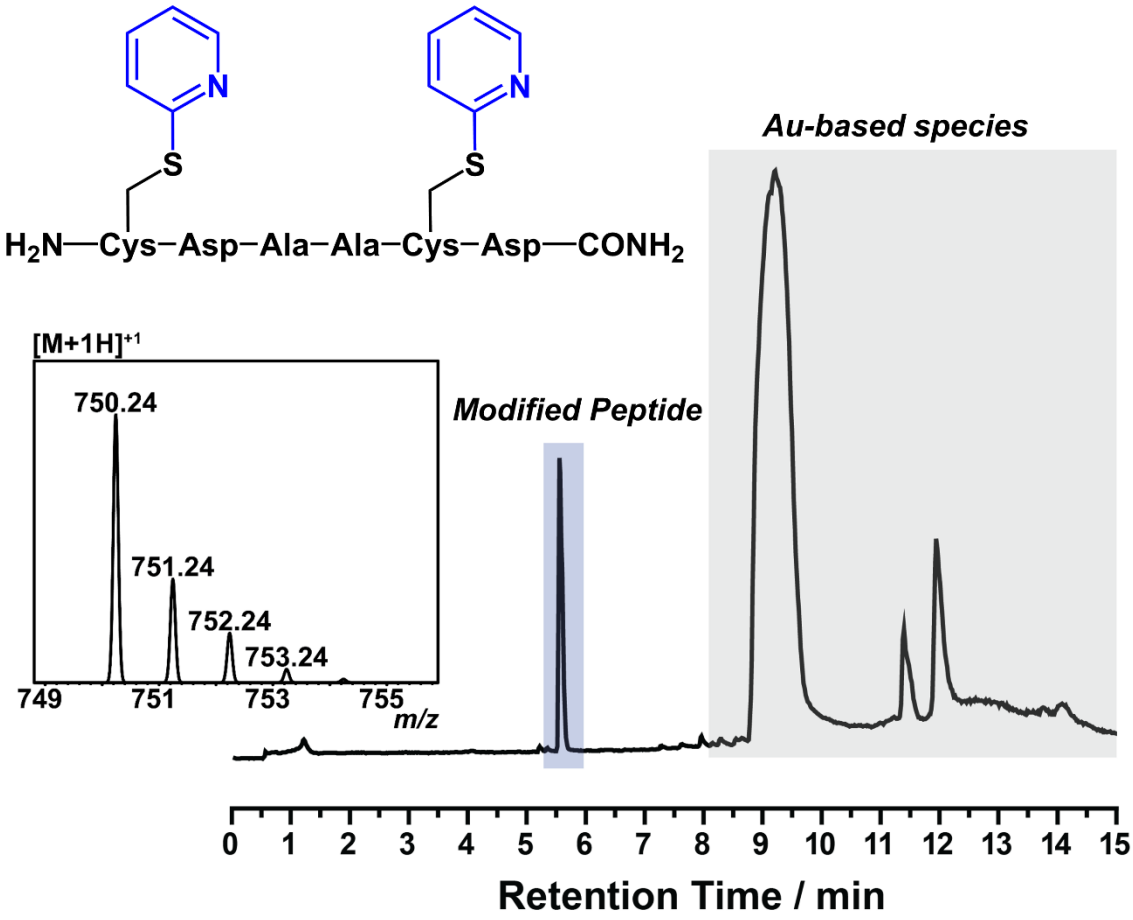

Figure D95. LC-MS trace of di-arylated peptide. 750.2395 (calc'd 750.2334) *m/z* for $C_{30}H_{39}N_9O_{10}S_2$.

5.5.22 Trypsin Digest and MS/MS experiments:

Trypsin digest experiment was performed by combining 50 µL of a 2 mM solution of peptide, 30 µL of water, and 20 µL of a 15 mM solution of [**2a**][SbF_6] or [**2i**][SbF_6], vortexing for <5 seconds

and sitting at room temperature for 1 minute. After 1 minute, 20 µL of a 1 mg/mL solution of trypsin in water was added, vortexed for <5 seconds, and heated to 37 °C for 10 minutes. A 20 µL aliquot was taken from the mixture and added to 100 µL of a 50:50 (H_2O:MeCN 0.1% TFA) solution and analyzed via LC-MS.

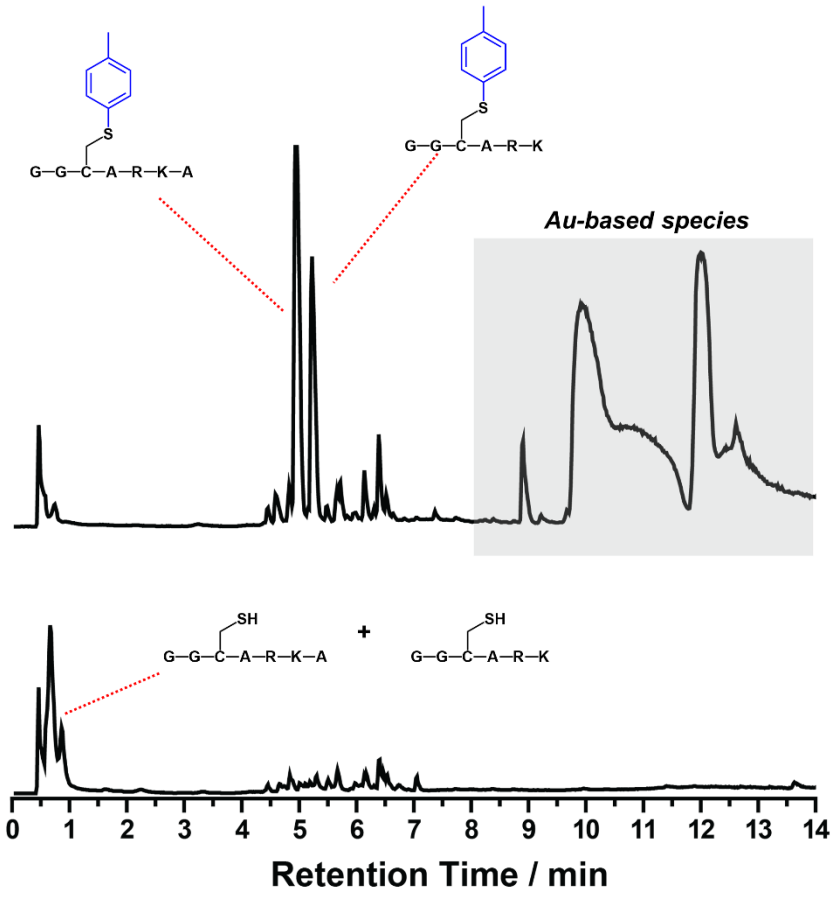

Figure D96. LC-MS traces of trypsin digest experiment of modified peptide (top) and native peptide (bottom).

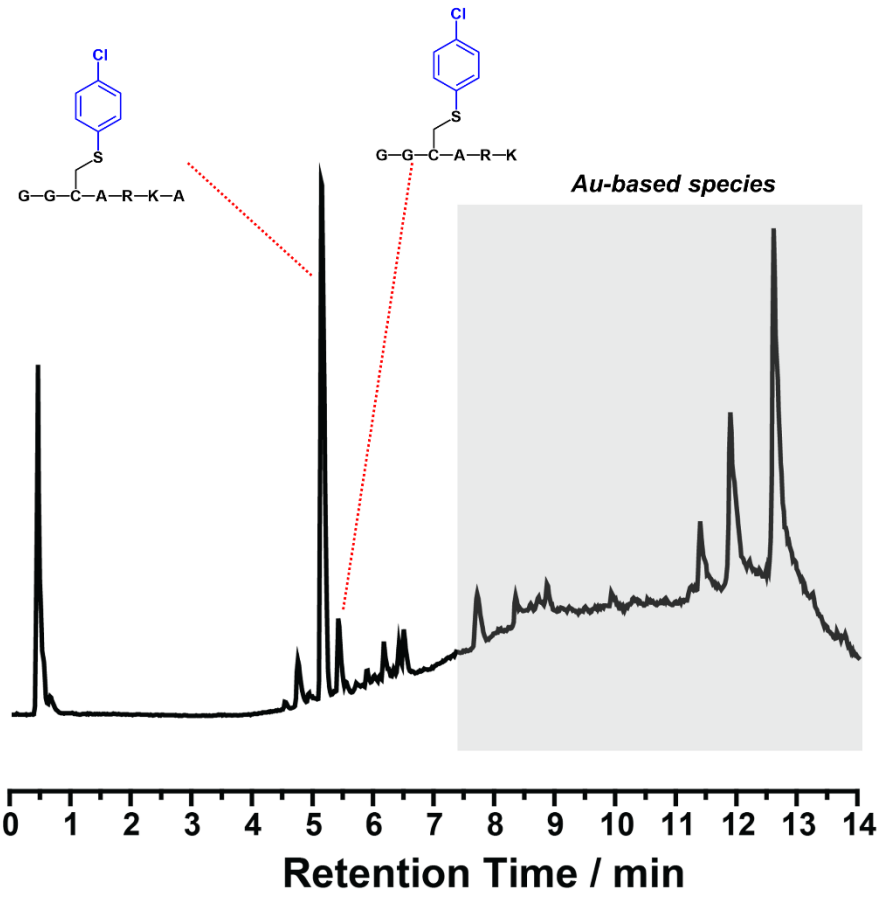

Figure D97. LC-MS trace of trypsin digested peptide modified with [**2i**][SbF_6].

Name	Ion Type	Ion Number	Theoretical Mass	Observed Mass
B3	B	3	290.0812	290.0839
B4	B	4	361.1184	361.1214
B5	B	5	464.1275	464.1304
Y1	Y	1	133.0615	133.0603
Y2	Y	2	236.0707	236.0729
Y3	Y	3	307.1078	307.1100
Y4	Y	4	378.1449	378.1470

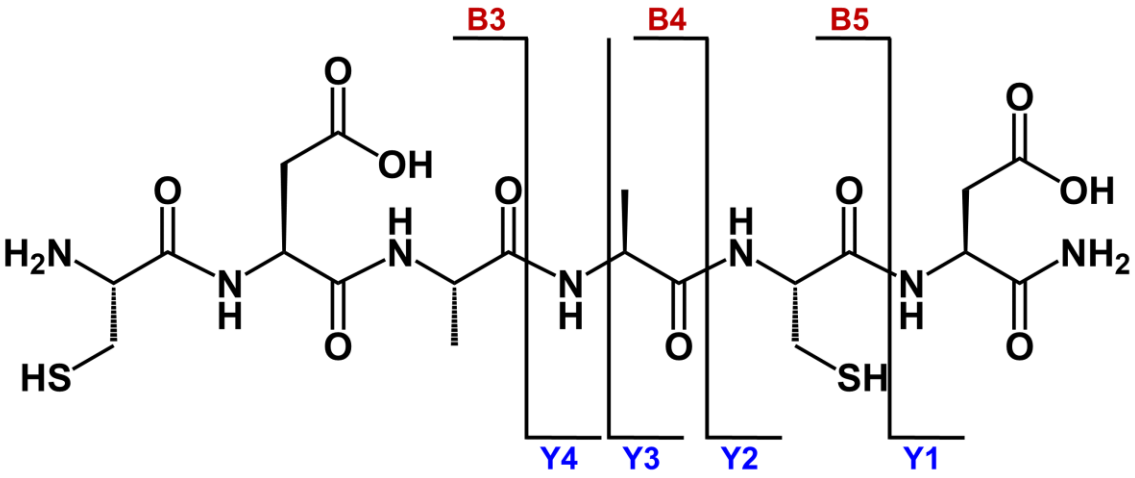

Figure D98. MS/MS analysis of dicysteine peptide, H_2N-CDAACD-$CONH_2$.

Name	Ion Type	Ion Number	Theoretical Mass	Observed Mass
B5	B	2	538.14	538.14

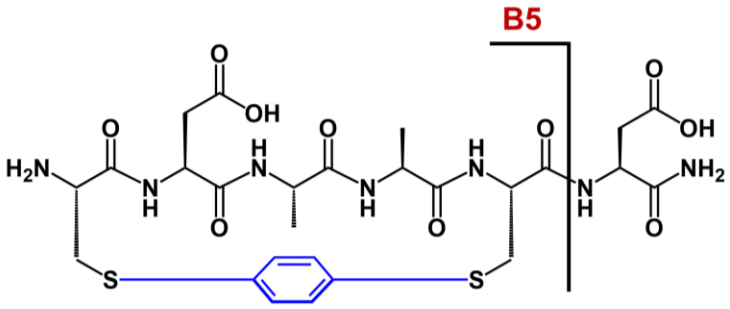

Figure D99. MS/MS analysis of stapled peptide.

Name	Ion Type	Ion Number	Theoretical Mass	Observed Mass
B4	B	4	314.1830	314.1292
B5	B	5	417.1922	417.1956
B7	B	7	644.3304	644.3294
Y2	Y	2	217.1666	217.1648
Y7	Y	7	661.3569	661.3562

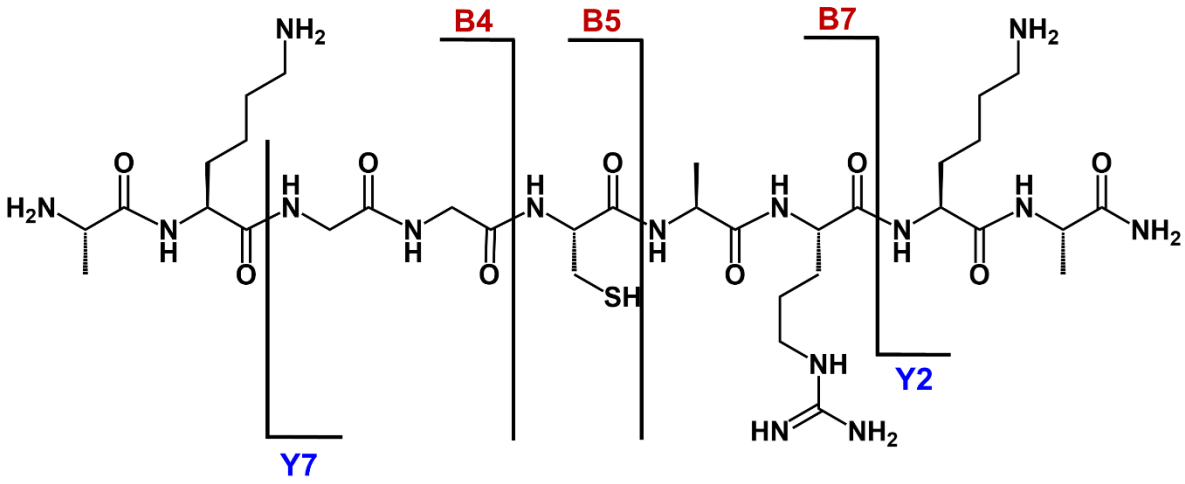

Figure D100. MS/MS analysis of native peptide sequence used for conjugation.

Name	Ion Type	Ion Number	Theoretical Mass	Observed Mass
B2	B	2	200.1401	200.1396
B5	B	5	527.1822	527.1848
B6	B	6	598.2193	598.2230
B7	B	7	754.3204	754.3204
B8	B	8	882.4154	882.4147
Y2	Y	2	217.1666	217.1663
Y3	Y	3	373.2677	373.2673
Y4	Y	4	444.3048	444.3040
Y6	Y	6	714.3255	714.3057
Y7	Y	7	771.3469	771.3470

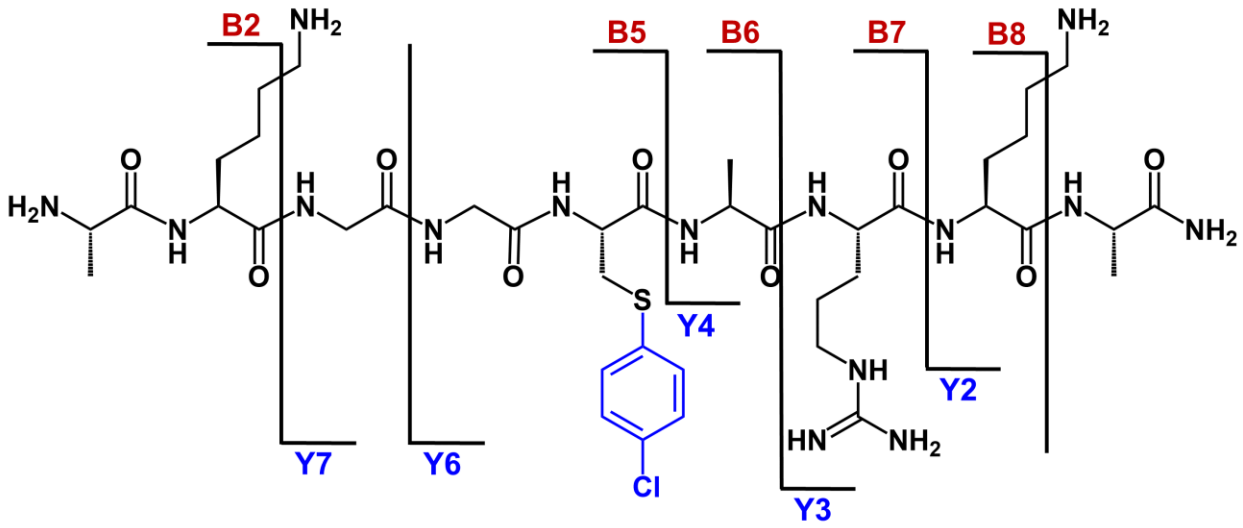

Figure D101. MS/MS analysis of arylated peptide.

5.5.23 Procedure for protein modifications

DARPin Modification: 50 µL of a 72.9 µM solution of DARPin in 20 mM Tris, 150 mM NaCl (pH: 7.5) was added to an Eppendorf tube. To this was added 45 µL of water and 5 µL of a 7.3 mM solution of **2a** in DMF. The solution was pipetted 20 times to ensure proper mixing and allowed to stand at room temperature for 30 min. After 30 min, a 20 µL aliquot of the reaction mixture was added to 100 µL of a 50:50 water/acetonitrile 0.1% TFA solution.

FGF2 Modification: 50 µL of a 0.66 µM solution of FGF2 in 200 mM Tris (pH 8.7) was added to an Eppendorf tube. To this solution was added 50 µL of a 9.93 µM solution of **2g** in water. The reaction m mixture was pipetted 20 times to ensure proper mixing and allowed to stand at room temperature for 30 min. After 30 min, a 20 µL aliquot of the reaction mixture was added to 100 µL of a 50:50 water/acetonitrile 0.1% TFA solution.

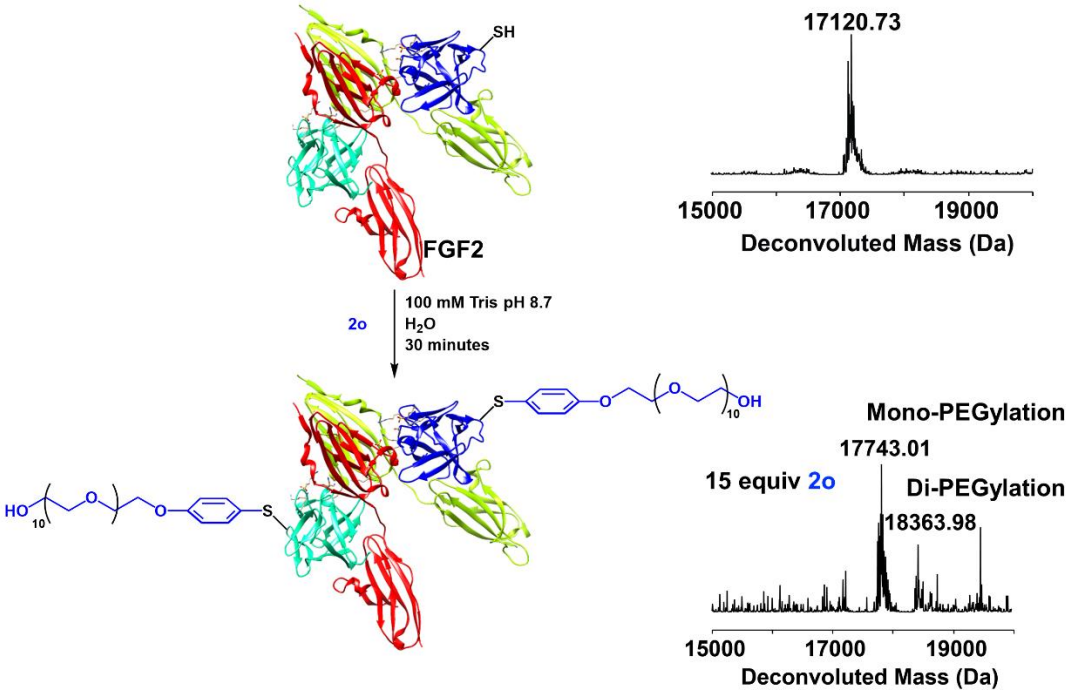

Figure D102. Modification of FGF2 using 2o and corresponding masses. Di-PEGylation is consistent with the presence of two accessible cysteine residues.

5.5.24 X-Ray Crystallographic Data

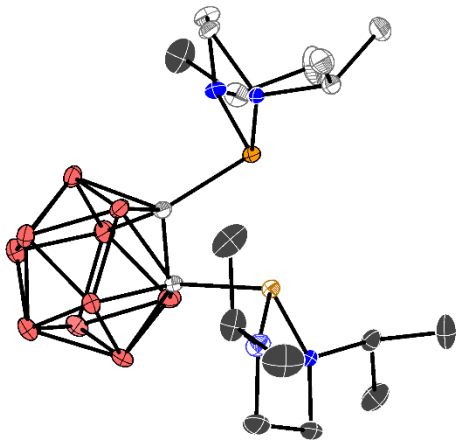

Solid-state structure of DPCb with thermal ellipsoids rendered at the 50% probability level and with hydrogen atoms omitted for clarity.

Crystallographic Data for 1,2-bis(1,3-diisopropyl-1,3-2-diaminophosphino)-1,2-dicarba-*closo*-dodecaborane (DPCb).

Identification code	MSM-A-2-221	
CCDC Code	1836204	
Empirical formula	C18 H46 B10 N4 P2	
Formula weight	488.63	
Temperature	100.15 K	
Wavelength	0.71073 Å	
Crystal system	Monoclinic	
Space group	$P2_1/n$	
Unit cell dimensions	a = 11.492(2) Å	α = 90°
	b = 19.277(3) Å	β = 99.819(5)°

	c = 13.003(2) Å γ = 90°
Volume	2838.3(8) Å^3
Z	4
Density (calculated)	1.143 Mg/m^3
Absorption coefficient	0.169 mm^{-1}
F(000)	1048
Crystal size	0.27 x 0.23 x 0.12 mm^3
Theta range for data collection	2.086 to 27.120°.
Index ranges	$-14 \leq h \leq 14$, $-24 \leq k \leq 22$, $-16 \leq l \leq 16$
Reflections collected	20897
Independent reflections	6265 [R(int) = 0.0409]
Completeness to theta = 25.242°	99.9%
Absorption correction	Semi-empirical from equivalents
Max. and min. transmission	0.2612 and 0.2263
Refinement method	Full-matrix least-squares on F^2
Data / restraints / parameters	6265 / 0 / 315
Goodness-of-fit on F^2	1.023
Final R indices [$I > 2\sigma(I)$]	R_1 = 0.0418, wR_2 = 0.0958
R indices (all data)	R1 = 0.0619, wR2 = 0.1062
Extinction coefficient	n/a
Largest diff. peak and hole	0.326 and -0.259 e.Å^{-3}

Atomic coordinates (x 10^4) and equivalent isotropic displacement parameters ($Å^2$x 10^3) for 1,2-bis(1,3-diisopropyl-1,3-2-diaminophosphino)-1,2-dicarba-*closo*-dodecaborane (DPCb). U(eq) is defined as one third of the trace of the orthogonalized U^{ij} tensor.

	x	y	z	U(eq)
P(1)	2021(1)	3922(1)	3137(1)	13(1)
P(2)	4592(1)	3186(1)	3011(1)	12(1)
N(1)	591(1)	4152(1)	2885(1)	19(1)
N(2)	2102(1)	4047(1)	4434(1)	16(1)
N(3)	4414(1)	3522(1)	1802(1)	14(1)
N(4)	5655(1)	2614(1)	2821(1)	16(1)
C(1)	3292(2)	2555(1)	2925(1)	13(1)
C(2)	2014(2)	2913(1)	3113(1)	13(1)
C(3)	4933(2)	3052(1)	1107(1)	16(1)
C(4)	5964(2)	2668(1)	1771(1)	20(1)
C(5)	4585(2)	4280(1)	1701(1)	17(1)
C(6)	3880(2)	4538(1)	677(2)	23(1)
C(7)	5884(2)	4485(1)	1817(2)	22(1)
C(8)	6593(2)	2450(1)	3714(1)	20(1)
C(9)	7507(2)	3026(1)	3935(2)	33(1)
C(10)	7169(2)	1761(1)	3555(2)	35(1)
C(11)	34(2)	4070(1)	3812(2)	27(1)

C(12)	976(2)	4251(1)	4728(2)	24(1)
C(13)	-165(2)	4261(1)	1868(2)	29(1)
C(14)	-851(2)	4931(1)	1856(2)	45(1)
C(15)	531(2)	4250(1)	986(2)	36(1)
C(16)	3200(2)	4336(1)	5035(1)	19(1)
C(17)	3295(2)	5119(1)	4910(2)	32(1)
C(18)	3322(2)	4124(1)	6172(2)	30(1)
B(9)	2865(2)	2481(1)	4131(2)	17(1)
B(4)	850(2)	2436(1)	2491(2)	16(1)
B(2)	3048(2)	1818(1)	2176(2)	16(1)
B(8)	3505(2)	1772(1)	3550(2)	18(1)
B(1)	2134(2)	2564(1)	1910(2)	15(1)
B(7)	2333(2)	1232(1)	2924(2)	21(1)
B(10)	2234(2)	1645(1)	4140(2)	21(1)
B(5)	1310(2)	2381(1)	3862(2)	18(1)
B(3)	1486(2)	1729(1)	1898(2)	19(1)
B(6)	981(2)	1614(1)	3122(2)	21(1)

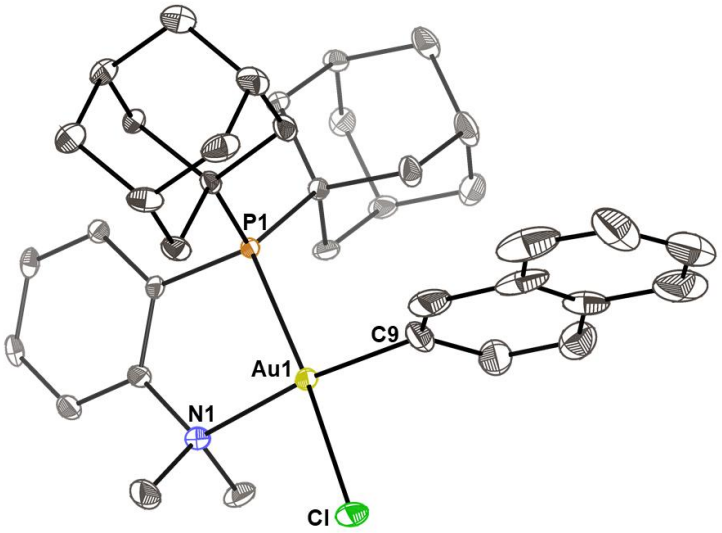

Solid-state structure of [**2c**][SbF_6] with thermal ellipsoids rendered at the 50% probability level and with hydrogen atoms, and $[SbF_6]^-$ counterion omitted for clarity.

Crystallographic Data for [**2c**][SbF_6].

Identification code	JS-06	
CCDC Code	1835370	
Empirical formula	C38 H47 Au Cl F6 N P Sb	
Formula weight	1016.90	
Temperature	100.0 K	
Wavelength	0.71073 Å	
Crystal system	Triclinic	
Space group	*P*-1	
Unit cell dimensions	*a* = 10.0473(12) Å	α = 100.731(4)°
	b = 11.3493(14) Å	β = 103.700(4)°
	c = 17.4404(18) Å	γ = 99.465(4)°
Volume	1852.5(4) $Å^3$	

Z	2
Density (calculated)	1.823 Mg/m^3
Absorption coefficient	4.859 mm^{-1}
$F(000)$	996
Crystal size	0.3 x 0.22 x 0.08 mm^3
Theta range for data collection	1.871 to 28.288°.
Index ranges	$-13 \leq h \leq 13$, $-15 \leq k \leq 15$, $-21 \leq l \leq 23$
Reflections collected	24139
Independent reflections	9144 [R(int) = 0.0292]
Completeness to theta = 25.242°	99.9%
Absorption correction	Semi-empirical from equivalents
Max. and min. transmission	0.5633 and 0.3777
Refinement method	Full-matrix least-squares on F^2
Data / restraints / parameters	9144 / 0 / 444
Goodness-of-fit on F^2	1.033
Final R indices [$I > 2\sigma(I)$]	$R1$ = 0.0359, w$R2$ = 0.0734
R indices (all data)	$R1$ = 0.0443, w$R2$ = 0.0762
Largest diff. peak and hole	2.306 and -2.007 $e.Å^{-3}$
SQUEEZE	Found 47e/uc; calc'd for CH_2Cl_2, 42e/uc

Atomic coordinates (x 10^4) and equivalent isotropic displacement parameters ($Å^2$x 10^3) for [**2c**][SbF_6]. U(eq) is defined as one third of the trace of the orthogonalized U^{ij} tensor.

	x	y	z	U(eq)
Au(1)	1025(1)	7043(1)	2269(1)	18(1)
Sb(1)	1335(1)	12273(1)	4024(1)	15(1)
Cl(1)	-1344(1)	7042(1)	1699(1)	28(1)
P(1)	3291(1)	6854(1)	2832(1)	13(1)
F(5)	2351(3)	13520(2)	3687(2)	29(1)
F(2)	327(3)	11051(2)	4384(2)	30(1)
N(1)	610(4)	6710(3)	3391(2)	18(1)
F(3)	1681(3)	13345(3)	5051(2)	31(1)
C(9)	1293(5)	7600(6)	1270(4)	34(1)
C(14)	1318(6)	8915(6)	1334(4)	38(1)
F(6)	999(3)	11198(3)	3014(2)	37(1)
C(13)	1360(6)	9415(5)	684(4)	40(1)
C(4)	1683(5)	6323(4)	4721(3)	19(1)
C(31)	3519(5)	2765(4)	1920(3)	23(1)
F(1)	-310(3)	12824(3)	3654(2)	39(1)
C(32)	4924(5)	3708(4)	2234(3)	19(1)
C(1)	-588(5)	5635(5)	3218(4)	31(1)
F(4)	2991(3)	11761(3)	4414(2)	31(1)

C(30)	5423(5)	3996(5)	1514(3)	25(1)
C(8)	3112(4)	6545(4)	3795(3)	14(1)
C(27)	2433(5)	3303(4)	1400(3)	23(1)
C(12)	1392(5)	8638(5)	-12(4)	33(1)
C(34)	4180(5)	5729(4)	1517(3)	21(1)
C(3)	1829(4)	6521(4)	3979(3)	16(1)
C(2)	197(5)	7859(5)	3750(3)	28(1)
C(33)	4730(4)	4879(4)	2764(3)	15(1)
C(20)	6165(4)	8111(4)	3446(3)	15(1)
C(19)	7225(4)	9364(4)	3678(3)	16(1)
C(25)	3651(4)	5447(4)	2237(3)	14(1)
C(26)	2240(4)	4476(4)	1923(3)	20(1)
C(10)	1290(5)	6883(6)	594(4)	41(2)
C(23)	5744(5)	10046(5)	2553(3)	30(1)
C(5)	2808(5)	6159(4)	5287(3)	18(1)
C(6)	4096(5)	6202(4)	5124(3)	17(1)
C(24)	4668(5)	8808(4)	2315(3)	24(1)
C(29)	4334(5)	4533(5)	999(3)	25(1)
C(16)	4282(4)	9234(4)	3707(3)	21(1)
C(7)	4242(4)	6385(4)	4389(3)	14(1)
C(21)	5355(5)	10958(4)	3182(4)	30(1)
C(28)	2922(5)	3600(5)	682(3)	29(1)
C(18)	6826(5)	10271(4)	4299(3)	21(1)

C(15)	4674(4)	8299(4)	3081(3)	17(1)
C(22)	7215(5)	9851(4)	2916(3)	25(1)
C(11)	1356(5)	7417(5)	-146(4)	43(2)
C(17)	5364(5)	10473(4)	3939(3)	24(1)
C(36)	1439(6)	8480(8)	-1435(4)	54(2)
C(37)	1434(6)	7235(9)	-1454(4)	60(2)
C(38)	1402(6)	6649(7)	-811(5)	61(2)
C(35)	1415(6)	9219(9)	-744(4)	60(2)

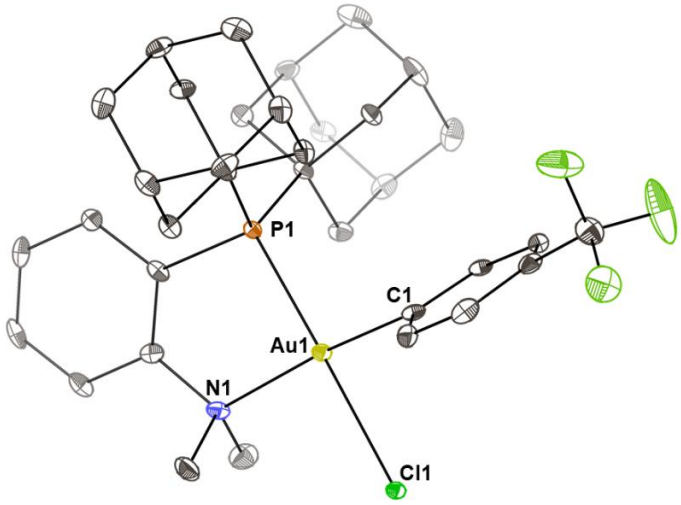

Solid-state structure of [**2d**][SbF_6] with thermal ellipsoids rendered at the 50% probability level and with hydrogen atoms, disorder and $[SbF_6]^-$ counterion omitted for clarity.

Crystal Data for [**2d**][SbF_6].

Identification code	JS-07	
CCDC Code	1835367	
Empirical formula	C35 H44 Au Cl0.86 F9 I0.14 N P Sb	
Formula weight	1047.65	
Temperature	100.0 K	
Wavelength	0.71073 Å	
Crystal system	Triclinic	
Space group	*P*-1	
Unit cell dimensions	*a* = 10.2214(4) Å	α = 108.9020(10)°
	b = 11.5151(4) Å	β = 99.9440(10)°
	c = 16.2248(6) Å	γ = 100.4260(10)°
Volume	1721.07(11) $Å^3$	
Z	2	

Density (calculated)	2.022 Mg/m^3
Absorption coefficient	5.358 mm^{-1}
F(000)	1018
Crystal size	0.3 x 0.27 x 0.21 mm^3
Theta range for data collection	1.916 to 28.267°.
Index ranges	$-12 \leq h \leq 13$, $-15 \leq k \leq 15$, $-21 \leq l \leq 21$
Reflections collected	23765
Independent reflections	8525 [*R*(int) = 0.0402]
Completeness to theta = 25.242°	99.9%
Absorption correction	Semi-empirical from equivalents
Max. and min. transmission	0.5633 and 0.4649
Refinement method	Full-matrix least-squares on F^2
Data / restraints / parameters	8525 / 0 / 436
Goodness-of-fit on F^2	1.035
Final *R* indices [$I > 2\sigma(I)$]	*R*1 = 0.0326, w*R*2 = 0.0604
R indices (all data)	*R*1 = 0.0459, w*R*2 = 0.0644
Extinction coefficient	n/a
Largest diff. peak and hole	2.688 and -1.864 $e.Å^{-3}$

Atomic coordinates (x 10^4) and equivalent isotropic displacement parameters ($Å^2$ x 10^3) for [**2d**][SbF_6]. U(eq) is defined as one third of the trace of the orthogonalized U^{ij} tensor.

	x	y	z	U(eq)
Au(1)	6102(1)	6560(1)	7210(1)	11(1)
Sb(1)	6396(1)	11976(1)	8925(1)	15(1)
Cl(1)	3712(2)	6382(2)	6713(1)	11(1)
P(1)	8366(1)	6482(1)	7673(1)	10(1)
F(6)	7311(3)	13222(3)	8563(2)	28(1)
F(5)	7111(3)	13094(3)	10129(2)	27(1)
F(4)	5495(3)	10762(3)	9309(2)	34(1)
F(8)	4860(3)	12657(3)	8878(2)	26(1)
F(3)	6033(3)	9529(3)	4118(2)	33(1)
F(9)	7936(3)	11320(3)	9000(2)	36(1)
F(7)	5712(3)	10895(3)	7725(2)	41(1)
F(1)	8059(3)	9275(3)	4309(2)	43(1)
N(1)	5807(4)	6279(3)	8437(2)	13(1)
F(2)	6408(5)	7801(3)	3307(2)	60(1)
C(1)	6259(4)	7107(4)	6154(3)	13(1)
C(15)	9728(4)	7935(4)	7853(3)	11(1)
C(12)	9416(5)	6292(4)	10188(3)	15(1)
C(4)	6490(4)	8096(4)	4822(3)	16(1)

C(27)	9059(5)	5024(4)	6115(3)	14(1)
C(26)	8623(4)	4934(4)	6963(3)	10(1)
C(6)	6355(4)	6330(4)	5321(3)	13(1)
C(34)	9730(4)	4501(4)	7489(3)	14(1)
C(13)	9489(4)	6389(4)	9365(3)	13(1)
C(11)	8181(5)	6157(4)	10417(3)	18(1)
C(5)	6471(4)	6825(4)	4659(3)	14(1)
C(16)	9471(5)	9046(4)	8606(3)	14(1)
C(22)	11203(4)	7807(4)	8136(3)	15(1)
C(24)	10528(5)	10281(4)	8777(3)	16(1)
C(9)	7075(4)	6265(4)	9019(3)	12(1)
C(18)	10387(5)	10581(4)	7918(3)	17(1)
C(2)	6210(4)	8358(4)	6299(3)	17(1)
C(30)	9863(4)	3201(4)	6877(3)	16(1)
C(3)	6333(4)	8852(4)	5642(3)	16(1)
C(19)	10658(5)	9500(4)	7174(3)	16(1)
C(10)	7012(5)	6148(4)	9841(3)	17(1)
C(28)	9159(5)	3722(4)	5520(3)	20(1)
C(21)	12245(5)	9068(4)	8319(3)	17(1)
C(35)	7775(5)	2744(4)	5253(3)	21(1)
C(14)	8305(4)	6373(4)	8769(3)	11(1)
C(25)	9607(4)	8257(4)	6988(3)	14(1)
C(31)	8505(4)	2215(4)	6609(3)	15(1)

C(29)	10284(5)	3328(4)	6044(3)	22(1)
C(017)	6733(5)	8661(4)	4129(3)	22(1)
C(7)	4705(5)	5111(4)	8243(3)	23(1)
C(20)	12113(5)	9372(4)	7461(3)	18(1)
C(32)	7384(5)	2620(4)	6089(3)	17(1)
C(33)	7249(4)	3924(4)	6682(3)	14(1)
C(23)	11979(5)	10133(4)	9064(3)	18(1)
C(8)	5364(5)	7447(4)	8925(3)	21(1)
I(1)	3551(3)	6512(3)	6725(2)	11(1)

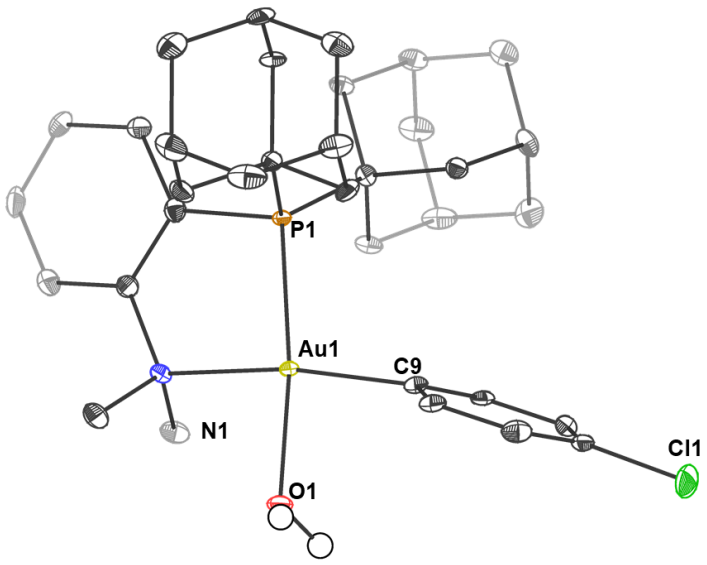

Solid-state structure of [(Me-DalPhos)Au(*p*-Cl-C_6H_4)OH_2][SbF_6]$_2$ with thermal ellipsoids rendered at the 50% probability level and with selected hydrogen atoms, disorder, two [SbF_6]$^-$ counterions and one DCM molecule omitted for clarity.

Crystallographic Data for [(Me-DalPhos)Au(*p*-Cl-C_6H_4)OH_2][SbF_6]$_2$.

Identification code	JS-08	
CCDC Code	1835368	
Empirical formula	C70 H95 Au2 Cl6 F18 N2 O2 P2 Sb3	
Formula weight	2372.30	
Temperature	100.0 K	
Wavelength	0.71073 Å	
Crystal system	Triclinic	
Space group	*P*-1	
Unit cell dimensions	*a* = 10.3978(4) Å	α = 90.4650(10)°
	b = 10.8778(4) Å	β = 90.5830(10)°
	c = 17.7061(7) Å	γ = 94.1330(10)°

Volume	1997.26(13) $Å^3$
Z	1
Density (calculated)	1.972 Mg/m^3
Absorption coefficient	4.989 mm^{-1}
F(000)	1150
Crystal size	0.25 x 0.2 x 0.15 mm^3
Theta range for data collection	1.877 to 28.297°.
Index ranges	$-13 \leq h \leq 13$, $-14 \leq k \leq 14$, $-20 \leq l \leq 23$
Reflections collected	35922
Independent reflections	9931 [*R*(int) = 0.0460]
Completeness to theta = 25.242°	100.0%
Absorption correction	Semi-empirical from equivalents
Max. and min. transmission	0.7457 and 0.6326
Refinement method	Full-matrix least-squares on F^2
Data / restraints / parameters	9931 / 3 / 483
Goodness-of-fit on F^2	1.010
Final *R* indices [$I > 2\sigma(I)$]	*R*1 = 0.0294, w*R*2 = 0.0529
R indices (all data)	*R*1 = 0.0411, w*R*2 = 0.0560
Extinction coefficient	n/a
Largest diff. peak and hole	1.184 and -1.134 $e.Å^{-3}$

Atomic coordinates (x 10^4) and equivalent isotropic displacement parameters ($Å^2$x 10^3) for [(Me-DalPhos)Au(*p*-Cl-C_6H_4)OH_2][SbF_6]$_2$. U(eq) is defined as one third of the trace of the orthogonalized U^{ij} tensor.

	x	y	z	U(eq)
Au(1)	4358(1)	3696(1)	3656(1)	9(1)
Sb(1)	8445(1)	2689(1)	4772(1)	19(1)
Sb(2)	0	0	0	25(1)
P(1)	3440(1)	3112(1)	2514(1)	9(1)
Cl(1)	7351(1)	9156(1)	3384(1)	26(1)
Cl(2)	5598(1)	7420(1)	1479(1)	32(1)
Cl(3)	7534(1)	6345(1)	558(1)	41(1)
F(6)	9644(2)	2832(2)	5568(1)	32(1)
F(2)	7790(2)	4204(2)	5056(2)	31(1)
O(1)	5134(2)	4002(2)	4720(1)	14(1)
F(4)	7193(2)	2579(2)	3987(1)	34(1)
F(1)	9016(2)	1159(2)	4506(2)	37(1)
F(3)	7214(2)	1901(2)	5407(1)	31(1)
F(5)	9606(2)	3510(3)	4123(2)	44(1)
N(1)	3293(3)	2092(3)	4115(2)	12(1)
C(35)	5792(3)	3617(3)	1786(2)	15(1)
C(22)	3046(3)	5347(3)	1805(2)	13(1)

F(8)	-578(3)	-488(3)	941(2)	74(1)
C(9)	5296(3)	5362(3)	3403(2)	13(1)
C(2)	4230(3)	1262(3)	4454(2)	17(1)
C(16)	1291(3)	3663(3)	1583(2)	13(1)
F(9)	-1691(3)	-237(4)	-334(2)	87(1)
C(23)	1558(3)	4624(3)	2867(2)	14(1)
C(33)	4129(3)	2294(3)	1061(2)	14(1)
C(7)	1699(3)	1020(3)	2281(2)	16(1)
C(26)	4687(3)	2611(3)	1852(2)	12(1)
C(30)	6846(3)	3171(3)	1270(2)	18(1)
C(31)	6281(4)	2858(3)	481(2)	19(1)
C(11)	7253(3)	6669(3)	3299(2)	17(1)
C(15)	2297(3)	4229(3)	2161(2)	11(1)
C(14)	4612(3)	6407(3)	3495(2)	11(1)
C(13)	5229(3)	7577(3)	3476(2)	15(1)
C(1)	2484(3)	2601(3)	4722(2)	17(1)
C(21)	2095(3)	6323(3)	1596(2)	17(1)
C(5)	912(4)	-289(3)	3284(2)	21(1)
C(17)	366(3)	4650(3)	1362(2)	16(1)
C(6)	921(4)	20(3)	2524(2)	20(1)
C(10)	6623(3)	5498(3)	3320(2)	13(1)
C(32)	5194(4)	1842(3)	555(2)	17(1)
C(29)	7385(4)	2023(4)	1617(2)	23(1)

C(20)	1388(4)	6715(3)	2305(2)	24(1)
C(24)	627(3)	5597(3)	2643(2)	19(1)
C(18)	-346(3)	5047(4)	2064(2)	21(1)
C(25)	1119(3)	5770(3)	1013(2)	18(1)
C(4)	1677(3)	388(3)	3796(2)	18(1)
C(3)	2460(3)	1390(3)	3556(2)	13(1)
C(8)	2463(3)	1742(3)	2802(2)	14(1)
C(27)	5235(4)	1445(3)	2199(2)	18(1)
F(7)	-224(4)	1600(3)	284(3)	113(2)
C(12)	6558(3)	7697(3)	3379(2)	15(1)
C(36)	7161(4)	7618(4)	1118(3)	34(1)
C(34)	5725(4)	697(3)	899(2)	24(1)
C(28)	6306(4)	1013(4)	1678(2)	23(1)

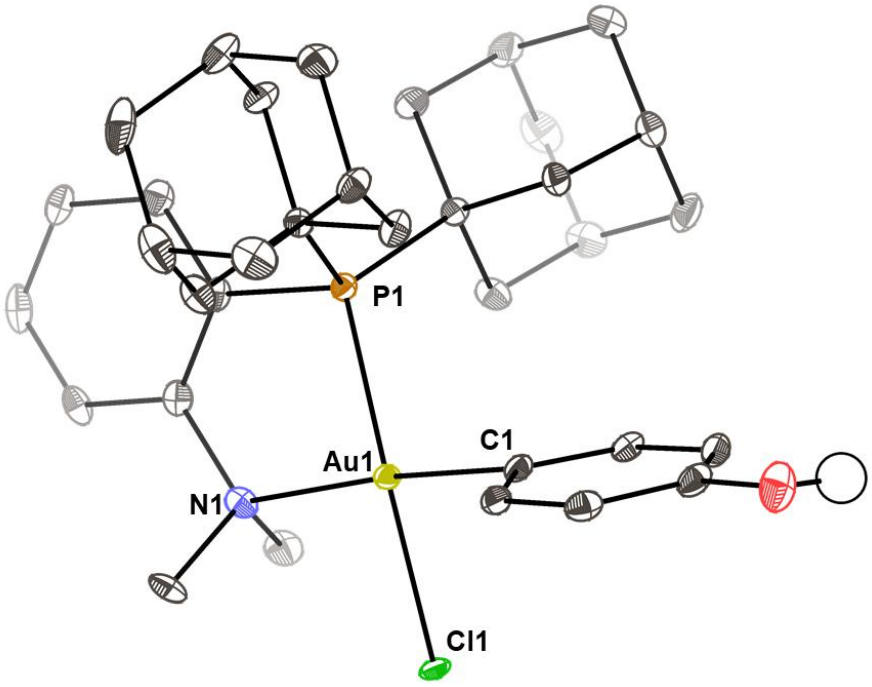

Solid-state structure of [**2f**][SbF_6]·H_2O with thermal ellipsoids rendered at the 50% probability level and with selected hydrogen atoms, one water molecule, and $[SbF_6]^-$ counterion omitted for clarity.

Crystallographic Data for [**2f**][SbF_6]·H_2O.

Identification code	JS-13
CCDC Code	1835373
Empirical formula	C34 H47 Au Cl F6 N O2 P Sb
Formula weight	1000.86
Temperature	100.0 K
Wavelength	0.71073 Å
Crystal system	Triclinic
Space group	*P*-1
Unit cell dimensions	a = 9.5384(10) Å α = 112.015(2)°

	b = 13.2116(13) Å β = 105.708(2)°
	c = 15.7777(11) Å γ = 91.052(3)°
Volume	1758.4(3) Å^3
Z	2
Density (calculated)	1.890 Mg/m^3
Absorption coefficient	5.121 mm^{-1}
F(000)	980
Crystal size	0.3 x 0.28 x 0.18 mm^3
Theta range for data collection	1.459 to 28.284°.
Index ranges	$-11 \leq h \leq 12$, $-17 \leq k \leq 17$, $-18 \leq l \leq 21$
Reflections collected	31512
Independent reflections	8736 [R(int) = 0.0381]
Completeness to theta = 25.242°	99.9%
Absorption correction	Semi-empirical from equivalents
Max. and min. transmission	0.5633 and 0.4270
Refinement method	Full-matrix least-squares on F^2
Data / restraints / parameters	8736 / 0 / 438
Goodness-of-fit on F^2	1.024
Final R indices [$I > 2\sigma(I)$]	$R1$ = 0.0256, w$R2$ = 0.0516
R indices (all data)	$R1$ = 0.0337, w$R2$ = 0.0543
Extinction coefficient	n/a
Largest diff. peak and hole	1.022 and -0.862 e.Å^{-3}

Atomic coordinates (x 10^4) and equivalent isotropic displacement parameters ($Å^2$ x 10^3)

For [**2f**][SbF_6]·H_2O. U(eq) is defined as one third of the trace of the orthogonalized U^{ij} tensor.

	x	y	z	U(eq)
Au(1)	8596(1)	4062(1)	2777(1)	11(1)
Sb(1)	10000	5000	0	15(1)
Sb(2)	10000	0	5000	22(1)
Cl(1)	11133(1)	4665(1)	3506(1)	15(1)
P(1)	6074(1)	3560(1)	2242(1)	12(1)
F(1)	10141(4)	4357(3)	867(2)	81(1)
F(2)	12018(3)	5138(2)	260(2)	64(1)
F(3)	10179(3)	6378(2)	998(2)	51(1)
F(4)	11012(3)	-884(2)	4190(2)	49(1)
F(5)	8253(3)	-605(2)	3998(2)	50(1)
F(6)	10222(3)	1120(2)	4585(2)	48(1)
O(1)	10888(3)	-417(2)	1248(2)	26(1)
O(2)	11532(3)	-1563(2)	2394(2)	33(1)
N(1)	8118(3)	5775(2)	3277(2)	15(1)
C(1)	9215(3)	2529(2)	2280(2)	14(1)
C(2)	9654(3)	2231(3)	1454(2)	16(1)
C(3)	10211(4)	1244(3)	1121(2)	18(1)
C(4)	10337(4)	548(3)	1614(2)	19(1)

C(5)	9921(3)	859(3)	2445(2)	18(1)
C(6)	9388(3)	1861(3)	2786(2)	15(1)
C(7)	8916(4)	6355(3)	2854(3)	22(1)
C(8)	8713(4)	6281(3)	4348(2)	21(1)
C(9)	6531(4)	5863(3)	2991(2)	15(1)
C(10)	6091(4)	6911(3)	3186(2)	17(1)
C(11)	4612(4)	7020(3)	2965(2)	21(1)
C(12)	3567(4)	6105(3)	2582(2)	18(1)
C(13)	3998(4)	5071(3)	2388(2)	17(1)
C(14)	5485(3)	4931(3)	2580(2)	14(1)
C(15)	5526(3)	2895(2)	2984(2)	13(1)
C(16)	6569(4)	3505(3)	4020(2)	17(1)
C(17)	6215(4)	2992(3)	4681(2)	22(1)
C(18)	4619(4)	3108(3)	4687(3)	25(1)
C(19)	3590(4)	2492(3)	3674(3)	21(1)
C(20)	3800(4)	1271(3)	3319(3)	23(1)
C(21)	5388(4)	1171(3)	3306(2)	20(1)
C(22)	5683(4)	1658(3)	2616(2)	16(1)
C(23)	3926(4)	3011(3)	3014(3)	19(1)
C(24)	6435(4)	1784(3)	4320(3)	23(1)
C(25)	5286(3)	2848(2)	908(2)	13(1)
C(26)	3584(3)	2599(3)	558(2)	18(1)
C(27)	3048(4)	2058(3)	-547(2)	21(1)

C(28)	3543(4)	2850(3)	-945(3)	28(1)
C(29)	5211(4)	3085(3)	-619(2)	25(1)
C(30)	5865(4)	2009(3)	-965(2)	24(1)
C(31)	5363(4)	1229(3)	-564(2)	18(1)
C(32)	5903(4)	1749(3)	533(2)	17(1)
C(33)	5776(4)	3632(3)	488(2)	19(1)
C(34)	3684(4)	980(3)	-905(2)	21(1)

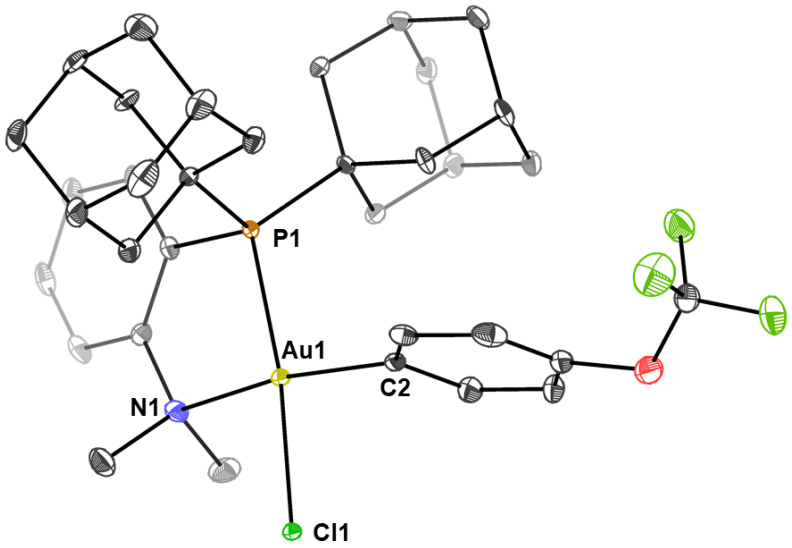

Solid-state structure of [**2g**][SbF_6] with thermal ellipsoids rendered at the 50% probability level and with hydrogen atoms, disorder, and $[SbF_6]^-$ counterion omitted for clarity.

Crystal data and structure refinement for [**2g**][SbF_6].

Identification code	JS-09	
CCDC Code	1835371	
Empirical formula	C35 H44 Au Cl0.95 F9 I0.05 N O P Sb	
Formula weight	1055.42	
Temperature	100.0 K	
Wavelength	0.71073 Å	
Crystal system	Triclinic	
Space group	*P*-1	
Unit cell dimensions	a = 10.0238(6) Å	α = 106.082(2)°
	b = 11.7115(7) Å	β = 106.450(2)°
	c = 16.7522(11) Å	γ = 97.925(2)°
Volume	1761.65(19) $Å^3$	

Z	2
Density (calculated)	1.990 Mg/m^3
Absorption coefficient	5.166 mm^{-1}
$F(000)$	1028
Crystal size	0.29 x 0.28 x 0.26 mm^3
Theta range for data collection	1.344 to 28.316°.
Index ranges	$-13 \leq h \leq 13$, $-14 \leq k \leq 15$, $-21 \leq l \leq 22$
Reflections collected	30660
Independent reflections	8761 [R(int) = 0.0353]
Completeness to theta = 25.242°	100.0%
Absorption correction	Semi-empirical from equivalents
Max. and min. transmission	0.7457 and 0.5596
Refinement method	Full-matrix least-squares on F^2
Data / restraints / parameters	8761 / 2 / 456
Goodness-of-fit on F^2	1.026
Final R indices [$I > 2\sigma(I)$]	$R1$ = 0.0267, w$R2$ = 0.0587
R indices (all data)	$R1$ = 0.0327, w$R2$ = 0.0611
Extinction coefficient	n/a
Largest diff. peak and hole	2.624 and -0.785 e.$Å^{-3}$

Atomic coordinates (x 10^4) and equivalent isotropic displacement parameters ($Å^2$x 10^3) for [**2g**][SbF_6]. U(eq) is defined as one third of the trace of the orthogonalized U^{ij} tensor.

	x	y	z	U(eq)
Au(1)	6146(1)	5645(1)	7174(1)	10(1)
Sb(1)	2359(1)	-1787(1)	1095(1)	14(1)
Cl(1)	8027(2)	5307(2)	6550(1)	10(1)
P(1)	4358(1)	6222(1)	7717(1)	9(1)
F(2)	1233(3)	226(2)	4611(2)	29(1)
F(8)	1863(3)	-1783(2)	-77(2)	33(1)
F(9)	3668(3)	-274(2)	1457(2)	28(1)
F(4)	918(3)	-980(3)	1244(2)	35(1)
F(7)	3774(3)	-2607(3)	913(2)	38(1)
F(3)	1732(3)	-1167(2)	3677(2)	30(1)
F(1)	1301(3)	446(3)	3399(2)	38(1)
F(6)	1044(3)	-3292(2)	704(2)	32(1)
C(26)	3254(3)	5011(3)	7950(2)	10(1)
F(5)	2888(3)	-1761(3)	2259(2)	43(1)
O(1)	3331(3)	497(3)	4410(2)	27(1)
C(33)	4315(4)	4622(3)	8639(2)	12(1)
C(23)	2125(4)	6138(3)	6218(2)	15(1)
C(27)	2106(4)	5479(3)	8334(2)	13(1)

N(1)	7641(3)	7112(3)	8328(2)	14(1)
C(12)	7262(4)	9179(3)	10352(2)	18(1)
C(14)	4924(4)	7997(3)	9387(2)	12(1)
C(28)	1317(4)	4453(3)	8561(2)	14(1)
C(16)	3333(3)	7044(3)	7032(2)	9(1)
C(32)	3504(4)	3617(3)	8869(2)	13(1)
C(2)	5010(4)	4042(3)	6210(2)	13(1)
C(34)	2475(4)	3879(3)	7114(2)	13(1)
C(4)	3474(4)	2691(4)	4767(3)	22(1)
C(13)	5801(4)	8877(3)	10180(2)	16(1)
C(30)	1676(4)	2870(3)	7350(2)	15(1)
C(35)	2388(4)	4097(3)	9249(2)	15(1)
C(29)	558(4)	3339(3)	7731(2)	16(1)
C(22)	1398(4)	6830(4)	5623(3)	21(1)
C(18)	3656(4)	8444(4)	6149(3)	19(1)
C(11)	7845(4)	8598(3)	9739(2)	17(1)
C(10)	6967(4)	7709(3)	8949(2)	12(1)
C(3)	4088(4)	3890(4)	5379(2)	17(1)
C(011)	2484(5)	7516(4)	5338(3)	24(1)
C(8)	8648(4)	6447(4)	8760(3)	22(1)
C(17)	4421(4)	7754(3)	6732(3)	16(1)
C(1)	1935(4)	23(4)	4034(2)	18(1)
C(24)	2696(4)	7991(3)	7562(2)	14(1)

C(21)	738(4)	7744(4)	6150(3)	23(1)
C(5)	3819(4)	1718(4)	5020(3)	22(1)
C(31)	2752(4)	2501(3)	8030(2)	15(1)
C(25)	1916(4)	8664(3)	6965(3)	17(1)
C(19)	3003(4)	9363(3)	6678(3)	19(1)
C(15)	5484(4)	7387(3)	8759(2)	11(1)
C(6)	4733(4)	1855(4)	5831(3)	22(1)
C(9)	8456(4)	8050(4)	8075(3)	21(1)
C(7)	5344(4)	3021(4)	6431(3)	19(1)
I(1)	8258(7)	5184(9)	6574(5)	27(2)

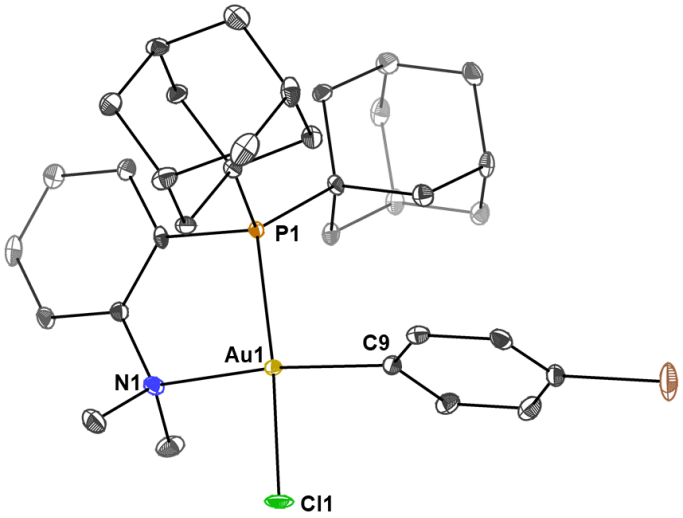

Solid-state structure of [**2j**][SbF_6] with thermal ellipsoids rendered at the 50% probability level and with hydrogen atoms, disorder, and $[SbF_6]^-$ counterion omitted for clarity.

Crystallographic Data for [**2j**][SbF_6].

Identification code	JS-12	
CCDC Code	1835371	
Empirical formula	C34 H44 Au Br Cl0.77 F6 I0.23 N P Sb	
Formula weight	1066.78	
Temperature	100.0 K	
Wavelength	0.71073 Å	
Crystal system	Triclinic	
Space group	*P*-1	
Unit cell dimensions	a = 10.1820(10) Å	α = 109.033(4)°
	b = 11.4038(13) Å	β = 100.165(3)°
	c = 16.3043(16) Å	γ = 100.426(4)°
Volume	1702.7(3) $Å^3$	

Z	2
Density (calculated)	2.081 Mg/m^3
Absorption coefficient	6.646 mm^{-1}
$F(000)$	1029
Crystal size	0.26 x 0.24 x 0.18 mm^3
Theta range for data collection	1.926 to 28.275°.
Index ranges	$-13 \leq h \leq 13$, $-14 \leq k \leq 15$, $-21 \leq l \leq 21$
Reflections collected	30650
Independent reflections	8451 [R(int) = 0.0374]
Completeness to theta = 25.242°	100.0%
Absorption correction	Semi-empirical from equivalents
Max. and min. transmission	0.7457 and 0.5487
Refinement method	Full-matrix least-squares on F^2
Data / restraints / parameters	8451 / 2 / 418
Goodness-of-fit on F^2	1.028
Final R indices [$I > 2\sigma(I)$]	$R1$ = 0.0276, w$R2$ = 0.0582
R indices (all data)	$R1$ = 0.0348, w$R2$ = 0.0604
Extinction coefficient	n/a
Largest diff. peak and hole	1.913 and -3.742 e.$Å^{-3}$

Atomic coordinates (x 10^4) and equivalent isotropic displacement parameters ($Å^2$x 10^3) for [**2j**][SbF_6]. U(eq) is defined as one third of the trace of the orthogonalized U^{ij} tensor.

	x	y	z	U(eq)
Au(1)	1103(1)	1550(1)	7182(1)	9(1)
Sb(1)	1382(1)	6967(1)	8946(1)	12(1)
Br(1)	1456(1)	3684(1)	3837(1)	30(1)
P(1)	3370(1)	1458(1)	7651(1)	8(1)
F(1)	2285(3)	8172(2)	8535(2)	25(1)
F(2)	647(3)	5811(3)	7764(2)	32(1)
F(3)	2930(3)	6303(2)	9026(2)	30(1)
F(4)	497(3)	5794(2)	9376(2)	27(1)
F(5)	2132(2)	8154(2)	10132(2)	23(1)
F(6)	-160(2)	7656(2)	8884(2)	22(1)
N(1)	786(3)	1234(3)	8386(2)	12(1)
C(1)	-320(4)	25(4)	8158(3)	21(1)
C(2)	312(4)	2383(4)	8881(3)	20(1)
C(3)	2045(4)	1211(3)	8975(2)	11(1)
C(4)	3299(4)	1341(3)	8731(2)	10(1)
C(5)	4484(4)	1370(3)	9345(2)	12(1)
C(6)	4412(4)	1277(4)	10164(2)	15(1)
C(7)	3147(4)	1123(4)	10380(3)	16(1)

C(8)	1967(4)	1087(4)	9787(2)	14(1)
C(9)	1281(4)	2111(4)	6130(2)	12(1)
C(10)	1367(4)	1315(4)	5305(2)	12(1)
C(11)	1432(4)	1796(4)	4623(3)	15(1)
C(12)	1380(4)	3051(4)	4778(3)	18(1)
C(13)	1240(4)	3833(4)	5582(3)	18(1)
C(14)	1185(4)	3362(4)	6263(3)	15(1)
C(15)	3649(4)	-107(3)	6946(2)	10(1)
C(16)	4731(4)	-547(3)	7489(2)	13(1)
C(17)	4888(4)	-1848(3)	6887(3)	13(1)
C(18)	3504(4)	-2849(4)	6593(3)	16(1)
C(19)	2412(4)	-2440(4)	6051(3)	16(1)
C(20)	2855(5)	-2319(4)	5226(3)	21(1)
C(21)	4242(4)	-1321(4)	5528(3)	18(1)
C(22)	2254(4)	-1133(3)	6640(3)	12(1)
C(23)	5337(4)	-1728(4)	6066(3)	19(1)
C(24)	4119(4)	-3(4)	6118(2)	14(1)
C(25)	4739(4)	2926(3)	7845(2)	10(1)
C(26)	4626(4)	3268(4)	6991(2)	13(1)
C(27)	5689(4)	4543(4)	7199(3)	15(1)
C(28)	5411(4)	5616(4)	7947(3)	15(1)
C(29)	5546(4)	5290(3)	8791(2)	13(1)
C(30)	6999(4)	5149(4)	9088(3)	16(1)

C(31)	7274(4)	4078(4)	8334(3)	16(1)
C(32)	6226(4)	2800(3)	8139(3)	13(1)
C(33)	4475(4)	4039(3)	8600(2)	12(1)
C(34)	7150(4)	4403(4)	7488(3)	17(1)
I(1)	-1468(1)	1453(1)	6680(1)	19(1)
Cl(1)	-1166(1)	1459	6725	19(1)

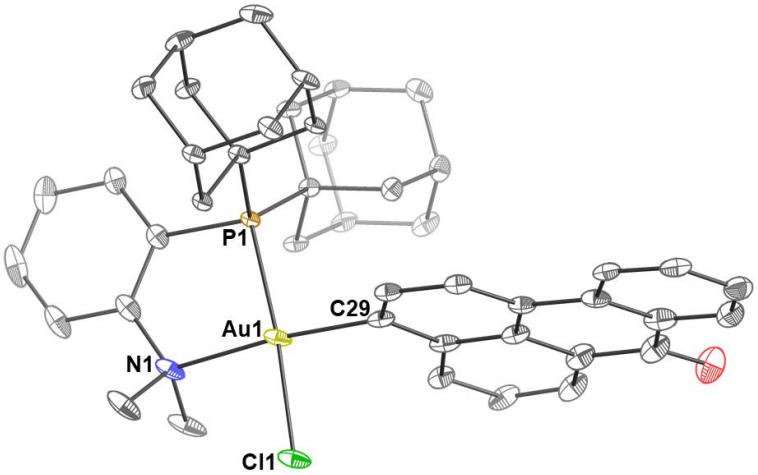

Solid-state structure of [**2r**][SbF_6] with thermal ellipsoids rendered at the 50% probability level and with hydrogen atoms, disorder, and $[SbF_6]^-$ counterion omitted for clarity.

Crystallographic Data for [**2r**][SbF_6].

Identification code	JS-17	
CCDC Code	1835366	
Empirical formula	C45 H49 Au Cl0.85 F6 I0.15 N O P Sb	
Formula weight	1132.70	
Temperature	100.0 K	
Wavelength	0.71073 Å	
Crystal system	Triclinic	
Space group	*P*-1	
Unit cell dimensions	*a* = 10.0424(11) Å	α = 101.463(3)°
	b = 12.0230(13) Å	β = 101.135(3)°
	c = 19.663(2) Å	γ = 100.103(3)°
Volume	2225.8(4) $Å^3$	
Z	2	

Density (calculated)	1.690 Mg/m^3
Absorption coefficient	4.149 mm^{-1}
F(000)	1111
Crystal size	0.25 x 0.22 x 0.18 mm^3
Theta range for data collection	1.773 to 26.452°.
Index ranges	$-12 \leq h \leq 12$, $-15 \leq k \leq 15$, $-24 \leq l \leq 24$
Reflections collected	61519
Independent reflections	9174 [*R*(int) = 0.0487]
Completeness to theta = 25.242°	100.0 %
Absorption correction	Semi-empirical from equivalents
Max. and min. transmission	0.6465 and 0.5276
Refinement method	Full-matrix least-squares on F^2
Data / restraints / parameters	9174 / 0 / 526
Goodness-of-fit on F^2	1.114
Final *R* indices [$I \leq 2\sigma(I)$]	*R*1 = 0.0460, w*R*2 = 0.0956
R indices (all data)	*R*1 = 0.0624, w*R*2 = 0.1054
Extinction coefficient	n/a
Largest diff. peak and hole	2.770 and -3.305 $e.Å^{-3}$

Atomic coordinates (x 10^4) and equivalent isotropic displacement parameters ($Å^2$x 10^3) for [**2r**][SbF_6]. U(eq) is defined as one third of the trace of the orthogonalized U^{ij} tensor.

	x	y	z	U(eq)
Au(1)	8747(1)	8127(1)	2346(1)	28(1)
Sb(1)	8659(1)	2683(1)	819(1)	54(1)
P(1)	6451(2)	8178(1)	1870(1)	17(1)
Cl(1)	11102(3)	8142(3)	2743(3)	39(1)
F(6)	7153(5)	3379(4)	666(3)	58(1)
F(3)	8074(5)	1772(4)	-108(3)	60(1)
F(5)	9733(5)	3803(5)	500(3)	71(2)
C(19)	5165(6)	6772(5)	1714(3)	21(1)
F(2)	10188(7)	2025(9)	993(4)	132(4)
O(1)	8334(7)	4433(4)	5181(3)	57(2)
C(10)	5593(6)	9333(5)	3041(3)	22(1)
C(29)	8585(6)	7911(5)	3334(4)	26(1)
C(25)	2690(6)	5642(5)	1247(4)	28(2)
N(1)	9124(6)	8318(5)	1318(3)	33(1)
F(4)	7577(7)	1522(8)	1114(4)	116(3)
C(8)	6625(7)	8400(5)	996(3)	27(1)
C(26)	3666(6)	6845(5)	1394(4)	24(1)

C(9)	6024(6)	9523(5)	2354(3)	21(1)
C(20)	5621(6)	5870(5)	1177(4)	24(1)
C(24)	2739(7)	5250(6)	1944(4)	35(2)
C(21)	4626(7)	4674(5)	1033(4)	28(2)
C(16)	7392(6)	10480(5)	2543(3)	22(1)
C(15)	7175(6)	11617(5)	2977(4)	25(1)
C(27)	5209(7)	6372(5)	2411(3)	27(1)
C(28)	3156(7)	4763(5)	713(4)	31(2)
C(32)	8622(6)	7682(5)	4742(4)	28(1)
C(30)	8688(6)	8862(5)	3878(4)	30(2)
C(11)	5428(7)	10496(5)	3480(4)	31(2)
C(39)	8451(8)	5404(6)	5061(4)	43(2)
C(3)	7910(8)	8446(5)	818(4)	33(2)
C(31)	8686(6)	8740(5)	4566(4)	28(1)
C(34)	8756(7)	8489(6)	6047(4)	33(2)
C(44)	8561(6)	6802(5)	3486(4)	31(2)
C(22)	4683(7)	4289(5)	1727(4)	36(2)
C(38)	8564(8)	6450(6)	5629(5)	42(2)
C(33)	8649(7)	7551(6)	5473(4)	32(2)
C(43)	8565(7)	5800(5)	2969(4)	32(2)
C(7)	5496(7)	8497(5)	486(4)	30(2)
C(14)	6004(7)	12027(5)	2529(4)	31(2)
C(45)	8542(7)	6691(5)	4189(4)	30(2)

C(23)	4221(7)	5165(6)	2258(4)	34(2)
C(18)	6793(7)	11411(5)	3662(4)	28(2)
C(35)	8806(7)	8353(7)	6728(4)	38(2)
C(40)	8472(8)	5570(6)	4342(4)	38(2)
C(17)	4875(7)	9952(5)	1904(4)	28(1)
C(42)	8487(8)	4736(6)	3125(4)	40(2)
C(13)	4661(7)	11085(5)	2347(4)	34(2)
C(6)	5642(10)	8650(6)	-176(4)	44(2)
C(12)	4274(7)	10898(6)	3037(4)	38(2)
C(4)	8047(9)	8599(6)	150(4)	43(2)
C(5)	6930(11)	8712(6)	-340(4)	53(3)
C(2)	10305(8)	9355(7)	1426(4)	47(2)
C(41)	8437(8)	4627(6)	3807(4)	42(2)
C(36)	8737(8)	7278(7)	6876(4)	45(2)
F(1)	9258(7)	3616(12)	1740(3)	171(5)
C(37)	8610(8)	6327(7)	6324(5)	45(2)
C(1)	9561(8)	7223(6)	1016(5)	49(2)
I(1)	11428(5)	8134(4)	3083(3)	36(2)

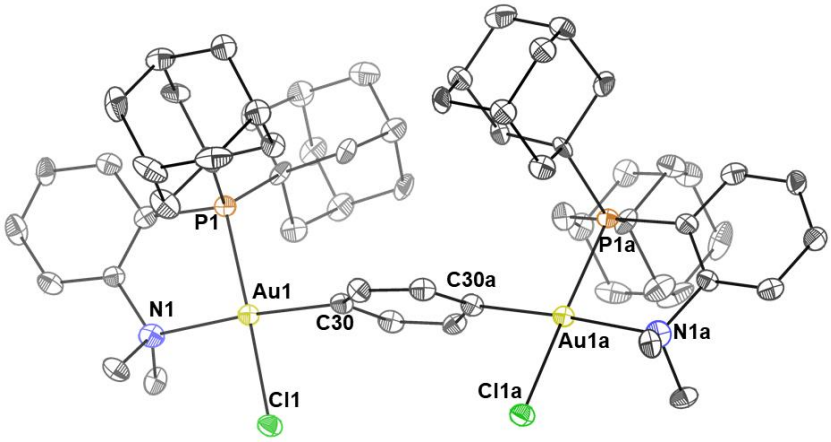

Solid-state structure of [**2s**][SbF_6]$_2$ with thermal ellipsoids rendered at the 50% probability level and with hydrogen atoms, one co-crystallized DCM molecule and two [SbF_6]$^-$ counterions omitted for clarity.

Crystallographic Data for [**2s**][SbF_6]$_2$·DCM.

Identification code	JS-03	
CCDC Code	1835365	
Empirical formula	C64 H88 Au2 Cl6 F12 N2 P2 Sb2	
Formula weight	2025.43	
Temperature	100.0 K	
Wavelength	0.71073 Å	
Crystal system	Orthorhombic	
Space group	*Pccn*	
Unit cell dimensions	a = 20.8838(10) Å	α = 90°
	b = 17.9885(10) Å	β = 90°
	c = 18.4736(10) Å	γ = 90°
Volume	6939.9(6) Å^3	
Z	4	

Density (calculated)	1.939 Mg/m^3
Absorption coefficient	5.336 mm^{-1}
F(000)	3944
Crystal size	0.22 x 0.08 x 0.05 mm^3
Theta range for data collection	1.857 to 24.998°.
Index ranges	$-24 \leq h \leq 24$, $-21 \leq k \leq 21$, $-21 \leq l \leq 21$
Reflections collected	36322
Independent reflections	6107 [*R*(int) = 0.1193]
Completeness to theta = 24.998°	99.9%
Absorption correction	Semi-empirical from equivalents
Max. and min. transmission	0.7452 and 0.4798
Refinement method	Full-matrix least-squares on F^2
Data / restraints / parameters	6107 / 0 / 396
Goodness-of-fit on F^2	1.059
Final *R* indices [$I > \sigma(I)$]	*R*1 = 0.0468, w*R*2 = 0.1034
R indices (all data)	*R*1 = 0.0913, w*R*2 = 0.1292
Extinction coefficient	n/a
Largest diff. peak and hole	2.319 and -2.320 $e.Å^{-3}$

Atomic coordinates (x 10^4) and equivalent isotropic displacement parameters ($Å^2$x 10^3) for [**2s**][SbF_6]$_2$. U(eq) is defined as one third of the trace of the orthogonalized U^{ij} tensor.

	x	y	z	U(eq)
Au(1)	2084(1)	5662(1)	4609(1)	18(1)
Sb(1)	3955(1)	3336(1)	3471(1)	27(1)
Cl(1)	1940(1)	6015(1)	3399(1)	27(1)
P(1)	2190(1)	5276(1)	5803(1)	18(1)
Cl(3)	5138(1)	2465(2)	523(2)	49(1)
Cl(2)	4936(2)	4028(2)	835(2)	58(1)
F(2)	3431(3)	3244(3)	4286(3)	30(1)
F(6)	3227(3)	3496(4)	2901(3)	44(2)
F(5)	4476(3)	3436(4)	2652(3)	48(2)
F(1)	4011(3)	4360(3)	3638(3)	46(2)
F(4)	3887(3)	2315(3)	3295(4)	48(2)
F(3)	4666(3)	3165(4)	4065(4)	50(2)
N(1)	1760(4)	4539(5)	4385(4)	25(2)
C(30)	2346(5)	6740(5)	4739(5)	21(2)
C(28)	1955(4)	6579(5)	6623(5)	21(2)
C(32)	3136(5)	7723(6)	4726(5)	22(2)
C(3)	1742(5)	4038(5)	5038(5)	20(2)
C(31)	2985(5)	6982(6)	4704(5)	23(2)

C(23)	1481(5)	7052(6)	7056(5)	26(2)
C(27)	377(5)	6040(6)	7094(5)	28(2)
C(4)	1600(5)	3300(6)	4949(6)	26(2)
C(19)	1641(4)	5819(5)	6404(5)	17(2)
C(8)	1876(4)	4345(5)	5708(5)	20(2)
C(26)	1030(5)	5976(6)	5963(5)	25(2)
C(7)	1822(5)	3858(6)	6307(5)	24(2)
C(24)	883(5)	7177(5)	6597(6)	28(3)
C(2)	2216(5)	4219(6)	3823(5)	27(3)
C(25)	557(5)	6437(6)	6411(6)	28(2)
C(14)	4212(5)	5295(6)	6983(5)	26(2)
C(20)	1451(5)	5402(6)	7106(5)	27(3)
C(21)	983(5)	5894(6)	7555(6)	30(3)
C(6)	1672(5)	3126(6)	6211(6)	28(3)
C(17)	3142(5)	4686(6)	6761(5)	27(2)
C(22)	1296(5)	6637(6)	7741(6)	34(3)
C(1)	1107(4)	4566(5)	4070(6)	25(2)
C(15)	4125(5)	5747(6)	6296(5)	26(2)
C(9)	3050(4)	5142(5)	6056(5)	22(2)
C(5)	1560(5)	2843(6)	5549(6)	31(3)
C(29)	4401(5)	5326(7)	5649(5)	34(3)
C(10)	3355(5)	4712(7)	5413(6)	34(3)
C(18)	3861(5)	4550(6)	6906(6)	28(3)

C(11)	4070(5)	4582(7)	5570(6)	36(3)
C(16)	3397(5)	5884(6)	6167(6)	26(2)
C(33)	5175(6)	3166(6)	1186(6)	40(3)
C(12)	4147(5)	4129(6)	6261(6)	40(3)

4.5.25 Appendix D References

1. Ahrland, S.; Dreisch, K.; Norén, B; Oskarsson, Å. *Mater. Chem. Phys.* **1993**, *35* 281-289.
2. Vinogradova, E. V.; Zhang, C.; Spokoyny, A. M.; Pentelute, B. L.; Buchwald, S. L. *Nature* **2014**, *526*, 687-691.
3. Joost, M.; Zeineddine, A.; Estévez, L; Mallet-Ladeira, S.; Miqueu, K.; Amgoune, A.; Bourissou, D. *J. Am. Chem. Soc.* **2014**, *136*, 14654-14657.
4. Neises, B.; Steglich, W. *Angew. Chem. Int. Ed.* **1978**, *17*, 522-524.
5. Zeineddine, A.; Estévez, L.; Mallet-Ladeira, S.; Miqueu, K.; Amgoune, A.; Bourissou, D. *Nat. Commun.* **2017**, *565*, 1-8.
6. Chen, R.; John, J.; Lavrentieva, A.; Muller, S.; Tomala, M.; Zhao, Y. X.; Zweigerdt, R.; Beutel, S.; Hitzmann, B.; Kasper, C.; Martin, U.; Rinas, U.; Stahl, F.; Scheper, T. *Eng. Life Sci*, **2012**, *12*, 29-38.